

Performance modeling of Arabian asphalt using HP-GPC chromatography

Ibrahim Mohammed Khalil Asi

Civil Engineering

June 1996

Abstract

In the Gulf countries, asphalt pavements show signs of high severity distresses in the early stages of service. One of the main factors contributing to these distresses is the asphalt cement. Asphalt cement is characterized by its viscous and elastic properties. Two tests are used in the Gulf countries to classify and test for the suitability of an asphalt cement for usage under certain loading and environmental conditions. They are penetration and viscosity. These tests, however, can't be used to predict the performance of the asphalt. SHRP has developed a new set of tests which has the ability to predict asphalt performance because it relies on fundamental asphalt properties. SHRP tests are time consuming and require expensive and complicated equipment set-up and highly trained operators. Therefore there is a need to find a simple, reliable, and fundamental test that can be used by asphalt manufacturers for process control and performance prediction.

High Pressure Gel Permeation Chromatography (HP-GPC) is one of the most advanced techniques used in characterizing the molecular distribution of liquid materials. It is available in quite a number of local institutions and oil refineries. It is possible to use this device to predict asphalt performance if a set of models that relate produced HP-GPC profiles to performance properties can be developed. HP-GPC has not been used as a standard test for the evaluation of asphalt cement.

In this study, Arabian neat asphalt samples were collected from the different asphalt producing refineries in the Gulf countries. An additional set of polymer modified samples was included in this study. All collected asphalt samples were subjected to two aging processes to simulate heating, mixing and compaction, and in-service aging. The asphalt samples at the different aging stages were subjected to rheological and performance-based testing. HP-GPC was used to produce profiles of the molecular size distribution of the test samples. Models were built to predict the rheological and performance-based properties from the produced HP-GPC profiles. These models will be used to determine the suitability of using a given asphalt for a specific environmental condition within the Gulf region.

INFORMATION TO USERS

This manuscript has been reproduced from the microfilm master. UMI films the text directly from the original or copy submitted. Thus, some thesis and dissertation copies are in typewriter face, while others may be from any type of computer printer.

The quality of this reproduction is dependent upon the quality of the copy submitted. Broken or indistinct print, colored or poor quality illustrations and photographs, print bleedthrough, substandard margins, and improper alignment can adversely affect reproduction.

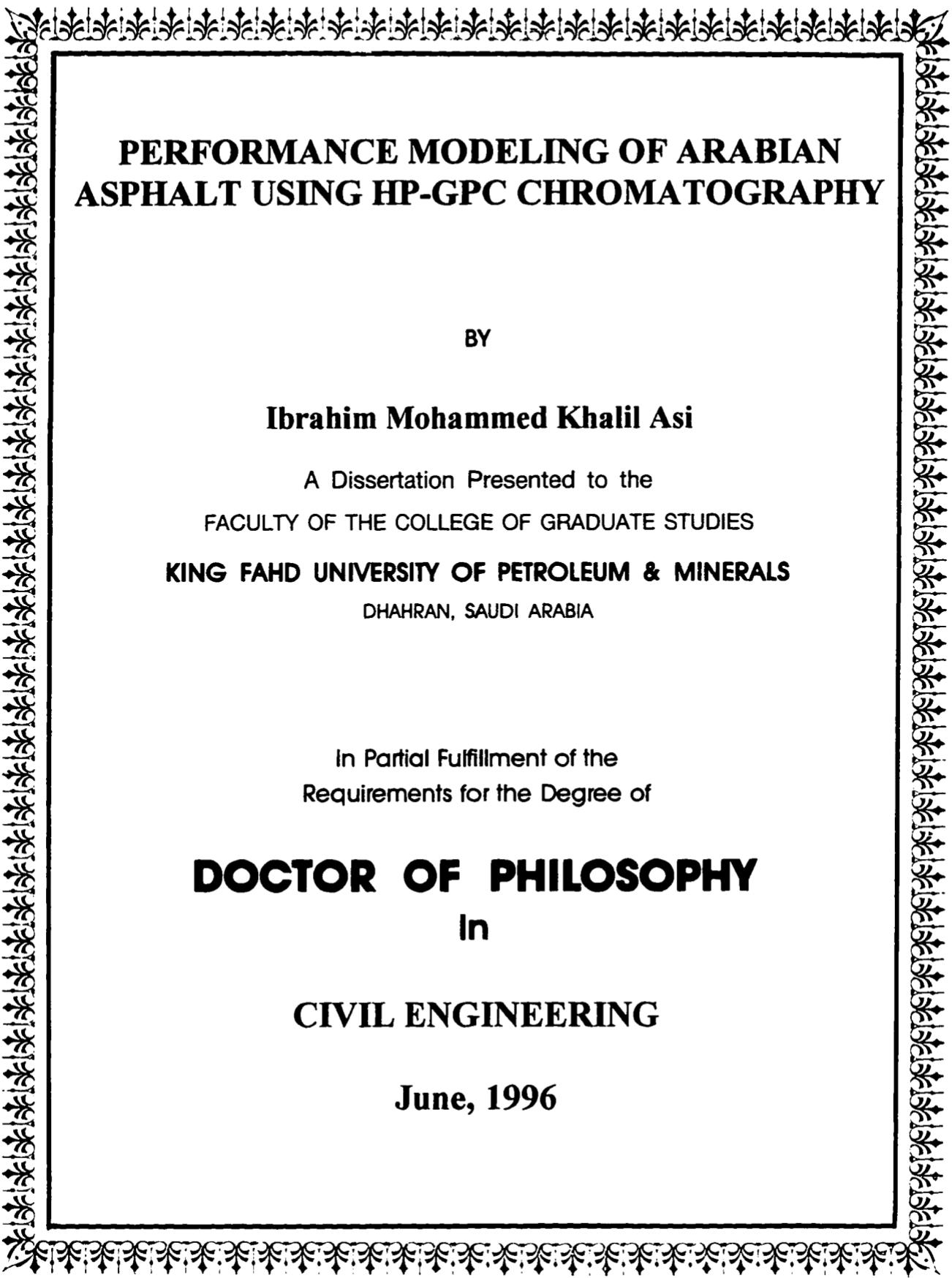
In the unlikely event that the author did not send UMI a complete manuscript and there are missing pages, these will be noted. Also, if unauthorized copyright material had to be removed, a note will indicate the deletion.

Oversize materials (e.g., maps, drawings, charts) are reproduced by sectioning the original, beginning at the upper left-hand corner and continuing from left to right in equal sections with small overlaps. Each original is also photographed in one exposure and is included in reduced form at the back of the book.

Photographs included in the original manuscript have been reproduced xerographically in this copy. Higher quality 6" x 9" black and white photographic prints are available for any photographs or illustrations appearing in this copy for an additional charge. Contact UMI directly to order.

UMI

A Bell & Howell Information Company
300 North Zeeb Road, Ann Arbor MI 48106-1346 USA
313/761-4700 800/521-0600



**PERFORMANCE MODELING OF ARABIAN
ASPHALT USING HP-GPC CHROMATOGRAPHY**

BY

Ibrahim Mohammed Khalil Asi

A Dissertation Presented to the
FACULTY OF THE COLLEGE OF GRADUATE STUDIES
KING FAHD UNIVERSITY OF PETROLEUM & MINERALS
DHAHRAN, SAUDI ARABIA

In Partial Fulfillment of the
Requirements for the Degree of

DOCTOR OF PHILOSOPHY
In

CIVIL ENGINEERING

June, 1996

UMI Number: 9715447

UMI Microform 9715447
Copyright 1997, by UMI Company. All rights reserved.

**This microform edition is protected against unauthorized
copying under Title 17, United States Code.**


UMI
300 North Zeeb Road
Ann Arbor, MI 48103

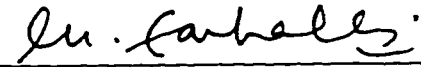
King Fahd University of Petroleum and Minerals
Dhahran 31261, Saudi Arabia

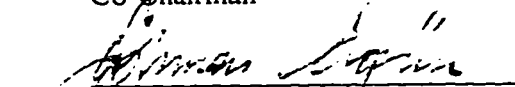
COLLEGE of GRADUATE STUDIES

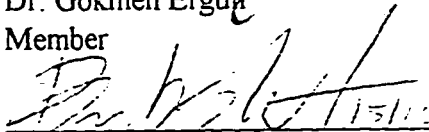
This dissertation, written by **IBRAHIM MOHAMMED KHALIL ASI** under the direction of his Dissertation Advisor and approved by his Dissertation Committee, has been presented to and accepted by the Dean of the College of Graduate Studies, in partial fulfillment of the requirements of the degree of **DOCTOR OF PHILOSOPHY in CIVIL ENGINEERING**.

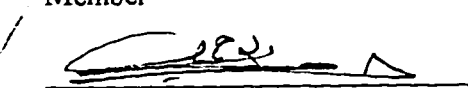
Dissertation Committee

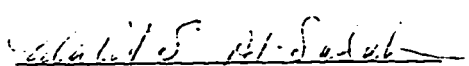

Dr. Hamad I. Al-Abdul Wahhab
Dissertation Committee Chairman

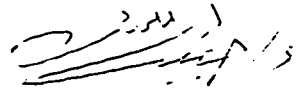

Dr. Mohammed F. Ali
Co-Chairman

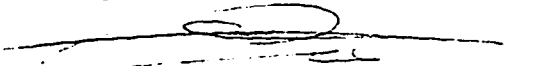

Dr. Gokmen Ergun
Member


Dr. Abdulaziz Bubshait
Member

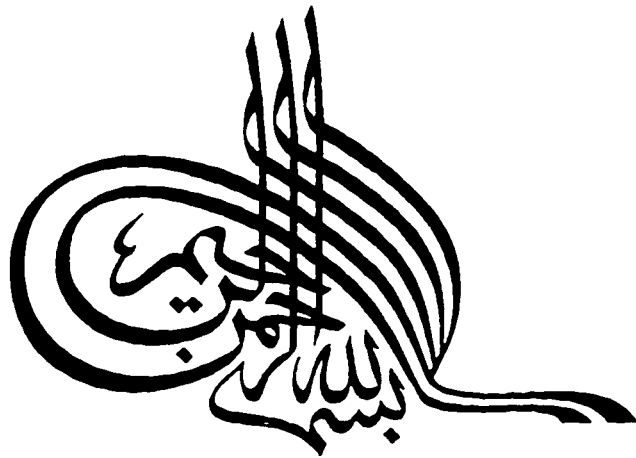

Dr. Hasan M. Al-Ahmadi
Member


Dr. Walid Al-Sabah
Member


Dr. Sahel N. Abduljawwad
Department Chairman


Dr. Aballah M. Al-Shehri
Dean, College of Graduate Studies

10-11-96
Date



{In the Name of Allah the Most Beneficent, the Most Merciful}

أهدي نتاجي هذا إلى:

والدي رحمهما الله وغفر لهما

وزوجتي رعاها الله

وأبنائي أحمد وآية وفقهما الله

وإلى كل من كان وراء هذا العمل.....

إبراهيم عاصي

ACKNOWLEDGEMENTS

ALL GRATITUDE IS TO ALLAH

Praise and Glory be to the Almighty ALLAH for bestowing me with the health, spirit, strength and perseverance to complete this work.

Acknowledgement is due to King Fahd University of Petroleum and Minerals for the support given to this research.

I wish to express my deep appreciation to my major advisor and chairman of my dissertation committee, Dr. Hamad I. Al-Abdul Wahhab for his encouragement, helpful suggestions and valuable guidance. Appreciation and thanks are also extended to the other members of my dissertation committee, Dr. Mohammed F. Ali, Dr. Gokmen Ergun, Dr. Abdulaziz Bubshait, Dr. Hasan M. Al-Ahmadi, and Dr. Walid Al-Sabah for their assistance and advice during my thesis research.

Also, my deepest appreciation to my brother Eng. Omer Ahmed and to all my friends who in one way or the other provided assistance during this research, to mention a few, Ibrahim Al-Dubabe, Hassan Zakariyah, Sobh Jebreel, Mohommad Tawabini and Solano Cruz, and to the souls of Mohammed Ashraf and Esam El-Deeb (peace upon them).

Last but not the least, my deepest thanks to my wife and children for their support and patience.

TABLE OF CONTENTS

<i>Chapter</i>		<i>Page</i>
	List of Tables	viii
	List of Figures	xi
	List of Plates	xiv
	ABSTRACT	xv
	Used Abbreviations	xvii
1	INTRODUCTION	1
1.1	General	1
1.2	Problem Statement	4
1.3	Objectives	6
2	LITERATURE REVIEW	7
2.1	General	7
2.2	Rheological Properties of Asphalt	7
	2.2.1 Consistency Tests	11
	2.2.1.1 Penetration Test	11
	2.2.1.2 Absolute Viscosity	12
	2.2.1.3 Kinematic Viscosity	12
	2.2.1.4 Softening Point	13
	2.2.1.5 Flash Point	13

2.2.2	Asphalt Aging	14
2.2.3	Temperature Susceptibility	16
2.2.3.1	Penetration Index.....	17
2.2.3.2	Penetration Ratio	19
2.2.3.3	Penetration Viscosity Number	19
2.2.3.4	Viscosity Temperature Susceptibility	20
2.3	Performance Related Properties	20
2.3.1	Aging of Binders for Performance Testing	22
2.3.2	Rotational Viscometer (RV) Testing	25
2.3.3	Dynamic Shear Rheometer (DSR) Testing	26
2.3.4	Bending Beam Rheometer (BBR) Testing	31
2.3.5	Direct Tension Tester (DTT) Testing	32
2.3.6	SHRP Binder Specifications	33
2.3.7	The Linear Viscoelastic Model (LVE) of Asphalt.	38
2.4	Chemical Composition of Asphalt	50
2.4.1	Asphalt Chemistry	50
2.4.2	Asphalt Composition	58
2.4.2.1	Corbett and Swarbrick Method	60
2.4.2.2	Rosstler and Sternberg Method	62

	2.4.2.3 The Clay-Gel Method	64
	2.4.2.4 High Pressure Gel Permeation Chromatography	67
	2.5 Summary	72
3	RESEARCH METHODOLOGY	74
	3.1 Introduction	74
	3.2 Experimental Design	76
	3.3 Rheological Tests	77
	3.4 Performance-Related Tests	79
	3.5 High Pressure Gel Permeation Chromatography.....	81
	3.6 Modeling of Rheological and Performance- Related Properties	83
4	DATA COLLECTION AND ANALYSIS	87
	4.1 Collection of Test Samples	87
	4.2 Physical Testing	90
	4.2.1 Consistency Testing	90
	4.2.2 Heat Hardening and Temperature Susceptibility Indices	93
	4.3 Performance Based Testing	98
	4.3.1 Rotational Viscosity	98
	4.3.2 Aging of Asphalt Samples	101

4.3.3	Dynamic Shear Rheometer Testing	103
4.3.4	Bending Beam Rheometer (BBR) Testing	110
4.3.5	Direct Tension Testing	116
4.3.6	Grading of Collected Asphalt Samples	121
4.4	Construction of the Master Curves	129
4.5	Chemical Composition	145
4.5.1	HP-GPC Testing	145
4.5.2	Fractionating Procedure of the HP-GPC Chromatograms	151
4.5.3	Fractionation of HP-GPC Chromatograms	158
4.6	Summary	173
5	MODELING OF ASPHALT PROPERTIES USING HP-GPC CHROMATOGRAMS	174
5.1	Generation of Models	174
5.2	Testing of Models	188
5.2.1	Sign Testing	188
5.2.2	Homoscedasticity Testing	190
5.2.3	Normality Testing	191
5.2.4	Autocorrelation Testing	191
5.2.5	Multicollinearity and Singularity Testing	194
5.3	Model Validation	197

5.4	Summary	201
6	CONCLUSIONS AND RECOMMENDATIONS	202
6.1	Conclusions	202
6.2	Recommendations	204
	REFERENCES	206
	APPENDICES	
	Appendix A : Performed SHRP Tests	
	Appendix B : Input and Output for LVE Development and Developed LVE Curves	
	Appendix C : Chemical Testing Results	
	Appendix D : Fractionating Procedures for the Produced HP-GPC Chromatograms	
	Appendix E : Statistical Analysis of the Produced Models	

LIST OF TABLES

<u>Table No.</u>		<u>Page</u>
2.1	Elemental analyses of representative petroleum asphalts (Petersen, 1984)	53
2.2	Analytical procedures used to test asphalt composition (Thenoux, 1987; Goodrich et al., 1986)	59
3.1	Experimental design matrix for the rheological properties of Ras Tanura samples	78
3.2	Experimental design matrix for the performance related properties of Ras Tanura samples	80
3.3	Used fractionating procedures for the fresh samples	82
3.4	Used properties and indices	84
3.5	A priori hypothesis for the models which will be predicted in the study	85
4.1	Physical properties of the different asphalt samples	92
4.2	Heat hardening and temperature susceptibility indices of the different asphalt samples	95
4.3	Testing the differences in PVN values between various refineries using ANOVA	99
4.4	Acquired data from the DSR testing machine for the different asphalt samples	108
4.5	Calculated complex shear moduli for the PAV residue samples at test frequencies and temperature after DSR tests ..	109
4.6	Acquired data from the BBR testing machine for the different asphalt samples	114

4.7	Stiffness values of the residue samples at the different loading times after BBR testing	115
4.8	Summary of DTT test results	122
4.9	SHRP grading of the collected samples	127
4.10	Calculated complex shear moduli for the PAV residue samples at the test frequencies and temperatures after BBR tests	132
4.11	Calculated parameters for the construction of the master curves for the neat samples	138
4.12	Calculated parameters for the construction of the master curves for the polymer modified samples	140
4.13	Example for calculating cumulative percentage area for a sliced HP-GPC produced chromatogram	155
4.14	HP-GPC fractions - using three equal times fractions	161
4.15	HP-GPC fractions - using three (30%-40%-30%) corresponding areas fractions	169
5.1	Used properties and indices	177
5.2	Correlation matrix - using three equal times fractions	178
5.3	R-square of the different models using stepwise regression	180
5.4	R-square of the different models for the extra suggested fractions	182
5.5	Generated models for the different parameters	185
5.6	Model fitting results and analysis of variance for the prediction of the upper grading limit model	187
5.7	Durbin-Watson test for autocorrelation	195

5.8	Validation of generated models for the different parameters ..	199
5.9	Prediction of the generated models for the performance grades of the validation samples	200

LIST OF FIGURES

<u>Figure No.</u>		<u>Page</u>
2.1	Typical relationship between shear stress and rate of shear strain for asphalt cement (Monismith et al., 1985)	8
2.2	Typical response of asphalt cement to creep (Monismith et al., 1985)	10
2.3	Variation of viscosity with temperature for two typical asphalts (McLeod, 1989)	18
2.4	Graphical representation of both G^* and δ (Asphalt Institute, 1993)	27
2.5	Stress strain relation for elastic and viscous materials (Asphalt Institute, 1993)	28
2.6	SHRP performance-graded asphalt binder specifications chart (Harrigan et. al., 1994)	35
2.7	General shape of the group complex modulus and phase angle versus loading time (Anderson et al., 1994)	43
2.8	Graphical representation of the time shift factors (Harrigan et. al., 1994)	45
2.9	Dynamic master curve for RT1 sample, with important parameters described (Al-Abdul Wahhab et al., 1995)	48
2.10	Adsorption/desorption chromatography Corbett-Swarbrick, ASTM D 4124	61
2.11	Chemical precipitation Rosstler-Sternberg, ASTM D 2006 ...	63
2.12	Adsorption/desorption chromatography "Clay-Gel", ASTM D 2007	65

2.13	Typical HP-GPC chromatogram showing the three elution times' fractions (Jennings, 1982)	70
3.1	Flow chart of the planned work	75
4.1	Sample identification scheme	89
4.2	Temperature-viscosity relationship for the tested samples	97
4.3	Typical printout of DSR fixed frequency testing for sample RT1R tested at 64°C	107
4.4	Typical printout of BBR test results for sample RY1P tested at -12°C	112
4.5	Typical BBR graphical presentation of load & force during testing	113
4.6	Direct tension test (DTT) setup assembly	117
4.7	Typical DTT test results for RT5P sample	120
4.8	Classification testing - unaged binders	123
4.9	Classification testing - RTFO aged binders	124
4.10	Classification testing - low starting point temperature (PG-64)	125
4.11	Classification testing - established low temperature binder grade with creep stiffness m-value, and tensile failure strain .	126
4.12	Graphical representation of performance grades of collected samples	128
4.13	Master curves of RY1 sample at test temperatures and at the defining temperature	142
4.14	Master curves of RY2 modified sample with different percentages of SBS	143

4.15	HP-GPC system setup	148
4.16	Typical produced HP-GPC chromatogram for BH-CRT-5-F sample	150
4.17	Produced HP-GPC chromatogram for KW2 sample at different stages of aging	152
4.18	HP-GPC chromatogram for BH1 sample after processing and slicing to eight slices	156
4.19	Bar chart representation of HP-GPC produced chromatogram for BH1 sample	157
4.20	Effect of polymer percentage on the skewness of the produced HP-GPC chromatogram	159
4.21	HP-GPC chromatograms for RT samples	164
4.22	HP-GPC chromatogram for RY samples	165
4.23	HP-GPC chromatogram for BH samples	166
4.24	HP-GPC chromatogram for KW samples	167
4.25	HP-GPC chromatogram for sample # 1 from each asphalt source	168
5.1	Change of R-square value with the change of number of fractions	183
5.2	Plot of predicted values versus the measured ones for the prediction of the upper grading limit model	189
5.3	Plot of predicted values versus residuals for prediction of the upper grading limit model	192
5.4	Normal probability plot for the residuals of the upper grading limit model	193

LIST OF PLATES

<u>Plate No.</u>		<u>Page</u>
4.1	Used Brookfield viscometer	100
4.2	Used rolling thin film oven (RTFO)	102
4.3	Used pressure aging vessel (PAV)	104
4.4	Dynamic shear rheometer (DSR) with all accessories	105
4.5	Bending beam rheometer (BBR) with all accessories	111
4.6	Fabricated direct tension tester (DTT)	118
4.7	High pressure gel permeation chromatography system	147

خلاصة الرسالة

إسم الطالب : إبراهيم محمد خليل عاصي.
عنوان الدراسة : تطوير نماذج لتحديد أداء الأسفلت العربي باستخدام جهاز نفاذية الجمل الكروماتوغرافي عالي الضغط (HP-GPC).
التخصص : هندسة مدنية.
تاريخ الشهادة : يونيو ١٩٩٦م.

تظهر في المراحل الأولى من أعمار الرصفات الأسفلتية في دول الخليج العربي تشوهات مرتفعة الشدة وتعتبر مادة الأسفلت المستخدمة في هذه الرصفات إحدى أهم العوامل التي تساهم في حدوث تلك التشوهات. يستخدم في دول الخليج حالياً اختباران لتصنيف أنواع الأسفلت وفحص ملائمة الأسفلت للاستخدام في الظروف البيئية السائدة. هذان الاختباران هما اختبار الإحتراق واختبار اللزوجة. ولا يملك أي من هذين الاختبارين المقدرة على التنبؤ بأداء الأسفلت عند الاستخدام في الطرق. وقد قام مؤرخاً المشروع البحثي الإستراتيجي للطرق في الولايات المتحدة الأمريكية (شارب - SHRP) بتطوير وتبني بعض الاختبارات التي يمكن من خلالها توقع أداء الأسفلت وذلك لكون هذه الاختبارات تعتمد على خصائص الأسفلت الأساسية. وأحد العيوب الموجودة في اختبارات شارب حاجتها إلى أجهزة مرتفعة التكاليف وكذلك فنيين متخصصين. ولذلك فإن هناك حاجة لإيجاد اختبار سهل، وموثوق ومبني على أسس علمية ومن الممكن إستخدامه من قبل مصنعي ومستخدمي الأسفلت للتحكم بنوعية المنتج وكذلك إمكانية تحديد أداء الأسفلت.

يعتبر جهاز نفاذية الجمل الكروماتوغرافي - عالي الضغط (HP-GPC) من أكثر الأجهزة تطوراً في مجال تمييز توزع الذرات في المواد المسائلة. ويميز هذا الجهاز وجوده في عدد من المؤسسات العلمية المحلية وكذلك مصافي البترول. ومن الممكن إستخدام هذا الجهاز لتحديد أداء الأسفلت إذا تم تطوير نماذج رياضية تستطيع الربط بين الرسومات البيانية المنتجة من جهاز (HP-GPC) وخصائص الأداء الأسفلتي. تم في هذه الدراسة جمع عينات أسفلتية من مصافي البترول المنتجة للأسفلت في دول الخليج العربي، وتم كذلك إستخدام عينات أسفلتية معالجة باللدائن. عُرِضَت جميع العينات المستخدمة في هذا البحث إلى عمليتي تعتيق وذلك لتمثيل التأثير الحاصل على الأسفلت نتيجة تسخينه وخلطه ورصه وكذلك لتمثيل الهرم الحاصل في الأسفلت أثناء الخدمة. فُحصت الخصائص الريولوجية (المرونة واللزوجة واللدانة) وخصائص الأداء لجميع عينات البحث، وكذلك تم إستخدام جهاز (HP-GPC) لإيجاد الرسم البياني لتوزيع أحجام الجزيئات المكونة للعينات المختلفة. وفي النهاية طورت نماذج رياضية للتنبؤ بالخصائص الريولوجية وخصائص الأداء من الرسومات البيانية المنتجة من جهاز (HP-GPC). بالإمكان إستخدام النماذج المطورة لمعرفة صلاحية أي أسفلت للاستخدام في الظروف البيئية السائدة.

درجة الدكتوراه في الفلسفة
جامعة الملك فهد للبترول والمعادن
الظهران، المملكة العربية السعودية
يونيو ١٩٩٦م

DISSERTATION ABSTRACT

NAME : IBRAHIM MOHAMMED KHALIL ASI

**TITLE OF STUDY : PERFORMANCE MODELING OF ARABIAN
ASPHALT USING HP-GPC CHROMATOGRAPHY**

MAJOR FIELD : CIVIL ENGINEERING

DATE OF DEGREE: JUNE, 1996

In the Gulf countries, asphalt pavements show signs of high severity distresses in the early stages of service. One of the main factors contributing to these distresses is the asphalt cement. Asphalt cement is characterized by its viscous and elastic properties. Two tests are used in the Gulf countries to classify and test for the suitability of an asphalt cement for usage under certain loading and environmental conditions. They are penetration and viscosity. These tests, however, can't be used to predict the performance of the asphalt. SHRP has developed a new set of tests which has the ability to predict asphalt performance because it relies on fundamental asphalt properties. SHRP tests are time consuming and require expensive and complicated equipment set-up and highly trained operators. Therefore there is a need to find a simple, reliable, and fundamental test that can be used by asphalt manufacturers for process control and performance prediction.

High Pressure Gel Permeation Chromatography (HP-GPC) is one of the most advanced techniques used in characterizing the molecular distribution of liquid materials. It is available in quite a number of local institutions and oil refineries. It is possible to use this device to predict asphalt performance if a set of models that relate produced HP-GPC profiles to performance properties can be developed. HP-GPC has not been used as a standard test for the evaluation of asphalt cement.

In this study, Arabian neat asphalt samples were collected from the different asphalt producing refineries in the Gulf countries. An additional set of polymer modified samples was included in this study. All collected asphalt samples were subjected to two aging processes to simulate heating, mixing and compaction, and in-service aging. The asphalt samples at the different aging stages were subjected to rheological and performance-based testing. HP-GPC was used to produce profiles of the molecular size distribution of the test samples. Models were built to predict the rheological and performance-based properties from the produced HP-GPC profiles. These models will be used to determine the suitability of using a given asphalt for a specific environmental condition within the Gulf region.

**DOCTOR OF PHILOSOPHY DEGREE
KING FAHD UNIVERSITY OF PETROLEUM AND MINERALS
DHAHRAN, SAUDI ARABIA
JUNE, 1996**

USED ABBREVIATIONS

<u>Property</u>	<u>Abbreviation</u>
* High Pressure - Gel Permeation Chromatography	- HP-GPC
* Strategic Highway Research Program	- SHRP
* Ras-Tanura samples	- RT
* Riyadh samples	- RY
* Bahrain samples	- BH
* Kuwait	- KW
* Penetration at 25°C	- PEN25
* Softening point	- SP
* Flash point	- FP
* Absolute viscosity at 60°C	- VIS60
* Kinematic viscosity at 135°C	- VIS135
* Rotational viscosity at 135°C	- RV135
* Retained penetration at 4°C	- RP4
* Reclaimed penetration at 25°C	- RP25
* Viscosity ratio at 60°C	- VR60
* Viscosity ratio at 135°C	- VR135

* Penetration index	- PI
* Penetration ratio	- PR
* Penetration-viscosity number	- PVN
* Viscosity-temperature susceptibility	- VTS
* Large molecular size	- LMS
* Medium molecular size	- MMS
* Small molecular size	- SMS
* Thin film oven	- TFO
* Rolling thin film oven	- RTFO
* Pressure Aging Vessel Test	- PAV
* Dynamic Shear Rheometer	- DSR
* Complex modulus	- G^*
* Phase angle	- δ
* Glassy modulus	- G_g
* Cross over frequency	- ω_o
* Test frequency	- ω_i
* Rheological index	- R
* Steady-state viscosity	- η_o
* Bending Beam Rheometer	- BBR
* Creep stiffness	- S
* Logarithmic creep rate	- m-value

- * Direct Tension Testing - DTT
- * Performance grade - PG
- * Linear visco-elastic model - LVE

Chapter 1

INTRODUCTION

1.1 GENERAL

Asphalt cement is a rheological, thermoplastic and visco-elastic material. It is considered a rheological material because its deformation characteristics vary not only with load, but also with time rate of load application. It is considered thermoplastic because its consistency or degree of hardness varies with temperature. Asphalt cement (AC) is neither purely elastic nor purely viscous in behavior. When loaded rapidly or when at low temperature, it exhibits elastic behavior. When loaded slowly or when at high temperature, it exhibits viscous behavior. For an intermediate range of load rate or temperature, AC exhibits a combination of elastic and viscous behavior. The properties of asphalt are also affected by its age since its consistency increases with age due to the oxidation process the asphalt is subjected to during its life cycle. Therefore, when testing for asphalt's physical properties, time, temperature, and aging should be taken into consideration. Another factor which should be considered when defining the physical properties of asphalt is the possibility of correlating the properties to field performance, i.e., the field performance of the AC may be predicted from those properties. A new set of tests have been adopted by the Strategic Highway Research Program (SHRP). These

tests can be used to evaluate the adequacy of an asphalt cement for a specified temperature and traffic load, from a performance point of view.

Asphalt chemistry is extremely complex; even utilizing highly technical analytical tools, it is impossible to identify and quantify all the components of even a single asphalt. The complexity of asphalt comes from its being a product of crude oil, which is formed from plant life by a natural process which occurs over thousands of years under varied conditions of temperature and pressure. Another factor is that asphalt is actually the residue left after all volatile fractions of the petroleum have been distilled off. Therefore, asphalt characteristics are affected by heating temperature and heating time in the distillation tower and the source and nature of the crude oil from which it's produced. The principal elements in asphalt are carbon and hydrogen. Small amounts of sulphur, nitrogen, and oxygen are present in asphalt. In addition, there are trace amounts of other materials such as vanadium and nickel. The most important factors affecting the behavior of asphalt are the way the atoms are incorporated into molecules and the type of molecular structures that are formed. These factors are more important than the total amounts of each element. Many molecular structural and chemical variations can be reduced to classes or types that produce similar effects on asphalt properties (Branthaver et al., 1993).

One of the methods which was developed to study the molecular structures of materials is High Pressure-Gel Permeation Chromatography (HP-GPC). HP-GPC is an advanced technique which was originally developed to determine the distribution of molecules in polymers. This technique can also be used to study the molecular size distribution of liquids such as asphalt. HP-GPC determines the degree of association of the molecules, which has a great influence on the behavior of the material. It is expected that comparing the distribution of the molecules between two asphalts will lead to understanding the difference in behavior between both asphalts. The molecular distribution of asphalt may have the fingerprint of its behavior when subjected to heating, construction, and/or field performance.

In this research, the possibility of using the HP-GPC chromatograms to predict asphalt performance behavior was evaluated. Mathematical models were generated to predict performance of asphalt cement based on its molecular size. Those models will hopefully help in understanding asphalt behavior and the suitability of using a specific asphalt under prevailing loading and temperature conditions.

In the Gulf countries, there are currently four asphalt producing refineries. They are the Ras Tanura and Riyadh refineries in Saudi Arabia, the Al-Ahmadi refinery in Kuwait, and the BAPCO refinery in Bahrain. The asphalt produced by

these refineries is referred to as “Arabian Asphalt”. Asphalts produced by these refineries are included in this study.

1.2 PROBLEM STATEMENT

In the Gulf countries, asphalt pavements show signs of high severity distresses in the early stages of service. One of the main factors contributing to these distresses is the asphalt cement. Asphalt cement is characterized by its viscous and elastic properties. Two tests are used in the Gulf countries to classify and test for the suitability of an asphalt cement for usage under certain loading and environmental conditions. They are penetration and viscosity. These tests, however, can't be used to predict the performance of the asphalt (Bahia and Anderson, 1994). SHRP has developed a new set of tests which has the ability to predict asphalt performance because it relies on fundamental asphalt properties. SHRP tests are time consuming and require expensive and complicated equipment set-up and highly trained operators. Therefore there is a need to find a simple, reliable, and fundamental test that can be used by asphalt manufacturers for process control and performance prediction.

High Pressure Gel Permeation Chromatography (HP-GPC) is one of the most advanced techniques used in characterizing the molecular distribution of liquid materials. It is available in quite a number of local institutions and oil

refineries. It is possible to use this device to predict asphalt performance if a set of models that relate produced HP-GPC profiles to performance properties can be developed. HP-GPC has not been used as a standard test for the evaluation of asphalt cement, and no models have been generated to predict asphalt performance based on HP-GPC profiles. There are certain features of the HP-GPC that make the technique more attractive than other chemical testing procedures. Some of those features include the following:

- it has a minimum disturbance on the forces associating the different molecules making up the asphalt, and it can detect interactions between molecules,
- it has a very high degree of repeatability,
- after setting up the machine, it is simple to operate,
- it can be used to monitor changes during manufacturing, hot mix processing, or the life cycle of the asphalt, and
- it is available at low cost to asphalt manufacturers compared to performance testing equipment,

In this research, HP-GPC was used to characterize the asphalts produced by Gulf countries. Models to predict both the rheological and performance-based properties of both neat and polymer modified Arabian asphalts, considering in-service conditions, were generated. These models will be used to determine the

suitability of using a given asphalt for a specific environmental condition within the Gulf region.

1.3 OBJECTIVES

The main goal of this research was to investigate the feasibility of using HP-GPC chromatograms to build models that can be used to predict performance and rheological properties of Arabian asphalt. Such models can be used to fingerprint asphalts suitable for each temperature range within the Gulf region. To achieve this goal, the research had the following objectives:

- 1- Study rheological, performance related properties and high pressure-gel permeation chromatography of Arabian asphalts.
- 2- Using the results obtained in the above item, calibrate and validate models for predicting the performance and rheological properties of Arabian asphalt from HP-GPC chromatograms.
- 3- Study the effects of aging and polymer modification on the molecular size distribution of asphalt.
- 4- Recommend and modify a suitable procedure for analysis of the different chromatograms produced by the HP-GPC.

Chapter 2

LITERATURE REVIEW

2.1 GENERAL

Emphasis in this literature review is on three major subjects that relate to the theme of this research. The first is rheology of asphalt and the traditional means of measuring rheological properties and temperature susceptibility. The second is the need for performance related properties, the aim of the Strategic Highway Research Program (SHRP), the performance tests included in SHRP, and the parameters which are determined from the performance tests. The third is the compositional characteristics of AC and the use of high pressure gel permeation chromatography to draw profiles of the molecular size distribution for the different samples.

2.2 RHEOLOGICAL PROPERTIES OF ASPHALT

Asphalt cement is a rheological material since its behavior depends on both temperature and rate of loading. In other words, its stress strain characteristics are time and/or temperature dependent. Fig. 2.1 shows the relation between the shear strain rate and shear stress for a typical asphalt, where the asphalt exhibits shear thinning characteristics with the increase of the shear strain. The viscosity of the asphalt (η) at any point is the instantaneous slope of the curve at any particular

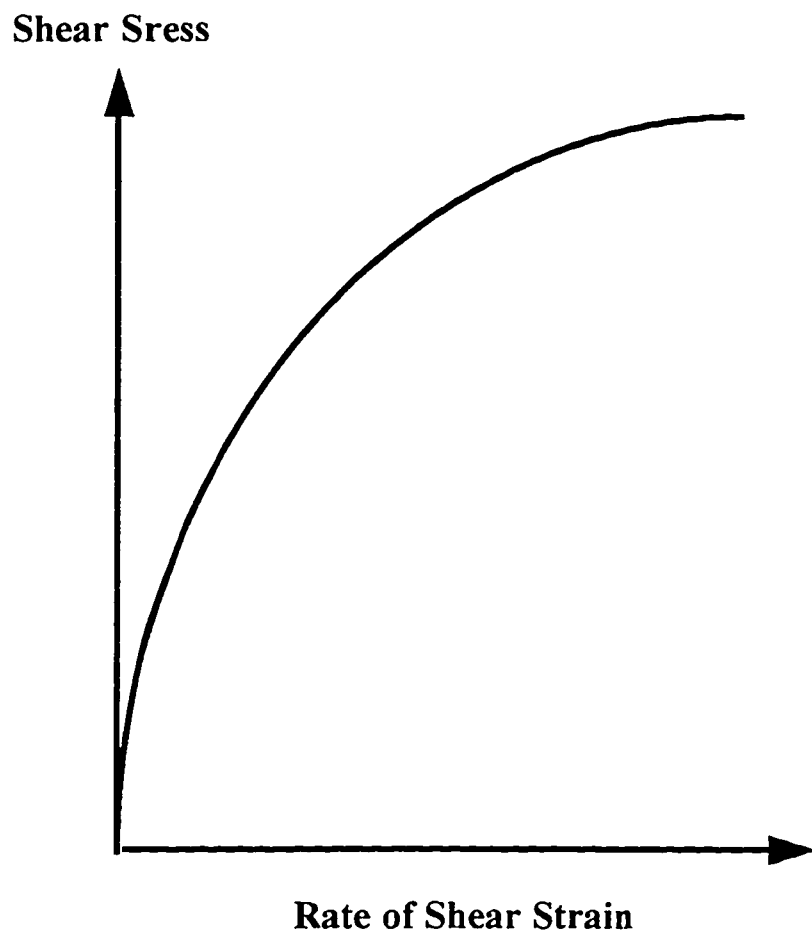


Figure 2.1: Typical Relationship between Shear Stress and Rate of Shear Strain for Asphalt Cement (Monismith et al., 1985).

shear rate. The viscosity decreases with the increase of shear rate. Time and temperature affects are interchangeable; high temperature and short loading times are, in general, equivalent to low temperature and long loading times. Asphalt will behave nearly as an elastic material when loaded at high load rate or when at low temperature. It will behave as a viscous material when loaded very slowly or when at high temperature. At intermediate ranges of load rate and/or temperature, asphalt behaves as a visco-elastic material, where a delayed elastic response governs the behavior. Fig. 2.2 shows a typical response of asphalt under creep loading. Three components of strains are shown in this curve. They are elastic, visco elastic, and viscous strains in the loading and unloading cycles. The magnitudes of these strains and the relative shape of the creep curve will change with loading time and test temperature (Monismith et al., 1985).

Another factor which should be considered when talking about rheological properties is age hardening of asphalt. Asphalt under the effect of time (age) and heat reacts with oxygen from the environment or loses some of its volatile materials. This leads to a more brittle asphalt; this process is called age hardening. Aging occurs at a faster rate in hot climates, compared with cold climates, in a process referred to as a seasonal hardening (Asphalt Institute, 1993). Due to the effect of time on aging, older asphalts are more brittle than new ones, and they are more prone to cracking. Aging of asphalt occurs even at the initial stages of

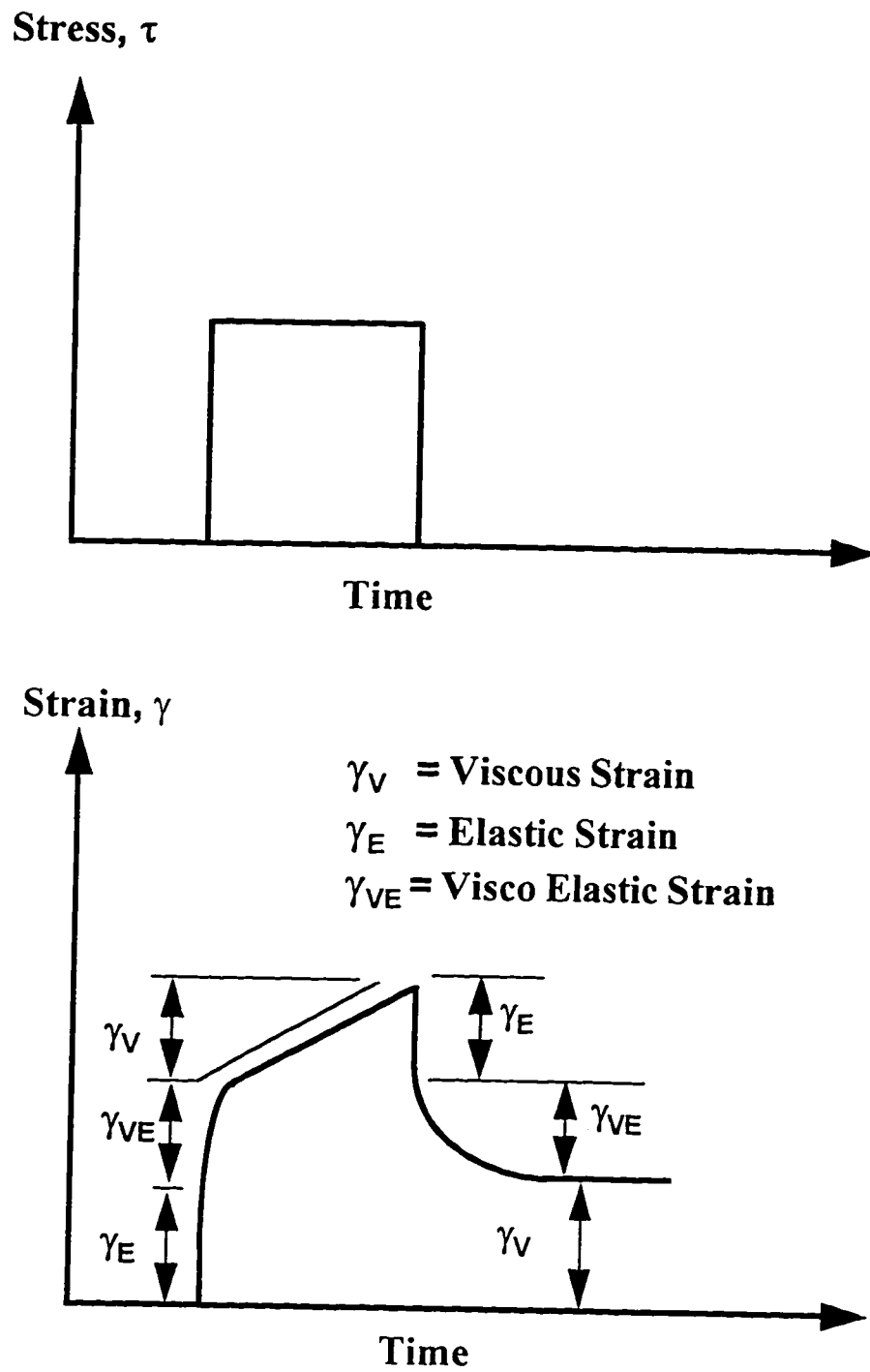


Figure 2.2: Typical Response of Asphalt Cement to Creep (Monismith et al., 1985).

construction, and it happens at a fast rate when the asphalt is being heated for mixing. Aging continues at nearly the same rate when the asphalt is mixed with aggregate and compacted.

2.2.1 Consistency Tests

Consistency describes the degree of fluidity or plasticity of the asphalt at any particular temperature. There are two main grading approaches which are used presently to grade the different asphalts according to their consistency. Those grading approaches use either the penetration or the viscosity test. Usually these tests are performed at pre-specified standard temperatures. Another type of consistency test is the softening point, which determines the temperature at which there will be a change in the asphalt phase from solid to liquid. A brief explanation about some currently used consistency tests follows:

2.2.1.1 Penetration test (ASTM D-5)

The penetration test is an empirical test which is used to measure consistency of asphalt. It was developed by Bowen in 1889. In this test, a needle of prescribed dimensions is loaded with a 100 g weight and allowed to penetrate freely the asphalt sample for five seconds. The depth of penetration of the needle is measured in units of 0.1 mm (Roberts et al., 1991; ASTM, 1993). The penetration test is temperature sensitive and is usually performed at 25°C. This temperature

was chosen since it represents an approximate average service temperature of asphalt pavement in a moderate temperature region (Roberts et al., 1991). The penetration test can be performed at a lower temperature, which is usually 4°C using a load of 200 g. This test is neither a measure of viscosity nor a measure of elasticity.

2.2.1.2 Absolute viscosity (ASTM D-2171)

Viscosity in general is a measure of the resistance of the fluid to flow. It is measured by using capillary tubes such as Cannon-Manning or Asphalt Institute viscometers. This test is performed at 60°C, which represents the highest temperature the asphalt pavement is subjected to in the United States. A vacuum is used to drive the asphalt into the tube, and the time required for the asphalt to flow between two marks is used to calculate the viscosity in poises (Thenoux, 1981; Roberts et al., 1991; ASTM, 1993).

2.2.1.3 Kinematic viscosity (ASTM D-2170)

Kinematic viscosity is measured using the Zeitufuchs Cross-Arm viscometer. This test is performed at 135°C, which represents the mixing and compaction temperature of the asphalt. At this temperature no vacuum is needed because the asphalt is liquid enough to flow into the capillary tube under gravitational force alone. The required time in seconds for the asphalt to flow

between two marks on the viscometer is measured and used to calculate the kinematic viscosity in centistokes (Roberts et al., 1991; ASTM, 1993).

2.2.1.4 Softening point (ASTM D-36)

The softening point is a measure of the temperature at which the asphalt will change from solid state into liquid state. It is performed by placing a steel ball on top of an asphalt film which is placed in a brass ring. The whole assembly is placed in a water bath and heated at a rate of 5°C/minute. The temperature, in °C, when the asphalt cannot hold the weight of the ball is marked as the softening point. This test is referred to as the ring and ball test (Roberts et al., 1991; ASTM, 1993).

2.2.1.5 Flash point (ASTM D-92)

Flash point is not considered a consistency test but is a safety test which is introduced to find the highest temperature that the asphalt cement can be heated to without flashing or ignition. The standard test that finds the flash point of the AC is the “Cleveland Open Cup for Flash Point”. In this test, the AC is heated at a rate of 5°C per minute. Heating is continued, and a flame is passed periodically over the cup containing the AC until the vapor ignites. The temperature at the instant of flashing is called the flash point (Roberts et al., 1991; ASTM, 1993).

2.2.2 Asphalt Aging

The asphalt binder, being composed of organic molecules, reacts with oxygen from the environment. This oxidation reaction changes the structure and composition of asphalt molecules. Due to the presence of air voids in asphaltic concrete pavements, a certain amount of air penetrates the mixture causing some degree of oxidative hardening. This process is rapid during asphalt-aggregate mixing at elevated temperatures (more than 150° C) and slow when in service. Another form of hardening which occurs during the hot mixing and compaction of asphalt concrete mixtures is volatilization. Volatilization is when the volatile light constituents of the asphalt binder evaporate. Physical hardening is a time-dependent increase in the stiffness of asphalt cement that occurs at moderate or in-service temperatures and is associated with time-dependent shrinkage of the binder.

The objective of the aging testing procedures was to simulate the hardening that occurs during mixing, construction, and service of the asphalt pavement. Aging of asphalt results mainly from oxidation reactions affecting certain functionalities in the more or less complex fabric molecules that constitute their structures (Button et al. 1993). This generally leads to loss of adhesion, reduction in ductility, increase in brittleness, and eventually to reduction in serviceability under induced traffic and climatic conditions (Majidzadeh and Schweyer 1968). The asphalt binder during its life in pavements is usually subjected to two types of aging. The first is rapid aging

during manufacturing and laying (heating, mixing, compaction, and cooling). The short-term aging can be simulated by using the thin film oven test (TFO) (ASTM D-1754) or the rolling thin film oven test (RTFO) (ASTM D-2982). Before the Strategic Research Program (SHRP) there was no means of simulating the long-term aging which occurs during the life cycle (7-10 years) of asphalt cement while in service. SHRP has introduced a pressure aging vessel (PAV) test to simulate long-term aging. This test is discussed in section 2.3.1.

The thin film oven test is performed by pouring 50 g of asphalt into a flat pan forming a thin layer 3.2 mm thick, then placing the pan on a rotating shelf at a speed of 5 to 6 revolutions per minute in an oven at 163°C for 5 hours. The aged asphalt is then tested to meet a specified minimum retained penetration or maximum viscosity and weight loss (Roberts et al., 1991; ASTM, 1993).

The rolling thin film oven test has the same function as the thin film oven test except that some modification has been incorporated to shorten the heating time. In this test, asphalt samples are poured into bottles and an air jet is blown into the sample while it rotates inside an oven at 163°C for a period of 75 minutes (Roberts et al., 1991; ASTM, 1993).

To evaluate the effect of aging on the asphalt, consistency tests are usually performed on fresh samples. Those samples are then aged using the TFO or the

RTFO and the consistency tests are repeated on the aged samples. The following indices are usually used to quantify the amount of heat hardening:

- Retained penetration @ 25°C,

$$RP_{25} = \frac{\text{Pen @ 25° C of aged samples}}{\text{Pen @ 25° C of fresh samples}} \quad (2.1)$$

Larger RP25 indicates lower heat hardening.

- Retained penetration @ 4°C,

$$RP_4 = \frac{\text{Pen @ 4° C of aged samples}}{\text{Pen @ 4° C of fresh samples}} \quad (2.2)$$

Larger RP4 indicates lower heat hardening.

- Viscosity ratio @ 60°C,

$$VR_{60} = \frac{\text{Absolute viscosity @ 60° C of aged samples}}{\text{Absolute viscosity @ 60° C of fresh samples}} \quad (2.3)$$

Larger VR60 indicates larger heat hardening.

- Viscosity ratio @ 135°C,

$$VR_{135} = \frac{\text{Kinematic viscosity @ 135° C of aged samples}}{\text{Kinematic viscosity @ 135° C of fresh samples}} \quad (2.4)$$

Larger VR135 indicates larger heat hardening.

2.2.3 Temperature Susceptibility

Asphalt cement is a thermoplastic material since its consistency changes with temperature. Temperature susceptibility describes the rate of change of

consistency with temperature. The higher the change in the rate of consistency, or the greater the slope of the temperature viscosity plot or temperature penetration graph, the higher the temperature susceptibility. For proper design and construction, the temperature susceptibility of asphalt should be taken into consideration. Asphalt specifications limit the temperature consistency of the asphalt for pumping, spray applications, mixing, and compaction of the asphalt concrete. Fig. 2.3 shows two types of asphalt; asphalt A has more temperature susceptibility than asphalt B (McLeod, 1989; Button et al., 1983).

There are different techniques that are usually used to indicate the temperature susceptibility of asphalt cement. A brief discussion of some follows.

2.2.3.1 Penetration Index, PI

This index combines the results of penetration at 25°C and the softening point of asphalt.

$$PI = \frac{30}{1 + 90 \text{ PTS}} * 10 \quad (2.5)$$

where

PTS = Penetration Temperature Susceptibility, and

$$PTS = \frac{\text{Log } 800 - \text{Log Pen @ } 25^{\circ}\text{C}}{\text{R\&B soft. pt., } ^{\circ}\text{F} - 77} \quad (2.6)$$

where

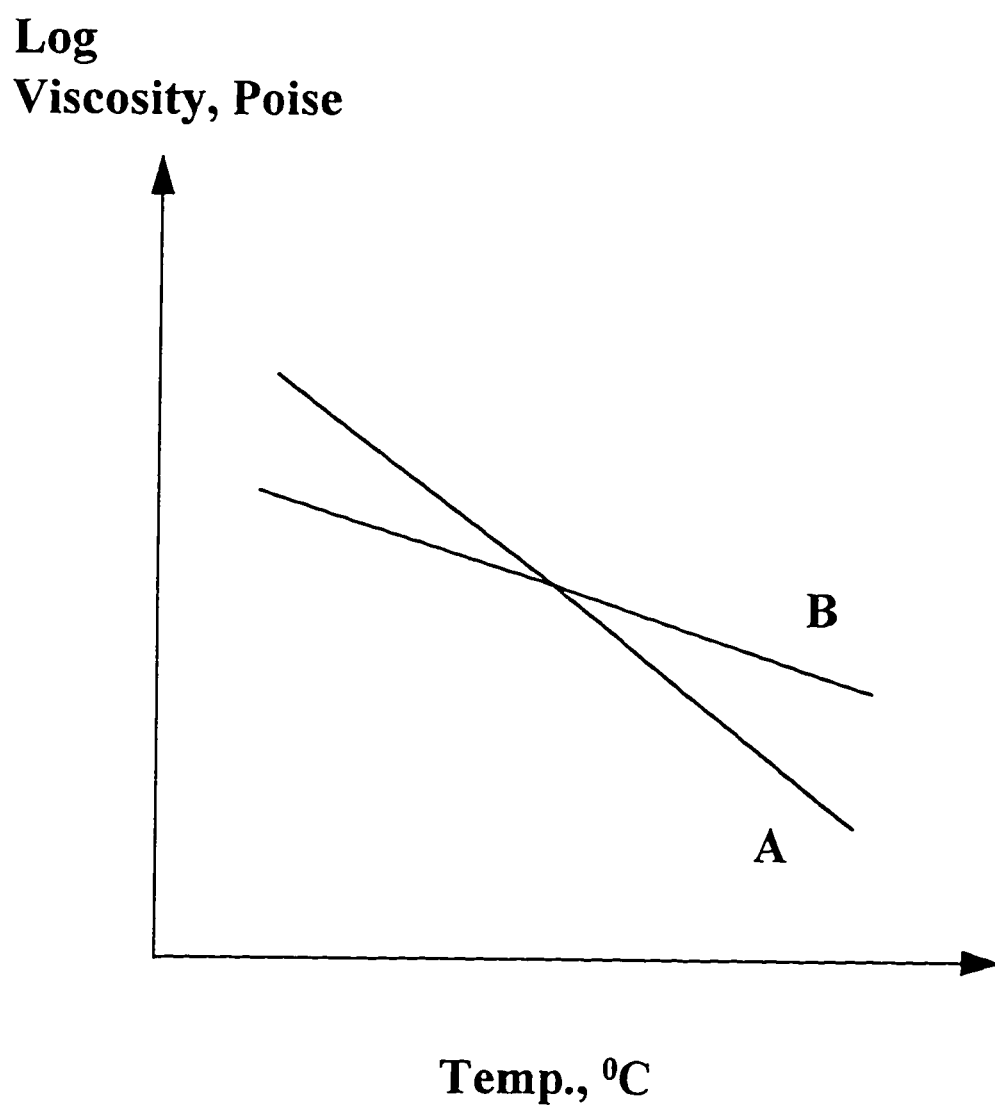


Figure 2.3: Variation of Viscosity with Temperature for Two Typical Asphalts (Mcleod, 1989).

Pen @ 25° C = penetration value measured at 25° C, dmm; and

R&B soft. pt. °F = Ring and Ball softening point measured in °F.

Typical acceptable asphalt grades have values of penetration index between +2 and -2. The larger negative values of PI indicates greater temperature susceptibility (Monismith et al., 1985).

2.2.3.2 Penetration Ratio, PR

This ratio combines the results of the penetration test at 4°C using a load of 200 g for 60 seconds and the penetration at 25°C using a load of 100 g for 5 seconds.

$$PR = \frac{\text{Pen at } 4^{\circ}\text{C}}{\text{Pen at } 25^{\circ}\text{C}} * 100 \quad (2.7)$$

where

Pen at 4°C = penetration value measured at 4° C, dmm; and

Pen at 25°C = penetration value measured at 25° C, dmm.

Lower PR indicates greater temperature susceptibility (Garrick, 1986).

2.2.3.3 Penetration-Viscosity Number, PVN

This test combines the results of the penetration test at 25°C and the kinematic viscosity. Lower PVN indicates greater temperature susceptibility (Mcleod, 1989).

$$PVN = \left(\frac{4.258 - 0.7967 \log \text{Pen} - \log \eta}{0.7951 - 0.1858 \log \text{Pen}} \right) (-1.5) \quad (2.8)$$

where

Pen = penetration value measured at 25° C, dmm; and

η = viscosity measured at 135° C, centistocks.

2.2.3.4 Viscosity-Temperature Susceptibility, VTS

VTS is based on the viscosity at two temperatures. A large VTS number indicates higher temperature susceptibility. VTS is calculated by the following formula (Roberts et al., 1991; Puzinauskas, 1967; Terrel et al., 1988):

$$VTS = \frac{\text{Log Log } \eta \text{ at } T_2 - \text{Log Log } \eta \text{ at } T_1}{\text{Log } T_1 - \text{Log } T_2} \quad (2.9)$$

where

η_1 = viscosity measured at T_1 , poises;

η_2 = viscosity measured at T_2 , poises; and

T_1 and T_2 = Temperature # 1 and Temperature # 2, °C.

2.3 PERFORMANCE RELATED PROPERTIES

The penetration and softening point tests are empirical tests that cannot be expressed in engineering units. They do not consider loading rate dependency, and they do not give an indication of whether the asphalt at the test temperature is more

elastic or more viscous (Bahia and Anderson, 1994). Moreover, the penetration test considers consistency at a medium temperature. On the other hand, although viscosity is a fundamental measure of flow, it only provides information about higher temperature viscous behavior not about the lower temperature elastic behavior, which is needed to completely predict performance. Moreover, none of the above mentioned physical properties can be used with confidence to predict the field performance of asphalt.

For all those reasons, the Strategic Highway Research Program (SHRP) developed a set of new testing methods that can be used to characterize the rheological, failure, and durability properties of asphalt binders. One of the factors which affects performance of the pavement is asphalt aging. To simulate both aging during mixing and compaction and aging in the field, SHRP has suggested to use the pressure aging vessel (PAV) and the rolling thin film oven test simultaneously. The most common asphalt pavement failures that the asphalt cement plays an important role in are rutting, fatigue cracking, and thermal cracking. These types of failures and distresses were kept in mind when selecting the new set of asphalt tests, which are (Bahia and Anderson, 1992)

- The rotational viscometer (RV) measures the flow properties at high temperature, which represent pumping and mixing temperature.

- The dynamic shear rheometer (DSR) measures the asphalt's properties at temperatures that represent high and intermediate pavement temperatures and at different loading rates representing traffic loading. This test gives an idea about the resistance of the asphalt cement to rutting when testing fresh asphalt and resistance to fatigue cracking when testing aged samples.
- The bending beam rheometer (BBR) measures the asphalt's properties at the lowest expected pavement temperatures and resembles the loading conditions that result from thermal cooling.
- The direct tension test is used to measure asphalt's failure properties at lowest pavement temperatures. This resembles loading that results from thermal cooling.

In this research, emphasis was placed on the rotational viscometer, the dynamic shear rheometer, the bending beam rheometer, and the direct tension test.

2.3.1 Aging of Binders for Performance Testing

The asphalt binder, during its life in pavements, is usually subjected to two types of aging. The first is rapid aging during manufacturing and laying (heating,

mixing, and compaction). The second is slow in-service aging due to climatic factors (heat and solar radiation). The factors affecting in-service aging include (Verhasselt and Choquet, 1993) the following:

1. Susceptibility of the binder to aging (i.e. ease of oxidation);
2. Porosity of asphaltic pavement, as characterized by the percentage of voids;
3. Oxidation reactions, which are stimulated by an increase in the exposure temperature;
4. Solar radiation, of which the ultraviolet component affects only a very thin layer of the binder at the surface, and the infrared (IR) spectrum increases the mean temperature of the pavement as it is absorbed;
5. Nature of the aggregate;
6. Other factors such as moisture, precipitation, and de-icing salts.

Asphalt hardening increases the stiffness and modulus of asphalt cement but lowers the strain required to produce cracking. Therefore, it is imperative that strain be limited to an acceptable level corresponding to the asphalt hardness attained during the life of the pavement. The only method for reducing the potential of low temperature cracking is to use a lower asphalt viscosity or reduce its hardening.

Kumar and Goetz (1977) have conducted a series of laboratory tests to measure the influence of permeability and asphalt film thickness on hardening. The film thickness was calculated as the percentage of asphalt available to coat an aggregate particle divided by the surface area of that aggregate particle. They found that air voids and asphalt film thickness had the greatest effects on the hardening rate such that when the air voids increase, the hardening rate increases. The most important factor associated with asphalt hardening is the oxidation of the asphalt throughout the entire thickness of the asphaltic concrete pavement. However, surface hardness is higher due to high temperature and ultra-violet light (Page et al. 1985).

Lee (1968) has developed a laboratory procedure for evaluating the durability of paving asphalt by simulating its two-stage hardening during the mixing process and subsequent pavement service. This test is capable of accelerating the hardening of asphalt into a relatively short period of time. The procedure consists of running the TFOT for a period of 5 hours at 163°C to simulate the changes that may occur in asphalt during hot-mixing, then exposing the TFOT residue to oxygen at the high pressure of 0.2 MPa (29 psi) at 60°C, for 24, 48, 96, and 240 hours to simulate the changes in the asphalt during its pavement service life. This aging procedure was recently adopted by SHRP after modification in terms of replacing the TFOT by the RTFOT test to reduce the testing time to only 85 minutes. The pressure-oxidation procedure was replaced by the Air Pressurized Aging Vessel

(PAV) (Button et al. 1993 and “Standard Practice” 1994). The test is performed at a pressure of 2.1 MPa (300 psi) at 90° to 110°C for 20 hours. This new aging procedure is capable of simulating 7 to 10 year aging of asphalt (Kulash, 1994 and Petersen et al., 1993).

2.3.2 Rotational Viscometer (RV) Testing

The Rotational Viscometer (RV) measures the rotational viscosity of the asphalt cement at pre-specified temperatures. This test was available before the SHRP project as a standard ASTM D4402 test, and it was included as part of SHRP’s binder specification testing. This test is performed to assure the possibility of handling and pumping the AC at the refinery, terminal, or hot mixing facility. Therefore, the RV will determine the flow characteristics of the asphalt at the elevated temperatures used in the refineries and mixing plants.

The RV is a rotational coaxial cylinder viscometer. One of the good features of the RV is that it can be used for polymer modified binders that have high viscosity since a set of spindles that can be used with materials with different viscosities are available with the instrument. Unlike capillary tube viscometers, the RV has large clearances between the rotating components and therefore can be used for binders with different types of additives. The RV has its own heating and digital reading unit (Asphalt Institute, 1993).

2.3.3 Dynamic Shear Rheometer (DSR) Testing

The device is used to measure the rheological properties of asphalt by measuring the viscous and elastic behavior of asphalt. Both loading rate and test temperature of the DSR can be controlled. In this test, asphalt is sandwiched between a fixed plate and a plate which rotates in an oscillatory (back and forth) manner. The frequency of oscillation, which is the length of time for each cycle, is controlled to simulate traffic speed. The oscillating plate is connected to a torque or strain gauge, which will record either of those values when the motion is created. From the recorded value, both the complex shear modulus (G^*) and phase angle (δ) of the asphalt sample are calculated. G^* is a measure of the total resistance of the asphalt to deformation. It consists of an elastic (recoverable) part and a viscous (non-recoverable) part. δ is an indicator of the relative amounts of elastic and viscous deformation (Asphalt Institute, 1993). Fig. 2.4 shows graphically the meaning of both G^* and δ . In this figure, although both asphalts A and B have the same G^* (length of the diagonal), asphalt A has a smaller elastic part while asphalt B has a lower viscous part. This indicates the need to define both G^* and δ for each asphalt. Fig. 2.5 shows the shape of the resulting shear strain for elastic and viscous materials due to an applied shear stress. This type of figure provides necessary information to calculate both G^* and δ . G^* is the ratio of the maximum

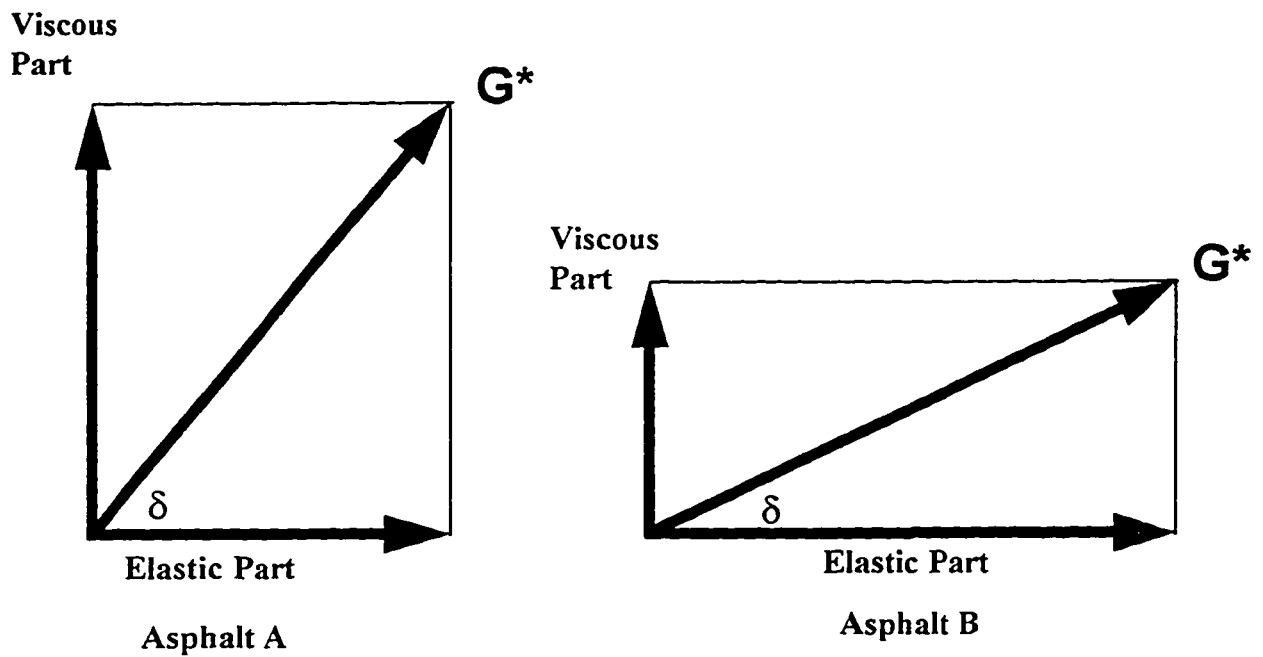


Figure 2.4: Graphical Representation of both G^* and δ
(Asphalt Institute, 1993).

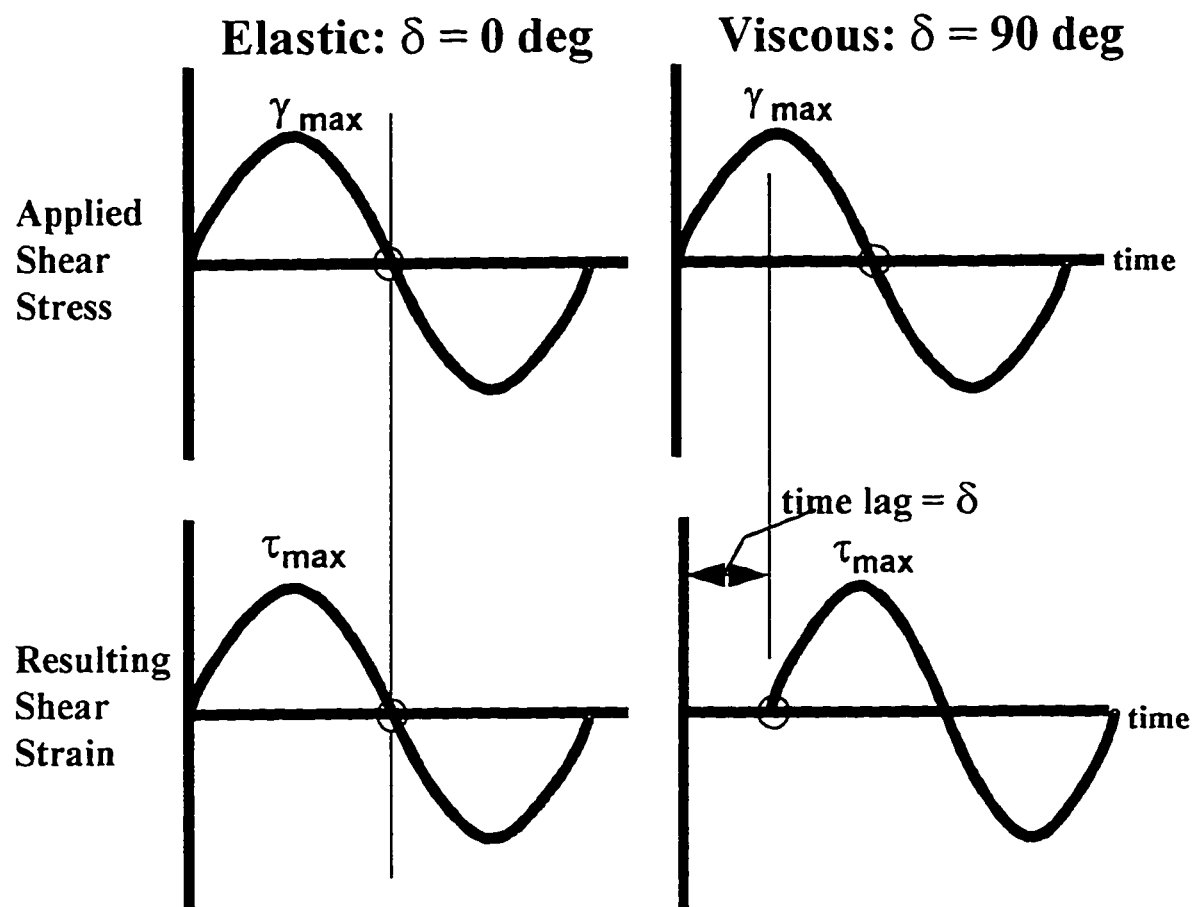


Figure 2.5: Stress Strain Relation for Elastic and Viscous Materials (Asphalt Institute, 1993).

shear stress (τ_{\max}) to maximum shear strain (γ_{\max}). The time lag between the applied stress and the resulting strain (for constant stress rheometer) is the phase angle. So, for perfectly elastic material, the applied stress coincides with the resulting strain, and the time lag or phase angle is zero. The phase angle increases with the increase of viscosity of the material (Asphalt Institute, 1993).

According to SHRP, permanent deformation (rutting) is controlled by limiting the minimum value of $(G^*/\sin \delta)$ at the required test temperature. This means that asphalt will better resist rutting if its shear modulus is higher and/or its $\sin \delta$ (viscous part/ G^*) is lower. On the other hand, fatigue cracking is controlled by limiting the maximum value of $G^* \sin \delta$ on PAV-aged samples. The limiting value concentrates on increasing the elastic part of the asphalt to be able to dissipate the applied stress and rapidly relax and/or have a lower value of G^* , which leads to a softer asphalt that can deform without developing large stresses. Performing the DSR test on samples aged by the pressure aging vessel provides the information needed to describe the binder resistance to fatigue cracking at intermediate pavement temperature.

Three other parameters are usually reported with the results of the dynamic shear rheometer: the storage modulus (G'), the loss modulus (G''), and the loss tangent ($\tan \delta$). These parameters are directly related to both the complex modulus and the phase angle. The storage modulus represents the in-phase component of the

complex modulus. Part of this modulus is due to the elastic component of the asphalt response. The formula for calculating G' (elastic component of G^*) is

$$G'(\omega) = G^*(\omega) \cos \delta \quad (2.10)$$

where

$G'(\omega)$ = dynamic storage modulus at frequency ω , Pa;

$G^*(\omega)$ = dynamic complex modulus at frequency ω , Pa; and

δ = phase angle, degrees.

The loss modulus represents the out-of-phase component of the complex modulus. Part of this modulus is due to the viscous component of the asphalt response. The formula for G'' (viscous component of G^*) is

$$G''(\omega) = G^*(\omega) \sin \delta \quad (2.11)$$

where

$G''(\omega)$ = dynamic loss modulus at frequency ω , Pa.

The loss tangent is the ratio of the loss modulus to the storage modulus, and it is represented by

$$\tan \delta(\omega) = \frac{G''(\omega)}{G'(\omega)} \quad (2.12)$$

where

$\delta(\omega)$ = phase angle at frequency ω , degrees.

2.3.4 Bending Beam Rheometer (BBR) Testing

Due to the disability of the DSR to measure the asphalt properties at the lowest pavement temperature, SHRP has introduced a new test, which is the BBR. It uses engineering beam theory to measure the deflection of a small asphalt beam sample under a creep load. It measures the amount a binder will deflect (creep) under a constant load. Creep load is used to simulate the stresses that gradually build-up in a pavement when temperature drops. The test is performed by loading an asphalt beam for four minutes with a constant load of 100 g and measuring the deflection at the center of the beam. The results of the BBR test are the creep stiffness (S) and creep rate (m). Creep stiffness is a measure of the asphalt's resistance to deformation due to constant loading, and it is calculated by measuring the deflection of the beam after 60 seconds of loading and substituting its value in the following equation:

$$S(t) = P L^3 / b h^3 \delta(t) \quad (2.13)$$

where,

$S(t)$ = creep stiffness at time, $t = 60$ seconds

P = applied constant load, 100 g

L = distance between beam supports, 102 mm

b = beam width, 12.5 mm

h = beam thickness, 6.25 mm

$\delta(t)$ = deflection at time, $t = 60$ seconds

Creep stiffness is desired at the minimum pavement design temperature after 2 hours of load. However, SHRP has utilized a Temperature-Time superposition, i.e., by raising the test temperature 10°C , an equal stiffness is obtained after a 60 second loading (Asphalt Institute, 1993). If the creep stiffness is too high, the asphalt will behave in a brittle manner and cracking will be more likely. SHRP recommends a maximum value of creep stiffness. The m -value is the rate of change of binder stiffness with load. It is the slope of the log stiffness versus log time curve at any time t . A higher m -value is desirable because it means when there is a change of temperature, the thermal stresses will accumulate but the stiffness will change fast, which will lead to absorbing the stresses and preventing the buildup of stresses. SHRP recommends a minimum value for m (Asphalt Institute, 1993). This test is a means for measuring the resistance of the AC to thermal cracking.

2.3.5 Direct Tension Tester (DTT) Testing

The pre-failure properties for some of the asphalts, especially modified asphalts, do not correlate very well with the failure properties. Therefore, the stiffness will not have correct relation with the failure properties, i.e. some modified binders might have a high creep stiffness but can stretch further before breaking

than other binders (Bahia and Anderson, 1994; Asphalt Institute, 1993). For those reasons, SHRP has developed a device which can directly measure the failure strain for the binder at the lowest expected pavement temperature. This device is called the direct tension tester. In this device a small "dog bone" shaped asphalt sample is stretched at a constant, slow rate of loading until failure. The failure strain, which is an indication of whether the asphalt will behave in a brittle or ductile manner at the test temperature, can be measured. SHRP defines failure as the stress where the load on the specimen reaches its maximum value and not necessarily the stress when the specimen breaks. Failure stress is the maximum load divided by the original sample cross section. At the failure stress, SHRP recommends a minimum failure strain of 1%. This test is an alternate procedure to measure the resistance of the asphalt binder to thermal cracking.

2.3.6 SHRP Binder Specifications

SHRP has developed or adopted the above mentioned performance tests to be used in their SHRP binder specifications. The binder specification is intended to control permanent deformation (rutting), low-temperature cracking, and fatigue cracking in asphalt pavements. The SHRP specifications can be used to grade any asphalt, i.e. they can specify the suitability of a certain asphalt for a certain environmental region. This is accomplished by specifying

two temperatures (lower and upper) for any asphalt that can perform satisfactorily within. As an example, a PG-78-10 (read performance grade 76 minus 10) grade asphalt means that the asphalt is suitable for a region with an average seven dry maximum pavement temperature of 76°C and a minimum pavement design temperature of -10°C.

Fig. 2.6 shows the Performance-Graded Asphalt specification chart, which was developed by the SHRP team. It can be seen from this chart that the performance properties remain constant for all grades but the temperature at which these properties must be achieved vary depending on the climate in which the binder is expected to serve.

Unusually rutting occurs at high service temperatures. The $G^*/\sin \delta$ factor is introduced for controlling rutting because it represents the high temperature viscous component of overall binder stiffness. This factor is measured by the DSR test machine. It is specified that for a binder to be able to resist rutting at any temperature, the value of $G^*/\sin \delta$ at the specified temperature must be at least 1.00 kPa for the fresh asphalt sample and must have a value greater than 2.20 kPa on samples that have been aged by the rolling thin film oven.

To verify the ability of the binder to resist fatigue cracking at a certain temperature, both G^* and δ are used. Since fatigue occurs at low to moderate

Figure 2.6. SHRP performance-graded asphalt binder specification chart (Harrigan et. al., 1994).

PERFORMANCE GRADE	PG 46-			PG 52-						PG 58-					PG 64-						
	34	40	46	10	16	22	28	34	40	46	16	22	28	34	40	10	16	22	28	34	40
Average 7-day Maximum Pavement Design Temperature, °C*	<46			<52						<58					<64						
Minimum Pavement Design Temperature, °C*	> -34	> -40	> -46	> -10	> -16	> -22	> -28	> -34	> -40	> -46	> -16	> -22	> -28	> -34	> -40	> -10	> -16	> -22	> -28	> -34	> -40
ORIGINAL BINDER																					
Flash Point Temp, T48: Minimum °C	230																				
Viscosity, ASTM D4402 [†] : Maximum, 3 Pa·s, Test Temp, °C	135																				
Dynamic Shear, TP5 [‡] : G*/sinδ, Minimum, 1.00 kPa Test Temp @ 10 rad/s, °C	46			52						58					64						
ROLLING THIN FILM OVEN (T240) OR THIN FILM OVEN RESIDUE (T179)																					
Mass Loss, Maximum, percent	1.00																				
Dynamic Shear, TP5 [‡] : G*/sinδ, Minimum, 2.20 kPa Test Temp @ 10 rad/s, °C	46			52						58					64						
PRESSURE AGING VESSEL (PAV) RESIDUE (TP1)																					
PAV Aging Temperature, °C*	90			90						100					100						
Dynamic Shear, TP5 [‡] : G*/sinδ, Maximum, 5000 kPa Test Temp @ 10 rad/s, °C	10	7	4	25	22	19	16	13	10	7	25	22	19	16	13	31	28	25	22	19	16
Physical Hardening [§]	Report																				
Creep Stiffness, TP1 [¶] : S, Maximum, 300 MPa, m - value, Minimum, 0.300 Test Temp @ 60s, °C	-24	-30	-36	0	-6	-12	-18	-24	-30	-36	-6	-12	-18	-24	-30	0	-6	-12	-18	-24	-30
Direct Tension, TP3 : Failure Strain, Minimum, 1.0% Test Temp @ 1.0 mm/min, °C	-24	-30	-36	0	-6	-12	-18	-24	-30	-36	-6	-12	-18	-24	-30	0	-6	-12	-18	-24	-30

- * Pavement temperatures may be estimated from air temperatures using an algorithm contained in the SUPERPAVE software program, provided by the specifying agency, or found by following the procedures as outlined in PPX.
- † This requirement may be waived at the discretion of the specifying agency if the supplier warrants that the asphalt binder can be adequately pumped and mixed at temperatures that meet all applicable safety standards.
- ‡ For quality control of unmodified asphalt cement production, measurement of the viscosity of the original asphalt cement may be substituted for dynamic shear measurements of G*/sinδ at test temperatures where the asphalt is a Newtonian fluid. Any suitable standard means of viscosity measurement may be used, including capillary or rotational viscometry (AASHTO T201 or T202).
- § The PAV aging temperature is based on simulated climatic conditions and is one of three temperatures: 90°C, 100°C or 110°C. The PAV aging temperature is 100°C for PG 58- and above, except for paving materials to be used in desert climates, where it is 110°C.
- ¶ Physical Hardening—TP1 is performed on a set of asphalt beams according to section 13.1, except the conditioning time is extended to 24 hrs ± 10 minutes at 10°C above the minimum performance temperature. The 24-hour stiffness and m-value are reported for information purposes only.
- || If the creep stiffness is below 300 MPa, the direct tension test is not required. If the creep stiffness is between 300 and 600 MPa, the direct tension failure strain requirement can be used in lieu of the creep stiffness requirement. The m-value requirement must be satisfied in both cases.

Figure 2.6. Continued.

PERFORMANCE GRADE	PG 70-						PG 76-					PG 82-				
	10	16	22	28	34	40	10	16	22	28	34	10	16	22	28	34
Average 7-day Maximum Pavement Design Temperature, °C*	< 70						< 76					< 82				
Minimum Pavement Design Temperature, °C*	> -10	> -16	> -22	> -28	> -34	> -40	> -10	> -16	> -22	> -28	> -34	> -10	> -16	> -22	> -28	> -34
ORIGINAL BINDER																
Flash Point Temp, T49: Minimum °C	230															
Viscosity, ASTM D4402: Maximum, 3 Pa·s, Test Temp, °C	135															
Dynamic Shear, TP5: G*/sinδ, Minimum, 1.00 kPa Test Temp @ 10 rad/s, °C	70						76					82				
ROLLING THIN FILM OVEN (T240) OR THIN FILM OVEN (T179) RESIDUE																
Mass Loss, Maximum, percent	1.00															
Dynamic Shear, TP5: G*/sinδ, Minimum, 2.20 kPa Test Temp @ 10 rad/s, °C	70						76					82				
PRESSURE AGING VESSEL (PAV) RESIDUE (TP1)																
PAV Aging Temperature, °C*	100(110)						100(110)					100(110)				
Dynamic Shear, TP5: G*/sinδ, Maximum, 5000 kPa Test Temp @ 10 rad/s, °C	34	31	28	25	22	19	37	34	31	28	25	40	37	34	31	28
Physical Hardening ¹	Repet															
Creep Stiffness, TP1: S, Maximum, 300.0 MPa, m - value, Minimum, 0.300 Test Temp @ 60s, °C	0	-6	-12	-18	-24	-30	0	-6	-12	-18	-24	0	-6	-12	-18	-24
Direct Tension, TP3: Failure Strain, Minimum, 1.0% Test Temp @ 1.0 mm/min, °C	0	-6	-12	-18	-24	-30	0	-6	-12	-18	-24	0	-6	-12	-18	-24

pavement temperatures after certain in-service periods, the fatigue resistance is verified on PAV residue. The controlling factor for fatigue cracking is $G^* \sin \delta$. SHRP binder specifications place a maximum limit on the value $G^* \sin \delta$ of 5000 kPa. This factor represents the ability of the binder to dissipate or relax stress leading to fatigue cracking. The DSR test only provides part of the information needed to describe good cracking properties. The test of the information is provided by the BBR and sometimes by the DTT.

The other factors which were introduced to verify ability to resist low-temperature cracking were the creep stiffness and m-value. If the creep stiffness is too high, the asphalt will behave in a brittle manner and cracking will be more likely. Therefore, a maximum limit of 300 MPa was set on the creep stiffness value to verify that no cracking will happen. The m-value is an indicator of the rate of change of stiffness with load. A high value of m means that if there is a change of temperature, there will be a buildup of thermal stresses and a high change of stiffness. This change of stresses will tend to dissipate stresses that would otherwise build up to a level where low-temperature cracking would occur (Asphalt Institute, 1993). So, a value of m greater than 0.300 is required.

The other limit which was introduced to account for the ability of the binder to withstand stresses that build up due to the decrease in temperature is

the failure strain. When the temperature decreases, shrinkage will occur in the binder, which leads to shrinkage stresses. The set limit on the failure strain is 1%. So, if the binder when loaded slowly can take up to 1% strain without cracking, it is expected that it can withstand shrinkage cracks as long as other BBR requirements are met (creep stiffness between 300 and 600 MPa).

Three other limits which were included in the specification were introduced to control ease of handling, safety, and aging. For handling and pumpability of binders, an upper limit on rotational viscosity was specified to be 3000 CP. This limit can be waived if the binder supplier warrants that the binder can be pumped and mixed at higher but safe temperatures. For safety precautions, a lower limit on the flash point of fresh samples was set to be 230°C. Finally, to insure against excessive aging (volatilization) during binder mixing and compaction, an upper limit on mass loss of RTFO residue was set to be 1.0 percent.

2.3.7 The Linear Viscoelastic Model (LVE) of Asphalt

Asphalt cement is a rheological material because its behavior depends on both temperature and rate of loading. In other words, its stress-strain characteristics are time and temperature dependent. Time and temperature effects are interchangeable; high temperature and short loading time is, in general, equivalent to long loading times and low temperatures. Asphalt will

behave nearly as an elastic material when loaded at a fast load rate or when at low temperature. It will behave as a viscous material when loaded very slowly or at high temperature. At intermediate ranges of load rate and/or temperature, asphalt behaves as a visco-elastic material, where a delayed elastic response governs the behavior. A mathematical model was developed by the SHRP team in order to describe asphalt behavior at different test temperatures and different frequencies. Analysis of the data collected by the SHRP team indicate that asphalt binders, including plain and most modified asphalt cements, can effectively be treated as a linear-visco-elastic (LVE) material under loading conditions likely to be encountered in a pavement when exposed to traffic and environment.

Anderson and his co-workers (1994) listed the following reasons for developing a mathematical model to describe the linear visco-elastic response of asphalt cements:

1. Since the mechanical response of asphalt cement, like other visco-elastic materials, is a continuous function of time and temperature, an infinite number of loading conditions and responses constitute its overall behavior. By expressing this behavior with a mathematical model, the responses can be reduced to a limited number of variables.

2. By mathematically modeling the LVE response and reducing the characterization to a few rational variables, relating the rheological behavior to chemical compositional parameters is simpler, more efficient, and more rational. This approach is in contrast to correlating individual response variables, obtained under arbitrary loading conditions, to chemical variables.

3. In some situations, it is necessary to know the response of an asphalt cement at loading frequencies (or times) and temperatures different from those for which directly measured data are available. Mathematical models allow such calculations to be made directly and quickly in a repeatable fashion.

4. In many approximate conversions from one viscoelastic function to another, numerical methods are used that require data at specific frequency or time intervals, which may not be the same as those used for the measurement. Using mathematical models simplifies the application of such approximate conversions.

5. Through the use of mathematical models, the testing needed to control various performance-related properties can be simplified. For example, the finding that over a limited

temperature range the shift factors for plain asphalts at temperatures below about 0°C (32°F) could be approximated by a simple logarithmic relationship, allowed a simplified testing scheme in which a creep test is performed for only 2 minutes at a temperature 10°C (18°F) above the expected minimum pavement temperature. Using this common shift factor allows the creep compliance after 2 hours loading time to be approximated by the compliance measured after a 60 second loading time.

6. In order to predict the mechanical behavior of paving mixtures within the context of a rational microstructural model, the behavior of the binder must be described under a broad range of conditions - a task accomplished efficiently through the use of mathematical models.

7. In order to effectively model pavement response and predict pavement performance, it is necessary to accurately predict the stress-strain response of the binder over a wide range of temperatures, loading times, and stresses or strains. This prediction can only be realistically made with the use of reasonably accurate mathematical models of the binder's visco-elastic behavior.

The developed model, which explains the behavior of AC at different loading and temperature conditions, is called the LVE model because it explains both the linear and viscous behavior of the AC. A graphical representation of the LVE model is usually referred to as a master curve of asphalt. In a master curve of dynamic mechanical data of an asphalt, one or more of the visco-elastic functions are plotted against frequency. Fig. 2.7 presents a typical plot showing the variation of the complex modulus and the phase angle with frequency drawn on a log-log scale. This type of curve is called the master curve of asphalt for both $G^*(\omega)$ and $\delta(\omega)$. At high frequencies, G^* approaches a limiting value, which is called the glassy modulus in shear. It is normally about 1 GPa. At low frequencies, the slope of the complex modulus curve approaches 1, which implies that viscous flow has been reached and that the asphalt behaves as a Newtonian fluid. At intermediate frequencies, the behavior of the asphalt changes gradually from a glassy solid to a simple fluid. In this region the asphalt behaves as a visco-elastic material. On the other hand, at very low frequencies, δ approaches 90° and at very high frequencies it approaches 0 degrees. At intermediate frequencies, δ will range between those two values (Anderson et al., 1991, 1994).

The SHRP team came up with different mathematical models that represent $G^*(\omega)$ and $\delta(\omega)$. The following two models to represent asphalt behavior are the product of SHRP:

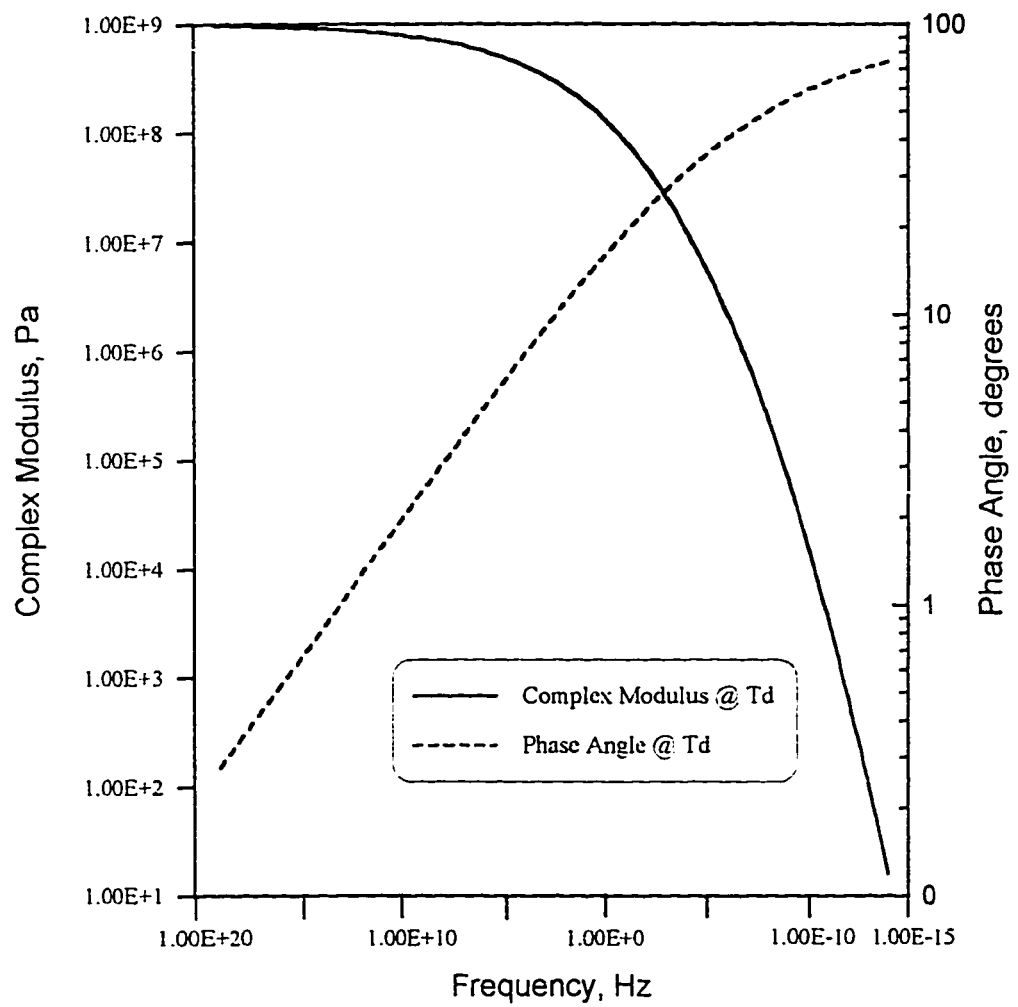


Figure 2.7: General shape of the group complex modulus and phase angle versus loading time (Anderson et al., 1994).

$$G^*(\omega) = G_g [1 + (\omega_o/\omega)^{(\log 2)R}]^{-R/(\log 2)} \quad (2.14)$$

$$\delta(\omega) = 90/[1 + (\omega_o/\omega)^{(\log 2)R}] \quad (2.15)$$

where

$G^*(\omega)$ = complex dynamic modulus, in Pa, at frequency ω ;

G_g = glassy modulus, typically 1 GPa;

ω_o = the cross over frequency, rad/s;

ω = the test frequency, rad/s;

R = the rheological index; and

$\delta(\omega)$ = the phase angle, in degrees, at frequency ω .

The resulting model requires three parameters: a location parameter that indicates the hardness of asphalt (G_g), a temperature dependency parameter that indicates the temperature dependency of the asphalt (R), and a shape parameter that indicates the time dependency of the asphalt (ω_o). The visco-elastic materials are affected by both the rate of loading and temperature. The above mentioned LVE considers the effect of rate of loading on the visco-elastic properties of asphalt. The effect of temperature on the visco-elastic properties is considered through the use of shift factors, which are used to shift the master curve horizontally to achieve the mechanical response at the defining temperatures. Fig. 2.8 shows a graphical

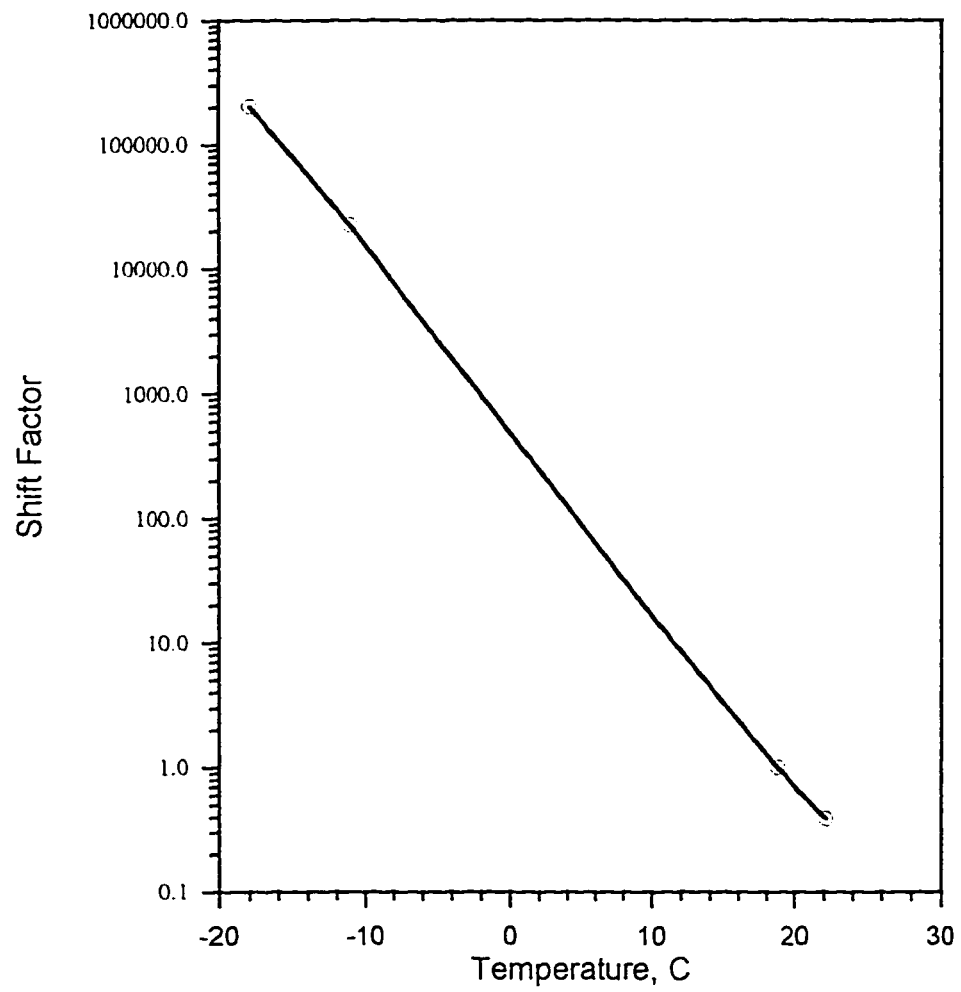


Figure 2.8: Graphical representation of the time shift factors (Harrigan, 1993).

representation of the shift factors. Two mathematical models were produced to represent the shift factors:

$$\text{Log } (aT)_d = -C_1 (T - T_d)/(C_2 + T - T_d) \quad (2.16)$$

$$\text{Log } (aT)_d = 2.303 E_a / r (1/T - 1/T_d) \quad (2.17)$$

where

$(aT)_d$ = the shift factor relative to the defining temperature, T_d ;

C_1, C_2 = empirically determined constants, fixed at 19 and

92 (Anderson et al., 1994);

T = the selected temperature, in °C;

T_d = the defining temperature, in °C, which is a characteristic parameter for each asphalt cement,

E_a = the activation energy for flow below T_d , fixed at 261 kJ/mol; and

r = the ideal gas constant, 8.34 J/mol-°K.

Eqn. (1.3) is the Williams-Landel-Ferry (WLF) equation and is usually used when the test temperature is above the defining temperature. Eqn. (1.4) is Arrhenius's function and is used when the test temperature is below the defining temperature. The reliability of estimating T_d is considered low due to the fact that asphalt is an amorphous material with a very wide glass transition region.

Anderson and his co-workers (1994) have given the following explanation for the parameters which are used in the LVE (these parameters are illustrated on the master curve shown in Fig. 2.9):

- *The glassy moduli, G_g^** - The value that the complex modulus or stiffness modulus approaches at low temperatures and high frequencies or short loading times; the glassy modulus is normally very close to 1 GPa in shear loading for most asphalt cements. A single value of 1 GPa may be assumed for most purposes.
- *The steady-state viscosity, η_o* - In dynamic testing, the steady-state, or Newtonian viscosity, is approximated as the limit of the dynamic viscosity, η^* , as the phase angle approaches 90° . The 45° line that the dynamic master curve approaches at low frequencies is often referred to as the viscous asymptote. It is indicative of the steady-state viscosity, and the value of η_o is asphalt specific.
- *The crossover frequency, ω_o , or crossover time, t_o* - The frequency at a given temperature where $\tan \delta$ is 1. At this point, the storage and loss moduli are equal. For most asphalt cements, the crossover frequency is nearly equal to the point at which the viscous asymptote intersects the glassy modulus. The crossover frequency can be thought of as a hardness parameter that indicates the general consistency of a

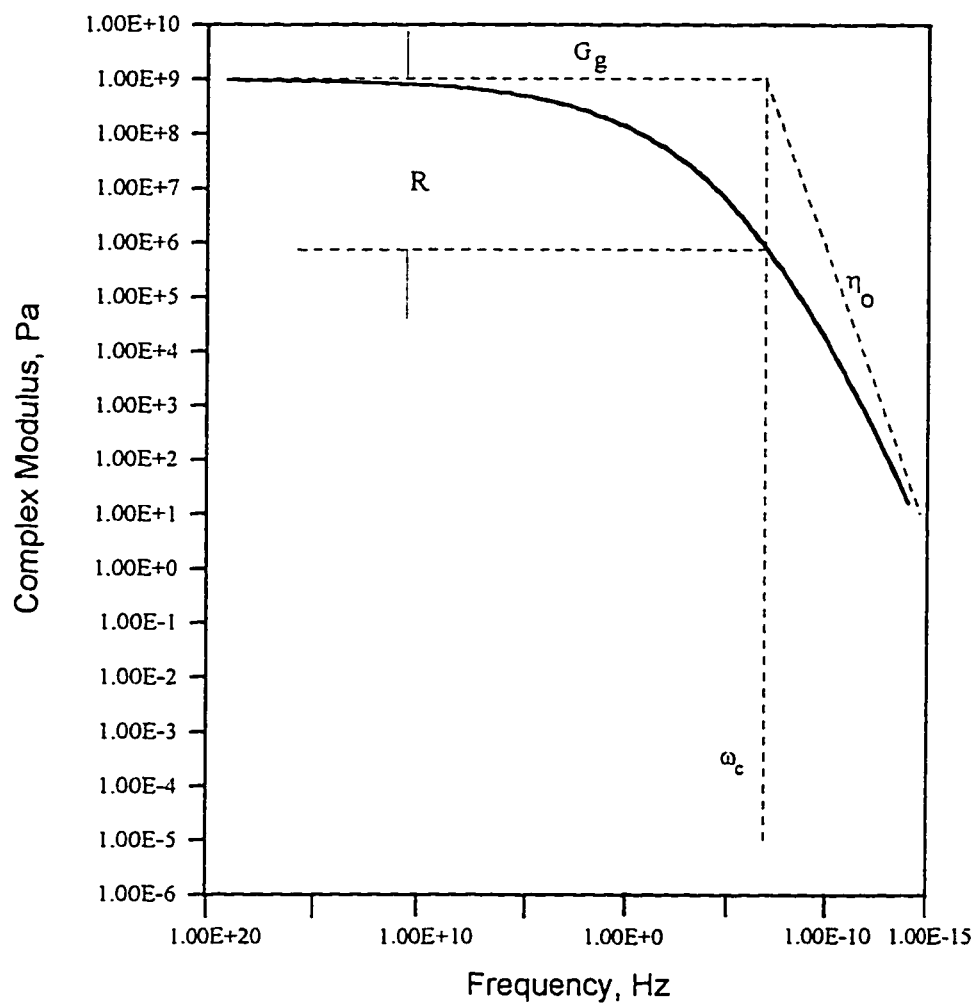


Figure 2.9: Dynamic master curve for RT1 sample, with important parameters described (Al-Abdul Wahhab et al., 1995)

given asphalt at the selected temperature and is asphalt specific. The crossover frequency is the reciprocal of the crossover time, $t_0 = 1/\omega_0$.

- *The rheological index, R* - the difference between the glassy modulus, G_g , and the dynamic complex modulus at the crossover frequency, $G^*(\omega_0)$. The rheological index is directly proportional to the width of the relaxation spectrum and indicates rheologic type. R is not a measure of temperature but reflects the change in modulus with frequency or loading time and therefore is a measure of the shear-rate dependency of asphalt cement. R is asphalt specific.

From the above discussion, it can be seen that the behavior of any asphalt at any temperature can be predicted using only three parameters: the defining temperature T_d , the crossover frequency ω_0 (or crossover time t_0), and the rheological index R. The defining temperature uniquely characterizes the shift factors as a function of temperature. The rheological index is a representation of the rheological behavior of asphalt and is directly proportional to the elastic behavior of asphalt at intermediate temperatures. The crossover frequency indicates the location of the master curve at the selected reference temperature and is an indication of the hardness of the asphalt (Anderson et al., 1991). These parameters are asphalt specific and can be used in analyzing the rheological properties of each

asphalt, comparing asphalts, and in developing chemical-physical property relationships.

2.4 CHEMICAL COMPOSITION OF ASPHALT

2.4.1 Asphalt Chemistry

Asphalt chemistry is extremely complex. Even with the presence of high-tech analytical tools, it would be impossible to identify and quantify all the components of even a single asphalt. The complexity of asphalt comes from its being a product of crude oil, which is formed by natural processes primarily from plant life. The plants were buried in sediment before they were consumed by microorganisms and were transformed into crude oil by a process not yet completely understood. This process occurs over millions of years under varied conditions of temperature and pressure. all petroleums basically consist mainly of hydrogen and carbon; however, crudes vary widely in the amount and nature of the hydrocarbons they contain. Another factor contributing to the complexity of asphalt structure is that it is actually the residue left after all the volatile fractions of the petroleum have been distilled off. So, the characteristics of asphalt are affected by the heating temperature and the heating time in the distillation tower, the manufacturing procedure, and the source of the crude oil. Crudes from different locations contain different percentages of asphalt residue. Corbett (1969) gave

examples of three crude oils from different sources (Nigeria light, Arabian heavy, and Boscan Venezuela) having an amount of bitumen residue ranging from 1%-58%. A third factor is that sometimes additional treatments of the residue are required. One of these may be treatment of the residue with a solvent such as propane or butane to precipitate asphaltic constituents from the residue. The remaining portion is used for manufacturing lubricating oils. Sometimes it is required to blend two asphalts together, add polymers, or air blow the asphalt to make it suitable for use. This adds to the complexity of the structure of asphalt.

When considering physical properties, it is well known that physical tests - excluding SHRP tests - are not good predictors of pavement performance. It is possible to have asphalts with the same viscosity grading and similar physical test results but that perform differently when in a pavement (Anderton, 1988; Goodrich and Dimpfi, 1986; Kalidindi et al., 1986; Rossler and White, 1959). Both physical and chemical tests have been considered to study asphalt properties. In chemical tests, chemists try to define and characterize asphalts by chemical composition and structure, which till now has not led to mix design input. Engineers have conducted physical tests and tried to correlate the test results with the performance of the asphalt mixtures. These have met with some success but have drawbacks, such as the high degree of variability in the tests themselves (Price and Burati, 1990).

The principal elements in asphalt are carbon and hydrogen. Sulfur is the next most abundant element followed by nitrogen and oxygen. There might also be trace amounts of other materials such as vanadium and nickel. Table 2.1 shows the constituents of four asphalts collected from different places in the U.S. The most important factors affecting the behavior of asphalt is the ways in which atoms are incorporated into molecules and the types of molecular structures. These factors are more important than the total amounts of each element. Normally, in hydrocarbons carbon atoms are linked to each other in one of the following three manners. They may be linked in straight or branched chains; in this case the materials are called aliphatic or paraffinic types. They might be linked together in either simple or complex saturated rings; in this structure the highest possible ratio of hydrogen to carbon is present. These materials are referred to as naphthenic. Finally, they may be aromatic, which is made of one or more especially stable six-atom rings that form the basis of compounds such as benzene and toluene. Asphalts are very complex combinations of all the three types of components (Halstead, 1985; Pfeiffer, 1950). Petersen (1984) has reported that the percentages of aliphatic or paraffinic carbon content of asphalts range from 35 to 60%. While the ranges for naphthenic and aromatic carbon are 15 to 30% and 25 to 35% respectively. The molecular weight of asphalt ranges between 300 and 2000. This includes

Table 2.1: Elemental analyses of representative petroleum asphalts
(Petersen, 1984)

Source	Mexican Blend	Arkansas- Louisiana	Boscan	California
Carbon, percent	83.77	85.78	82.90	86.77
Hydrogen, percent	9.91	10.19	10.45	10.93
Nitrogen, percent	0.28	0.26	0.78	1.10
Sulfur, percent	5.25	3.41	5.43	0.99
Oxygen, percent	0.77	0.36	0.29	0.20
Vanadium, ppm	180	7	1380	4
Nickel, ppm	22	0.4	109	6

molecules with about 24 to 150 carbons. Some of the useful known chemical properties of asphalt, summarized by Goodrich (1986), follow:

- Asphalt has a significant heteroatom content. This includes nitrogen, oxygen, sulfur, vanadium, nickel, and iron.
- Heteroatoms play an important role in the physical properties of an asphalt. The polar heteroatom-containing compounds are capable of intermolecular associations that affects such physical properties as boiling point, solubility, and viscosity. These polar compounds tend to be concentrated in the asphalt fraction of a crude oil.
- The molecular weight of asphalt compounds ranges from about 300 to 2000. Yet, as a result of molecular associations, asphalt behaves as if it has a much higher molecular weight.
- Aging of an asphalt is associated with oxidation. An increase in the polar fractions on aging, among other things, results in increased asphalt viscosity.
- The composition, rheology, and durability of an asphalt are unique to the crude blend from which the asphalt was refined. Yet asphalts from many sources perform well in roads.

Thus, one of the important factors affecting the behavior of the asphalt molecules between each other and with surfaces and/or molecules from other materials such as

aggregate is the presence of hetroatoms, which are referred to as functional or polar groups. Thus, polarity is due to an imbalance of electrochemical forces within the molecule, which produces a dipole. The dipole molecule has both electropositive and electronegative characteristics like a magnet having both north and south poles. This dipole tends to cause molecules to organize themselves into preferred structural orientations. This structure is held together by electrostatic and other short-range forces, which are weak compared to covalent chemical bonds. Short-range (non-covalent) forces range from about 1 to 10 kcal/mole, while covalent bonds between two carbon atoms are more than 80 kcal/mole and between carbon and hydrogen are around 100 kcal/mole (Branthaver et al., 1993). It follows then that the organized structure may be subject to rearrangement or may be scrambled either from physical stress or by increased temperature. This will not be associated with chemical changes where all of the molecular species remain the same; although, it will affect the physical properties. Therefore, the more randomized the structure of the molecules of the asphalt, the weaker will be the bonds and the lower will be the viscosity of the asphalt.

Depending on polarity of asphalt molecules, asphalt can be defined as a collection of polar and non-polar molecules. The polar molecules tend to associate strongly to form organized structures throughout the continuous phase of the non-polar materials. On the other hand, the non-polar phase has the ability to

disassociate the organized structure, which varies from one asphalt to another (Branthaver et al., 1993). The oxidation of asphalt leads to increases in both the amount of polarity and the number of polar sites present among asphalt molecules. Plancher, Dorrence, and Petersen (1977) used the model of polarity of asphalt molecules to explain the bonding between asphalt and aggregate. This model suggests that some of the polar heads of the organic components find themselves near the aggregate surface and bind to it allowing their less polar tails to extend into the asphalt matrix.

Due to the large number of molecules with different chemical structures in asphalt, chemists have not seriously attempted to separate and identify all the different molecules present in asphalt. All efforts have been focused on trying to separate or characterize asphalt by determining different groupings or generic fractions based on polarity, reactivity, and/or the molecular size of the various molecular types present in the asphalt.

Early researchers (Pfeiffer and Saal, 1940; Barth, 1984; Girdler and Saal, 1965) represented asphalt cement as a colloidal dispersion of high molecular weight hydrocarbons called asphaltenes in a dispersion medium called maltenes, which is a combination of resins and oils.

The asphaltenes are the high molecular weight materials and are primarily of an aromatic nature with very few side chains attached. Both sulfur and nitrogen are

present in the asphaltene molecules. Asphaltenes comprise the fraction of asphalt that has the highest polarity and tendency to interact and associate. They are the major fraction that determines asphalt viscosity. Asphaltenes are defined by ASTM (1973) as the component of the bitumen in petroleum, petroleum products, malphas, asphalt cements, and solid native bitumens which are soluble in carbon disulfide but insoluble in paraffin naphthas.

When the asphalt is dissolved in a non-polar solvent such as pentane, hexane, or heptane, asphaltene will not dissolve; it will precipitate. Rosstler and White (1962) described the asphaltene fraction as the component of asphalt primarily responsible for asphalt viscosity and colloidal behavior due to its limited solubility in the remaining components. The part which will dissolve and remain solution will be a mixture of resins and oils and is called "maltenes".

The resins are intermediate molecular weight materials and contain more side chains than the asphaltenes. Sulfur and nitrogen are present in those materials but to a lesser extent than in the asphaltenes. The polar nature of the resins gives them the ability to be adsorbed by and to dissolve the asphaltenes. So, the resins are the agents that disperse the asphaltenes through the oils to provide a homogeneous liquid (Halstead, 1985).

The oils are the lightest molecular weight materials in asphalt and generally have a large number of chains in proportion to their number of rings.

The relative amounts of asphaltenes, resins, and oils, and their characteristics vary considerably from asphalt to asphalt (Rosstler and White, 1962). Asphaltenes, resins, and oils differ also in their carbon to hydrogen ratio (C/H). In asphaltenes, the C/H ratio is greater than 0.8; in resins, the C/H ratio is greater than 0.6; and in oils, the C/H ratio is less than 0.6. In proceeding from oils to asphaltenes, the aromaticity increases, the sulfur content increases, the C/H ratio increases, the molecular weight increases, and the number of side chains decreases (Monismith et al., 1985).

2.4.2 Asphalt Composition

Asphalt composition means separating the asphalt into smaller and simpler fractions. Separations are commonly based on separating hydrocarbon molecules by groups depending on their different boiling ranges and the different shapes of their molecules. Such materials are then purified and finally identified through physical and chemical means. Chemical characterization of asphalt by separation into generic fraction rather than separating and identifying the individual molecular types, is due to the presence of many different types of molecules in the asphalt.

A variety of analytical procedures have been used to study asphalt. Goodrich et al. (1986) presented a summary of all laboratory techniques being used in asphalt technology. Table 2.2 gives a listing of the most popular tests that have

Table 2.2: Analytical procedures used to test asphalt composition
(Thenoux, 1987; Goodrich et al., 1986)

Group	Subgroup	Reference
Fractionation by Precipitation	<ul style="list-style-type: none"> - Solvent Precipitation - Chemical Precipitation 	ASTM D 2006
Fractionation by Precipitation	<ul style="list-style-type: none"> - Vacuum Distillation - Thermogravimetric Analysis 	
Chromatographic Separation	<ul style="list-style-type: none"> - Gas Chromatography - Inverse Gas/Liquid Chromatography - Liquid Chromatography · Adsorption 	ASTM D 4124 ASTM D 2007
	<ul style="list-style-type: none"> · Size Exclusion · Thin Layer · Ion Exchange · Coordination - Mass Spectrometry - Vapor Pressure Osmometry 	ASTM D 3593
Chemical Analysis	<ul style="list-style-type: none"> - Spectrophotometric Techniques <ul style="list-style-type: none"> · Infrared · Ultraviolet · Nuclear Magnetic Resonance · X-ray · Neutron Activation - Titrametric Gravimetric - Elemental Analysis 	Petersen (1984)
Molecular Weight Analysis	<ul style="list-style-type: none"> - Mass Spectrometry - Vapor Pressure Osmometry 	
Others	<ul style="list-style-type: none"> - Internal Dispersion Stability - Asphalt Purity <ul style="list-style-type: none"> · Solubility in Carbon Disulfide · Solubility in Carbon Tetrachloride · Ash Content 	Plancher (1979) Heithaus (1960) ASTM D 4 ASTM D 156 ASTM D 482

been used in asphalt analysis. Those tests have been grouped into six categories. A description of some of most popular ones follows in the proceeding paragraphs.

2.4.2.1 Corbett and Swarbrick Method (Corbett, 1969)

The Corbett and Swarbrick method defines the asphalt in terms of adsorption and desorption on a chromatographic column. The procedure is now an ASTM D 4124 standard procedure. A schematic of the procedure is shown in Fig.

2.10. The asphalt is fractionated into the following fractions:

- A - Asphaltenes
- PA - Polar-Aromatics
- NA - Naphthene-Aromatics
- S - Saturates.

Both saturates and naphthene-aromatics are liquids which act as plasticizers for the polar-aromatic and asphaltene solids. Saturates are better plasticizers than naphthene-aromatics. The asphaltenes are solution thickeners, while the presence of saturates and asphaltenes produce low temperature sensitivity. The ductility of an asphalt depends on the presence of polar-aromatics. Thenoux (1987) made the following observations on this method:

1. The fractions obtained by this procedure are still mixtures of molecular groups and not well-defined chemical species.

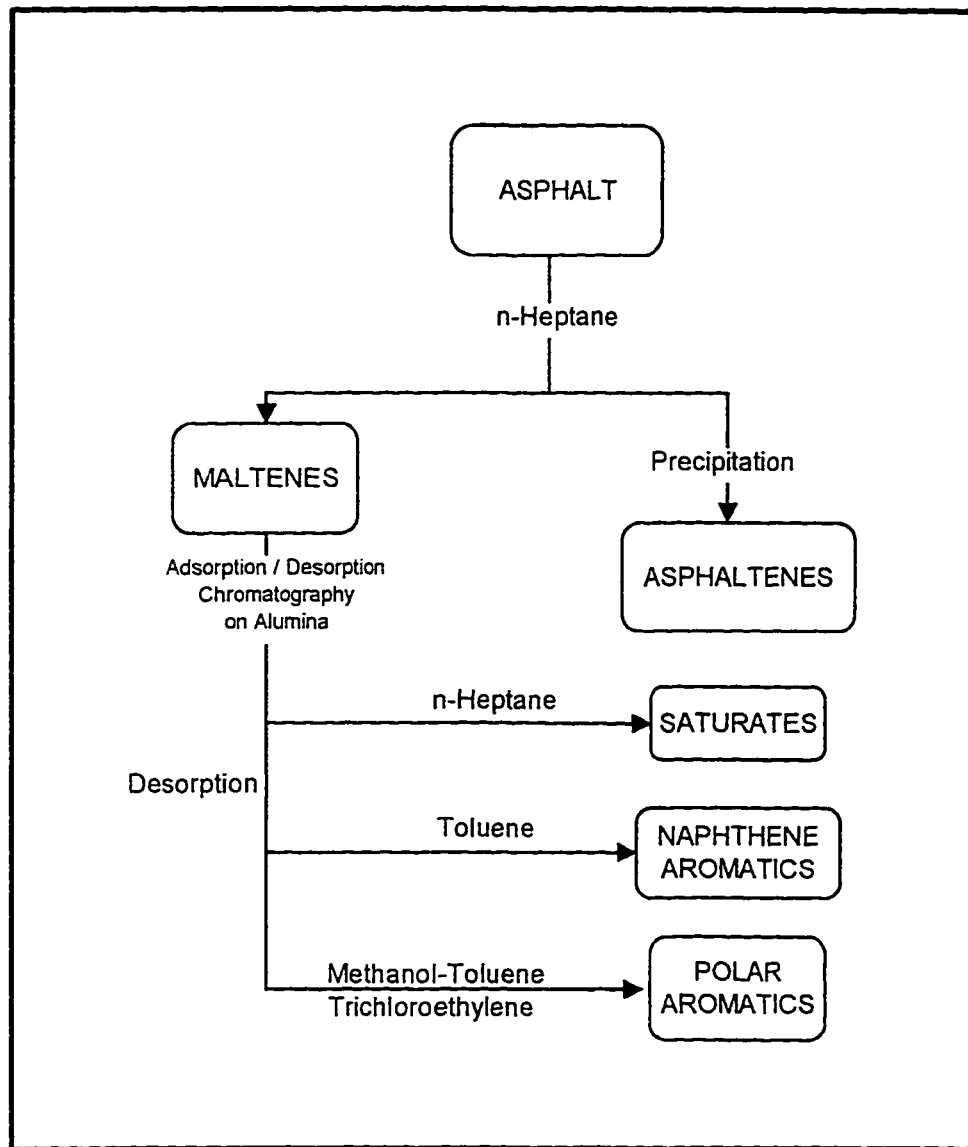


Figure 2.10: Adsorption/desorption chromatography Corbett-Swarbrick, ASTM D 4124.

2. The asphaltene obtained by this procedure is different from asphaltene obtained by other procedures because it is precipitated by n-heptane rather than n-pentane.
3. The method is nondestructive and further analysis or separation can be done over the remaining fractions.
4. A shortened procedure has been approved by the ASTM Committee.
5. The description of the method in the ASTM is considered insufficiently explained, which leads to bad reproducibility of the results from one lab to another.

2.4.2.2 Rosstler and Sternberg Method (Rosstler, 1962)

This was an ASTM D 2006 method, but it was discontinued in 1976. A schematic of the procedure is shown in Fig. 2.11. It fractionates asphalt components according to their solubility in sulfuric acid. The fractions are

- A - Asphaltenes
- N - Nitrogen gases
- A₁ - First Acidaffins
- A₂ - Second Acidaffins
- P - Paraffins.

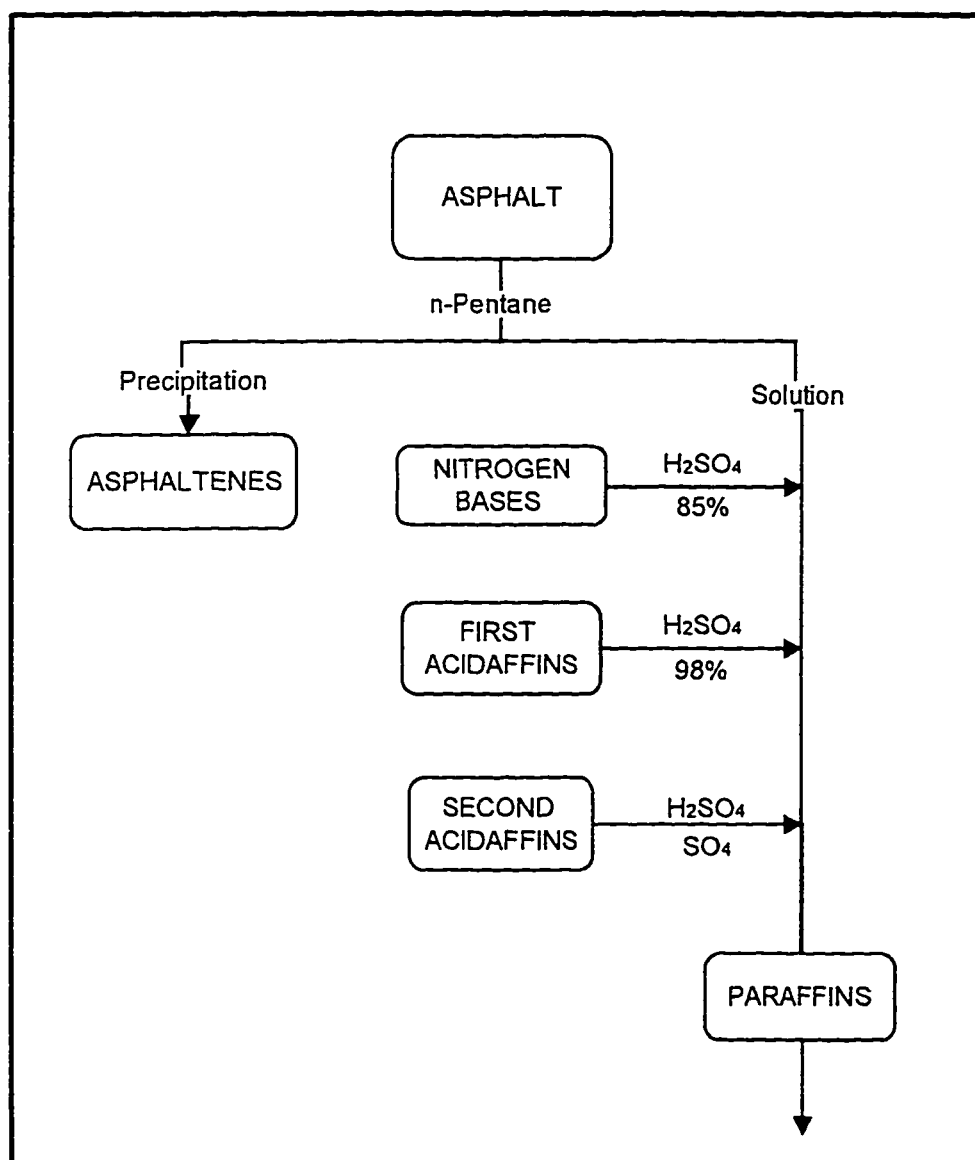


Figure 2.11: Chemical precipitation Rossler-Sternberg, ASTM D 2006.

Rosstler has suggested the following two parameters, which are related to some extent, to pavement performance and to asphalt aging:

$$\text{The chemical reactivity ratio (durability parameter)} = (N+A_1)/(P+A_2) \quad (2.18)$$

$$\text{The compatibility parameter} = N/P \quad (2.19)$$

The durability parameter gives an indication of the asphalt's durability, the lower the number the higher the durability.

2.4.2.3 The Clay-Gel Method

This procedure was developed to replace the Rosstler-Sternberg method. It is designated as ASTM D 2007. As shown in Fig. 2.12, n-pentane is added to the asphalt to separate the asphaltene. The remaining fraction is then added to a pair of columns which are assembled in series. The upper column is packed with attapulugus clay, and the lower column is packed with activated silica gel with a layer of clay on top. Results from the clay-gel technique have been used for characterization of both virgin and aged asphalts and recycling agents.

This procedure is claimed to be simple, relatively inexpensive, free of hazardous concentrated acid, yields repeatable results, and the data obtained by this procedure are almost identical to the results from the Rosstler-Sternberg analysis (Pavlovich, 1985).

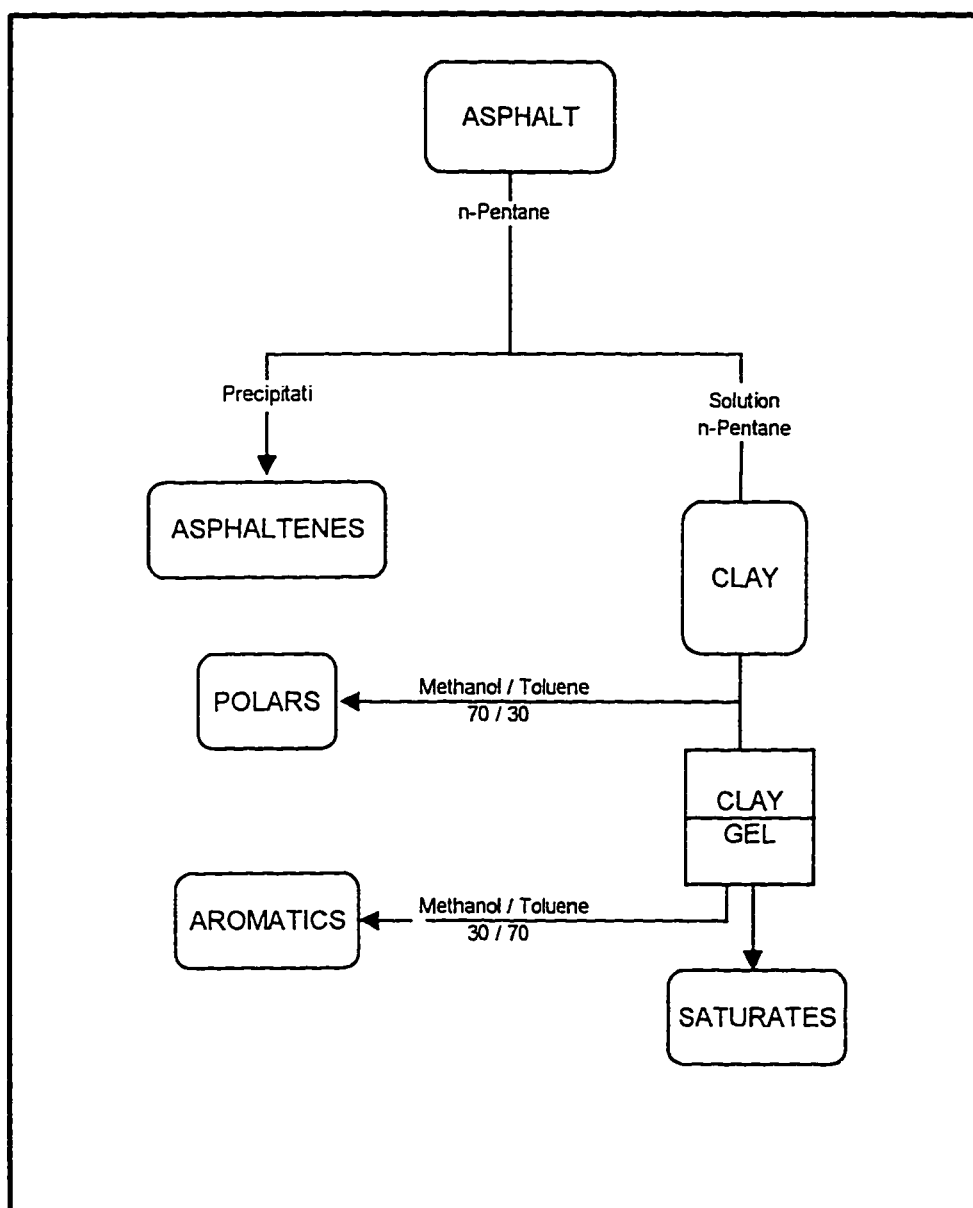


Figure 2.12: Adsorption/desorption chromatography "Clay-Gel", ASTM D 2007

It is noted that the above three separation procedures share the same idea. They involve precipitating an asphaltene fraction by mixing the whole asphalt sample in a specific solvent. The solubles are then separated on a least-polar to most-polar basis through increasing reactivity with sulfuric acid (Rosstler), or increasing absorption (Corbett and clay-gel) on a specific media. Those types of fractional separations of asphalt do not provide well-defined chemical components. To get a whole idea about these fractions, their names should be associated with the procedure followed and the materials used for separation. The chemistry of the fractions has been only broadly defined (Rosstler and White, 1962; Hattingh, 1984). Goodrich and Dimphi (1986) compared the weight percentages of those fractions for the same asphalts, where they mentioned that the fractional parts of the saturates and paraffins are similar. The middle parts of the fractions are not comparable at all. Despite what has been mentioned, it does not mean that the separations are of little value. This is due to the fact that fractional separation techniques provide a method for following changes in an asphalt, whether during laboratory studies, refinery processing, field mixing, or field aging, or recycling. In controlled studies using one asphalt, changes in composition measured by fractional separation may be informative. Little reliable correlation has been achieved between fractional separation and field performance (Goodrich and Dimphi, 1986).

2.4.2.4 High Pressure Gel Permeation Chromatography

This procedure is another type of separation technique used to differentiate between asphalt molecules on the basis of their molecular size. It obtains a chromatogram of the relative amounts of large, medium, and small molecules in an asphalt but does not result in physical separation by molecular size. The technique is most accurately described as high pressure liquid chromatography in the gel permeation mode. It is generally referred to as "HPLC" or "HP-GPC" (High Pressure Gel Permeation Chromatography), or sometimes as "SEC" (Size Exclusion Chromatography).

Gel permeation chromatography (GPC) was developed in 1963 to determine the molecular weight distribution of polymers. In the mid 1960's, GPC was adopted for analyzing macro-molecular non-polymers including asphalt. Early studies of asphalt on GPC showed that GPC could be used to distinguish asphalts of different compositions (Richman, 1967; Breen and Stephens, 1969). In 1970, Bynum and Traxler showed that aging and weathering of asphalt made systematic changes in the GPC profiles. However, gel permeation chromatography only began to attract widespread attention in the asphalt industry in 1980. This was due to improved equipment, which made the procedure quicker, more efficient, and more reliable (Garrick, 1986).

A survey of research in the use of GPC in characterizing asphalt molecules showed that it can be used to fingerprint asphalts and to monitor and study changes in asphalt due to mixing, heating, and aging. The GPC is good for studying the degree of molecular association because the system causes the least disturbance to the association. HP-GPC allows differentiation between asphalts of the same grades but with different compositions.

Usually in the GPC procedure, tetrahydrofuran (THF) is used as a carrier solvent, where a solution of the asphalt sample plus the THF solution is injected into the system and passed through the separation columns. Separation in GPC takes place in columns which contain porous silica-gel packing with pores of various known diameters. The asphalt molecules, which are dissolved in the solution, flow through the columns at different rates depending on their sizes. Small molecules enter the pores of the packing, and their movement are slowed to a lesser extent. This is why the larger molecules emerge from the system first and are followed by progressively smaller molecules. A detector, such as a differential refractometer, will detect the molecules as they emerge from the columns and will produce a chromatogram of the relative amount of molecules being eluted from the system at different times.

Chromatograms produced from HP-GPC have been analyzed differently by different analysts. Jennings (1982) classified the molecules eluted during the first

third of the elution period as large molecular size (LMS), those eluted during the second third as medium molecular size (MMS), and those eluted in the last third as small molecular size (SMS). Fig. 2.13 shows a typical chromatogram showing the three parts of the elution time.

It is expected that when the molecular size distributions of the different asphalts are similar, their performance will be similar. Also, if the distributions are different, then the performance will be different. Studies using three part fractionating found that greater relative amounts of LMS are associated with poor pavement performance and that a balance between the three parts is an important attribute relating to pavement performance. Glover et al. (1988) found high correlation between the LMS region and the asphaltene content. Hattingh (1984) concluded that too high asphaltene or LMS percentage causes cracking and that too low percentage causes rutting. Jennings and his co-workers (1980-1985) have concluded that LMS can play a significant role in cracking and that low LMS is desired to reduce cracking. Jennings and Pribanic (1985) suggested that the HP-GPC can be used not only to predict the performance of a pavement but also to design an asphalt to meet a target LMS content and thereby obtain improved performance with regard to transverse cracking. Garrick and Wood (1988) and Price and Burati (1990) found a correlation with physical properties such as viscosity, penetration, temperature susceptibility, and viscosity ratio. Noureldin

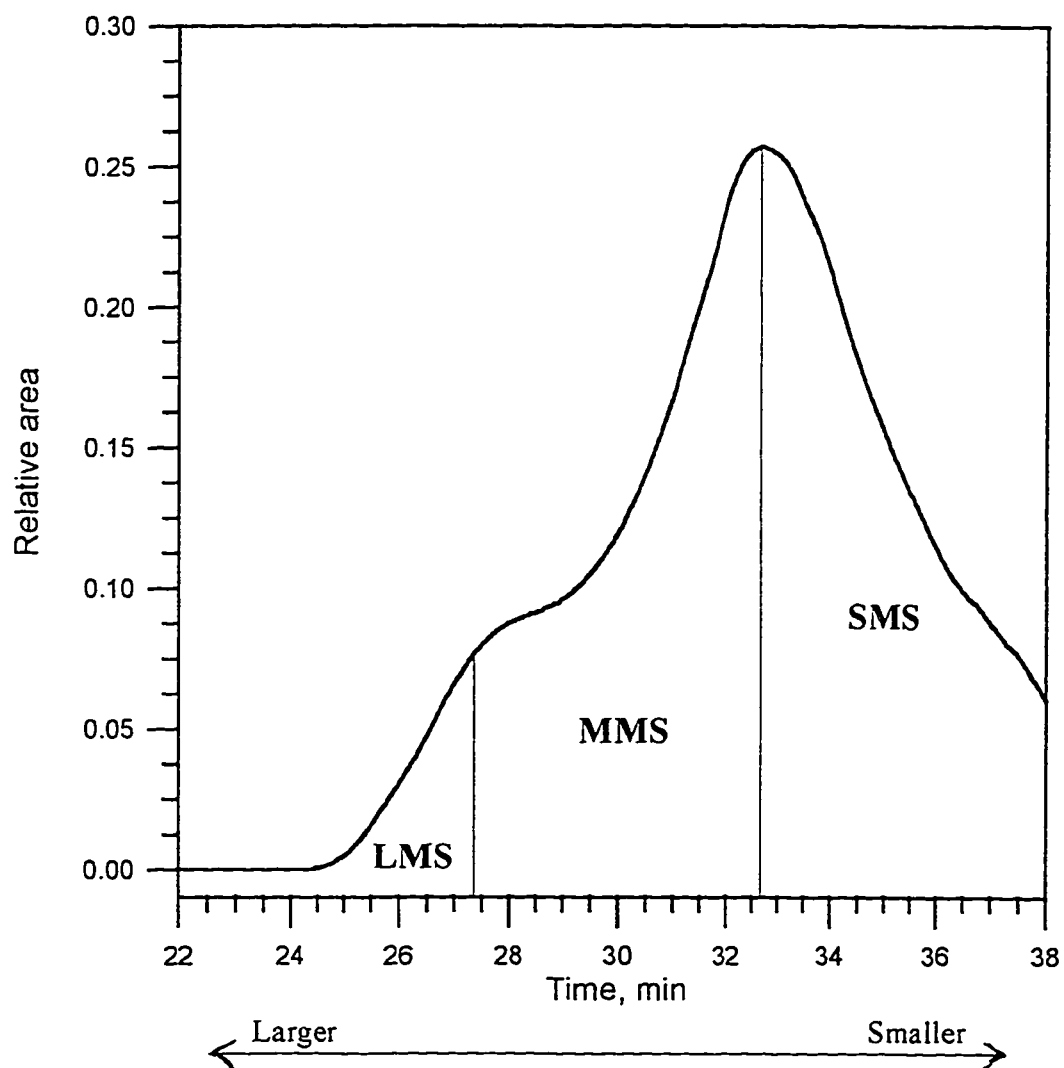


Figure 2.13: Typical HP-GPC chromatogram showing the three elution times' fractions (Jennings, 1982)

(1982) reported that low percentages of asphaltene (less than 20%) in the asphalt result in a highly temperature susceptible paving mixture with potential for rutting. Other studies (Button, 1983; Zenewitz and Tran, 1987; Garrick and Wood, 1988) related the amounts of small molecular size fractions to rutting and tender mixtures.

Garrick and Wood (1988) partitioned the HP-GPC profile into eight partitions and got a correlation between penetration, viscosity, and heat hardening. Also, correlations were established with asphalt concrete properties including resilient modulus and indirect tensile strength. Price and Burati (1990) partitioned the profile into ten partitions and got good correlation for modified asphalts with some physical tests. Garrick and Biskur (1990) divided the profile into twelve equal partitions and got good correlation with temperature susceptibility and viscosity ratio.

In spite of all the above mentioned correlations with the HP-GPC, some authorities (Stock, 1986) have expressed reservations about the interpretation of the data obtained by this technique. This could be due to the fact that there are several test parameters that must be carefully controlled to insure inter-laboratory comparison of results. Some of the suggested factors by Stock (1986) to reduce variability of HP-GPC results are (i) the solution should be injected into the instrument as soon as possible after preparation to avoid molecular swelling, (ii) to secure comparability between chromatograms produced by different laboratories,

(iii) the column system used in the instrument and the solvent used as the mobile phase should be the same.

2.5 SUMMARY

Emphasis of this chapter was on the available literature on the rheological properties of asphalt, recently adapted performance-related properties, and on asphalt chemistry with an added emphasis on the HP-GPC technique and its use in predicting the physical performance of asphalt.

Rheological properties included consistency testing, asphalt aging and its indices, and asphalt temperature susceptibility and its indices.

SHRP-developed performance related properties were discussed. Discussion included the idea behind performance-based testing and parameters, rotational viscometer testing, dynamic shear rheometer testing, bending beam rheometer testing, direct tension tester testing, and SHRP performance grading. Discussion about the linear viscoelastic model for asphalt, its usefulness, and its parameters was also discussed.

The literature review also included discussion about asphalt chemistry and asphalt composition and its analytic procedures. Emphasis was placed on the high pressure gel permeation chromatography technique, its development, operational procedure, and its use in asphalt characterization. Previous work on

the use of HP-GPC to predict asphalt properties and asphalt performance was also presented.

Chapter 3

RESEARCH METHODOLOGY

3.1 INTRODUCTION

The flow of the work in this research is shown in Fig. 3.1. Asphalt samples were collected from all asphalt producing refineries in the Gulf countries in addition to one set of polymer modified samples. Collected samples were tested at three aging stages, i.e., fresh, rolling thin film oven (RTFO) residue, and pressure aging vessel (PAV) residue. The asphalt samples were subjected to rheological tests to get the rheological properties and to calculate the age hardening indices and temperature susceptibility indices. The asphalt samples were also subjected to performance-related tests to get their performance indices and to develop the linear visco-elastic models (LVE) of the test samples from which the asphalt specific properties were calculated. The asphalt samples at the three aging stages were finally subjected to fractionation by HP-GPC. Produced chromatograms were fractionated using different fractionating procedures. All obtained results were used to develop models to relate both rheological and performance-related properties to HP-GPC produced chromatograms.

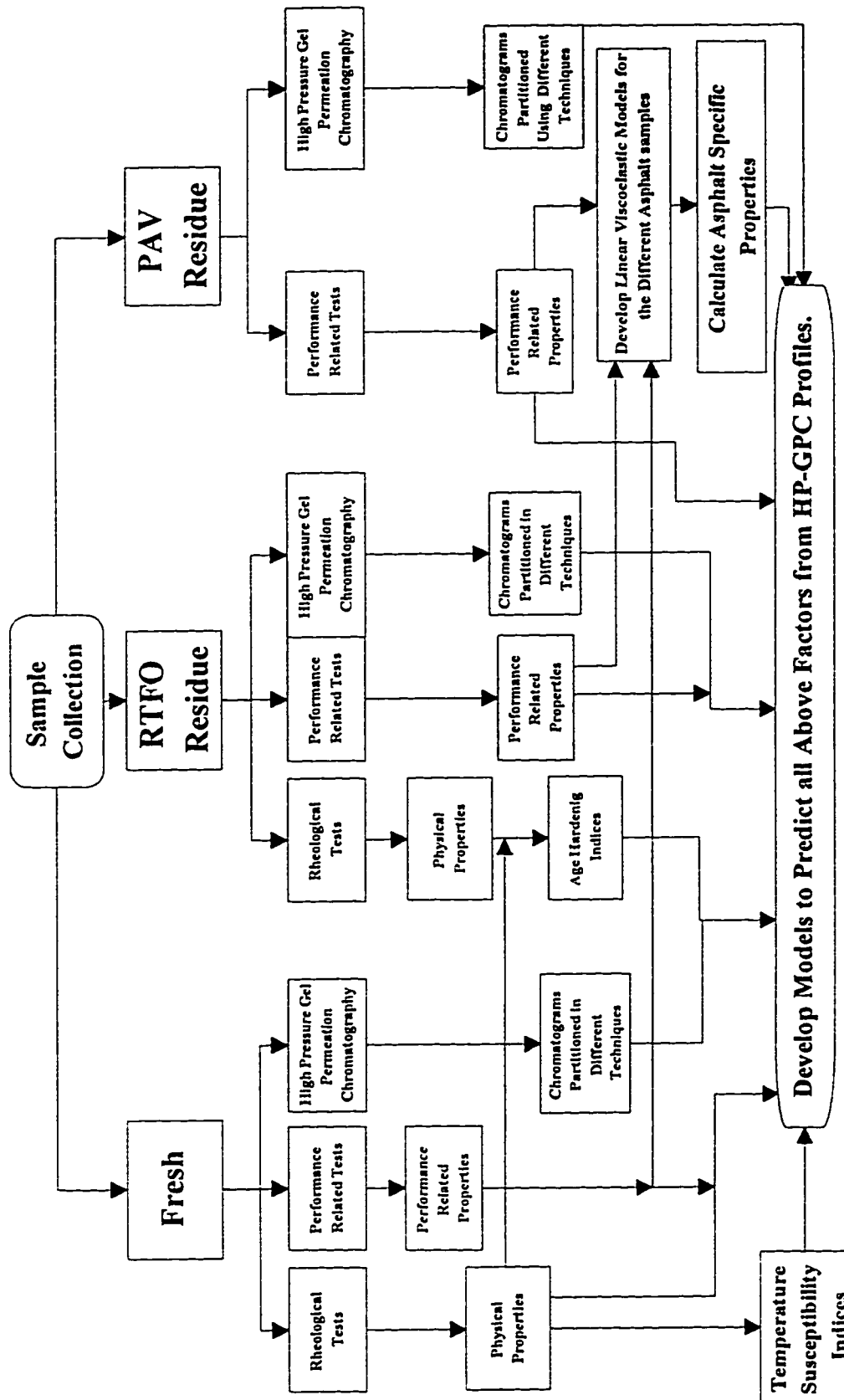


Figure 3.1: Flow chart of the planned work

3.2 EXPERIMENTAL DESIGN

To check the required number of samples to generate the different models, a confidence limit of 80% for the selected parameters was chosen. Additionally, the acceptable amount of error in estimating the dependent variables was limited to 10%. Anderson et al. (1994) have estimated performance parameters for a number of selected asphalt samples, and the standard deviations for all the calculated samples ranged between 0.0194 and 0.4025. So, the minimum required sample size using the above standard deviations range was as follows (Montgomery and Peck, 1982):

$$n = \left(\frac{Z_{\alpha/2} \sigma}{e} \right)^2 \quad (3.1)$$

$$z_{0.1} = 1.28, e = 0.1, \sigma = 0.4025$$

$$n \text{ (required number of samples)} = \left(\frac{1.28 * 0.4025}{0.1} \right)^2 = 26.5 \quad (3.2)$$

With an objective to cover all Gulf countries, five asphalt samples were collected from every asphalt producing refinery in the Gulf countries. Those refineries included Ras Tanura, Riyadh, Al-Ahmadi (Kuwait), and the Bapco (Bahrain) refineries. Collected samples covered a five month production period (one sample every month) to study the variability of production with time. Another set of polymer modified samples was also tested to find the effect of polymer modification on the HP-GPC produced

chromatograms. The total number of replicates for each test and parameter are shown in the following sections.

3.3 RHEOLOGICAL TESTS

Collected asphalt samples were subjected to the following rheological tests: Penetration at 4°C and 25°C, softening point, absolute viscosity, and kinematic viscosity. Temperature susceptibility factors included penetration index, penetration ratio, penetration viscosity number, and viscosity temperature susceptibility. Neat Arab asphalt samples were aged using the thin film oven test to study the effect of aging on their rheological properties. Age hardening indices, including retained penetration at 4°C and 25°C and viscosity ratio at 60°C and 135°C, were also determined. The experimental design matrix for the rheological testing of Ras Tanura refinery samples is shown in Table 3.1. The same experimental design was followed with the other samples from the Riyadh, Bapco, and Al-Ahmadi refineries in addition to the polymer modified samples. Table 3.1 shows the number of replicates for each test at each aging condition. The number of replicates was judged from the repeatability of the test and the applicability of the test at the specific aging and modification condition. For example, usually the flash point test was just performed on fresh samples and was not performed on RTFO or PAV residues. Also, capillary viscosities were not performed for polymer modified samples.

3.4 PERFORMANCE-RELATED TESTS

Performed performance-related tests included the rotational viscosity test, which was performed on fresh samples. The dynamic shear rheometer test was performed at different temperatures and frequencies on fresh samples. Aged samples were tested using the rolling thin film oven and the pressure aging vessel. The bending beam and direct tension tests were performed on samples aged with the pressure aging vessel. Complex shear modulus, phase angle, creep stiffness, creep rate, failure strain, and all related parameters were calculated.

Master curves for all asphalt collected samples were constructed. In addition, the shift factors, which were used to shift the master curves to the required temperatures, were calculated. Asphalt specific primary parameters, which can fully characterize the linear visco-elastic model of the different asphalt cement samples, were also calculated. These parameters included glassy moduli, steady state viscosity, crossover frequency, rheological index, and reference temperature. The experimental design matrix for the performance-related testing of Ras Tanura refinery samples is shown in Table 3.2. The same experimental design was followed with the other samples from the Riyadh, Bapco, Al-Ahmadi refineries, and the polymer modified samples. Table 3.2 shows the number of replicates for each calculated parameter. Each parameter was calculated after a set of tests was performed.

Table 3.2: Experimental design matrix for the performance related properties of Ras Tanura samples.

Group	Property	RT																													
		NEAT										POLYMER MODIFIED																			
		RT1			RT2			RT3			RT4			RT5			RT-CRT-5			RT-CRT-10			RT-SBS-3			RT-SBS-6			RT-SBS-9		
		FRSH	RTFO	PAV	FRSH	RTFO	PAV	FRSH	RTFO	PAV	FRSH	RTFO	PAV	FRSH	RTFO	PAV	FRSH	RTFO	PAV	FRSH	RTFO	PAV	FRSH	RTFO	PAV	FRSH	RTFO	PAV	FRSH	RTFO	PAV
Grading																															
	Lower grading temp. (°C)																														
	Upper grading temp. (°C)																														
LVE Model Parameters																															
	Gg (Gpa)																														
	R																														
	ω_0 @ Td (Hz)																														
LVE Model Parameters																															
	η_0 @ Td (Gpa-s)																														
Design Parameters																															
	$G^* / \sin \delta$ @ 64°C (MPa)																														
	$G^* \times \sin \delta$ @ 25°C (MPa)																														
	S(60) @ 0°C (MPa)																														
	m(60) @ 0°C																														

3.5 HIGH PRESSURE GEL PERMEATION CHROMATOGRAPHY

High pressure gel permeation chromatography was used to characterize the chemical composition of all asphalt samples (neat and modified) at all aging stages.

Different techniques were used to fraction all produced HP-GPC profiles:

- 1- fractionating according to elution times:
 - i) three fractions with equal elution times,
 - ii) three fractions at 25%, 50%, and 25% of total elution time,
 - iii) eight fractions with equal elution times, and
 - iv) twelve fractions with equal elution times

- 2- fractionating according to average areas:
 - i) three fractions with equal average areas,
 - ii) three fractions at 25%, 50%, and 25% of average areas,
 - iii) eight fractions with equal average areas, and
 - iv) twelve fractions with equal average areas.

An additional fractionation procedure was used by fractionating areas under each profile into three areas of 30%, 40%, and 30% of average area taking each asphalt source by itself. Areas under each fraction were calculated to be used in the correlation models. The used fractionating procedures for fresh samples are shown in Table 3.3. The same fractionating procedures were followed for both RTFO- and PAV-aged samples.

3.6 MODELING OF RHEOLOGICAL AND PERFORMANCE-RELATED PROPERTIES

Models for the selected rheological and performance-related parameters were generated using the HP-GPC produced profiles. Table 3.4 shows the properties and indices which were used in the study. The total number of samples used to generate those models was forty five, i.e. twenty-one fresh samples and twenty-four polymer modified samples. Out of these forty five samples, thirty-seven samples were used for generating the different models. The other eight samples were chosen randomly for model validation.

The developed models depended on the results of the fractions of the HP-GPC profiles. Table 3.5 shows a list of the a priori hypothesis for all the factors which were modeled in this research.

Since the total number of variables in each model is high (might reach fourteen variables) and since it is difficult to predict which fraction contributes more to any of the properties, especially in the high number of fractions, it was decided to use stepwise regression. Stepwise Forward-Selection Regression was used to correlate each factor with the different fractions of each fractionating process. An example of a model to correlate the steady state viscosity, η_{ss} , with the areas under the twelve equal time fractions is as follows:

Table 3.4: Used properties and indices.

Group	Used symbol	Property	Use
Rheological Properties	PEN25	Penetration at 25°C, dmm	Consistency Test
	PEN4	Penetration at 4°C, dmm	Consistency Test
	SP	Softening Point, °C	Consistency Test
	FP	Flash Point, °C	Consistency Test
	VIS60	Viscosity at 60°C, Poise	Consistency Test
	RV135	Rotational Viscosity at 135°C, cPa.s	Consistency Test
	VIS135	Viscosity at 135°C, cSt	Consistency Test
	RP25	Retained Penetration at 25°C	Heat Hardening Index
	RP4	Retained Penetration at 4°C	Heat Hardening Index
	VR60	Viscosity Ratio at 60°C	Heat Hardening Index
	VR135	Viscosity Ratio at 135°C	Heat Hardening Index
	PI	Penetration Index	Temperature Susceptibility Index
	PR	Penetration Ratio	Temperature Susceptibility Index
	PVN	Penetration Viscosity Number	Temperature Susceptibility Index
	VTs	Viscosity Temperature Susceptibility	Temperature Susceptibility Index
Performance Related Properties	Lower	Lower grading temp., °C	Performance Grading Temperature
	Upper	Upper grading temp., °C	Performance Grading Temperature
	Gg	Glassy Moduli, Gpa	LVE Model Parameters
	R	Rheological Index	LVE Model Parameters
	w_0	Crossover Frequency at Td, Hz	LVE Model Parameters
	η_0	Steady-State Viscosity at Td, Gpa.s	LVE Model Parameters
	$G^* / \sin \delta$	$G^* / \sin \delta$ @ 64°C, MPa	Rutting Parameter
	$G^* \times \sin \delta$	$G^* \times \sin \delta$ @ 25°C, MPa	Fatigue Parameter
	S	Creep Stiffness at 60Hz @ 0°C, MPa	Thermal Cracking Parameter
	m	Creep Rate @ 0°C	Thermal Cracking Parameter

Table 3.5: A priori Hypothesis for the models which will be predicted in the study.

Predicted Factor	Purpose	Hypothesis	Explanation
Performance Related Properties:			
Upper Grading Temperature	Asphalt grading	Proportional to LMS	Higher LMS means higher stiffness.
Lower Grading Temperature	Asphalt grading	Proportional to MMS	Higher MMS gives ductility.
Steady-State Viscosity, η_0	Asphalt specific property	Proportional to LMS	Higher LMS means higher viscosity.
Crossover Frequency, ω_c	Asphalt specific property	Proportional to LMS	Depends on asphaltene percentage.
Rheological Index, R	Asphalt specific property	Proportional to LMS	Increases with increase of molecular weight.
Reference Temperature, T_d	Asphalt specific property	Proportional to LMS	Increases with increase of molecular weight.
$G^* / \sin \delta$ (for fresh samples)	Control of Rutting	Proportional to LMS	Rutting resistance is proportional to LMS.
$G^* \sin \delta$ (for PAV aged samples)	Control of Fatigue Cracking	Inversely proportional to LMS	Cracking resistance is inversely proportional to LMS.
Creep Stiffness, S	Control of Thermal Cracking	Inversely proportional to LMS	Cracking resistance is inversely proportional to LMS.
Creep Rate, m	Control of Thermal Cracking	Inversely proportional to LMS	Cracking resistance is inversely proportional to LMS.
Present Rheological Factors:			
Penetration Index	Indicator of asphalt susceptibility	Negatively related to LMS	It is related to penetration.
Penetration Ratio	Indicator of asphalt susceptibility	Negatively related to LMS	It is related to penetration.
Penetration Viscosity Number	Indicator of asphalt susceptibility	Negatively related to MMS	Depending on the shape of the relationship.
Viscosity Temperature Susceptibility	Indicator of asphalt susceptibility	Positively related to LMS	It is related to viscosity.
Retained Penetration @25C	Indicator of Asphalt Hardening	Negatively related to LMS	It is related to penetration.
Retained Penetration @4c	Indicator of Asphalt Hardening	Negatively related to LMS	It is related to penetration.
Retained Viscosity @60C	Indicator of Asphalt Hardening	Positively related to LMS	It is related to viscosity.
Retained Viscosity @135C	Indicator of Asphalt Hardening	Positively related to LMS	It is related to viscosity.
Penetration @25C	Related to Consistency of Asphalt	Negatively related to LMS	Higher LMS means higher association .
Penetration @4C	Related to Consistency of Asphalt	Negatively related to LMS	Higher LMS means higher association .
Softening Point	Related to Consistency of Asphalt	Positively related to LMS	Higher LMS means higher association .
Absolute Viscosity	Related to Consistency of Asphalt	Positively related to log LMS	Higher LMS means higher association .
Kinematic Viscosity	Related to Consistency of Asphalt	Positively related to log LMS	Higher LMS means higher association .

$$\eta_o = \beta_o + \beta_1 \text{Frac.1} + \beta_2 \text{Frac.2} + \beta_3 \text{Frac.3} + \dots + \beta_{12} \text{Frac.12} + \varepsilon \quad (3.3)$$

where

Frac.i = the area under the “i”th fraction;

β_1 = regression coefficient for “i”th fraction; and

ε = error.

The purpose of using stepwise regression is to help in selecting a smaller subset that will adequately explain the response from the total number of dependent variables. The criteria for including any factor in the regression model was set to be 1.0, i.e., the variable will be included in the model if it adds to the significance level of F-ratio a value of 1.0 or greater. The following preliminary analyses were performed on the collected data which were used in creating the models:

- check of normality of the dependent variable,
- type of relation between the dependent variable and any of the independent variables,
- homoscedasticity,
- autocorrelation (Durbin Watson), and
- multicollinearity and singularity (VIF or Pearson correlation matrix).

These tests will be explained thoroughly in Chapter 5.

Chapter 4

DATA COLLECTION AND ANALYSIS

4.1 COLLECTION OF TEST SAMPLES

It was decided to collect asphalt samples from all asphalt producing refineries in the Gulf Countries. A list of the selected refineries follows:

- a. Ras Tanura Refinery, located in Eastern Saudi Arabia,
- b. Riyadh Refinery, located in Central Saudi Arabia,
- c. Al-Ahmadi Refinery, located in Kuwait,
- d. Bapco Refinery, located in Bahrain, and
- e. Awazel Company, located in Riyadh. This company receives AC from the Riyadh refinery (60/70 pen. asphalt) and air blows it to produce a harder asphalt (40/50 pen. asphalt).

Every month a sample was collected from each refinery, totaling five samples per refinery. This was done to have variability within samples collected from the same refinery. In addition, one sample was collected from the Awazel Company. The total number of collected neat samples was 21.

Another set of samples was collected from the batch of polymer modified samples prepared for the “Adaptation of SHRP Performance Based Asphalt Specifications to the Gulf Countries” project. In the polymer modification process,

one sample from each refinery was modified using 5, 10, and 15% crumb rubber (CRT) and 3, 6, and 9% styrene-butadiene-styrene (SBS). Details of mixing procedures of the polymers with the fresh asphalts can be found in Al-Abdul Wahhab et al. (1995). The total number of collected polymer modified samples was 24. So, the total number of samples used in this research was 45.

The neat samples were categorized and coded using a four-digit label ($X_1X_2X_3X_4$); the first two digits, X_1X_2 , indicate sample source: RT = Ras Tanura, RY = Riyadh, BH = Bahrain, KW = Kuwait, and AZ = AWAZEL; the third digit, X_3 , indicates sample number (1 to 5); and finally the fourth digit, X_4 , indicates sample age condition: No code = fresh sample, R = RTFO residue, and P = Pressure Aging Vessel residue. For modified samples, the coding label was $X_1X_2-X_3X_4X_5-X_6-X_7$; the first two digits, X_1X_2 , indicate sample source; the next three digits ($X_3X_4X_5$) indicate the polymer type (SBS or CRT), while X_6 indicates the polymer percentage and X_7 indicates sample age condition: F = fresh sample, R = RTFO aging and P = Pressure Aging Vessel residue. Fig. 4.1 shows the identification scheme followed for both neat and modified samples.

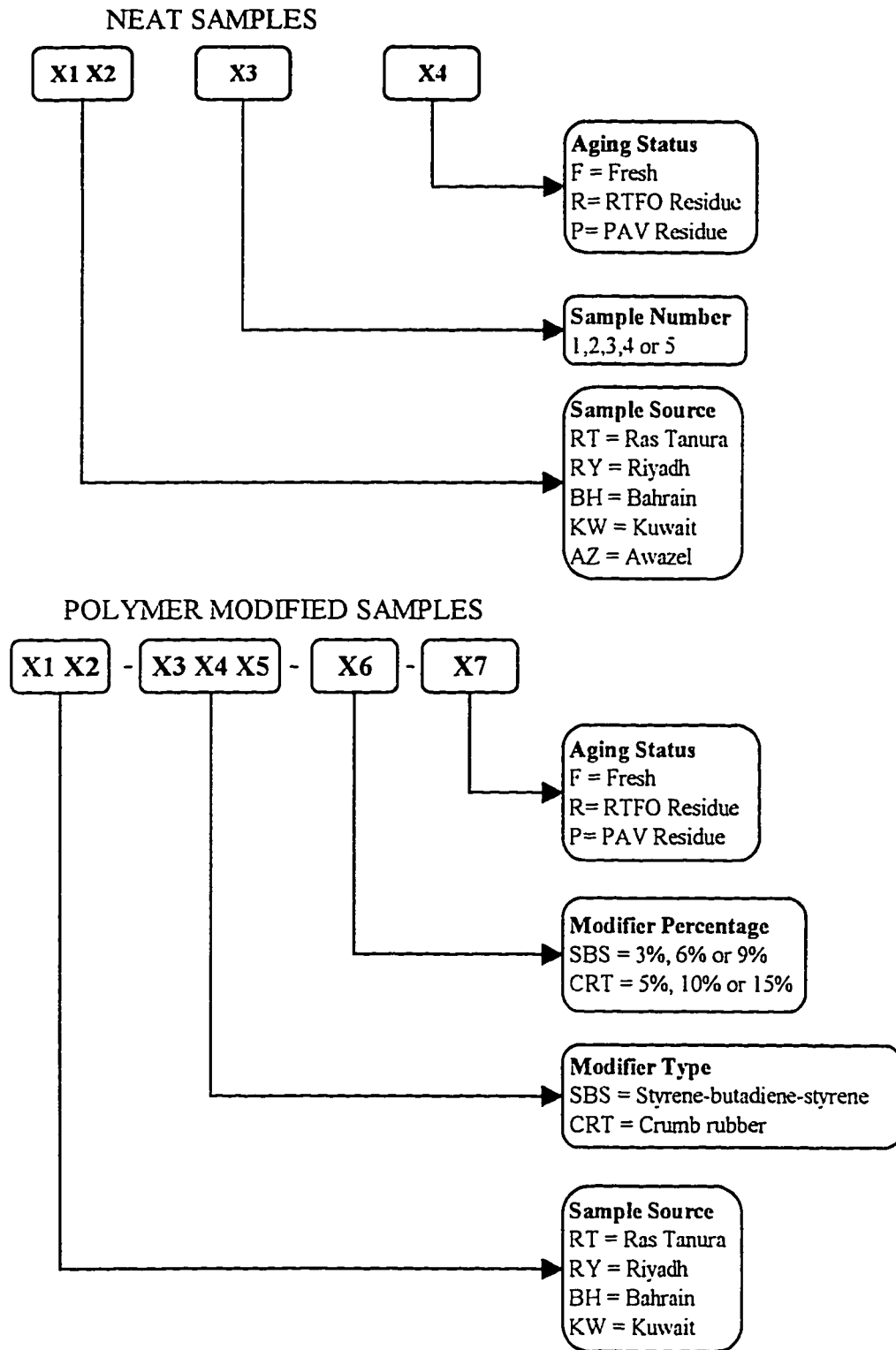


Figure 4.1: Sample identification scheme.

4.2 PHYSICAL TESTING

4.2.1 Consistency Testing

Neat asphalts were subjected to the following tests to determine their physical properties:

1. Penetration at 4°C and 25° ASTM D545, AASHTO T-49-80
2. Absolute viscosity at 60°C ASTM D2171, AASHTO T-202-80
3. Kinematic viscosity at 135°C ASTM D2170, AASHTO T-201-80
4. Rotational viscosity at 135°C ASTM D4402
5. Softening point ASTM D36, AASHTO T-53-81
6. Flash point ASTM D92, AASHTO T-73

Furthermore, fresh samples were aged using the thin film oven (TFO) (ASTM D-1754), which simulates the short-term aging of asphalts that occurs during heating, mixing, and compaction. TFO residue samples were subjected to the following set of testing to study the effect of aging on the physical properties:

1. Penetration at 4°C and 25°C - PEN4 and PEN25
2. Absolute viscosity at 60°C - VIS60
3. Kinematic viscosity at 135°C - VIS135
4. Softening point - SP

The polymer modified samples were subjected to the penetration test at 25°C, the softening point test, the flash point test, and the rotational viscosity test at 135°C. Results of all performed tests are shown in Table 4.1. As can be noticed from the above discussion, the flash point and the rotational viscosity were not performed on the TFO samples because the flash point test is a safety test which is usually performed on fresh samples. Usually the flash point is lowered by aging. The rotational viscosity test for asphalt was originally suggested by SHRP to test the ability of handling and pumping the AC at the refinery, terminal, and/or the hot mixing facility. So, this test was originally suggested for fresh (not aged) samples. For the polymer modified samples, the rotational viscometer was used in place of the kinematic and absolute viscometers because the latter two viscometers are capillary and cannot be used for polymer modified samples since the polymers can clog the viscometer. Some of the observations that can be said about Table 4.1 include the following:

- For both PEN25 & PEN4, samples from RT have the highest variability.
- Regarding penetration grading, all samples from BH can be said to have 40-50 pen. grade, while all other refineries' samples had different penetration grades.
- The softening point and viscosity (VIS60, VIS135, and RV135)

Table 4.1: Physical properties of the different asphalt samples.

Sample ID	PEN ₂₅	PEN ₄	SP (°C)	FP (°C)	VIS ₆₀ (Pulse)	RV ₁₃₅ (Pa.s)	VIS ₁₃₅ (cSt)
RT1	60	29	50	310	3164	0.468	408
RT1R	54	26	59	-	5111	-	554
RT2	63	29	51	308	3205	0.460	492
RT2R	54	27	56	-	5666	-	587
RT3	56	31	50	308	3350	0.460	492
RT3R	50	25	57	-	5931	-	568
RT4	51	32	51	309	3558	0.480	489
RT4R	46	26	55	-	8960	-	675
RT5	56	32	51	306	2986	0.445	441
RT5R	52	29	54	-	7033	-	568
BH1	45	17	50	338	3399	0.465	482
BH1R	35	16	54	-	5581	-	609
BH2	47	17	50	336	3043	0.485	486
BH2R	35	16	54	-	6136	-	619
BH3	48	22	49	334	2852	0.460	451
BH3R	38	18	55	-	5025	-	629
BH4	50	21	50	336	2978	0.455	452
BH4R	40	17	56	-	5202	-	598
BH5	48	23	50	335	2933	0.450	447
BH5R	38	17	55	-	4993	-	573
RY1	54	21	49	332	2622	0.530	412
RY1R	42	19	54	-	4656	-	543
RY2	57	23	50	324	2693	0.490	439
RY2R	39	19	56	-	5910	-	551
RY3	50	21	50	322	3097	0.490	468
RY3R	39	16	57	-	6546	-	585
RY4	54	23	50	320	2631	0.460	523
RY4R	42	18	56	-	5097	-	547
RY5	51	21	51	326	2935	0.500	556
RY5R	36	19	57	-	5738	-	574
KW1	53	24	50	294	3187	0.500	530
KW1R	39	16	62	-	6500	-	736
KW2	51	23	51	298	3453	0.565	584
KW2R	32	19	58	-	6002	-	686
KW3	54	25	52	290	3865	0.575	530
KW3R	35	18	56	-	6992	-	760
KW4	56	25	50	284	3304	0.590	533
KW4R	36	19	58	-	7631	-	791
KW5	55	24	51	288	3562	0.565	573
KW5R	29	18	59	-	5839	-	726
AZ1	38	23	55	326	6172	0.620	526
AZ1R	31	17	59	-	10750	-	594
RT-CRT-5-F	57	-	59	300	-	1.381	-
RT-CRT-10-F	46	-	62	300	-	2.743	-
RT-CRT-15-F	36	-	75	304	-	11.193	-
RT-SBS-3-F	43	-	60	308	-	1.436	-
RT-SBS-6-F	35	-	86	304	-	4.169	-
RT-SBS-9-F	26	-	94	310	-	6.077	-
RY-CRT-5-F	36	-	61	316	-	1.399	-
RY-CRT-10-F	42	-	59	294	-	1.641	-
RY-CRT-15-F	36	-	69	306	-	7.170	-
RY-SBS-3-F	25	-	64	328	-	1.562	-
RY-SBS-6-F	18	-	75	330	-	4.526	-
RY-SBS-9-F	15	-	93	324	-	4.359	-
BH-CRT-5-F	31	-	60	322	-	1.085	-
BH-CRT-10-F	33	-	58	320	-	1.604	-
BH-CRT-15-F	39	-	68	316	-	5.401	-
BH-SBS-3-F	50	-	60	332	-	1.372	-
BH-SBS-6-F	22	-	82	336	-	3.241	-
BH-SBS-9-F	32	-	92	330	-	4.491	-
KW-CRT-5-F	19	-	63	304	-	1.865	-
KW-CRT-10-F	38	-	62	296	-	3.649	-
KW-CRT-15-F	35	-	71	306	-	9.003	-
KW-SBS-3-F	44	-	58	296	-	1.354	-
KW-SBS-6-F	28	-	72	306	-	3.462	-
KW-SBS-9-F	24	-	85	310	-	9.333	-

increased with aging and with the introduction of polymers. While penetration was decreased.

- The highest value of SP for fresh non-modified samples was 51°C. Polymer modification allowed SP to reach 94°C for some types and percentages of polymers.
- For the used polymers, there was no major change in the flash point value.
- The flash points of all studied samples were within acceptable limits.
- The addition of polymers seems to have increased the values of the viscosity for some samples over the maximum allowable limit set by SHRP.

4.2.2 Heat Hardening and Temperature Susceptibility Indices

Durability is a very important factor affecting the behavior of AC. Durability is the resistance of the AC to change in properties when subjected to processing and weathering and is manifested by resistance to hardening with time. To get an indication about the durability of the collected asphalt samples, the following heat hardening indices were calculated:

- Retained penetration @ 4°C - RP4

- Retained penetration @ 25°C - RP25
- Viscosity ratio @ 60°C - VR60
- Viscosity ratio @ 135°C - VR135

These indices are shown in Table 4.2. Larger values of retained penetration indicate little or no heat hardening, i.e. more durable asphalt, while larger values of viscosity ratio indicate a significant amount of heat hardening in the thin film oven.

To find the temperature susceptibility, which is a measure of rate of consistency change with temperature, of the collected samples, the following indices were calculated:

- Penetration Index - PI

The larger negative values of PI indicate greater temperature susceptibility.

- Penetration Ratio - PR

Lower PR indicates greater temperature susceptibility.

- Penetration-Viscosity Number - PVN

Lower PVN indicates greater temperature susceptibility.

- Viscosity-Temperature Susceptibility - VTS

Large VTS indicates higher temperature susceptibility.

These indices were calculated for the test samples and presented in Table 4.2. Some of the observations that can be said about Table 4.2 include the following:

Table 4.2: Heat hardening and temperature susceptibility indices of the different asphalt samples.

Sample ID	RP25	RP4	VR60	VR135	PI	PR	PVN	VTs
RT1	0.90	0.89	1.62	1.36	-0.72	48.81	-0.75	3.65
RT2	0.86	0.91	1.77	1.19	-0.44	46.21	-0.42	3.50
RT3	0.89	0.83	1.77	1.15	-0.95	54.86	-0.56	3.52
RT4	0.91	0.82	2.52	1.38	-0.98	63.21	-0.66	3.55
RT5	0.92	0.92	2.36	1.29	-0.73	56.74	-0.70	3.56
BH1	0.76	0.95	1.64	1.26	-1.41	36.79	-0.79	3.54
BH2	0.75	0.94	2.02	1.27	-1.45	35.21	-0.74	3.49
BH3	0.79	0.79	1.76	1.39	-1.53	46.34	-0.82	3.53
BH4	0.80	0.78	1.75	1.32	-1.25	42.08	-0.78	3.54
BH5	0.78	0.74	1.70	1.28	-1.27	47.38	-0.83	3.54
RY1	0.78	0.88	1.78	1.32	-1.20	39.17	-0.83	3.56
RY2	0.69	0.82	2.19	1.26	-0.98	39.82	-0.70	3.53
RY3	0.79	0.77	2.11	1.25	-1.28	42.32	-0.74	3.53
RY4	0.78	0.80	1.94	1.05	-1.01	41.87	-0.50	3.37
RY5	0.70	0.93	1.95	1.03	-0.86	40.38	-0.48	3.37
KW1	0.74	0.66	2.04	1.39	-1.01	45.39	-0.51	3.43
KW2	0.63	0.84	1.74	1.18	-0.93	45.54	-0.42	3.39
KW3	0.64	0.71	1.81	1.43	-0.63	46.21	-0.48	3.50
KW4	0.64	0.76	2.31	1.48	-0.93	44.54	-0.44	3.45
KW5	0.52	0.73	1.64	1.27	-0.86	44.45	-0.36	3.42
AZ1	0.78	0.61	2.04	1.13	-0.59	78.39	-0.45	3.55

- From the values of RP25 and RP4, on the average, RT samples are more durable than other samples.
- Variability of VR60 and VR135 was small between all samples from all sources.
- The value of the PI ranged between -0.44 and -1.53 . RT samples have the lowest temperature susceptibility, while BH samples have the highest temperature susceptibility.
- The penetration viscosity number for all samples ranged from -0.42 to -0.83 .
- The variability in the values of viscosity temperature was not high.

The relation between temperature and viscosity for all neat samples is shown in Fig. 4.2. As can be noticed from Table 4.2, the different indices for the same property gave conflicting results. For example, comparing the values of RP25 for both RY2 and RY3 indicate that RY3 has a lower heat hardening index, while values of RP4 indicate that RY2 has a lower heat hardening index. The same is noticed when comparing the values of PI and PR (which are temperature susceptibility indices) for RT3 and RT4. This indicates the need for a better set of tests to evaluate the suitability of the asphalt cement for certain environmental and loading conditions.

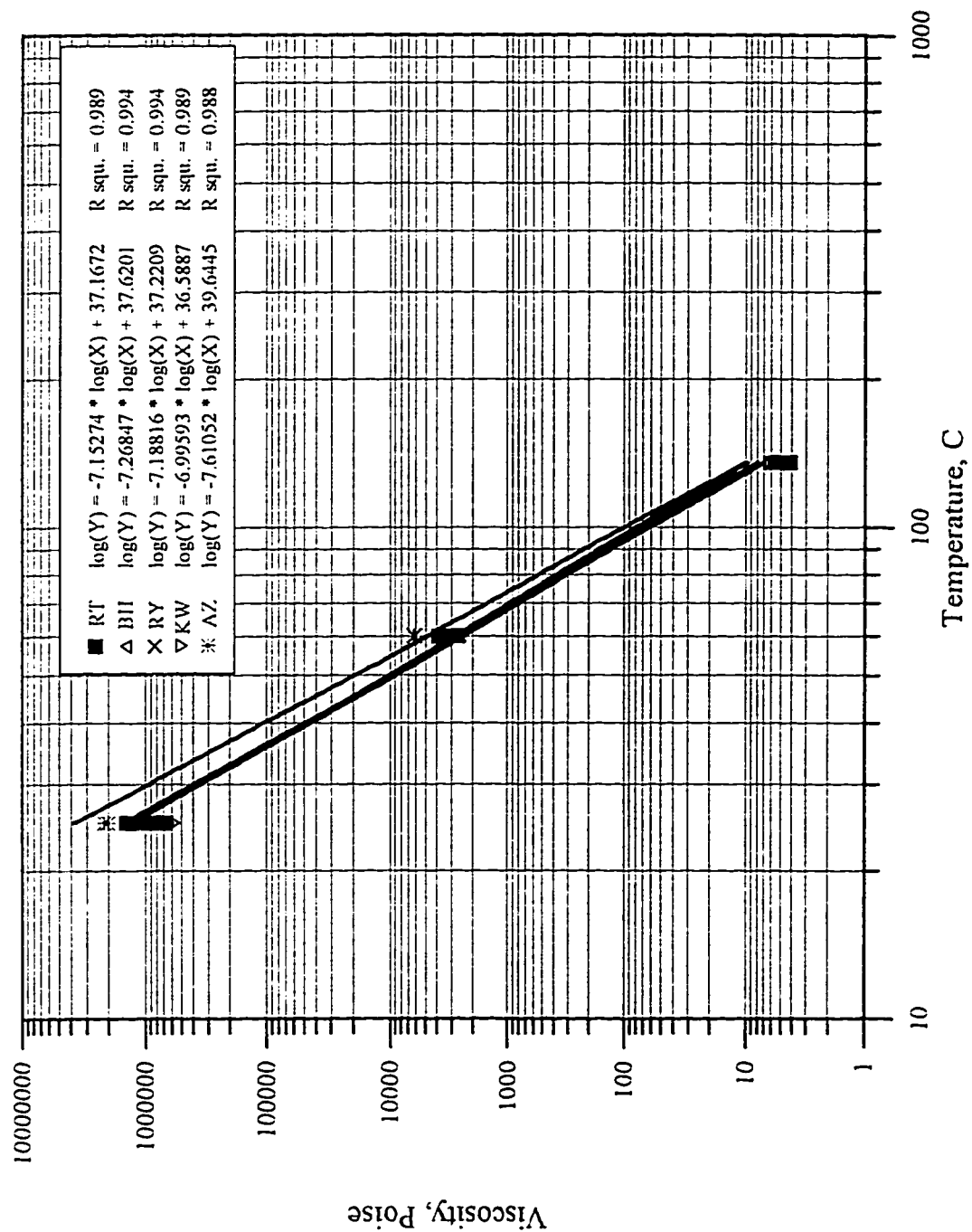


Figure 4.2: Temperature - viscosity relationship for the tested samples.

Statistical analysis was performed to check variability between refineries for all the performed rheological tests and calculated indices. Table 4.3 shows the results of the performed statistical analysis. The statistical tests showed that, at 95% confidence, there are significant differences between the refineries for all tested properties, except for VR60 and VR135 where the significant levels were 37% and 87%, respectively. These results indicate that there is variability in production between refineries and there is variability between the collected samples which increases the significance of the generated models. These differences between refineries were expected because the sources of the crude oil are different and the distillation processes are different (Al-Abdul Wahhab et. al., 1995).

4.3 PERFORMANCE BASED TESTING

Recommended SHRP performance tests were performed on all the collected asphalt samples to grade these samples according to the SHRP grading system and to find the performance-related properties of these samples for further correlations with HP-GPC chromatograms.

4.3.1. Rotational Viscosity

A Brookfield viscometer was used to measure the rotational viscosity of the different asphalt samples. Plate 4.1 shows a close picture of the used Brookfield viscometer. The ASTM D4402 method “Viscosity Determination of Unfilled

Table 4.3: Testing of differences in pavement characteristics between various refineries using ANOVA.

Characteristics	Average Value									F-ratio	Sig. level
	RT	BH	RY	KW	AZ	RT-P	BH-P	RY-P	KW-P		
PEN25	57	48	53	54	38	41	35	29	31	9.79	0.0000
PEN4	31	20	22	24	23	-	-	-	-	25.38	0.0000
SP (oC)	51	50	50	51	55	73	70	70	68	6.11	0.0001
FP (oC)	308	336	325	291	326	304	326	316	303	20.83	0.0000
VIS60 (Poise)	3252	3041	2796	3474	6172	-	-	-	-	49.21	0.0000
RV135 (Pa.s)	0.46	0.46	0.49	0.56	0.62	4.50	2.87	3.44	4.78	3.71	0.0030
VIS135 (cSt)	464	464	480	550	526	-	-	-	-	4.39	0.0139
RP25	0.89	0.78	0.75	0.63	0.78	-	-	-	-	18.76	0.0000
RP4	0.87	0.84	0.84	0.74	0.61	-	-	-	-	4.64	0.0111
VR60	2.01	1.77	2.00	1.91	2.04	-	-	-	-	0.66	0.6314
VR135	1.27	1.31	1.18	1.35	1.13	-	-	-	-	2.11	0.1270
PI	-0.76	-1.39	-1.06	-0.87	-0.59	-	-	-	-	11.42	0.0001
PR	53.97	41.56	40.71	45.23	78.39	-	-	-	-	20.51	0.0000
PVN	-0.62	-0.79	-0.65	-0.44	-0.45	-	-	-	-	7.52	0.0013
VTS	3.56	3.53	3.47	3.44	3.55	-	-	-	-	3.32	0.0368

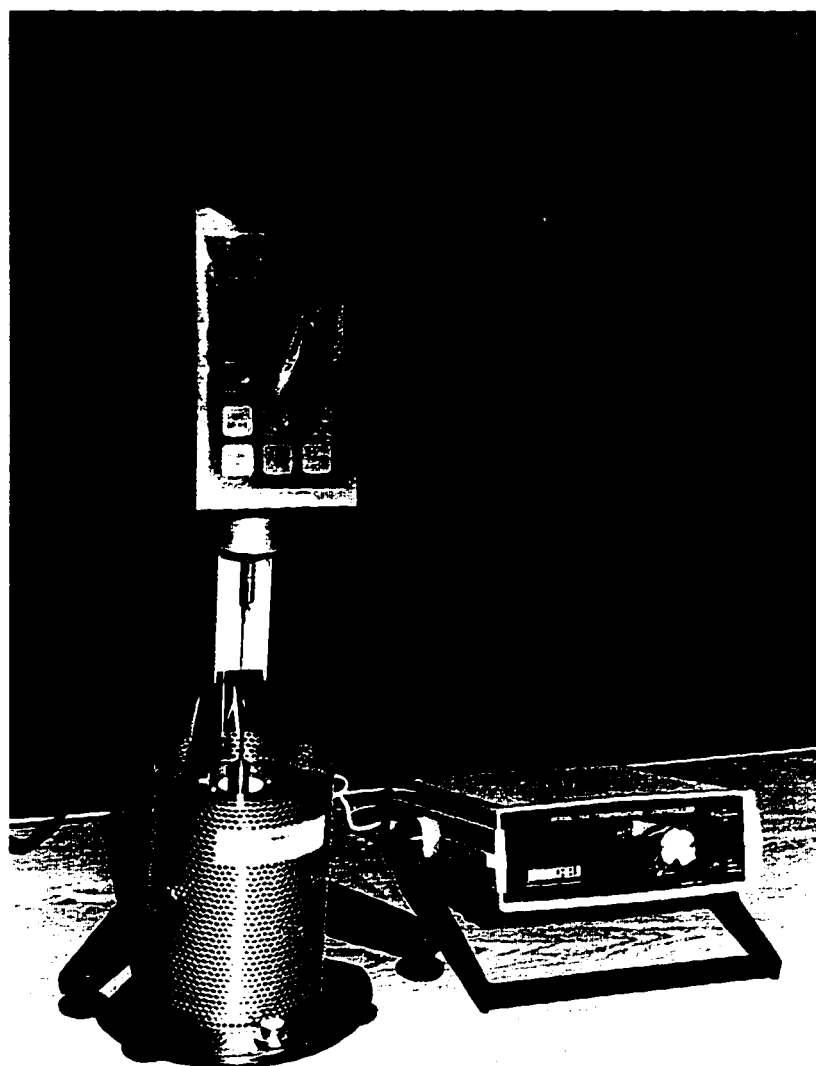


Plate 4.1: Used Brookfield viscometer.

Asphalts Using the Brookfield Thermosel Apparatus” was followed in performing the tests. The followed test procedure is summarized in Appendix A.

The rotational viscosity test was performed on all test samples and the results of the tests are included in Table 4.1. On the average, KW samples had the highest rotational viscosity values for both neat and modified samples. All neat samples had values of rotational viscosity less than 1.0 Pa.s. Adding polymers to the asphalt cement increased the rotational viscosity. The increase in the rotational viscosity was proportional to the polymer percentage. Some of the polymers increased the rotational viscosity to a value higher than the maximum limit (3.0 Pa.s) specified by SHRP.

4.3.2 Aging of Asphalt Samples

Two stages of aging were applied to the collected asphalt samples. The first aging procedure simulated the short-term aging of asphalt which occurs due to heating, mixing, and compaction of asphalt. This aging process was performed using the RTFO. The other aging process was performed using PAV, and it simulates eight to ten years of in-service aging. These aging processes were required to prepare the asphalt samples for further testing.

In this research, both aging procedures were performed. The rolling thin film oven was used to get the required RTFO residue of all samples. Plate 4.2 shows Cox & Sons’ RTFO, which was used in this research. The AASHTO T240, ASTM D2872

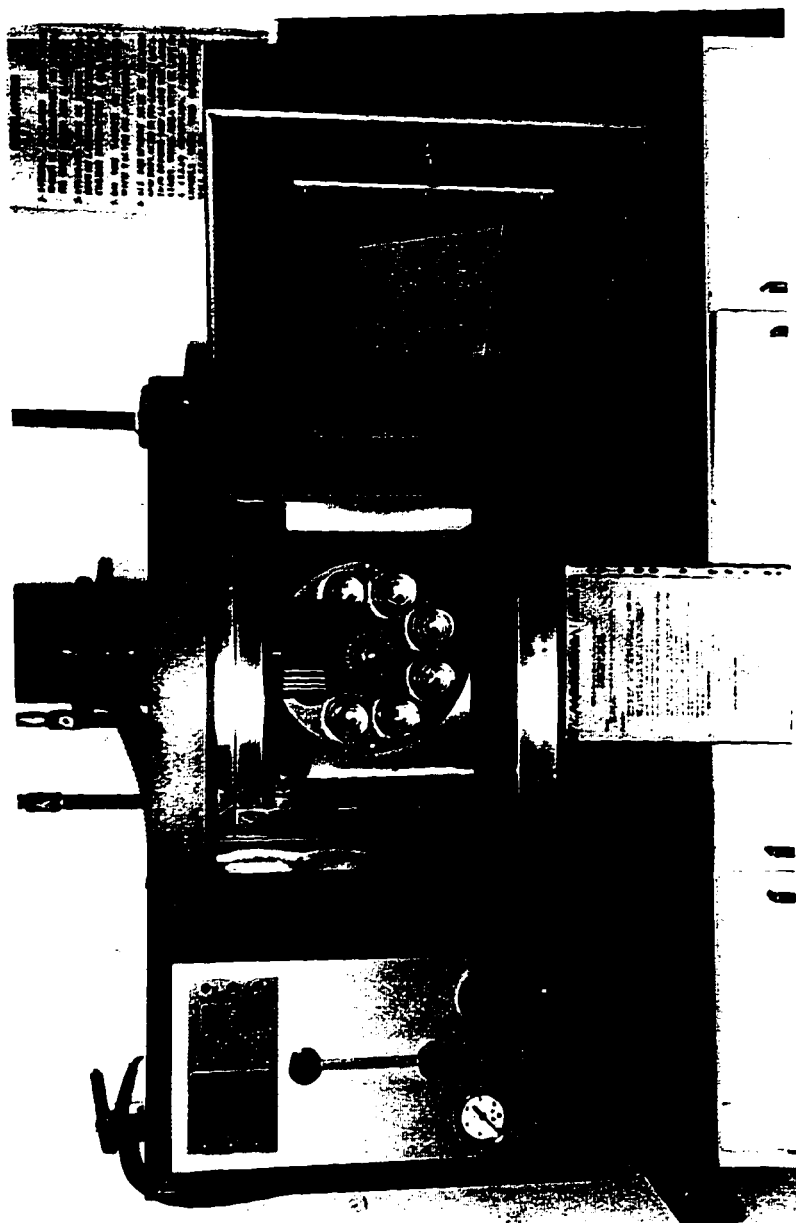


Plate 4.2: Used rolling thin film oven (RTFO).

standard test procedure was followed in RTFO aging. The followed RTFO aging procedure is summarized in Appendix A.

The RTFO aging process was performed on all test samples. Aged samples were grouped into two groups. The first group was subjected to all other required tests on RTFO residue, while the second group was subjected to PAV aging. Emptying the RTFO bottles was difficult because of the shape of the bottle opening. This was taken care of by using a specially shaped spatula.

The pressure aging vessel, shown in Plate 4.3, was used according to the AASHTO PP1 “Accelerated Aging of Asphalt Binder Using a Pressurized Aging Vessel” test procedure. All pressure aging was performed on samples previously aged by RTFO. The used PAV aging procedure is summarized in Appendix A.

PAV aging was performed on all required samples, and PAV residues from all samples were ready for the next set of tests.

4.3.3 Dynamic Shear Rheometer Testing

A Bohlin Dynamic Shear Rheometer (DSR) was used to determine the complex modulus (G^*) and the phase angle (δ) for all test samples. The AASHTO TP5 standard method of test for “Determining the Rheological Properties of Asphalt Binder Using a Dynamic Shear Rheometer” was followed. The test apparatus consisted of a dynamic shear rheometer (DSR), a temperature controller, and a computer that controls the rheometer and acquires data. Plate 4.4 shows the DSR

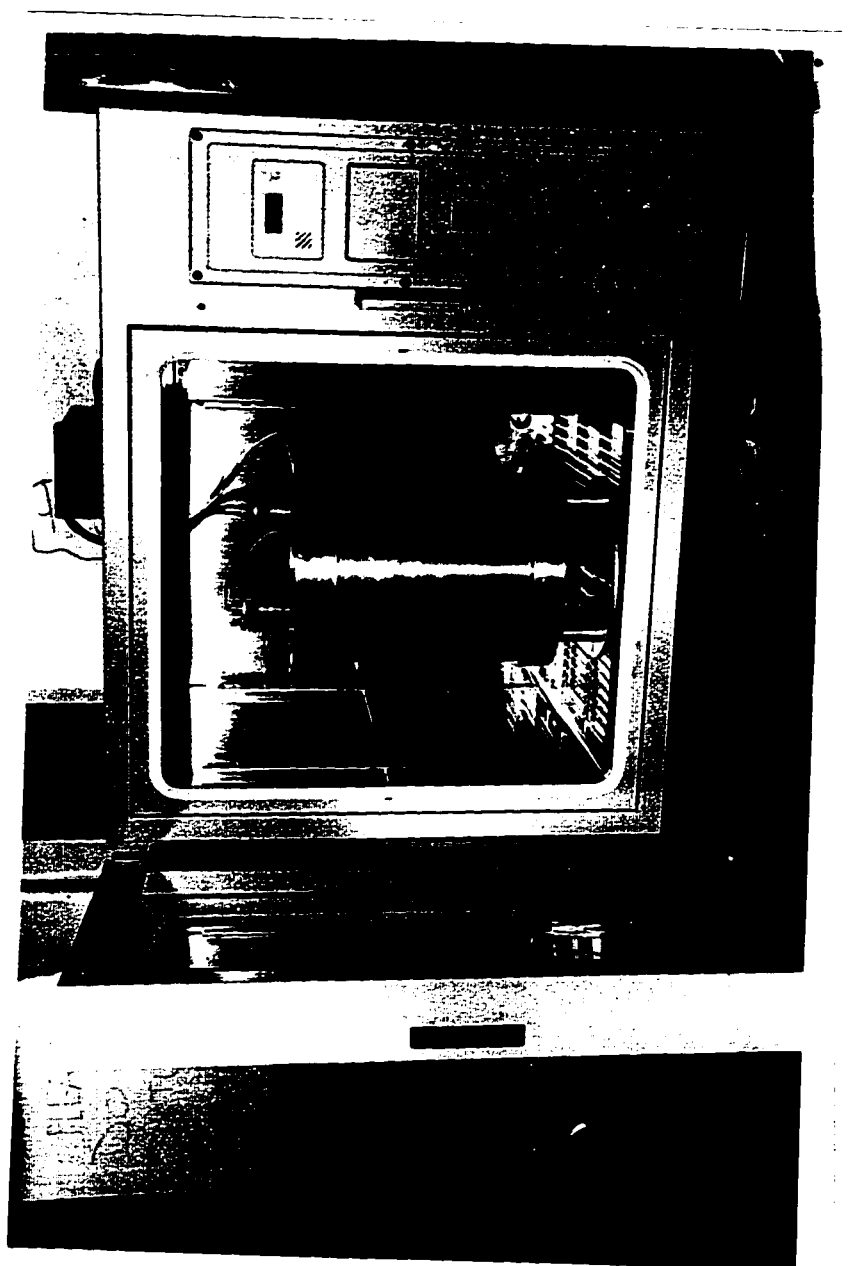


Plate 4.3: Used pressure aging vessel (PAV).

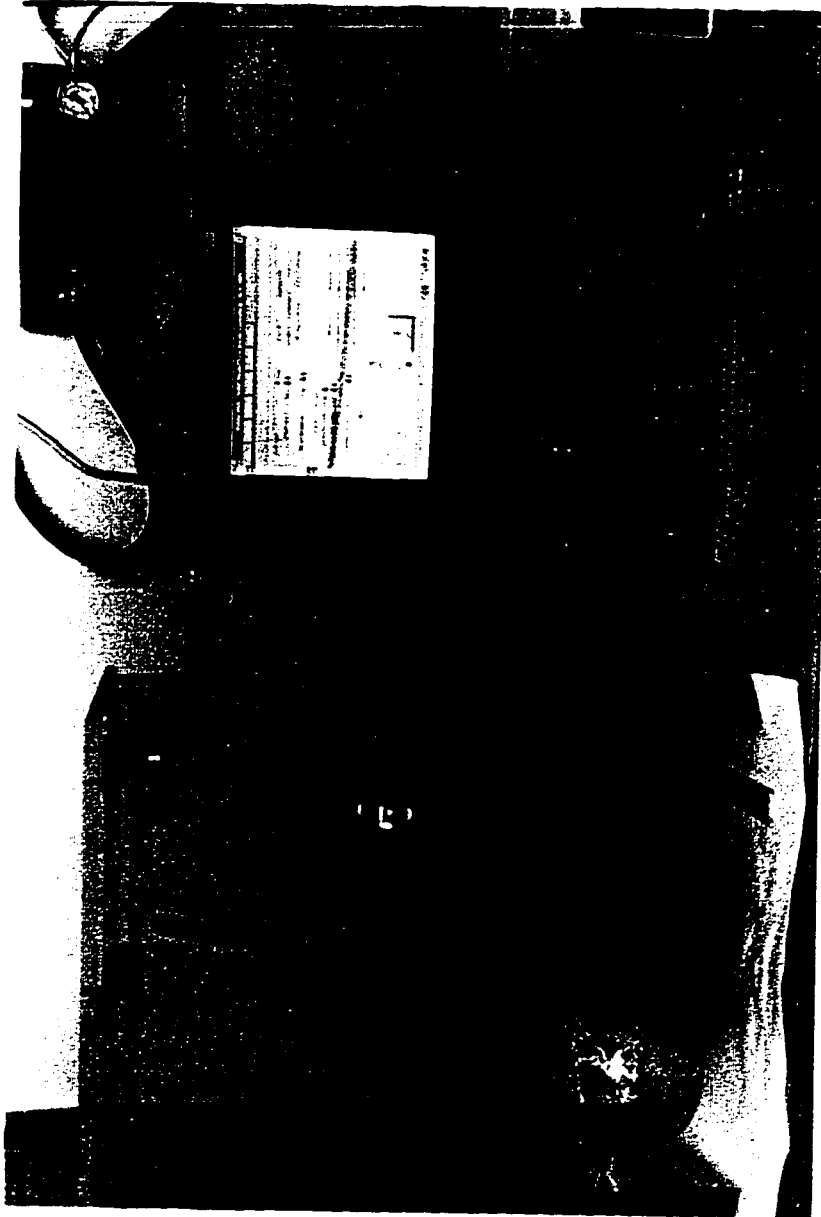


Plate 4.4: Dynamic shear rheometer (DSR) with all accessories.

apparatus with all needed accessories. The DSR test was performed on fresh binders and binders that had been aged by the rolling thin film oven and pressure aging vessel. The followed test procedure is summarized in Appendix A.

Fig. 4.3 shows a typical output of the fixed frequency DSR testing. In this figure there is a field called “test status”, and it shows “PASSED”. This is done automatically by the software, where it checks the value of $G^*/\sin \delta$ for the fresh samples and the RTFO residue, $G^* \sin \delta$ for PAV residue and compares it with the grading limits set by SHRP. The limiting value for $G^*/\sin \delta$ for fresh samples is to have a value higher than 1.00 kPa. For RTFO residue, the limiting value for $G^*/\sin \delta$ is to have a value greater than 2.20 kPa, while the limiting value for PAV residue is set so that the value of $G^* \sin \delta$ should be lower than 5000 kPa.

Table 4.4 shows the acquired results from the DSR fixed frequency testing for grading the different asphalt samples. Table 4.5 shows the values of G^* at the different test temperatures and different frequencies for PAV residues. Just the PAV residue results are presented because they are the ones that were used for generating the LVE models of the different asphalts.

All neat fresh samples had values for $G^*/\sin \delta$ greater than 1.00 kPa at 64°C, and for all RTFO samples the values for $G^*/\sin \delta$ were over 2.2 kPa at 64°C. Therefore, the upper grading temperature for those samples was 64°C. For the polymer modified samples, the upper grading temperature ranged between 70°C and

DSR Project - SHRP Binder Test - Strain Controlled
(Created by Version 2.05)

Parameters:

Measurement Type: High Temperature Range
Target Temperature: 64.0 °C
Strain Amplitude: 10.00 percent
Plate Diameter: 25.0 mm
Plate Gap: 1.0 mm
Equilibration Time: 0.5 minutes

Ancillary Info:

Operator ID: Operator 001
Sample ID: SampleQC01
Sample Type: Rolling Thin Film Oven Test Residue
Test Number: 0001

Measurement Results:

Completed: 11/7/94 10:24:07 AM
Modulus (G*): 3.7726E3 Pascal
Phase Angle (delta): 79.2 degrees
G*/sin(delta): 3.8403E3 Pascal
Strain Amplitude: 4.85 percent
Final Temperature: 64.0 °C
Osc. Frequency: 10.08 radians/second
Test Status: PASSED

Operator Notes:

RT1R @ 64C

Figure 4.3: Typical printout of DSR fixed frequency testing for sample RT1R tested at 64°C.

Table 4.4: Acquired data from the DSR testing machine for the different asphalt samples.

Sample ID	Fresh			Fresh			RTFO			RTFO			PAV			PAV		
	Temp.(°C)	G* \backslash sinδ (kPa)	Temp.(°C)	G* \backslash sinδ (kPa)	Temp.(°C)	G* \backslash sinδ (kPa)	Temp.(°C)	G* \backslash sinδ (kPa)	Temp.(°C)	G* \backslash sinδ (kPa)	Temp.(°C)	G* \backslash sinδ (kPa)	Temp.(°C)	G* \backslash sinδ (kPa)	Temp.(°C)	G* \backslash sinδ (kPa)		
RT1	64.00	1.76	70.00	0.68	64.00	3.69	70.00	1.82	22.00	2.30	19.00	3.13						
RT2	64.00	1.43	70.00	0.69	64.00	3.19	70.00	1.61	22.00	2.94	19.00	3.94						
RT3	64.00	1.37	70.00	0.67	64.00	3.29	70.00	1.64	22.00	2.80	19.00	3.54						
RT4	64.00	1.55	70.00	0.71	64.00	4.02	70.00	1.96	22.00	3.12	19.00	4.06						
RT5	64.00	1.52	70.00	0.72	64.00	2.99	70.00	1.46	19.00	3.79	16.00	4.93						
BH1	64.00	1.31	70.00	0.64	64.00	3.00	70.00	1.45	25.00	3.79	22.00	5.14						
BH2	64.00	1.46	70.00	0.70	64.00	2.84	70.00	1.36	25.00	3.57	22.00	4.73						
BH3	64.00	1.25	70.00	0.62	64.00	2.79	70.00	1.33	19.00	4.61	16.00	6.54						
BH4	64.00	1.33	70.00	0.67	64.00	2.78	70.00	1.32	25.00	2.63	22.00	3.55						
BH5	64.00	1.23	70.00	0.60	64.00	2.63	70.00	1.21	22.00	4.21	19.00	5.01						
RY1	64.00	1.31	70.00	0.64	64.00	2.73	70.00	1.30	22.00	4.98	19.00	6.55						
RY2	64.00	1.31	70.00	0.67	64.00	3.62	70.00	1.71	25.00	4.41	22.00	5.80						
RY3	64.00	1.42	70.00	0.69	64.00	3.92	70.00	1.75	25.00	4.06	22.00	5.35						
RY4	64.00	1.24	70.00	0.61	64.00	3.03	70.00	1.47	22.00	3.44	19.00	5.17						
RY5	64.00	1.44	70.00	0.68	64.00	4.42	70.00	1.98	22.00	4.02	19.00	5.64						
KW1	64.00	1.60	70.00	0.81	64.00	3.34	70.00	1.65	22.00	4.54	19.00	6.66						
KW2	64.00	1.50	70.00	0.73	64.00	3.74	70.00	1.74	22.00	4.68	19.00	6.87						
KW3	64.00	1.58	70.00	0.81	64.00	3.63	70.00	1.76	22.00	4.81	19.00	6.93						
KW4	64.00	1.48	70.00	0.76	64.00	3.78	70.00	1.92	25.00	3.25	22.00	5.98						
KW5	64.00	1.55	70.00	0.80	64.00	3.59	70.00	1.67	22.00	4.34	19.00	6.52						
AZ1	70.00	1.24	76.00	0.62	70.00	2.83	76.00	1.30	25.00	4.65	22.00	5.99						
RT-CRT-5-F	76.00	0.81	80.00	0.32	76.00	1.87	80.00	0.53	25.00	1.87	22.00	2.39						
RT-CRT-10-F	76.00	1.42	80.00	0.93	76.00	3.20	80.00	2.09	25.00	1.49	22.00	1.60						
RT-CRT-15-F	76.00	6.59	80.00	4.58	76.00	13.45	80.00	9.47	25.00	0.70	22.00	0.99						
RT-SBS-3-F	76.00	1.50	80.00	0.91	76.00	3.27	80.00	2.02	25.00	1.71	22.00	2.16						
RT-SBS-6-F	76.00	5.24	80.00	3.31	76.00	6.28	80.00	4.54	25.00	1.10	22.00	1.43						
RT-SBS-9-F	76.00	12.38	80.00	8.60	76.00	12.64	80.00	9.55	25.00	0.54	22.00	0.59						
RY-CRT-5-F	76.00	0.97	80.00	0.43	76.00	2.16	80.00	0.63	25.00	2.33	22.00	3.55						
RY-CRT-10-F	76.00	1.73	80.00	1.13	76.00	2.26	80.00	1.50	25.00	2.34	22.00	3.23						
RY-CRT-15-F	76.00	3.70	80.00	2.49	76.00	6.17	80.00	4.33	25.00	1.31	22.00	1.62						
RY-SBS-3-F	76.00	2.20	80.00	1.40	76.00	4.08	80.00	2.59	25.00	3.36	22.00	4.38						
RY-SBS-6-F	76.00	5.67	80.00	3.75	76.00	8.51	80.00	5.93	25.00	1.60	22.00	2.30						
RY-SBS-9-F	76.00	8.51	80.00	6.12	76.00	14.61	80.00	10.09	25.00	1.16	22.00	1.34						
BH-CRT-5-F	76.00	1.48	80.00	0.90	76.00	1.97	80.00	1.24	25.00	2.02	22.00	3.55						
BH-CRT-10-F	76.00	1.10	80.00	0.73	76.00	1.98	80.00	0.87	25.00	2.50	22.00	3.30						
BH-CRT-15-F	76.00	2.01	80.00	1.53	76.00	4.67	80.00	3.37	25.00	0.92	22.00	1.38						
BH-SBS-3-F	76.00	1.11	80.00	0.64	76.00	2.22	80.00	1.45	25.00	3.24	22.00	5.28						
BH-SBS-6-F	76.00	2.92	80.00	1.97	76.00	5.32	80.00	3.44	25.00	3.50	22.00	4.29						
BH-SBS-9-F	76.00	12.49	80.00	13.21	76.00	16.28	80.00	13.11	25.00	2.22	22.00	2.84						
KW-CRT-5-F	76.00	2.25	80.00	1.38	76.00	4.22	80.00	2.76	25.00	2.02	22.00	3.07						
KW-CRT-10-F	76.00	1.98	80.00	1.14	76.00	4.71	80.00	3.28	25.00	2.07	22.00	1.99						
KW-CRT-15-F	76.00	4.94	80.00	3.56	76.00	6.93	80.00	4.92	25.00	1.30	22.00	1.84						
KW-SBS-3-F	76.00	1.02	80.00	0.63	76.00	2.58	80.00	1.75	25.00	2.10	22.00	2.80						
KW-SBS-6-F	76.00	2.95	80.00	1.96	76.00	8.11	80.00	5.20	25.00	2.76	22.00	3.73						
KW-SBS-9-F	76.00	11.98	80.00	7.90	76.00	12.57	80.00	8.25	25.00	2.15	22.00	2.78						

Table 4.5: Stiffness values of the residue samples at the different loading times after BBR testing.

Sample ID	Temp.	Loading Time (sec)						Temp.	Loading Time (sec)					
		8	15	30	60	120	240		8	15	30	60	120	240
RT1	-18.00	319188625	268811094	221019188	180517906	146459516	118038184	-11.10	197892641	162542016	129694547	102538658	80327336	62351652
RT2	-18.00	2184296	5877523	15434189	18194165	28932182	293269672	-	-	-	-	-	-	-
RT3	-18.10	586578063	503137688	422085594	351699813	291072500	239269672	-12.00	293861094	245375156	199383094	160409203	127776938	100776289
RT4	-24.20	526859688	450147781	375328781	310246125	254237203	206542344	-18.10	312264125	260783016	212096875	171060984	138813781	108510180
RT5	-24.10	639551875	548271663	455809583	373189125	300877188	238871219	-18.20	373853906	308615375	245943734	192830953	148744688	112883000
BH1	-18.20	647700438	562184500	475665500	397599063	328536719	268303344	-12.00	377741743	256048203	204890141	161775719	126056000	95454500
BH2	-18.30	630304688	545857313	460449781	383733875	315952563	257014856	-12.10	381009825	318089719	257257453	205190906	161405969	125214008
BH3	-18.30	565448750	487620781	409375688	339522469	278177875	225166109	-12.10	369888563	307811656	248363203	197885906	155692063	120960484
BH4	-18.30	670274875	579132313	486960031	404257406	331338408	268123408	-12.20	359191083	298053156	239518750	189887875	148517703	114594469
BH5	-18.30	546225438	474040656	401452688	336463875	279079125	229087344	-12.20	287571906	239318281	193382000	154537203	122131117	95454500
RY1	-18.30	580592813	500282083	418837000	345711969	281333908	225719469	-12.10	359912888	299511656	241863422	193027953	152252266	118686258
RY2	-18.30	581196188	50087188	421390563	351237125	290059281	237325172	-12.20	299803790	250345078	203323453	163414172	129971094	102295766
RY3	-18.30	506029825	432899594	362159906	300760594	247998062	203040578	-12.20	287090313	228666953	180551594	145015094	115369594	90916055
RY4	-18.30	535248188	463303844	391641188	327998250	272154125	223272094	-12.10	261570750	218408078	176888250	143425453	114864773	91271616
RY5	-18.30	609613625	528001063	444511438	368908656	301815844	243418188	-12.10	375525000	308803813	246623547	195084234	152843344	118606008
KW1	-18.30	617157813	533568313	448167281	370970813	302814219	243270172	-12.10	370190438	305223656	244178250	193226000	151253408	117117328
KW2	-18.30	579588438	510980750	438636344	371147625	309549281	254460734	-12.10	384755281	321401313	260359031	208219313	164386953	128141656
KW3	-18.30	676628000	583748563	491605813	409425594	337209094	274656469	-12.10	410766031	342042844	276176625	220202891	173376578	134797719
KW4	-18.20	653550313	556267375	460081875	375717594	302845000	241180313	-12.10	380224406	312761313	248782963	195112938	150872250	115024547
KW5	-18.30	615899313	536738250	457904281	387784438	328019563	272082438	-12.10	364075188	304705656	247998328	199819922	159376594	125843727
AZ1	-18.20	2412994	6442810	24845094	29713007	46644473	63461206	-12.10	1692246	5681472	18426269	22287811	37318274	49708428
RT-CRT-5-F	-18.00	218187219	202552734	165638953	134828516	108758169	87324742	-12.00	128977281	105483328	83693509	65735438	51110082	39338012
RT-CRT-10-F	-18.00	219855984	185736203	153578469	128438652	103642468	84567313	-12.00	103668188	84959805	67926445	42635891	33787137	33787137
RT-CRT-15-F	-18.00	147700547	122071188	98688602	79577133	63998652	51337469	-12.00	89677102	56109180	44092316	34589070	27040098	21102025
RT-SBS-3-F	-18.00	275638125	235658668	197461594	164893172	137228109	113816266	-12.00	164994203	136879438	111240570	90272695	73150500	59189664
RT-SBS-6-F	-12.00	169299188	142700234	117064102	95076070	76448164	60857106	-6.00	88160289	73977112	59740845	47845863	38003367	29936568
RY-CRT-5-F	-18.00	457081000	391693219	327491219	271301469	222699922	181114078	-12.00	191928813	167785188	126788648	100302945	79108547	61942723
RY-CRT-10-F	-18.00	319143083	272023281	228408766	186982313	153228969	124597555	-12.00	184898063	150288375	118914258	93399297	72825383	56370504
RY-CRT-15-F	-18.00	226142922	189749083	156720989	125997750	101485383	81116836	-12.00	131350166	107008781	84824552	66216141	51340908	39425981
RY-SBS-3-F	-18.00	4509338281	388868469	328287000	275336750	229463438	190009250	-12.00	253845031	215301672	178096406	146070719	118787647	95780789
RY-SBS-6-F	-18.00	408780000	354864968	301614781	254586656	213409203	177658156	-12.00	227680359	190901734	156418891	127501414	103392078	83407578
BH-CRT-5-F	-12.00	208805172	178331609	148758094	123133273	101137648	82431438	6.00	153651656	128529859	104887289	85019344	68452398	54743863
BH-CRT-10-F	-18.00	368950400	313739100	260838900	215736656	223230547	183545484	-12.00	238922203	189185563	155784908	102516016	81924825	61924825
BH-CRT-15-F	0.12	121445273	97371500	76679750	58292234	44199145	33666659	-12.00	207630547	172002094	136019281	109304398	85433320	65903531
BH-SBS-3-F	-12.00	323188908	274818156	227674108	186781328	151692787	121998895	-6.00	152542922	124107398	98134297	77002489	59958152	46328961
BH-SBS-6-F	-12.00	263468188	220396156	183062126	150971484	123635967	97831567	-6.00	116387164	102854039	84789164	78788594	63968563	53383668
BH-SBS-9-F	-18.00	342370844	302882469	262208813	224841875	190971083	160670078	-12.00	193133313	164110378	135055328	111360266	90392408	72631672
KW-CRT-10-F	-12.00	340803531	290427031	242239750	200980531	165666076	136166984	-6.00	165283766	136255516	107287719	83934438	65241750	50385469
KW-CRT-15-F	-18.00	454185438	384811031	319077531	263320719	218279000	176800594	-12.00	217853391	178414266	141319719	110437742	83147808	64709181
KW-SBS-3-F	-18.00	273873250	232798453	192968928	129101672	104200305	82637375	-12.00	162637154	13441047	106820023	85061078	67378008	53092370
KW-SBS-6-F	-18.00	511046408	439889563	369596556	307733938	253902483	207588158	-12.00	217984031	177272359	139258859	108031481	82839500	62368758
KW-SBS-9-F	-18.00	490608313	428918900	366326250	309745781	259290872	21487872	-12.00	274307600	231378844	189731359	153828906	123317008	97744594
KW-SBS-12-F	-12.00	24047391	204888781	170323891	140382813	114689461	92867258	-6.00	153438719	125632822	99689408	78229258	60684086	46560731

80°C. The starting lower grading temperature for all test samples was decided depending on the $G^* \sin \delta$ value.

4.3.4 Bending Beam Rheometer (BBR) Testing

Fisher's BBR was used in this research to measure the creep stiffness (S) and logarithmic creep rate (m -value) of all test samples. Plate 4.5 shows the BBR and all accessories used in this study. The BBR test can be performed on PAV residue or fresh samples. But for SHRP grading, it must be performed on PAV residue. In this research, AASHTO TP1 "Determining the Flexural Creep Stiffness of Asphalt Binder Using the Bending Beam Rheometer" test procedure was followed. In the BBR test, a beam specimen with dimensions of $125 \times 12.5 \times 6.2$ mm is loaded with 100 gms for a period of 240 seconds. The effective length of the test beam is 102 mm. The followed procedure in testing for S and m is summarized in Appendix A.

Fig. 4.4 shows a typical printout of BBR test results, and Fig. 4.5 shows a typical graphical presentation of load and force which are usually displayed during testing. Table 4.6 presents the calculated S and m -values for the different test samples at the different test temperatures. Since the stiffness values of the tested samples at the different loading times (8, 15, 30, 60, 120, and 240 seconds) were needed for the construction of the asphalt master curves, they are displayed in Table 4.7. Lower grading temperatures and the need for subjecting the test samples for DTT were

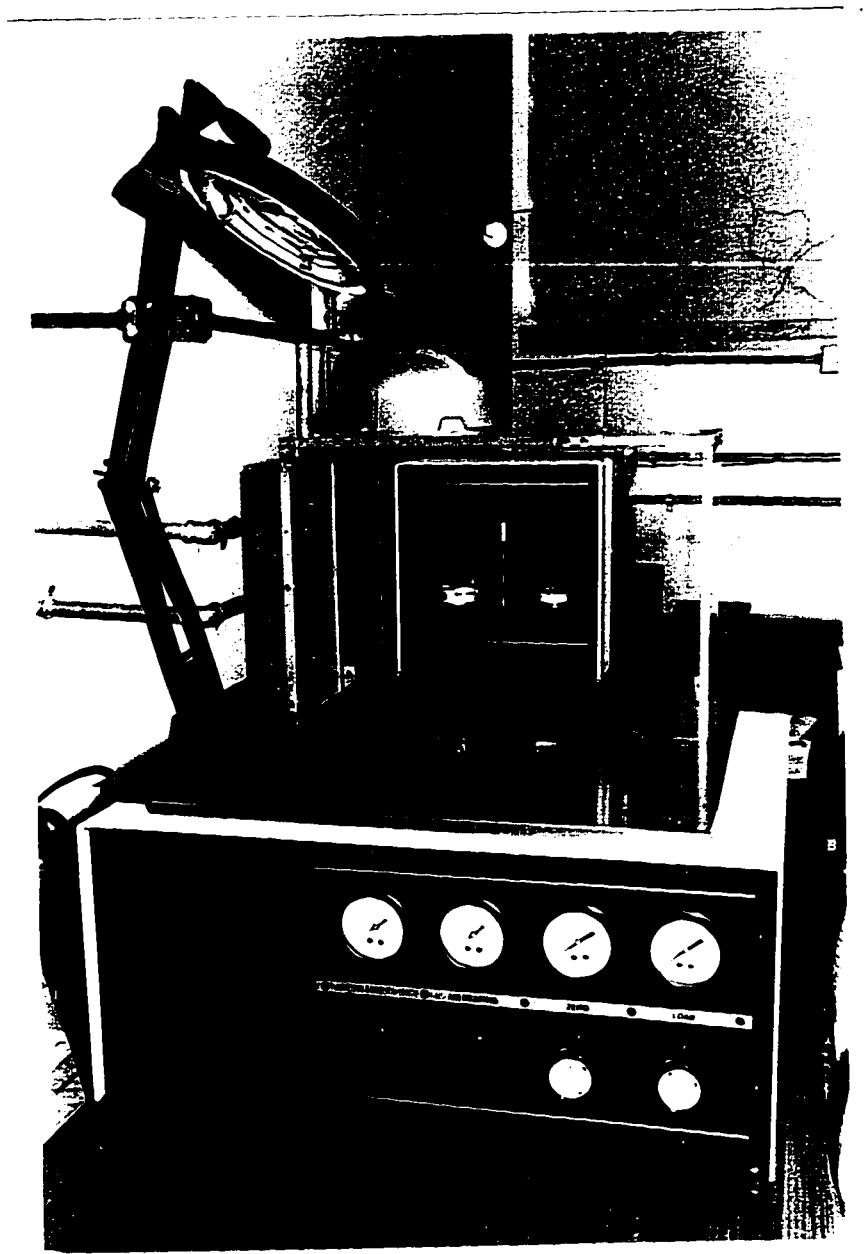


Plate 4.5: Bending beam rheometer (BBR) with all accessories.

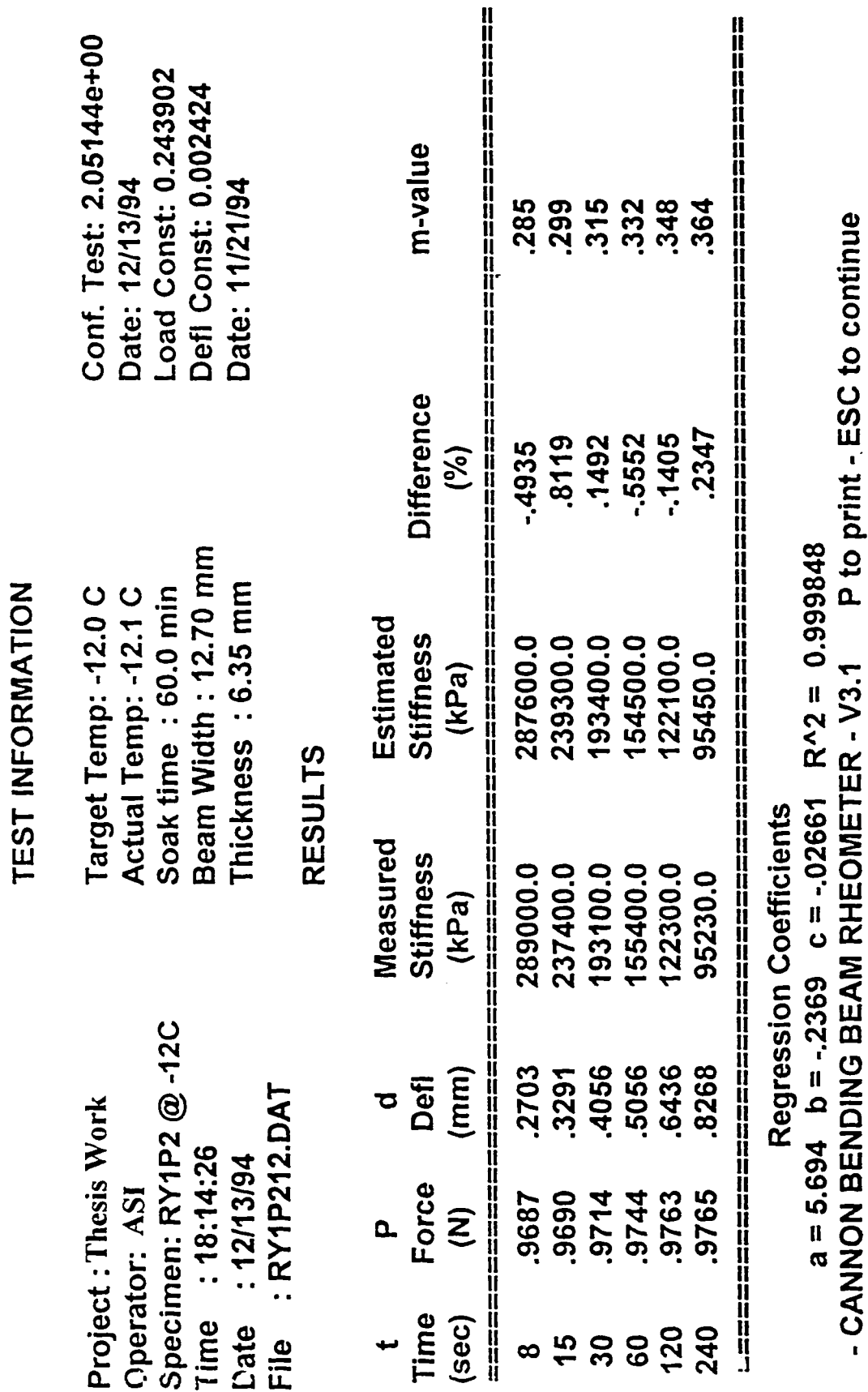


Figure 4.4: Typical printout of BBR test results for sample RY1P tested at -12°C.

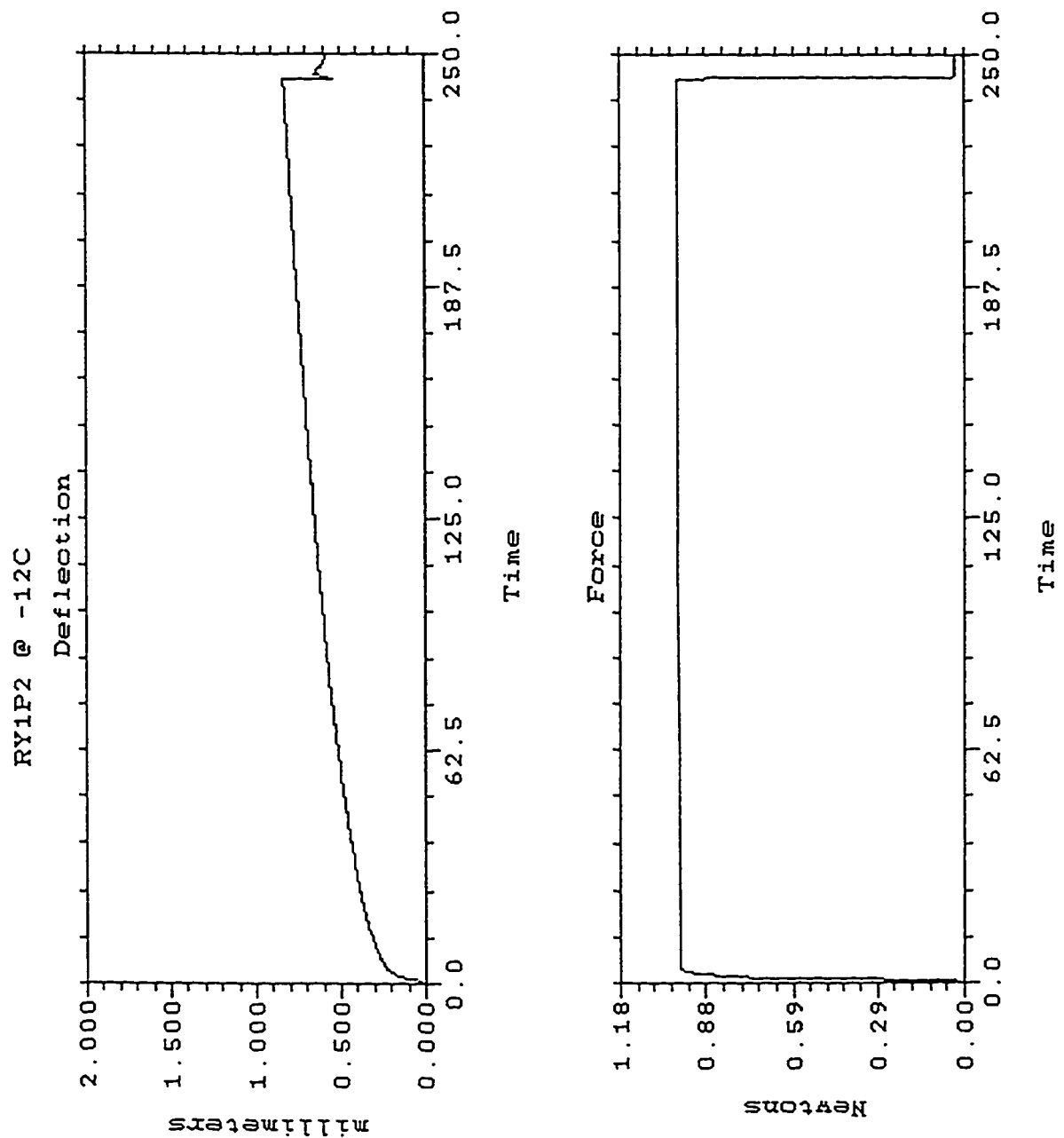


Figure 4.5: Typical BBR graphical presentation of load & force during testing.

Table 4.6: Acquired data from the BBR testing machine for the different asphalt samples.

Sample ID	Temp.(°C)	S (MPa)	m value	Temp.(°C)	S (MPa)	m value	Temp.(°C)	S (MPa)	m value
RT1	-12.00	102.00	0.35	-18.00	180.70	0.30	-12.00	64.69	0.35
RT2	-12.00	96.72	0.34	-18.00	169.70	0.30	-12.00	49.08	0.34
RT3	-18.00	163.87	0.29	-24.00	433.10	0.24	-12.00	35.50	0.35
RT4	-18.00	170.65	0.32	-24.00	351.40	0.27	-12.00	89.36	0.31
RT5	-18.00	174.50	0.32	-24.00	309.80	0.28	-12.00	88.17	0.30
BH1	-12.00	191.50	0.36	-18.00	372.00	0.30	-12.00	58.01	0.30
BH2	-12.00	206.50	0.33	-18.00	397.00	0.27	-12.00	105.50	0.33
BH3	-12.00	221.00	0.31	-18.00	383.00	0.27	-12.00	90.36	0.35
BH4	-12.00	194.00	0.34	-18.00	340.00	0.28	-12.00	64.56	0.36
BH5	-12.00	184.00	0.35	-18.00	405.00	0.27	-12.00	155.77	0.30
RY1	-12.00	153.60	0.33	-18.00	336.00	0.26	-12.00	139.37	0.30
RY2	-12.00	193.00	0.34	-18.00	343.20	0.29	-12.00	121.77	0.28
RY3	-12.00	164.00	0.32	-18.00	351.40	0.27	-12.00	129.10	0.31
RY4	-12.00	144.00	0.33	-18.00	302.20	0.27	-12.00	111.40	0.35
RY5	-12.00	147.60	0.32	-18.00	326.90	0.28	-12.00	60.98	0.36
KW1	-12.00	193.60	0.35	-18.00	366.90	0.26	-12.00	155.03	0.30
KW2	-12.00	190.90	0.35	-18.00	372.30	0.26	-12.00	167.00	0.27
KW3	-12.00	208.20	0.33	-18.00	371.80	0.25	-12.00	118.63	0.29
KW4	-12.00	217.80	0.34	-18.00	410.80	0.27	-12.00	210.63	0.26
KW5	-12.00	198.70	0.34	-18.00	344.00	0.29	-12.00	113.37	0.36
AZ1	-12.00	199.20	0.32	-18.00	369.00	0.25	-12.00	78.21	0.34
							-12.00	121.60	0.37
							-12.00	154.60	0.31
							-12.00	146.37	0.29
							-12.00	214.39	0.22
							-12.00	342.43	0.22
							-18.00	289.13	0.28
							-18.00	171.77	0.28
							-18.00	318.17	0.28
							-18.00	315.10	0.25
							-18.00	214.39	0.22

Table 4.7: Stiffness values of the residue samples at the different loading times after BBR testing.

Sample ID	Temp.	Loading Time (sec)					Temp.	Loading Time (sec)					
		8	15	30	60	120		240	8	15	30	60	120
RT1	-18.00	319186625	268811094	221019188	180517906	146459516	118038164	197892841	162542016	129694547	102538656	80327336	62351652
RT2	-18.00	2194296	5877523	15434189	18194165	28932182	37573782
RT3	-18.10	586578063	503137688	422085594	351699813	291072500	239269672	293661094	245375156	199383094	160409203	127776938	100776289
RT4	-24.20	526859688	450147781	310246125	254237203	206542344	206542344	312284125	260783011	212096875	171060984	136813781	108510180
RT5	-24.10	639551875	548216563	458095593	373189125	300877188	238871219	373853906	308815375	245943734	192830953	148744688	112803000
BH1	-18.20	647700438	562184500	475565500	397599063	328536719	268303344	377473713	315877969	256088203	204890141	161775719	126056000
BH2	-18.30	630304688	545857313	460449781	383733875	315952563	257014656	381009625	318089719	257257453	205190906	161405969	125214008
BH3	-18.30	565448750	487620781	409375688	339522469	278177875	225156109	369888563	307811656	248363203	197885908	155892063	120960484
BH4	-18.30	670274875	579132313	486960031	404257406	331338406	268123406	359191063	298053156	239516750	188887875	148517703	114598469
BH5	-18.30	546225438	474040656	401452688	336463875	279079125	229087344	287571906	239318281	193382000	154537203	122131117	95454500
RY1	-18.30	580528213	500282063	418837000	345711969	281333906	225719469	359912688	299511656	241863422	193027953	152252266	118666258
RY2	-18.30	581196188	500887188	421390563	351237125	290059281	237325172	299603750	250345078	203323453	163414172	129971094	102295766
RY3	-18.30	508029625	439999594	362159906	300760594	247990062	203040578	267090313	222666953	180551594	145015094	115369594	90915055
RY4	-18.30	535248188	463303844	391641188	327998250	272154125	223727094	261570750	218408078	177686250	143425453	114864773	91271516
RY5	-18.30	609613625	528001063	444511438	368908656	301815844	243418188	375525000	308003813	246623547	195084234	152843344	118606008
KW1	-18.30	617157813	533568313	448167281	370970813	302614219	243270172	370190438	305223656	244176250	193226000	151253406	117117328
KW2	-18.30	579588438	510980750	438636344	371147625	309549281	254480734	384755281	321401313	260359031	208219313	164396953	128141656
KW3	-18.30	675828000	583748563	491605813	409425594	337290984	274656469	410766031	342042844	276176625	220202891	173375578	134977719
KW4	-18.20	635550313	558267375	460081875	375717594	302945000	241180313	380224406	312761313	248782953	195112938	150872250	115024547
KW5	-18.30	615989313	536738250	457904281	387794438	326019563	272082438	364075188	304705656	247998328	199815922	159378594	125843727
AZ1	-18.20	24122994	8442810	24845094	29713007	48684473	63481208	1692248	5661472	18426289	22267811	37311824	49708428
RT-CRT-5-F	-18.00	241817219	202552734	165638953	134628516	108758156	87324742	128977281	105483328	83693609	65735438	51110082	39338012
RT-CRT-10-F	-18.00	219855984	183736203	153579469	126438852	103642469	84587313	103668188	84959805	67928445	54063414	42835891	33787137
RT-CRT-15-F	-18.00	147700547	122071188	98688602	79577133	63998652	51337469	69677102	56109180	44092316	34569098	21102025	15024098
RT-SBS-3-F	-18.00	275838125	235658688	197461594	16483172	137228109	113816266	164998203	136879438	111240370	90272695	73150500	59186644
RT-SBS-6-F	-12.00	169299188	142700234	117064102	95076070	76448164	60857106	89160289	739771172	59740645	47845863	38003387	29936568
RT-SBS-9-F	-12.00	203159025	171240281	140476922	114091284	91737797	73028527
RY-CRT-5-F	-18.00	457081000	391683219	327491219	271301469	222890922	181114078	191928813	157785188	128258848	100302945	79108547	61942723
RY-CRT-10-F	-18.00	319143063	270232281	228408766	186982313	153228969	124597555	184689063	150296375	118914258	83399297	72825383	56370504
RY-CRT-15-F	-18.00	226142922	189749063	155220969	125987750	101488383	81118836	131350156	107008781	84582852	66216141	51340908	39425961
RY-SBS-3-F	-18.00	450938281	38888469	328267000	275338750	229483438	190009250	253845031	215301672	178096406	146070719	118787547	95780789
RY-SBS-6-F	-18.00	408790000	354864969	301614781	254586656	213409203	177658158	227680359	190901734	156418891	127501414	103392078	83407578
RY-SBS-9-F	-12.00	208805172	178331609	148758094	123133273	101137648	82431438	153651656	128529859	104887289	85019344	68452388	54743863
BH-CRT-5-F	-18.00	444846156	384112844	324239313	271306658	225230547	185345484	223892203	189185583	155784906	127006109	102515016	81924825
BH-CRT-10-F	-18.00	368950400	313739100	260839900	215516200	176967000	144414200	207630547	172002094	138018281	109304398	85433320	65903531
BH-CRT-15-F	0.12	321445273	97377500	75679750	58292234	44499145	33666859
BH-SBS-3-F	-12.00	323186906	274818156	227874109	188781328	151692797	121998695	152542922	124107398	98134297	77002469	59958152	46328961
BH-SBS-6-F	-12.00	307872156	263468188	220396156	183068125	150977484	123635867	116387164	102854039	88789164	75788594	63968563	53383688
BH-SBS-9-F	-18.00	342370844	302882469	262206813	224841875	190974063	160670078	193133313	164110375	135855328	111363268	90392406	72651672
KW-CRT-5-F	-12.00	340803531	290427031	242239750	200980531	165868078	136166984	168293766	136255516	107287719	83934438	65241750	50385469
KW-CRT-10-F	-18.00	454195438	384811031	319077531	263320719	216279000	178800594	178414266	178414266	141319719	110437742	85147609	64789191
KW-CRT-15-F	-18.00	273873250	23278453	192968828	158539719	129101872	104203005	162537375	133441047	106820023	85081078	67378008	5392570
KW-SBS-3-F	-18.00	511046406	439899563	389596856	307733938	253802453	207588156	217844031	177272359	139328659	108031481	82839500	62365758
KW-SBS-6-F	-18.00	49060813	428918000	366326250	309745781	259290672	214887672	274307500	231379844	189731359	153828906	123317008	97744594
KW-SBS-9-F	-12.00	240447391	204888781	1770323891	140362813	114689461	92867258	153436719	125632922	99698406	78229258	60694088	46560731

determined using the data shown in Table 4.6. The lowest grading temperatures ranged between -16°C and -28°C .

4.3.5 Direct Tension Testing

As required by SHRP, if the creep stiffness of any asphalt sample at any test temperature is below 300 MPa, the direct tension test is not required. If the creep stiffness is between 300 and 600 MPa, the direct tension failure strain requirement can be used in lieu of the creep stiffness requirement (Asphalt Institute, 1993). In any case, the m -value should be greater than 0.30. Therefore, this test is only performed for samples that have an m -value greater than 0.30 and S value between 300 and 600 MPa. However, in this study for the purpose of comparing the BBR and DTT tests results, all neat asphalt aged samples were subjected to the DTT test at the same temperature that the asphalts were graded in the BBR test regardless of the stiffness and m -values. In performing the direct tension test, the AASHTO TP3 "Determining the Fracture Properties of Asphalt Binder in Direct Tension" standard test method was followed. The Direct Tension Test (DTT) setup was completely fabricated, assembled, calibrated, and verified in house. Fig. 4.6 and Plate 4.6 show all the parts the DTT system. It consists of a universal loading machine, which has a frame with a cross-head speed of 1.00 mm/min; a load cell with an accuracy of 0.01 mm; a locally made double-wall Plexiglas environmental chamber; a CO_2 temperature control unit; a circulating bath with ethyl alcohol; a temperature readout; and an x - y graphic chart

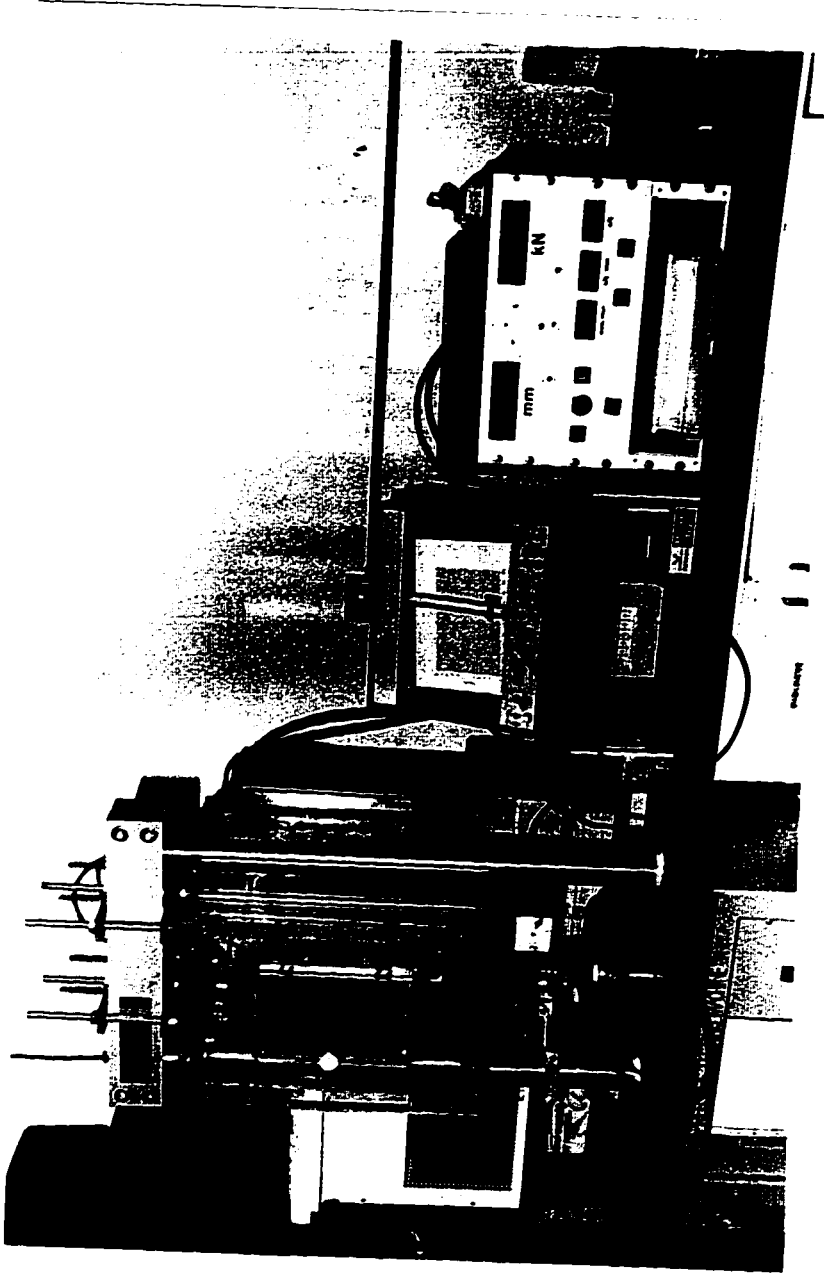


Plate 4.6: Fabricated direct tension tester (DTT).

recorder for load and elongation recording. The sample preparation for DDT testing and the test procedure are given in Appendix A.

In this study, the DTT was performed on all collected asphalt samples, regardless of the BBR test results, at the same temperature at which the BBR test was used to grade the asphalt. Table 4.8 gives a summary of all DTT results where the average values of the four tested specimens for each asphalt type are reported.

Fig. 4.7 shows typical test results for RT5P (Ras Tanura produced asphalt, sample number 5, aged by PAV) tested at -18°C . This testing temperature was the one at which the BBR test was performed and at which the asphalt was graded for low temperature. This test was repeated for four test specimens. The failure strain range was 2.04 to 3.7%, while the failure stress range was 17.99 to 24.53 MPa. Fig. 4.7 also shows that the rate at which the stress and strain increase is very high, as an indication of brittleness. Each test specimen took less than one minute to break, and all test specimens failed under brittle fracture. For grading purposes, it is required to perform the DTT test only if the BBR test results show that the creep stiffness is between 300 and 600 MPa and the m -value is greater than 0.300, in which case the DTT will govern the lower temperature grading of the asphalt binder. If the tensile strain is greater than or equal to 1%, then the lower temperature grading determined by the BBR test is correct. Otherwise, a new BBR test is required at a higher grade (higher temperature) for that asphalt binder.

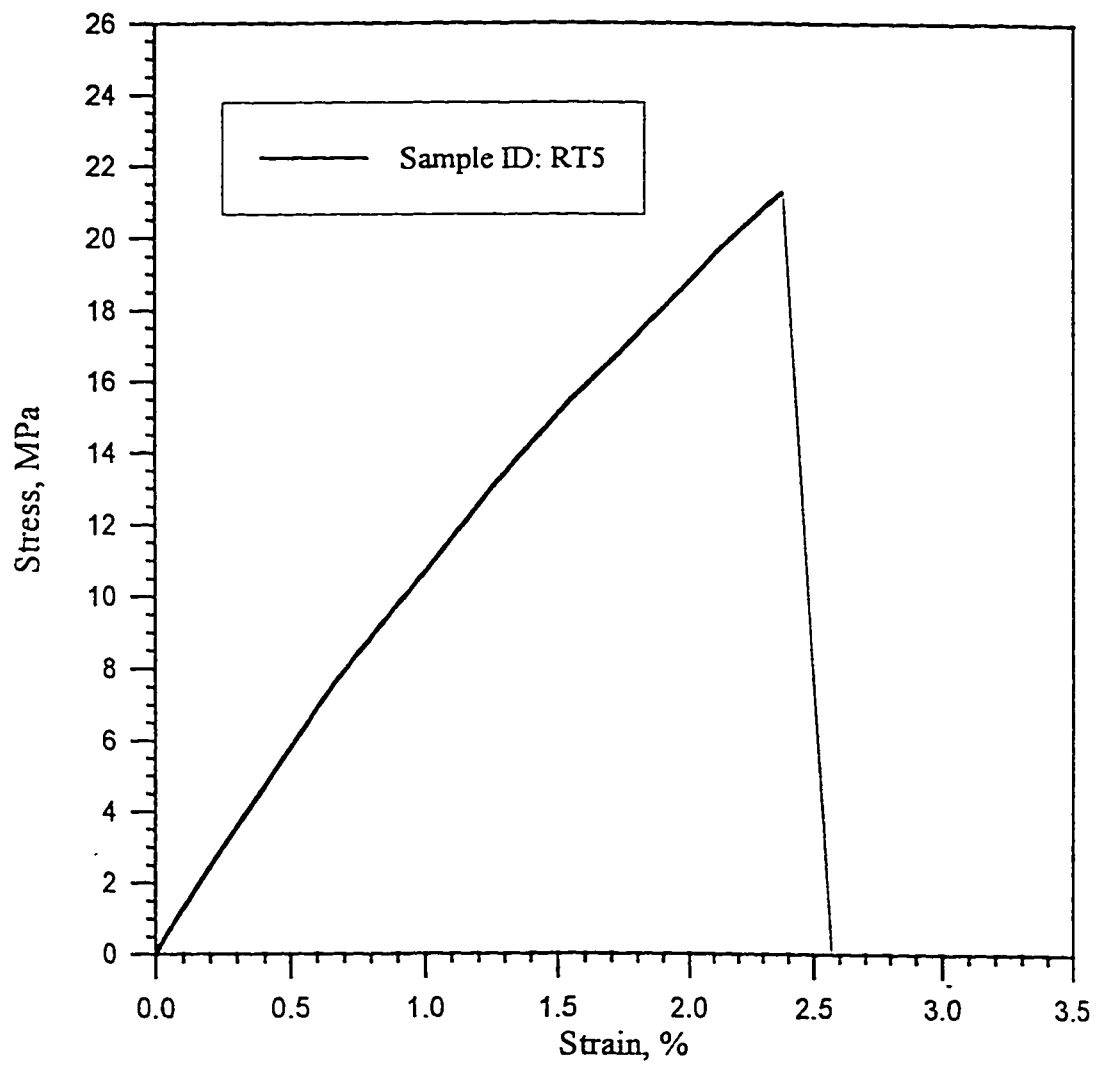


Figure 4.7: Typical DTT test results for RT5P sample.

As can be seen from Table 4.8, there was no improvement on the lower grading temperature for all tested samples, and the lower grading temperatures obtained from the BBR testing were unchanged. This shows that the results of both the BBR and DTT testings were consistent, and the DTT results confirm and supplement the BBR results. In general, BH samples had the highest failure stress values in both BBR and DTT testing.

4.3.6 Grading of Collected Asphalt Samples

All above performance tests are required for grading the collected samples. SHRP grading criteria were followed to grade all the collected samples. Figs. 4.8-4.11 present SHRP recommended performance grading procedures. The performance grading of all collected samples is shown in Table 4.9, while Fig. 4.12 shows a graphical representation of the samples grades. As noticed from the grading Table, some of the polymer modified samples failed the criteria set on maximum allowable rotational viscosity, but were included in the grading with an asterisk showing that. This was done because SHRP grading allows this as long as it is assured that it is safe to pump and mix the binder at a higher temperature than the normally used temperature.

It can be observed that all neat samples had either PG grade PG 64-22 or PG 64-28. Polymer modification changed the grades of the samples into grades with higher upper limits. This limit reached as high as 82°C in some samples. Since

Table 4.8: Summary of DTT test results.

Sample ID	Test Temp.	Failure Strain (%)	Failure Stress (MPa)
RT1	-18.00	1.03	12.90
RT2	-12.00	1.58	13.27
RT3	-18.00	0.84	10.88
RT4	-18.00	1.83	12.54
RT5	-18.00	2.82	21.67
BH1	-12.00	1.28	25.25
BH2	-12.00	2.35	23.17
BH3	-12.00	4.37	25.89
BH4	-12.00	3.20	17.72
BH5	-12.00	2.48	23.58
RY1	-12.00	1.30	12.74
RY2	-12.00	1.73	15.81
RY3	-12.00	1.70	14.92
RY4	-12.00	1.53	15.35
RY5	-12.00	2.00	81.00
KW1	-12.00	1.72	17.35
KW2	-12.00	1.89	16.35
KW3	-12.00	1.25	13.35
KW4	-12.00	1.85	16.26
KW5	-18.00	0.83	16.08
AZ1	-12.00	2.08	21.86

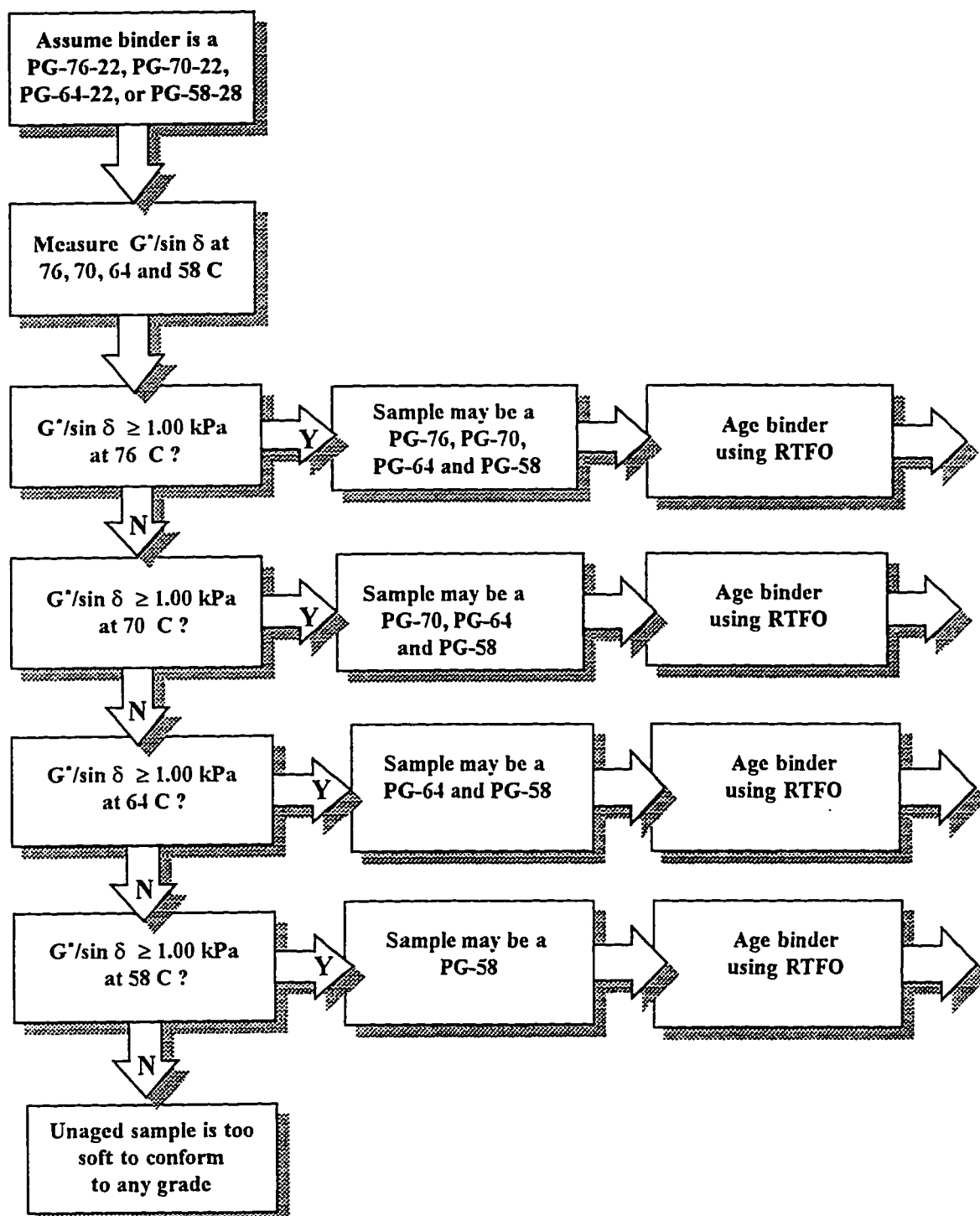


Figure 4.8: Classification testing - unaged binders (Asphalt Institute, 1993)

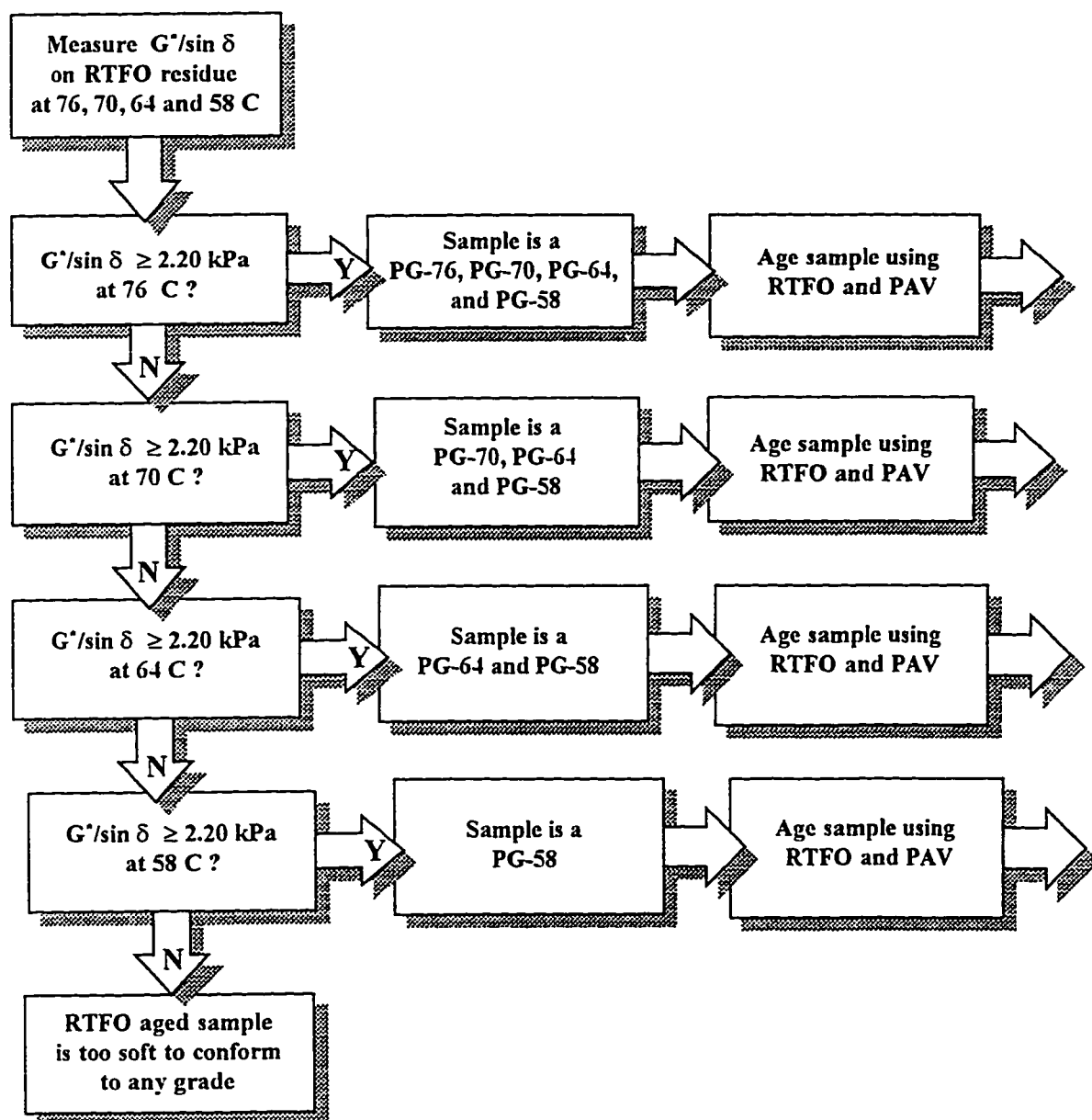


Figure 4.9: Classification testing - RTFO aged binders (Asphalt Institute, 1993)

PG-64

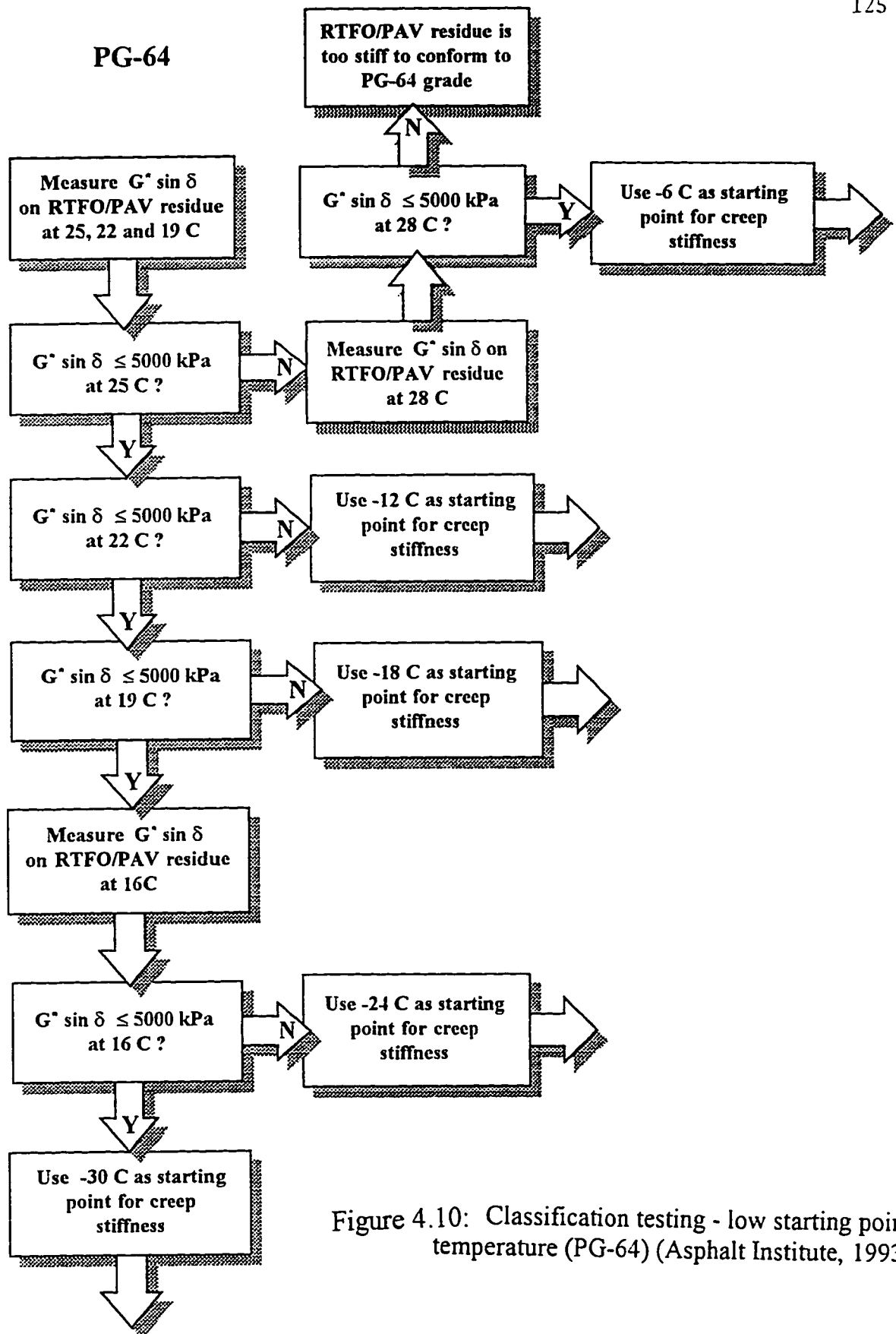


Figure 4.10: Classification testing - low starting point temperature (PG-64) (Asphalt Institute, 1993)

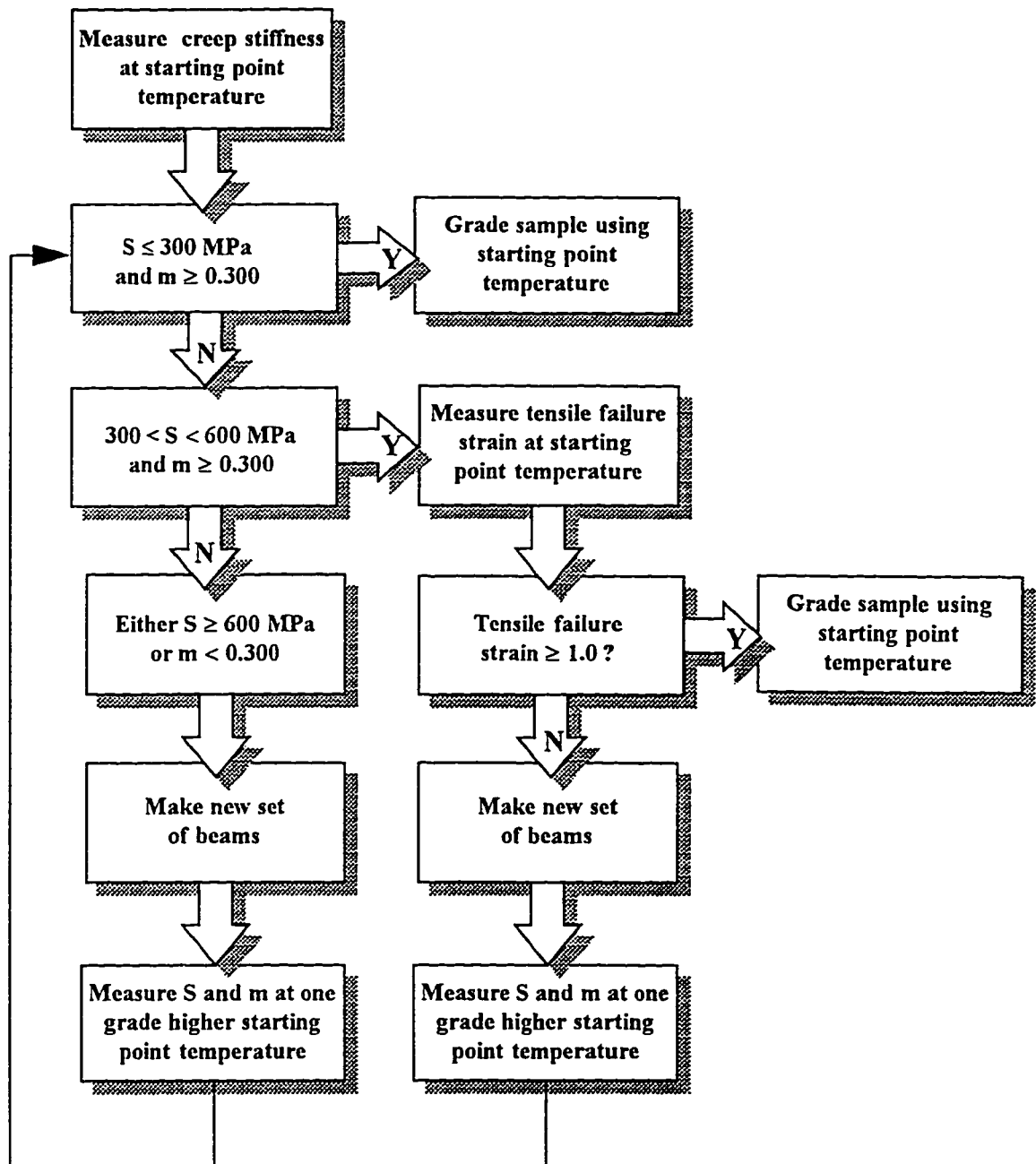


Figure 4.11: Classification testing - established low temperature binder grade with creep stiffness m-value, and tensile failure strain (Asphalt Institute, 1993).

Table 4.9: SHRP grading of the collected samples.

Sample ID	Grading	Sample ID	Grading
RT1	PG 64 - 22	RT-CRT-5-F	PG 70 - 28
RT2	PG 64 - 22	RT-CRT-10-F	PG 76 - 22
RT3	PG 64 - 22	RT-CRT-15-F	PG 82 - 28*
RT4	PG 64 - 28	RT-SBS-3-F	PG 76 - 22
RT5	PG 64 - 28	RT-SBS-6-F	PG 82 - 22*
BH1	PG 64 - 28	RT-SBS-9-F	PG 82 - 22*
BH2	PG 64 - 22	RY-CRT-5-F	PG 70 - 22
BH3	PG 64 - 22	RY-CRT-10-F	PG 76 - 22
BH4	PG 64 - 22	RY-CRT-15-F	PG 82 - 28*
BH5	PG 64 - 22	RY-SBS-3-F	PG 82 - 22
RY1	PG 64 - 22	RY-SBS-6-F	PG 82 - 22*
RY2	PG 64 - 22	RY-SBS-9-F	PG 82 - 16*
RY3	PG 64 - 22	BH-CRT-5-F	PG 70 - 22
RY4	PG 64 - 22	BH-CRT-10-F	PG 70 - 22
RY5	PG 64 - 22	BH-CRT-15-F	PG 82 - 28*
KW1	PG 64 - 22	BH-SBS-3-F	PG 76 - 22
KW2	PG 64 - 22	BH-SBS-6-F	PG 82 - 16*
KW3	PG 64 - 22	BH-SBS-9-F	PG 82 - 16*
KW4	PG 64 - 22	KW-CRT-5-F	PG 82 - 16
KW5	PG 64 - 22	KW-CRT-10-F	PG 82 - 22*
AZ1	PG 70 - 22	KW-CRT-15-F	PG 82 - 22*
		KW-SBS-3-F	PG 76 - 22
		KW-SBS-6-F	PG 82 - 22*
		KW-SBS-9-F	PG 82 - 16*

* Rotational viscosity is higher than 3000 cPa.s.

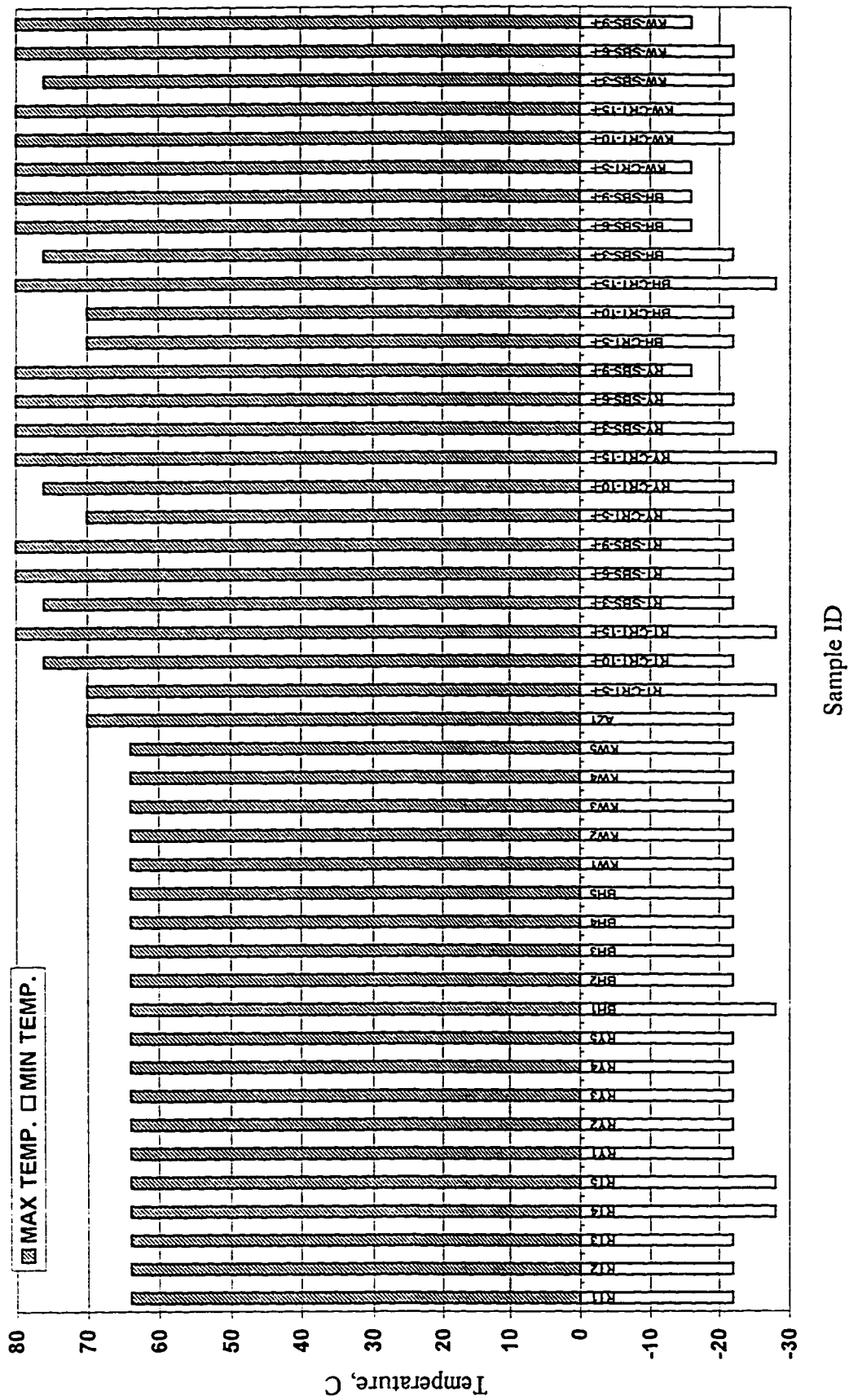


Figure 4.12: Graphical representation of performance grades of collected samples.

pavement temperatures in the Gulf countries reach values higher than the 64°C limit of the neat asphalt, it implies that polymer modification should be used in a large region of the Gulf countries. For the lower limit grades, polymer modification improved (lowered) the limit for some samples but had an adverse effect on other samples. Therefore, the suitability of any polymer for asphalt modification should be verified prior to use according to the temperature limits of the region.

4.4 CONSTRUCTION OF THE MASTER CURVES

Since one of the objectives of the study was to correlate performance-based properties with molecular size distribution of the asphalt samples, it was found that the best way to achieve this was by finding some asphalt specific properties (independent of temperature and rate of loading) and correlate them with the molecular size distribution. These properties were obtained through the use of the linear viscoelastic model (LVE) of each asphalt. It is called the linear viscoelastic model because it is used to explain both the linear and the visco-elastic behavior of asphalt cement. The following procedure was adopted to construct the LVE models of the tested samples:

- A non-linear statistical procedure was selected to fit the collected data to the suggested LVE model since it gives more reliable results and error is reduced (Bahia, 1995).

- Combining the test results for the asphalts at the different aging stages confounds the construction of the master curve; therefore, the fitted model was restricted to PAV-aged samples.
- The stiffnesses measured by the bending beam at the different testing times were converted to complex shear moduluses (G^*) by the following approximation (Anderson et al., 1994):

$$G^*(1/t) = S(t) / 3 \quad (4.1)$$

$$\delta(1/t) = m(t) * 90 \quad (4.2)$$

For example, if the measured stiffness at 60 seconds is 300 MPa and the m -value is 0.3, then

$$G^* \text{ (at } (1/60) \text{ rad/s)} = 300/3 = 100 \text{ MPa, and}$$

$$\delta \text{ (at } (1/60) \text{ rad/s)} = 0.3 * 90 = 27 \text{ degrees}$$

Since in the BBR testing, stiffness was reported at six intervals, there are six values of G^* and δ at the test temperature for each of the tested BBR beams.

- The dynamic shear test was performed on the test samples using frequency sweep. At each test temperature, the DSR test was conducted using six frequencies (0.01, 0.10, 1.00, 1.50, 5.00, and 10.00 Hz).

- The G^* data obtained from the DSR frequency sweep test and the transformed BBR data at each test temperature were compiled in tabular form. Table 4.5 shows the G^* values for the test samples at the different frequencies and test temperatures obtained using the DSR frequency sweep testing. The transformed G^* values from the creep stiffness values after BBR testing are shown in Table 4.10.
- NLIN (non-linear regression) routine in statistical analysis system (SAS) software was used to fit the linear viscoelastic model parameters, which is of the following form:

$$G^* = G_g [1 + (\omega_o / \omega_r)^{\log 2/R}]^{-R/\log 2} \quad (4.3)$$

All parameters were defined in the literature review (section 2.3.7).

The NLIN method uses an iterative process, where a starting (seed) value of the parameters to be estimated is used in the equation and the error sum of squares in estimating the dependent variable is calculated. The values of the parameters are continually improved until the error sum of squares is minimized. The NLIN is similar to a series of linear regressions. Details of NLIN calculation procedures can be found in SAS (1994).

To include all the data for the sample at the different test temperatures and to allow the software to calculate the shift factors simultaneously with the other parameter, ω_r was calculated using the following formula:

Table 4.10: Calculated complex shear moduli for the PAV residue samples at the test frequencies and temperatures after BBR tests.

Sample ID	Temp.	Test Frequency (Hz)						Temp.	Test Frequency (Hz)					
		0.125	0.067	0.033	0.017	0.008	0.004		0.125	0.067	0.033	0.017	0.008	0.004
RT1	-18.00	106396208	89603698	73673063	60172635	48819839	39346055	-11.10	65964214	54180672	43231516	34179552	26775719	20763884
RT2	-18.00	7314322	1959174	5144730	6064727	9644061	12524594	-	-	-	-	-	-	-
RT3	-18.10	195266021	167712563	140695198	117233271	97024167	79756537	-12.00	97887031	81791719	66461031	53469734	42592313	33592096
RT4	-24.20	175619896	150049260	125109594	103415375	84745734	68047448	-18.10	104088042	86927672	70639858	57020328	45804594	36170060
RT5	-24.10	213183958	182738654	151936521	124396375	100292396	79623740	-18.20	124617969	102871792	81981245	64276984	49581563	37627687
BH1	-18.20	215900146	187394833	158521833	132533021	109512240	89434448	-12.00	125915771	105292656	85362734	68296714	53925240	42018687
BH2	-18.30	210101563	181952438	153483260	127911292	105317521	85671552	-12.10	127003206	106029906	85752484	68396969	53801990	41738003
BH3	-18.30	168482917	162540260	136458563	113747156	92725958	75052036	-12.10	123296188	102603885	82787734	65961969	51897354	40320161
BH4	-18.30	223424958	193044104	162320010	134752469	110446135	89374469	-12.20	119730354	99351052	79838917	63295958	49505901	38199490
BH5	-18.30	182075146	158013552	133817563	112154625	93026375	76362448	-12.20	95857302	79772760	64460667	51512401	40710372	31818167
RY1	-18.30	193530938	166760688	139612333	115237323	93777969	75239823	-12.10	119970896	99837219	80621141	64342651	50750755	39582088
RY2	-18.30	193732063	166962396	140463521	117079042	96866427	79108391	-12.20	99867917	83448359	67774484	54471391	43323698	34098569
RY3	-18.30	168676542	144333198	120719969	100255331	82666021	67680193	-12.20	89030104	74222318	60183665	48338365	38456531	30305018
RY4	-18.30	178416063	154434615	130547063	109332750	90718042	74575698	-12.10	97190250	72802693	59228750	47808484	38288258	30423839
RY5	-18.30	203204542	176000354	148170479	122969552	100605281	81139396	-12.10	125175000	102934604	82207849	65028078	50947781	39535336
KW1	-18.30	205719271	177856104	149389094	123658938	100871406	81090057	-12.10	123396813	101741219	81392083	64408667	50417802	39039109
KW2	-18.30	193196146	170326917	146212115	123715875	103183094	84826911	-12.10	128251760	107133771	86786344	69406438	54798984	42713865
KW3	-18.30	225209333	194582854	163868604	136475198	112403031	91552156	-12.10	136920010	114014281	92058875	73400984	57791659	44932573
KW4	-18.20	217650104	185422458	153360625	125239198	100981987	80393438	-12.10	128741489	104253771	82927651	65037848	50290750	38341516
KW5	-18.30	205329771	178912750	152634760	129264813	108673188	86964146	-12.10	121356396	101569552	82668109	66605307	53125531	41947909
A21	-18.20	804331	2814203	8315031	9904336	16221491	21160402	-12.10	564082	1887157	6142090	7422604	12437208	16589478
RT-CRT-5-F	-18.00	80605740	67517578	55212084	44876172	36525719	29108247	-12.00	42992427	35161109	27697870	21911813	17036694	13112671
RT-CRT-10-F	-18.00	73285328	61912068	51193156	42148284	34547490	28195771	-12.00	34556063	28319935	22842148	18021138	14278630	11262379
RT-CRT-15-F	-18.00	49235316	40690396	32868201	26523711	21332317	17112490	-12.00	23225701	18703060	14997439	11523023	9013366	7034008
RT-SBS-3-F	-18.00	91946042	78552896	65820531	45742703	37938755	31937555	-12.00	54999401	45626479	37080190	30090898	24393500	19729888
RT-SBS-6-F	-12.00	56433063	47568745	39021387	31692023	25482721	20285702	-8.00	29120096	24659057	19913548	15948821	12667789	9978656
RT-SBS-9-F	-12.00	67719675	57080094	48825841	38030428	30579266	24342842	-	-	-	-	-	-	-
RY-CRT-5-F	-18.00	152360333	130584406	109163740	90433823	74230307	60371359	-12.00	63976271	52595063	42088218	33434315	26389518	20647574
RY-CRT-10-F	-18.00	106381021	90674427	75488922	62327438	51076323	41532518	-12.00	61566021	50099458	39638088	31133099	24275128	18790168
RY-CRT-15-F	-18.00	75380974	63249688	51740323	41992250	33829461	27038945	-12.00	43783385	35669594	28194284	22072047	17113635	13141867
RY-SBS-3-F	-18.00	150312760	129622823	109422333	91778917	76487813	63336417	-12.00	84815010	71787224	59365469	48890740	39595849	31926930
RY-SBS-6-F	-18.00	138263333	118288323	100538260	84862219	71136401	59219385	-12.00	75893453	63633911	52139630	42500471	34484028	27802528
RY-SBS-9-F	-12.00	69601724	59443870	49586031	41044424	33712549	27477146	6.00	51217219	42843286	34962430	28339781	22817466	18247961
BH-CRT-5-F	-18.00	148215385	128037615	108079771	90462221	75076649	61781828	-12.00	74584068	63082188	51928302	42335370	34171872	27308208
BH-CRT-10-F	-18.00	122903467	104579700	86946300	71830733	58989000	48138067	-12.00	69210182	57334031	46006427	36434799	28477773	21967844
BH-CRT-15-F	0.12	40481758	32459167	25226583	19430745	14633048	11222588	-	-	-	-	-	-	-
BH-SBS-3-F	-12.00	107728969	91806052	75891370	62253776	50564266	40665565	-6.00	50847841	41369133	32711432	25667490	19986051	1542987
BH-SBS-6-F	-12.00	102624052	87822729	73465385	61020708	50325828	41211958	-8.00	38795721	34284680	29596388	25262665	21322188	17794558
BH-SBS-9-F	-18.00	114123815	100980823	87402271	74947282	63658021	53556893	-12.00	84377771	54703458	45285109	37121089	30130802	24217224
KW-CRT-5-F	-12.00	113601177	96809010	80746583	66993510	55289359	45388895	-8.00	56097922	45419505	35762573	27978148	21747250	16795158
KW-CRT-10-F	-18.00	151398479	128270344	106359177	87773573	72093000	59933531	-12.00	72617797	59471422	47106573	36812581	28382536	21589730
KW-CRT-15-F	-18.00	91291083	77599484	64322943	52846573	43033891	34733435	-12.00	54179125	44480349	35606674	28353693	22459669	17697523
KW-SBS-3-F	-18.00	170348802	146623188	123198805	102577979	84634151	69106052	-12.00	72661344	59090786	46442286	36010487	27548500	20786586
KW-SBS-6-F	-18.00	163536271	142972667	122108750	103246594	86430224	71629824	-12.00	91435833	77126615	63243786	51276302	41105669	32581531
KW-SBS-9-F	-12.00	80149130	68296260	56774630	48787604	38223154	30955753	-6.00	51145573	41877641	33232802	26076419	20231362	15520244

$$\omega_r = \omega_i * 10^{(A_1 * I_1 + A_2 * I_2 + A_3 * I_3) \dots} \text{ (up to the number of temperatures that the test was performed at less than the selected reference temperatures).} \quad (4.4)$$

A_i = time-temperature shift factors

I_i = indicator variables that have the value of 1 if data are for the temperature of A_i , otherwise they take a value of 0.

As an example, if the test is performed at four temperatures (−18, −12, 19, and 25°C) and if 19 is chosen as the reference temperature, then

at test temperature of −18°C, $I_1 = 1$, and all other I 's are = 0's

at test temperature of −12°C, $I_2 = 1$, and all other I 's are = 0's

at test temperature of 25°C, $I_3 = 1$, and all other I 's are = 0's

At test temperature 19, all I_i 's equal 0 because 19 is selected as a reference temperature and all curves are shifted to that temperature.

The SAS program shifted the frequency scale for each temperature such that it fit the model and calculated the shift factors (A_i 's) as part of the fitting. Therefore, the SAS software estimated the model coefficients G_g , ω_a , and R and the shift factors simultaneously.

- For neat asphalts, the value of G_g should be about 1 GPa (Anderson et al., 1994). So, in fitting the collected data to the LVE, G_g was fixed to be 1×10^9 Pa. The other parameters were estimated by the SAS software. In the case of modified samples, the value of G_g was not restricted and was estimated by the software as well as all other parameters.
- When using the LVE model to replace the power functions for programing purposes, it was decided to take the logarithm of both sides of the LVE function. Therefore, the logarithm of G_g and G^* were used in place of the original values. Therefore, the used LVE model had the following form:

$$\begin{aligned} \text{Log } G^* = \log G_g - ((R/\log 2) * \log (1 + (\omega_o/\omega_i * 10^{**} \\ (A1 * I1 + A2 * I2 + A3 * I3))))^{**} (\log 2/R))) \end{aligned} \quad (4.5)$$

where

G^* = complex dynamic modulus, in Pa;

G_g = glassy modulus, typically 1 GPa;

ω_o = the cross over frequency, rad/s;

ω_i = the test frequency, rad/s;

R = the rheological index; and

A_i 's & I_i 's = previously defined.

The software examined the seed values given by the programmer for the parameters R , ω_o , $A1$, $A2$, and $A3$ and evaluated the residual sum of squares (RSS) at those values. The

software then started changing the values of those parameters and evaluated the RSS at each combination of values to determine the best set of values that fit the model (SAS, 1994). The iterations continued till the convergence criteria were met. The convergence criteria were met when

$$\frac{SSE_{i-1} - SSE_i}{SSE_i + 10^{-6}} < 10^{-8} \quad (4.6)$$

where

SSE_i = sum of squares of error for the specified (i) iteration; and

SSE_{i-1} = sum of squares of error for the previous (i-1) iteration.

This means that the software will at each step calculate SSE and use its value with the value of SSE of the previous step in Eqn. (4.6). If the criteria of the above mentioned equation are met, then regression will stop, otherwise, the estimated values of the parameters will be changed and Eqn. (4.6) will be reevaluated and the stopping criteria will be rechecked. Samples of the program and computer output for BH1 samples are shown in Appendix B, Figs. B1, and B2 respectively.

- To estimate the defining temperature T_d , the WLF equation was used (Branthaver et al., 1993). The WLF equation is as follows:

$$\text{Log } (aT)_{i,d} = - C_1 (T_i - T_d) / (C_2 + T_i - T_d) \quad (4.7)$$

where $(aT)_{i,d}$ is the shift factor between the test temperature and T_d . C_1 and C_2 are the WLF constants and are assumed to have the values of 19 and 92 respectively. The value of these constants was verified by the SHRP team and found appropriate (Branthaver et al., 1993). The test temperatures versus the shift factors corresponding to those temperatures, which were obtained from the previous regression, were re-tabulated. The NLIN regression procedure in the SAS program was reused to fit these data into the reformatted WLF equation shown below:

$$\text{Log } (aT)_{i,R} = -\log (aT)_{R,d} - C_1 (T_i - T_d) / (C_2 + T_i - T_d) \quad (4.8)$$

where

$(aT)_{i,R}$ = the shift factor between the test temperature and the reference temperature

$(aT)_{R,d}$ = the shift factor between the reference temperature and the defining temperature

T_i = the test temperature.

The regression will estimate $\log (aT)_{R,d}$ and T_d . Since the lowest test temperature is not far below T_d , it was decided to use the WLF equation and not go into the complications of using the linear model - Eqn. 1.4 previously mentioned in the literature review (section 1.1) - for evaluating the shift factor for test temperatures below the defining temperature.

- The following equation was used to estimate the crossover frequency at the defining temperature (Branthaver et al., 1993):

$$\text{Log } (\omega_o)_d = \log (\omega_o)_R - \log (aT)_{R,d} \quad (4.9)$$

- The steady-state viscosity (η_o) at any temperature is equal to the glassy modulus divided by the frequency at any point along that viscous asymptote. It can be calculated by dividing the glassy modulus by the crossover frequency. To calculate the value of η_o at the defining temperature, the value of G_g was divided by crossover frequency at the defining temperature.

The above procedure was performed for all research samples. Results for neat samples are shown in Table 4.11, while Table 4.12 shows the results for the modified samples. A plot of the master curves for RY1 samples at all test temperatures and at the defining temperature is shown in Fig. 4.13. Fig. 4.14 shows the master curves for the SBS polymer modified RY2 samples. Figs. B3-B23 in Appendix B show the master curves drawn at the defining temperature for all the neat samples, while Figs. B24-B30 are for polymer modified samples.

From the above mentioned figures (Figs. 4.13 and 4.14 and Figs. B3-B30) and tables (Tables 4.11-4.12), it is observed that for neat asphalt samples the master curve at T_d is the highest in stiffness, which is reasonable since T_d was lower than all test temperatures. For polymer modified samples, it was noticed that the shift in the

Table 4.11: (Continued)

[illegible]

Table 4.12: Calculated parameters for the construction of the master curves for the polymer modified samples.

	RT (CRB-5%)		RT (CRB-10%)		RT (CRB-15%)		RT (SBS-3%)		RY (CRB-5%)		RY (CRB-10%)		RY (CRB-15%)		RY (SBS-3%)		RY (SBS-6%)		RY (SBS-9%)		BH (CRB-10%)	
	temp	log (aT) _h	temp	log (aT) _h	temp	log (aT) _h	temp	log (aT) _h	temp	log (aT) _h	temp	log (aT) _h	temp	log (aT) _h	temp	log (aT) _h	temp	log (aT) _h	temp	log (aT) _h	temp	log (aT) _h
T1	-18	4.3488	-18	5.4565	-18	4.9983	-18	5.7106	-18	5.385	-18	5.0473	-18	5.7312	-18	4.9188	-18	5.7768	-12	6.5752	-18	5.0968
T2	-12	3.5966	-12	4.262	-12	3.9269	-12	4.775	-12	3.9707	-12	4.03	-12	4.7192	-12	3.8599	-12	4.7181	-6	5.8835	-12	4.1577
T3=T _R	22	0	19	0	19	0	22	0	22	0	21.9	0	22	0	22	0	22.2	0	22	0	22	0
T4	24.9	-0.2951	21.6	-0.3123	24.7	-0.8379	24.5	-0.4508	25.2	-0.5256	24.7	-0.3196	24.5	-0.4251	25.3	-0.3735	25.1	-0.4171	25.2	-0.112	25	-0.3941
T _g	-33.2764	7.1042	-17.7885	5.4041	-20.904	5.5982	-18.574	5.5282	-21.4018	5.9238	-24.8879	6.3688	-16.7768	5.5566	-26.7077	6.5264	-16.9315	5.6124	-15.1197	4.3665	-23.697	6.2483
Q ₁ (GPa.s)	1.1290		0.8557		0.6097		0.8874		2.3142		2.3676		3.7297		1.3164		1.1285		1.1478		1.5893	
R	2.6883		2.7699		2.8849		2.8256		3.0927		3.0035		4.2523		2.5914		2.7764		3.3501		2.7228	
ω ₀ @ T _R (Hz)	0.4572		0.7314		0.3363		0.3706		0.1429		0.4874		0.1659		0.2061		0.3172		0.3465		0.6535	
ω ₀ @ T _g (Hz)	3.6E-08		2.88E-06		8.48E-07		1.1E-06		1.7E-07		2.08E-07		4.61E-07		6.13E-08		7.74E-07		1.48E-05		3.68E-07	
η ₀ @ T _g (GPa.s)	31390178		296650		718742		807969		13588383		11355715		8098954		21464561		1457360		77037		4307789	
R ² for T _g evaluation	0.9995		0.9999		0.9983		0.9982		0.9982		0.9999		0.9989		0.9987		0.9994		0.9901		0.9995	
R ² for R & ω ₀ evaluation	0.9782		0.9999		0.9874		0.9999		0.9997		0.9982		0.98		0.9905		0.9926		0.9943		0.9949	

Table 4.12: (Continued)

	BH (CRB-15%)		BH (SBS-3%)		BH (SBS-5%)		BH (SBS-8%)		KW (CRB-6%)		KW (CRB-10%)		KW (CRB-15%)		KW (PPU-15%)		KW (SBS-3%)		KW (SBS-6%)		KW (SBS-9%)	
	temp	log (aT) _R	temp	log (aT) _R	temp	log (aT) _R	temp	log (aT) _R	temp	log (aT) _R	temp	log (aT) _R	temp	log (aT) _R	temp	log (aT) _R	temp	log (aT) _R	temp	log (aT) _R	temp	log (aT) _R
T1	-12	4.0485	-12	4.527	-12	4.4977	-18	5.0913	-12	5.6795	-18	5.862	-18	5.8266	-12	4.3889	-12	4.6752	-18	5.4209	-18	5.4635
T2	.	.	-6	3.301	-6	3.3205	-12	4.1113	-6	4.1363	-12	4.4821	-12	4.656	-6	3.5158	-6	3.8176	-12	4.3236	-12	4.4262
T3=T _R	18.9	0	22	0	22.2	0	21.5	0	22	0	21.9	0	21.9	0	22.1	0	21.6	0	22.2	0	22	0
T4	24.7	-0.7996	24.6	-0.4237	25.2	-0.2433	25	-0.3433	25	-0.3999	24.6	-0.4139	25	-0.4374	24.5	-0.3051	24.6	-0.2797	25	-0.3295	24.5	-0.3899
T _d	-19.2531	5.4501	-18.6507	5.721	-20.6397	6.0433	-23.9962	6.2757	-17.2696	4.5412	-18.1417	5.6844	-16.5566	5.538	-19.7722	5.8617	-15.7758	5.5178	-21.182	6.0532	-19.7722	5.8617
G ₁ (GPa)	2.5462		1.2286		1.6334		2.2398		10.9496		5.4891		2.7002		1.2158		0.9391		1.1535		2.9478	
R	4.1941		2.6327		2.7427		3.0113		4.5393		3.4863		3.3631		2.7306		2.5478		2.5055		2.7828	
ω ₀ @ T _R (Hz)	0.767		0.2083		0.2547		0.3065		0.0682		0.35		0.4603		0.0602		0.4693		0.4029		0.7359	
ω ₀ @ T _d (Hz)	2.72E-06		3.96E-07		2.31E-07		1.62E-07		1.96E-06		7.24E-07		1.33E-06		8.28E-08		1.42E-06		3.58E-07		1.01E-06	
n ₀ @ T _d (Cpa-s)	935847		3102492		7085509		13786992		5582332		7562841		2024692		14685599		659249		3235957		2913273	
R ² for T _d	0.9981		0.9979		0.9987		0.9999		0.9987		0.9996		0.9997		0.9994		0.9987		0.9999		0.9995	
R ² for R & ω ₀	0.9831		0.9999		0.9881		0.9944		0.919		0.9994		0.9948		0.9834		0.9876		0.9913		0.9897	
evaluation																						

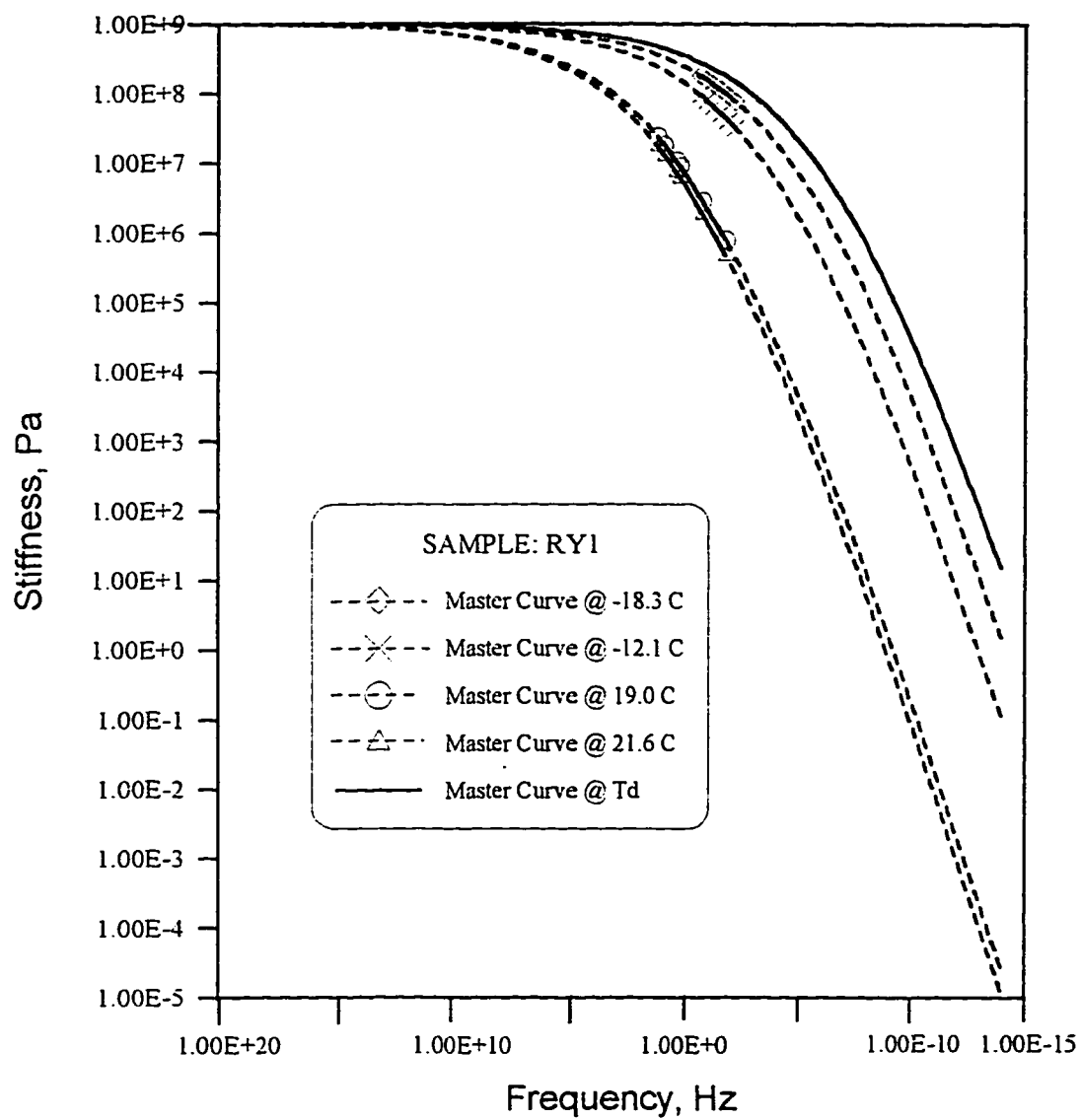


Figure 4.13: Master curves of RY1 sample at test temperatures and at the defining temperature.

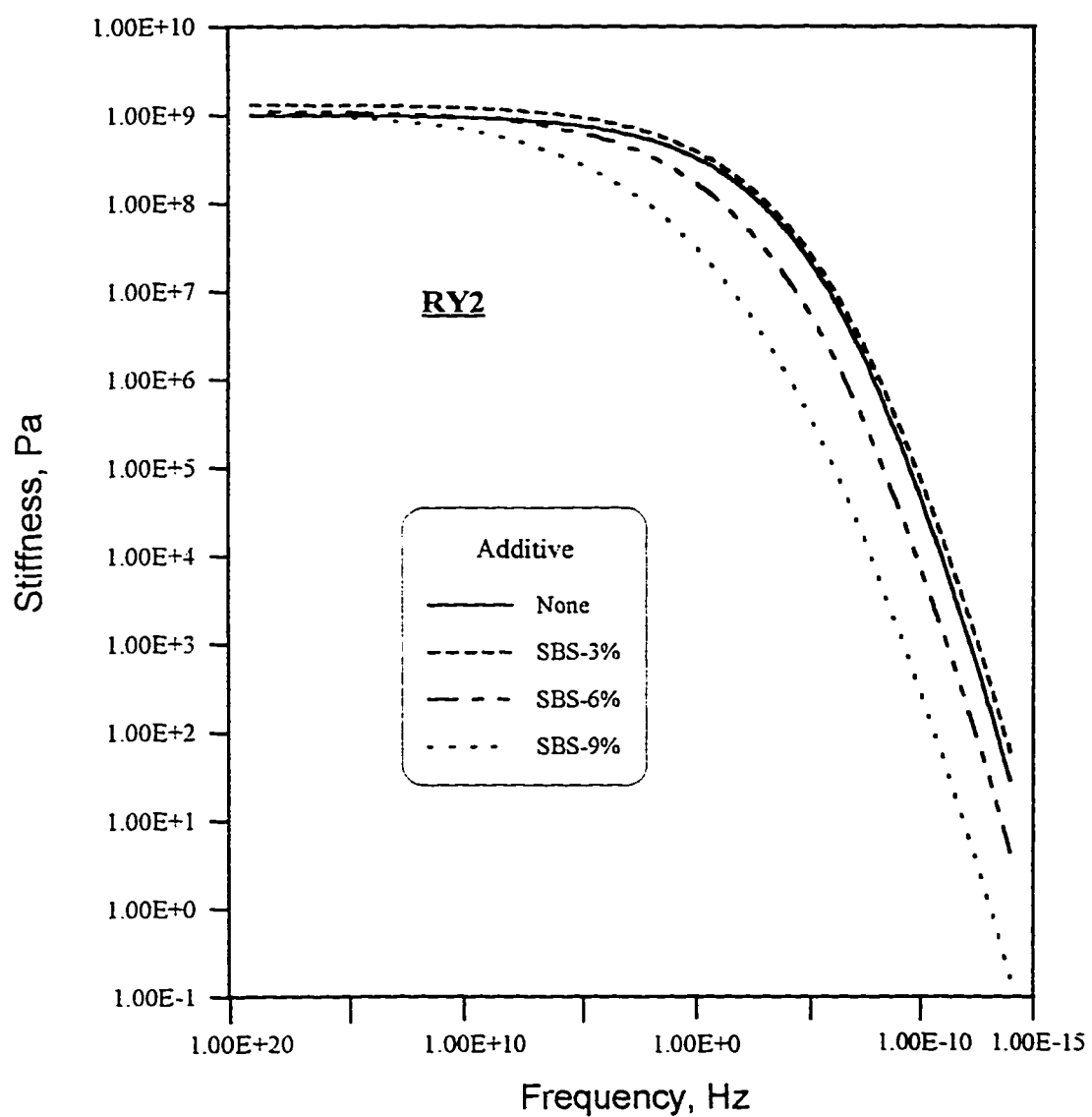


Figure 4.14: Master curves of RY2 modified sample with different percentages of SBS.

location of the master curve due to polymer modification was not consistent for all samples.

It was impossible to fit LVE for RT-SBS-6, RT-SBS-9, and BH-CRT-5 because it seems that these samples no longer behaved as linear visco-elastic materials. For the other samples, the asphalt specific properties (rheological index, R , crossover frequency at the defining temperature, $\omega_o @ T_d$, defining temperature, T_d , and the steady state viscosity at the defining temperature, $\eta_o @ T_d$) are shown in Table 4.11 for neat samples and 4.12 for modified ones. The following parameters can be calculated and used to predict field performance of the asphalt:

- * $G^*/\sin \delta$ can be restricted to limit rutting
- * $G^* \sin \delta$ can be restricted to limit fatigue
- * S and m are means for measuring the resistance of the AC to thermal cracking.

These performance parameters are affected by both test temperature and rate of loading. So, for comparison and modeling purposes, all of these parameters should be measured at the same rate of loading and temperature.

Since $G^*/\sin \delta$ is a rutting predicting parameter, and since rutting occurs at high temperature, a temperature of 64°C was fixed to calculate this parameter. Usually fatigue occurs at moderate temperatures; therefore, $G^*\sin\delta$, which is a fatigue

indicator, was calculated at 25°C using the developed LVE models. Thermal cracking is most critical at the lowest temperature the pavement is subjected to, and since measuring S and m after 60 seconds of loading and specific test temperature will give an idea about resistance of the AC to thermal cracking at a temperature which is lower by 10°C than the test temperature, it was decided to calculate these parameters at 0°C and at a 60 seconds loading time. Models were generated to relate those properties with HP-GPC produced profiles.

4.5 CHEMICAL COMPOSITION

4.5.1 HP-GPC Testing

High pressure gel permeation chromatography is widely used in the analysis of petroleum residues and asphalts. Although the interpretation of the HP-GPC output is not as straightforward with asphalts as it is with polymers, the method allows at least relative determinations of molecular size and molecular weight.

Waters' HPLC system 840 was used in this research with a Model 501 pump, 712 WISP auto injector, and R-401 refractometer as a detector. To control the HP-GPC system and collect, analyze, save, and retrieve the collected data for future use, Millennium 2010 Chromatography Manager software was attached to the above system. Four micro styra-gel columns, connected in the following order according to porosity size: 10,000, 1,000, 500, and 100 Å were all attached prior to the differential

refractive index (R.I.) detector. This detector was used to detect differences in refractive index between the carrier solution and the sample stream. The greater the difference the greater the response. Tetrahydrofuran (THF) (HPLC grade) was used to dilute the asphalt samples and was used as the mobile phase. Plate 4.7 and Fig. 4.15 show the used instrument with all its accessories and the HP-GPC system setup, respectively. The experimental procedure followed in this research was based on published methods in Branthaver et al., (1993); Brule, Raymond and Such, (1986); Donaldson et al., (1988); Jennings et al., (1988) with the introduction of needed modifications. The followed procedure was as follows:

- About 2.0 to 2.5 g of asphalt sample (fresh, RTFO residue, or PAV residue, either neat or modified) was dissolved in about 25 ml THF. The solution was sonified for 15 min. at room temperature.
- The solution was transferred to a 50-ml volumetric flask and volume was made with THF.
- An aliquot was then filtered through a 0.2 μm membrane.
- The diluted sample was then transferred into the HP-GPC special vial and was placed into the auto injector.
- The Millenium 2010 Chromatography Manager was set to automatically inject an exact volume of 100 μml into the four column system.



Plate 4.7: High pressure gel permeation chromatography system.

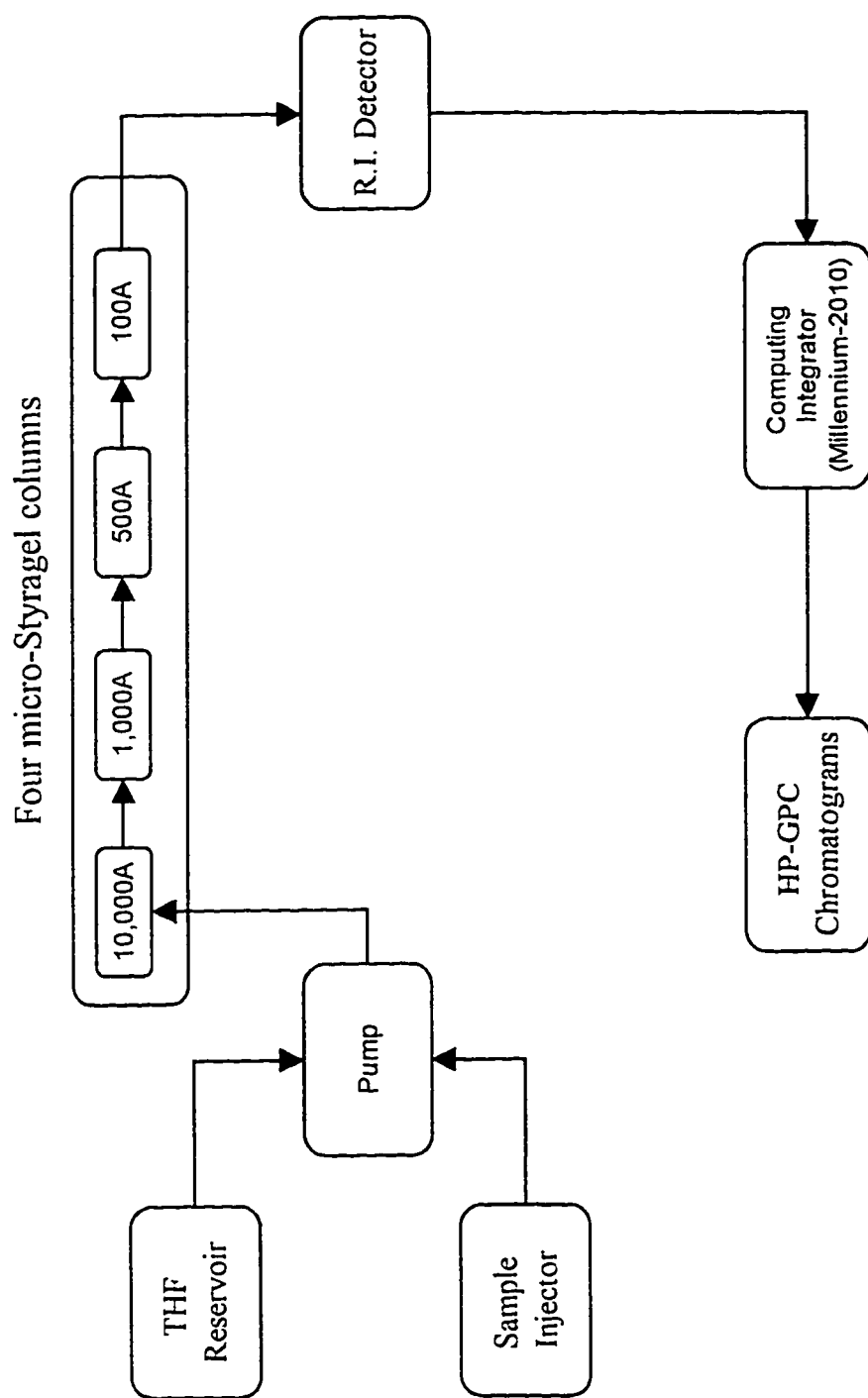


Figure 4.15: HP-GPC system setup.

- The differential reflectometer was located after the column system and was used to detect the eluted volumes of the molecules.
- The software then received the data from the differential refractometer and drew a graphical representation of the eluted volumes with time. Fig. 4.16 shows a typical output of the HP-GPC chromatogram without processing for the BH-CRT-5-F sample.

In summary, the following was used in the HP-GPC testing:

- Mobile phase : Tetrahydrofuran (THF)
- Solvent : THF
- Test temperature : 24°C
- Sample concentration : 5.0 percent
- Injection volume : 100 μ l
- Flow rate : 1.0 μ l/min
- Detector : Differential refractive index
- Column porosity : 10,000, 1,000, 500 and 100 A
- Packing gel : micro-styra-gel

All asphalt samples were analyzed using the HP-GPC technique. Processing and fractionation of produced chromatograms are given in the next section. The HP-

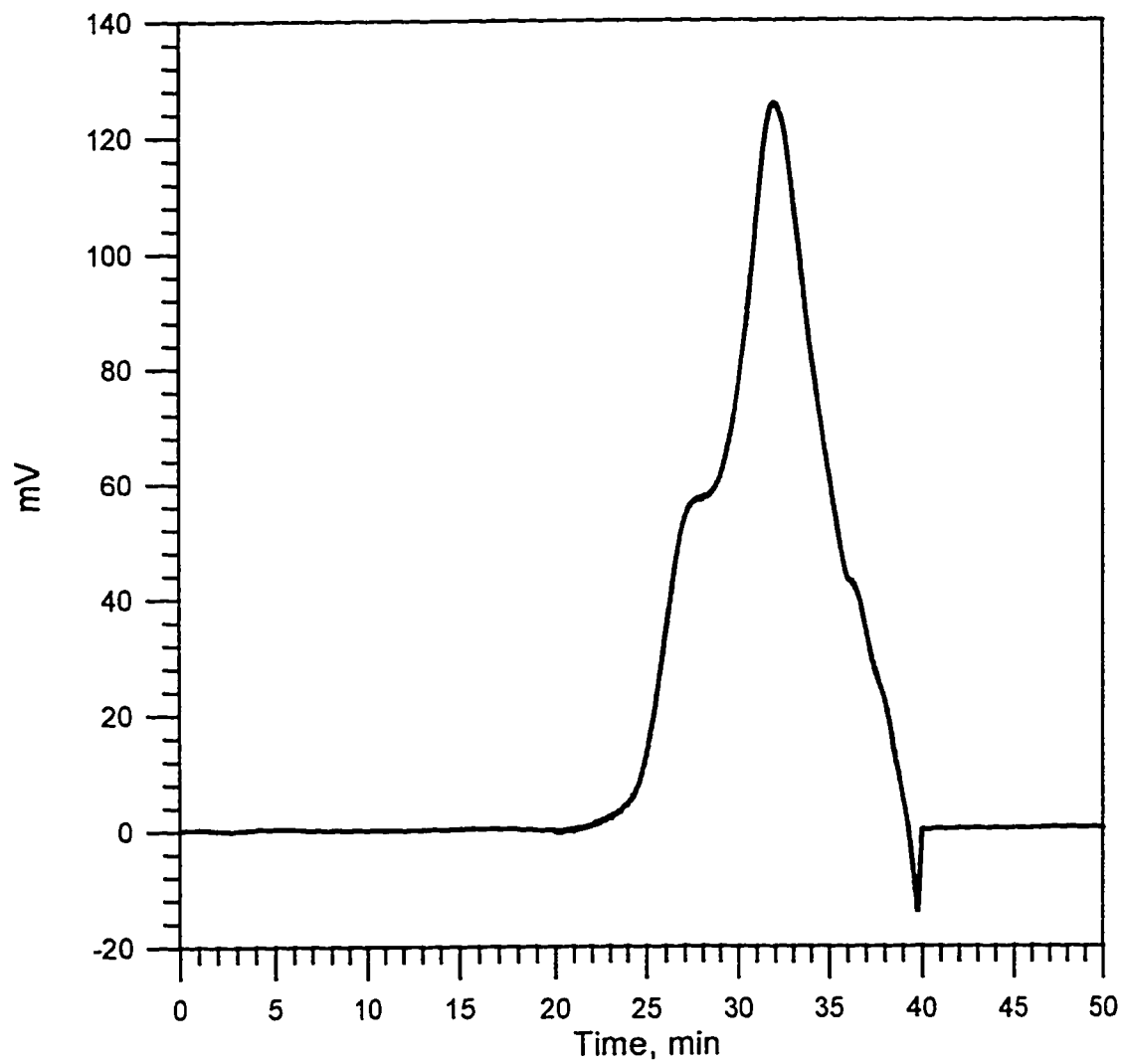


Figure 4.16: Typical produced HP-GPC chromatogram for BH-CRT-5-F sample.

GPC system was calibrated using polystyrene standards with molecular weights 1350, 9100, 37900, and 190,000 amu.

In general, the following can be noticed. The column assembly was suitable to provide different profiles for different samples at different aging conditions. Also, the effect of molecular size affected the start of the elution time from the HP-GPC columns. Aged and polymer modified samples started earlier than fresh ones. The negative peak noticed in Fig. 4.16 at the end of the elution time was noticed in most of the samples, which seems to be an inherited feature of the system since it was noticed even if plain solution was used. Therefore, the analysis of the produced profiles was truncated at 38 minutes.

4.5.2 Fractionating Procedure of the HP-GPC Chromatograms

The initial output of the computer after running the asphalt samples through the porous columns was a graphical presentation of the change in voltage (in mV) sensed by the differential refractometer due to the difference of the refractive index between the carrier solution and the sample stream versus time of elution in minutes. Fig. 4.17 shows the produced chromatograms for KW2, KW2R, and KW2P superimposed on top of each other. This figure shows the ability of the system in detecting differences between asphalts exposed to different aging processes. There is a clear difference between the general shapes of the three chromatograms, i.e., there is an increase in the amount of LMS due to aging. The negative peaks on the trailing edge of the

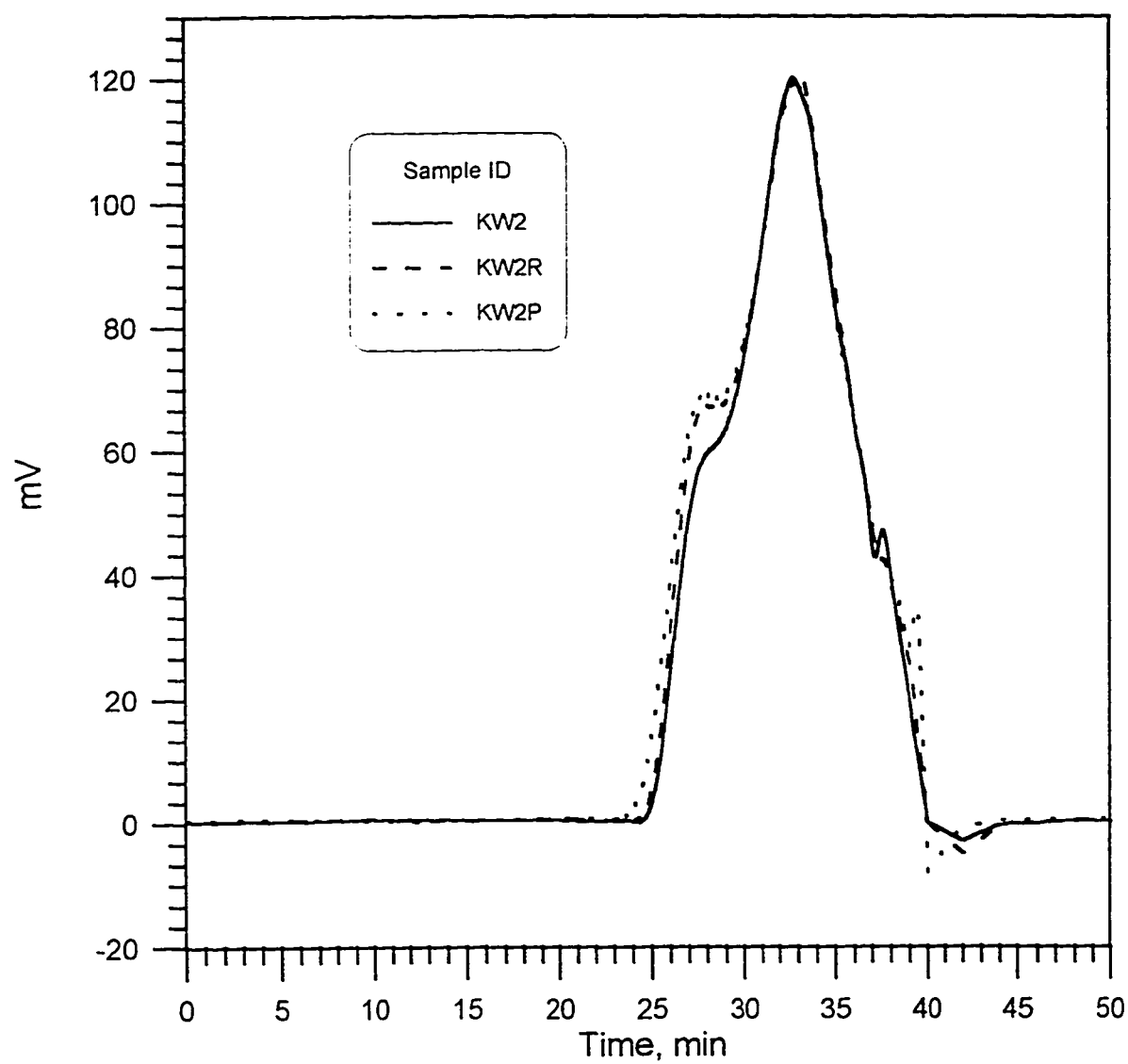


Figure 4.17: Produced HP-GPC chromatogram for KW2 sample at different stages of aging.

chromatograms seem to be inherent in the system and occur even when only the solvent is injected.

Looking at the chromatograms shown in Figs. 4.16 and 4.17 and studying the other chromatograms produced for all other samples, it was decided to restrict the analysis of the data to the elution period 22-38 minutes. The Millennium Chromatography Manager was reused to slice the area under the chromatograms into one thousand slices. The program gave the timing for each slice and the area under each slice. The data for each sample were then copied from the Millennium program and transferred into Excel software for further analysis.

The following procedure was followed to standardize the data:

1. From the 1000 slices, the highest slice area was determined.
2. Area under each slice was divided by the maximum area found in step #1.

This step was performed to standardize the areas of all the slices.

3. The sum of the standardized areas under all slices was calculated.
4. The standardized area under each slice was then divided by the summation of all standardized areas (step # 3) and multiplied each by hundred. This was done to extract the percentage of the area under each slice from the total area.
5. Finally, the cumulative percentage of the areas was found by cumulatively adding the area under each slice.

Table 4.13 shows a typical example for calculating the cumulative percentage area for an extracted subset of chromatographic slice data for BH1 samples for the region of data between 24.5 and 25.0 minutes.

To fraction the data for any chosen set of fractions, the following was done:

1. The number of fractions and the required fractionating procedure were specified.
2. The times (between 22 and 28 minutes) corresponding to each fraction were evaluated.
3. The cumulative percentage area at each fractionating time was found.
4. Finally, to get the area under each fraction, the cumulative percentage area for each fraction was subtracted from the one before it.

Fig. 4.18 shows a typical HP-GPC profile after being processed. The variable on the x-axis is the time required for a particular size to emerge from the system. The reading on the y-axis is the detector response, which is an indicator of the concentration of asphalt molecules in solution. The profile was divided into eight areas. The cut-off points were selected to have equal elution times. The divided areas were numbered from left to right. Consequently, apparent molecular sizes decrease progressively from section 1 to section 8. Fig. 4.19 is a graphical representation (using bar charts) of the area under each slice using eight slices of equal elution time.

Table 4.13: Example for calculating cumulative percentage area for a sliced HP-GPC produced chromatogram.

Elution Time	Area of Slice	Standardized Areas	Percentage	Cumulative Percentage
24.5	169	0.071	0.502	0.502
24.517	123	0.051	0.366	0.868
24.533	303	0.127	0.901	1.769
24.55	389	0.163	1.156	2.925
24.567	340	0.142	1.011	3.935
24.583	401	0.168	1.192	5.127
24.6	546	0.228	1.623	6.750
24.617	528	0.221	1.569	8.319
24.633	540	0.226	1.605	9.925
24.65	610	0.255	1.813	11.738
24.667	742	0.310	2.205	13.943
24.683	759	0.317	2.256	16.199
24.7	766	0.320	2.277	18.476
24.717	876	0.366	2.604	21.080
24.733	914	0.382	2.717	23.796
24.75	989	0.413	2.940	26.736
24.767	972	0.406	2.889	29.625
24.783	1089	0.455	3.237	32.862
24.8	1162	0.486	3.454	36.316
24.817	1228	0.513	3.650	39.966
24.833	1282	0.536	3.810	43.776
24.85	1520	0.635	4.518	48.294
24.867	1528	0.639	4.542	52.836
24.883	1586	0.663	4.714	57.550
24.9	1805	0.755	5.365	62.915
24.917	1846	0.772	5.487	68.401
24.933	1951	0.816	5.799	74.200
24.95	1990	0.832	5.915	80.115
24.967	2138	0.894	6.355	86.470
24.983	2160	0.903	6.420	92.890
25	2392	1.000	7.110	100.000
Max. Area =	2392			
Sum of Areas =		14.065		

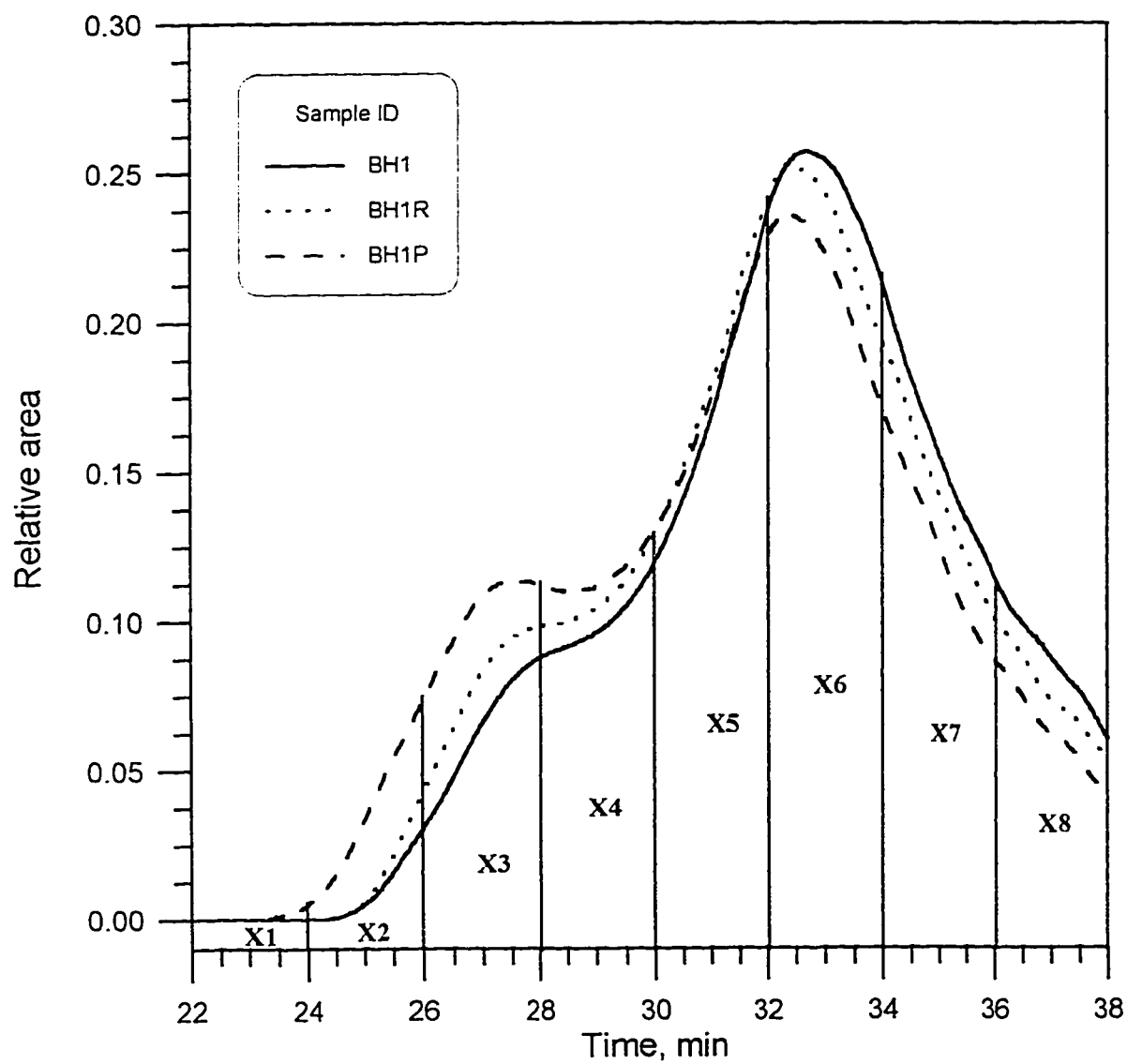


Figure 4.18: HP-GPC chromatogram for BH1 sample after processing and slicing to eight slices.

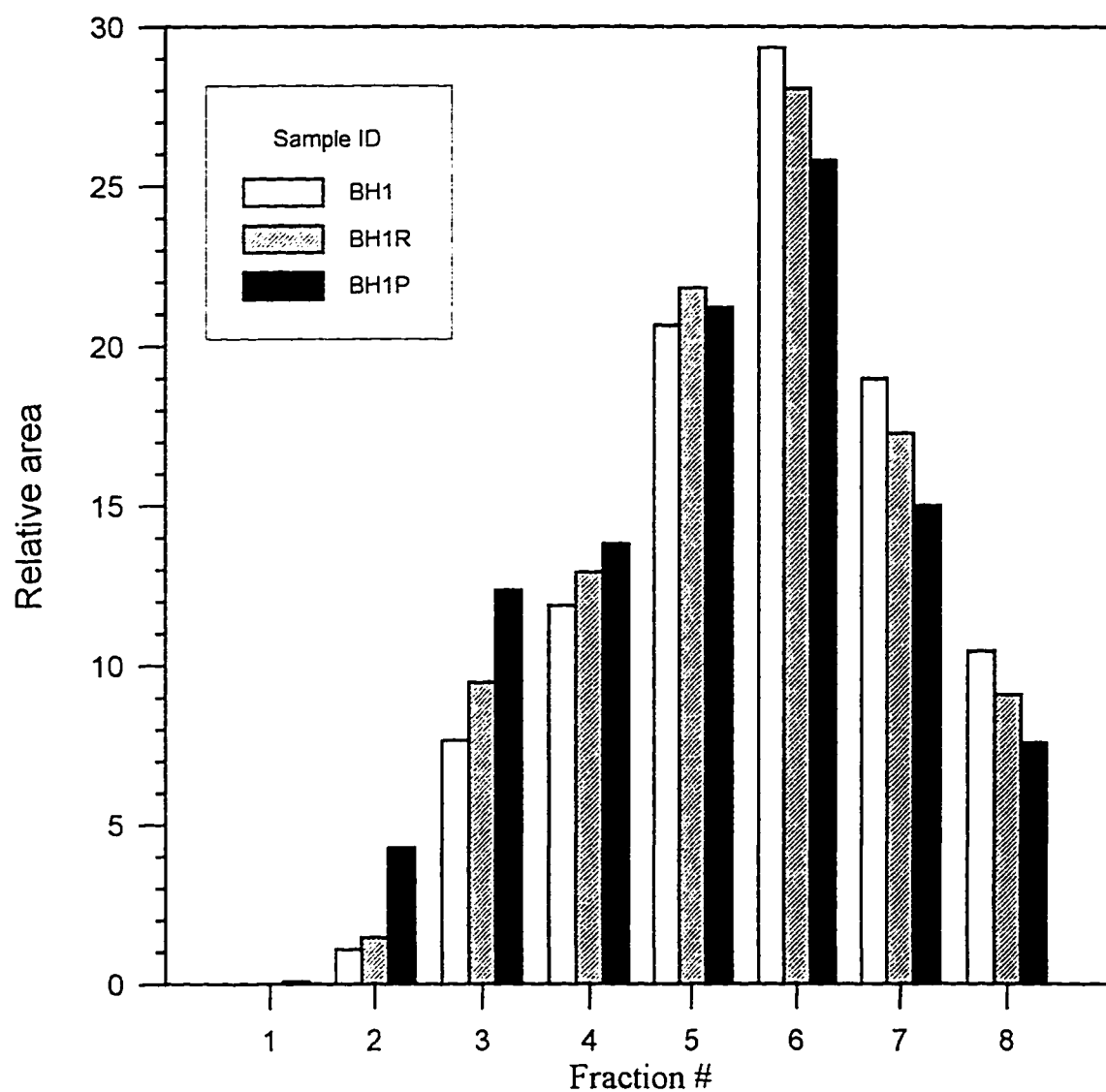


Figure 4.19: Bar chart representation of HP-GPC produced chromatogram for BH1 sample.

From this figure a direct judgment about the distribution of areas can be drawn immediately. Figs. C1- C21 in Appendix C show a bar chart representation of all neat samples under study at different aging stages. From these figures, it can be noticed that there is a shift in the bar charts to the left with aging, i.e., increase in the amount of the larger molecular size fraction. Therefore, the HP-GPC system was able to detect the change in the molecular size distribution due to aging of the samples.

To study the effect of polymer quantity and polymer type on the produced HP-GPC profiles, Fig. 4.20 was drawn. In this figure, skewness factors for the produced HP-GPC chromatograms of the polymer modified samples were drawn. It can be noticed that there was an increase in the value of skewness with the increase in the percentage of polymer. The increase in skewness means that there was a pileup of cases with lower scores, i.e. there was a shift in the profile to the left since there was an increase in the larger size molecules. Also, it can be seen from Fig. 4.20 that the affect of SBS is more than that of CRT in shifting the molecular size distribution to the left and increasing the relative amounts of the large molecular size.

4.5.3 Fractionation of HP-GPC Chromatograms

The purpose of fractionating the produced HP-GPC chromatograms was to quantify them. Different fractionating procedures were tried in this research to find the most appropriate one that could explain the shape of the produced profiles. These procedures included the following:

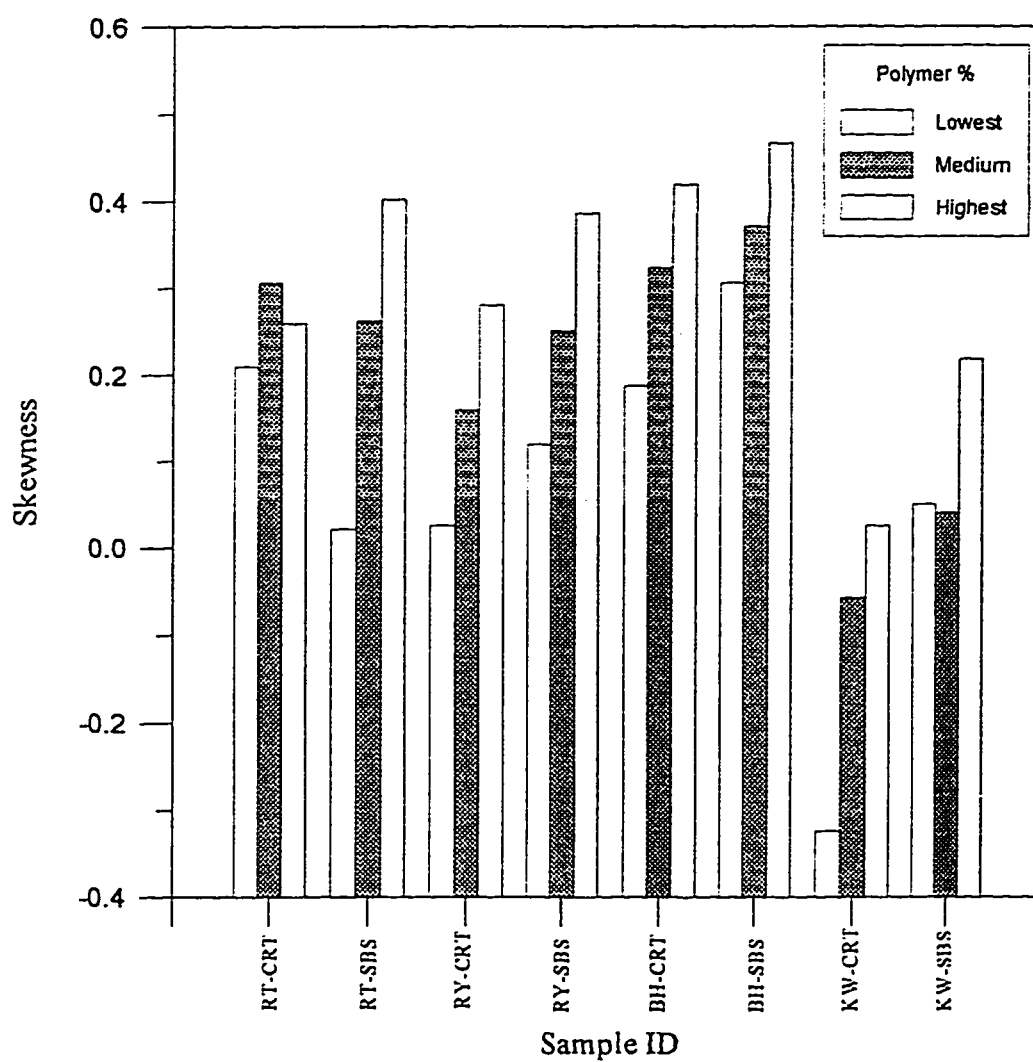


Figure 4.20: Effect of polymer percentage on the skewness of the produced HP-GPC chromatogram.

1. Three fractions of equal elution periods. This was accomplished by dividing the chromatograms at 27.33 and 32.67 minutes. Table 4.14 shows the areas under the HP-GPC fractions with equal elution periods for neat and modified asphalts.
2. Three fractions with equal average areas. This was obtained by finding the corresponding elution times corresponding to 1/3rd and 2/3rd of the average areas for each profile of the asphalt samples at all aging stages. Then the average of the times at these two fractions was obtained and used to divide all the profiles on those times. Table D-1 in Appendix D shows the HP-GPC fractions using this technique.
3. Three fractions partitioned at 25%, 50%, and 25% of total elution time. Table D-2 in Appendix D shows the results of this procedure.
4. Three fractions partitioned at 25%, 50%, and 25% of average areas. Table D-3 in Appendix D shows results of this procedure.
5. Eight fractions at equal elution periods. Results are shown in Table D-4 in Appendix D.
6. Eight fractions with equal average area. Results are shown in Table D-5 in Appendix D.
7. Twelve equal period fractions (Table D-6 in Appendix D).
8. Twelve equal average areas (Table D-7 in Appendix D).

Table 4.14: HP-GPC fractions - using three equal times fractions.

Partition	1st	2nd	3rd	Skew	Standard
Corr. time	27.33	32.67	38.00	Factor	Deviation
RT1	13.5	48.9	37.6	-1.00	18.10
RT1R	14.6	48.6	36.7	-0.85	17.25
RT1P	17.4	46.9	35.8	-0.72	14.91
RT2	12.0	48.1	40.0	-1.39	18.95
RT2R	14.0	49.2	36.8	-0.85	17.84
RT2P	16.9	47.0	36.0	-0.78	15.21
RT3	11.8	48.1	40.0	-1.38	19.05
RT3R	14.0	49.0	37.1	-0.90	17.81
RT3P	18.8	47.1	34.0	-0.22	14.17
RT4	14.7	48.4	36.9	-0.90	17.17
RT4R	14.7	48.7	36.6	-0.83	17.23
RT4P	19.4	45.3	35.3	-0.68	13.06
RT5	13.1	47.6	39.3	-1.33	18.05
RT5R	14.7	47.9	37.4	-1.01	17.01
RT5P	18.5	46.7	34.9	-0.48	14.17
RY1	8.5	48.9	42.6	-1.57	21.71
RY1R	7.4	58.3	34.2	-0.16	25.44
RY1P	12.0	55.1	32.9	0.10	21.54
RY2	9.3	55.4	35.3	-0.38	23.15
RY2R	7.9	55.9	36.2	-0.53	24.12
RY2P	13.5	54.5	32.0	0.30	20.52
RY3	9.2	48.5	42.2	-1.56	21.12
RY3R	7.6	56.6	35.7	-0.44	24.57
RY3P	15.1	54.2	30.6	0.61	19.69
RY4	10.0	55.1	34.9	-0.30	22.62
RY4R	9.1	55.5	35.4	-0.40	23.25
RY4P	16.5	52.8	30.8	0.62	18.30
RY5	10.7	53.7	35.6	-0.47	21.58
RY5R	9.1	55.5	35.4	-0.39	23.23
RY5P	15.3	53.9	30.8	0.59	19.45
BH1	5.4	45.8	48.7	-1.70	24.22
BH1R	7.1	48.5	44.4	-1.67	22.84
BH1P	12.2	48.8	39.0	-1.22	18.99
BH2	5.6	46.7	47.8	-1.73	24.06
BH2R	7.9	48.5	43.6	-1.64	22.12
BH2P	11.1	48.9	40.1	-1.35	19.79
BH3	5.5	47.0	47.5	-1.73	24.09
BH3R	7.2	48.5	44.3	-1.67	22.74
BH3P	12.7	47.9	39.4	-1.32	18.33
BH4	6.1	47.2	46.7	-1.73	23.56
BH4R	8.2	48.5	43.3	-1.62	21.93
BH4P	10.5	48.7	40.8	-1.44	20.20
BH5	5.8	47.9	46.3	-1.72	23.84
BH5R	7.5	48.8	43.7	-1.63	22.53
BH5P	10.7	48.9	40.4	-1.39	20.09
KW1	6.8	46.1	47.0	-1.73	22.94
KW1R	7.4	46.8	45.9	-1.73	22.48
KW1P	12.0	46.4	41.6	-1.60	18.66
KW2	7.4	46.7	46.0	-1.73	22.48
KW2R	8.9	46.4	44.7	-1.72	21.21
KW2P	10.9	45.7	43.4	-1.70	19.46
KW3	7.1	46.1	46.8	-1.73	22.71
KW3R	8.5	46.6	44.9	-1.72	21.54
KW3P	12.0	45.9	42.1	-1.65	18.57
KW4	6.4	47.1	46.4	-1.73	23.30
KW4R	9.0	46.4	44.6	-1.72	21.10
KW4P	13.1	51.8	35.1	-0.42	19.41
KW5	6.5	46.9	46.6	-1.73	23.23
KW5R	8.8	46.6	44.6	-1.71	21.30
KW5P	13.1	51.8	35.2	-0.42	19.41
AZ1	9.5	48.1	42.4	-1.59	20.85
AZ1R	10.3	48.2	41.5	-1.52	20.22
AZ1P	13.1	47.7	39.2	-1.31	18.06

Table 4.14: (Continued)

Partiton	1st	2nd	3rd	Skew Factor	Standard Deviation
Corr time	27.33	32.67	38.00		
RT-CRT-5-F	12.1	51.1	36.8	-0.78	19.70
RT-CRT-5-R	16.1	48.7	35.2	-0.52	16.37
RT-CRT-5-P	17.7	47.8	34.4	-0.33	15.07
RT-CRT-10-F	16.0	48.6	37.4	-1.10	15.72
RT-CRT-10-R	17.1	48.9	36.0	-0.77	15.04
RT-CRT-10-P	21.4	45.9	32.7	0.22	12.27
RT-CRT-15-F	12.3	51.2	36.5	-0.70	19.63
RT-CRT-15-R	14.3	48.2	37.5	-1.03	17.36
RT-CRT-15-P	17.6	46.1	36.3	-0.88	14.46
RT-SBS-3-F	17.1	45.4	37.5	-1.17	14.65
RT-SBS-3-R	19.4	45.4	35.1	-0.61	13.11
RT-SBS-3-P	19.7	46.7	33.7	-0.11	13.49
RT-SBS-6-F	13.6	49.3	37.0	-0.88	18.12
RT-SBS-6-R	15.8	48.0	36.2	-0.77	16.29
RT-SBS-6-P	22.3	45.2	32.5	0.34	11.47
RT-SBS-9-F	18.9	44.8	36.3	-0.96	13.19
RT-SBS-9-R	19.7	44.1	36.1	-0.97	12.42
RT-SBS-9-P	14.8	37.7	47.6	-1.08	16.63
RY-CRT-5-F	9.7	51.7	38.5	-1.03	21.49
RY-CRT-5-R	12.5	50.4	37.1	-0.84	19.24
RY-CRT-5-P	17.0	49.6	33.5	-0.04	16.29
RY-CRT-10-F	12.6	49.9	37.5	-0.94	19.01
RY-CRT-10-R	13.5	50.0	36.4	-0.73	18.46
RY-CRT-10-P	16.5	49.5	34.0	-0.19	16.51
RY-CRT-15-F	8.2	51.1	40.7	-1.31	22.38
RY-CRT-15-R	11.5	50.1	38.3	-1.06	19.77
RY-CRT-15-P	16.8	47.9	35.3	-0.55	15.60
RY-SBS-3-F	15.6	50.7	33.7	-0.08	17.56
RY-SBS-3-R	16.7	51.1	32.2	0.31	17.22
RY-SBS-3-P	16.2	55.5	28.2	1.07	20.15
RY-SBS-6-F	16.3	50.2	31.5	0.50	18.03
RY-SBS-6-P	19.5	48.8	31.7	0.48	14.73
RY-SBS-6-P	23.9	47.0	29.1	1.39	12.11
RY-SBS-9-F	17.6	50.2	32.1	0.33	16.33
RY-SBS-9-R	18.7	49.1	32.2	0.35	15.25
RY-SBS-9-P	21.8	48.6	29.6	1.12	13.77
BH-CRT-5-F	11.1	51.7	37.2	-0.82	20.59
BH-CRT-5-R	14.5	50.2	35.3	-0.48	17.91
BH-CRT-5-P	15.3	50.8	33.9	-0.13	17.76
BH-CRT-10-F	9.5	52.2	38.3	-0.97	21.74
BH-CRT-10-R	12.3	50.5	37.2	-0.86	19.35
BH-CRT-10-P	15.5	49.7	34.9	-0.40	17.14
BH-CRT-15-F	7.9	52.3	39.7	-1.16	22.90
BH-CRT-15-R	9.1	51.5	39.4	-1.15	21.81
BH-CRT-15-P	15.7	48.7	35.5	-0.58	16.61
BH-SBS-3-F	10.2	52.0	37.7	-0.89	21.25
BH-SBS-3-R	12.7	51.2	36.2	-0.64	19.39
BH-SBS-3-P	11.9	51.7	36.4	-0.66	20.08
BH-SBS-6-F	11.6	49.2	39.1	-1.22	19.46
BH-SBS-6-R	11.6	49.2	39.2	-1.23	19.46
BH-SBS-6-P	17.0	47.4	35.6	-0.66	15.32
BH-SBS-9-F	10.0	50.5	39.5	-1.20	20.94
BH-SBS-9-R	10.9	50.1	38.9	-1.15	20.19
BH-SBS-9-P	15.1	50.7	34.2	-0.21	17.79
KW-CRT-5-F	19.2	47.9	32.9	0.15	14.38
KW-CRT-5-R	19.6	46.8	33.5	-0.07	13.60
KW-CRT-5-P	22.6	45.7	31.6	0.67	11.54
KW-CRT-10-F	16.8	48.1	35.0	-0.48	15.71
KW-CRT-10-R	16.3	48.2	35.5	-0.61	16.06
KW-CRT-10-P	20.9	46.0	33.0	0.10	12.57
KW-CRT-15-F	11.8	51.0	37.2	-0.84	19.87
KW-CRT-15-R	14.3	49.3	36.4	-0.76	17.69
KW-CRT-15-P	19.3	47.0	33.7	-0.12	13.82
KW-SBS-3-F	10.0	52.0	38.0	-0.94	21.34
KW-SBS-3-R	12.6	51.2	36.2	-0.66	19.43
KW-SBS-3-P	14.5	49.7	35.7	-0.60	17.73
KW-SBS-6-F	14.4	49.2	36.3	-0.75	17.57
KW-SBS-6-R	14.8	49.2	36.0	-0.68	17.38
KW-SBS-6-P	18.2	48.5	33.3	0.00	15.16
KW-SBS-9-F	19.7	46.0	34.2	-0.30	13.17
KW-SBS-9-R	14.5	49.3	36.2	-0.72	17.59
KW-SBS-9-P	14.9	48.6	36.5	-0.80	17.06

9. In this procedure, it was decided to check if the profiles for the samples from each source (RT, RY, BH, and KW) had unique shapes characterizing them from asphalts belonging to other sources. Therefore, neat samples from each source were drawn on the same graph as shown in Figs. 4.21 through 4.24. Also, a profile of sample #1 from each source was drawn in Fig. 4.25. From Figs. 4.21-4.25, it is observed that samples from each source (other than RY) carry some shape characteristics which differentiate them from samples from other sources. For RY samples, it looks that RY1 and RY3 belong to one batch and RY2, RY4, and RY5 belong to another batch. So it was decided to find the cut of points for each source by themselves and to have three fractions at 30%, 40%, and 30% of the areas. These percentages were chosen to represent sort of an average procedure between slicing the profiles into equal areas and slicing them into 25%, 50%, and 25% areas. Table 4.15 shows selected fractionating times for each source and area under each fraction.

Two more factors, standard deviation and skewness, which give an idea about the shape of the profiles are included in Tables 4.14 and 4.15 and in the tables which are included in Appendix D. The standard deviation is a measure of how widely values are dispersed from the average value (the mean), while skewness characterizes the degree of asymmetry of a distribution around its mean. Positive skewness

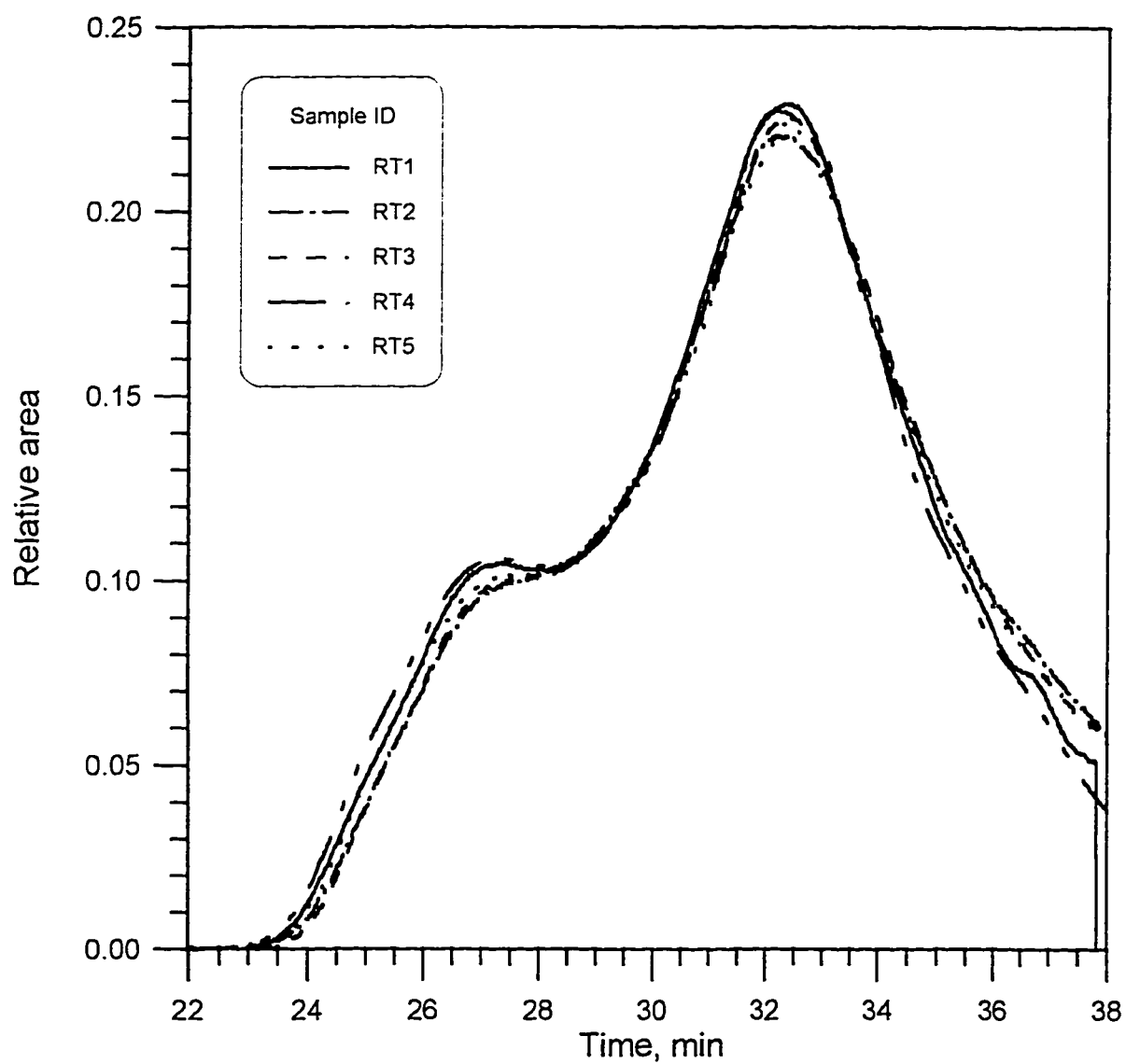


Figure 4.21: HP-GPC chromatograms for RT samples.

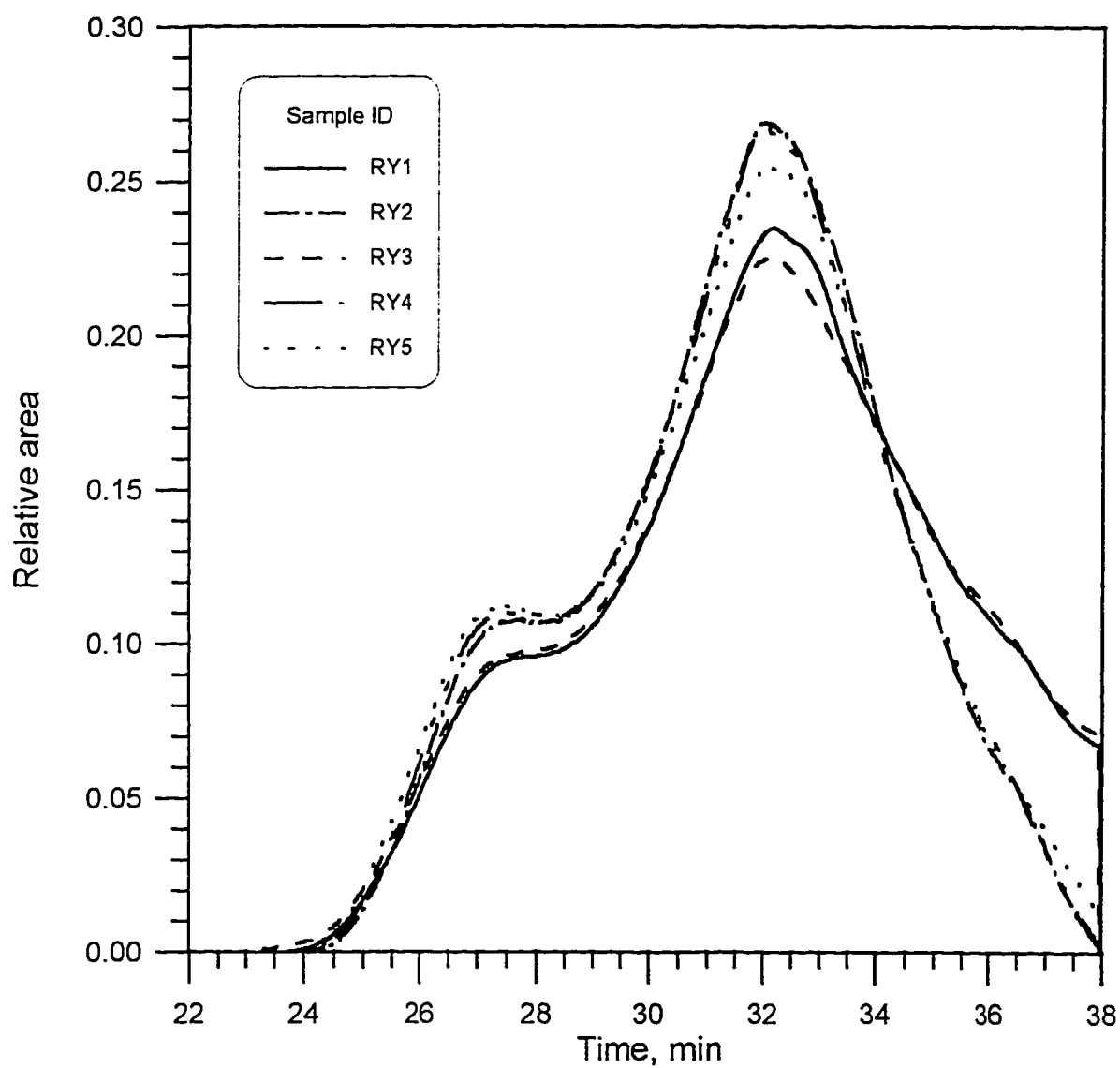


Figure 4.22: HP-GPC chromatogram for RY samples.

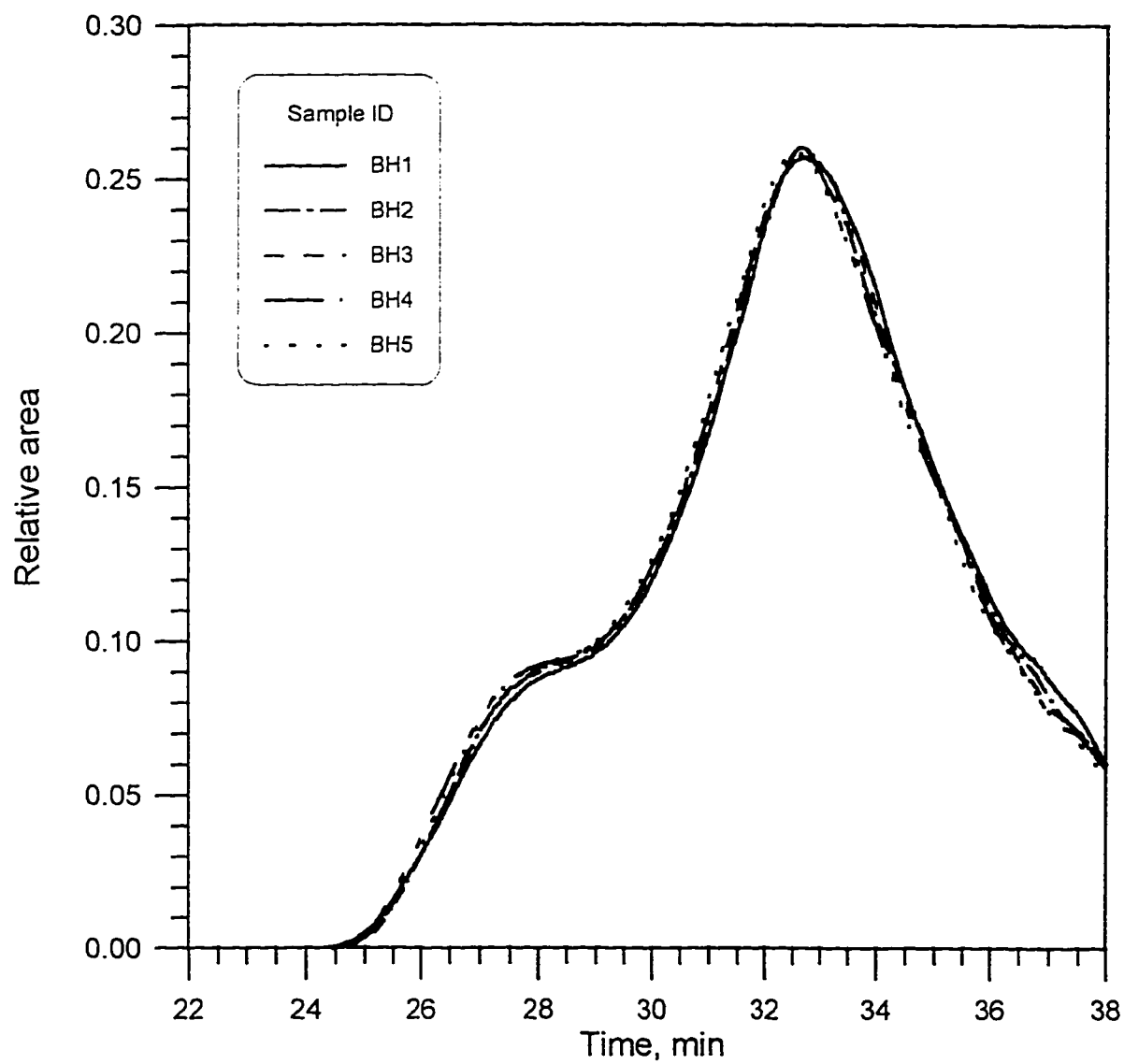


Figure 4.23: HP-GPC chromatogram for BH samples.

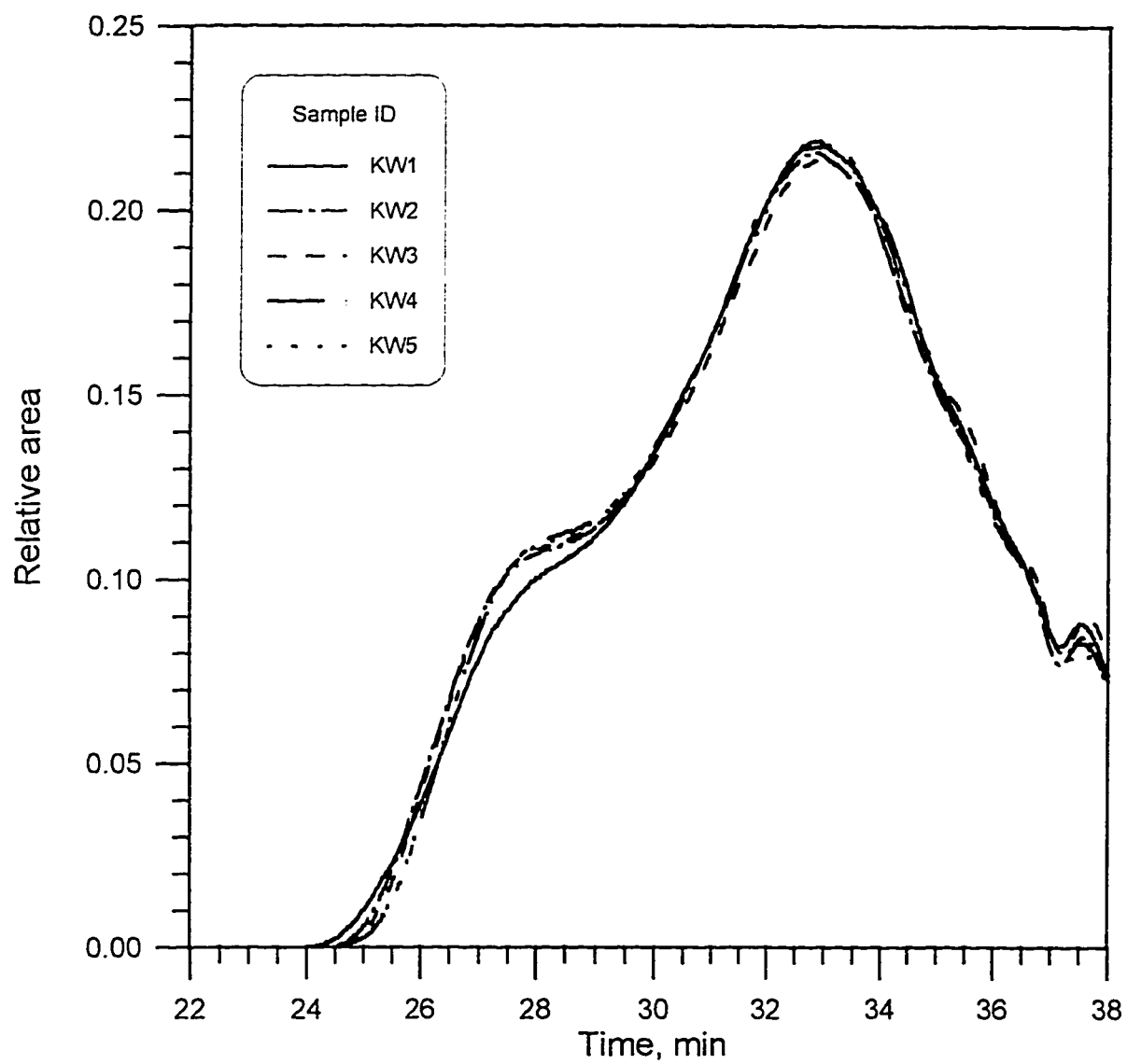


Figure 4.24: HP-GPC chromatogram for KW samples.

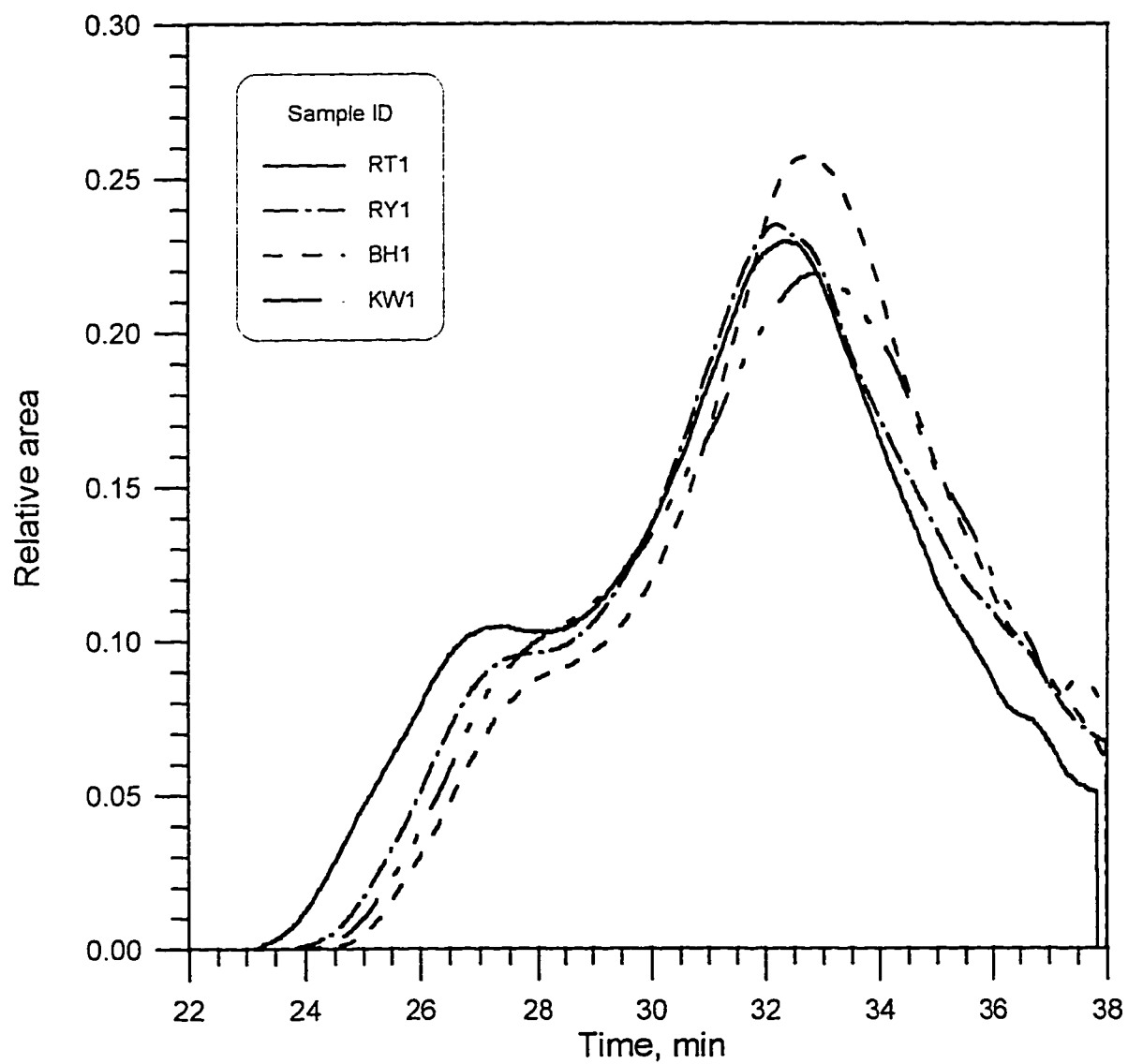


Figure 4.25: HP-GPC chromatogram for sample # 1 from each asphalt source.

Table 4.15: HP-GPC fractions - using three (30%-40%-30%)
corresponding areas fractions.

Partition	1st	2nd	3rd	Skew Factor	Standard Deviation
Corr. time	29.92	33.37	38.00	-	-
RT1	30.6	40.7	28.7	1.56	6.49
RT1R	32.4	39.5	28.1	0.73	5.78
RT1P	35.0	37.5	27.5	-1.31	5.17
Corr. time	29.92	33.37	38.00	-	-
RT2	29.0	39.7	31.2	1.44	5.66
RT2R	31.7	40.3	28.0	1.09	6.30
RT2P	34.4	37.9	27.7	-0.90	5.16
Corr. time	29.92	33.37	38.00	-	-
RT3	28.8	40.1	31.2	1.42	5.95
RT3R	31.6	39.9	28.5	1.19	5.90
RT3P	36.6	37.5	25.9	-1.69	6.43
Corr. time	29.92	33.37	38.00	-	-
RT4	31.8	40.3	28.0	1.05	6.31
RT4R	32.3	39.9	27.8	0.74	6.12
RT4P	36.4	36.1	27.5	-1.72	5.05
Corr. time	29.92	33.37	38.00	-	-
RT5	30.0	39.3	30.6	1.71	5.20
RT5R	32.1	39.3	28.6	0.97	5.49
RT5P	35.9	37.6	26.5	-1.59	5.98
Corr. time	30.46	33.69	38.00	-	-
RY1	29.5	40.8	29.7	1.73	6.44
RY1R	33.0	46.1	20.9	0.11	12.61
RY1P	37.0	43.5	19.5	-1.20	12.43
Corr. time	30.12	33.03	38.00	-	-
RY2	29.2	40.9	29.8	1.72	6.60
RY2R	29.8	39.0	31.3	1.56	4.93
RY2P	35.1	37.9	27.0	-1.29	5.70
Corr. time	30.46	33.69	38.00	-	-
RY3	30.5	39.6	29.8	1.70	5.46
RY3R	33.0	44.2	22.7	0.12	10.74
RY3P	40.1	41.9	18.0	-1.70	13.34
Corr. time	30.12	33.03	38.00	-	-
RY4	30.1	40.5	29.5	1.71	6.19
RY4R	29.8	40.4	29.9	1.73	6.08
RY4P	37.9	36.2	25.9	-1.61	6.49
Corr. time	30.12	33.03	38.00	-	-
RY5	30.7	39.0	30.3	1.72	4.89
RY5R	29.5	40.6	29.9	1.73	6.33
RY5P	36.9	37.3	25.6	-1.73	6.51
Corr. time	31.0	33.9	38.0	-	-
BH1	29.1	39.9	30.9	1.55	5.79
BH1R	33.0	39.3	27.7	0.29	5.80
BH1P	39.5	36.7	23.8	-1.52	8.39
Corr. time	31.0	33.9	38.0	-	-
BH2	29.9	39.9	30.2	1.73	5.70
BH2R	33.9	39.0	27.1	-0.45	5.99
BH2P	36.2	37.1	24.8	-1.69	7.45
Corr. time	31.0	33.9	38.0	-	-
BH3	29.9	40.2	29.9	1.73	5.98
BH3R	32.9	39.4	27.7	0.30	5.87
BH3P	39.4	36.1	24.5	-1.38	7.83
Corr. time	31.0	33.9	38.0	-	-
BH4	30.8	39.8	29.4	1.61	5.68
BH4R	34.3	38.7	27.0	-0.70	5.92
BH4P	37.2	37.6	25.3	-1.73	6.96
Corr. time	31.0	33.9	38.0	-	-
BH5	30.8	40.2	29.0	1.57	6.06
BH5R	33.5	39.4	27.1	-0.12	6.15
BH5P	37.6	37.3	25.0	-1.73	7.18
Corr. time	30.6	34.0	38.0	-	-
KW1	29.5	40.4	30.1	1.71	6.13
KW1R	31.2	39.6	29.2	1.48	5.49
KW1P	35.9	37.5	26.6	-1.59	5.92
Corr. time	30.6	34.0	38.0	-	-
KW2	30.7	40.0	29.3	1.62	5.85
KW2R	32.9	38.6	28.4	0.34	5.11
KW2P	34.9	37.6	27.6	-1.21	5.17
Corr. time	30.6	34.0	38.0	-	-
KW3	30.4	39.5	30.1	1.73	5.34
KW3R	32.6	39.0	28.4	0.59	5.31
KW3P	36.2	37.2	26.5	-1.67	5.91
Corr. time	30.6	34.0	38.0	-	-
KW4	30.1	40.4	29.5	1.71	6.13
KW4R	32.9	38.8	28.2	0.35	5.31
KW4P	39.7	40.7	19.8	-1.72	11.90
Corr. time	30.6	34.0	38.0	-	-
KW5	30.1	40.2	29.7	1.72	5.98
KW5R	32.8	39.0	28.2	0.46	5.42
KW5P	39.8	41.1	19.1	-1.71	12.33
Corr. time	30.6	34.0	38.0	-	-
AZ1	32.6	41.8	25.6	0.42	8.12
AZ1R	33.9	41.1	24.9	-0.33	8.12
AZ1P	37.1	39.6	23.4	-1.58	8.72

Table 4.15: (Continued)

Parison	1st	2nd	3rd	Skew	Standard
Corr. time	29.92	33.37	38.00	Factor	Deviation
RT-CRT-5-F	30.3	41.8	27.7	1.50	7.56
RT-CRT-5-R	34.1	38.0	26.8	-0.58	6.13
RT-CRT-5-P	35.8	38.2	26.2	-1.41	6.38
Corr. time	29.92	33.37	38.00	-	-
RT-CRT-10-F	32.5	38.4	25.1	0.79	4.72
RT-CRT-10-R	34.1	38.3	27.6	-0.81	5.43
RT-CRT-10-P	38.8	36.2	25.1	-1.48	7.29
Corr. time	29.92	33.37	38.00	-	-
RT-CRT-15-F	30.0	42.5	27.4	1.53	8.04
RT-CRT-15-R	31.1	39.9	29.0	1.48	5.81
RT-CRT-15-P	34.1	37.8	28.0	-0.65	4.97
Corr. time	29.92	33.37	38.00	-	-
RT-SBS-3-F	34.0	36.6	29.4	-0.75	3.87
RT-SBS-3-R	36.4	36.2	27.4	-1.73	5.10
RT-SBS-3-P	37.4	36.6	26.0	-1.70	6.37
Corr. time	29.92	33.37	38.00	-	-
RT-SBS-6-F	31.2	40.3	28.5	1.38	6.19
RT-SBS-6-R	33.3	38.7	28.0	0.01	5.37
RT-SBS-6-P	39.7	35.4	24.9	-1.13	7.85
Corr. time	30.48	33.69	38.00	-	-
RT-SBS-9-F	35.1	36.6	28.2	-1.52	4.50
RT-SBS-9-R	35.9	36.1	28.0	-1.73	4.65
RT-SBS-9-P	29.1	31.6	39.3	1.33	5.29
Corr. time	30.12	33.03	38.00	-	-
RY-CRT-5-F	30.0	36.2	33.8	-0.70	3.15
RY-CRT-5-R	32.7	34.7	32.6	1.73	1.19
RY-CRT-5-P	37.8	32.9	29.3	0.48	4.28
Corr. time	30.48	33.69	38.00	-	-
RY-CRT-10-F	31.7	35.3	33.0	0.89	1.83
RY-CRT-10-R	33.4	34.6	32.0	-0.19	1.34
RY-CRT-10-P	36.9	33.3	29.8	0.05	3.55
Corr. time	30.12	33.03	38.00	-	-
RY-CRT-15-F	26.3	38.0	35.7	-1.45	6.19
RY-CRT-15-R	30.4	36.0	33.6	-0.42	2.82
RY-CRT-15-P	36.1	33.0	31.0	0.63	2.56
Corr. time	30.12	33.03	38.00	-	-
RY-SBS-3-F	36.1	34.4	29.5	-1.31	3.42
RY-SBS-3-R	37.5	34.6	28.0	-1.07	4.67
RY-SBS-3-P	37.5	38.8	23.7	-1.68	8.38
Corr. time	31.00	33.88	38.00	-	-
RY-SBS-6-F	38.6	33.9	27.5	-0.47	5.57
RY-SBS-6-R	39.4	32.8	27.8	0.43	5.81
RY-SBS-6-P	43.8	30.9	25.3	1.09	9.45
Corr. time	31.00	33.88	38.00	-	-
RY-SBS-9-F	37.5	34.5	28.0	-1.00	4.88
RY-SBS-9-R	38.8	33.3	28.1	0.03	5.26
RY-SBS-9-P	42.0	32.1	25.9	0.68	8.13
Corr. time	31.00	33.88	38.00	-	-
BH-CRT-5-F	40.0	37.2	22.9	-1.56	9.18
BH-CRT-5-R	43.1	34.9	22.0	-0.65	10.65
BH-CRT-5-P	44.7	34.8	20.5	-0.53	12.15
Corr. time	31.00	33.88	38.00	-	-
BH-CRT-10-F	37.8	38.8	23.3	-1.71	6.74
BH-CRT-10-R	40.1	37.1	22.8	-1.53	9.21
BH-CRT-10-P	43.6	34.8	21.6	-0.58	11.07
Corr. time	31.00	33.88	38.00	-	-
BH-CRT-15-F	37.9	38.8	23.3	-1.71	6.74
BH-CRT-15-R	36.2	39.4	24.4	-1.43	7.91
BH-CRT-15-P	43.6	34.8	21.6	-0.58	11.07
Corr. time	31.00	33.88	38.00	-	-
BH-SBS-3-F	38.5	36.6	22.9	-1.73	9.00
BH-SBS-3-R	41.2	36.6	22.3	-1.31	8.88
BH-SBS-3-P	41.0	36.5	22.4	-1.32	8.70
Corr. time	30.59	33.99	38.00	-	-
BH-SBS-6-F	38.4	37.0	24.6	-1.67	7.56
BH-SBS-6-R	38.0	37.8	24.2	-1.73	7.92
BH-SBS-6-P	43.8	34.1	22.1	-0.32	10.90
Corr. time	30.59	33.99	38.00	-	-
BH-SBS-9-F	36.7	36.9	24.4	-1.56	7.78
BH-SBS-9-R	37.5	38.3	24.2	-1.72	7.90
BH-SBS-9-P	44.8	34.5	20.7	-0.44	12.07
Corr. time	30.59	33.99	38.00	-	-
KW-CRT-5-F	44.3	36.0	19.7	-0.82	12.55
KW-CRT-5-R	44.4	35.2	20.3	-0.68	12.16
KW-CRT-5-P	47.1	34.0	18.9	-0.20	14.09
Corr. time	30.59	33.99	38.00	-	-
KW-CRT-10-F	41.4	37.6	21.0	-1.49	10.83
KW-CRT-10-R	40.9	37.7	21.4	-1.56	10.44
KW-CRT-10-P	44.8	35.2	20.0	-0.65	12.52
Corr. time	30.59	33.99	38.00	-	-
KW-CRT-15-F	37.2	40.7	22.1	-1.48	9.92
KW-CRT-15-R	39.2	38.9	21.9	-1.73	9.89
KW-CRT-15-P	43.5	36.2	20.3	-1.02	11.86
Corr. time	30.59	33.99	38.00	-	-
KW-SBS-3-F	36.2	40.9	22.9	-1.24	8.35
KW-SBS-3-R	38.7	39.8	21.4	-1.71	10.33
KW-SBS-3-P	40.4	37.8	21.7	-1.61	10.12
Corr. time	30.59	33.99	38.00	-	-
KW-SBS-6-F	39.6	38.1	22.3	-1.68	9.82
KW-SBS-6-R	40.2	37.9	21.9	-1.82	9.96
KW-SBS-6-P	43.7	36.3	20.0	-1.02	12.13
Corr. time	30.59	33.99	38.00	-	-
KW-SBS-9-F	43.5	35.4	21.1	-0.79	11.36
KW-SBS-9-R	39.7	38.3	22.0	-1.69	9.87
KW-SBS-9-P	39.7	38.0	22.3	-1.67	9.56

indicates a distribution with an asymmetric tail extending towards more positive values, which means that there is a piling of data to the left. Negative skewness indicates a distribution with an asymmetric tail extending towards more negative values, which means that there is piling of data to the right. These two factors give an indication about the general shape of the produced profiles. They were used in the correlation studies between the HP-GPC and the other suggested properties.

Out of the above fractionating procedures, one procedure will be selected depending on its ability to characterize and quantify the produced profiles and its ability to relate to asphalt rheological and performance based properties. It is expected that having more fractions will explain the produced profiles in a better way, but in the next chapter it will be verified if the extra number of fractions will produce enough profile explanation to justify its usage. It can be noticed from the tables and figures shown in this section that the effect of both aging and polymer modification is an increase in the larger molecular size fraction. It is expected that the increase in the percentage of the larger molecular size fraction is responsible for the decrease in the penetration value and increase in the asphalt viscosity and the jump from one performance grade to a higher grade.

Figs. 4.21 through 4.25 show the repeatability of the HP-GPC system since it gave the same shape characteristics for all samples belonging to each refinery. It can

be noticed from these figures that RT and RY samples had more LMS fraction than BH and KW samples.

In general, the following can be said about the produced HP-GPC chromatograms:

- 1- The HP-GPC system was effective in detecting the effects of aging, polymer modification, asphalt source, and asphalt production on the molecular size distribution.
- 2- There is an increase in the amount of large molecular size fractions as a result of aging.
- 3- The addition of polymer increased the amount of large molecular size fractions.
- 4- The styrene-butadiene-styrene (SBS) has higher effect in increasing the amount of large molecular size fraction than crumb rubber (CRT).
- 5- Transformation of molecular size seems to be the reason behind the change in physical properties which occurs due to aging.
- 6- The increase in the amount of LMS leads to decrease in the penetration value and increase in the viscosity of the AC in line with the a priori hypothesis mentioned in Chapter 3.

4.6 SUMMARY

This chapter provided details about the selected test samples and the experimental work and calculations performed on those samples. Test samples were collected from the different refineries producing asphalts in the Gulf countries in addition to some polymer modified samples. Performed tests were grouped into three groups. The first group was the physical testing. It included details of testing and test results for the performed consistency tests and heat hardening and temperature susceptibility indices. The second group was performance-based testing. It included all SHRP required performance tests, which lead to the grading of all collected samples. The linear visco-elastic models for all the collected samples were developed. The third group of testing was the performance of the HP-GPC testing on the collected samples. Resulted chromatograms were sliced using different techniques.

Chapter 5

MODELING OF ASPHALT PROPERTIES USING HP-GPC CHROMATOGRAMS

5.1 GENERATION OF MODELS

The main objective of this study was the generation of models that can be used to predict the different properties of asphalt using HP-GPC chromatograms. The physical and performance properties that were used in this research are listed in Tables 4.1 and 4.2 and Tables 4.4 through 4.9. The HP-GPC chromatograms which have been tried to build the prediction models were those presented in Tables 4.14 to 4.15 and D-1 to D-7 in Appendix D.

As explained in Chapter 4, nine methods of fractionating the produced chromatograms were tried as follows:

- 1- Using three equal time slices
- 2- Using three equal average area slices
- 3- Fractionating into three slice of 25, 50, and 25% of total time
- 4- Fractionating into three slice of 25, 50. and 25% of total area
- 5- Fractionating into eight equal time slices
- 6- Slicing into eight equal time fractions
- 7- Slicing into twelve equal time fractions

8- Slicing into twelve equal area fractions

9- Slicing into three slices of 30, 40, and 30% of total area but taking each source average area separately.

As mentioned in the research methodology chapter (section 3.6), one sample from each group of the collected samples was selected at random for model verification. The collected samples were grouped into eight categories according to source and modification. The eight categories were as follows:

- 1- neat samples produced from the Ras Tanura refinery. This included samples from RT1, RT2, RT3, RT4, and RT5;
- 2- neat Riyadh refinery samples (RY1 and RY5);
- 3- neat Bapco refinery (Bahrain) samples (BH1 to BH5);
- 4- neat Al-Ahmadi refinery (Kuwait) samples (KW1 to KW5);
- 5- modified RT samples (RT-CRT-5 to RT-CRT-15 and RT-SBS-3 to RT-SBS-9);
- 6- modified RY samples (6 samples);
- 7- modified BH samples (6 samples); and
- 8- modified KW samples (6 samples).

The AZ sample was added to group number 6 since the sample was originally obtained from the Riyadh refinery and modified with SBS. The selected samples for

model verification were RT3, RY1, BH3, KW5, RT-SBS-3, RY-CRT-10, BH-CRT-15, and KW-SBS-3.

In the produced prediction models, the dependent variables were the rheological or performance-based properties of the AC. Table 5.1 shows a list of these properties. The independent variables were those fractions in which the HP-GPC profiles were fractionated into, and the skewness factors and the standard deviations of the distributions, taking each fractionating procedure separately.

To have a preliminary idea about the relationships between the variables used in models, correlation matrices were obtained. Table 5.2 shows an example of the correlation matrix for the three equal time fractions. Correlation coefficients provide a normalized and scale-free measure of the association between two variables. A positive correlation coefficient indicates that the variables vary in the same direction, while a negative coefficient indicates that the variables vary in the opposite direction. Statistically independent variables have an expected correlation coefficient of zero. Tables E-1 to E-7 in Appendix E show the correlation matrices for all the other fractionating procedures.

The modeling effort involved 225 equations (25 dependent variables times 9 fractions). Therefore, as an initial trial, the stepwise regression method was used to find which fractionating method produced better models. The criterion which was used for this was R^2 of the regression, which was the percent of variance in the dependent variable

Table 5.1: Used properties and indices.

Group	Used symbol	Property
Rheological Properties	PEN25	Penetration at 25°C, dmm
	PEN4	Penetration at 4°C, dmm
	SP	Softening Point, °C
	FP	Flash Point, °C
	VIS60	Viscosity at 60°C, Poise
	RV135	Rotational Viscosity at 135°C, cPa.s
	VIS135	Viscosity at 135°C, cSt
Heat Hardening	RP25	Retained Penetration at 25°C
	RP4	Retained Penetration at 4°C
	VR60	Viscosity Ratio at 60°C
	VR135	Viscosity Ratio at 135°C
Temp. Susc.	PI	Penetration Index
	PR	Penetration Ratio
	PVN	Penetration Viscosity Number
	VTs	Viscosity Temperature Susceptibility
Grading	Lower	Lower grading temp., °C
	Upper	Upper grading temp., °C
LVE Parameters	Gg	Glassy Moduli, GPa
	R	Rheological Index
	ω_0	Crossover Frequency at Td, Hz
	η_0	Steady-State Viscosity at Td, GPa.s
Design Param.	$G^* / \sin \delta$	$G^* / \sin \delta$ @ 64°C, MPa
	$G^* \times \sin \delta$	$G^* \times \sin \delta$ @ 25°C, MPa
	S	Creep Stiffness at 60Hz @ 0°C, MPa
	m	Creep Rate @ 0°C

Table 5.2: Correlation matrix - using three equal times fractions.

Partition	1st	2nd	3rd	Skew Factor	Standard Deviation
Corr. time	27.33	32.67	38.00		
PEN25	-0.6*	0.0	0.5*	-0.6*	0.5*
PEN4	0.8*	0.0	-0.4	0.2	-0.8*
SP (°C)	0.6*	0.0	-0.5*	0.5*	-0.6*
FP (°C)	-0.2	0.3	0.0	0.1	0.2
VIS60 (Poise)	0.0	-0.3	0.2	-0.3	-0.1
RV135 (cPa.s)	0.5*	0.0	-0.4*	0.4*	-0.5*
VIS135 (cSt)	-0.2	-0.1	0.2	-0.1	0.3
RP25	0.7	0.0	-0.4	0.2	-0.7*
RP4	0.2	0.1	-0.2	0.3	-0.2
VR60	0.4	0.2	-0.3	0.2	-0.3
VR135	-0.2	-0.6*	0.5	-0.5*	0.0
PI	0.6*	0.1	-0.4	0.2	-0.6*
PR	0.5	-0.1	-0.2	-0.1	-0.6*
PVN	0.1	0.1	-0.1	0.1	-0.1
VTs	0.3	-0.3	0.0	-0.2	-0.4
Lower grading temp. (°C)	0.3	0.0	-0.2	0.3	-0.3
Upper grading temp. (°C)	0.7*	0.1	-0.6*	0.6*	-0.6*
Gg (Gpa)	0.3	-0.2	-0.2	0.3	-0.3
R	0.5*	0.2	-0.5*	0.5*	-0.5*
ω_0 @ Td (Hz)	0.3	0.0	-0.3	0.4*	-0.3
η_0 @ Td (Gpa-s)	0.1	-0.1	0.0	-0.1	-0.1
$G^* / \sin \delta$ @ 64°C (MPa)	-0.1	0.0	0.1	-0.1	0.1
$G^* \times \sin \delta$ @ 25°C (MPa)	0.3*	0.0	-0.3	0.2	-0.3*
S(60) @ 0°C (MPa)	0.4*	-0.1	-0.3	0.2	-0.4*
m(60) @ 0°C	0.3	0.1	-0.4*	0.4*	-0.3
1st Partition	1.0*	0.0	-0.8*	0.8*	-1.0*
2nd Partition		1.0*	-0.5*	0.5*	0.2
3rd Partition			1.0*	-0.9*	0.7*
Skew Factor				1.0*	-0.6*
Standard Deviation					1.0*

* Significantly correlated at 5% level.

explained by the model. Once the best fractionating method was selected, a further effort was made for fine tuning the models. The criteria for including any factor in the regression model was set to be 1.0, i.e., the variable will be included in the model if it adds to the significance level of F-ratio a value of 1.0 or greater. After the addition of each factor, starting with the one that contributed the most to the F-value, the contribution of each factor to the F-value of the model was recalculated. If the value of the contribution for any of the included factors dropped under 1.0, it was dropped from the model. The selection procedure continued until the contribution of all factors inside the model was greater than or equal to one and the contribution of the factors not included in the model was less than 1.0.

Table 5.3 gives a list of the values of R^2 obtained from the stepwise regression for the different models using the different fractionating procedures. The average values of R^2 in addition to their standard deviations are included in the table. It can be seen from the table that there was an increase in the average value of R^2 . The number of fractions increased. A large increase in the average value of R^2 was obtained for three to eight fractions and a moderate increase occurred from eight to twelve fractions. Equal time fractions gave better results than equal area fractions. Average R^2 value increased from 0.24 when using three equal time fractions to 0.59 when using twelve equal time fractions, indicating that the increase in the number of fractions will add to the degree of explanation of the model. It should also be noted

Table 5.3: R-square of the different models using stepwise regression.

Property	HP-GPC Fractioning Procedure								
	3 equal times	3 equal areas	3 times (25,50,25%)	3 areas (25,50,25%)	8 equal times	8 equal areas	12 equal times	12 equal areas	3 relative areas
PEN25	0.5055	0.3586	0.3818	0.3618	0.5344	0.6066	0.5627	0.6084	0.7536
PEN4	0.7127	0.7256	0.6964	0.7605	0.8667	0.7708	0.8470	0.7967	0.0000
SP (°C)	0.3578	0.2992	0.4475	0.3069	0.7790	0.5691	0.8416	0.6221	0.4061
FP (°C)	0.1491	0.3787	0.0853	0.5274	0.4769	0.7104	0.6156	0.7223	0.1222
VIS60 (Poise)	0.1969	0.1514	0.0825	0.1766	0.4449	0.9041	0.5953	0.9186	0.7544
RV135 (cPa.s)	0.2092	0.1956	0.2471	0.1876	0.6849	0.7014	0.6704	0.7564	0.2651
VIS135 (cSt)	0.0651	0.1640	0.1232	0.1776	0.5722	0.5261	0.8305	0.5507	0.0000
RP25	0.5473	0.5134	0.7601	0.8052	0.9008	0.8951	0.8852	0.9006	0.0966
RP4	0.1900	0.2269	0.0975	0.0746	0.2767	0.6130	0.2792	0.4559	0.3550
VR60	0.1386	0.2926	0.1218	0.1687	0.1442	0.1443	0.4255	0.2168	0.0000
VR135	0.3409	0.4215	0.3675	0.4318	0.3487	0.5482	0.3136	0.6189	0.0000
PI	0.3580	0.5720	0.2467	0.5732	0.6898	0.8206	0.7035	0.7607	0.1084
PR	0.4255	0.4373	0.2036	0.4279	0.7232	0.6277	0.7808	0.7611	0.7933
PVN	0.0000	0.2616	0.0000	0.1093	0.7787	0.7818	0.7049	0.8234	0.0000
VTS	0.2300	0.1860	0.4115	0.0000	0.4771	0.5583	0.5955	0.6000	0.1036
Lower grading temp. (°C)	0.0852	0.2368	0.1087	0.1555	0.5364	0.3588	0.6497	0.4769	0.4298
Upper grading temp. (°C)	0.4420	0.4281	0.4842	0.4185	0.7111	0.6947	0.7155	0.6391	0.6013
Gg (Gpa)	0.0673	0.2763	0.0000	0.3570	0.8235	0.1310	0.9784	0.2270	0.6982
R	0.2705	0.2898	0.3000	0.3569	0.6708	0.2548	0.6923	0.3722	0.4878
ω_0 @ Td (Hz)	0.2275	0.1571	0.1131	0.1392	0.1715	0.1680	0.2570	0.1617	0.1454
η_c @ Td (Gpa.s)	0.0000	0.1217	0.0000	0.2152	0.2694	0.3459	0.3549	0.2074	0.0530
$G^* / \sin \delta$ @ 64°C (MPa)	0.0000	0.0522	0.0000	0.0389	0.0336	0.0494	0.3775	0.1127	0.1601
$G^* \times \sin \delta$ @ 25°C (MPa)	0.1214	0.0972	0.1403	0.1058	0.1382	0.1176	0.3207	0.1533	0.0000
S(60) @ 0°C (MPa)	0.1506	0.1072	0.1737	0.1210	0.2735	0.1737	0.3554	0.3190	0.0000
m(60) @ 0°C	0.1692	0.1344	0.1243	0.1176	0.4341	0.5372	0.5037	0.7281	0.2806
Average	0.2384	0.2834	0.2287	0.2846	0.5104	0.5123	0.5943	0.5404	0.2646
Standard Deviation	0.1838	0.1645	0.2079	0.2149	0.2519	0.2716	0.2113	0.2533	0.2757

that R^2 increases as the number of independent variables increase. Therefore, part of the increase in R^2 is due to the increasing number of independent variables and not necessarily the improvement in the explanatory power of the models. To have a complete idea about the increase in the value of R^2 with the increase in the number of fractions, an additional fractionating procedure of five equal times was tried. The R^2 results of the regression analysis are shown in Table 5.4. Fig. 5.1 shows the increase in the value of average R^2 with the increase in the number of fractions. It is noticed from the figure that the rate of increase in R^2 with the increase in the number of fractions was high, but this rate decreased gradually with the increase in the number of fractions. Therefore, it was decided that twelve fractions of equal times would be used in the modeling work for the rest of this study. Increasing the number of fractions more than twelve was not feasible because a large number of samples would have been needed for model development and there would have been other problems such as multicollinearity as explained below.

Asphalt properties are known to be affected by the aging of the asphalt cement, since RTFO residue represents the asphalt after being heated, mixed, and compacted, which is the case with the AC in the field. It was believed that using the HP-GPC produced profiles for the RTFO residue in the prediction models would give better determination coefficients. The produced profiles for the RTFO residue of the different asphalt samples were partitioned into twelve fractions. Stepwise regression

Table 5.4: R-square of the different models for the extra suggested fractions .

Property	HP-GPC Fractioning Procedure	
	12 equal times (RTFO Residue)	5 equal times
PEN25	0.6676	0.6581
PEN4	0.8739	0.7661
SP (°C)	0.9232	0.7875
FP (°C)	0.7119	0.3814
VIS60 (Poise)	0.7214	0.7312
RV135 (cPa.s)	0.4273	0.3775
VIS135 (cSt)	0.8647	0.6529
RP25	0.8459	0.8885
RP4	0.6874	0.3005
VR60	0.4306	0.1521
VR135	0.7159	0.3973
PI	0.8138	0.6520
PR	0.7882	0.3197
PVN	0.7741	0.6928
VTS	0.7014	0.4102
Lower grading temp. (°C)	0.3285	0.3847
Upper grading temp. (°C)	0.8693	0.6855
Gg (Gpa)	0.9427	0.8919
R	0.5816	0.2791
ω_0 @ Td (Hz)	0.1807	0.1325
η_0 @ Td (Gpa.s)	0.5001	0.0000
$G^* / \sin \delta$ @ 64°C (MPa)	0.0000	0.0000
$G^* \times \sin \delta$ @ 25°C (MPa)	0.3961	0.3568
S(60) @ 0°C (MPa)	0.4650	0.3949
m(60) @ 0°C	0.5848	0.4052
Average	0.6318	0.4679
Standard Deviation	0.2405	0.2588

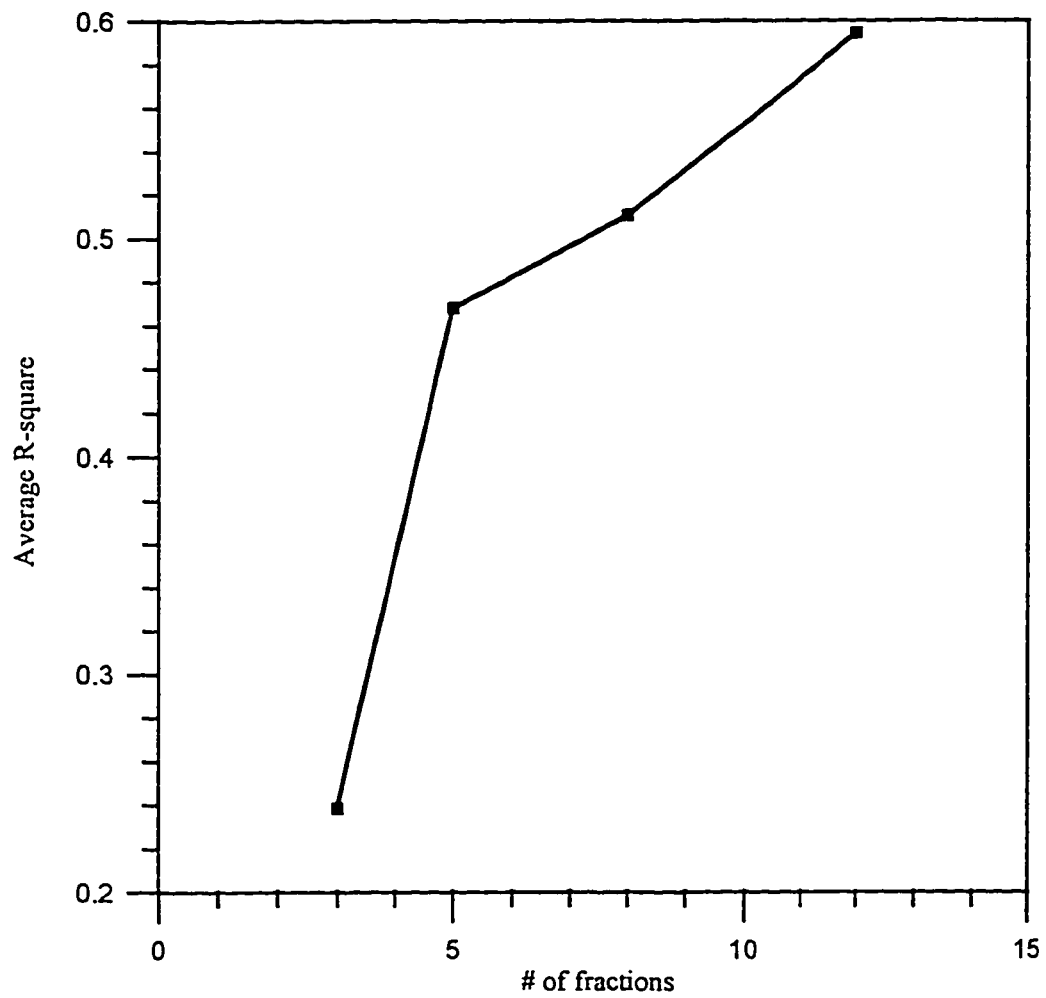


Figure 5.1: Change of R-square value with the change of number of fractions.

was used to produce models for all the prediction parameters. R^2 for all produced models are shown in Table 5.4. The average R^2 value was 0.63, which clearly shows an increase in the average value of R^2 when using RTFO chromatograms. Therefore, twelve fractions of equal time for the RTFO residue were used in model generation.

After selecting twelve fractions with equal times for modeling based on average R^2 , further efforts were made to improve the fit. First, the possibility of improving the fit through transformations was investigated. To do this, the relations between the dependent variables (DV) and the independent variables (IV) were drawn. The shapes of these graphs were studied to check if the relation was linear. If they were not linear, some sort of mathematical transformation for either the DV or the IV or both was performed to linearize them. Required transformations were made, and the models were rebuilt. Table 5.5 shows the transformed models with their R^2 and significance levels. In these models, “XI’s” represent the fraction number, “skew” represents the measured skewness factor between the different fractions, and “STDEV” represents the standard deviation of the twelve fractions. R^2 represents the coefficient of determination, which gives the amount of variability in the DV explained by the suggested model. All R^2 values for all the models were found to be over 0.5 except for VR60 (viscosity ratio at 60°C), which is not a fundamental property of asphalt and is only an indicator variable. All suggested models had a confidence level greater than 98%. Table 5.6 gives the model fitting

Table 5.5: Generated models for the different parameters.

Property	Suggested Model	R ²	SIG. LEVEL
PEN25	$PEN25 = (-8.338 - 1.059 X_2 + 1.396 X_3 - 1.337 X_4 + 1.283 X_5 + 0.622 X_9)^2$	0.7268	0.0000
PEN4	$PEN4 = -11.218 + 7.875 X_2 + 3.277 X_5 + 0.551 X_{11}$	0.8739	0.0000
SP (°C)	$SP = 51.379 + 15.377 X_1$	0.9232	0.0000
FP (°C)	$FP = -1530.538 + 45.734 X_1 + 40.798 X_2 + 86.306 X_4 - 66.539 X_5 + 65.555 X_6 - 28.154 X_7 + 12.160 X_8 - 14.572 X_{10} + 19.367 X_{11} + 55.547 X_{12} + 183.819 STDEV$	0.9316	0.0000
VIS60 (Poise)	$VIS60 = -5.941E04 + 1261.669 X_4 + 2655.203 X_5 - 915.448 X_7 + 1945.649 X_8 + 1792.497 X_{12}$	0.7214	0.0078
RV135 (cPa.s)	$RV135 = EXP (69.804 - 1.129 X_1 - 1.789 X_3 - 2.039 X_5 + 0.327 X_6 - 0.409 X_9 + 0.305 X_{10} - 0.528 X_{11} - 1.284 X_{12} - 5.217 STDEV)$	0.9268	0.0000
VIS135 (cSt)	$VIS135 = 7100.710 + 3542.734 X_1 - 385.749 X_2 - 321.343 X_5 - 96.242 X_8 - 109.289 X_{10} - 133.739 X_{12} - 661.481 SKEW$	0.8647	0.0027
RP25	$RP25 = 0.605 + 0.150 X_2 + 0.018 X_{12} + 0.232 SKEW$	0.8459	0.0000
RP4	$RP4 = -7.911 - 3.750 X_1 + 0.253 X_3 + 0.365 X_6 + 0.375 X_{10} + 1.125 SKEW$	0.6874	0.0139
VR60	$VR60 = 0.764 + 28.752 X_1 - 0.412 X_2 + 0.120 X_6$	0.4306	0.0555
VR135	$VR135 = -5.097 + 4.381 X_1 + 0.139 X_3 + 0.214 X_7 + 0.224 X_{10} + 0.109 X_{12}$	0.7159	0.0086
PI	$PI = -1.820 - 15.438 X_1 + 0.347 X_4 - 0.103 X_9 + 0.035 X_{11}$	0.8138	0.0002
PR	$PR = -925.416 + 649.389 X_1 - 6.484 X_3 + 34.848 X_4 + 35.469 X_8 + 27.232 X_{12} - 125.971 SKEW$	0.7883	0.0061
PVN	$PVN = -3.480 + 0.377 X_5 - 0.120 X_6 + 0.046 X_9$	0.7741	0.0002
VTS	$VTS = 4.407 - 0.241 X_2 + 0.169 X_3 - 0.129 X_4 - 0.023 X_9$	0.7014	0.0037

Table 5.5: Continued.

Property	Suggested Model	R ²	SIG. LEVEL
Lower grading temp. (°C)	(LOWER) = 1 / (- 0.191 - 0.017 X1 + 0.005 X4 + 0.014 X6 - 0.004 X8 + 0.012 X10 - 0.018 STDEV + 0.090 SKEW)	0.6926	0.0000
Upper grading temp. (°C)	UPPER = (23.419 - 0.309 X3 - 0.595 X5 - 0.216 X9 - 0.350 X12 - 0.679 STDEV - 0.741 SKEW) ²	0.8802	0.0000
Gg (Gpa)	Gg = 126.506 - 1.330 X3 - 4.113 X5 - 6.817 X6 + 2.719 X7 - 1.125 X8 - 1.954 X9 - 22.904 SKEW	0.9427	0.0000
R	R = EXP (5.698 - 0.339 X5 - 0.057 X9 - 0.163 X12 - 0.793 SKEW)	0.7156	0.0000
ω_0 @ Td (Hz)	$\omega_0 = 1 / (1.335E08 - 4.047E07 X2 + 3.531E07 X3 - 1.404E07 X4 - 1.373E07 X8 + 2.301E07 STDEV + 7.085E07 SKEW)$	0.5432	0.0007
η_0 @ Td (Gpa-s)	$\eta_0 = 5.044E07 - 3.615E07 X2 + 3.111E07 X3 - 1.533E07 X4 + 1.599E07 SKEW$	0.5001	0.0003
G* / sin δ @ 64°C (MPa)	G* / sin δ = EXP (51.210 - 1.615 X2 + 2.434 X3 - 6.698 X4 + 9.953 X5 - 6.422 X6 - 1.008 X9 - 2.604 X11)	0.6367	0.0001
G* x sin δ @ 25°C (MPa)	G* X sin δ = EXP (- 176.868 + 2.994 X2 + 1.460 X3 + 9.338 X5 + 2.254 X8 + 3.076 X10 + 3.010 X12 + 15.321 SKEW)	0.6367	0.0001
S(60) @ 0°C (MPa)	S = 1 / (- 7.435E08 + 2.131E07 X1 + 3.354E07 X2 + 3.210E07 X8 + 1.374E07 X9 - 8.334E06 X10 + 1.191E07 X12 - 2.244E08 SKEW)	0.7788	0.0000
m(60) @ 0°C	m = 1 / (4.785 - 0.155 X2 - 0.100 X7 - 0.091 X8 + 0.263 X9 - 0.319 X10)	0.5962	0.0000

Table 5.6: Model fitting results and analysis of variance for the prediction of the upper grading limit model.

Model fitting results for: (UPPER) ^{1/2}					
Independent variable	coefficient	std. error	t-value	sig.level	
CONSTANT	23.418924	1.711578	13.6826	0.0000	
R-3/12	-0.309291	0.050817	-6.0863	0.0000	
R-5/12	-0.594722	0.116338	-5.1120	0.0000	
R-9/12	-0.215934	0.052514	-4.1119	0.0003	
R-12/12	-0.350226	0.064739	-5.4098	0.0000	
STANDARD DEV.	-0.679037	0.155798	-4.3584	0.0001	
SKEW	-0.741092	0.277232	-2.6732	0.0120	
R-SQ. (ADJ.) = 0.8563 SE= 0.165225 MAE= 0.112406 DurbWat= 1.720					
37 observations fitted, forecast(s) computed for 0 missing val. of dep. var.					
Analysis of Variance for the Full Regression					
Source	Sum of Squares	DF	Mean Square	F-Ratio	P-value
Model	6.01879	6	1.00313	36.7455	0.0000
Error	0.818982	30	0.0272994		
Total (Corr.)	6.83777	36			
R-squared = 0.880227 Std. error of est. = 0.165225					
R-squared (Adj. for d.f.) = 0.856272 Durbin-Watson statistic = 1.71955					

results and the analysis of variance for predicting the upper performance grading limit. In the model fitting results, the coefficient of all introduced variables in the model are given, in addition to their t-value statistics and significance levels. It is worth noting that all of the used parameters are confidence at a level of 98.8%. It is also observed that when fitting the models, there was a transformation in the DV where the square root of the upper grading temperature was used. In the analysis of variance table, the confidence level of the fitted model is 99.99%, and the R^2 for that model is 88%. The model fitting results and the analysis of variance tables for the rest of the prediction parameters are given in Appendix E.

Fig. 5.2 gives a plot of the predicted values versus the measured values for the upper grading temperature. The figure shows the distribution of the points around the 45° line. Data points are shown in steps because the grading temperatures are reported in steps of 6°C. Similar figures for the other prediction parameters are given in Appendix E. In those figures, all the points were located around the forty five degree line with some disturbance, since not all models had high R^2 values.

5.2 TESTING OF MODELS

5.2.1 Sign Testing

The sign test was performed to check if the parameter signs in the developed models were according to the ones set in the a priori hypothesis; however, it was

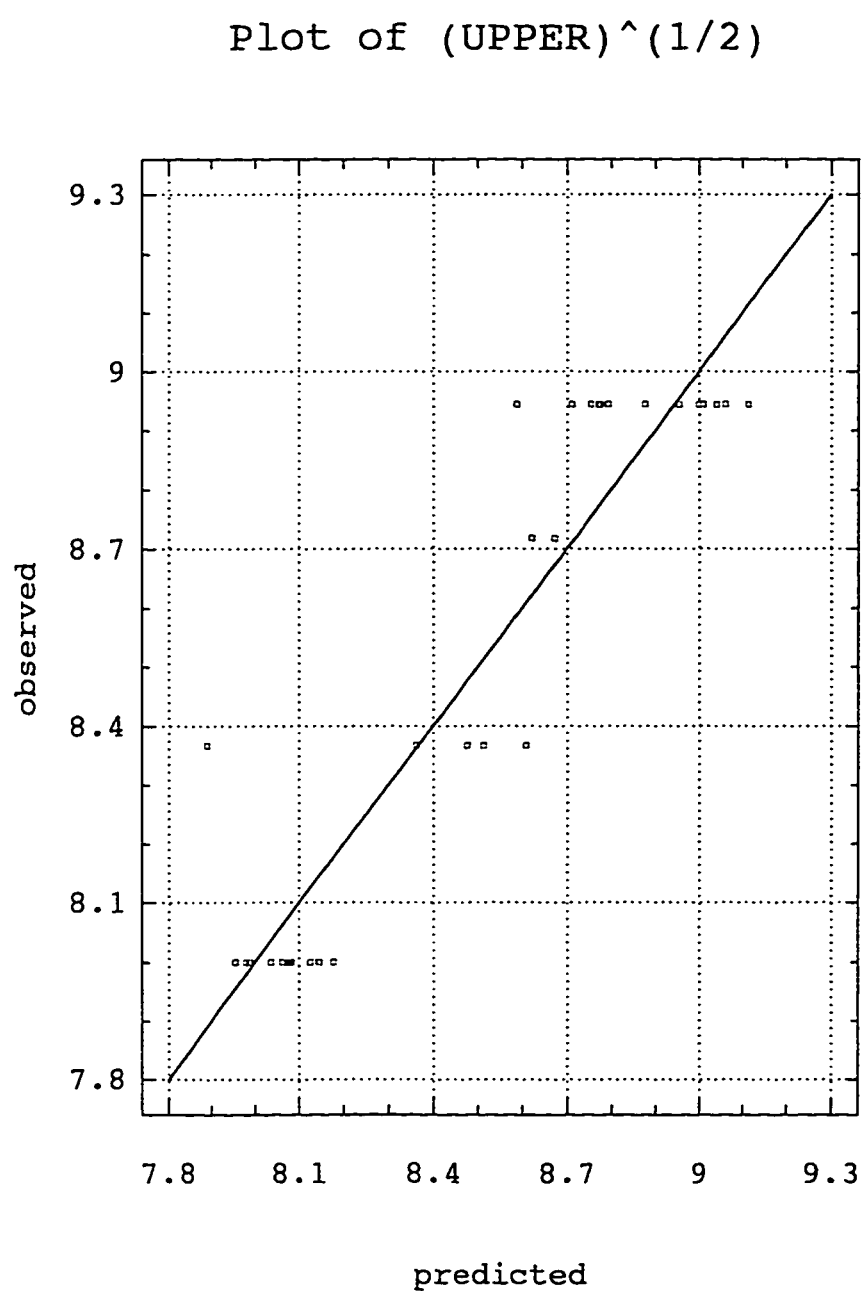


Figure 5.2: Plot of predicted values versus the measured ones for the prediction of the upper grading limit model.

difficult to detect this because quite a number of variables were used in the models and there were some sort of intercorrelations between those variables. In addition to that, there were no clear cut off points between LMS, MMS, and SMS, especially when using twelve fractions. Some of the general observations about the used signs in the developed models follow:

- X2, which represents part of LMS, is negatively related to PEN25,
- X1, which represents part of LMS, is positively related to SP,
- PI is negatively related to LMS (X1)
- Used parameters in the upper grading temperature model are not used in the lower grading temperature model.

The above mentioned observations are all according to the set a priori hypothesis.

5.2.2 Homoscedasticity Testing

One of the main assumptions that must be satisfied when using the ordinary least square method is that errors have constant variance. This implies that there should be a scatter of errors around all points of the independent variables. This assumption is called homoscedasticity. To check for homoscedasticity of the used variables, plots of predicted values of DV against residuals (difference between measured and predicted values) will reveal any violation of this assumption (Ergun, 1985). The plot of predicted values versus residuals of estimation of upper grading

temperature is shown in Fig. 5.3. Figures for the other parameters are shown in Appendix E. From Fig. 5.3 it is noticed that although there is one outlier, which has shifted the zero residuals line up, for the most part it can be said that the homoscedasticity conditions were met for the model of the upper grading temperature. The same can be said about the plots which are shown in Appendix E for the predicted values versus residuals of the other models.

5.2.3 Normality Testing

In multiple regression, normality is part of significance testing. Normal probability plots were drawn for the residual to ensure that the errors were normally distributed. Fig. 5.4 is the normal probability plot for the residuals of the upper grading limit model. From visual inspection of this line it appears that it is, to a certain extent, linear. Therefore the normality assumption of the error is met for the upper grading model. Normality plots for the other models are given in Appendix E. It is noticed from these figures that the normality assumption of the error is met for all the models.

5.2.4 Autocorrelation Testing

One of the fundamental assumptions of linear regression is that the error terms (ϵ_i) are uncorrelated (Montgomery and Peck, 1982). The Durbin-Watson test can be used in detecting autocorrelation. The value of the Durbin-Watson statistic (d) is

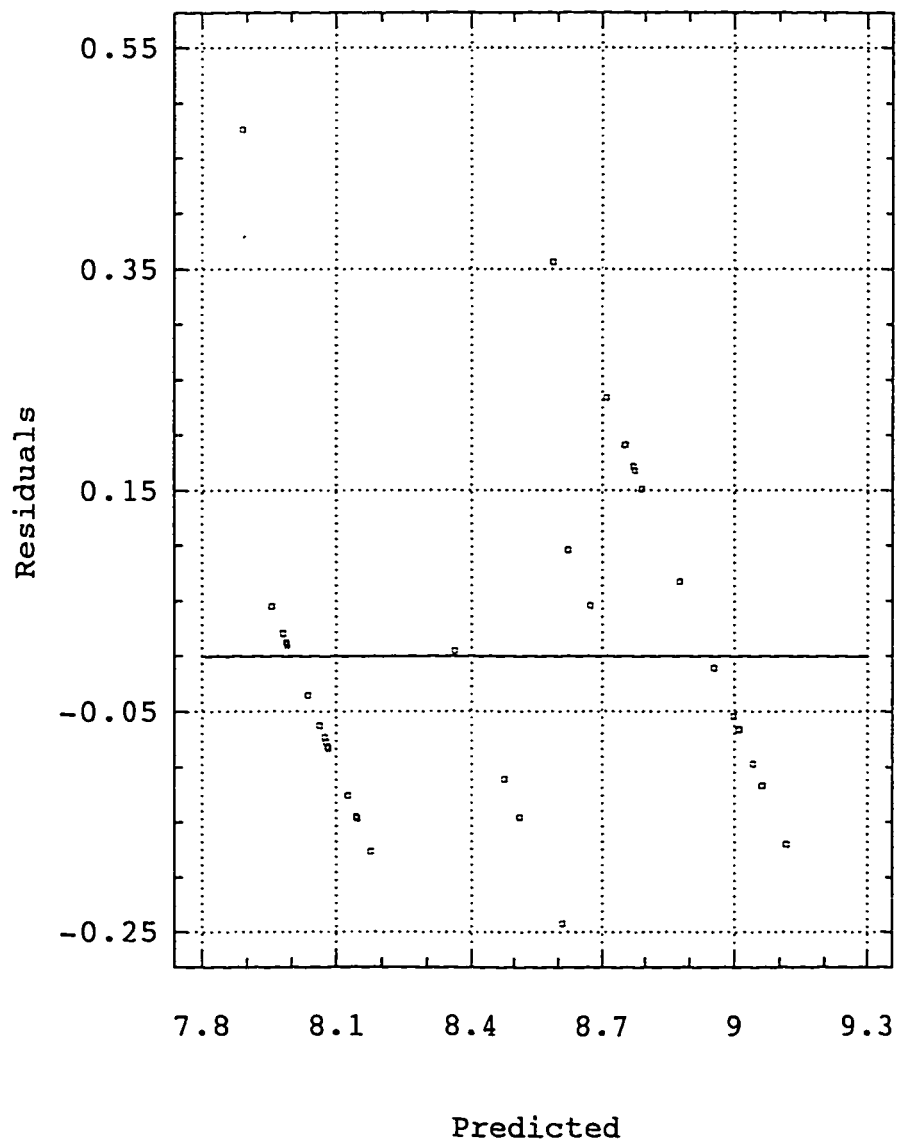
Residual Plot for $(UPPER)^{(1/2)}$ 

Figure 5.3: Plot of predicted values versus residuals for prediction of the upper grading limit model.

Norm. Prob. Plot for $(UPPER)^{1/2}$

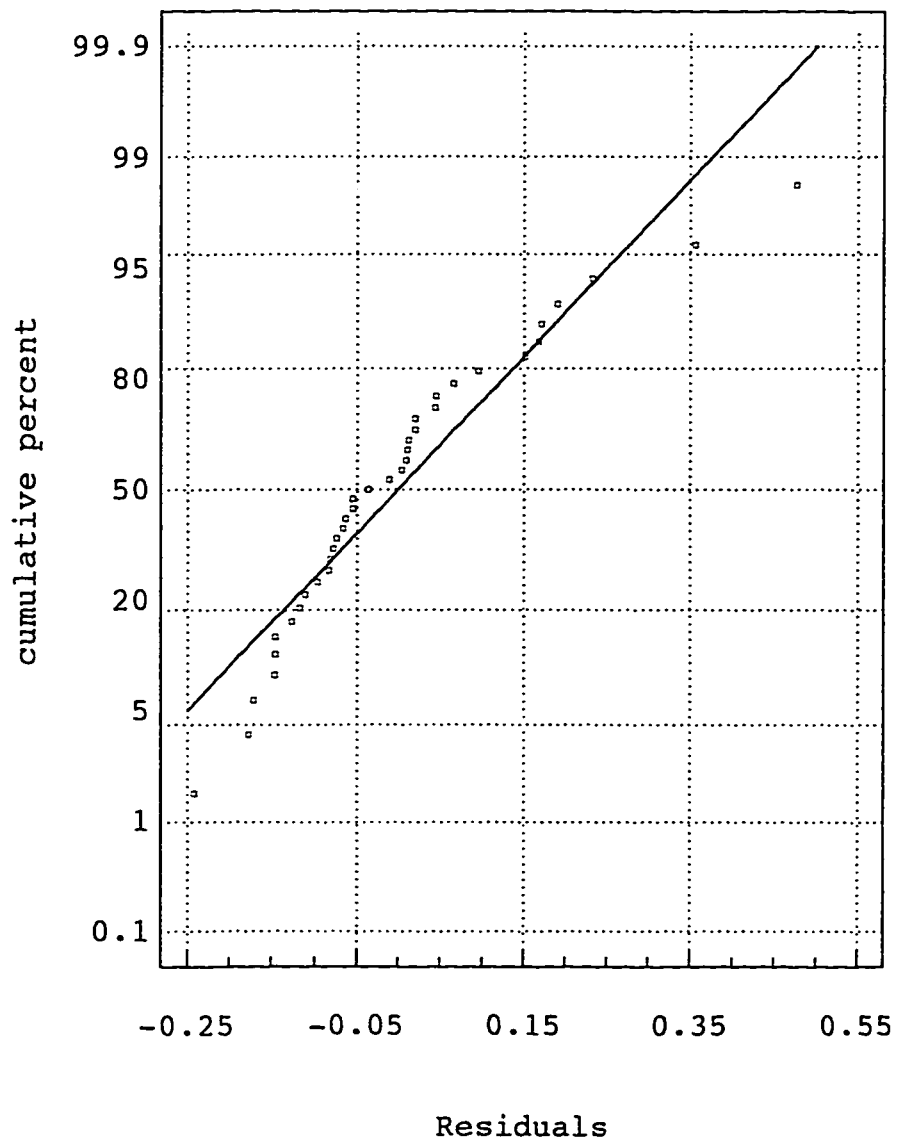


Figure 5.4: Normal probability plot for the residuals of the upper grading limit model.

given in the analysis of variance computer output. Table 5.7 shows the value of Durbin-Watson statistics in addition to lower and upper limits (d_L & d_U) on the value of (d) at the 5% significant level. A small d value indicates a positive autocorrelation, while a large d value indicates a negative autocorrelation. While a value in between is for random series (Ergun, 1985). The limits of the d value follow:

- if $d < d_L$ reject the null hypothesis of non-autocorrelated u 's
 in favor of the hypothesis of positive autocorrelation,
- if $d > d_U$ do not reject the null hypothesis,
- if $d_L < d < d_U$ the test is inconclusive.

In the case of $d > 2$, the test is for negative autocorrelation. In this case, $4-d$ was calculated and the same criteria of positive autocorrelation was used. Results show that for all the models at both significance levels either the test is inconclusive or that we don't reject the null hypothesis of non-autocorrelated errors. Hence, autocorrelation does not seem to be a problem.

5.2.5 Multicollinearity and Singularity Testing

Two other threats to regression are multicollinearity and singularity. Multicollinearity occurs when two variables in the correlation matrix are perfectly (or near perfectly) correlated when they show a similar pattern of correlation with other variables. Singularity occurs when one of the IV's is a linear combination of others

Table 5.7: Durbin-Watson test for autocorrelation.

Property	$\alpha = 0.05$		$\alpha = 0.01$		# Variables	# Samples	d(+ve)	d(-ve)	Ho (.05)	Ho (.01)
	d_L	d_U	d_L	d_U						
PEN25	1.19	1.8	1	1.59	5	37	2.322	1.678	Inc.*	N.R.**
PEN4	0.9	1.71	0.67	1.43	3	17	1.514	-	Inc.	N.R.
SP (°C)	1.13	1.38	1.22	1.32	1	37	2.280	1.720	N.R.	N.R.
FP (°C)	1.19	1.8	1	1.59	11	37	2.254	1.746	Inc.	N.R.
VIS60 (Parse)	0.67	2.1	0.48	1.85	5	17	2.561	1.439	Inc.	Inc.
RV135 (cPa.s)	1.19	1.8	1	1.59	9	37	2.194	1.806	N.R.	N.R.
VIS135 (cSt)	0.67	2.1	0.48	1.85	7	17	2.050	1.950	Inc.	N.R.
RP25	0.9	1.71	0.67	1.43	3	17	2.222	1.778	N.R.	N.R.
RP4	0.67	2.1	0.48	1.85	5	17	2.164	1.836	Inc.	Inc.
VR60	0.9	1.71	0.67	1.43	3	17	1.645	-	Inc.	N.R.
VR135	0.67	2.1	0.48	1.85	5	17	2.333	1.667	Inc.	Inc.
PI	0.78	1.9	0.57	1.63	4	17	2.985	1.015	Inc.	Inc.
PR	0.67	2.1	0.48	1.85	6	17	2.398	1.602	Inc.	Inc.
PVN	0.9	1.71	0.67	1.43	3	17	2.464	1.536	Inc.	N.R.
VTS	0.78	1.9	0.57	1.63	4	17	2.522	1.478	Inc.	Inc.
Lower grading temp. (°C)	1.19	1.8	1	1.59	7	37	2.515	1.485	Inc.	Inc.
Upper grading temp. (°C)	1.19	1.8	1	1.59	6	37	1.720	-	Inc.	N.R.
Gg (Gpa)	0.71	2.06	0.52	1.8	7	18	2.555	1.445	Inc.	Inc.
R	1.22	1.73	1.03	1.51	4	35	1.955	-	N.R.	N.R.
ω_1 @ Td (Hz)	1.19	1.8	1	1.59	6	35	1.449	-	Inc.	Inc.
n_0 @ Td (Gpa.s)	1.22	1.73	1.03	1.51	4	35	1.576	-	Inc.	N.R.
$G^* / \sin \delta$ @ 64°C (MPa)	1.19	1.8	1	1.59	7	35	2.171	1.829	N.R.	N.R.
$G^* \times \sin \delta$ @ 25°C (MPa)	1.19	1.8	1	1.59	7	35	2.085	1.935	N.R.	N.R.
S(60) @ 0°C (MPa)	1.19	1.8	1	1.59	7	35	2.101	1.899	N.R.	N.R.
m(60) @ 0°C	1.19	1.8	1	1.59	5	35	1.862	-	N.R.	N.R.

* Inc. = Hypotheses test is inconclusive.

** N.R. = Don't reject Ho

(Ergun, 1985). Usually using stepwise regression will take care of these threats, since it drops the variables that are explained by other variables. As an extra check against multicollinearity, the variance inflation factor (VIF) is usually used.

$$VIF = C_{jj} = (1 - R_j^2)^{-1} \quad (5.1)$$

where

VIF = variance inflation factor;

C_{jj} = the j 'th diagonal element of the matrix $C = (X'X)^{-1}$; and

R_j^2 = the coefficient of determination obtained when X_j is regressed on the remaining $(j-1)$ regressors.

If X_j is nearly orthogonal to the remaining regressors, R_j^2 is small and C_{jj} is close to unity, while if X_j is nearly linearly dependent on some subset of the remaining regressors, R_j^2 is near unity and C_{jj} is large. VIF was calculated for the IV's which were used in the models for predicting the upper and lower asphalt grading temperatures. A value of VIF greater than 10 might be an indication of multicollinearity between the IV's. For the upper grading temperature, VIF for all the IV were less than 10 except for the standard deviation factor, where its VIF value was 16, which is not considered far from 10. In the model for lower grading temperature, VIF values were higher than those for upper grading temperature and VIF values

reached 50. It was decided to try to decrease the values of VIF by either dropping some of the correlated variables, combining related variables, and/or using some sort of transformation to those variables. All efforts were unsuccessful because the model was very sensitive and any change in the factors led to a drastic drop in the value of R^2 . Another procedure was tried, which was to use eight fractions instead of twelve because it was thought that this would take care of combining some variables that were thought to be intercorrelated. Although the value of R^2 dropped from 0.70 to 0.60, this process was also unsuccessful because the VIF test was performed on the IV's which were used in the new model and results showed high values of VIF. No combining, dropping, or transformation procedure was capable of reducing their values. Therefore it was decided to stick to the models presented in Table 5.5 but check the suitability of the models in predicting the dependent variables through the validation samples.

5.3 MODEL VALIDATION

As stated previously, one sample was selected randomly from each group of samples totaling eight samples. Four of these samples were polymer modified samples and four were non-modified samples. Unfortunately, not all the rheological tests were applicable to polymer modified samples. Therefore, for these tests, the total number of samples available for model validation was 4. In addition to that,

even for the tests with eight validation samples, the number of variables in the suggested models reached eleven variables, which did not give the ability to make solid statistical validation tests. Montgomery and Peck (1982) have suggested a procedure to test for validation testing by fitting the validation data for the developed models and calculating the coefficient of determination (R^2) for the newly fitted data then comparing this value with the R^2 of the model with the original data. This test was performed for the developed models. Results of this test are shown in Table 5.8. Since there are a small number of samples to account for the errors (i.e. not enough degrees of freedom for the error), the test was very sensitive and availability of any outlier gave erroneous results. Therefore, for some samples, the sum of squares for error was even higher than the total sum of square of the model. For these cases, the test was marked not applicable (N.A.) For the rest of the properties, the test gave acceptable results. The values of R^2 were higher than 0.6 (except for the steady-state viscosity model, where the value of R^2 was 0.13), which supports the validity of the majority of models. The few models that were not validated may need to be checked by new data in future research.

It was decided to visually check the ability of the models to predict the dependent variables using the verification samples. Table 5.9 shows the prediction of the generated models for the performance grades of the validation data. Out of the eight validation samples, the upper and lower temperature grading models were used

Table 5.8: Validation of generated models for the different parameters.

Property	R ² (Model)	# Samples (Model)	# Samples (Valid.)	SSE (Valid.)	Syy (Valid.)	R ² (Valid.)
PEN25	0.73	37	8	692.70	305.89	N.A.*
PEN4	0.87	17	4	16.16	2473.24	0.99
SP (°C)	0.92	37	8	361.93	324.19	N.A.
FP (°C)	0.93	37	8	1051	97206	0.99
VIS60 (Poise)	0.72	17	4	333426	38922590	0.99
RV135 (cPa.s)	0.93	37	8	4967947	19241221	0.74
VIS135 (cSt)	0.86	17	4	22240	943440	0.98
RP25	0.85	17	4	0.02	2.30	0.99
RP4	0.69	17	4	0.02	2.62	0.99
VR60	0.43	17	4	1.35	12.08	0.89
VR135	0.72	17	4	0.04	6.62	0.99
PI	0.81	17	4	1.12	5.44	0.79
PR	0.79	17	4	412.48	8666.76	0.95
PVN	0.77	17	4	0.04	1.80	0.98
VTS*	0.70	17	4	0.01	49.23	1.00
Lower grading temp. (°C)	0.69	37	8	40.02	31.50	N.A.
Upper grading temp. (°C)	0.88	37	8	42.27	350.00	0.88
Gg (Gpa)	0.94	18	4	7.98	20.58	0.61
R	0.72	35	7	1.00	10.90	0.91
ω_0 @ Td (Hz)	0.54	35	7	1.34E-11	6.98E-12	N.A.
η_0 @ Td (Gpa.s)	0.50	35	7	8.32E+14	9.59E+14	0.13
G' / sin δ @ 64°C (MPa)	0.64	35	7	2.49	0.06	N.A.
G' x sin δ @ 25°C (MPa)	0.64	35	7	2675	1862	N.A.
S(60) @ 0°C (MPa)	0.78	35	7	378772	306545	N.A.
m(60) @ 0°C	0.60	35	7	0.01	0.21	0.97

* Not applicable.

Table 5.9: Prediction of the generated models for the performance grades of the validation samples.

Sample	Performance Grade (measured)	Upper Temperature (predicted)	Lower Temperature (predicted)	Performance Grade (predicted)
RT3	PG 64 - 22	66.24	-21.26	PG 64 - 22
RY1	PG 64 - 22	62.46	-19.65	PG 64 - 22
BH3	PG 64 - 22	63.84	-19.94	PG 64 - 22
KW5	PG 64 - 22	65.19	-20.80	PG 64 - 22
RT-SBS-3-F	PG 76 - 22	80.83	-17.08	PG 80 - 16
RY-CRT-10-F	PG 76 - 22	73.94	-21.31	PG 76 - 22
BH-CRT-15-F	PG 80 - 28	79.51	-26.81	PG 80 - 28
KW-SBS-3-F	PG 76 - 22	73.62	-20.52	PG 76 - 22

to predict their grades. Seven samples were graded correctly, while the eighth was wrongly graded. This is an acceptable amount of error since the R^2 for the upper and lower grading models are 0.88 and 0.69.

5.4 SUMMARY

Analysis and discussion of test results and generation of models for the Arabian asphalt's rheological and performance properties using the HP-GPC techniques were presented in this chapter. Inconsistency in the conventional rheological tests results were noticed, which indicates the need for a new set of tests that depends on fundamental properties of asphalt and that can predict the in-service performance of the AC. Performance grading indicated the need for polymer modification for locally produced asphalts. An analysis procedure was suggested to quantify the molecular weight distribution of the asphalts. Finally, models with reasonable reliability and validity were generated for the Arabian asphalt's rheological and performance properties using the HP-GPC techniques.

Chapter 6

CONCLUSIONS AND RECOMMENDATIONS

6.1 CONCLUSIONS

In this study, Arabian neat asphalt samples were collected from the different asphalt producing refineries in the Gulf countries. An additional set of polymer modified samples was included in this study. All collected asphalt samples were subjected to two aging processes to simulate heating, mixing and compaction, and in-service aging. The asphalt samples at the different aging stages were subjected to rheological and performance-based testing. HP-GPC was used to produce profiles of the molecular size distribution of the test samples. Models were built to predict the rheological and performance-based properties from the produced HP-GPC profiles. This study has achieved the set objectives and the following conclusions can be drawn:

1. There were a lot of inconsistencies in the conventional presently used physical testing results and heat hardening and temperature susceptibility indices, which gave conflicting results or indications.
2. SHRP performance-based properties are good indicators of field performance since they depend on fundamental properties of asphalt cement.

3. Mathematical linear visco-elastic models that can be used to predict asphalt performance over a wide range of temperatures, loading times, and stresses or strains were developed for locally produced modified and neat asphalts.
4. HP-GPC produced profiles that were capable of detecting the effects of aging and source on the molecular size distribution of the asphalts.
5. There was an increase in the amount of larger molecular size fractions of the asphalt samples due to aging and polymer modification.
6. Styrene-butadiene-styrene (SBS) was more effective than crumb rubber (CRT) in increasing the relative amounts of larger molecular size fractions, which led to increased stability of the AC.
7. Transformation of the distribution of molecular size seems to be the reason behind the change in the asphalt's physical properties.
8. Slicing the HP-GPC chromatograms into twelve fractions with equal elution times produced the best results for predicting rheological and performance-based properties.
9. Two additional factors proved to be helpful in characterizing the shape of the produced chromatograms. They were skewness and standard deviation of the different sliced fractions.

10. Since RTFO residue represents the AC after being processed, using HP-GPC chromatograms of rolling thin film oven (RTFO) or thin film oven (TFO) residue gives better prediction results than that of fresh samples.
11. Prediction models were generated for the different rheological and performance-based properties from HP-GPC chromatograms. Generated models have reasonable coefficient of determination and high levels of significance. R^2 values of the generated models to predict the lower and upper performance grading temperatures of asphalt were 0.69 and 0.88, respectively.
12. Asphalt producing factories can check with reasonable confidence the suitability of produced asphalts for local environmental and loading conditions using available HP-GPC machines without obtaining SHRP performance test equipment.

6.2 RECOMMENDATIONS

The objective of this study was to produce models that use HP-GPC equipment to predict asphalt performance. Further steps can be taken by others to introduce additional chemical analysis tests. These might include ion exchange chromatography to study the polar-hetroatoms available in the asphalt, which are thought to have high influence on the properties of asphalt. This test was beyond the scope of this study since it needed other equipment and materials, but the results from the HP-GPC study

can be included in such a study to refine developed models and to better understand asphalt behavior. New sets of samples would be required in order to verify and fine tune the produced models.

REFERENCES

- Al-Abdul Wahhab, H.I., Ali, M.F., Asi, I.M. and Al-Dubabe, I.A., "Adaptation of SHRP Performance Based Specifications for Gulf Countries," Progress Report No. 4, KACST Project, Riyadh, 1995.
- American Society for Testing and Materials (ASTM), Annual Book of ASTM Standards, Philadelphia, Pa., 1993.
- Anderson, D.A., Christensen, D.W. and Bahia, H. "Physical Properties of Asphalt Cement and the Development of Performance-Related Specifications," Proc. AAPT, Vol. 60, 1991, pp. 437-475.
- Anderson, D.A., Christensen, D.W., Bahia, H.U., Dongre, R., Sharma, M.G., Antle, C.E, and Button, J., "Binder Characterization and Evaluation, Volume 3: Physical Characterization," SHRP Publication, SHRP-A-369, 1994, pp. 3-122.
- Anderson, G.L., "Modified Binders for Asphalt Airfield Pavements," presented at the 67th Annual Meeting of the TRB, Washington, D.C., 1988.
- Asphalt Institute Research Center, "Background of SHRP Asphalt Binder Test Methods," National Asphalt Training Center Demonstration Project 101, Federal Highway Administration Office of Technology Application, Washington, DC, 1993, pp. 1-79.
- Bahia, H.U. and Anderson, D.A., "Physical Hardening of Asphalt Binders and Relation to Compositional Parameters," Preprints of the 204th American

Chemical Society (ACS) National Meeting, Division of Fuel Chemistry,
Vol. 37, No. 3 and 4. 1992.

Bahia, H.U. and Anderson, D.A., "The New Rheological Properties of Asphalt Binders: Why are They Required and How They Compare to Conventional Properties," Physical Properties of Asphalt Cement Binders, ASTM STP 1241, C. Harden, Ed., American Society for Testing and Materials, 1994.

Barth, R.J., Asphalt Science and Technology, Gordon and Breach Science Publishers, 1984.

Branthaver, J.F., Petersen, J.C., Robertson, R.E., Duvall, J.J., Kim, S.S., Harnsberger, P.M., Mill, T., Ensley, E.K., Barbour, F.A., and Schabron, J.F., "Binder Characterization and Evaluation, Volume 2: Chemistry," SHRP Publication, SHRP-A-368, 1993, pp. 1-76.

Breen, J.J. and Stephens, J.E., "The Interrelationship Between the Glass Transition Temperature and Molecular Characteristics of Asphalt," Proc. AAPT, Vol. 38, 1969, pp. 706-712.

Brule, B., Raymond, G. and Such, C., "Relationship Between Composition, Structure, and Properties of Road Asphalts: State of Research at the French Public Works Central Laboratory," Trans. Res. Rec. 1096, 1986, pp. 22-34.

- Button, J.W., Little, D.N., and Gallaway, B.M., "Influence of Asphalt Temperature Susceptibility on Pavement Construction and Performance," NCHRP Report 268, TRB, 1983.
- Bynom, D. and Traxler, R.N., "Gel Permeation Chromatography Data on Asphalts Before and After Service in Pavements," Proc. AAPT, Vol. 39, 1970, pp. 683-702.
- Corbett, L.W., "Composition of Asphalt Based on Generic Fractionation Using Solvent Deasphalting, Elution-Adsorption Chromatography, and Densimetric Characterization," Analytical Chemistry, Vol. 41, 1969, pp. 576-579.
- Donaldson, G.R., Hlanlinka, M.W., Bullin, J.A., Glover, C.J. and Davison, R.R., "The Use of Toluene as a Carrier Solvent for Gel Permeation Chromatography Analyses of Asphalt," Liquid Chromatography, Vol. 11, 1988, pp. 749-765.
- Epps, J.A., "Paving with Asphalt Cements Produced in the 1980's," NCHRP Report 269, TRB, 1983.
- Ergun, G., "CE 572 Methods of Analysis for Planners," Class Notes, Dept. of Civil Engineering, KFUPM, Dhahran, 1985.
- Garrick, N.W., "Using High Pressure-Gel Permeation Chromatography to Evaluate the Chemical Composition of Blended Asphalts," Unpublished Ph.D. Dissertation, Purdue University, 1986, pp. 6-77.

- Garrick, N.W. and Wood, L.E., "Predicting Asphalt Properties from HP-GPC Profiles," Proc. AAPT, Vol. 57, 1988, pp. 26-40.
- Garrick, N.W. and Biskur, R.R., "A Classification System for Interpreting GPC Profiles of Asphalts," Proc. AAPT, Vol. 59, 1990.
- Girdler, J.P. and Saal, R., "Constitution of Asphaltenes and Related Studies," Proc. AAPT, Vol. 33, 1965.
- Glover, C.J., Davison, R.R., Bullin, J.A., Button, J.W., and Donaldson, G.R., "Chemical Characterization of Asphalt Cement and Performance-Related Properties," TRR 1171, 1988, pp. 71-81.
- Goodrich, J.L. and Dimpfi, L.H., "Performance and Supply Factors to Consider in Paving Asphalt Specifications," Proc. AAPT, Vol. 55, 1986.
- Halstead, W.J., "Relation of Asphalt Chemistry to Physical Properties and Specifications," Proc. AAPT, Vol. 54, 1985.
- Hattingh, M.H., "The Fractionation of Asphalt," Proc. AAPT, Vol. 53, 1984, pp. 197-215.
- Jennings, P.W., "High Pressure Liquid Chromatography as a Method of Measuring Asphalt Composition," Research Report FHWA-MT-7930, Montana Department of Highway, Helena, 1980.
- Jennings, P.W., Pribanic, J.A.S., Dawson, K.R. and Bricca, C.E., "Use of HPLC and NMR Spectroscopy to Characterize Asphaltic Materials," Preprints,

Division of Petroleum Chemistry, American Chemical Society, Vol. 26, 1981, pp. 915-922.

Jennings, P.W., "Uses of High Pressure Liquid Chromatography to Determine the Effects of Various Additives and Fillers on Characteristics of Asphalt," Report FHWA/MT-82/001, Montana Department of Highways, Helena, 1982, 24 pp.

Jennings, P.W. and Pribanic, J.A.S., "The Expanded Montana Asphalt Quality Study Using High Pressure Liquid Chromatography," Research Report FHWA/MT-85/001, Montana Department of Highways, Helena, 1985.

Jennings, P.W., Pribanic, J.A., Dawson, K.R., Smith, J.A. and Koontz, S., "Uses of High Performance Gel Permeation Chromatography for Asphalt Analysis," presented at 64th Annual Meeting of the Transportation Research Board, Washington, D.C., January 1985.

Jennings, P.W., Pribanic, J.A., Smith, J. and Mendes, T.M., "Predicting the Performance of Montana Test Sections by Physical and Chemical Testing," Transp. Res. Rec. 1171, 1988, pp. 59-65.

Kalidindi, S., "Variability in Asphalt Cement Properties based on Source and Time," Engineering Report, Department of Civil Engineering, Clemson University, 1986.

Kulash, D.J., "Towards Performance-Based Specifications for Bitumen and Asphalt Mixtures," Proc., Inst. of Civil Engrs. Transp., 1994, pp. 187-194.

- Kumar, A. and Goetz, W.H., "Asphalt Hardening as Affected by Film Thickness, Voids, and Permeability in Asphaltc Pavements," Proc., Assoc. of Asphalt Pavng Technologists, Vol. 46, 1977, pp. 571-605.
- Majizadeh, K. and Schweyer, H.E., "Viscoelastic Response of Aged Asphalt Cements," Hwy. Res. Rec. 231, National Research Council, Washington, D.C., 1968, pp. 50-61.
- McLeod, N.W., "Relationship of Paving Asphalt Temperature Susceptibility as Measured by PVN to Paving Asphalt Specifications, Asphalt Paving Mixture Design and Asphalt Pavement Performance," Proc. AAPT, Vol. 58, 1989.
- Monismith, C.L., Epps, J.S. and Finn, F.N., "Asphalt Pavements Mixtures: Design, Construction and Performance," Course Notes, Institute of Transportation Studies, University of California, Berkeley, 1985, pp. 1-75.
- Montgomery, D.C. and Peck, E.A., Introduction to Linear Regression Analysis, John Wiley, New York, 1982.
- Noureldin, A.S., "Experimental and Statistical Evaluation and Improvements of Local 60/70 Asphalt Cement," M.Sc. Thesis, Faculty of Engineering, Cairo University, 1982, pp. 191-197.
- Pavlovich, R.D., et al., "Asphalt Fractional Composition: Correlation Between Rosstler and Clay-Gel Components," TRB 1034, 1985.

- Petersen, J.C., Branthaver, J.F., Robertson, , R.E., Harnsberger, P.M., Duvall, J.J. and Ensley, E.K., "Effect of Physicochemical Factors on Asphalt Oxidation Kinetic," Transp. Res. Rec. 1391, National Research Council, Washington, D.C., 1993, pp. 1-10.
- Pfeiffer, J.P. and Saal, R., "Asphaltic Bitumen as Colloid Systems," Journal Physics and Chemistry, Vol. 44, 1940.
- Pfeiffer, J.P. and Van Doormal, P., The Properties of Asphaltic Bitumen, Elsevier Publishing Company, 1950.
- Plancher, H., Dorrence, S.M. and Petersen, J.C., "Identification of Chemical Types in Asphalts Strongly Absorbed at the Asphalt-Aggregate Interface and Their Relative Displacement by Water," Proc. AAPT, Vol. 46, 1977, pp. 151-175.
- Price, R.P. and Burati, Jr., J.L., "Predicting Laboratory Results for Modified Asphalts Using HP-GPC," Proc. AAPT, Vol. 59, 1990, pp. 1-32.
- Puzinauskas, V.P., "Evaluation of Properties of Asphalt Cements with Emphasis on Consistencies at Low Temperatures," Proc. AAPT, Vol. 36, 1967, p. 489.
- Richman, W.B., "Molecular Weight Distribution of Asphalts," Proc. AAPT, Vol. 36, 1967, pp. 106-113.

- Roberts, F.L., Kandhal, P.S., Brow, E.R., Dah-Yinn Lee and Kennedy, T.W., "Hot Mix Asphalt Materials, Mixture Design and Construction," National Centre for Asphalt Technology, 1991, pp. 21-62.
- Rosstler, F.S. and White, R.M., "Influence of Chemical Composition of Asphalts on Performance, Particularly Durability," ASTM Special Technical Report 277, 1959.
- Rosstler, F.S. and White, R.M., "Composition and Changes in Composition of Highway Asphalts," Proc. AAPT, Vol. 31, 1962.
- SAS Institute, Inc., SAS User's Guide, 1994.
- Stock, A.F., "Review of the Application of High-Pressure Liquid Chromatography to Pavements," TRB 1096, 1986.
- Terrel, R.L., Epps, J.A. and Crawford, C., "Making the Most of Temperature/Viscosity Characteristics," National Pavement Association Information Series 102/88, 1988.
- Thenoux, G., "Chemical Characterization of Asphalt Cements Using Chromatographic Techniques: Relation to Rheological Properties and Field Performance," Ph.D. Dissertation, Oregon State University, 1987, pp. 21-50.
- Verhasselt, A.F. and Choquet, F.S., "Comparing Field and Laboratory Aging of Bitumen on a Kinetic Basis," Transp. Res. Rec. 1391, National Research Council, Washington, D.C., 1993, pp. 30-38.

Zenewitz, J.A. and Tran, K.T., "A Further Statistical Treatment of the Expanded Montana Asphalt Quality Study," Public Roads, Vol. 51, No. 3, 1987, pp. 72-81.

APPENDICES

Appendix A

SHRP Performed Tests

Summary of the Different Test Procedures Followed

1. Rotational Viscosity

The test procedure is summarized as follows:

1. Approximately 30 g of binder was heated until it was sufficiently fluid.
2. The temperature of the thermo-container was set at 135°C.
3. 10.5 g of AC were poured into the Brookfield sample chamber.
4. When the 135°C temperature of the thermo-container was attained, the sample chamber was placed into the thermo-container.
5. Then the preheated spindle (spindle # 27 was used in this research) was placed into the sample chamber.
6. The sample was left in the thermo-container for about 30 minutes to equilibrate.
7. The spindle was set to a speed of 20 rpm.

When the reading of the viscosity in the display unit was constant, the viscosity in centipoises was recorded.

2. Rolling Thin Film Oven Test (RTFO)

The followed RTFO aging procedure is summarized as follows:

1. About 350 g of the required asphalt sample to be aged was heated until sufficiently fluid.
2. RTFO bottles were filled with 35 ± 0.5 g of binder.
3. Eight bottles were loaded into the oven, which was set at 163°C.
4. Rotation of the bottles was started at a rate of 15 rpm, in addition, an air jet at a rate of 4000 ml/min was applied.
5. The test was continued for 85 minutes.
6. The bottles were emptied into either PAV containers or other containers to be used in further tests required on RTFO residue.

3. Pressure Aging Vessel Test (PAV)

The used PAV aging procedure is summarized as follows:

1. The pressure vessel was preheated to 120°C.
2. The required asphalt sample was heated until sufficiently fluid.
3. 50 g of asphalt were poured into each PAV pan.
4. Filled pans were placed in the sample rack.
5. The sample rack was then placed into the pressure vessel.
6. The pressure vessel was placed into the oven, which was set at 110°C.
7. 2070 kPa (300 psi) pressure was applied to the samples inside the pressure vessel.
8. Heating under pressure was continued for 20 hours.
9. At the end, pressure was released and the samples were collected.

4. Dynamic Shear Rheometer Testing

The followed test procedure is summarized as follows:

1. An approximate amount of 10 g of the test sample (either fresh, RTFO residue, or PAV residue) was placed into a small container and heated until it was sufficiently fluid.
2. A thin stream of asphalt was poured into the center of a small silicon rubber mold (25 mm diameter for fresh and RTFO samples and 8 mm diameter for PAV samples).
3. The rheometer was then prepared. The air supply, the computer, and the temperature control system were turned on.
4. Then the rheometer was set into oscillatory loading mode, and the temperature control system was set to the required test temperature.
5. The appropriate upper plate (25 mm plate for fresh and RTFO samples and 8 mm for PAV samples) was attached to the rheometer spindle, and the gap between the upper and lower plates was set to 1 mm for the 25 mm plates and 2 mm for the other 8 mm plate.
6. Additional clearance of 50 microns was added to the gap. This extra clearance was dialed out prior to testing but was included just to achieve the proper sample shape during testing.

7. The upper plate was removed, and the silicon mold was flexed. The molded sample was applied directly to the upper plate.
8. The upper plate was reinstalled in the rheometer, and it was brought back to the original plate with required gap and the additional 50 microns.
9. At that time, the sample was squeezed between the lower and upper plates for trimming. The extra asphalt was trimmed with a heated trimmer, creating a sample with vertical sides flush with the upper plate.
10. The extra 50 microns were then dialed out by lowering the upper plate 50 microns.
11. The sample was then covered with water at the desired test temperature and left for 15 minutes to make sure that the sample had attained the desired temperature.
12. Two tests were performed on the sample at each test temperature. The first test was performed using a preset fixed frequency. This type of test is usually used to grade asphalt samples according to SHRP grading. The other test was performed using the frequency sweep. The results of this test were used later for generating the linear viscoelastic model of each asphalt.

In the fixed frequency testing, according to SHRP recommendations, the frequency was set at 10 radians per second (1.59 Hz). The starting shear strain was based on the ample type.

- For fresh samples, the starting shear strain was 12.5%.
- For RTFO residue, the starting shear strain was 10%.
- For PAV residue, the starting shear strain was 1%.

In the frequency sweep testing, a set of test frequencies was selected. The selected frequencies were 0.01, 0.1, 1.0, 1.5, 5.0, and 10.0 Hz.

13. All the desired parameters were fed into the control software, and it took over the testing. The testing consisted of two phases, load conditioning and data acquisition. In the load conditioning phase, the required shear strain was applied for 10 cycles at a rate of 10 radians per second. No test results were recorded at this stage. In the second phase, the loading was reapplied at the desired shear strain and desired frequency or frequencies and the data were calculated and saved for each frequency.
14. If the test was required on another test temperature, that test temperature was fed into the software. Sufficient time was allowed for the sample to reach the desired temperature.

Then the test was repeated using the same sample.

5. *Bending Beam Rheometer (BBR) Testing*

The followed procedure in BBR testing is summarized as follows:

1. The asphalt sample (PAV residue) was heated till it became fluid.
2. The air system to the rheometer, the cooling system, and the test system were started and set at the desired temperature.
3. Calibration of the whole system and a test of compliance of the test device were then performed according to the steps required by the control software.
4. For sample preparation, aluminum bar molds were used. The inside faces of the molds were greased with a glycerin/talc releasing agent. Plastic strips were placed onto the coated surfaces of the mold. The molds were then assembled together.
5. The molds were then filled with asphalt. The samples were left to cool for 45 minutes, then the excess asphalt was trimmed away using a hot spatula.
6. The filled molds were then placed into a freezer for about 10 minutes. The beams were then demolded.
7. Beams were then placed in the test batch for 60 minutes prior to testing for thermal conditioning.

8. At the end of 60 minutes, each asphalt beam was placed on the supports and a four gram preload was manually applied to the beam to insure full seating of the beam on the supports.
9. A 100 gram seating load was applied automatically by the rheometer software for one second. This load was released, and the sample was left for 20 seconds to recover.
10. At the end of the recovery period, the 100 grams were reapplied to the beam for a total of 240 seconds. During this loading period, the software monitored both the load and deflection and plotted deflection versus time.
11. At the end of the test period, the software released the load and calculated the creep stiffness and m-value.

6. Direct Tension Testing

The sample preparation for DDT testing and the test procedure are summarized as follows:

The asphalt binder was heated until it was sufficiently fluid to pour and was then poured into preheated silicon rubber molds. The test specimens were left in the mold to cool to room temperature and then the excess asphalt binder was trimmed off with a heated straight edge. Prior to demolding, the mold containing the test specimens was placed in a freezer to get rigidity. After demolding, test specimens were stored in the environmental chamber for conditioning at the test temperature before testing.

The environmental chamber was prepared by initially cooling methyl alcohol in the circulating bath till the required testing temperature was reached and then circulating it through the radiator inside the chamber. The asphalt test specimen, after being prepared and demolded, was fixed in place between the two clamps using the two end inserts. When the required temperature inside the chamber was obtained, the CO₂ unit was utilized to control the test temperature to within $\pm 0.2^{\circ}\text{C}$ of the testing temperature and to avoid frost formation inside the chamber, on the test sample, or on any of the test fixtures. After conditioning the test specimen at the test temperature, the loading machine was started and the load and elongation were recorded and displayed on the x-y chart recorder.

The DTT gave graphically the load and elongation at failure of the test specimen. The failure stress was calculated by dividing the failure load by the original cross-sectional area of the test specimen, which was nominally 3.6 mm². The tensile strain at failure was calculated as the elongation at failure divided by the effective gauge length of the test specimen, which was the portion of the specimen that contributed to the majority of strain and had a value of 27.0 mm.

Appendix B

Input and Output for LVE Development and Developed LVE Curves

FILE: A1-11 SAS A1 KING FAHD UNIVERSITY OF PETROLEUM AND MINERALS, DHAHRAN

```

CMS F1 DD DISK BH PRN A;
OPTIONS NOCENTER;
DATA;
  INFILE DD FIRSTOBS=2;
  INPUT
    BH1G BH1T BH1F
    BH2G BH2T BH2F
    BH3G BH3T BH3F
    BH4G BH4T BH4F
    BH5G BH5T BH5F;
  LBH1G=LOG10(BH1G);
  IF BH1T=-12.0 THEN IT1=1;ELSE IT1=0;
  IF BH1T=-18.2 THEN IT2=1;ELSE IT2=0;
  IF BH1T= 24.7 THEN IT3=1;ELSE IT3=0;
;
PROC NLIN;
  PARMS
    B1=1 B2=1 B3=1 B4=1 B5=1;
  MODEL LBH1G= 9-((B1 /LOG10(2)))
    *LOG10(1+(B2/(BH1F *(10**(B3*(IT1+B4*IT2+B5*IT3))))))
    ** (LOG10(2)/ B1 ));
  OUTPUT OUT=OUT P=PREDICT R=RESIDUAL;

```

Fig. B-1: Written program to evaluate LVE parameters for BH1 sample

1The SAS System

19:43 Monday, December 25, 1995

Non-Linear Least Squares DUD Initialization					Dependent Variable LBH1C	
DUD	B1	B2	B3	B4	B5	Sum of Squares
-6	1.000000	1.000000	1.000000	1.000000	1.000000	26.245350
-5	1.000000	1.000000	1.000000	1.000000	1.000000	24.311549
-4	1.000000	1.000000	1.000000	1.000000	1.000000	25.906351
-3	1.000000	1.000000	1.000000	1.000000	1.000000	26.092265
-2	1.000000	1.000000	1.000000	1.000000	1.000000	25.889682
-1	1.000000	1.000000	1.000000	1.000000	1.000000	27.043803

Non-Linear Least Squares Iterative Phase					Dependent Variable LBH1C	
Iter	B1	B2	B3	B4	B5	Sum of Squares
0	1.100000	1.000000	1.000000	1.000000	1.000000	24.311549
1	2.274969	0.134164	3.011861	3.475774	-0.816184	1.120913
2	2.275957	0.151144	3.030519	3.501045	-0.815018	1.112650
3	2.269284	0.136486	3.041794	3.518416	-0.802104	1.046334
4	2.218091	0.216474	3.876191	4.742086	-0.619446	0.265217
5	2.200977	0.377689	4.091278	5.148177	-0.635804	0.073908
6	2.202261	0.386979	4.105912	5.178244	-0.635792	0.072386
7	2.296196	0.357771	4.019725	5.145428	-0.636520	0.049266
8	2.290153	0.341580	4.005210	5.110947	-0.632550	0.029276
9	2.284724	0.348185	3.997018	5.126625	-0.631490	0.028040
10	2.278215	0.346665	3.990553	5.133917	-0.627334	0.021453
11	2.270777	0.334128	3.987689	5.101999	-0.624502	0.013674
12	2.293316	0.280937	4.025744	5.084221	-0.628058	0.012254
13	2.315617	0.257834	4.036684	5.104961	-0.644269	0.011210
14	2.315732	0.256990	4.036739	5.105926	-0.644347	0.011205
15	2.315724	0.257017	4.036743	5.105920	-0.644353	0.011205
16	2.316234	0.256596	4.036716	5.106736	-0.644048	0.011205
17	2.316124	0.256637	4.036499	5.106469	-0.644134	0.011205
18	2.316239	0.256490	4.036764	5.106659	-0.644084	0.011205
19	2.316249	0.256480	4.036772	5.106666	-0.644090	0.011205

NOTE: Convergence criterion met.

Non-Linear Least Squares Summary Statistics

Source	DF	Sum of Squares	Mean Square	Dependent Variable LBH1C	
Regression	5	1305.5217843	261.1043569		
Residual	19	0.0112046	0.0005897		
Uncorrected Total	24	1305.5329889			
(Corrected total)	23	14.4281654			

Parameter	Estimate	Asymptotic Std. Error	Asymptotic Confidence Interval	95 %
B1	2.316248710	0.04270049152	2.2268761932	2.4056212278
B2	0.256480204	0.05280128838	0.1459666268	0.3669937809
B3	4.036771705	0.05596831744	3.9196295071	4.1539139024
B4	5.106666666	0.07355586631	4.9597734304	5.2606105574

Fig. B-2:

Computer output for the LVE calculated parameters for BH1 sample

B5 -0.644090132 0.02917781174 -0.7051595578 -0.5830207069
 1The SAS System

19:43 Monday, December 25, 199

Asymptotic Correlation Matrix

Corr	B1	B2	B3	B4	B5
-----	-----	-----	-----	-----	-----
B1	1				
B2	-0.972451944	1			
B3	0.7041764394	-0.597720298	1		
B4	0.7622970241	-0.676849933	0.6421738436	1	
B5	-0.261287333	0.4206690624	0.0813860591	0.0026067073	1

Fig B-2: (Continued)

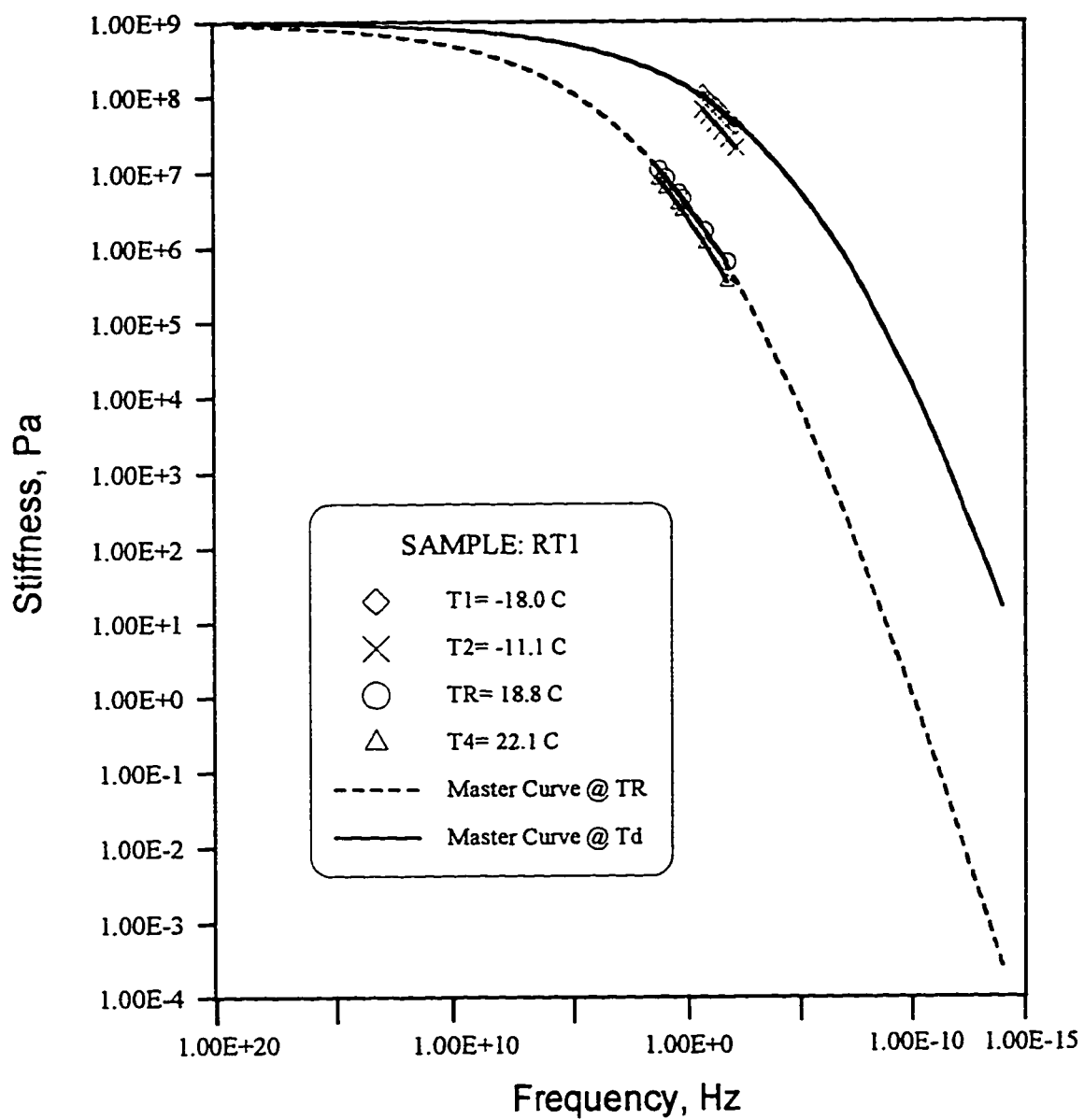


Fig. B-3: Master curve for RT1 sample

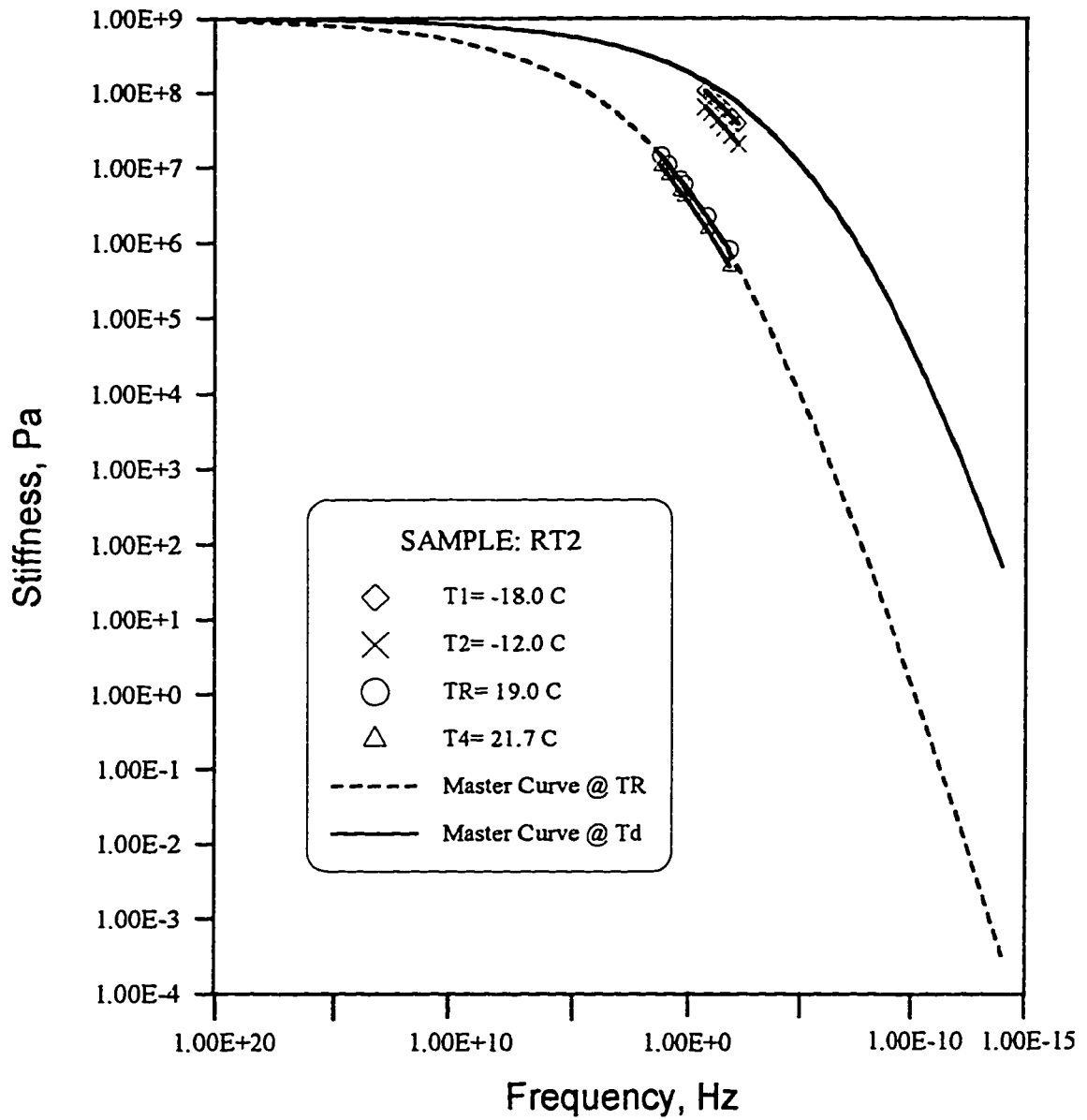


Fig. B-4: Master curve for RT2 sample

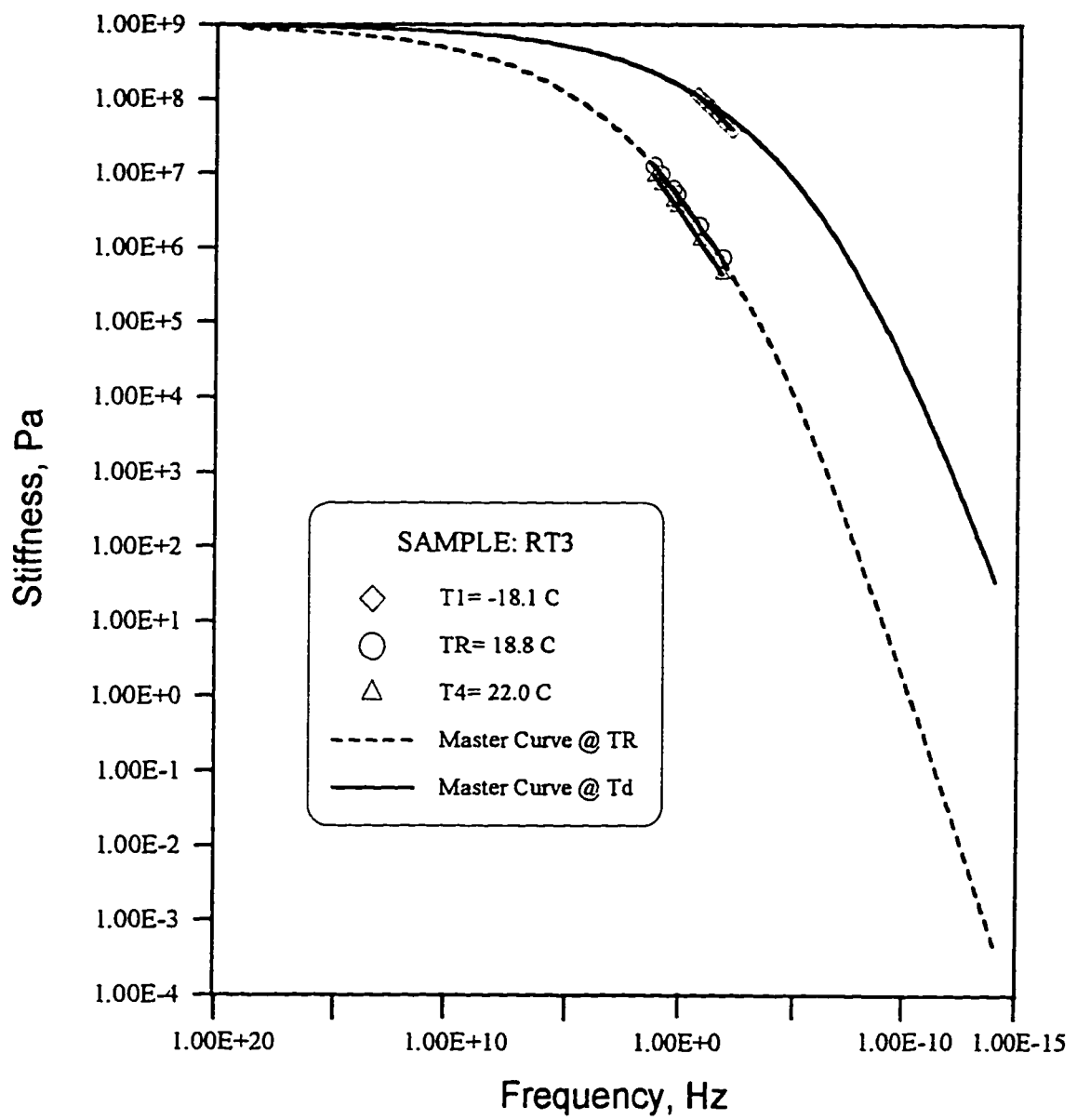


Fig. B-5: Master curve for RT3 sample

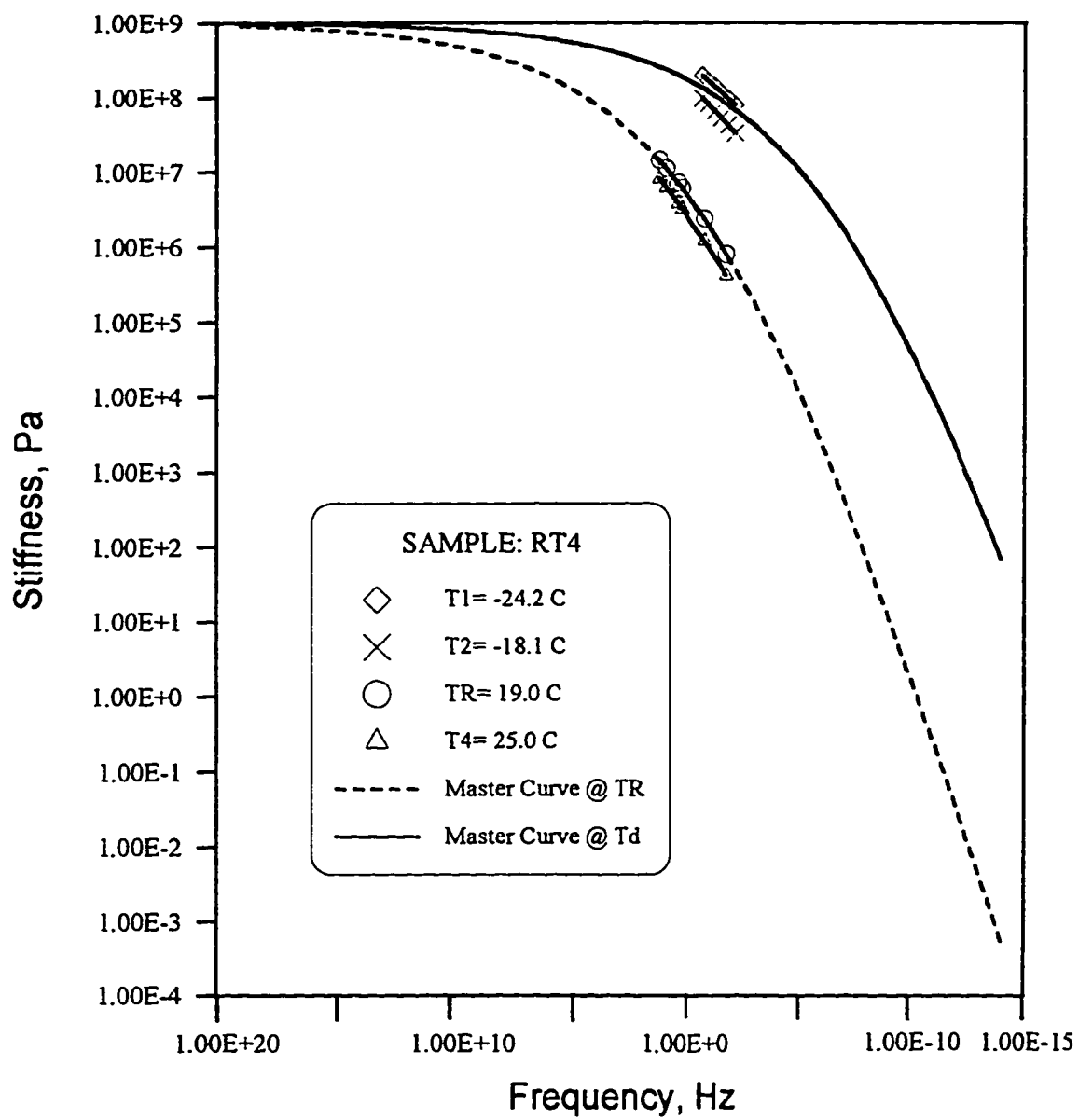


Fig. B-6: Master curve for RT4 sample

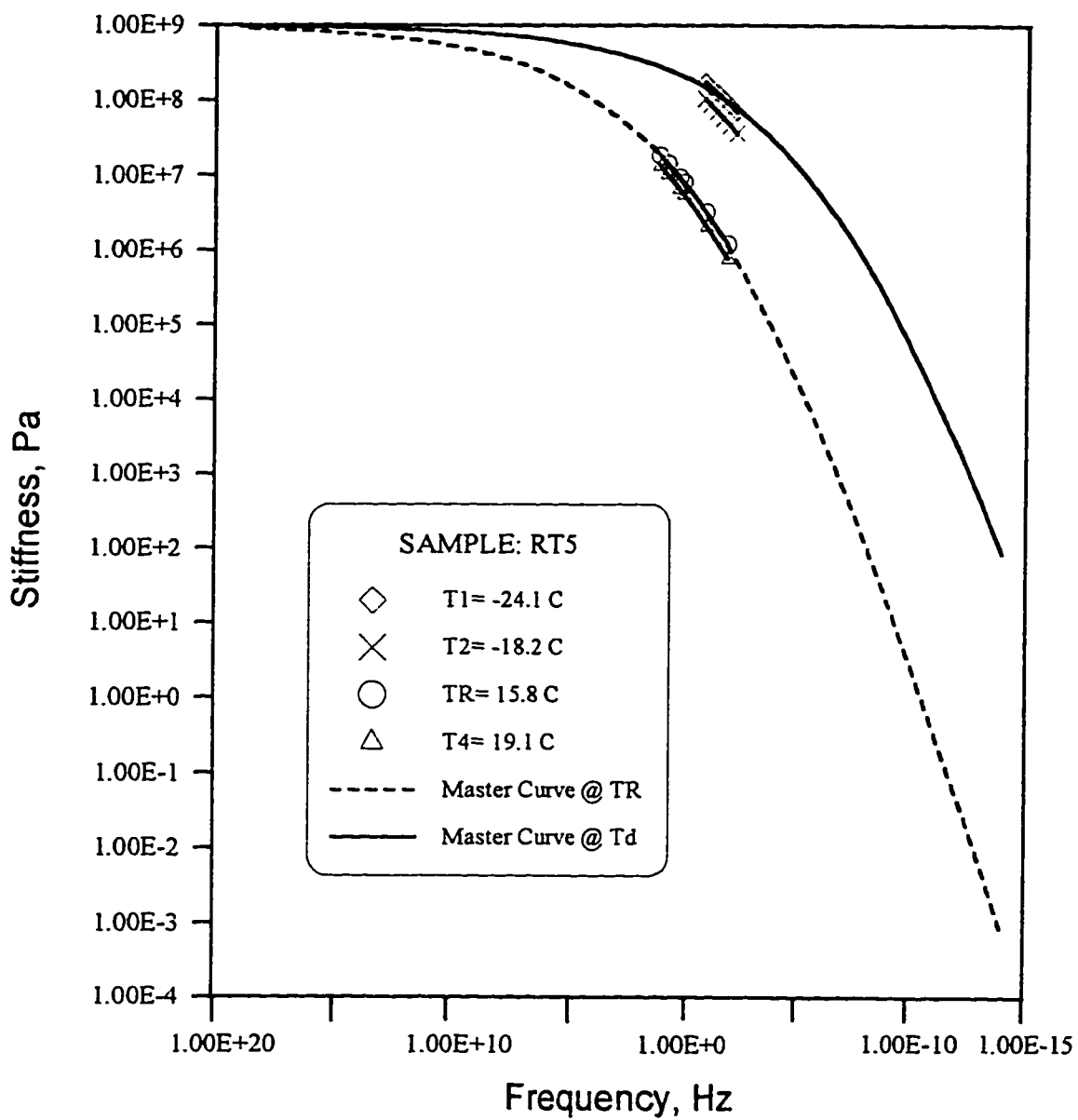


Fig. B-7: Master curve for RT5 sample

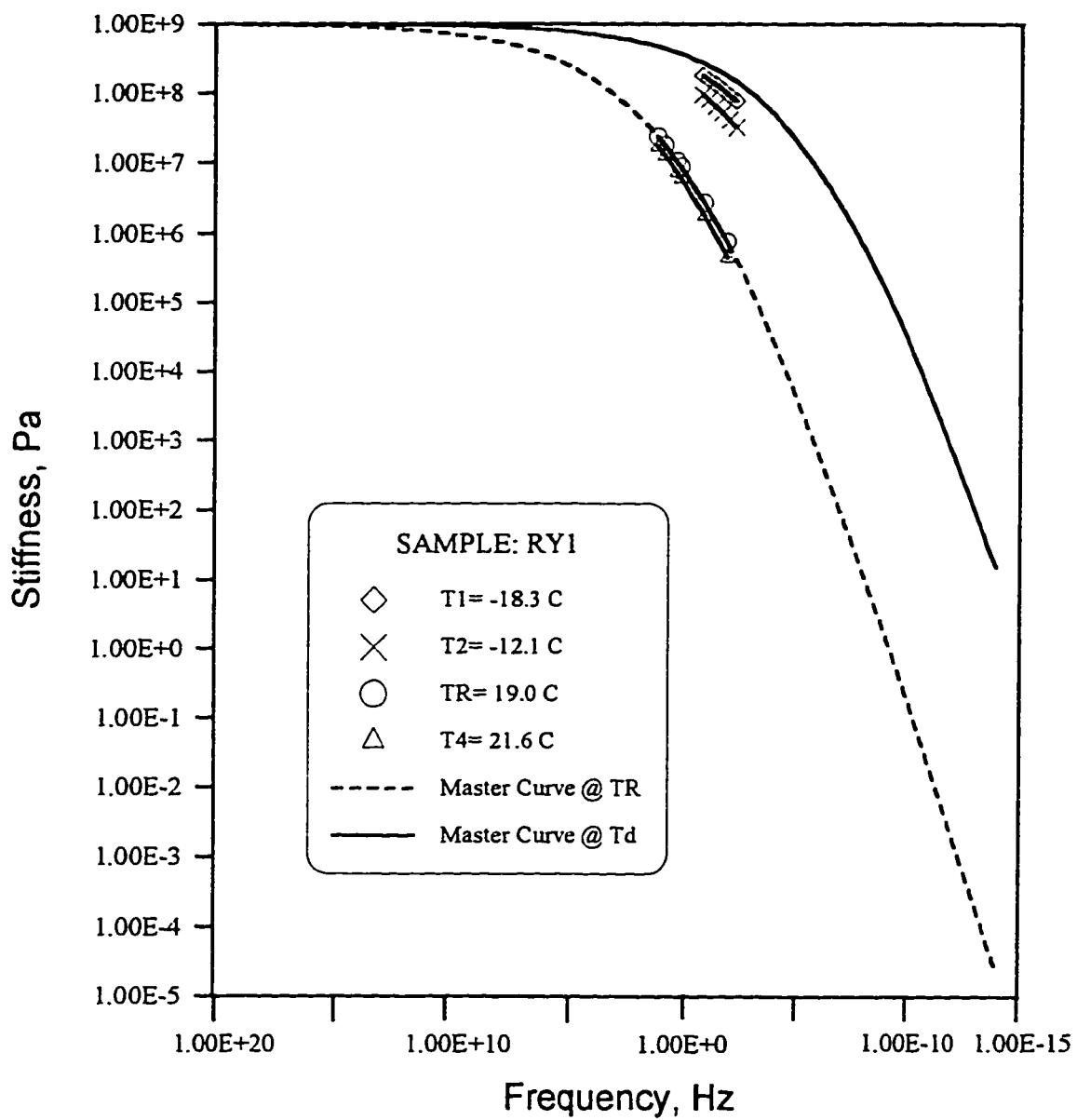


Fig. B-8: Master curve for RY1 sample

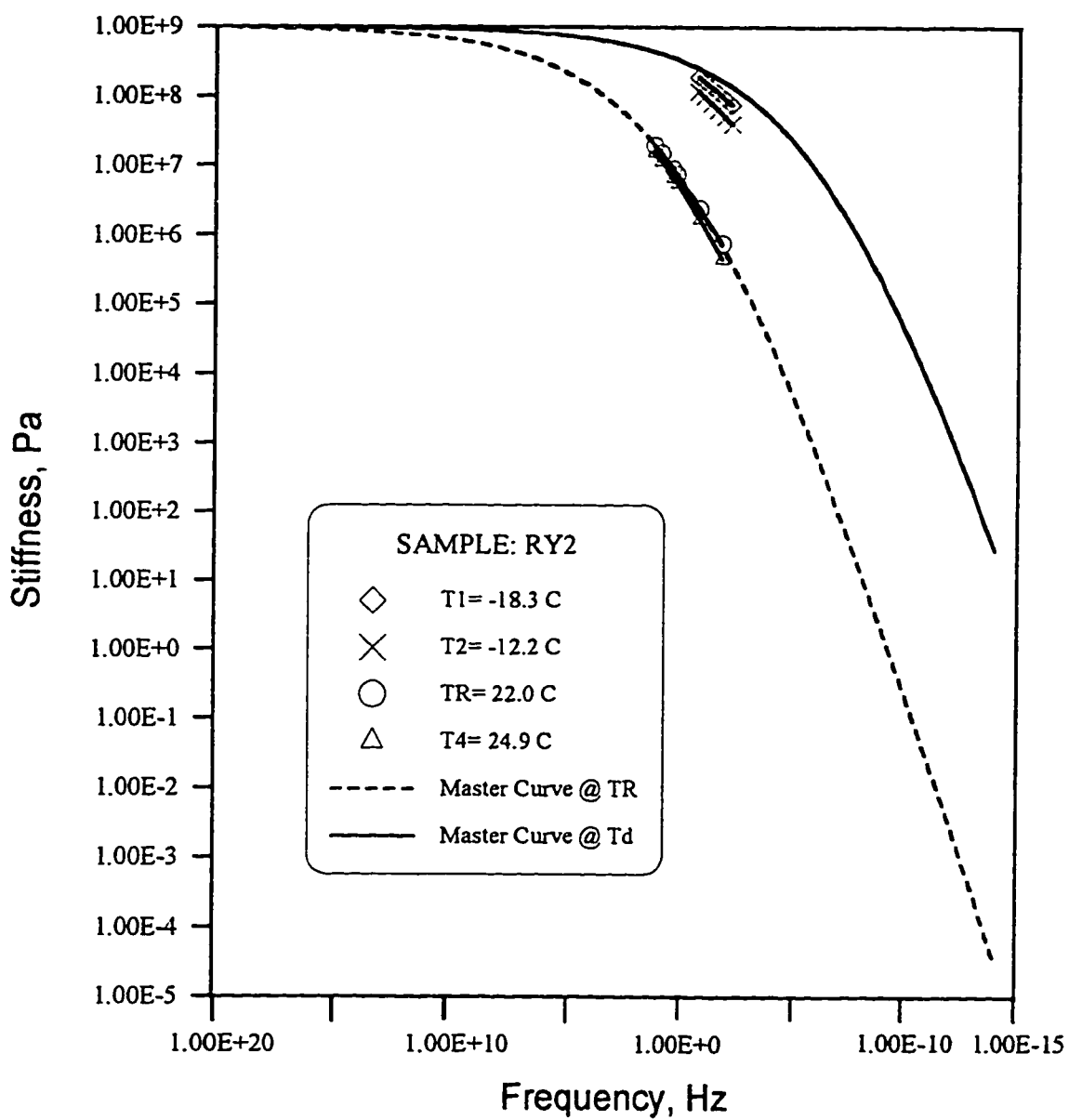


Fig. B-9: Master curve for RY2 sample

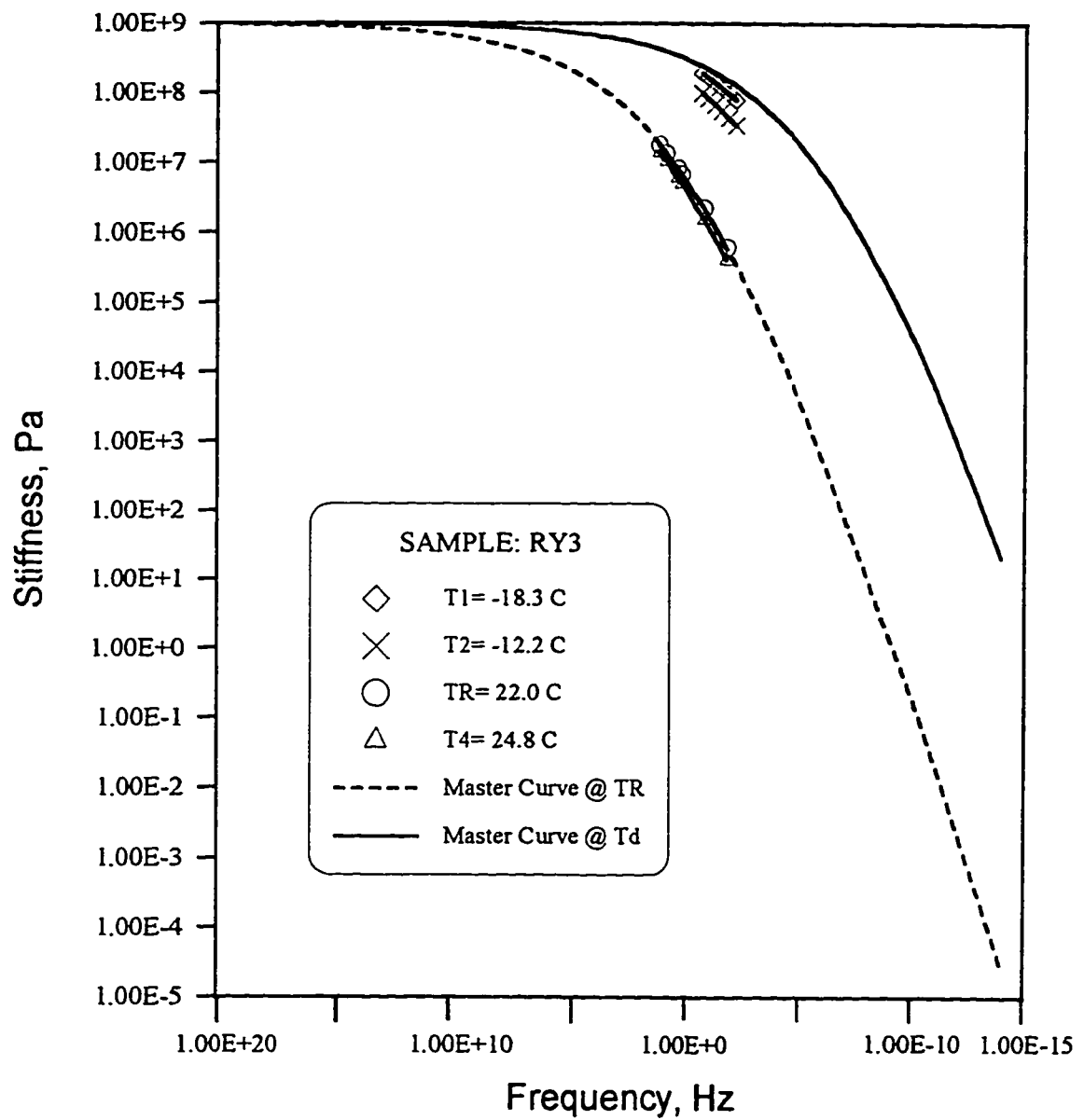


Fig. B-10: Master curve for RY3 sample

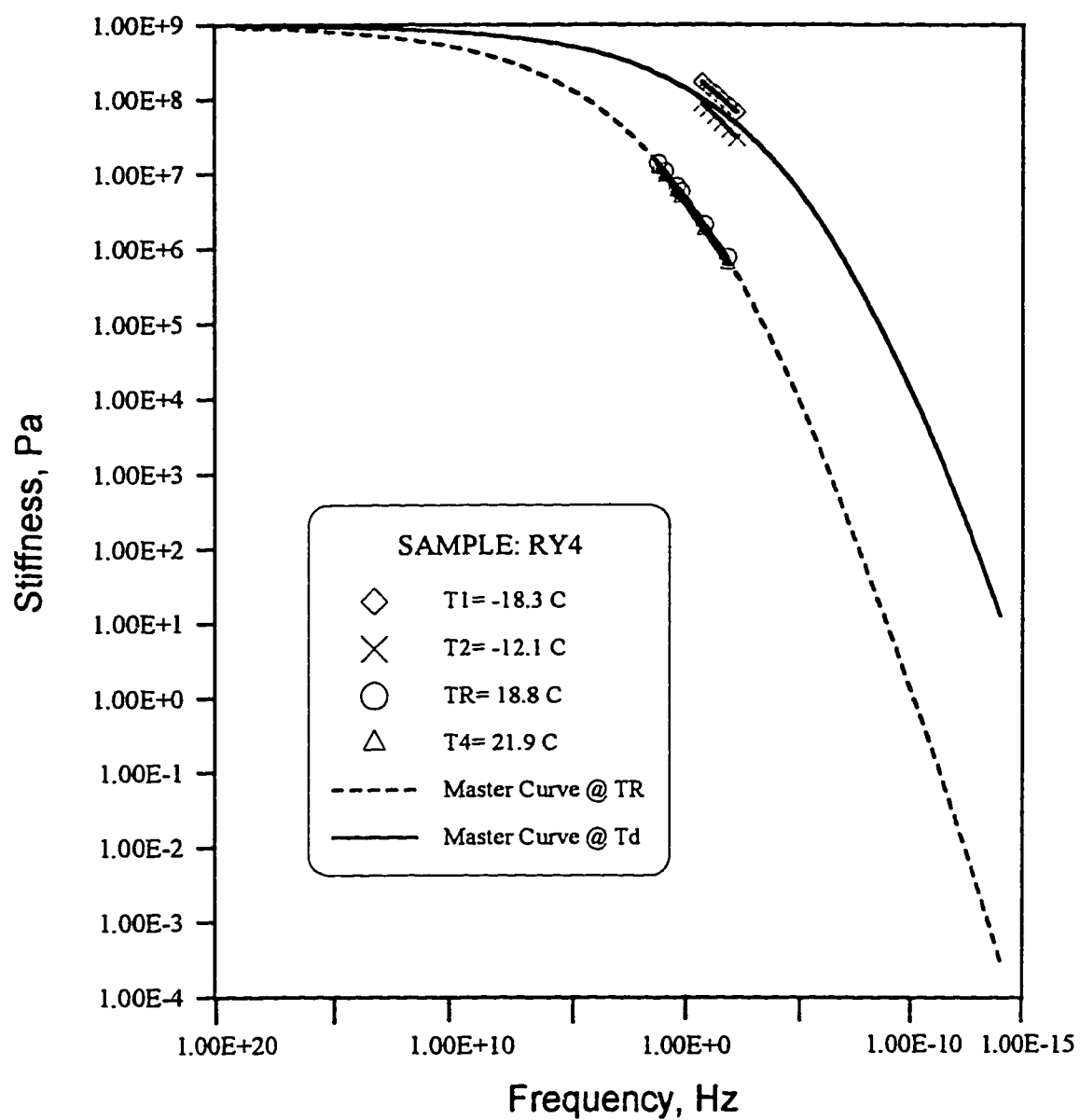


Fig. B-11: Master curve for RY4 sample

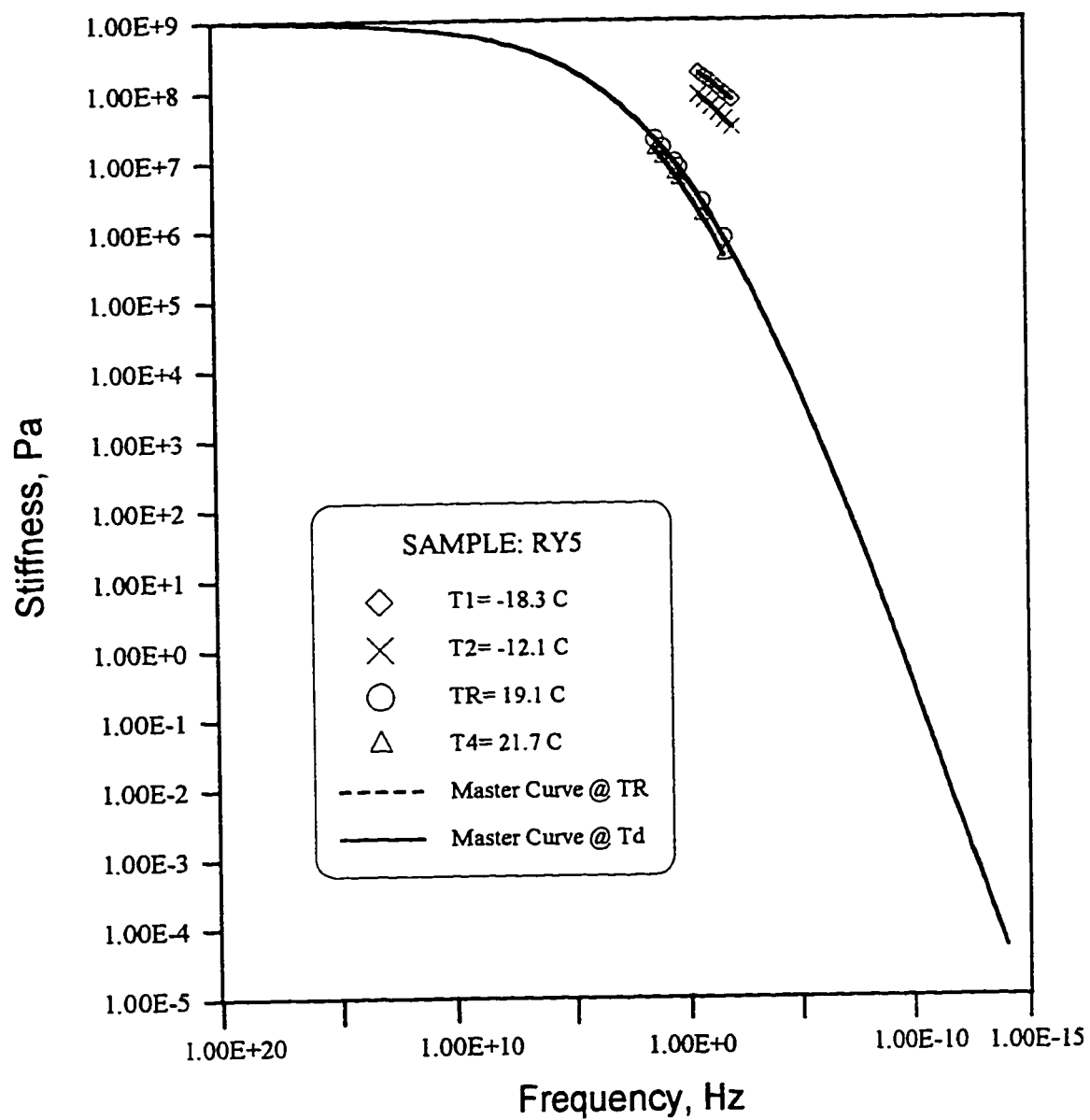


Fig. B-12: Master curve for RY5 sample

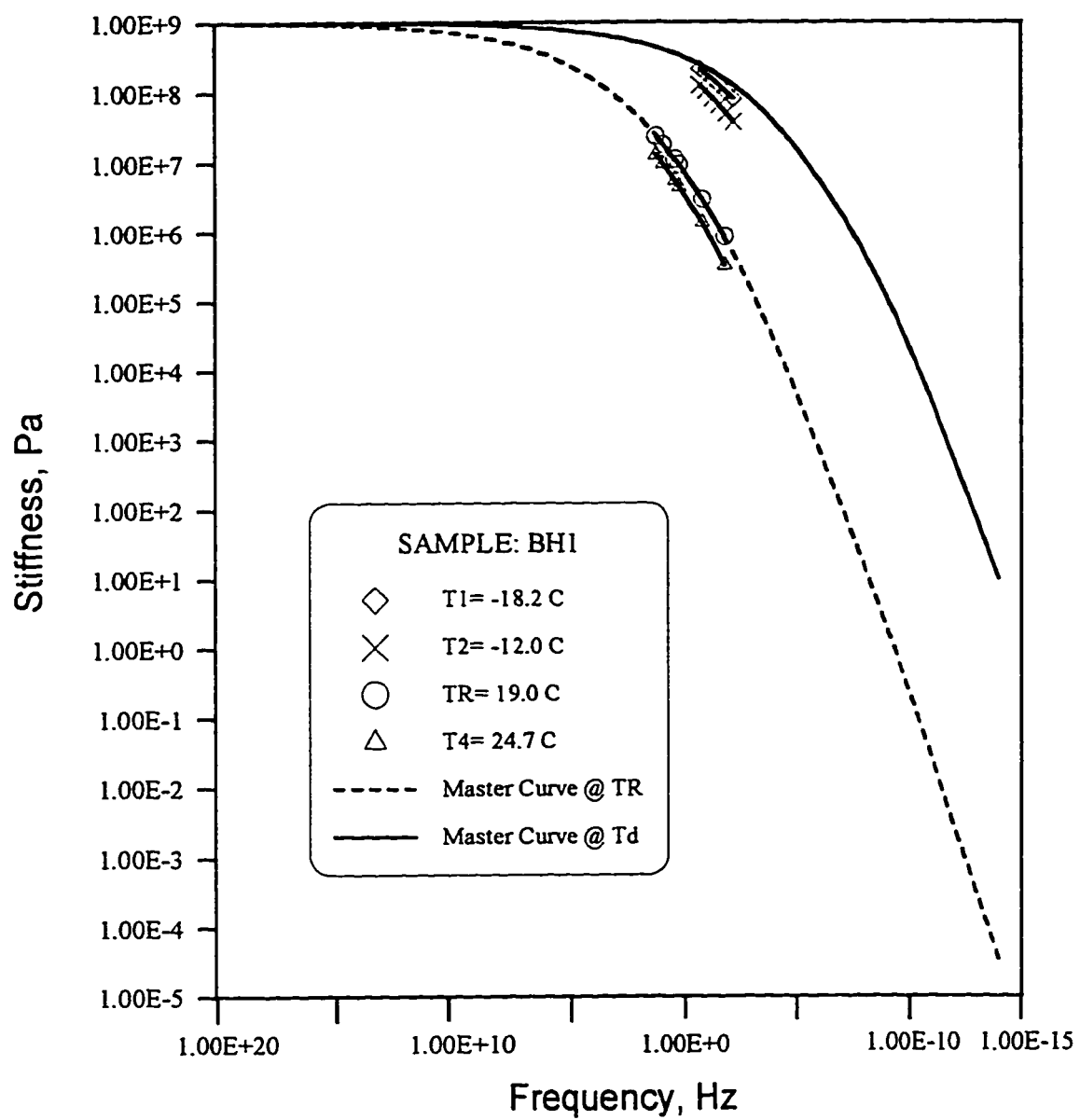


Fig. B-13: Master curve for BH1 sample

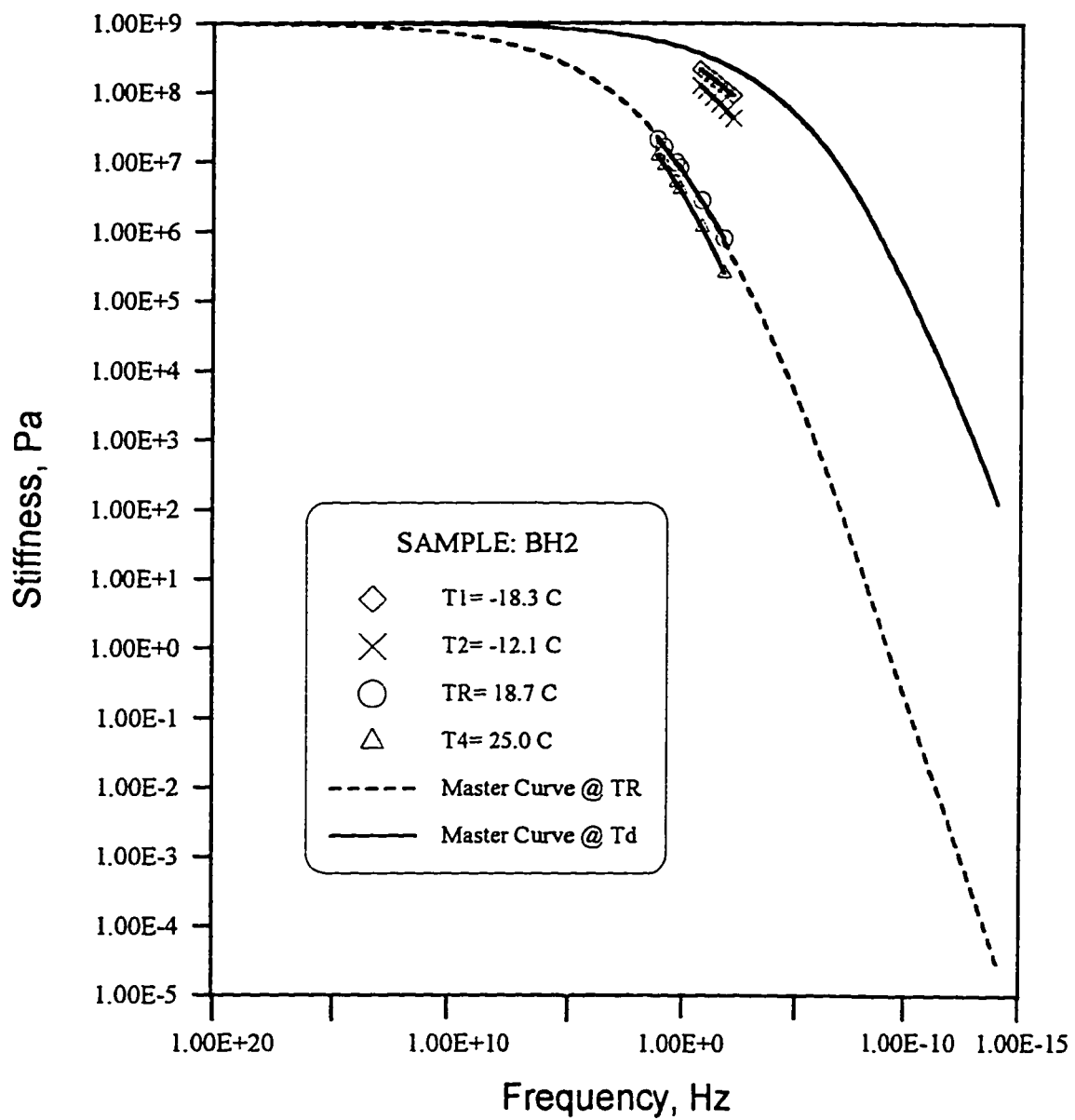


Fig. B-14: Master curve for BH2 sample

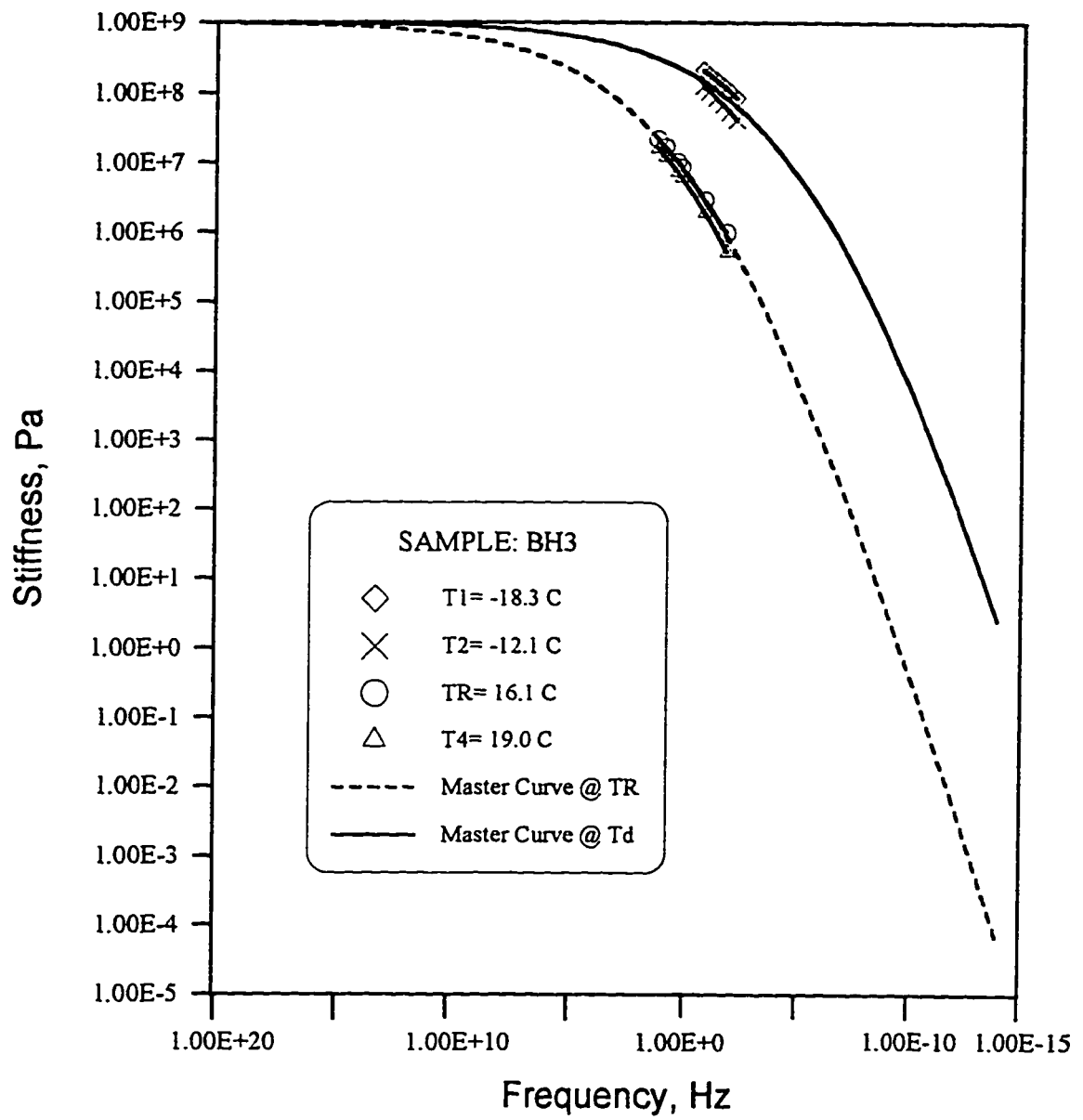


Fig. B-15: Master curve for BH3 sample

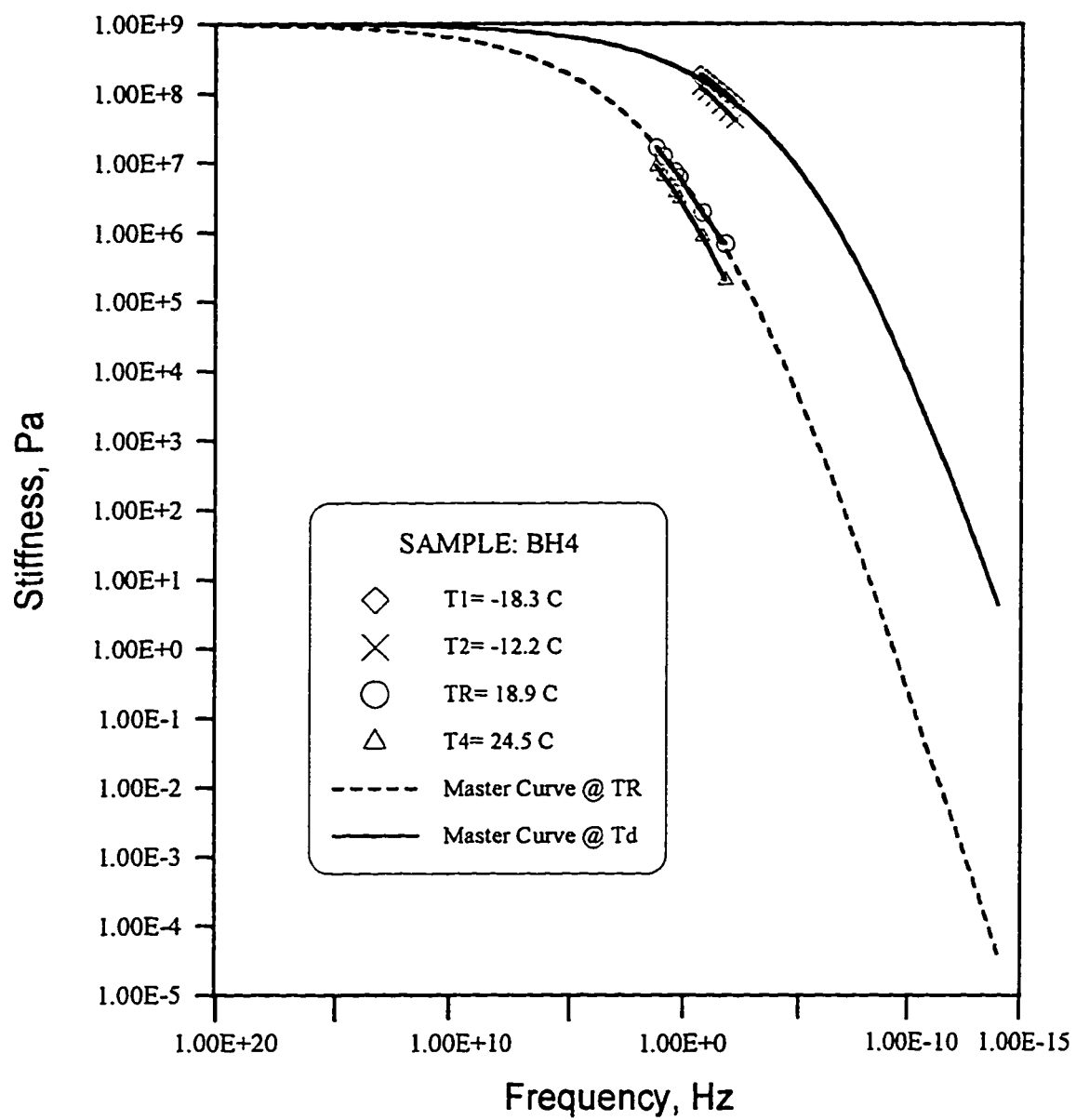


Fig. B-16: Master curve for BH4 sample

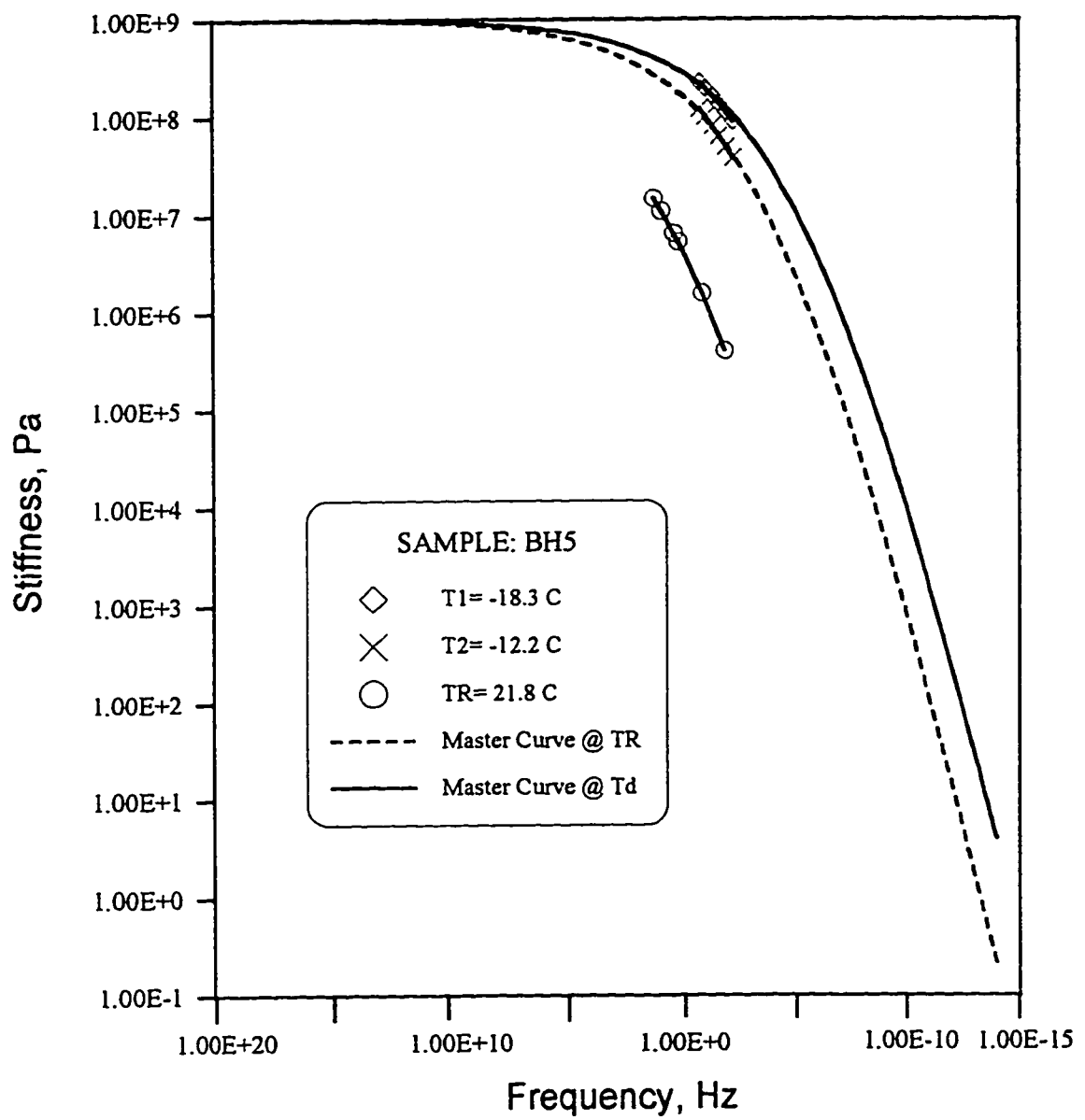


Fig. B-17: Master curve for BH5 sample

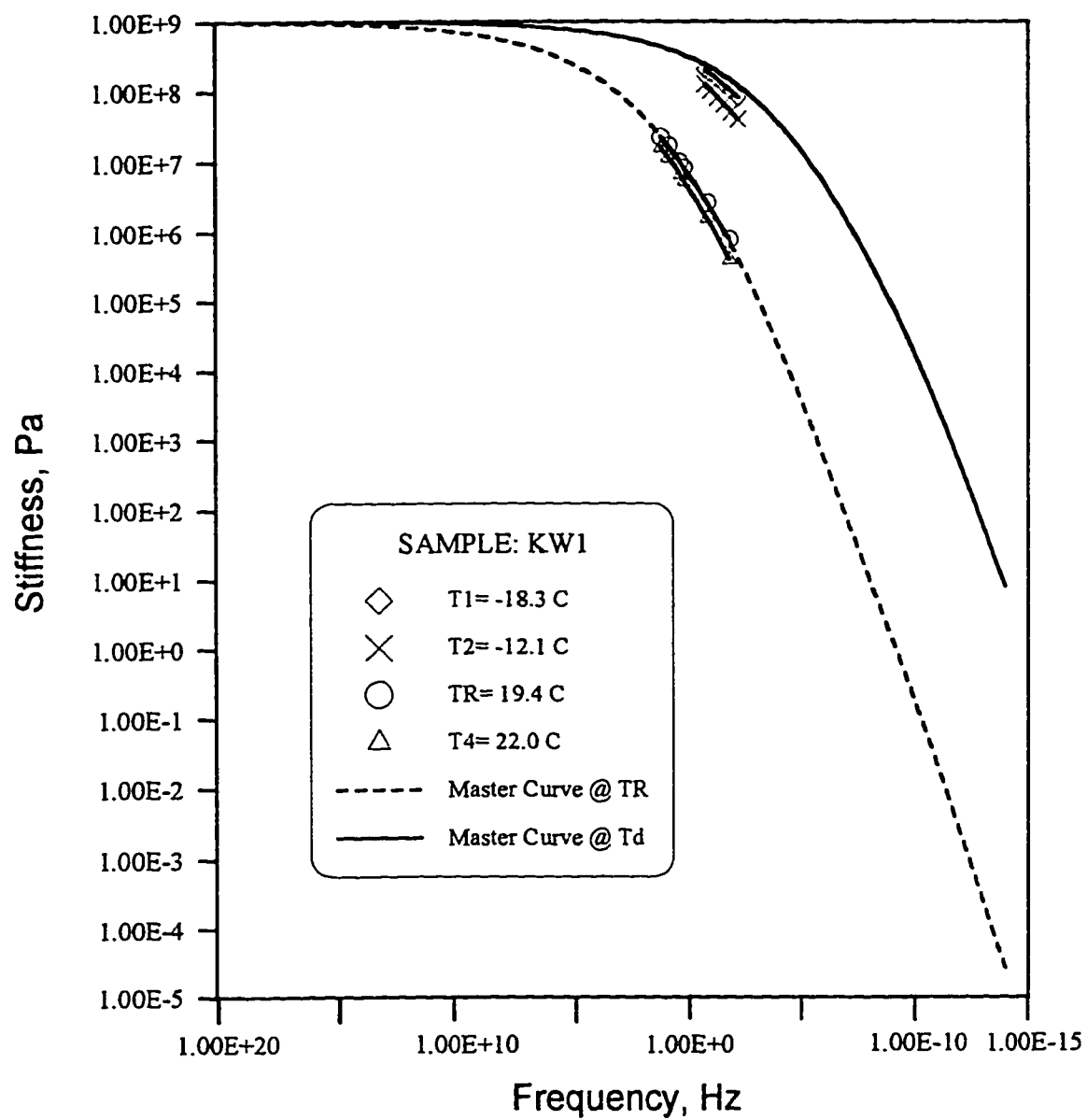


Fig. B-18: Master curve for KW1 sample

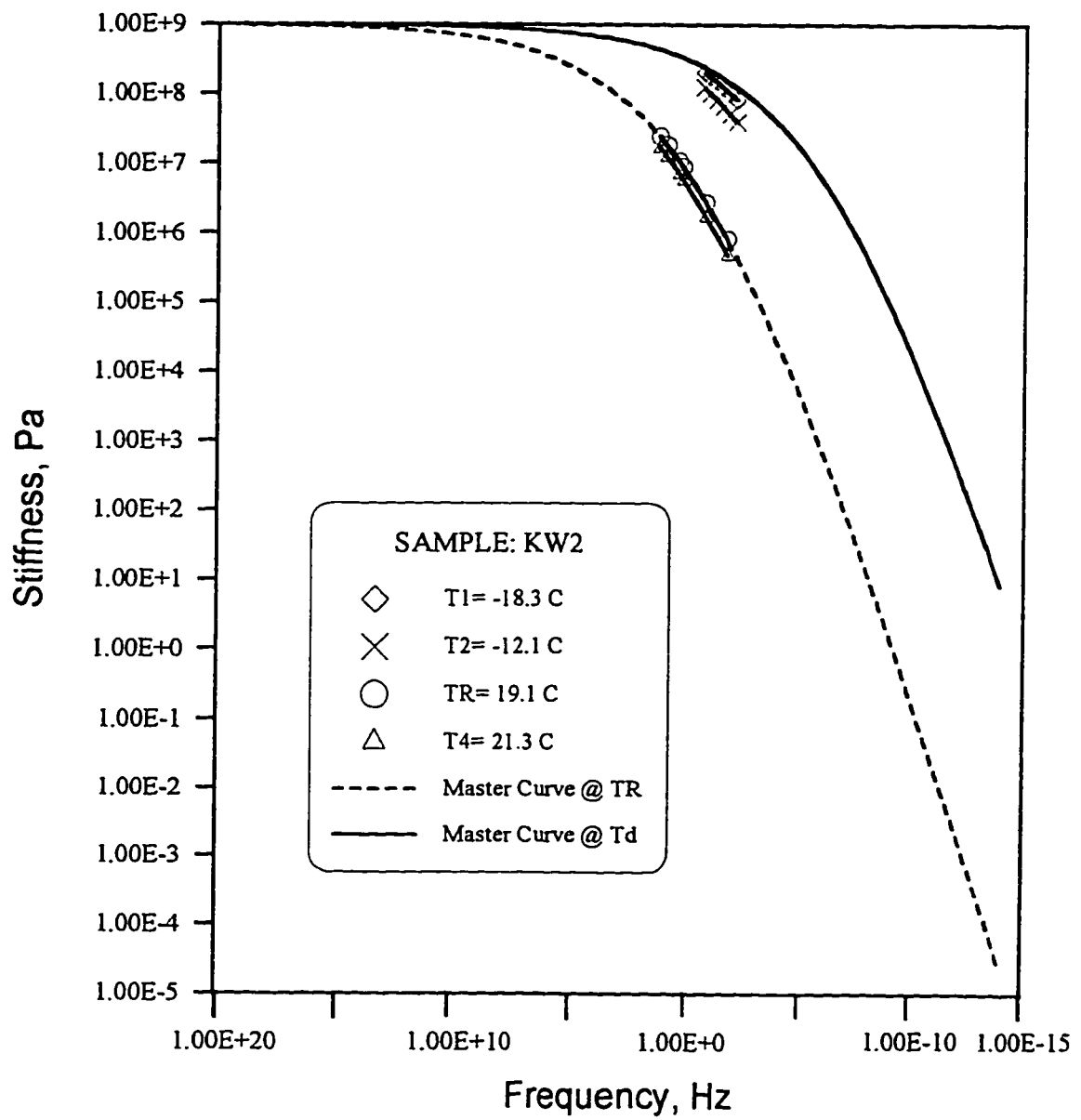


Fig. B-19: Master curve for KW2 sample

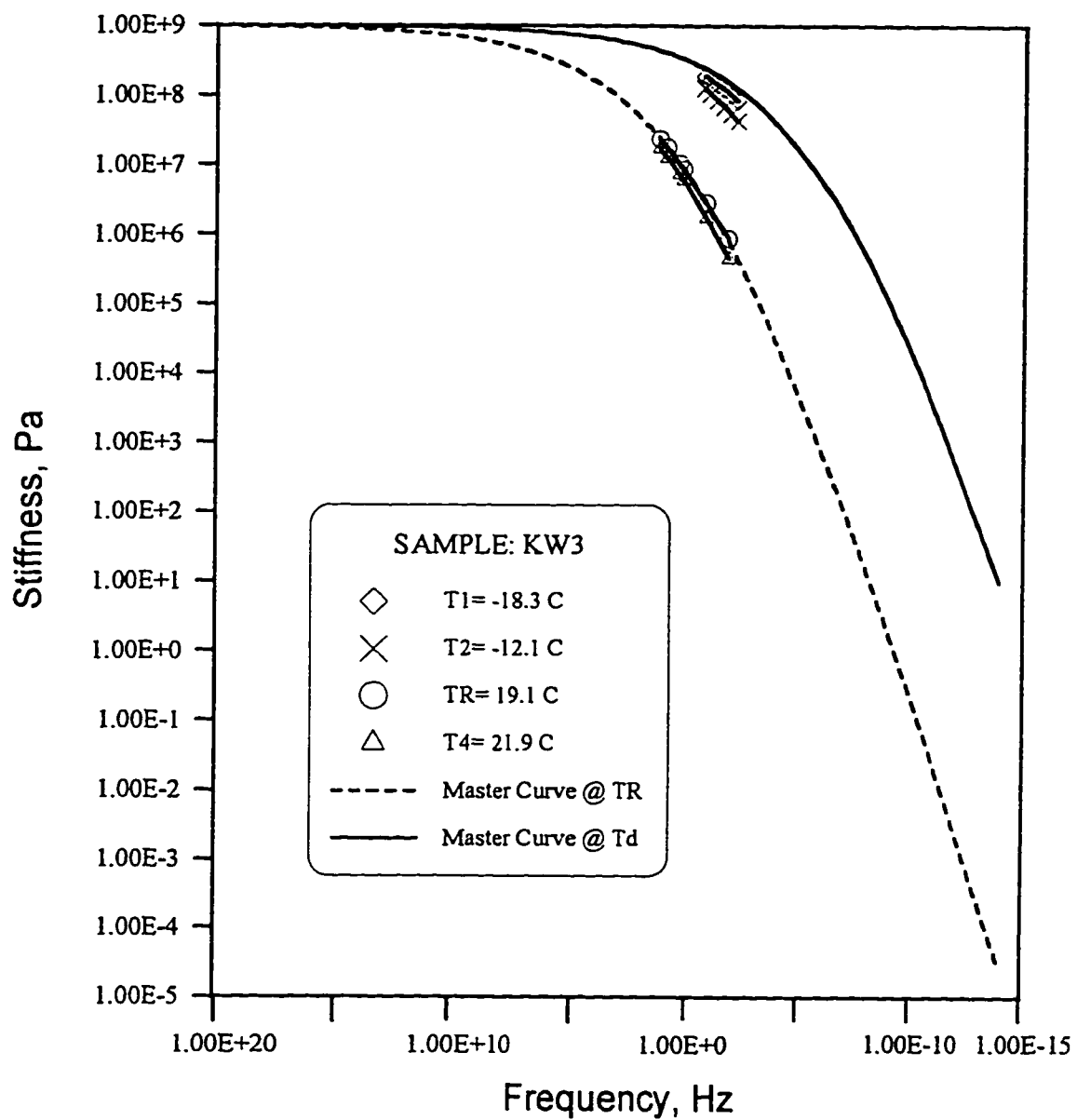


Fig. B-20: Master curve for KW3 sample

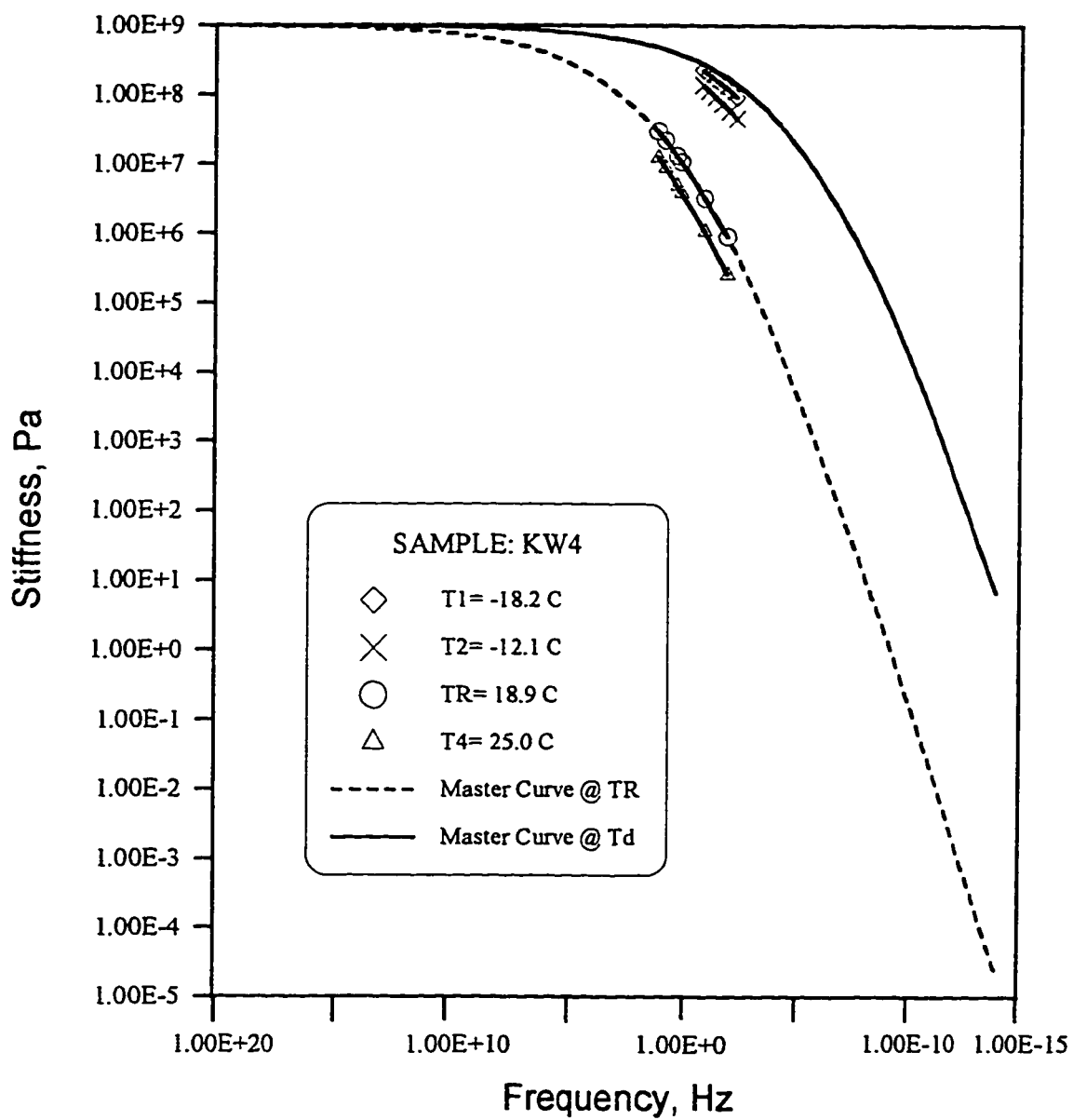


Fig. B-21: Master curve for KW4 sample

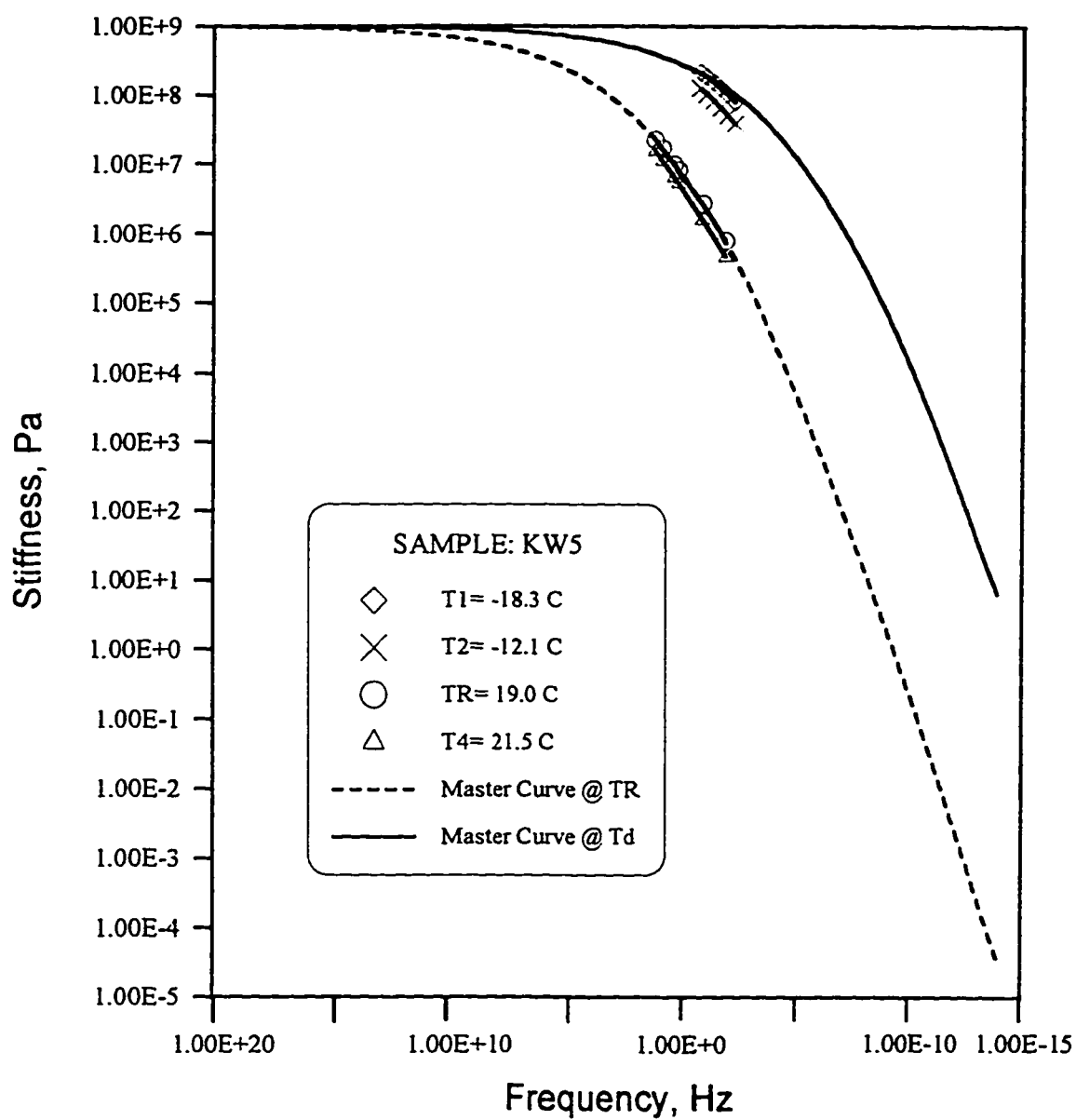


Fig. B-22: Master curve for KW5 sample

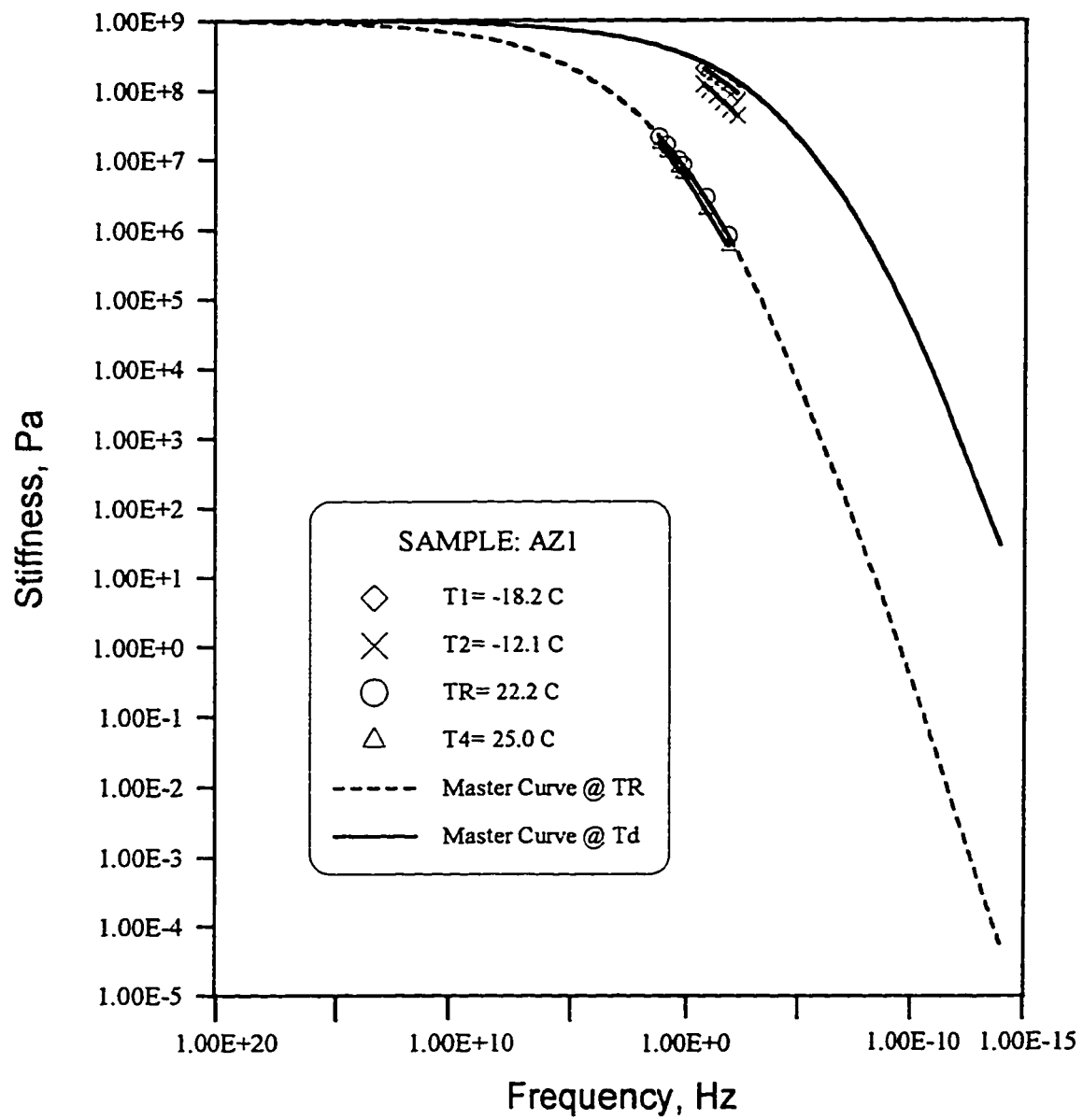


Fig. B-23: Master curve for AZ1 sample

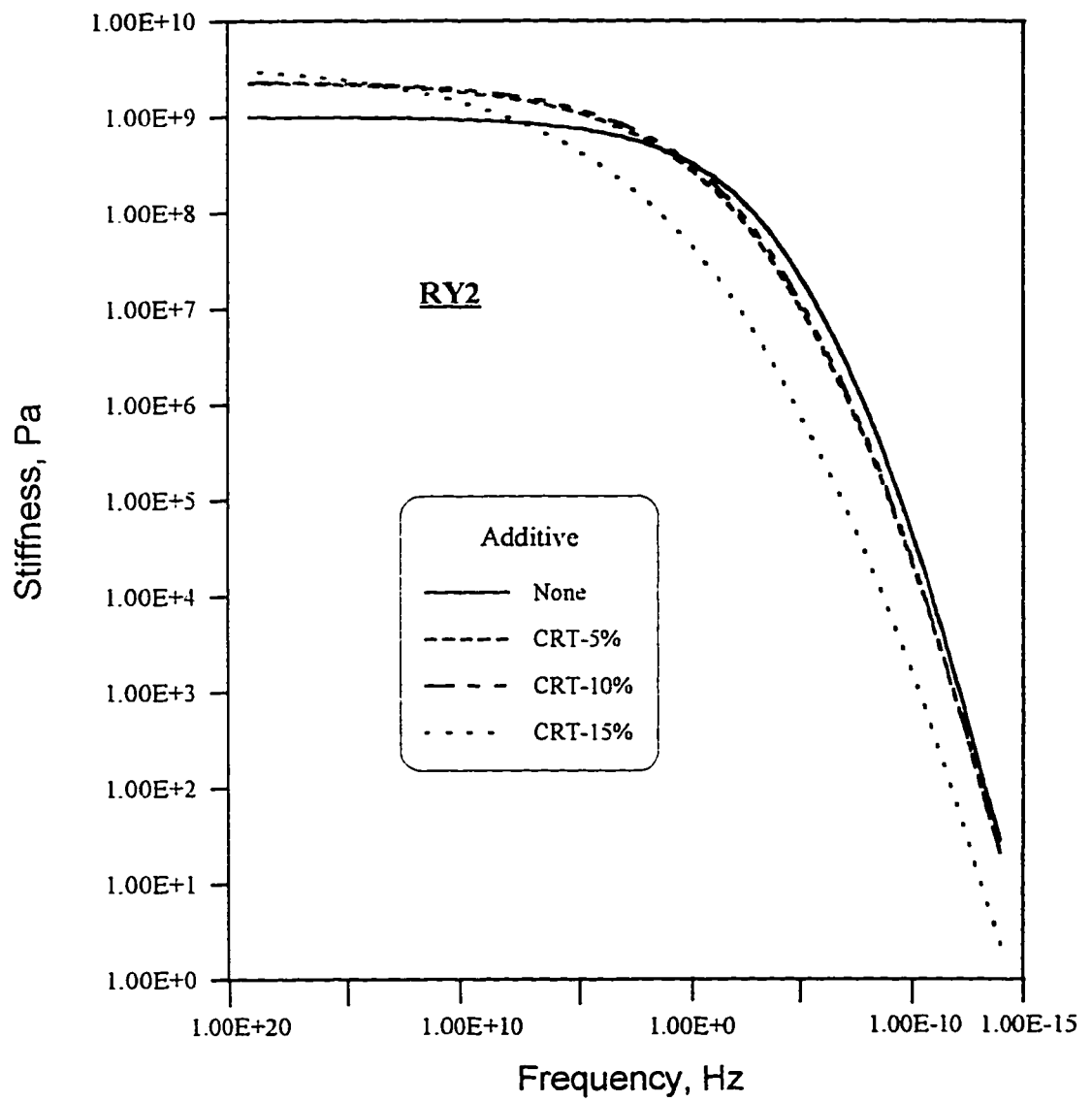


Fig. B-24: Master curves of RY2 modified samples with different percentages of CRT.

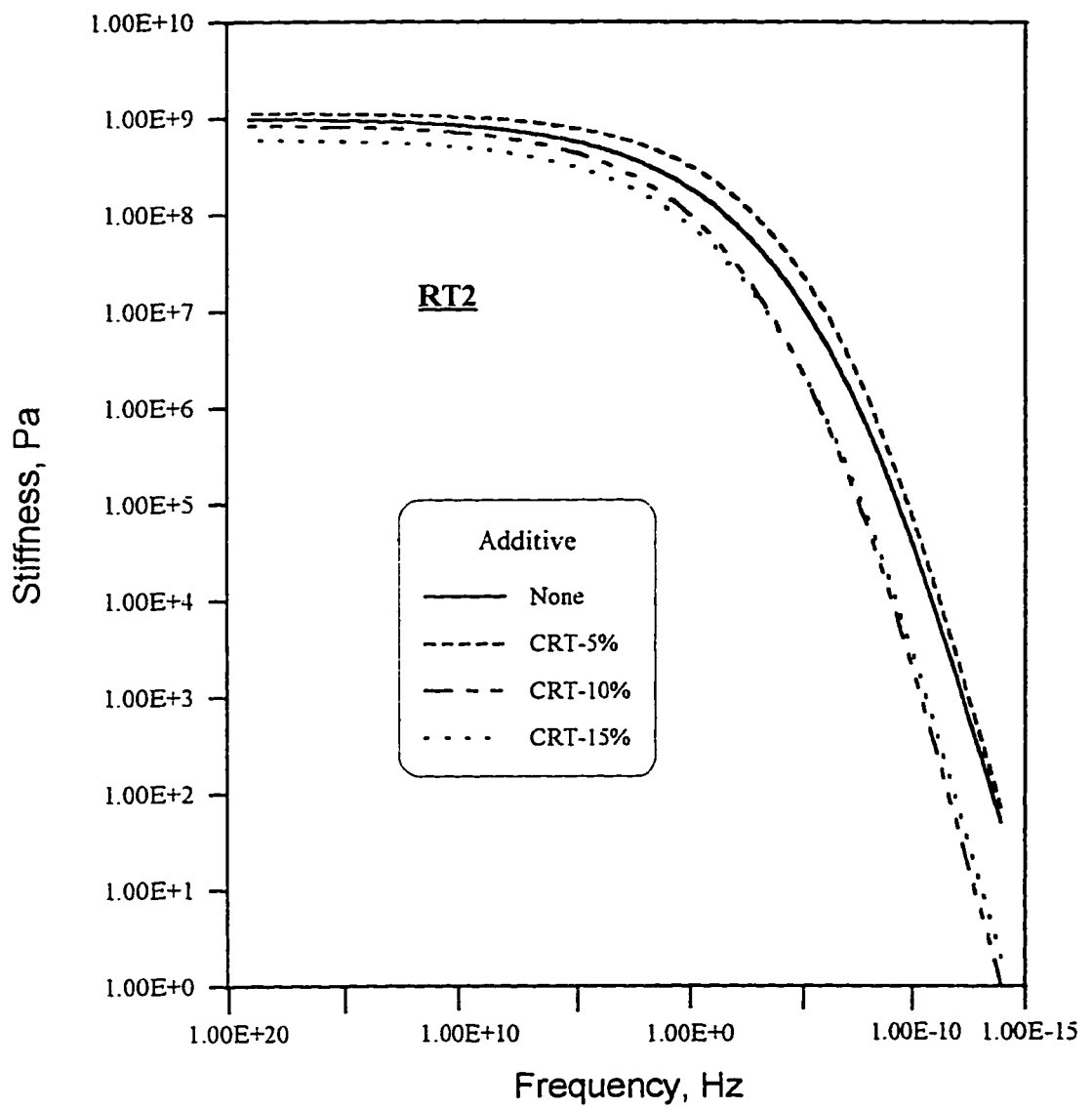


Fig. B-25: Master curves of RT2 modified samples with different percentages of CRT.

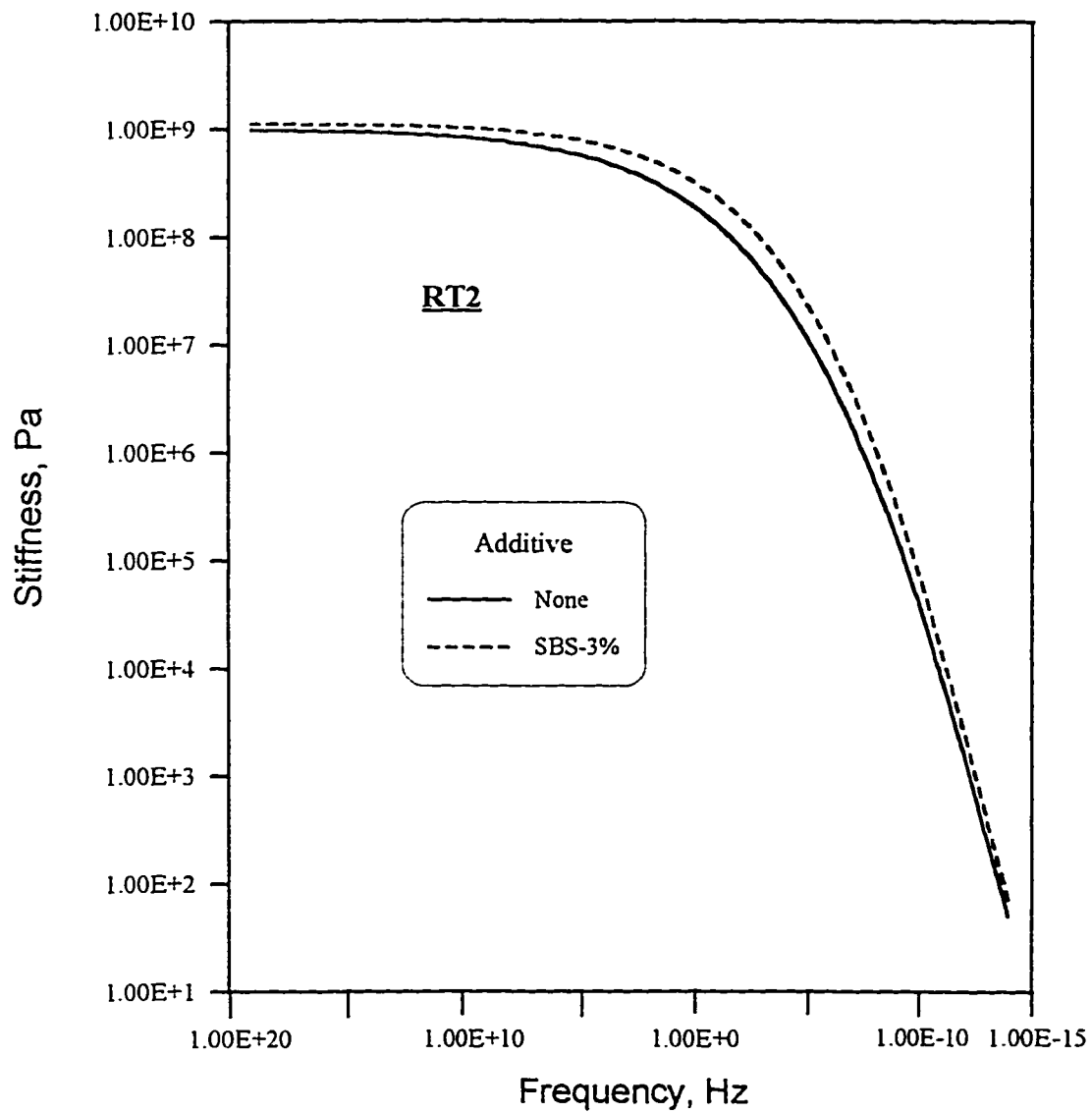


Fig. B-26: Master curves of RT2 modified samples with different percentages of SBS.

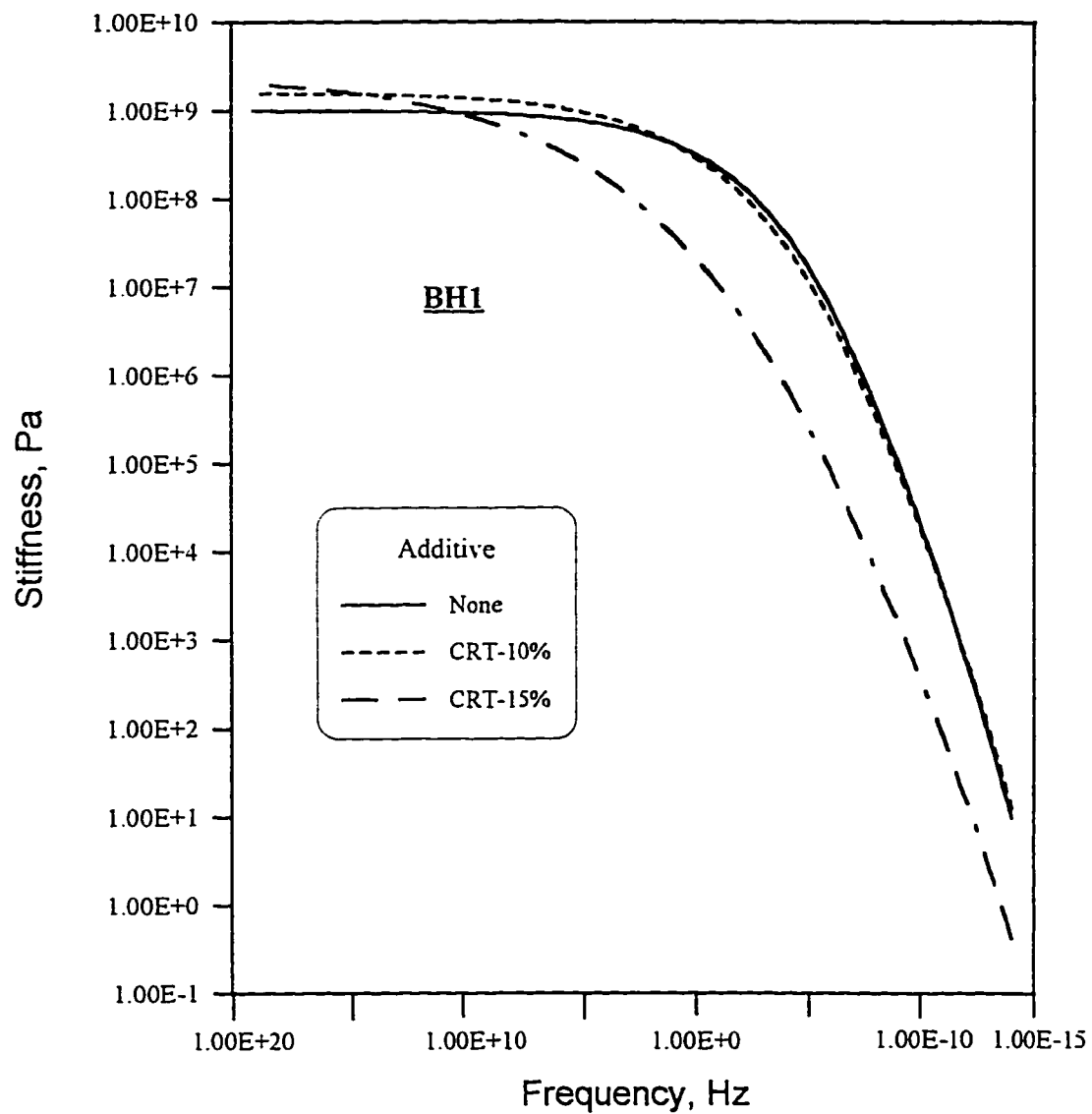


Fig. B-27: Master curves of BH1 modified samples with different percentages of CRT.

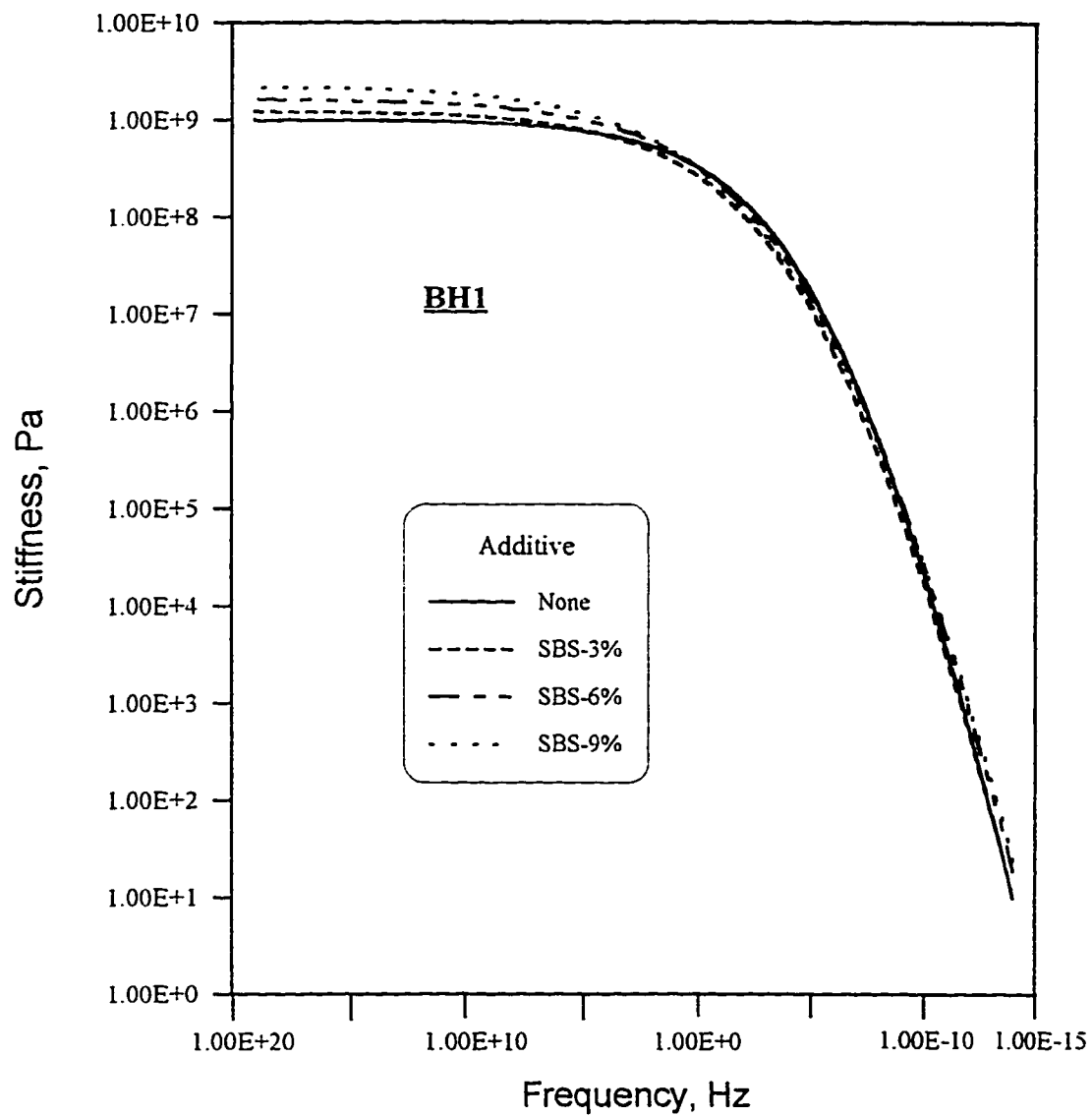


Fig. B-28: Master curves of BH1 modified samples with different percentages of SBS.

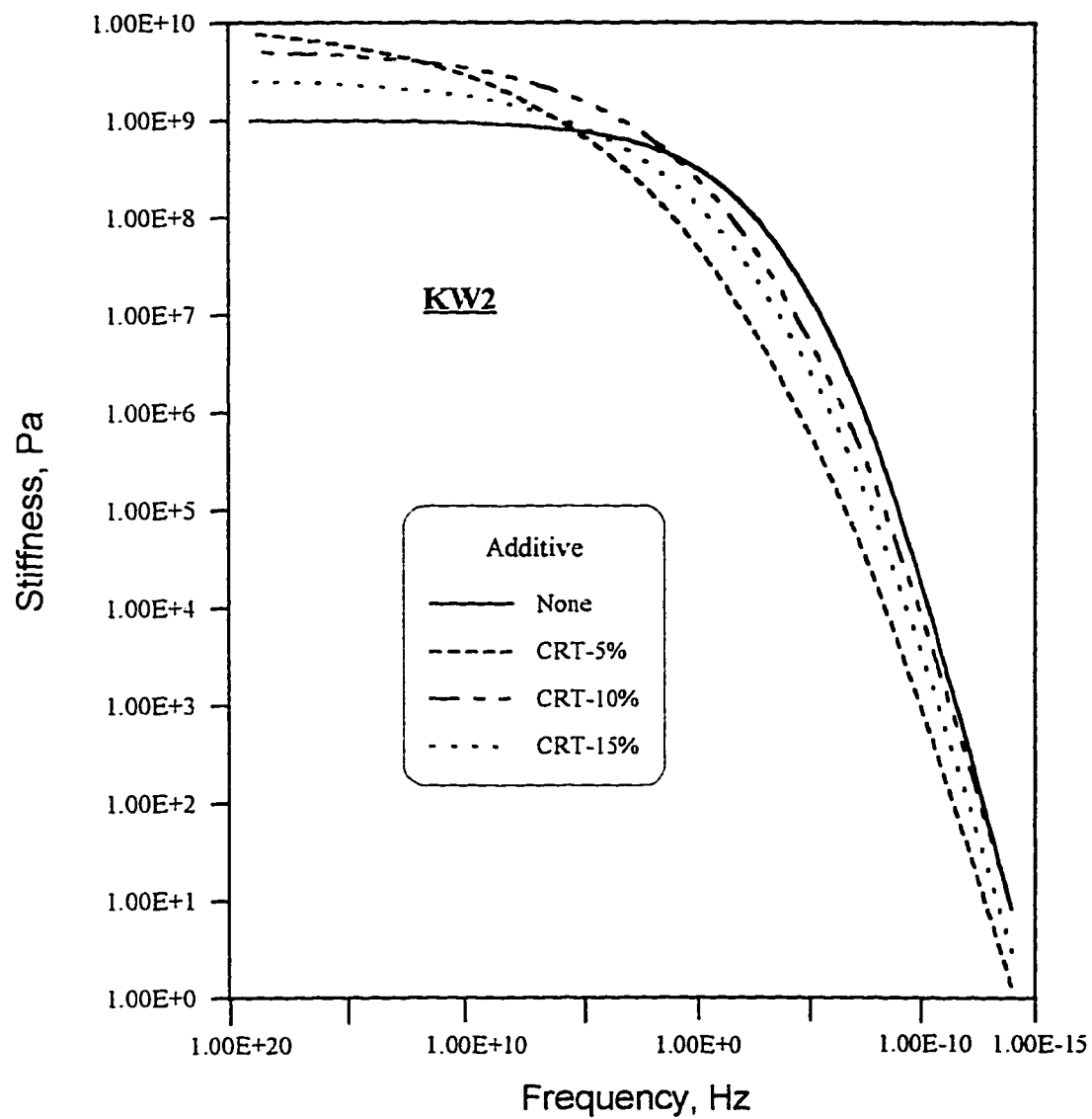


Fig. B-29: Master curves of KW2 modified samples with different percentages of CRT.

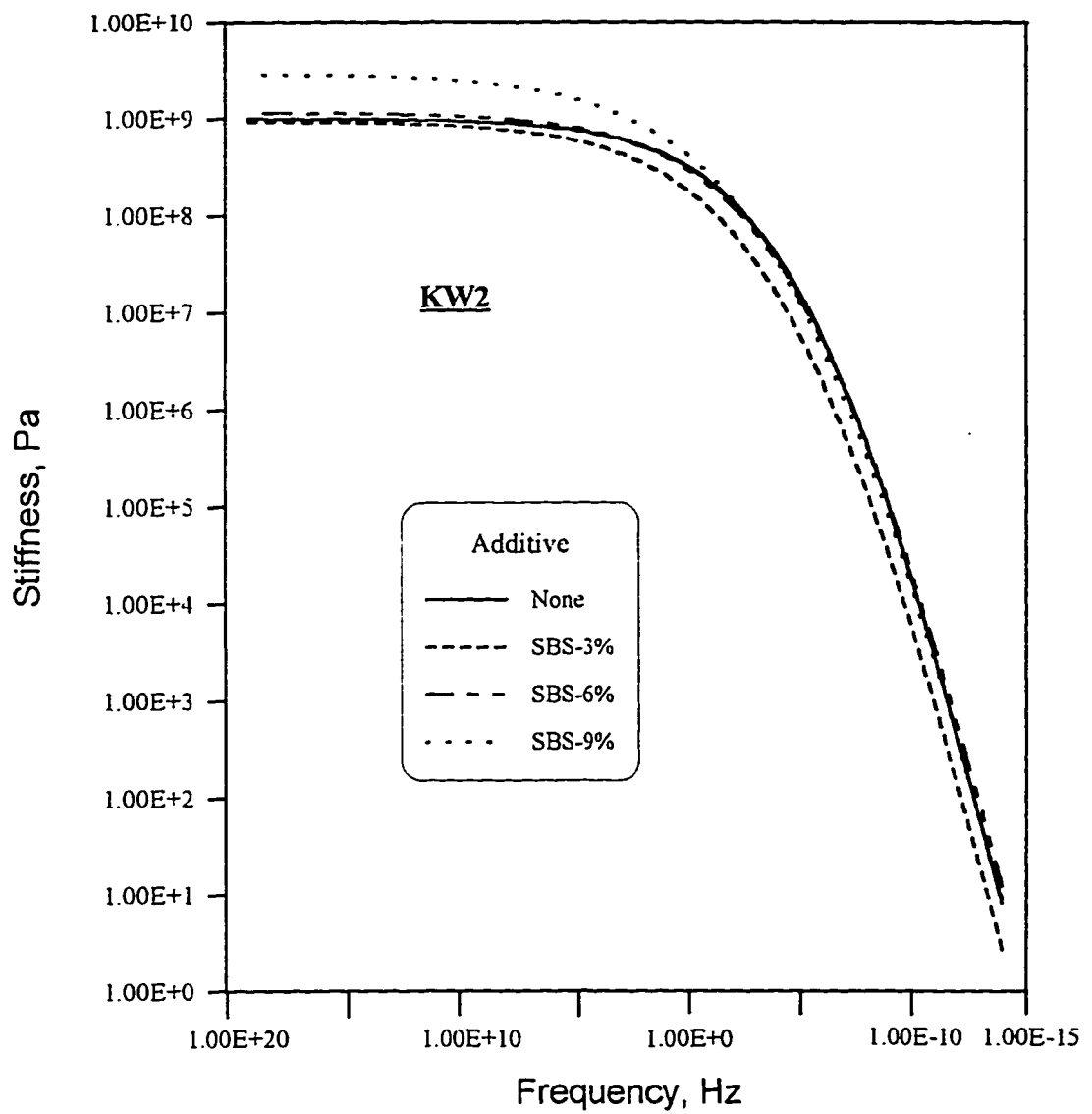


Fig. B-30: Master curves of KW2 modified samples with different percentages of SBS.

Appendix C

Chemical Testing Results

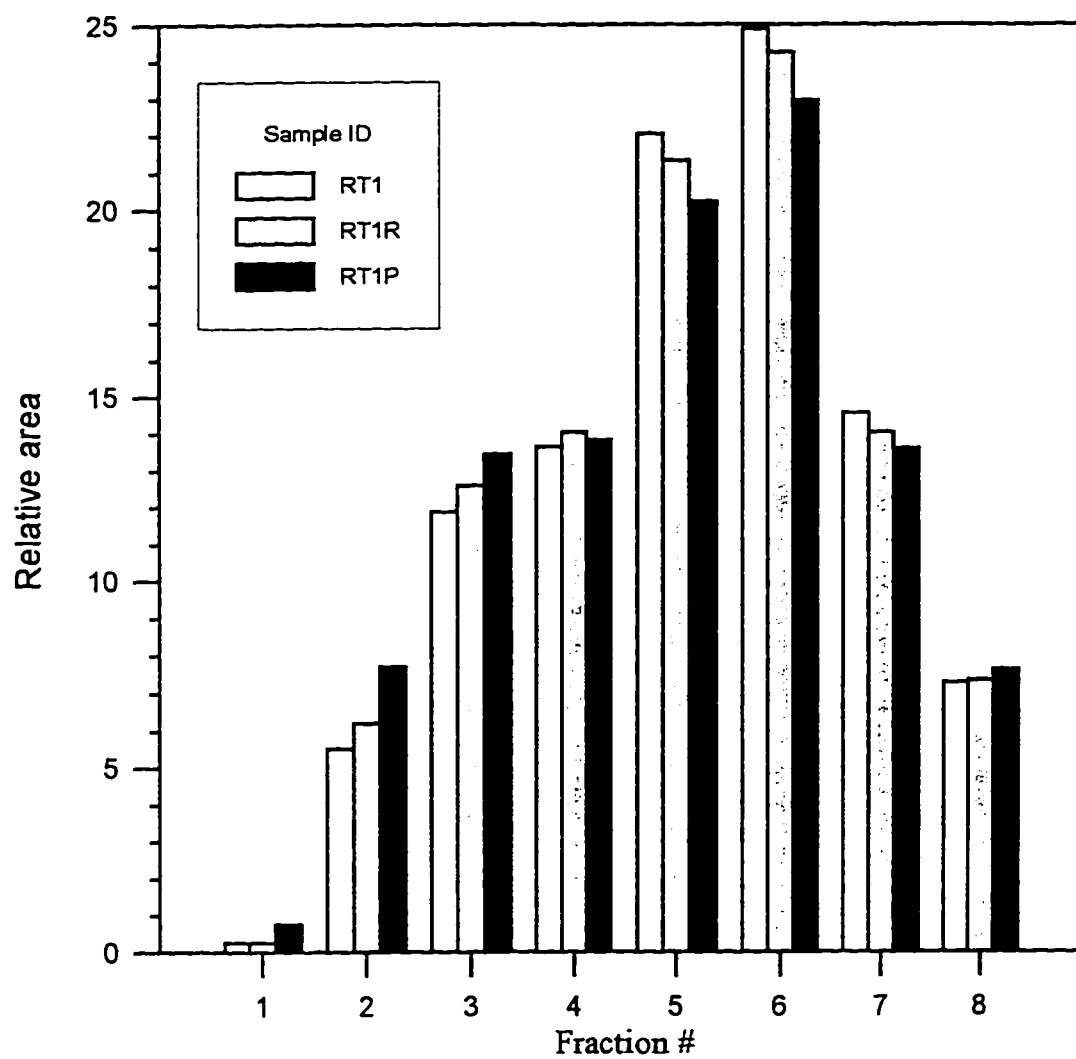


Fig. C-1 : Bar graph comparing molecular sizes of original asphalt (RT1) and its RTFO and PAV residues

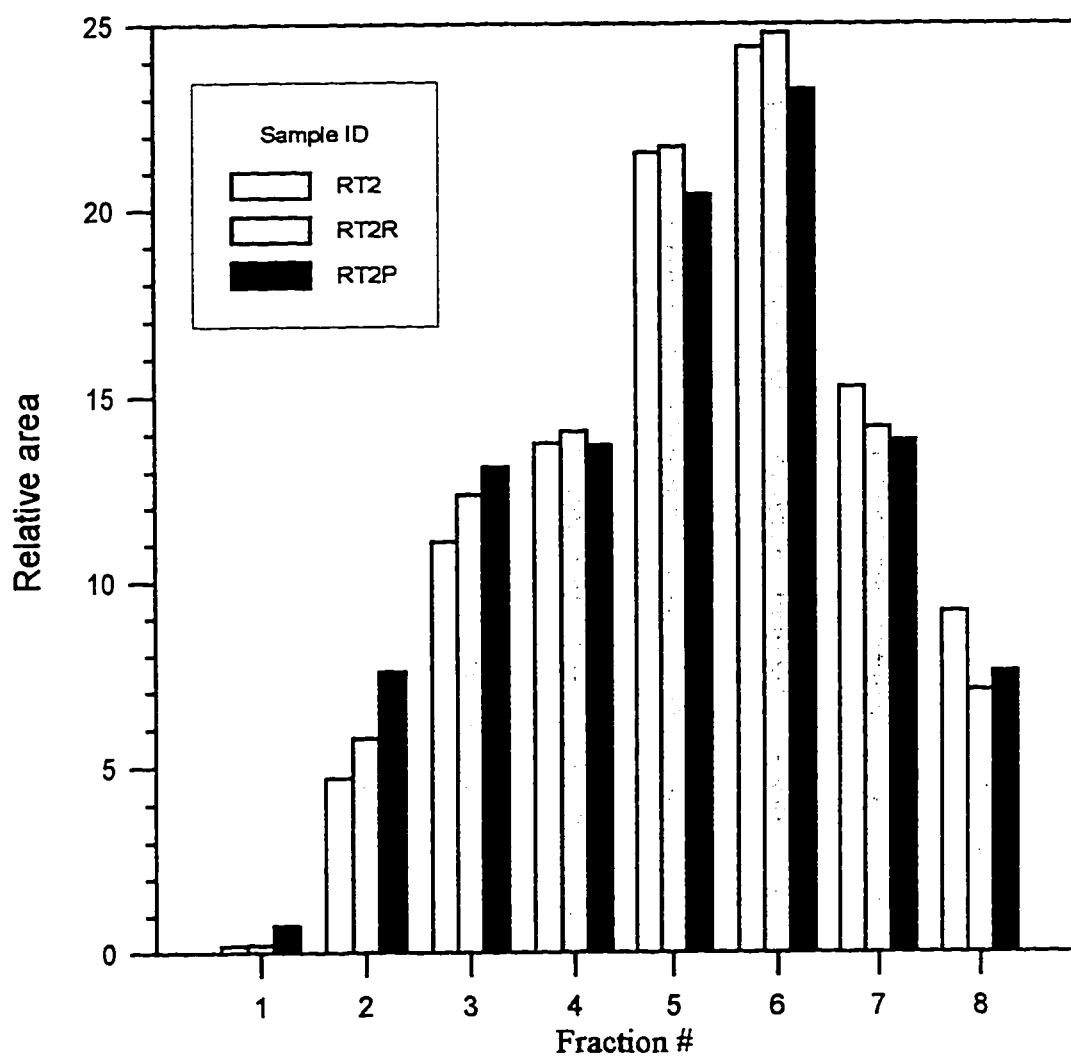


Fig. C-2 : Bar graph comparing molecular sizes of original asphalt (RT2) and its RTFO and PAV residues

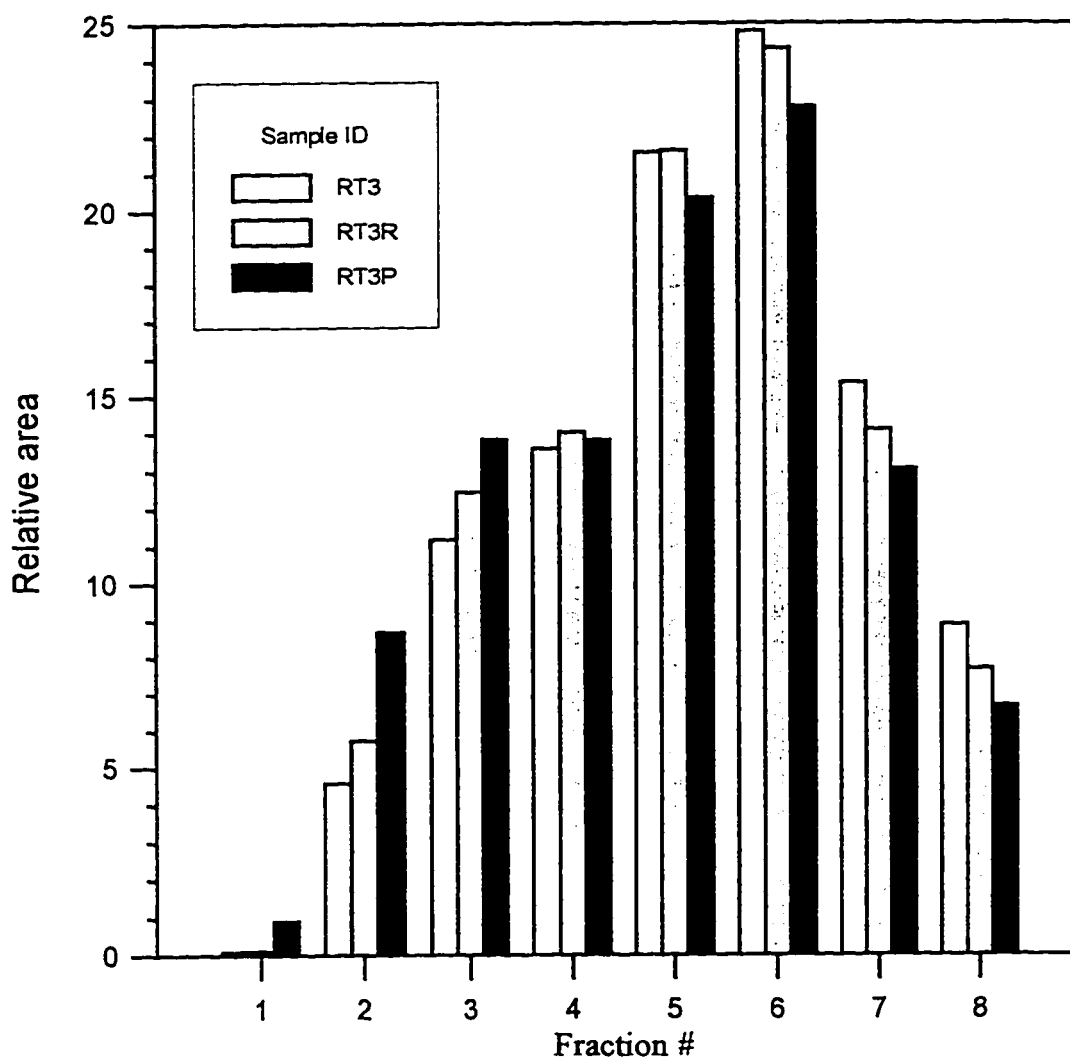


Fig. C-3 : Bar graph comparing molecular sizes of original asphalt (RT3) and its RTFO and PAV residues

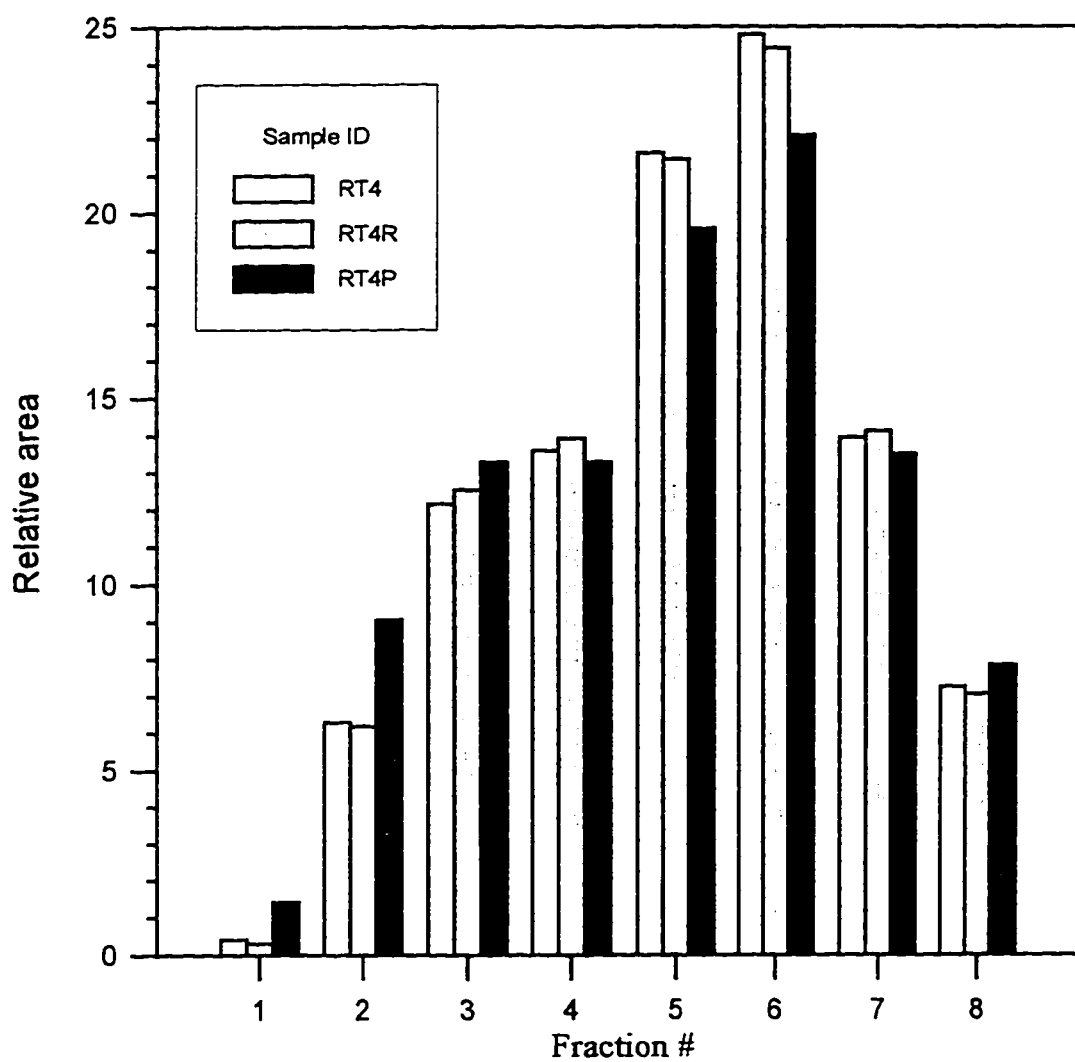


Fig. C-4 : Bar graph comparing molecular sizes of original asphalt (RT4) and its RTFO and PAV residues

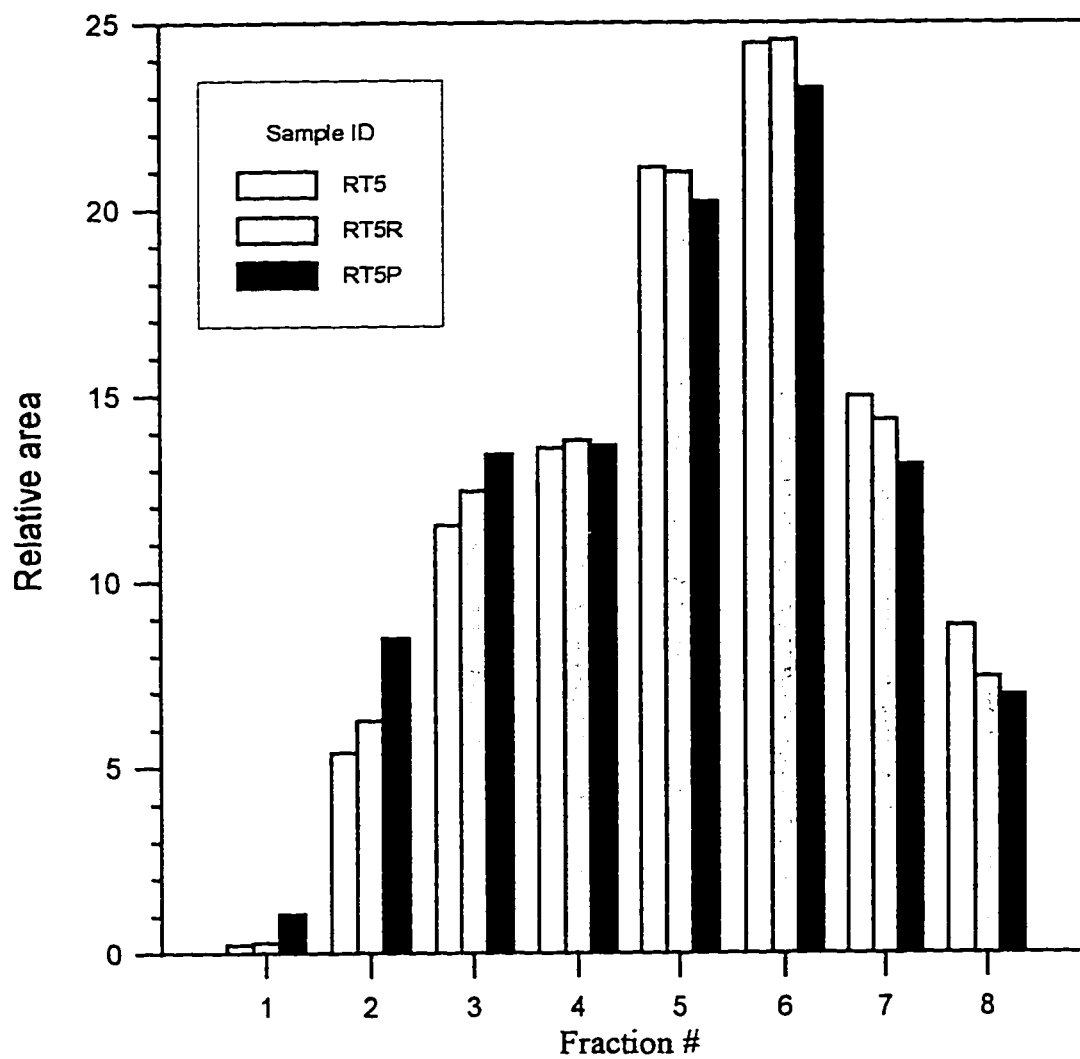


Fig. C-5 : Bar graph comparing molecular sizes of original asphalt (RT5) and its RTFO and PAV residues

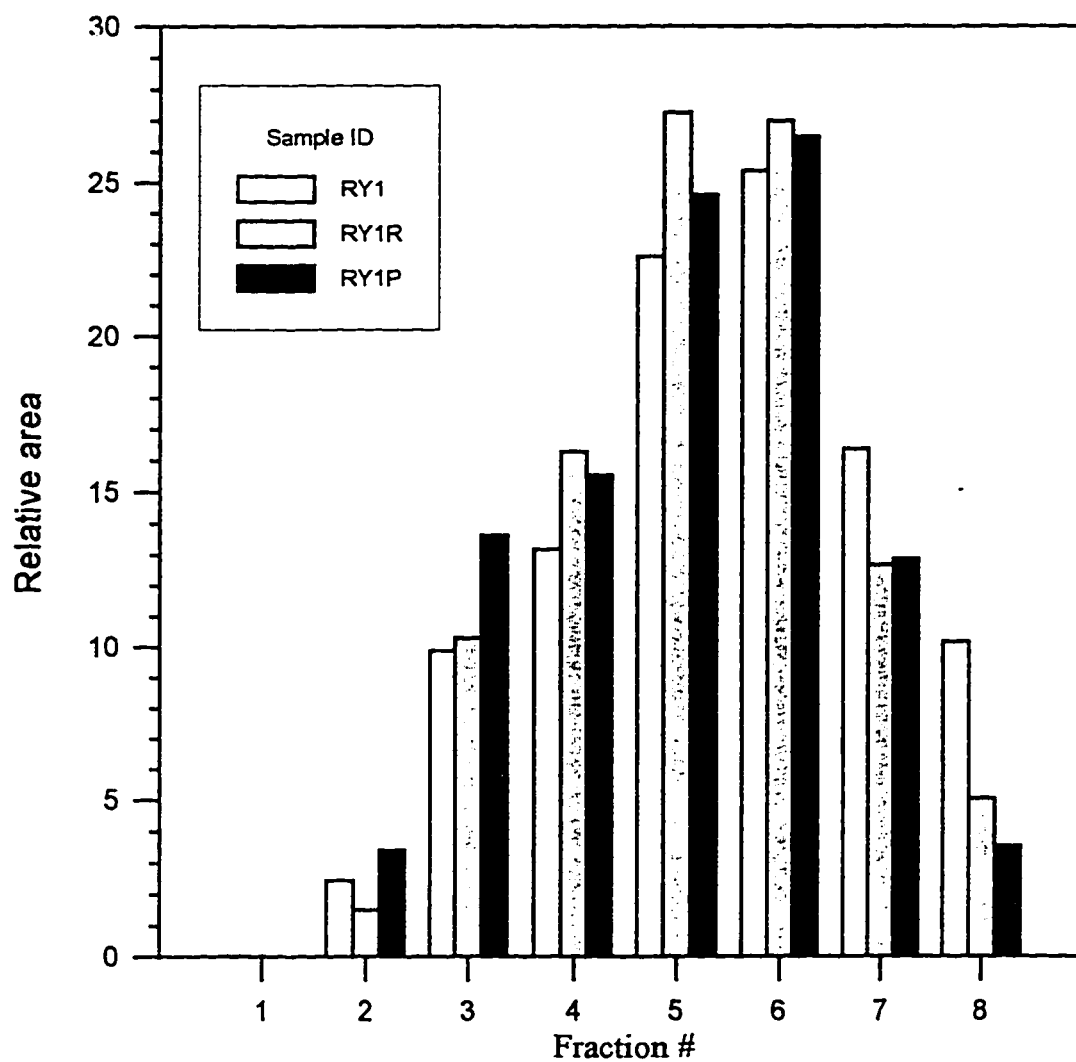


Fig. C-6 : Bar graph comparing molecular sizes of original asphalt (RY1) and its RTFO and PAV residues

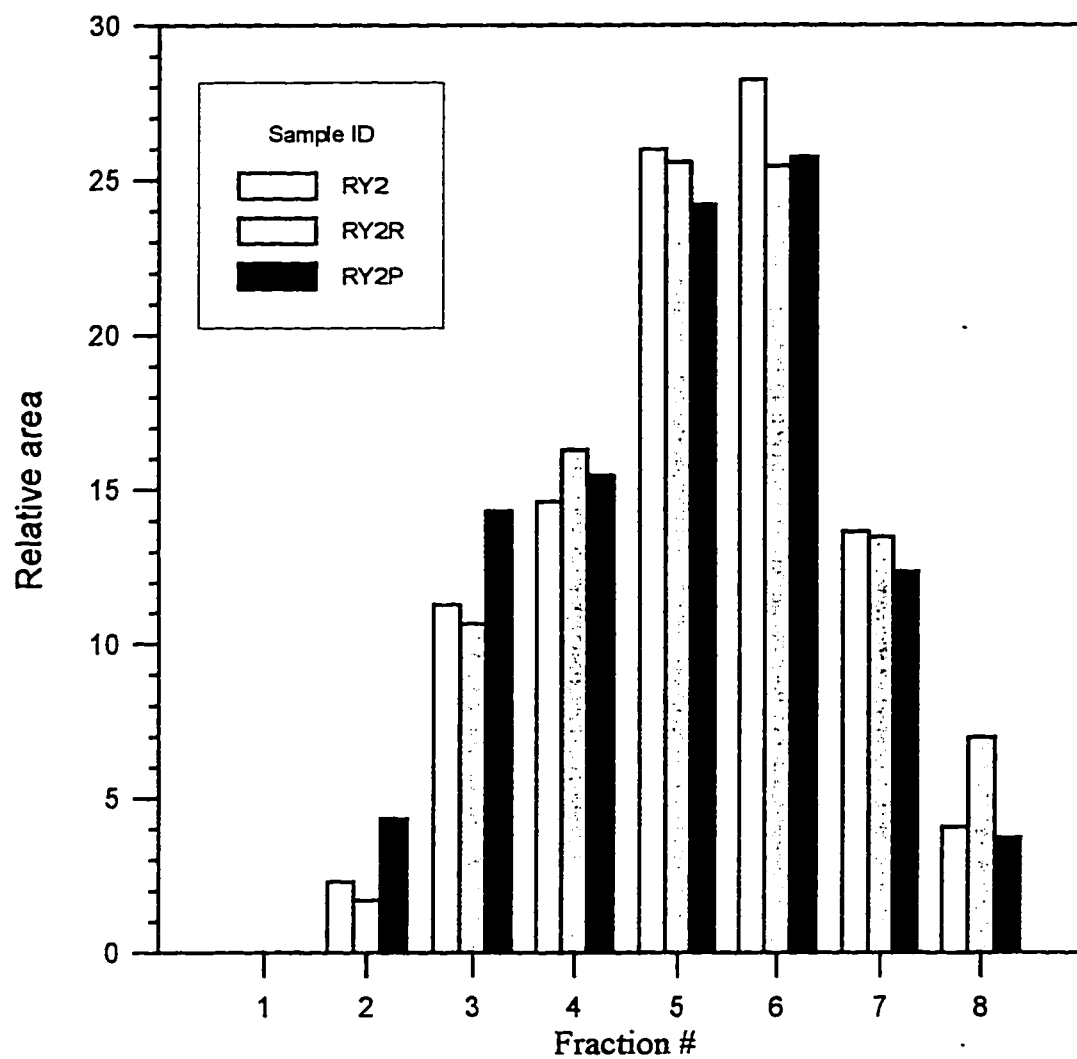


Fig. C-7 : Bar graph comparing molecular sizes of original asphalt (RY2) and its RTFO and PAV residues

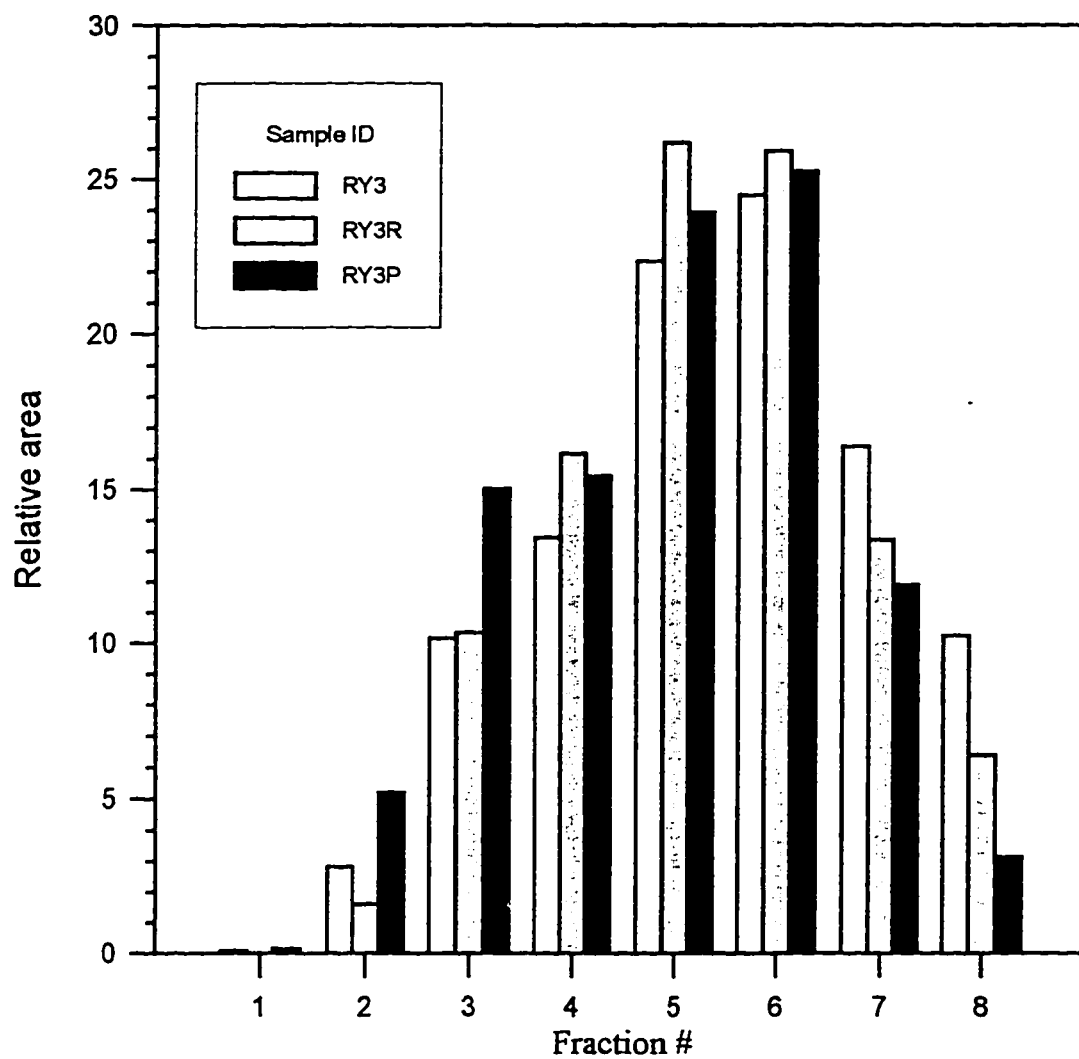


Fig. C-8 : Bar graph comparing molecular sizes of original asphalt (RY3) and its RTFO and PAV residues

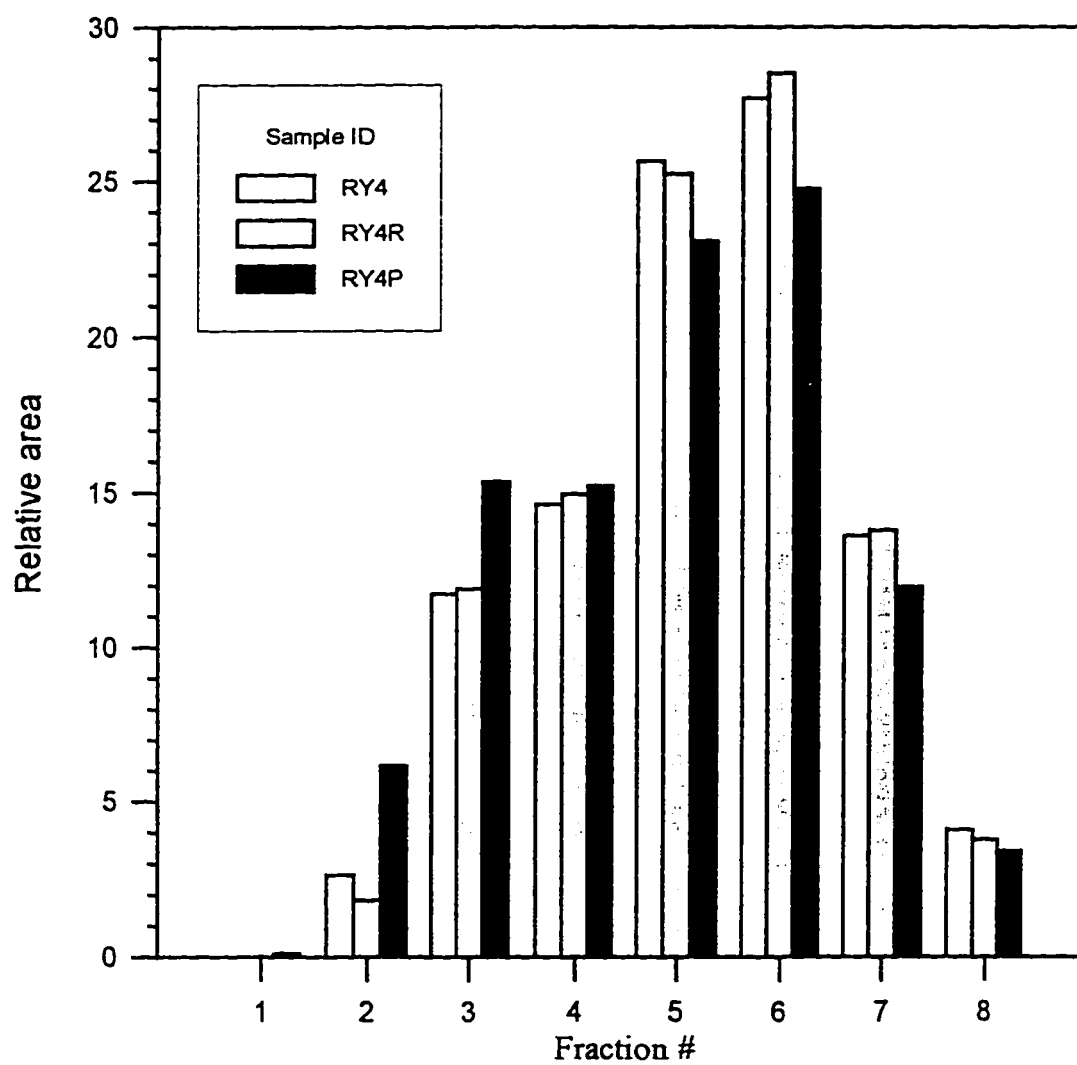


Fig. C-9: Bar graph comparing molecular sizes of original asphalt (RY4) and its RTFO and PAV residues

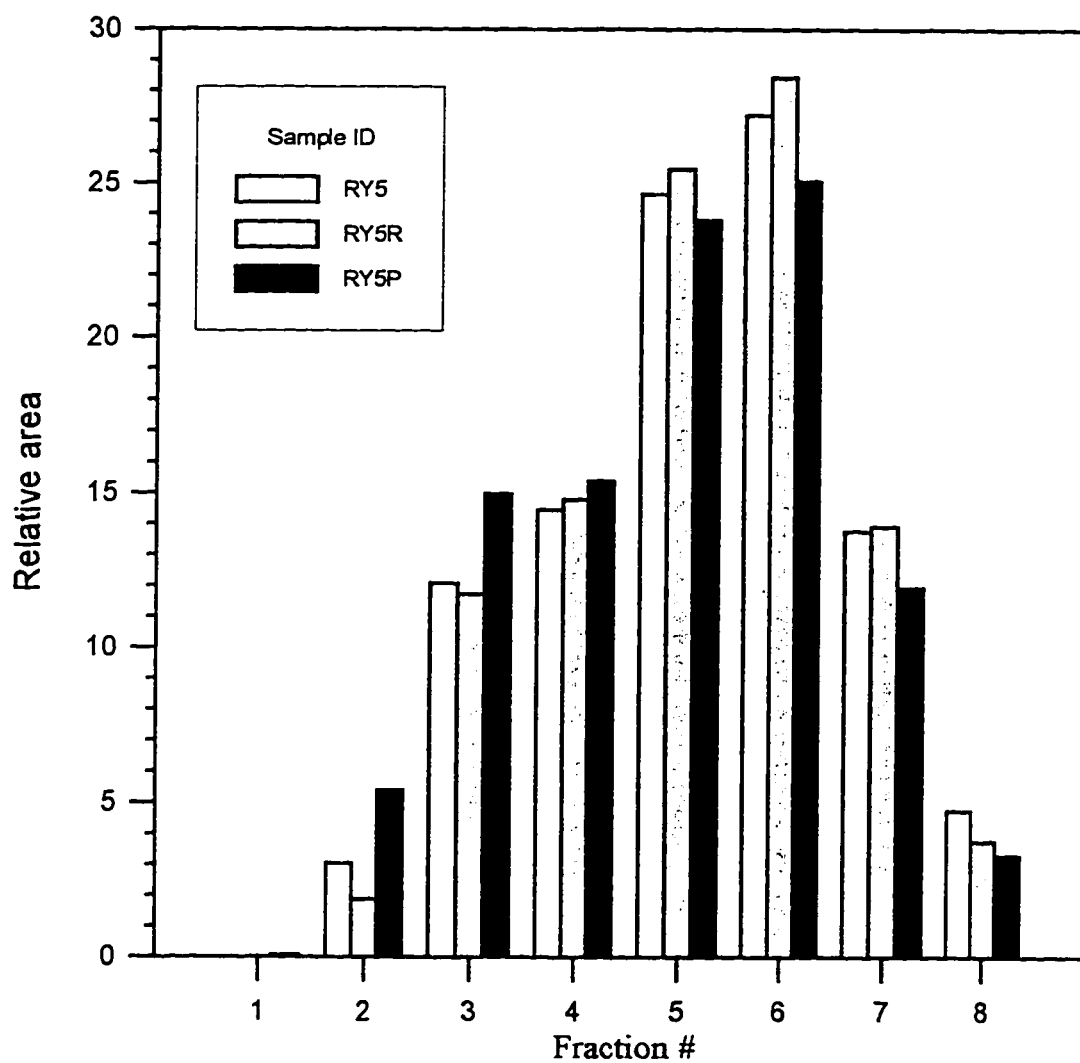


Fig. C-10 : Bar graph comparing molecular sizes of original asphalt (RY5) and its RTFO and PAV residues

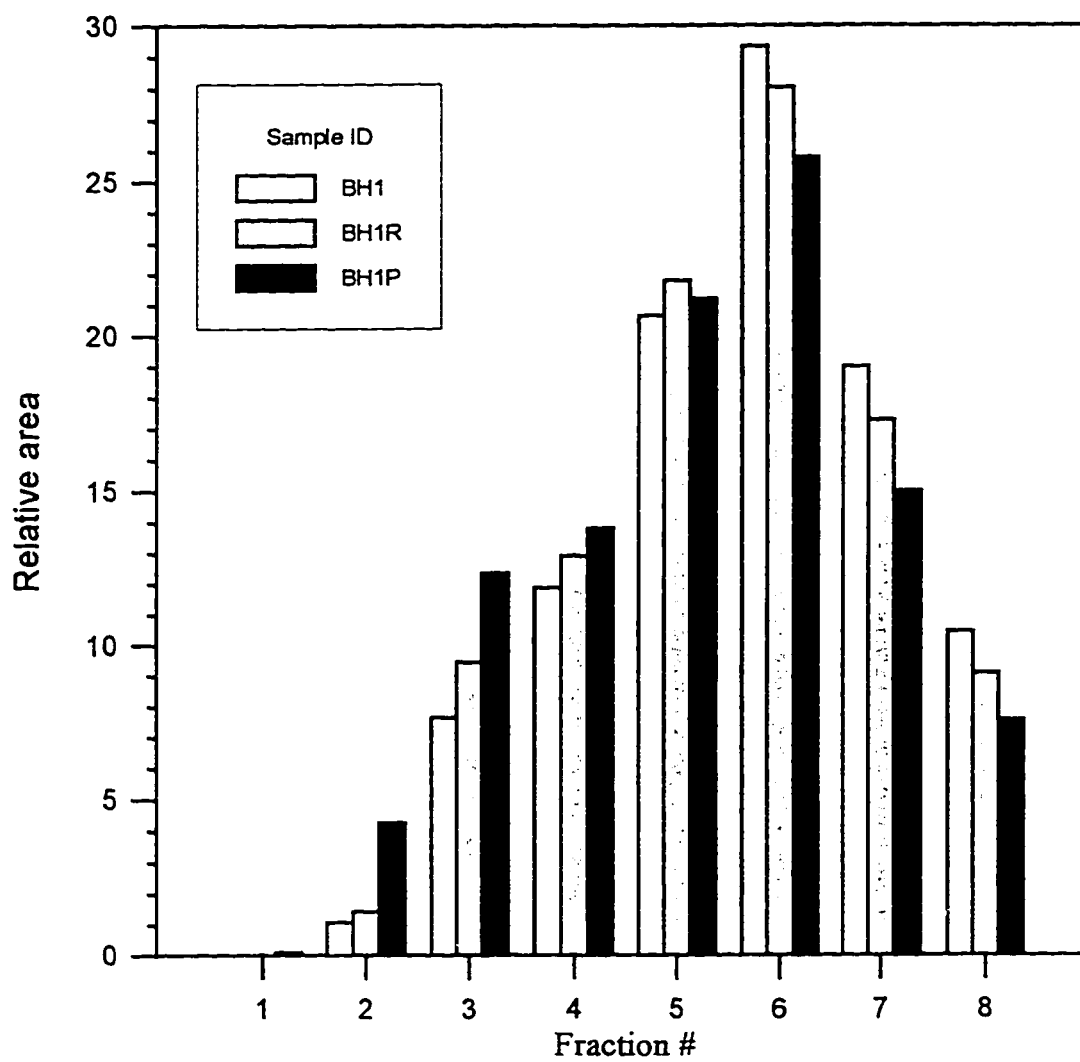


Fig. C-11 : Bar graph comparing molecular sizes of original asphalt (BH1) and its RTFO and PAV residues

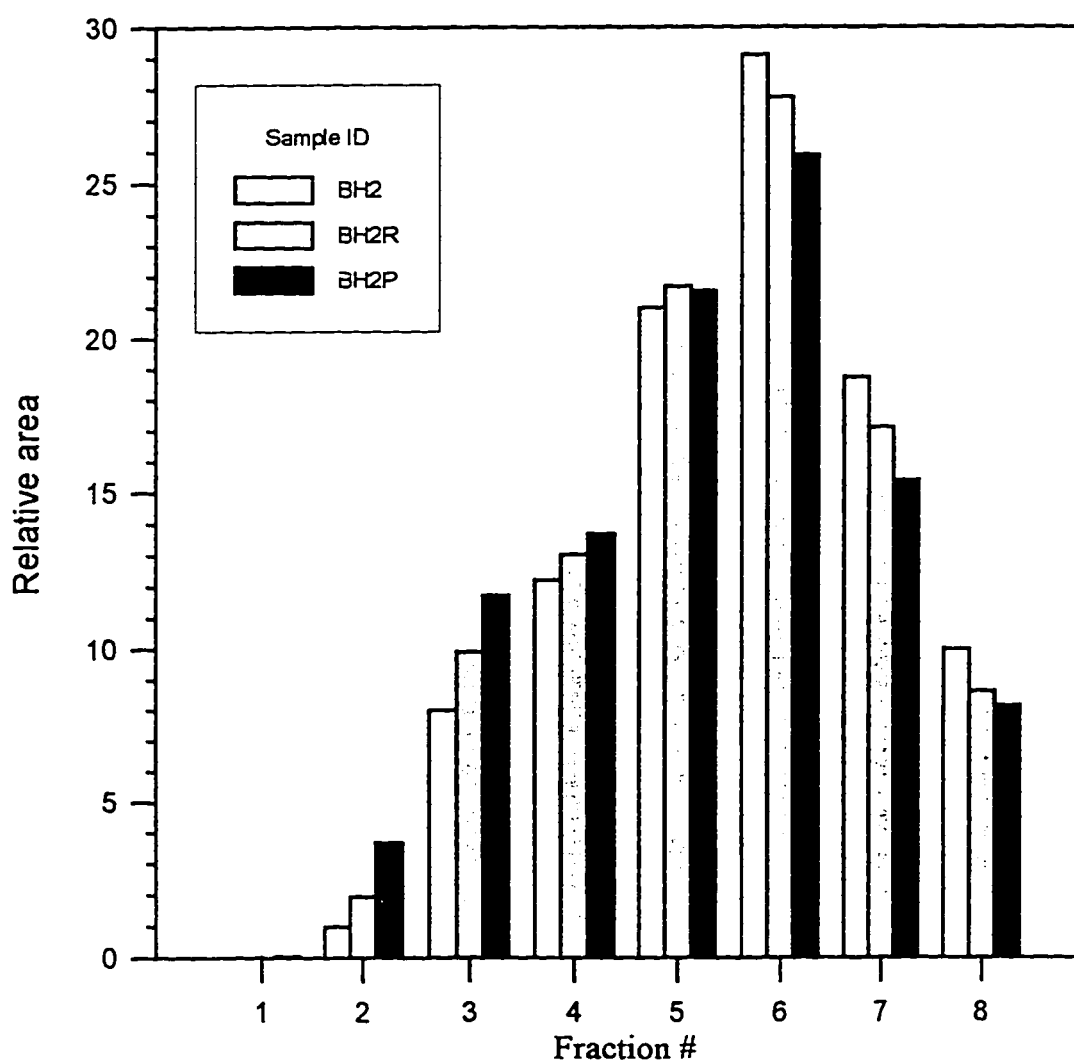


Fig. C-12 : Bar graph comparing molecular sizes of original asphalt (BH2) and its RTFO and PAV residues

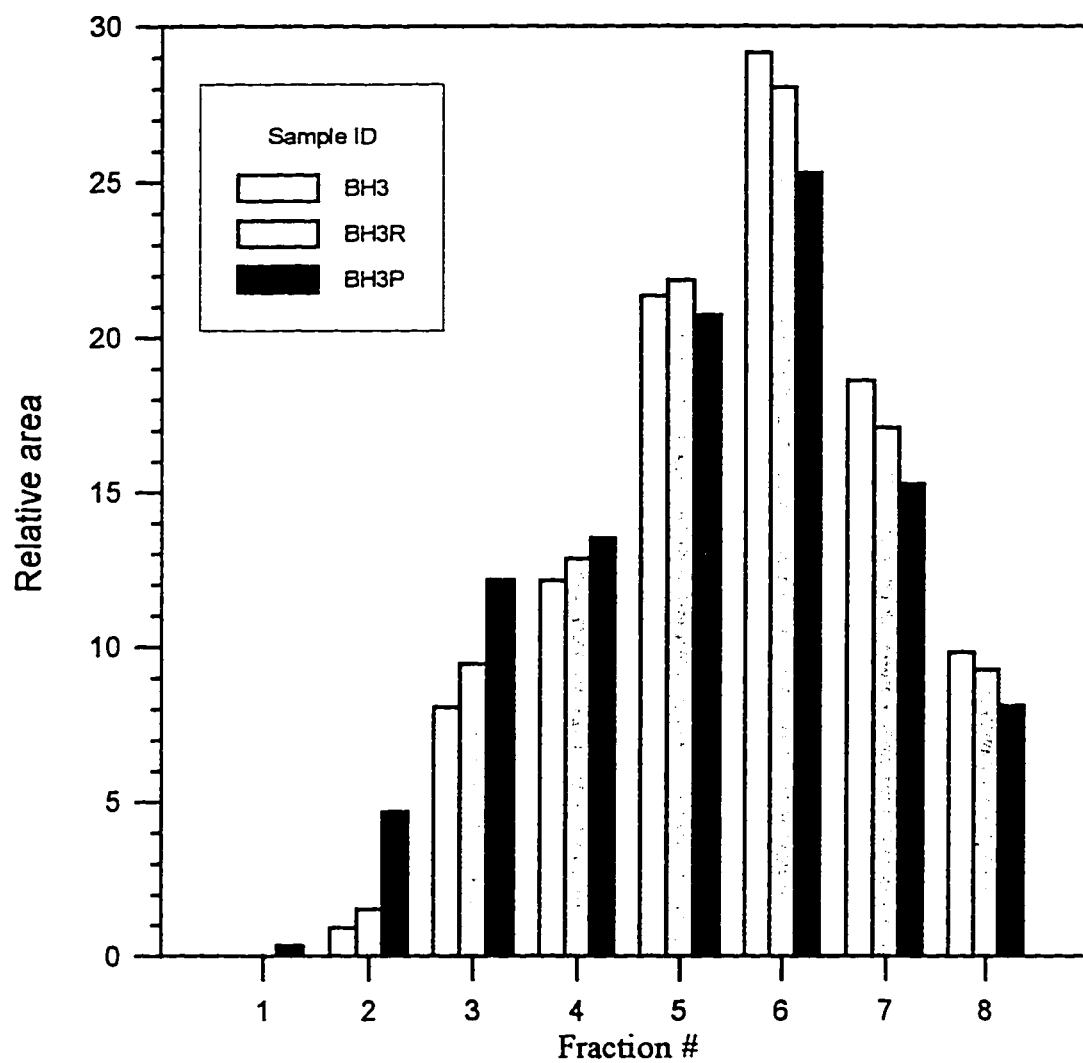


Fig. C-13 : Bar graph comparing molecular sizes of original asphalt (BH3) and its RTFO and PAV residues

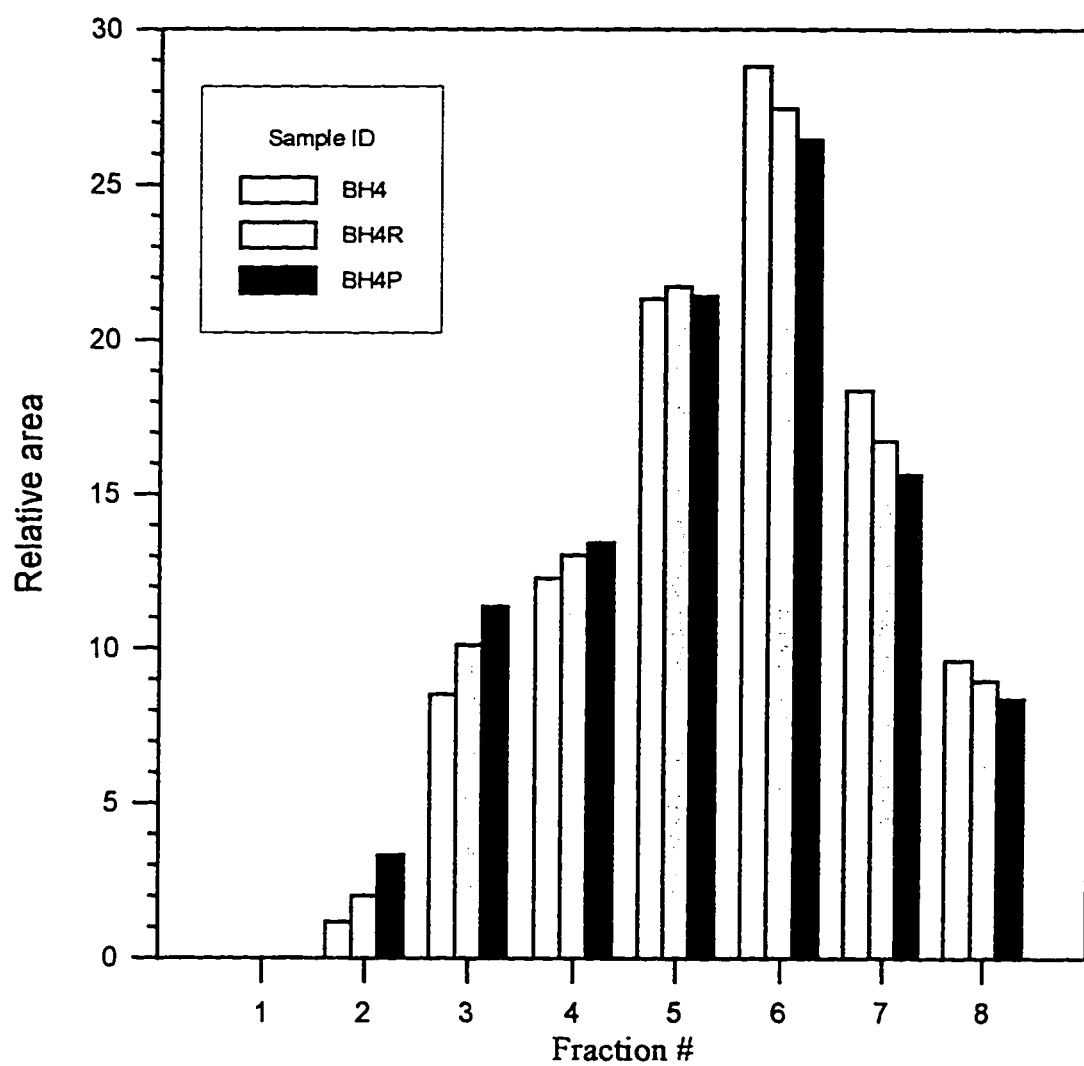


Fig. C-14 : Bar graph comparing molecular sizes of original asphalt (BH4) and its RTFO and PAV residues

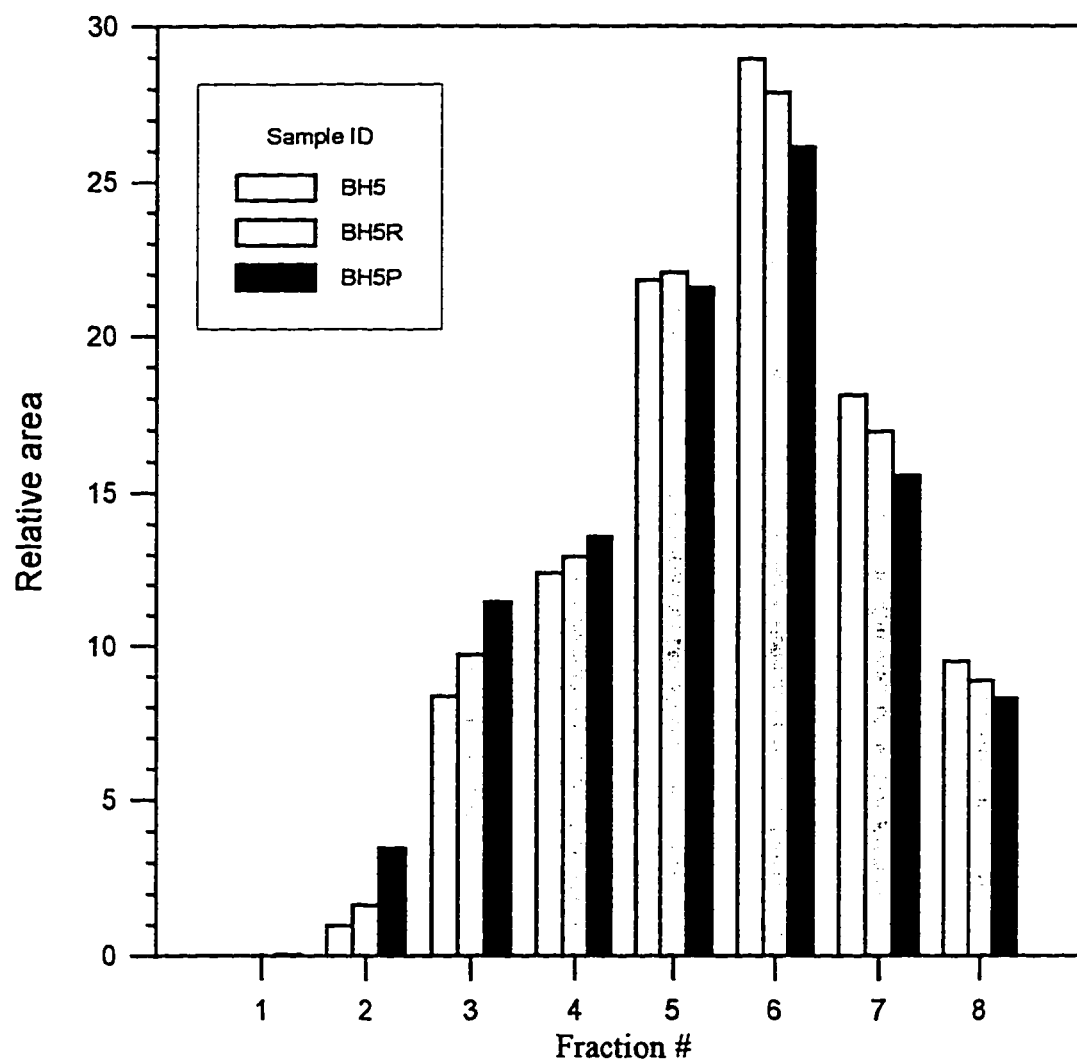


Fig. C-15 : Bar graph comparing molecular sizes of original asphalt (BH5) and its RTFO and PAV residues

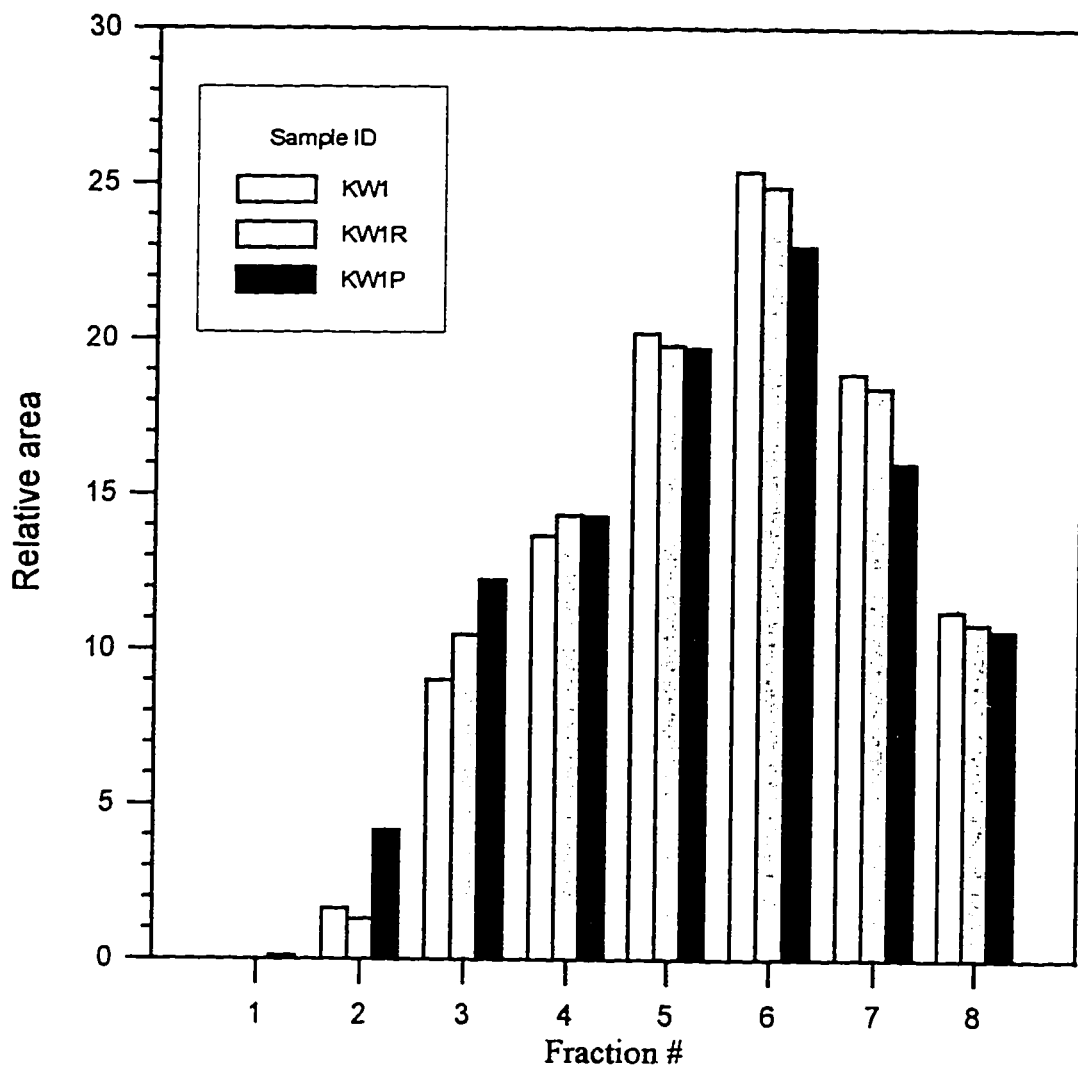


Fig. C-16 : Bar graph comparing molecular sizes of original asphalt (KW1) and its RTFO and PAV residues

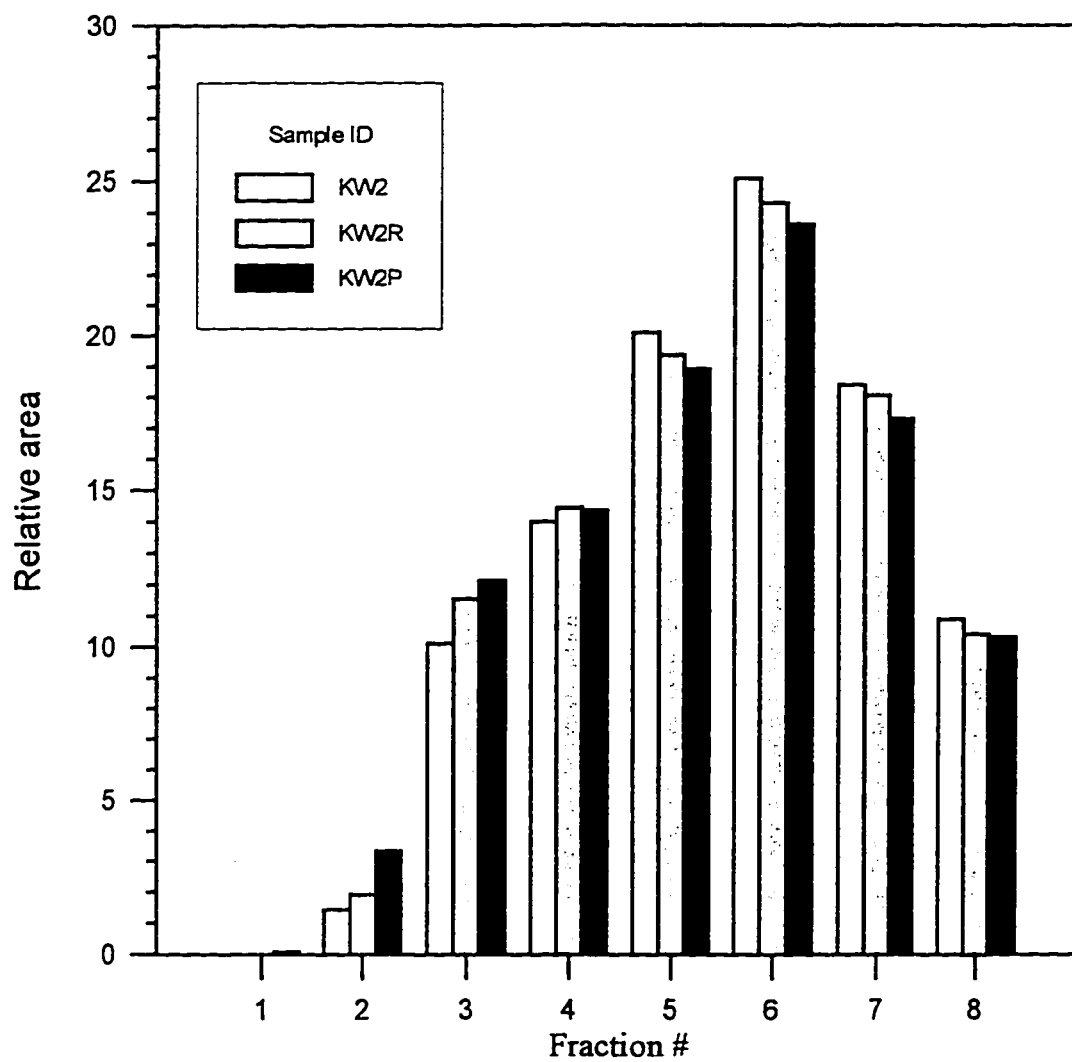


Fig. C-17 : Bar graph comparing molecular sizes of original asphalt (KW2) and its RTFO and PAV residues

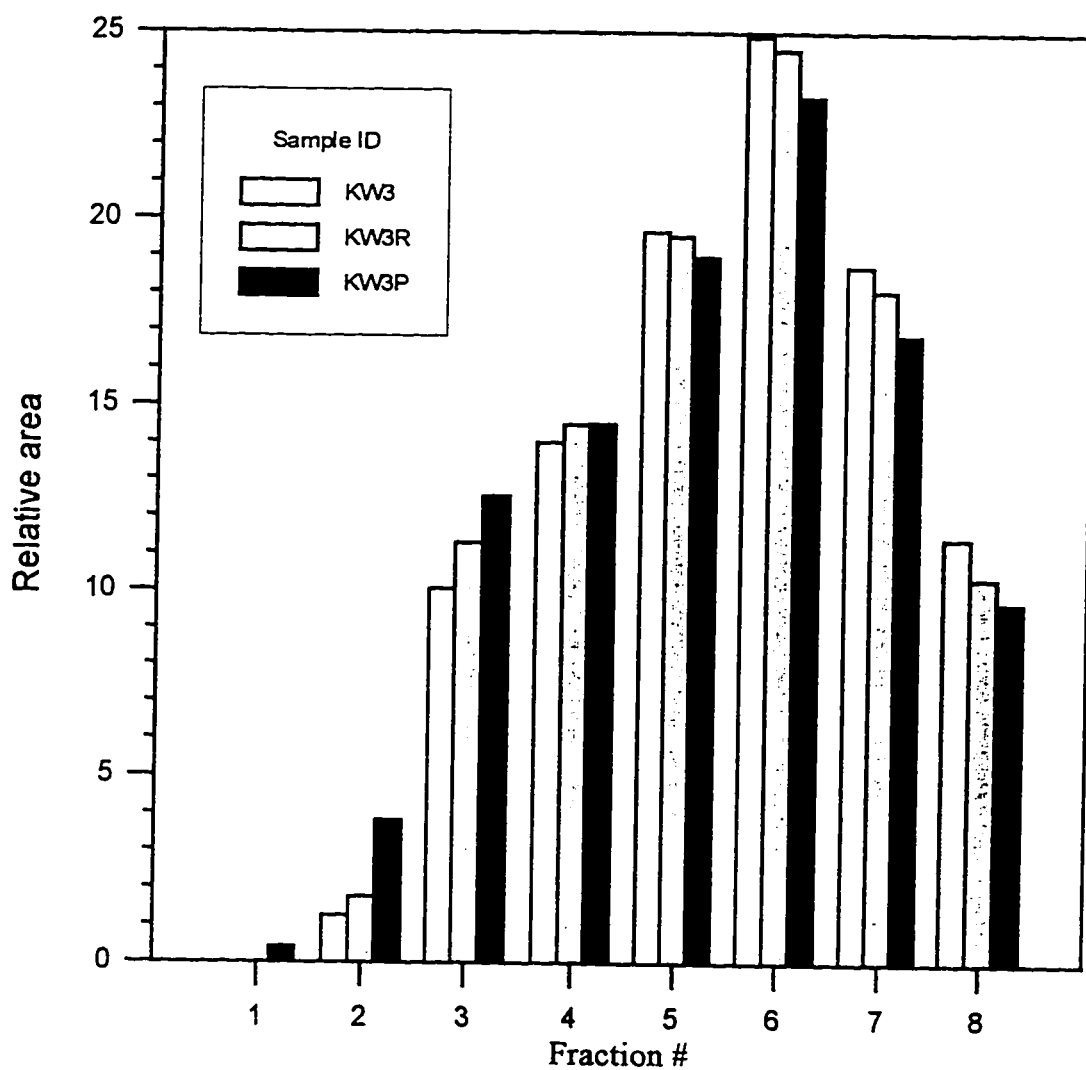


Fig. C-18 : Bar graph comparing molecular sizes of original asphalt (KW3) and its RTFO and PAV residues

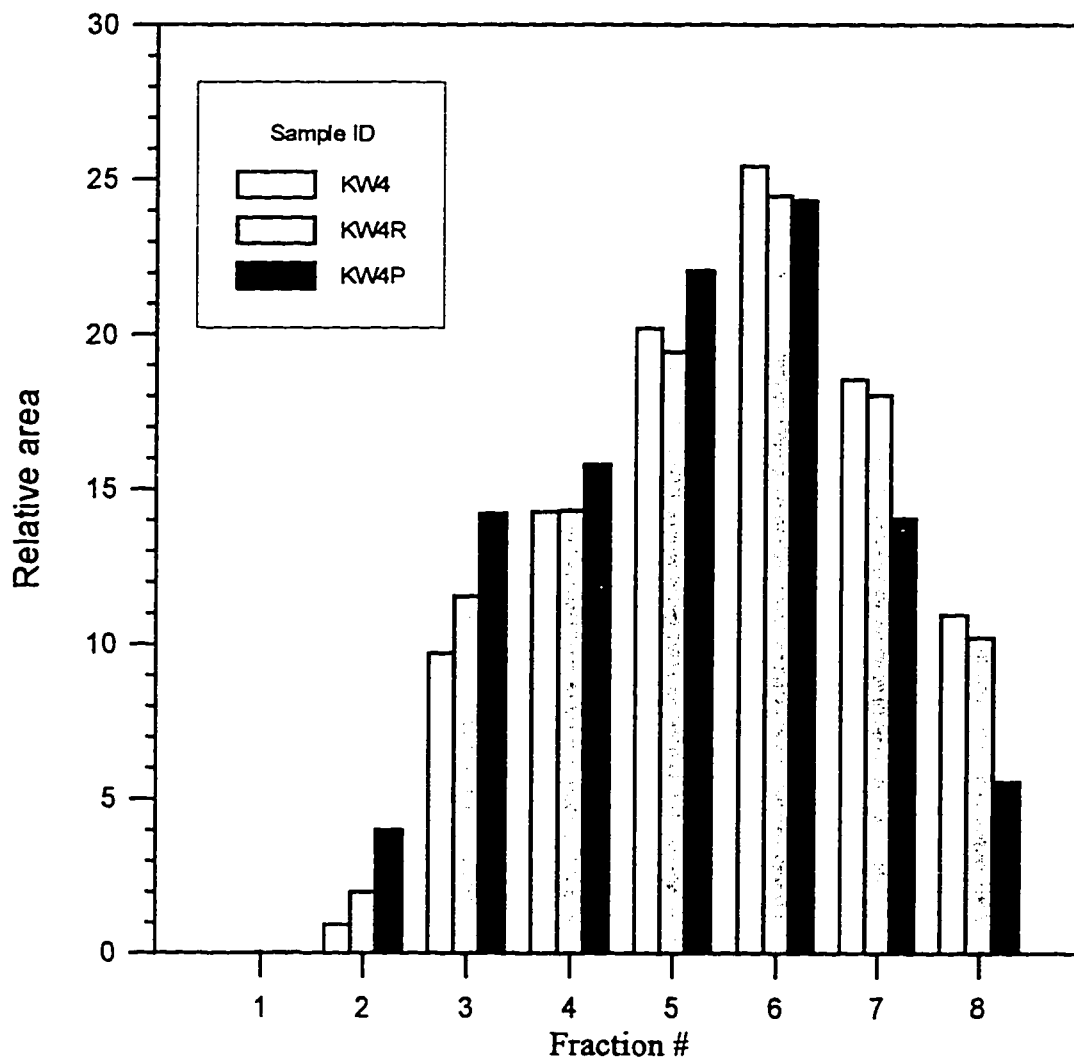


Fig. C-19 : Bar graph comparing molecular sizes of original asphalt (KW4) and its RTFO and PAV residues

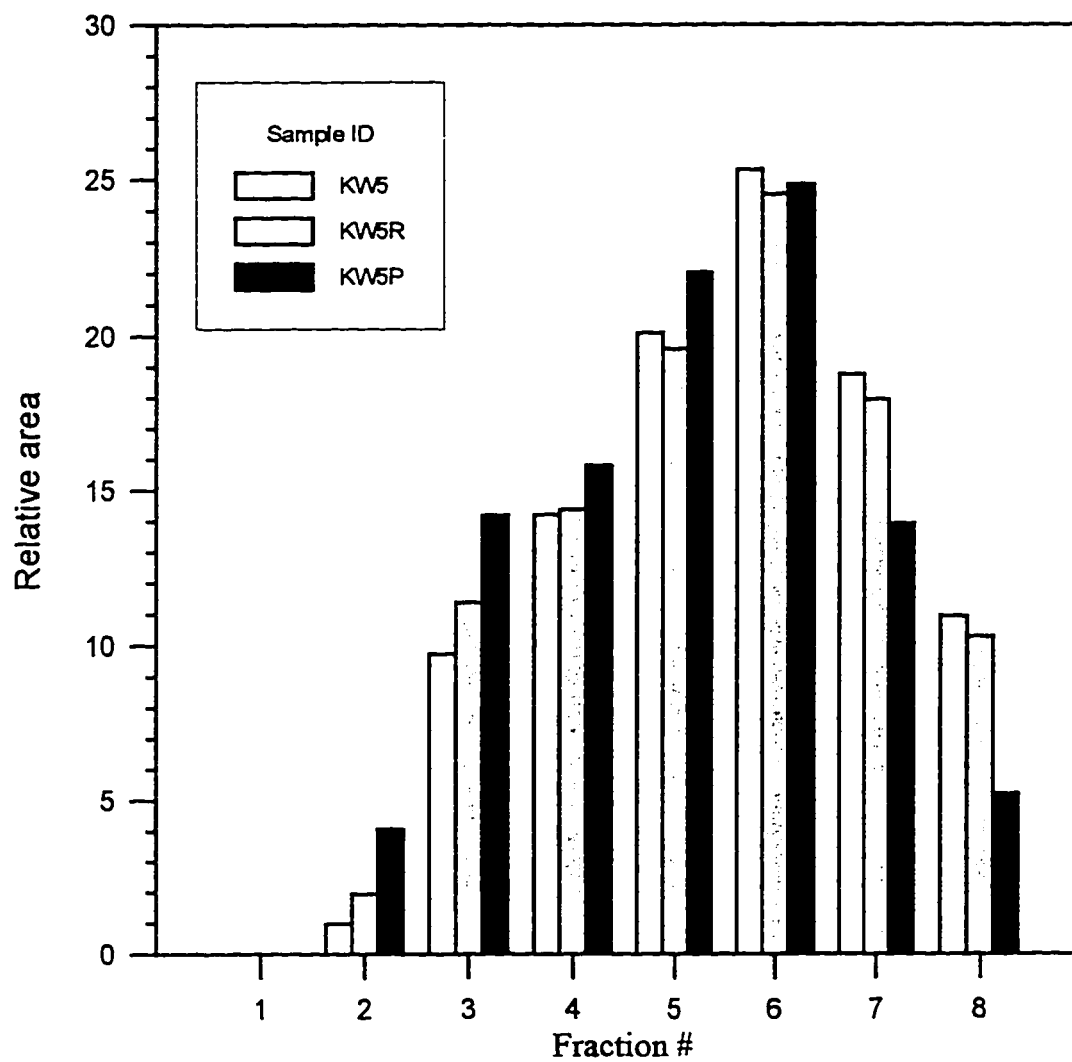


Fig. C-20 : Bar graph comparing molecular sizes of original asphalt (KW5) and its RTFO and PAV residues

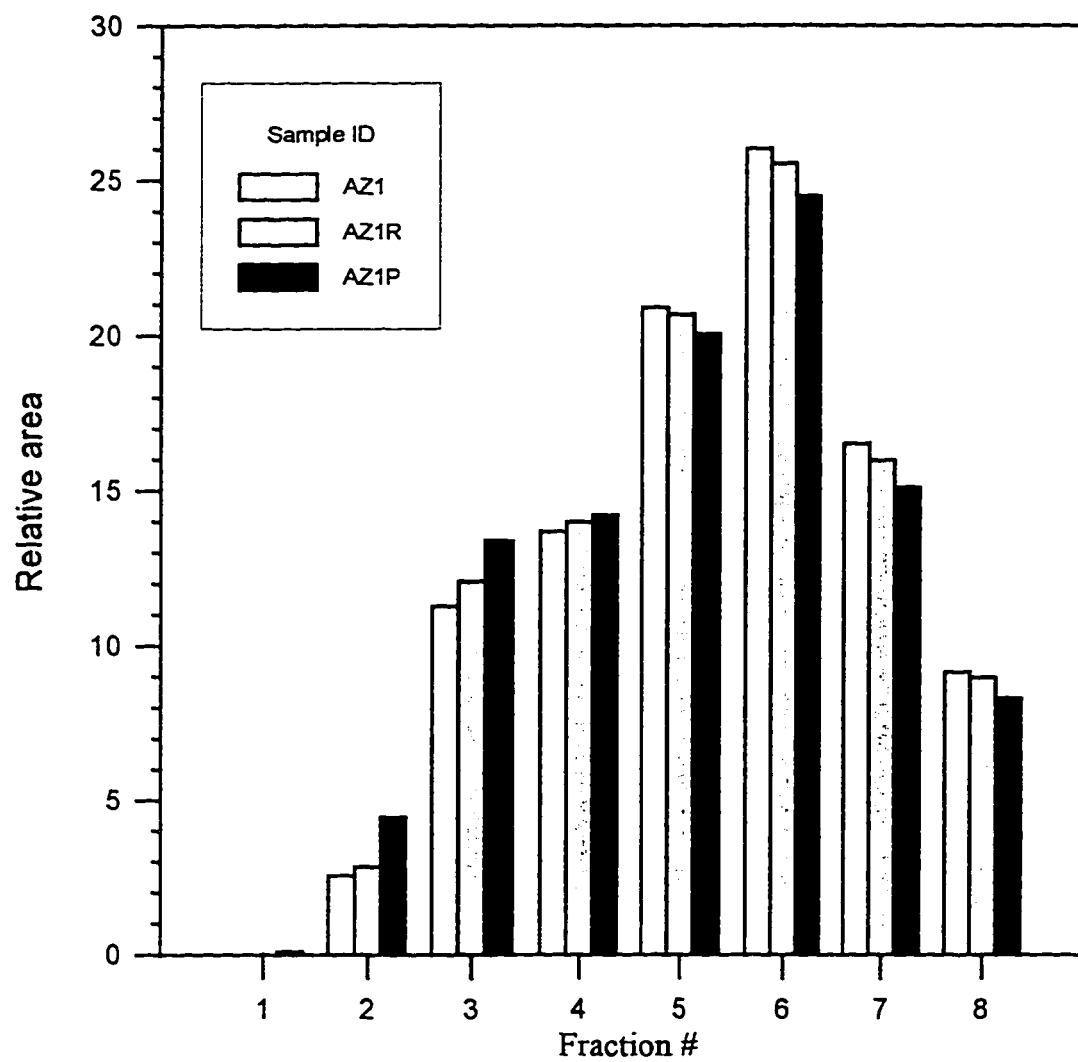


Fig. C-21 : Bar graph comparing molecular sizes of original asphalt (AZ1) and its RTFO and PAV residues

Appendix D

Fractionating Procedures for the Produced HP-GPC Chromatograms

Table D-1 : HP-GPC fractions - using three equal areas fraction

Partition	1st	2nd	3rd	Skew	Standard
Corr. time	30.49	33.17	38.00	Factor	Deviation
RT1	35.5	33.4	31.1	-0.10	2.24
RT1R	37.2	32.3	30.5	1.21	3.51
RT1P	39.6	30.6	29.8	1.69	5.48
RT2	33.9	32.4	33.6	-1.48	0.79
RT2R	36.6	33.0	30.4	0.54	3.12
RT2P	39.0	31.0	30.0	1.66	4.97
RT3	33.7	32.8	33.6	-1.68	0.48
RT3R	36.5	32.7	30.8	0.98	2.92
RT3P	41.2	30.7	28.1	1.47	6.93
RT4	36.6	33.0	30.4	0.42	3.12
RT4R	37.1	32.7	30.2	0.82	3.51
RT4P	40.9	29.5	29.6	1.73	6.55
RT5	34.8	32.1	33.0	0.96	1.37
RT5R	36.8	32.2	31.0	1.46	3.10
RT5P	40.5	30.7	28.8	1.56	6.30
RY1	29.8	34.2	36.0	-1.14	3.16
RY1R	33.4	39.3	27.3	-0.06	6.00
RY1P	37.3	36.8	25.9	-1.72	6.45
RY2	33.0	39.1	27.9	0.26	5.57
RY2R	33.8	36.7	29.6	-0.53	3.58
RY2P	38.7	36.0	25.2	-1.46	7.15
RY3	30.9	33.2	36.0	0.29	2.55
RY3R	33.4	37.6	28.9	-0.10	4.36
RY3P	40.5	35.6	24.0	-1.11	8.48
RY4	33.8	38.6	27.6	-0.39	5.50
RY4R	33.5	38.5	28.0	-0.15	5.29
RY4P	41.3	34.4	24.2	-0.57	8.59
RY5	34.3	37.1	28.5	-0.96	4.39
RY5R	33.2	38.8	28.0	0.07	5.41
RY5P	40.5	35.3	24.2	-1.02	8.35
BH1	24.4	34.5	41.1	-0.63	8.43
BH1R	27.9	35.1	37.1	-1.41	4.85
BH1P	34.5	33.3	32.2	0.25	1.13
BH2	25.0	34.9	40.1	-0.86	7.64
BH2R	28.9	34.8	36.3	-1.48	3.90
BH2P	33.1	33.6	33.3	1.03	0.23
BH3	25.0	35.2	39.8	-1.03	7.60
BH3R	27.8	35.1	37.1	-1.42	4.87
BH3P	34.6	32.7	32.7	1.73	1.07
BH4	25.8	35.1	39.1	-1.06	6.80
BH4R	29.2	34.8	36.1	-1.49	3.64
BH4P	32.2	33.9	34.0	-1.72	1.00
BH5	25.7	35.6	38.7	-1.32	6.80
BH5R	28.4	35.2	36.4	-1.58	4.34
BH5P	32.6	33.8	33.6	-1.49	0.66
KW1	28.4	31.1	40.5	1.40	6.34
KW1R	30.2	30.4	39.4	1.73	5.30
KW1P	34.9	29.5	35.6	-1.63	3.34
KW2	29.6	30.8	39.5	1.63	5.39
KW2R	31.9	29.6	38.5	1.25	4.60
KW2P	33.9	28.9	37.3	-0.55	4.24
KW3	29.3	30.3	40.4	1.69	6.11
KW3R	31.6	29.9	38.5	1.47	4.56
KW3P	35.2	28.7	36.1	-1.64	4.06
KW4	29.1	31.0	39.9	1.51	5.79
KW4R	31.9	29.8	38.3	1.31	4.45
KW4P	38.6	32.6	28.8	0.63	4.92
KW5	29.0	30.9	40.0	1.52	5.88
KW5R	31.7	30.0	38.3	1.42	4.39
KW5P	38.6	32.8	28.6	0.49	5.00
AZ1	31.5	32.9	35.6	0.93	2.08
AZ1R	32.9	32.3	34.8	1.34	1.32
AZ1P	36.1	31.1	32.8	0.89	2.51

Table D-1: Continued.

Partiton	1st	2nd	3rd	Skew	Standard
Corr. time	30.49	33.17	38.00	Factor	Deviation
RT-CRT-5-F	35.6	34.3	30.2	-1.32	2.81
RT-CRT-5-R	39.0	31.9	29.1	1.17	5.11
RT-CRT-5-P	40.4	31.2	28.4	1.35	6.28
RT-CRT-10-F	37.2	31.4	31.4	1.73	3.35
RT-CRT-10-R	38.8	31.4	29.9	1.54	4.78
RT-CRT-10-P	43.3	29.5	27.1	1.59	8.75
RT-CRT-15-F	35.3	34.8	29.9	-1.68	2.99
RT-CRT-15-R	36.0	32.7	31.3	1.11	2.43
RT-CRT-15-P	38.7	31.0	30.3	1.69	4.68
RT-SBS-3-F	38.5	29.9	31.6	1.47	4.52
RT-SBS-3-R	40.9	29.6	29.5	1.73	6.55
RT-SBS-3-P	42.1	29.8	28.1	1.63	7.62
RT-SBS-6-F	36.2	32.9	30.8	0.65	2.73
RT-SBS-6-R	38.2	31.5	30.2	1.56	4.30
RT-SBS-6-P	44.3	28.8	26.9	1.66	9.53
RT-SBS-9-F	39.6	30.0	30.4	1.72	5.46
RT-SBS-9-R	40.2	29.6	30.2	1.71	6.00
RT-SBS-9-P	32.9	25.3	41.7	0.21	8.19
RY-CRT-5-F	33.5	34.3	32.2	-0.66	1.06
RY-CRT-5-R	36.1	32.8	31.1	0.87	2.54
RY-CRT-5-P	41.1	31.0	27.9	1.35	6.94
RY-CRT-10-F	35.1	33.5	31.4	-0.35	1.87
RY-CRT-10-R	36.8	32.8	30.4	0.75	3.24
RY-CRT-10-P	40.3	31.4	28.3	1.27	6.22
RY-CRT-15-F	29.9	36.2	33.9	-0.78	3.17
RY-CRT-15-R	33.9	34.2	32.0	-1.65	1.20
RY-CRT-15-P	39.4	31.2	29.5	1.54	5.29
RY-SBS-3-F	39.7	32.3	28.1	0.79	5.87
RY-SBS-3-R	41.1	32.4	28.5	0.58	7.33
RY-SBS-3-P	41.4	36.4	22.2	-1.26	10.00
RY-SBS-6-F	42.1	31.7	28.1	0.85	8.14
RY-SBS-6-P	42.8	30.7	26.5	1.26	8.50
RY-SBS-6-R	47.1	28.8	24.1	1.43	12.15
RY-SBS-9-F	41.1	32.3	26.5	0.59	7.30
RY-SBS-9-R	42.1	31.2	26.7	1.12	7.92
RY-SBS-9-P	45.4	30.0	24.6	1.26	10.77
BH-CRT-5-F	34.3	34.9	30.8	-1.59	2.18
BH-CRT-5-R	37.7	33.0	29.3	0.41	4.20
BH-CRT-5-P	39.3	32.7	28.0	0.49	5.64
BH-CRT-10-F	31.9	36.4	31.7	1.71	2.65
BH-CRT-10-R	34.5	34.7	30.8	-1.71	2.17
BH-CRT-10-P	38.2	32.9	28.9	0.38	4.68
BH-CRT-15-F	29.4	37.9	32.7	0.64	4.27
BH-CRT-15-R	30.4	36.9	32.7	0.82	3.29
BH-CRT-15-P	37.1	33.4	29.5	-0.06	3.84
BH-SBS-3-F	32.7	38.2	31.0	1.00	2.65
BH-SBS-3-R	35.6	34.4	29.9	-1.43	3.02
BH-SBS-3-P	35.4	34.5	30.1	-1.52	2.86
BH-SBS-6-F	33.0	34.3	32.6	1.36	0.88
BH-SBS-6-R	32.7	34.8	32.5	1.69	1.27
BH-SBS-6-P	38.8	31.6	29.6	1.38	4.85
BH-SBS-9-F	31.0	36.2	32.7	0.97	2.64
BH-SBS-9-R	32.0	35.5	32.5	1.61	1.88
BH-SBS-9-P	39.6	32.3	28.1	0.74	5.62
KW-CRT-5-F	43.2	29.3	27.4	1.64	8.60
KW-CRT-5-R	43.4	28.4	28.2	1.73	8.69
KW-CRT-5-P	46.0	27.6	26.4	1.71	11.03
KW-CRT-10-F	40.3	30.5	29.3	1.66	6.03
KW-CRT-10-R	39.7	30.5	29.8	1.70	5.53
KW-CRT-10-P	43.8	28.5	27.7	1.72	9.03
KW-CRT-15-F	36.0	33.0	31.0	0.60	2.50
KW-CRT-15-R	38.0	31.4	30.6	1.64	4.06
KW-CRT-15-P	42.4	29.3	28.2	1.69	7.88
KW-SBS-3-F	34.9	33.3	31.8	0.13	1.55
KW-SBS-3-R	37.5	32.3	30.2	1.18	3.77
KW-SBS-3-P	39.2	30.8	30.0	1.88	5.13
KW-SBS-6-F	38.5	31.0	30.5	1.72	4.47
KW-SBS-6-R	39.1	30.6	30.3	1.73	4.96
KW-SBS-6-P	42.6	29.5	27.9	1.65	8.07
KW-SBS-9-F	42.4	28.7	28.8	1.73	7.89
KW-SBS-9-R	38.6	31.0	30.5	1.71	4.53
KW-SBS-9-P	38.5	30.7	30.7	1.73	4.48

Table D-2: HP-GPC fractions - using three (25%, 50% & 25%) times fractions.

Partition	1st	2nd	3rd	Skew	Standard
Corr. time	26.00	34.00	38.00	Factor	Deviation
RT1	5.8	72.4	21.8	1.33	34.78
RT1R	6.4	72.2	21.4	1.37	34.47
RT1P	8.4	70.4	21.2	1.44	32.71
RT2	4.9	70.7	24.4	1.11	33.81
RT2R	6.0	72.9	21.2	1.37	35.06
RT2P	8.3	70.4	21.3	1.43	32.75
RT3	4.7	71.1	24.2	1.12	34.17
RT3R	5.8	72.4	21.7	1.33	34.77
RT3P	9.6	70.8	19.7	1.55	32.80
RT4	6.7	72.1	21.2	1.39	34.36
RT4R	6.5	72.3	21.2	1.39	34.57
RT4P	10.5	68.2	21.3	1.49	30.68
RT5	5.6	70.6	23.8	1.18	33.55
RT5R	6.5	71.7	21.7	1.35	34.12
RT5P	9.5	70.5	20.0	1.53	32.59
RY1	2.4	71.0	26.5	0.85	34.80
RY1R	1.5	80.8	17.7	1.44	41.90
RY1P	3.4	80.2	16.4	1.54	41.14
RY2	2.3	80.0	17.7	1.46	41.17
RY2R	1.7	77.9	20.4	1.31	39.71
RY2P	4.4	79.6	16.0	1.57	40.52
RY3	2.9	70.5	26.7	0.84	34.27
RY3R	1.6	78.7	19.8	1.34	40.28
RY3P	5.3	79.7	15.0	1.62	40.41
RY4	2.6	79.7	17.7	1.47	40.85
RY4R	1.8	80.6	17.6	1.46	41.68
RY4P	6.3	78.4	15.3	1.63	39.30
RY5	3.0	78.4	18.5	1.44	39.82
RY5R	1.9	80.4	17.7	1.45	41.55
RY5P	5.5	79.3	15.3	1.62	40.08
BH1	1.1	69.5	29.4	0.51	34.38
BH1R	1.5	72.2	26.4	0.84	35.88
BH1P	4.3	73.1	22.6	1.24	35.62
BH2	1.0	70.3	28.7	0.59	34.89
BH2R	1.9	72.3	25.7	0.91	35.82
BH2P	3.7	72.8	23.5	1.15	35.59
BH3	0.9	70.7	28.4	0.62	35.14
BH3R	1.5	72.2	26.3	0.85	35.84
BH3P	5.0	71.6	23.3	1.20	34.42
BH4	1.2	70.9	28.0	0.67	35.16
BH4R	2.0	72.3	25.7	0.92	35.75
BH4P	3.3	72.6	24.0	1.10	35.57
BH5	1.0	71.5	27.5	0.71	35.60
BH5R	1.7	72.6	25.8	0.90	36.05
BH5P	3.5	72.7	23.8	1.12	35.57
KW1	1.6	68.3	30.1	0.43	33.45
KW1R	1.3	69.5	29.2	0.53	34.28
KW1P	4.3	69.2	26.6	0.88	32.99
KW2	1.4	69.3	29.3	0.53	34.11
KW2R	1.9	69.6	28.4	0.63	34.12
KW2P	3.4	69.0	27.6	0.76	33.17
KW3	1.2	68.6	30.1	0.42	33.81
KW3R	1.8	69.8	28.4	0.63	34.30
KW3P	4.2	69.3	26.5	0.89	33.06
KW4	0.9	69.6	29.5	0.50	34.49
KW4R	2.0	69.8	28.2	0.66	34.16
KW4P	4.0	76.4	19.6	1.41	38.09
KW5	1.0	69.3	29.7	0.47	34.32
KW5R	1.9	69.8	28.2	0.66	34.24
KW5P	4.1	76.8	19.1	1.44	38.42
AZ1	2.5	71.8	25.6	0.94	35.30
AZ1R	2.8	72.2	24.9	1.01	35.47
AZ1P	4.5	72.1	23.4	1.18	34.87

Table D-2: Continued.

Partition	1st	2nd	3rd	Skew	Standard
Corr. time	26.00	34.00	38.00	Factor	Deviation
RT-CRT-5-F	4.8	74.4	20.8	1.36	36.46
RT-CRT-5-R	7.7	71.8	20.5	1.46	33.95
RT-CRT-5-P	9.1	71.1	19.8	1.53	33.11
RT-CRT-10-F	8.8	68.6	22.6	1.36	31.29
RT-CRT-10-R	9.2	69.7	21.1	1.47	32.02
RT-CRT-10-P	12.1	68.7	19.2	1.63	30.80
RT-CRT-15-F	5.1	74.3	20.6	1.38	36.34
RT-CRT-15-R	7.2	70.5	22.2	1.34	33.08
RT-CRT-15-P	10.2	68.2	21.5	1.47	30.75
RT-SBS-3-F	8.9	68.0	23.0	1.34	30.87
RT-SBS-3-R	10.7	67.9	21.4	1.49	30.44
RT-SBS-3-P	10.5	69.5	20.0	1.56	31.69
RT-SBS-6-F	6.5	71.7	21.8	1.35	34.08
RT-SBS-6-R	8.3	70.2	21.5	1.42	32.59
RT-SBS-6-P	13.5	67.4	19.1	1.66	29.67
RT-SBS-9-F	11.2	66.8	22.0	1.47	29.52
RT-SBS-9-R	11.9	66.3	21.8	1.51	29.01
RT-SBS-9-P	9.4	59.0	31.5	0.32	24.87
RY-CRT-5-F	2.5	74.5	23.0	1.16	37.07
RY-CRT-5-R	4.7	73.1	22.2	1.27	35.56
RY-CRT-5-P	7.4	72.7	19.8	1.49	34.69
RY-CRT-10-F	5.3	72.2	22.4	1.27	34.77
RY-CRT-10-R	5.9	72.3	21.7	1.34	34.70
RY-CRT-10-P	7.7	72.3	19.9	1.49	34.32
RY-CRT-15-F	2.3	73.8	23.9	1.08	36.70
RY-CRT-15-R	5.0	72.4	22.6	1.25	34.97
RY-CRT-15-P	8.9	70.1	21.0	1.46	32.42
RY-SBS-3-F	7.4	72.5	20.1	1.47	34.53
RY-SBS-3-R	8.0	73.2	18.8	1.55	34.99
RY-SBS-3-P	6.7	79.4	13.9	1.67	40.05
RY-SBS-6-F	9.7	71.9	18.4	1.60	33.73
RY-SBS-6-P	11.0	70.1	18.9	1.61	32.10
RY-SBS-6-P	14.4	68.7	16.9	1.72	30.63
RY-SBS-9-F	9.5	71.8	18.6	1.59	33.64
RY-SBS-9-R	10.1	70.9	19.0	1.59	32.83
RY-SBS-9-P	12.5	70.0	17.4	1.69	31.89
BH-CRT-5-F	3.9	74.2	21.9	1.27	36.48
BH-CRT-5-R	6.3	72.6	21.1	1.39	34.82
BH-CRT-5-P	6.5	73.9	19.6	1.47	35.71
BH-CRT-10-F	3.1	74.8	22.0	1.24	37.17
BH-CRT-10-R	5.4	72.7	21.9	1.31	35.07
BH-CRT-10-P	7.3	72.1	20.5	1.45	34.24
BH-CRT-15-F	2.7	74.2	23.2	1.15	36.84
BH-CRT-15-R	3.6	73.0	23.4	1.16	35.76
BH-CRT-15-P	8.2	70.9	20.9	1.45	33.14
BH-SBS-3-F	3.6	74.7	21.8	1.27	36.93
BH-SBS-3-R	4.9	73.8	21.3	1.33	35.96
BH-SBS-3-P	4.6	74.1	21.3	1.33	36.25
BH-SBS-6-F	5.5	71.1	23.4	1.20	33.89
BH-SBS-6-R	5.4	71.4	23.2	1.22	34.12
BH-SBS-6-P	9.5	69.6	21.0	1.48	31.90
BH-SBS-9-F	4.8	71.8	23.4	1.18	34.62
BH-SBS-9-R	5.2	71.6	23.1	1.22	34.36
BH-SBS-9-P	6.0	74.3	19.7	1.46	36.13
KW-CRT-5-F	9.8	70.7	19.5	1.56	32.71
KW-CRT-5-R	10.1	69.5	20.3	1.53	31.74
KW-CRT-5-P	13.0	68.2	18.8	1.66	30.35
KW-CRT-10-F	8.3	70.8	20.9	1.46	33.06
KW-CRT-10-R	8.0	70.6	21.4	1.41	32.97
KW-CRT-10-P	11.8	68.4	19.9	1.60	30.63
KW-CRT-15-F	4.4	73.7	21.9	1.28	36.02
KW-CRT-15-R	6.7	71.4	21.9	1.35	33.83
KW-CRT-15-P	10.8	69.1	20.2	1.56	31.29
KW-SBS-3-F	3.5	73.8	22.7	1.20	36.33
KW-SBS-3-R	4.8	73.8	21.4	1.33	36.02
KW-SBS-3-P	6.2	72.2	21.6	1.35	34.54

Table D-3: HP-GPC fractions - using three (25%,50% &25%) areas fractions.

Partition	1st	2nd	3rd	Skew	Standard
Corr. time	29.39	33.89	38.00	Factor	Deviation
RT1	26.7	50.3	23.0	1.61	14.84
RT1R	28.4	49.0	22.5	1.39	13.92
RT1P	31.2	46.5	22.3	0.76	12.26
RT2	25.1	49.4	25.6	1.73	13.88
RT2R	27.7	49.9	22.4	1.47	14.60
RT2P	30.6	47.0	22.4	0.93	12.50
RT3	24.9	49.7	25.4	1.73	14.20
RT3R	27.7	49.4	22.9	1.51	14.13
RT3P	32.8	46.5	20.8	0.20	12.87
RT4	27.9	49.7	22.3	1.45	14.49
RT4R	28.4	49.3	22.3	1.38	14.18
RT4P	32.8	44.8	22.4	0.23	11.24
RT5	26.2	48.9	24.9	1.72	13.49
RT5R	28.2	48.9	22.9	1.44	13.73
RT5P	32.2	46.7	21.1	0.40	12.84
RY1	20.9	51.3	27.7	1.38	15.94
RY1R	22.4	58.7	18.9	1.68	22.07
RY1P	27.4	55.0	17.5	1.24	19.44
RY2	23.1	58.0	18.9	1.66	21.49
RY2R	23.0	55.4	21.5	1.72	19.17
RY2P	29.0	53.8	17.1	0.98	18.73
RY3	21.9	50.2	27.9	1.42	14.95
RY3R	22.5	56.6	20.9	1.72	20.17
RY3P	30.7	53.1	16.1	0.61	18.63
RY4	23.9	57.2	18.9	1.62	20.82
RY4R	23.6	57.6	18.8	1.64	21.16
RY4P	31.9	51.7	16.4	0.36	17.66
RY5	24.7	55.6	19.8	1.61	19.41
RY5R	23.3	57.7	18.9	1.65	21.25
RY5P	30.9	52.8	16.4	0.60	18.33
BH1	16.6	52.5	30.9	0.59	18.04
BH1R	19.5	52.8	27.7	1.30	17.33
BH1P	26.0	50.2	23.8	1.69	14.64
BH2	17.1	52.7	30.2	0.77	18.03
BH2R	20.5	52.4	27.1	1.44	16.85
BH2P	24.6	50.6	24.8	1.73	14.96
BH3	17.0	53.1	29.9	0.82	18.32
BH3R	19.5	52.8	27.7	1.31	17.39
BH3P	26.3	49.2	24.5	1.70	13.77
BH4	17.8	52.8	29.4	0.95	17.80
BH4R	20.8	52.2	27.0	1.47	16.60
BH4P	23.8	50.9	25.3	1.71	15.27
BH5	17.5	53.5	29.0	1.01	18.38
BH5R	20.0	52.9	27.1	1.41	17.35
BH5P	24.1	50.9	25.0	1.72	15.18
KW1	19.8	48.8	31.5	0.56	14.59
KW1R	21.5	47.9	30.6	0.89	13.43
KW1P	26.1	46.1	27.7	1.69	11.10
KW2	20.9	48.4	30.6	0.84	13.94
KW2R	23.3	46.9	29.8	1.21	12.20
KW2P	25.4	45.8	28.9	1.53	10.90
KW3	20.8	47.7	31.5	0.60	13.58
KW3R	22.9	47.3	29.8	1.17	12.61
KW3P	26.7	45.5	27.8	1.71	10.58
KW4	20.3	48.9	30.9	0.75	14.46
KW4R	23.3	47.1	29.6	1.25	12.32
KW4P	28.9	50.3	20.8	1.19	15.24
KW5	20.3	48.7	31.1	0.70	14.33
KW5R	23.1	47.3	29.6	1.23	12.55
KW5P	29.0	50.7	20.3	1.16	15.68
AZ1	23.0	50.1	26.9	1.60	14.65
AZ1R	24.4	49.4	26.2	1.70	13.97
AZ1P	27.7	47.8	24.6	1.62	12.59

Table D-3: Continued.

Partion	1st	2nd	3rd	Skew Factor	Standard Deviation
Corr. time	29.39	33.89	38.00		
RT-CRT-5-F	26.2	52.0	21.8	1.59	16.34
RT-CRT-5-R	30.1	48.4	21.5	1.01	13.73
RT-CRT-5-P	31.7	47.6	20.7	0.53	13.49
RT-CRT-10-F	28.7	47.7	23.6	1.42	12.73
RT-CRT-10-R	30.2	47.6	22.2	1.03	13.00
RT-CRT-10-P	35.1	44.9	20.0	-0.62	12.51
RT-CRT-15-F	25.9	52.5	21.6	1.61	16.77
RT-CRT-15-R	27.1	49.5	23.4	1.60	14.15
RT-CRT-15-P	30.3	47.2	22.5	1.01	12.61
RT-SBS-3-F	30.3	45.7	24.0	1.13	11.19
RT-SBS-3-R	32.6	45.0	22.4	0.29	11.28
RT-SBS-3-P	33.6	45.6	20.8	-0.09	12.38
RT-SBS-6-F	27.1	50.1	22.8	1.57	14.65
RT-SBS-6-R	29.2	48.2	22.6	1.28	13.27
RT-SBS-6-P	36.0	44.1	19.9	-0.93	12.30
RT-SBS-9-F	31.5	45.5	22.9	0.69	11.42
RT-SBS-9-R	32.3	44.9	22.8	0.43	11.10
RT-SBS-9-P	25.8	41.2	33.0	0.22	7.70
RY-CRT-5-F	23.9	52.0	24.0	1.73	16.20
RY-CRT-5-R	26.7	50.0	23.4	1.63	14.52
RY-CRT-5-P	32.0	47.2	20.7	0.43	13.31
RY-CRT-10-F	26.0	50.6	23.4	1.68	15.00
RY-CRT-10-R	27.4	49.7	22.9	1.54	14.38
RY-CRT-10-P	31.0	48.1	20.8	0.73	13.78
RY-CRT-15-F	20.5	54.5	25.0	1.62	18.49
RY-CRT-15-R	24.4	51.8	23.8	1.73	15.99
RY-CRT-15-P	30.4	47.6	21.9	0.95	13.08
RY-SBS-3-F	29.9	49.1	21.0	1.01	14.39
RY-SBS-3-R	31.3	49.0	19.8	0.62	14.72
RY-SBS-3-P	31.0	54.2	14.8	0.51	19.79
RY-SBS-6-F	32.6	48.2	19.2	0.24	14.51
RY-SBS-6-R	33.4	48.7	19.9	-0.02	13.43
RY-SBS-6-P	38.1	44.3	17.7	-1.35	13.92
RY-SBS-9-F	31.8	48.9	19.5	0.53	14.79
RY-SBS-9-R	32.6	47.4	20.0	0.24	13.74
RY-SBS-9-P	36.2	45.6	18.2	-0.89	13.92
BH-CRT-5-F	24.8	52.2	23.0	1.71	16.35
BH-CRT-5-R	28.5	49.3	22.1	1.35	14.22
BH-CRT-5-P	29.8	49.5	20.7	1.01	14.71
BH-CRT-10-F	22.5	54.4	23.1	1.73	18.27
BH-CRT-10-R	25.3	51.7	23.0	1.69	15.91
BH-CRT-10-P	29.2	49.3	21.4	1.18	14.37
BH-CRT-15-F	20.1	55.7	24.2	1.85	19.48
BH-CRT-15-R	21.1	54.3	24.6	1.66	18.26
BH-CRT-15-P	28.5	49.7	21.8	1.33	14.54
BH-SBS-3-F	23.5	53.7	22.8	1.73	17.65
BH-SBS-3-R	26.4	51.1	22.4	1.60	15.55
BH-SBS-3-P	26.1	51.6	22.3	1.62	15.97
BH-SBS-6-F	24.4	51.2	24.4	1.73	15.47
BH-SBS-6-R	24.0	51.6	24.4	1.73	15.85
BH-SBS-6-P	30.3	47.8	21.9	0.98	13.19
BH-SBS-9-F	22.0	53.4	24.6	1.69	17.46
BH-SBS-9-R	23.1	52.5	24.4	1.72	16.57
BH-SBS-9-P	30.6	48.9	20.6	0.84	14.36
KW-CRT-5-F	33.9	45.7	20.4	-0.21	12.67
KW-CRT-5-R	34.2	44.4	21.4	-0.34	11.55
KW-CRT-5-P	37.3	43.1	19.6	-1.30	12.23
KW-CRT-10-F	31.0	47.2	21.8	0.79	12.90
KW-CRT-10-R	30.2	47.3	22.5	1.04	12.69
KW-CRT-10-P	34.9	44.4	20.7	-0.59	11.90
KW-CRT-15-F	26.0	51.1	22.9	1.85	15.47
KW-CRT-15-R	28.3	48.7	23.0	1.45	13.56
KW-CRT-15-P	33.3	45.6	21.1	0.00	12.27
KW-SBS-3-F	24.6	51.7	23.7	1.73	15.89
KW-SBS-3-R	27.4	50.1	22.5	1.52	14.68
KW-SBS-3-P	29.5	48.0	22.5	1.20	13.15
KW-SBS-6-F	28.8	48.1	23.0	1.37	13.15
KW-SBS-6-R	29.2	47.8	23.0	1.29	12.88
KW-SBS-6-P	33.1	48.1	20.7	0.07	12.70
KW-SBS-9-F	33.5	44.7	21.8	-0.06	11.45
KW-SBS-9-R	28.7	48.2	23.1	1.38	13.19
KW-SBS-9-P	28.9	47.9	23.1	1.35	12.99

Table D-4: HP-GPC fractions - using eight equal times fractions.

Partition	1st	2nd	3rd	4th	5th	6th	7th	8th	Skew	Standard
Corr. time	24	26	28	30	32	34	36	38	Factor	Deviation
RT1	0.3	5.5	11.9	13.6	22.0	24.9	14.6	7.3	0.15	8.25
RT1R	0.3	6.2	12.6	14.0	21.3	24.3	14.0	7.3	0.04	7.90
RT1P	0.7	7.7	13.4	13.8	20.2	22.9	13.6	7.6	-0.13	7.15
RT2	0.2	4.7	11.1	13.7	21.5	24.4	15.2	9.2	0.02	8.08
RT2R	0.2	5.8	12.4	14.1	21.7	24.8	14.2	7.0	0.10	8.16
RT2P	0.7	7.5	13.1	13.7	20.4	23.2	13.8	7.5	-0.07	7.26
RT3	0.1	4.6	11.2	13.6	21.6	24.8	15.3	8.9	0.06	8.23
RT3R	0.1	5.7	12.4	14.0	21.6	24.3	14.1	7.7	0.03	8.02
RT3P	0.9	8.7	13.8	13.8	20.3	22.8	13.0	6.7	-0.13	7.11
RT4	0.4	6.3	12.1	13.6	21.6	24.8	13.9	7.2	0.17	8.02
RT4R	0.3	6.2	12.5	13.9	21.5	24.4	14.1	7.0	0.07	7.98
RT4P	1.4	9.1	13.3	13.3	19.6	22.1	13.5	7.8	-0.19	6.55
RT5	0.2	5.4	11.5	13.6	21.1	24.4	15.0	8.8	0.04	7.93
RT5R	0.3	6.2	12.4	13.8	21.0	24.5	14.3	7.4	0.06	7.90
RT5P	1.0	8.5	13.4	13.6	20.2	23.2	13.1	6.9	-0.03	7.13
RY1	0.0	2.4	9.9	13.2	22.6	25.4	16.4	10.2	0.06	8.89
RY1R	0.0	1.5	10.3	16.3	27.3	27.0	12.7	5.0	0.42	10.55
RY1P	0.0	3.4	13.6	15.5	24.6	26.5	12.8	3.5	0.22	9.80
RY2	0.0	2.3	11.2	14.6	26.0	28.2	13.6	4.0	0.45	10.47
RY2R	0.0	1.7	10.6	16.3	25.6	25.4	13.4	7.0	0.22	9.71
RY2P	0.0	4.3	14.3	15.4	24.2	25.7	12.3	3.7	0.18	9.44
RY3	0.1	2.8	10.2	13.4	22.3	24.5	16.4	10.2	-0.03	8.58
RY3R	0.0	1.6	10.4	16.2	26.2	25.9	13.3	6.4	0.30	9.99
RY3P	0.1	5.2	15.0	15.5	23.9	25.3	11.9	3.1	0.12	9.28
RY4	0.0	2.6	11.7	14.6	25.6	27.7	13.6	4.1	0.40	10.25
RY4R	0.0	1.8	11.9	15.0	25.2	28.5	13.8	3.8	0.39	10.51
RY4P	0.1	6.2	15.4	15.2	23.1	24.8	12.0	3.4	0.04	8.91
RY5	0.0	3.0	12.1	14.5	24.7	27.2	13.8	4.7	0.35	9.83
RY5R	0.0	1.9	11.7	14.8	25.5	28.4	13.9	3.8	0.40	10.53
RY5P	0.1	5.4	15.0	15.4	23.8	25.1	11.9	3.3	0.10	9.18
BH1	0.0	1.1	7.7	11.9	20.6	29.3	19.0	10.4	0.38	10.05
BH1R	0.0	1.5	9.4	12.9	21.8	28.0	17.3	9.1	0.28	9.64
BH1P	0.1	4.3	12.3	13.8	21.2	25.8	15.0	7.6	0.13	8.50
BH2	0.0	1.0	8.0	12.2	21.0	29.1	18.7	10.0	0.35	10.02
BH2R	0.0	1.9	9.9	13.0	21.7	27.7	17.1	8.6	0.27	9.47
BH2P	0.0	3.7	11.7	13.7	21.5	25.9	15.4	8.1	0.13	8.65
BH3	0.0	0.9	8.0	12.1	21.4	29.2	18.6	9.8	0.36	10.08
BH3R	0.0	1.5	9.4	12.8	21.8	28.0	17.1	9.2	0.29	9.61
BH3P	0.3	4.7	12.1	13.5	20.7	25.3	15.3	8.1	0.11	8.18
BH4	0.0	1.2	8.5	12.3	21.3	28.8	18.4	9.6	0.33	9.90
BH4R	0.0	2.0	10.1	13.0	21.7	27.4	16.7	9.0	0.24	9.34
BH4P	0.0	3.3	11.4	13.4	21.4	26.4	15.6	8.4	0.18	8.80
BH5	0.0	1.0	8.4	12.4	21.8	28.9	18.1	9.5	0.35	10.02
BH5R	0.0	1.7	9.7	12.9	22.1	27.9	16.9	8.9	0.28	9.58
BH5P	0.0	3.5	11.5	13.6	21.6	26.1	15.5	8.3	0.16	8.73
KW1	0.0	1.6	9.0	13.7	20.2	25.4	18.9	11.2	-0.11	8.91
KW1R	0.0	1.3	10.5	14.3	19.8	24.9	18.4	10.8	-0.25	8.73
KW1P	0.1	4.2	12.2	14.3	19.7	23.0	16.0	10.6	-0.40	7.60
KW2	0.0	1.4	10.1	14.0	20.1	25.1	18.4	10.9	-0.19	8.79
KW2R	0.0	1.9	11.5	14.4	19.4	24.3	18.1	10.4	-0.32	8.41
KW2P	0.1	3.3	12.1	14.4	18.9	23.6	17.3	10.3	-0.37	7.88
KW3	0.0	1.2	10.1	14.0	19.7	24.9	18.7	11.4	-0.25	8.75
KW3R	0.0	1.8	11.3	14.5	19.5	24.5	18.1	10.3	-0.29	8.51
KW3P	0.4	3.8	12.5	14.5	19.0	23.2	16.9	9.7	-0.36	7.66
KW4	0.0	0.9	9.7	14.3	20.2	25.4	18.5	10.9	-0.18	8.99
KW4R	0.0	2.0	11.6	14.3	19.4	24.5	18.0	10.2	-0.29	8.43
KW4P	0.0	4.0	14.2	15.8	22.1	24.3	14.1	5.5	-0.10	8.65
KW5	0.0	1.0	9.7	14.2	20.1	25.3	18.8	10.9	-0.19	8.97
KW5R	0.0	1.9	11.4	14.4	19.6	24.5	17.9	10.3	-0.28	8.46
KW5P	0.0	4.0	14.2	15.8	22.0	24.8	13.9	5.2	-0.05	8.78
AZ1	0.0	2.5	11.3	13.7	20.9	26.0	16.5	9.1	0.04	8.77
AZ1R	0.0	2.8	12.1	14.0	20.7	25.5	16.0	9.0	-0.03	8.57
AZ1P	0.1	4.4	13.4	14.2	20.0	24.5	15.1	8.3	-0.13	8.00

Table D-4: Continued.

Partiton	1st	2nd	3rd	4th	5th	6th	7th	8th	9th	10th	11th	12th	Skew	Standard
Corr. time	26.96	28.29	29.41	30.44	31.22	31.89	32.57	33.17	33.89	34.70	35.89	38.00	Factor	Deviation
RT-CRT-5-F	9.9	8.5	7.9	8.8	8.6	8.9	9.2	8.0	8.2	7.3	7.2	7.5	0.28	0.81
RT-CRT-5-R	13.6	13.0	3.7	8.2	8.0	8.1	8.9	7.4	7.6	6.8	7.2	7.5	0.63	2.66
RT-CRT-5-P	15.3	9.0	7.6	8.1	7.8	8.1	8.4	7.3	7.5	6.7	7.0	7.2	3.00	2.27
RT-CRT-10-F	13.9	7.8	7.1	8.0	7.8	8.1	8.6	7.3	7.6	7.1	7.7	8.9	2.98	1.82
RT-CRT-10-R	14.8	12.1	3.5	7.9	7.7	7.9	8.8	7.4	7.7	6.9	7.4	7.9	1.05	2.79
RT-CRT-10-P	18.8	9.0	7.4	7.7	7.4	7.7	8.0	6.8	6.9	6.3	6.7	7.1	3.21	3.37
RT-CRT-15-F	10.1	8.2	7.7	8.8	8.8	9.2	9.4	8.0	8.1	7.4	7.5	6.9	0.41	0.65
RT-CRT-15-R	12.2	11.6	3.5	8.2	8.1	8.3	9.1	7.6	7.9	7.4	7.8	8.3	-0.21	2.16
RT-CRT-15-P	15.5	7.9	7.1	7.8	7.7	8.1	8.4	7.2	7.6	7.1	7.5	8.1	3.27	2.29
RT-SBS-3-F	14.7	8.5	7.2	7.6	7.4	7.7	8.2	7.1	7.5	7.1	8.0	9.1	2.99	2.09
RT-SBS-3-R	17.0	12.5	3.4	7.6	7.4	7.6	8.3	6.8	7.1	6.8	7.5	8.1	1.66	3.37
RT-SBS-3-P	17.1	9.0	7.5	7.9	7.6	7.9	8.0	6.8	7.1	6.5	6.9	7.6	3.12	2.85
RT-SBS-6-F	11.5	8.1	7.6	8.5	8.3	8.6	8.9	7.5	7.8	7.2	7.6	8.1	2.30	1.10
RT-SBS-6-R	13.5	12.3	3.6	8.3	8.0	8.0	8.7	7.2	7.6	6.9	7.5	8.2	0.65	2.52
RT-SBS-6-P	19.8	8.9	7.4	7.7	7.3	7.4	7.8	6.7	6.9	6.2	6.7	7.2	3.28	3.68
RT-SBS-9-F	16.7	8.0	6.9	7.5	7.4	7.7	8.2	7.1	7.3	6.9	7.6	8.6	3.24	2.67
RT-SBS-9-R	17.5	11.8	3.2	7.4	7.1	7.4	8.3	7.2	7.4	6.7	7.5	8.6	1.77	3.44
RT-SBS-9-P	13.1	9.8	3.1	6.6	5.9	5.9	7.0	7.0	8.8	9.5	11.2	12.3	0.06	2.98
RY-CRT-5-F	7.4	8.7	8.0	8.9	8.8	9.1	9.2	7.7	8.0	7.5	8.0	8.6	-0.11	0.64
RY-CRT-5-R	10.1	13.0	3.8	8.7	8.5	8.6	9.0	7.2	7.7	7.3	7.7	8.4	0.14	2.12
RY-CRT-5-P	14.2	9.9	8.1	8.5	8.1	8.3	8.3	6.8	7.0	6.6	6.9	7.3	2.36	2.07
RY-CRT-10-F	10.4	8.2	7.5	8.5	8.5	9.0	9.0	7.4	7.8	7.3	7.9	8.4	1.08	0.86
RY-CRT-10-R	11.2	12.8	3.7	8.6	8.5	8.5	9.0	7.3	7.6	7.0	7.5	8.3	0.09	2.21
RY-CRT-10-P	13.9	9.3	8.0	8.6	8.3	8.3	8.3	6.9	7.3	6.7	6.9	7.4	2.47	1.93
RY-CRT-15-F	6.3	7.2	7.1	8.8	9.2	9.6	9.7	8.2	8.7	8.4	8.5	8.3	-0.58	1.03
RY-CRT-15-R	9.5	11.5	3.6	8.7	8.8	8.8	9.4	7.7	8.2	7.7	8.0	8.1	-1.26	1.82
RY-CRT-15-P	14.5	8.5	7.5	8.3	8.1	8.2	8.3	7.0	7.4	7.0	7.4	7.7	3.04	2.01
RY-SBS-3-F	13.2	8.9	8.0	9.1	8.8	8.8	8.4	6.8	7.0	6.5	6.9	7.8	1.88	1.79
RY-SBS-3-R	14.2	13.5	3.9	9.1	9.0	8.6	8.5	6.8	6.8	6.2	6.4	7.1	0.94	2.96
RY-SBS-3-P	13.5	9.4	8.2	9.7	10.0	10.1	9.6	7.4	7.2	6.2	5.6	3.1	-0.10	2.67
RY-SBS-6-F	15.8	9.0	7.9	8.9	8.7	8.6	8.3	6.6	6.7	6.1	6.5	6.7	2.44	2.58
RY-SBS-6-R	17.0	12.9	3.8	8.7	8.5	8.1	8.2	6.4	6.6	6.1	6.3	7.5	1.59	3.49
RY-SBS-6-P	21.3	9.2	7.7	8.4	7.9	7.8	7.8	6.1	6.3	5.6	5.7	6.5	3.03	4.24
RY-SBS-9-F	15.2	8.7	7.8	8.9	8.8	8.8	8.4	6.8	6.9	6.4	6.5	6.8	2.43	2.39
RY-SBS-9-R	16.2	12.9	3.7	8.7	8.5	8.3	8.3	6.6	6.7	6.1	6.8	7.1	1.42	3.29
RY-SBS-9-P	19.2	9.2	7.9	8.6	8.2	8.2	7.9	6.1	6.3	5.6	6.0	6.6	2.84	3.61
BH-CRT-5-F	8.8	12.6	3.7	8.7	8.8	9.1	9.7	7.8	7.8	7.1	7.5	8.4	-0.31	2.03
BH-CRT-5-R	12.1	13.0	3.7	8.5	8.4	8.6	9.2	7.2	7.2	6.9	7.3	8.0	0.37	2.42
BH-CRT-5-P	12.7	13.6	3.8	8.7	8.5	8.6	9.0	7.1	7.3	6.7	6.7	7.3	0.72	2.65
BH-CRT-10-F	7.5	7.8	7.3	8.8	9.3	9.8	9.7	8.0	8.4	7.5	7.8	8.2	0.67	0.90
BH-CRT-10-R	10.2	11.9	3.5	8.4	8.7	9.1	9.6	7.7	7.8	6.9	7.7	8.4	-0.81	2.02
BH-CRT-10-P	13.0	8.8	7.5	8.3	8.4	8.8	8.9	7.3	7.3	6.7	7.2	7.7	2.28	1.66
BH-CRT-15-F	6.1	7.1	7.1	8.7	9.3	10.2	10.4	8.5	8.4	7.7	8.1	8.5	0.05	1.26
BH-CRT-15-R	7.3	10.6	3.4	8.5	9.1	9.7	10.4	8.1	8.2	7.8	8.2	8.5	-1.64	1.85
BH-CRT-15-P	13.5	8.1	7.0	8.1	8.5	8.9	9.1	7.4	7.5	7.0	7.2	7.8	2.56	1.77
BH-SBS-3-F	8.1	8.2	7.4	8.6	9.0	9.8	9.9	8.1	8.1	7.3	8.0	7.7	0.84	0.84
BH-SBS-3-R	10.3	12.8	3.6	8.5	8.6	9.0	9.7	7.6	7.5	6.8	7.7	7.9	-0.11	2.19
BH-SBS-3-P	9.6	8.8	7.9	8.7	8.7	9.2	9.4	7.6	7.6	7.0	7.6	7.8	0.11	0.84
BH-SBS-6-F	9.6	7.8	7.1	8.1	8.4	9.1	9.5	7.8	8.0	7.3	8.1	9.2	0.23	0.83
BH-SBS-6-R	9.6	11.3	3.3	8.0	8.3	8.9	9.9	8.1	8.2	7.5	8.1	8.8	-1.49	1.89
BH-SBS-6-P	14.7	8.5	7.3	7.9	7.8	8.3	8.6	7.4	7.5	6.8	7.1	8.2	3.01	2.08
BH-SBS-9-F	8.2	10.6	3.4	8.4	8.9	9.4	10.3	8.2	8.1	7.7	8.3	8.6	-1.92	1.79
BH-SBS-9-R	9.0	11.0	3.4	8.2	8.6	9.3	10.2	7.9	8.1	8.2	8.3	7.9	-1.70	1.83
BH-SBS-9-P	12.4	10.0	8.3	8.4	8.0	8.5	8.8	7.4	7.3	6.6	6.7	7.4	1.58	1.59
KW-CRT-5-F	16.6	9.4	8.1	8.7	7.9	7.7	7.7	6.5	6.9	6.4	6.8	7.4	2.86	2.74
KW-CRT-5-R	17.0	13.7	3.8	8.4	7.6	7.1	7.7	6.4	6.9	6.6	7.1	7.7	1.71	3.53
KW-CRT-5-P	20.1	9.4	7.9	8.2	7.4	7.1	7.2	6.3	6.6	6.1	6.7	7.0	3.14	3.82
KW-CRT-10-F	14.4	8.9	7.9	8.7	8.0	7.9	8.0	6.9	7.3	6.7	7.1	8.1	2.83	2.01
KW-CRT-10-R	13.9	12.8	3.8	8.8	8.1	7.8	8.2	6.9	7.3	6.8	7.7	8.0	0.92	2.66
KW-CRT-10-P	18.4	8.9	7.7	8.3	7.6	7.4	7.5	6.4	6.9	6.5	7.1	7.2	3.18	3.24
KW-CRT-15-F	9.6	8.4	8.2	9.3	8.8	8.6	8.6	7.4	8.0	7.4	7.8	7.9	0.39	0.70
KW-CRT-15-R	12.0	12.6	3.9	9.0	8.4	8.0	8.5	7.1	7.5	7.1	7.7	8.2	0.35	2.26
KW-CRT-15-P	16.9	8.8	7.8	8.5	7.8	7.7	7.7	6.6	7.0	6.7	7.0	7.5	3.13	2.78
KW-SBS-3-F	7.9	8.4	8.5	8.6	8.9	8.7	8.7	7.5	7.9	7.5	8.0	8.4	0.51	0.62
KW-SBS-3-R	10.2	13.4	4.1	9.3	8.6	8.2	8.7	7.3	7.7	7.1	7.6	7.8	0.58	2.17
KW-SBS-3-P	12.0	9.2	8.4	9.1	8.3	8.0	8.0	6.9	7.3	7.0	7.6	8.1	1.94	1.37
KW-SBS-6-F	12.1	8.6	8.2	9.1	8.3	8.1	8.1	7.0	7.3	7.1	7.6	8.6	2.16	1.36
KW-SBS-6-R	12.4	13.1	4.0	9.1	8.2	7.8	8.2	6.9	7.3	7.0	7.6	8.4	0.67	2.42
KW-SBS-6-P	15.8	9.3	8.3	8.9	8.0	7.7	7.7	6.6	7.0	6.5	6.9	7.5	2.73	2.45
KW-SBS-9-F	17.4	8.5	7.7	8.4	7.7	7.5	7.5	6.5	6.9	6.5	7.2	8.3	3.15	2.94
KW-SBS-9-R	12.2	12.9	4.0	9.1	8.3	7.9	8.3	7.0	7.4	7.0	7.6	8.5	0.52	2.34
KW-SBS-9-P	12.7	8.3	8.0	9.0	8.3	8.1	8.0	6.9	7.5	7.0	7.7	8.5	2.53	1.50

Table D-5: HP-GPC fractions - using eight equal areas fractions.

Partition	1st	2nd	3rd	4th	5th	6th	7th	8th	Skew Factor	Standard Deviation
Corr. time	27.64	29.39	30.90	31.89	32.98	33.89	35.28	38.00		
RT1	15.5	11.2	13.1	12.0	14.9	10.4	11.5	11.5	0.82	1.82
RT1R	16.7	11.7	12.9	11.5	14.5	10.2	11.2	11.3	1.28	2.13
RT1P	19.5	11.7	12.3	10.9	13.6	9.6	10.7	11.5	2.07	3.07
RT2	13.8	11.2	13.0	11.7	14.4	10.4	11.9	13.6	-0.14	1.42
RT2R	16.1	11.7	13.0	11.7	14.8	10.4	11.4	11.0	1.01	1.99
RT2P	19.1	11.6	12.3	11.1	13.8	9.8	10.9	11.6	2.00	2.91
RT3	13.7	11.1	12.9	11.7	14.7	10.5	12.0	13.4	0.08	1.41
RT3R	16.0	11.7	12.9	11.8	14.6	10.1	11.2	11.7	0.95	1.93
RT3P	21.0	11.7	12.3	11.0	13.7	9.5	10.5	10.3	2.17	3.69
RT4	16.7	11.3	12.8	11.8	14.8	10.4	11.1	11.2	1.27	2.17
RT4R	16.8	11.6	12.8	11.7	14.6	10.2	11.3	11.0	1.28	2.17
RT4P	21.5	11.3	11.9	10.6	13.1	9.3	10.7	11.7	2.35	3.80
RT5	15.0	11.2	12.7	11.4	14.4	10.3	11.8	13.2	0.39	1.62
RT5R	16.7	11.5	12.6	11.4	14.5	10.4	11.5	11.4	1.42	2.09
RT5P	20.6	11.6	12.2	10.9	13.7	9.9	10.5	10.6	2.23	3.49
RY1	10.3	10.6	13.2	12.3	15.2	10.6	12.6	15.2	0.37	1.96
RY1R	9.4	12.9	16.3	14.7	16.8	10.8	10.6	8.3	0.21	3.21
RY1P	14.4	13.0	14.6	13.4	16.2	10.8	10.9	6.7	-0.97	2.99
RY2	11.3	11.8	14.9	14.3	17.2	11.6	11.4	7.5	-0.04	2.94
RY2R	9.9	13.1	15.7	13.7	15.7	10.4	10.8	10.7	0.44	2.37
RY2P	16.0	13.0	14.3	13.2	15.9	10.5	10.3	6.8	-0.72	3.13
RY3	11.0	10.9	13.3	12.1	14.5	10.3	12.5	15.3	0.44	1.79
RY3R	9.6	12.9	16.1	14.0	16.1	10.5	10.8	10.1	0.45	2.65
RY3P	17.7	13.1	14.3	13.0	15.7	10.2	10.1	6.0	-0.49	3.66
RY4	12.1	11.9	14.7	14.1	17.1	11.3	11.3	7.6	-0.09	2.83
RY4R	11.3	12.2	14.7	13.8	17.3	11.8	11.7	7.2	-0.22	2.95
RY4P	18.9	13.0	13.8	12.6	15.2	10.1	10.0	6.4	0.11	3.78
RY5	12.8	11.8	14.4	13.5	16.5	11.3	11.4	8.3	-0.08	2.41
RY5R	11.3	12.0	14.8	13.9	17.4	11.6	11.7	7.2	-0.15	2.99
RY5P	17.8	13.1	14.2	12.9	15.5	10.1	10.1	6.2	-0.37	3.61
BH1	6.9	9.7	11.5	11.5	16.5	13.0	15.0	16.0	-0.41	3.28
BH1R	8.9	10.6	12.4	12.0	16.3	12.0	13.7	14.0	0.12	2.26
BH1P	14.3	11.7	12.4	11.6	15.3	10.9	12.0	11.8	1.20	1.50
BH2	7.1	10.0	11.8	11.6	16.6	12.7	14.8	15.4	-0.45	3.08
BH2R	9.8	10.7	12.4	12.0	16.2	11.8	13.6	13.5	0.69	1.98
BH2P	13.1	11.5	12.5	11.8	15.3	10.9	12.2	12.5	1.44	1.32
BH3	7.1	9.9	11.9	11.9	16.6	12.7	14.7	15.2	-0.50	3.06
BH3R	9.0	10.5	12.4	12.1	16.3	12.0	13.4	14.2	0.17	2.25
BH3P	14.8	11.5	12.1	11.4	15.1	10.6	11.9	12.6	0.90	1.63
BH4	7.8	10.1	11.9	11.9	16.5	12.5	14.5	14.9	-0.28	2.80
BH4R	10.0	10.8	12.4	12.0	16.1	11.7	13.3	13.7	0.81	1.89
BH4P	12.5	11.3	12.4	11.8	15.7	11.1	12.4	12.9	1.78	1.42
BH5	7.5	10.1	12.2	12.1	16.7	12.5	14.4	14.6	-0.43	2.86
BH5R	9.3	10.6	12.5	12.3	16.3	11.9	13.3	13.8	0.37	2.09
BH5P	12.7	11.4	12.5	11.9	15.5	11.0	12.3	12.7	1.66	1.37
KW1	8.6	11.2	12.6	10.7	14.0	11.4	14.5	16.9	0.33	2.61
KW1R	9.4	12.1	12.5	10.5	13.7	11.2	14.2	16.4	0.44	2.22
KW1P	14.1	12.0	12.6	10.4	13.1	10.0	12.2	15.5	0.24	1.81
KW2	9.3	11.6	12.6	10.7	13.9	11.2	14.1	16.5	0.49	2.28
KW2R	11.0	12.3	12.4	10.2	13.3	11.0	13.9	15.8	0.70	1.83
KW2P	13.1	12.3	12.2	9.9	13.0	10.6	13.4	15.5	0.20	1.72
KW3	9.1	11.7	12.4	10.4	13.7	11.2	14.2	17.3	0.74	2.55
KW3R	10.6	12.3	12.5	10.3	13.4	11.1	14.0	15.8	0.55	1.86
KW3P	14.2	12.4	12.2	10.0	12.8	10.5	13.1	14.7	-0.30	1.63
KW4	8.4	11.9	12.7	10.7	14.0	11.5	14.4	16.5	-0.05	2.49
KW4R	11.1	12.2	12.3	10.3	13.4	11.1	14.0	15.5	0.57	1.74
KW4P	15.5	13.4	13.9	11.7	14.3	10.3	11.3	9.4	-0.07	2.13
KW5	8.4	11.8	12.7	10.7	14.0	11.4	14.4	16.6	0.07	2.52
KW5R	10.9	12.2	12.4	10.4	13.5	11.1	13.9	15.7	0.62	1.78
KW5P	15.5	13.4	13.9	11.7	14.5	10.7	11.4	8.9	-0.26	2.20
AZ1	11.5	11.5	12.4	11.4	15.1	11.2	12.9	14.0	1.02	1.41
AZ1R	12.5	11.9	12.4	11.2	14.8	11.0	12.5	13.7	0.78	1.23
AZ1P	15.4	12.3	12.2	10.8	14.2	10.5	11.9	12.6	0.74	1.62

Table D-5: Continued.

Partion	1st	2nd	3rd	4th	5th	6th	7th	8th	Skew	Standard
Corr. time	27.64	29.39	30.90	31.89	32.98	33.89	35.28	38.00	Factor	Deviation
RT-CRT-5-F	14.2	12.0	13.8	12.6	14.9	10.7	11.0	10.8	0.26	1.83
RT-CRT-5-R	18.2	11.8	13.0	11.5	14.1	9.7	10.7	10.8	1.57	2.69
RT-CRT-5-P	19.9	11.8	12.7	11.4	13.6	9.8	10.4	10.4	2.02	3.25
RT-CRT-10-F	17.8	10.9	12.5	11.5	13.8	10.0	11.1	12.4	1.68	2.45
RT-CRT-10-R	19.1	11.1	12.6	11.2	14.0	9.9	10.9	11.3	1.97	2.95
RT-CRT-10-P	23.5	11.5	12.1	10.9	12.8	9.1	9.8	10.2	2.44	4.62
RT-CRT-15-F	14.3	11.6	13.9	13.0	15.0	10.7	11.3	10.3	0.17	1.78
RT-CRT-15-R	16.1	11.0	13.1	11.8	14.5	10.1	11.6	11.8	0.93	1.98
RT-CRT-15-P	19.5	10.9	12.3	11.4	13.5	10.0	11.0	11.5	2.20	3.01
RT-SBS-3-F	19.1	11.2	11.9	10.9	13.2	9.7	11.1	12.9	2.03	2.89
RT-SBS-3-R	21.5	11.1	12.0	10.7	13.1	9.1	10.7	11.7	2.31	3.81
RT-SBS-3-P	21.8	11.7	12.4	11.1	12.8	9.2	10.0	10.8	2.34	3.95
RT-SBS-6-F	15.6	11.6	13.4	12.2	14.2	10.2	11.2	11.6	0.66	1.78
RT-SBS-6-R	17.8	11.5	13.1	11.5	13.8	9.8	11.0	11.6	1.57	2.46
RT-SBS-6-P	24.4	11.6	12.0	10.8	12.5	9.0	9.6	10.3	2.51	4.97
RT-SBS-9-F	20.8	10.7	11.8	10.9	13.2	9.6	10.7	12.2	2.31	3.54
RT-SBS-9-R	21.7	10.6	11.6	10.4	13.4	9.5	10.8	12.0	2.35	3.90
RT-SBS-9-P	16.3	9.6	10.1	8.3	11.8	11.0	15.4	17.6	0.43	3.44
RY-CRT-5-F	11.8	12.2	14.1	12.9	14.6	10.4	11.7	12.3	0.29	1.34
RY-CRT-5-R	14.6	12.0	13.8	12.3	14.1	9.9	11.4	11.9	-0.20	1.57
RY-CRT-5-P	19.3	12.7	13.3	11.8	13.1	9.1	10.2	10.5	1.62	3.14
RY-CRT-10-F	14.5	11.4	13.5	12.7	14.3	10.1	11.4	12.0	-0.04	1.54
RY-CRT-10-R	15.6	11.8	13.7	12.1	14.1	9.7	11.1	11.8	0.30	1.88
RY-CRT-10-P	18.7	12.4	13.5	11.9	13.2	9.5	10.2	10.8	1.56	2.87
RY-CRT-15-F	9.9	10.6	14.1	13.6	15.4	11.3	12.9	12.1	0.14	1.68
RY-CRT-15-R	13.4	11.0	14.0	12.6	14.8	10.4	12.1	11.7	0.23	1.49
RY-CRT-15-P	18.9	11.6	13.1	11.7	13.2	9.6	10.8	11.1	1.91	2.83
RY-SBS-3-F	17.7	12.2	14.3	12.5	13.2	9.1	10.0	10.9	0.86	2.70
RY-SBS-3-R	18.9	12.3	14.5	12.4	13.4	8.8	9.7	10.0	1.03	3.25
RY-SBS-3-P	18.5	12.6	15.5	14.4	14.8	9.5	9.2	5.6	-0.35	4.18
RY-SBS-6-F	20.4	12.1	14.1	12.3	13.0	8.8	9.4	9.8	1.50	3.71
RY-SBS-6-P	21.6	11.8	13.8	11.7	12.8	8.5	9.5	10.4	1.84	4.05
RY-SBS-9-F	26.1	11.9	13.1	11.1	11.8	8.2	8.5	9.1	2.31	5.79
RY-SBS-9-R	19.7	11.9	14.0	12.6	13.2	9.0	9.8	9.7	1.38	3.42
RY-SBS-9-P	20.8	11.8	13.9	11.9	13.0	8.7	9.7	10.3	1.73	3.78
RY-SBS-9-P	24.0	12.2	13.4	11.7	12.3	8.2	8.8	9.3	2.08	5.00
BH-CRT-5-F	13.1	11.7	14.0	13.0	15.2	10.1	11.2	11.8	0.22	1.63
BH-CRT-5-R	16.7	11.8	13.5	12.3	14.3	9.3	10.9	11.3	0.63	2.30
BH-CRT-5-P	17.6	12.3	13.7	12.3	14.0	9.4	10.3	10.4	0.90	2.63
BH-CRT-10-F	11.4	11.1	14.2	13.9	15.4	10.9	11.4	11.7	0.82	1.72
BH-CRT-10-R	14.3	11.1	13.6	12.9	15.1	10.1	11.0	12.0	0.12	1.76
BH-CRT-10-P	17.6	11.7	13.2	12.4	14.1	9.5	10.4	11.1	1.14	2.54
BH-CRT-15-F	9.6	10.5	14.0	14.3	16.5	11.0	12.0	12.2	0.57	2.27
BH-CRT-15-R	10.8	10.3	13.9	13.8	16.2	10.5	12.3	12.3	0.71	2.03
BH-CRT-15-P	17.7	10.8	13.0	12.6	14.3	9.8	10.8	11.1	1.27	2.55
BH-SBS-3-F	12.2	11.3	13.7	13.7	15.6	10.6	11.3	11.5	0.88	1.69
BH-SBS-3-R	14.8	11.6	13.6	12.8	15.1	9.7	10.8	11.6	0.06	1.91
BH-SBS-3-P	14.0	12.1	13.8	13.0	14.8	10.0	10.9	11.4	-0.12	1.68
BH-SBS-6-F	13.5	10.9	12.9	12.8	15.0	10.5	11.4	13.0	0.17	1.50
BH-SBS-6-R	13.5	10.5	12.9	12.6	15.6	10.5	11.8	12.5	0.67	1.65
BH-SBS-6-P	19.0	11.3	12.5	11.7	13.8	9.8	10.5	11.4	1.94	2.89
BH-SBS-9-F	11.7	10.3	13.6	13.3	16.1	10.5	12.2	12.4	0.79	1.87
BH-SBS-9-R	12.7	10.5	13.2	13.1	15.8	10.3	12.7	11.7	0.65	1.75
BH-SBS-9-P	17.5	13.0	13.2	12.0	14.1	9.6	10.1	10.5	0.95	2.60
KW-CRT-5-F	21.4	12.5	13.4	11.0	12.3	9.0	9.9	10.5	2.07	3.89
KW-CRT-5-R	21.9	12.3	13.1	10.4	12.2	8.8	10.4	11.0	2.18	4.03
KW-CRT-5-P	25.0	12.3	12.7	10.2	11.6	8.6	9.4	10.2	2.44	5.24
KW-CRT-10-F	18.9	12.0	13.5	11.3	12.9	9.6	10.4	11.3	1.83	2.89
KW-CRT-10-R	18.3	11.9	13.7	11.2	13.0	9.4	10.7	11.7	1.56	2.71
KW-CRT-10-P	23.0	11.9	12.8	10.6	12.0	8.9	10.1	10.7	2.40	4.43
KW-CRT-15-F	13.8	12.2	14.5	12.4	13.8	10.3	11.4	11.5	0.04	1.44
KW-CRT-15-R	16.3	12.0	14.1	11.5	13.5	9.6	11.3	11.7	0.72	2.05
KW-CRT-15-P	21.4	11.9	13.1	11.0	12.4	9.1	10.3	10.7	2.24	3.81
KW-SBS-3-F	12.0	12.8	15.0	12.4	14.0	10.3	11.7	12.1	0.43	1.43
KW-SBS-3-R	14.7	12.7	14.6	11.8	13.8	9.8	11.3	11.3	-0.01	1.77
KW-SBS-3-P	16.7	12.8	14.0	11.5	12.9	9.5	11.0	11.6	0.84	2.18
KW-SBS-6-F	16.5	12.3	14.0	11.8	13.0	9.6	11.0	12.0	0.78	2.08
KW-SBS-6-R	16.8	12.4	14.1	11.2	13.0	9.4	11.1	11.9	0.85	2.25
KW-SBS-6-P	20.4	12.7	13.6	11.1	12.3	9.1	10.1	10.7	1.88	3.51
KW-SBS-9-F	21.7	11.7	12.9	10.7	12.1	8.9	10.2	11.6	2.27	3.83
KW-SBS-9-R	16.5	12.2	14.2	11.4	13.2	9.5	11.1	12.0	0.72	2.14
KW-SBS-9-P	16.9	12.1	13.9	11.5	12.8	9.7	11.0	12.1	1.14	2.15

Table D-6: HP-GPC fractions - using twelve equal times fractions.

Partition	1st	2nd	3rd	4th	5th	6th	7th	8th	9th	10th	11th	12th	Skew	Standard
Corr. time	23.33	24.67	26.00	27.33	28.67	30.00	31.33	32.67	34.00	35.33	36.67	38.00	Factor	Deviation
RT1	0.0	1.2	4.6	7.7	8.3	9.5	13.4	17.7	15.8	10.7	7.0	4.1	0.21	5.48
RT1R	0.0	1.3	5.2	8.2	8.7	9.7	13.0	17.2	15.3	10.4	6.6	4.4	0.10	5.26
RT1P	0.2	2.1	6.1	8.9	8.9	9.4	12.3	16.2	14.6	10.0	6.7	4.5	-0.04	4.76
RT2	0.0	0.9	4.0	7.1	8.1	9.6	13.2	17.1	15.6	11.1	7.7	5.6	0.08	5.36
RT2R	0.0	1.1	4.9	8.0	8.7	9.7	13.2	17.6	15.7	10.5	6.6	4.1	0.16	5.44
RT2P	0.2	2.1	6.0	8.7	8.8	9.4	12.4	16.5	14.7	10.1	6.8	4.5	0.01	4.82
RT3	0.0	0.7	4.0	7.2	8.1	9.5	13.1	17.4	15.8	11.2	7.6	5.4	0.11	5.46
RT3R	0.0	1.0	4.9	8.1	8.7	9.7	13.2	17.5	15.3	10.4	6.8	4.5	0.10	5.34
RT3P	0.2	2.6	6.8	9.3	9.0	9.4	12.4	16.3	14.4	9.7	6.1	3.9	-0.03	4.75
RT4	0.1	1.5	5.2	8.0	8.4	9.4	13.0	17.6	15.7	10.3	6.7	4.2	0.23	5.34
RT4R	0.0	1.3	5.1	8.2	8.7	9.6	13.0	17.4	15.5	10.4	6.6	4.1	0.14	5.31
RT4P	0.4	3.2	6.9	8.9	8.6	9.1	12.0	15.6	14.0	9.9	6.7	4.8	-0.09	4.36
RT5	0.0	1.0	4.5	7.4	8.2	9.4	12.9	17.1	15.6	10.9	7.5	5.4	0.09	5.26
RT5R	0.0	1.3	5.2	8.1	8.6	9.5	12.8	17.1	15.7	10.6	6.7	4.4	0.11	5.25
RT5P	0.3	2.6	6.6	8.9	8.8	9.3	12.3	16.3	14.8	9.7	6.3	4.0	0.04	4.74
RY1	0.0	0.2	2.3	6.1	7.7	9.3	13.7	18.2	16.1	11.7	8.7	6.1	0.13	5.89
RY1R	0.0	0.0	1.5	6.0	9.1	11.5	16.8	20.9	16.5	9.7	5.2	2.8	0.47	7.01
RY1P	0.0	0.1	3.3	8.6	9.8	10.7	15.0	19.6	16.5	9.9	4.9	1.5	0.26	6.53
RY2	0.0	0.1	2.2	7.0	8.6	10.3	15.7	20.9	17.6	10.5	5.4	1.8	0.49	6.97
RY2R	0.0	0.0	1.7	6.2	9.2	11.5	15.9	19.3	15.8	10.0	6.3	4.2	0.27	6.43
RY2P	0.0	0.3	4.0	9.2	10.0	10.6	14.6	19.3	16.0	9.5	5.0	1.6	0.23	6.30
RY3	0.0	0.3	2.5	6.3	7.8	9.5	13.7	17.6	15.6	11.7	8.8	6.1	0.04	5.68
RY3R	0.0	0.0	1.6	6.0	9.0	11.5	16.3	19.8	16.0	10.0	6.0	3.8	0.35	6.62
RY3P	0.0	0.7	4.7	9.8	10.1	10.6	14.5	19.1	15.6	9.3	4.4	1.3	0.18	6.21
RY4	0.0	0.1	2.5	7.3	8.7	10.3	15.5	20.7	17.2	10.4	5.6	1.7	0.45	6.83
RY4R	0.0	0.0	1.8	7.3	9.1	10.5	15.3	20.6	17.8	10.7	5.3	1.6	0.42	6.99
RY4P	0.0	0.8	5.4	10.2	10.0	10.3	14.1	18.3	15.4	9.2	4.6	1.5	0.09	5.95
RY5	0.0	0.1	2.9	7.7	8.8	10.1	15.0	19.8	17.1	10.5	5.6	2.4	0.38	6.53
RY5R	0.0	0.0	1.9	7.3	8.9	10.4	15.5	20.8	17.7	10.8	5.2	1.7	0.44	7.00
RY5P	0.0	0.6	4.8	9.8	10.0	10.5	14.6	18.8	15.5	9.3	4.6	1.4	0.15	6.13
BH1	0.0	0.0	1.1	4.3	6.9	8.3	12.1	18.5	19.3	13.9	9.2	6.3	0.37	6.63
BH1R	0.0	0.0	1.4	5.6	7.8	8.9	12.9	18.9	18.1	12.7	8.2	5.4	0.31	6.38
BH1P	0.0	0.6	3.8	7.8	8.9	9.4	12.7	17.9	16.4	11.1	7.0	4.4	0.18	5.66
BH2	0.0	0.0	1.0	4.6	7.2	8.5	12.4	18.6	19.1	13.7	9.0	6.0	0.35	6.62
BH2R	0.0	0.1	1.9	6.0	7.9	9.0	12.9	18.7	17.9	12.6	8.0	5.1	0.31	6.27
BH2P	0.0	0.4	3.3	7.4	8.7	9.3	12.9	18.0	16.6	11.3	7.3	4.8	0.19	5.75
BH3	0.0	0.0	0.9	4.6	7.1	8.4	12.6	18.9	19.1	13.6	8.9	5.9	0.37	6.66
BH3R	0.0	0.0	1.5	5.7	7.7	8.9	13.0	18.9	18.0	12.5	8.3	5.5	0.32	6.36
BH3P	0.1	0.9	4.0	7.7	8.7	9.2	12.4	17.6	16.0	11.1	7.5	4.7	0.16	5.44
BH4	0.0	0.0	1.2	5.0	7.3	8.5	12.5	18.8	18.8	13.5	8.8	5.7	0.35	6.55
BH4R	0.0	0.1	2.0	6.2	8.0	9.0	12.9	18.6	17.6	12.3	8.0	5.3	0.28	6.19
BH4P	0.0	0.3	3.0	7.1	8.5	9.2	12.8	18.3	16.8	11.5	7.6	5.0	0.23	5.84
BH5	0.0	0.0	1.0	4.8	7.3	8.6	12.9	19.1	18.8	13.3	8.6	5.6	0.37	6.63
BH5R	0.0	0.0	1.6	5.8	7.8	9.0	13.1	19.0	17.9	12.4	8.1	5.3	0.32	6.34
BH5P	0.0	0.4	3.1	7.2	8.6	9.3	12.8	18.2	16.6	11.4	7.5	4.9	0.22	5.81
KW1	0.0	0.1	1.6	5.2	7.9	9.5	12.5	16.2	16.9	13.6	9.7	6.9	-0.08	5.87
KW1R	0.0	0.0	1.3	6.1	8.9	9.8	12.3	15.8	16.6	13.3	9.5	6.5	-0.20	5.76
KW1P	0.0	0.6	3.7	7.7	9.0	9.8	12.3	15.3	15.0	11.4	8.5	6.6	-0.36	5.01
KW2	0.0	0.0	1.4	5.9	8.5	9.6	12.5	16.0	16.7	13.2	9.5	6.6	-0.15	5.79
KW2R	0.0	0.1	1.9	6.9	9.3	9.8	12.1	15.3	16.3	13.0	9.2	6.2	-0.27	5.54
KW2P	0.0	0.4	3.0	7.5	9.3	9.7	11.8	14.9	15.8	12.4	8.9	6.2	-0.33	5.20
KW3	0.0	0.0	1.2	5.9	8.6	9.6	12.2	15.7	16.6	13.3	9.9	7.0	-0.21	5.75
KW3R	0.0	0.1	1.7	6.7	9.2	9.8	12.2	15.4	16.5	13.1	9.1	6.2	-0.24	5.61
KW3P	0.2	0.6	3.4	7.8	9.4	9.8	11.9	14.8	15.5	12.2	8.5	5.8	-0.32	5.06
KW4	0.0	0.0	0.9	5.5	8.7	9.8	12.5	16.1	17.0	13.4	9.4	6.7	-0.14	5.93
KW4R	0.0	0.0	2.0	7.0	9.2	9.7	12.1	15.4	16.4	13.1	9.0	6.1	-0.24	5.57
KW4P	0.0	0.3	3.7	9.1	10.2	10.8	13.7	17.1	15.5	10.5	6.1	3.0	-0.08	5.74
KW5	0.0	0.0	1.0	5.5	8.6	9.8	12.5	16.0	16.9	13.5	9.6	6.6	-0.15	5.91
KW5R	0.0	0.1	1.9	6.8	9.1	9.8	12.2	15.5	16.4	13.0	9.1	6.2	-0.23	5.58
KW5P	0.0	0.3	3.8	9.0	10.2	10.7	13.7	17.1	16.0	10.5	6.0	2.6	-0.04	5.82
AZ1	0.0	0.1	2.4	7.0	8.6	9.3	12.6	17.5	16.8	12.0	8.1	5.5	0.07	5.81
AZ1R	0.0	0.1	2.7	7.5	9.1	9.5	12.5	17.1	16.5	11.6	7.9	5.3	0.01	5.67
AZ1P	0.0	0.5	4.0	8.5	9.5	9.5	12.2	16.5	15.8	11.1	7.3	5.0	-0.09	5.31

Table D-6: Continued.

Partion	1st	2nd	3rd	4th	5th	6th	7th	8th	9th	10th	11th	12th	Skew	Standard
Corr. time	23.33	24.67	26.00	27.33	28.67	30.00	31.33	32.67	34.00	35.33	36.67	38.00	Factor	Deviation
RT-CRT-5-F	0.1	0.9	3.8	7.3	8.7	10.2	14.0	18.1	18.0	10.3	6.5	4.0	0.25	5.73
RT-CRT-5-R	0.5	1.8	5.4	8.4	8.9	9.8	13.0	17.1	14.6	10.0	6.5	4.0	0.14	5.03
RT-CRT-5-P	0.5	2.6	8.0	8.6	8.9	9.6	12.8	16.5	14.6	9.7	6.2	3.8	0.11	4.81
RT-CRT-10-F	1.5	2.4	4.8	7.2	7.9	9.2	12.7	16.7	14.8	10.5	7.1	5.0	0.36	4.71
RT-CRT-10-R	1.0	2.7	5.6	7.9	8.3	9.3	12.6	16.8	14.7	10.1	6.8	4.2	0.29	4.76
RT-CRT-10-P	0.9	3.8	7.4	9.2	8.8	9.2	12.1	15.7	13.6	9.2	6.1	3.8	-0.01	4.27
RT-CRT-15-F	0.1	1.1	3.9	7.2	8.4	10.0	14.3	18.5	15.9	10.6	6.5	3.5	0.31	5.81
RT-CRT-15-R	0.9	1.9	4.4	7.0	8.0	9.5	13.2	17.6	15.1	10.7	7.1	4.4	0.36	5.17
RT-CRT-15-P	1.3	3.3	5.6	7.4	8.0	9.1	12.6	16.5	14.8	10.3	6.8	4.4	0.38	4.58
RT-SBS-3-F	1.2	2.3	5.5	8.1	8.5	9.1	12.0	15.9	14.5	10.5	7.8	4.7	0.07	4.50
RT-SBS-3-R	1.2	2.9	6.6	8.7	8.5	9.1	12.1	16.0	13.6	9.9	7.4	4.0	0.06	4.32
RT-SBS-3-P	0.6	2.8	7.0	9.1	8.9	9.5	12.5	15.8	13.7	9.4	6.4	4.2	-0.07	4.45
RT-SBS-6-F	1.4	1.3	3.8	7.1	8.3	9.9	13.6	17.4	15.2	10.5	6.9	4.4	0.30	5.25
RT-SBS-6-R	1.8	1.9	4.6	7.5	8.5	9.7	13.1	16.8	14.5	10.2	6.9	4.4	0.31	4.81
RT-SBS-6-P	2.2	4.3	7.0	8.8	8.8	9.3	12.0	15.2	13.4	9.1	6.1	3.9	0.20	3.90
RT-SBS-9-F	2.8	2.9	5.5	7.7	8.0	8.8	12.0	15.9	14.3	10.1	7.3	4.6	0.44	4.20
RT-SBS-9-R	3.1	3.2	5.6	7.8	8.1	8.7	11.6	15.9	14.2	10.1	7.0	4.7	0.53	4.07
RT-SBS-9-P	2.0	3.3	4.1	5.4	6.9	8.1	9.7	13.2	15.8	14.5	10.4	6.7	0.35	4.48
RY-CRT-5-F	0.0	0.1	2.4	7.2	8.9	10.3	14.4	18.2	15.5	11.0	7.3	4.7	0.09	5.91
RY-CRT-5-R	0.3	0.8	3.5	7.8	9.0	10.1	13.9	17.6	14.7	10.6	7.1	4.5	0.09	5.44
RY-CRT-5-P	0.2	1.4	5.8	9.6	9.7	10.2	13.3	16.4	13.6	9.6	6.3	3.9	-0.15	4.96
RY-CRT-10-F	0.5	1.2	3.6	7.3	8.4	9.8	13.9	17.9	15.1	10.8	7.2	4.5	0.24	5.45
RY-CRT-10-R	0.6	1.4	3.8	7.6	8.8	10.0	13.8	17.6	14.5	10.3	7.0	4.4	0.20	5.27
RY-CRT-10-P	0.3	2.0	5.5	8.7	9.2	10.2	13.6	16.5	14.1	9.6	6.3	4.0	0.00	4.95
RY-CRT-15-F	0.0	0.1	2.2	5.9	7.4	9.6	14.9	19.2	16.8	12.1	7.4	4.4	0.33	6.37
RY-CRT-15-R	0.7	1.2	3.1	6.6	8.0	9.8	14.3	18.3	15.5	11.2	7.2	4.2	0.34	5.67
RY-CRT-15-P	1.2	2.5	5.2	8.0	8.6	9.6	13.3	16.4	14.3	10.2	6.6	4.2	0.20	4.72
RY-SBS-3-F	1.0	1.6	4.8	8.2	8.9	10.4	14.4	17.0	13.6	9.4	6.4	4.2	0.17	5.02
RY-SBS-3-R	0.9	1.7	5.3	8.8	9.2	10.4	14.6	17.0	13.2	9.0	6.0	3.8	0.18	5.03
RY-SBS-3-P	0.0	1.0	5.7	9.5	9.3	10.8	16.1	19.3	14.3	8.6	4.3	1.0	0.26	6.21
RY-SBS-6-F	2.0	2.4	5.3	8.6	9.0	10.3	14.3	16.7	13.1	8.8	6.1	3.5	0.29	4.73
RY-SBS-6-P	2.2	3.1	5.7	8.5	8.8	10.1	13.8	16.3	12.6	8.8	6.1	4.0	0.33	4.38
RY-SBS-6-R	2.0	4.7	7.8	9.5	9.0	9.8	13.1	15.1	12.2	8.0	5.5	3.4	0.05	3.97
RY-SBS-9-F	2.7	2.1	4.8	8.1	8.7	10.1	14.4	17.0	13.5	9.2	5.9	3.6	0.41	4.81
RY-SBS-9-R	2.4	2.3	5.4	8.6	8.8	10.0	13.9	16.5	13.0	9.0	6.3	3.6	0.30	4.57
RY-SBS-9-P	2.2	3.5	6.8	9.2	9.1	10.1	13.4	15.9	12.2	8.3	5.6	3.5	0.23	4.23
BH-CRT-5-F	0.3	0.8	2.9	7.1	8.7	10.0	14.4	18.9	15.1	10.4	6.9	4.5	0.30	5.80
BH-CRT-5-R	0.6	1.3	4.3	8.2	9.0	9.9	13.7	17.9	14.0	10.1	6.7	4.3	0.21	5.23
BH-CRT-5-P	0.2	1.3	5.0	8.8	9.4	10.1	13.9	17.7	14.1	9.5	6.2	3.9	0.11	5.29
BH-CRT-10-F	0.0	0.5	2.6	6.4	8.0	9.7	15.1	19.4	16.2	10.7	7.0	4.3	0.38	6.19
BH-CRT-10-R	0.6	1.4	3.4	6.9	8.2	9.5	14.1	18.8	15.1	10.2	7.4	4.3	0.42	5.60
BH-CRT-10-P	0.5	1.9	5.0	8.2	8.8	9.6	13.7	17.6	14.3	9.8	6.7	4.1	0.24	5.13
BH-CRT-15-F	0.2	0.5	1.9	5.3	7.4	9.5	15.0	20.5	16.6	11.3	7.3	4.5	0.52	6.49
BH-CRT-15-R	0.1	1.0	2.6	6.5	7.4	9.4	12.7	20.2	15.3	11.4	8.8	4.5	0.48	5.98
BH-CRT-15-P	0.9	2.3	5.0	7.5	8.1	9.1	13.7	17.9	14.6	10.1	6.6	4.2	0.44	5.11
BH-SBS-3-F	0.4	0.5	2.6	6.7	8.3	9.7	14.5	19.5	15.9	10.6	7.2	3.9	0.40	6.09
BH-SBS-3-R	0.8	0.7	3.4	7.8	8.8	9.7	14.0	18.8	14.6	10.0	7.6	3.7	0.30	5.62
BH-SBS-3-P	0.2	0.9	3.5	7.3	8.9	10.1	14.2	18.5	15.0	10.2	7.0	4.1	0.26	5.68
BH-SBS-6-F	1.7	1.3	2.5	6.2	8.0	9.2	13.6	18.5	15.7	10.7	7.9	4.8	0.45	5.53
BH-SBS-6-R	1.7	1.3	2.5	6.2	7.9	9.0	13.5	19.1	15.8	11.0	7.7	4.5	0.53	5.66
BH-SBS-6-P	1.7	3.0	4.8	7.5	8.5	9.2	12.8	16.8	14.7	9.8	6.7	4.5	0.44	4.66
BH-SBS-9-F	2.2	0.9	1.7	5.3	7.4	9.3	14.3	19.8	15.8	11.4	7.5	4.6	0.58	6.00
BH-SBS-9-R	2.4	0.9	1.9	5.7	7.6	9.2	13.9	19.6	15.6	11.8	7.2	4.1	0.56	5.89
BH-SBS-9-P	0.2	0.9	4.9	9.1	10.0	10.2	13.2	17.3	14.5	9.5	6.1	4.1	0.01	5.28
KW-CRT-5-F	0.3	2.6	6.8	9.4	9.3	10.3	13.1	15.2	13.3	9.3	6.3	3.9	-0.27	4.52
KW-CRT-5-R	0.4	2.7	7.0	9.5	9.4	10.1	12.6	14.9	13.0	9.7	6.6	4.1	-0.38	4.35
KW-CRT-5-P	0.7	4.1	8.2	9.8	9.2	9.9	12.3	14.2	12.8	8.9	6.3	3.6	-0.46	4.03
KW-CRT-10-F	0.7	2.1	5.5	8.5	8.9	10.1	13.3	15.8	14.2	9.8	6.7	4.3	-0.03	4.71
KW-CRT-10-R	0.8	2.0	5.2	8.3	8.8	10.2	13.4	16.0	13.9	10.0	7.5	3.9	-0.04	4.78
KW-CRT-10-P	1.0	3.6	7.2	9.2	8.9	9.8	12.6	14.8	13.2	9.5	6.6	3.7	-0.21	4.15
KW-CRT-15-F	0.0	0.7	3.7	7.4	8.7	10.7	14.5	17.1	15.3	10.8	7.0	4.1	0.05	5.60
KW-CRT-15-R	0.9	1.6	4.2	7.6	8.7	10.5	13.8	16.6	14.3	10.5	7.1	4.3	0.08	5.03
KW-CRT-15-P	1.4	3.2	6.2	8.6	8.8	10.0	12.9	15.3	13.5	9.7	6.4	4.0	0.01	4.29
KW-SBS-3-F	0.7	0.5	2.3	6.6	8.8	11.1	14.7	17.3	15.3	11.0	7.2	4.5	0.08	5.72
KW-SBS-3-R	0.6	0.6	3.5	7.8	9.2	10.9	14.2	17.0	14.6	10.5	6.9	4.0	0.01	5.42
KW-SBS-3-P	0.8	1.1	4.3	8.3	9.3	10.8	13.7	15.9	14.1	10.3	6.9	4.3	-0.11	4.99
KW-SBS-6-F	1.7	1.4	3.8	7.6	8.8	10.6	13.7	16.1	14.2	10.4	7.0	4.7	0.07	4.87
KW-SBS-6-R	1.8	1.5	3.9	7.6	9.0	10.7	13.6	16.1	13.9	10.3	7.1	4.5	0.06	4.81
KW-SBS-6-P	1.5	2.3	5.6	8.8	9.4	10.6	13.2	15.3	13.5	9.5	6.4	4.0	-0.05	4.47
KW-SBS-9-F	2.9	3.4	5.5	8.0	8.6	9.9	12.7	14.9	13.3	9.6	6.6	4.5	0.23	3.93
KW-SBS-9-R	2.1	1.3	3.6	7.5	8.9	10.6	13.8	16.2	14.1	10.3	7.1	4.5	0.10	4.88
KW-SBS-9-P	2.7	1.7	3.5	7.0	8.6	10.5	13.6	15.9	14.3	10.4	7.1	4.6	0.18	4.73

Table D-7: HP-GPC fractions - using twelve equal areas fractions.

Partition	1st	2nd	3rd	4th	5th	6th	7th	8th	9th	10th	11th	12th	Skew	Standard
Corr. time	26.96	28.29	29.41	30.44	31.22	31.89	32.57	33.17	33.89	34.70	35.89	38.00	Factor	Deviation
RT1	11.2	8.2	7.3	8.4	8.2	8.4	9.3	7.9	8.1	7.4	7.7	7.9	2.09	1.05
RT1R	12.2	8.6	7.6	8.3	7.9	8.1	9.1	7.6	7.9	7.3	7.3	7.9	2.56	1.34
RT1P	14.8	8.9	7.5	8.0	7.5	7.7	8.6	7.2	7.5	6.8	7.3	8.2	3.01	2.12
RT2	9.8	7.9	7.4	8.4	8.1	8.2	9.0	7.7	8.1	7.5	8.2	9.8	1.02	0.82
RT2R	11.6	8.5	7.6	8.4	8.0	8.3	9.3	7.8	8.1	7.3	7.5	7.6	2.25	1.18
RT2P	14.5	8.8	7.4	8.0	7.6	7.8	8.7	7.3	7.6	6.9	7.4	8.1	3.01	2.01
RT3	9.7	7.9	7.3	8.3	8.0	8.2	9.2	7.8	8.2	7.6	8.2	9.5	0.78	0.75
RT3R	11.6	8.6	7.6	8.4	8.0	8.3	9.2	7.6	7.9	7.2	7.4	8.3	2.18	1.16
RT3P	16.2	9.1	7.5	8.0	7.6	7.7	8.6	7.2	7.4	6.7	6.9	7.2	3.06	2.57
RT4	12.3	8.3	7.3	8.2	8.0	8.3	9.3	7.9	8.0	7.2	7.4	7.8	2.52	1.38
RT4R	12.3	8.6	7.5	8.3	8.0	8.3	9.2	7.7	7.9	7.2	7.5	7.6	2.58	1.36
RT4P	16.9	8.7	7.2	7.7	7.4	7.4	8.2	6.9	7.3	6.8	7.2	8.4	3.19	2.76
RT5	10.8	8.0	7.3	8.2	7.9	8.1	9.1	7.6	8.1	7.5	8.0	9.5	1.70	1.00
RT5R	12.3	8.5	7.5	8.2	7.8	8.0	9.0	7.7	8.1	7.3	7.6	8.0	2.76	1.33
RT5P	15.9	8.9	7.4	7.9	7.5	7.7	8.6	7.3	7.7	6.7	6.9	7.5	3.11	2.46
RY1	6.5	7.4	7.0	8.4	8.5	8.7	9.5	8.0	8.2	7.9	8.9	10.9	0.73	1.17
RY1R	5.3	8.4	8.6	10.5	10.3	10.3	10.8	8.5	8.4	7.0	6.4	5.5	-0.28	1.93
RY1P	9.3	9.8	8.3	9.4	9.2	9.4	10.3	8.4	8.4	7.2	6.4	3.9	-1.58	1.76
RY2	7.0	8.4	7.7	9.4	9.7	10.1	10.9	8.9	9.0	7.5	6.9	4.5	-0.73	1.73
RY2R	5.7	8.6	8.7	10.2	9.7	9.5	10.0	8.0	8.0	6.9	7.1	7.5	-0.33	1.37
RY2P	10.7	10.0	8.3	9.2	9.0	9.3	10.1	8.2	8.1	6.8	6.2	4.1	-1.04	1.87
RY3	7.2	7.5	7.1	8.5	8.4	8.5	9.2	7.6	8.1	7.8	9.0	11.0	1.44	1.07
RY3R	5.5	8.4	8.6	10.3	10.0	9.7	10.2	8.3	8.1	7.0	6.9	6.9	-0.22	1.54
RY3P	12.2	10.3	8.3	9.2	8.9	9.2	10.0	8.1	7.8	6.8	5.9	3.5	-0.60	2.24
RY4	7.6	8.6	7.7	9.4	9.5	9.9	10.8	8.8	8.7	7.4	6.9	4.6	-0.86	1.64
RY4R	6.7	9.0	7.9	9.4	9.4	9.7	10.9	9.0	9.1	7.7	6.9	4.2	-1.04	1.77
RY4P	13.5	10.2	8.2	8.9	8.6	8.8	9.6	7.9	7.8	6.6	6.1	3.8	0.27	2.36
RY5	8.3	8.7	7.7	9.1	9.2	9.5	10.4	8.6	8.8	7.5	7.0	5.2	-0.96	1.34
RY5R	6.7	8.7	7.8	9.4	9.5	9.8	11.0	9.0	9.0	7.7	7.0	4.2	-0.98	1.78
RY5P	12.4	10.2	8.3	9.1	9.0	9.0	9.8	8.0	7.8	6.6	6.0	3.7	-0.40	2.20
BH1	3.9	6.4	6.4	7.3	7.5	8.2	10.1	9.2	10.2	9.5	10.2	11.3	-0.69	2.13
BH1R	5.1	7.4	6.9	7.9	8.0	8.6	10.1	8.9	9.3	8.7	9.2	9.8	-1.04	1.38
BH1P	9.7	8.8	7.5	8.0	7.8	8.2	9.5	8.2	8.5	7.7	7.9	8.2	1.03	0.71
BH2	3.9	6.7	6.5	7.5	7.6	8.3	10.1	9.2	9.9	9.3	10.1	10.8	-0.94	1.98
BH2R	5.9	7.6	7.0	7.9	7.9	8.5	10.0	8.8	9.2	8.5	9.2	9.3	-0.70	1.13
BH2P	8.7	8.5	7.4	8.1	7.9	8.4	9.6	8.2	8.5	7.8	8.1	8.8	0.56	0.56
BH3	3.9	6.7	6.5	7.6	7.7	8.5	10.2	9.2	10.0	9.3	10.0	10.6	-1.05	1.97
BH3R	5.3	7.4	6.9	7.9	8.0	8.6	10.2	8.8	9.4	8.4	9.2	10.0	-0.84	1.39
BH3P	10.3	8.6	7.3	7.8	7.6	8.1	9.4	8.1	8.2	7.4	8.3	8.8	1.19	0.87
BH4	4.4	6.9	6.6	7.6	7.7	8.5	10.1	9.1	9.7	9.1	9.9	10.4	-0.94	1.78
BH4R	6.2	7.7	7.0	7.9	7.9	8.5	10.0	8.7	9.1	8.4	8.9	9.7	-0.46	1.09
BH4P	8.2	8.3	7.2	8.0	7.8	8.4	9.8	8.3	8.7	7.9	8.3	9.1	0.80	0.64
BH5	4.1	6.8	6.6	7.7	7.9	8.6	10.3	9.1	9.8	9.0	9.7	10.2	-1.17	1.82
BH5R	5.5	7.5	6.9	8.0	8.0	8.7	10.1	8.8	9.3	8.3	9.3	9.6	-0.88	1.27
BH5P	8.4	8.4	7.3	8.0	7.9	8.4	9.7	8.2	8.5	7.8	8.3	8.9	0.90	0.60
KW1	5.0	7.4	7.4	8.2	7.6	7.5	8.6	7.8	9.0	9.1	10.3	12.1	0.44	1.74
KW1R	5.2	8.5	7.8	8.2	7.4	7.3	8.4	7.7	8.9	8.9	10.0	11.7	0.28	1.56
KW1P	9.6	8.8	7.8	8.3	7.5	7.2	8.1	7.2	7.9	7.6	8.8	11.3	1.61	1.18
KW2	5.3	8.0	7.6	8.2	7.6	7.5	8.5	7.7	8.9	8.8	10.1	11.7	0.45	1.55
KW2R	6.5	8.9	7.9	8.2	7.3	7.1	8.2	7.5	8.7	8.6	9.9	11.2	0.91	1.28
KW2P	8.5	9.0	7.9	8.1	7.1	6.9	7.9	7.3	8.4	8.4	9.4	11.1	1.21	1.13
KW3	5.0	8.1	7.6	8.1	7.4	7.3	8.4	7.7	8.9	8.8	10.4	12.3	0.65	1.76
KW3R	6.2	8.8	7.9	8.2	7.4	7.2	8.2	7.6	8.8	8.8	9.8	11.2	0.67	1.29
KW3P	9.5	9.2	7.9	8.1	7.1	7.0	7.8	7.1	8.3	8.1	9.2	10.4	0.55	1.07
KW4	4.4	8.1	7.8	8.3	7.6	7.5	8.6	7.8	9.1	9.0	10.1	11.8	-0.30	1.74
KW4R	6.6	8.9	7.8	8.1	7.3	7.2	8.2	7.6	8.8	8.8	9.8	11.0	0.89	1.21
KW4P	10.3	10.1	8.6	9.1	8.3	8.2	9.0	7.7	8.0	7.3	7.4	6.1	0.00	1.19
KW5	4.5	8.1	7.7	8.3	7.6	7.5	8.5	7.9	9.0	9.0	10.3	11.8	-0.19	1.74
KW5R	6.5	8.8	7.8	8.2	7.4	7.2	8.2	7.6	8.7	8.7	9.7	11.1	0.86	1.23
KW5P	10.3	10.1	8.6	9.1	8.3	8.2	9.0	7.8	8.3	7.4	7.2	5.7	-0.36	1.26
AZ1	7.2	8.4	7.4	8.0	7.7	8.0	9.3	8.2	8.7	8.1	9.0	9.8	0.49	0.77
AZ1R	7.9	8.9	7.6	8.1	7.6	7.9	9.2	8.0	8.6	8.0	8.6	9.7	0.85	0.65
AZ1P	10.4	9.5	7.7	8.0	7.4	7.7	8.8	7.7	8.2	7.5	8.1	8.9	1.26	0.91

Table D-7: Continued.

Partition	1st	2nd	3rd	4th	5th	6th	7th	8th	9th	10th	11th	12th	Skew	Standard
Corr. time	26.96	28.29	29.41	30.44	31.22	31.89	32.57	33.17	33.89	34.70	35.89	36.00	Factor	Deviation
RT-CRT-5-F	9.9	8.5	7.9	8.8	8.6	8.9	9.2	8.0	8.2	7.3	7.2	7.5	0.26	0.81
RT-CRT-5-R	13.6	13.0	3.7	8.2	8.0	8.1	8.9	7.4	7.6	6.8	7.2	7.5	0.83	2.66
RT-CRT-5-P	15.3	9.0	7.6	8.1	7.8	8.1	8.4	7.3	7.5	6.7	7.0	7.2	3.00	2.27
RT-CRT-10-F	13.9	7.8	7.1	8.0	7.8	8.1	8.6	7.3	7.6	7.1	7.7	8.9	2.96	1.82
RT-CRT-10-R	14.8	12.1	3.5	7.9	7.7	7.9	8.8	7.4	7.7	6.9	7.4	7.9	1.05	2.79
RT-CRT-10-P	18.8	9.0	7.4	7.7	7.4	7.7	8.0	6.8	6.9	6.3	6.7	7.1	3.21	3.37
RT-CRT-15-F	10.1	8.2	7.7	8.8	8.8	9.2	9.4	8.0	8.1	7.4	7.5	6.9	0.41	0.95
RT-CRT-15-R	12.2	11.6	3.5	8.2	8.1	8.3	9.1	7.6	7.9	7.4	7.8	8.3	-0.21	2.16
RT-CRT-15-P	15.5	7.9	7.1	7.8	7.7	8.1	8.4	7.2	7.6	7.1	7.5	8.1	3.27	2.29
RT-SBS-3-F	14.7	8.5	7.2	7.8	7.4	7.7	8.2	7.1	7.5	7.1	8.0	9.1	2.99	2.09
RT-SBS-3-R	17.0	12.5	3.4	7.6	7.4	7.6	8.3	6.8	7.1	6.8	7.5	8.1	1.66	3.37
RT-SBS-3-P	17.1	9.0	7.5	7.9	7.6	7.9	8.0	6.8	7.1	6.5	6.9	7.6	3.12	2.85
RT-SBS-6-F	11.5	8.1	7.6	8.5	8.3	8.6	8.9	7.5	7.8	7.2	7.6	8.1	2.30	1.10
RT-SBS-6-R	13.5	12.3	3.6	8.3	8.0	8.0	8.7	7.2	7.6	6.9	7.5	8.2	0.65	2.52
RT-SBS-6-P	19.8	8.9	7.4	7.7	7.3	7.4	7.8	6.7	6.9	6.2	6.7	7.2	3.26	3.68
RT-SBS-9-F	16.7	8.0	6.9	7.5	7.4	7.7	8.2	7.1	7.3	6.9	7.6	8.6	3.24	2.67
RT-SBS-9-R	17.5	11.8	3.2	7.4	7.1	7.4	8.3	7.2	7.4	6.7	7.5	8.6	1.77	3.44
RT-SBS-9-P	13.1	9.8	3.1	6.6	5.9	5.9	7.0	7.0	8.8	9.5	11.2	12.3	0.06	2.98
RY-CRT-5-F	7.4	8.7	8.0	8.9	8.8	9.1	9.2	7.7	8.0	7.5	8.0	8.6	-0.11	0.64
RY-CRT-5-R	10.1	13.0	3.8	8.7	8.5	8.6	9.0	7.2	7.7	7.3	7.7	8.4	0.14	2.12
RY-CRT-5-P	14.2	9.9	8.1	8.5	8.1	8.3	8.3	6.8	7.0	6.8	6.9	7.3	2.36	2.07
RY-CRT-10-F	10.4	8.2	7.5	8.5	8.5	9.0	9.0	7.4	7.8	7.3	7.9	8.4	1.08	0.66
RY-CRT-10-R	11.2	12.8	3.7	8.6	8.5	8.5	9.0	7.3	7.6	7.0	7.5	8.3	0.09	2.21
RY-CRT-10-P	13.9	9.3	8.0	8.6	8.3	8.3	8.3	6.9	7.3	6.7	6.9	7.4	2.47	1.93
RY-CRT-15-F	6.3	7.2	7.1	8.8	9.2	9.6	9.7	8.2	8.7	8.4	8.5	8.3	-0.58	1.03
RY-CRT-15-R	9.5	11.5	3.6	8.7	8.8	8.8	9.4	7.7	8.2	7.7	8.0	8.1	-1.26	1.82
RY-CRT-15-P	14.5	8.5	7.5	8.3	8.1	8.2	8.3	7.0	7.4	7.0	7.4	7.7	3.04	2.01
RY-SBS-3-F	13.2	8.9	8.0	9.1	8.8	8.8	8.4	6.8	7.0	6.5	6.9	7.8	1.88	1.79
RY-SBS-3-R	14.2	13.5	3.9	9.1	9.0	8.6	8.5	6.8	6.8	6.2	6.4	7.1	0.94	2.96
RY-SBS-3-P	13.5	9.4	8.2	9.7	10.0	10.1	9.6	7.4	7.2	6.2	5.6	3.1	-0.10	2.67
RY-SBS-6-F	15.8	9.0	7.9	8.9	8.7	8.8	8.3	6.8	6.7	6.1	6.5	6.7	2.44	2.58
RY-SBS-6-R	17.0	12.9	3.8	8.7	8.5	8.1	8.2	6.4	6.6	6.1	6.3	7.5	1.59	3.49
RY-SBS-6-P	21.3	9.2	7.7	8.4	7.9	7.8	7.6	6.1	6.3	5.6	5.7	6.5	3.03	4.24
RY-SBS-9-F	15.2	8.7	7.8	8.9	8.8	8.8	8.4	6.8	6.9	6.4	6.5	6.8	2.43	2.39
RY-SBS-9-R	16.2	12.9	3.7	8.7	8.5	8.3	8.3	6.6	6.7	6.1	6.8	7.1	1.42	3.29
RY-SBS-9-P	19.2	9.2	7.9	8.6	8.2	8.2	7.9	6.1	6.3	5.8	6.0	6.6	2.84	3.61
BH-CRT-5-F	8.8	12.6	3.7	8.7	8.8	9.1	9.7	7.8	7.8	7.1	7.5	8.4	-0.31	2.03
BH-CRT-5-R	12.1	13.0	3.7	8.5	8.4	8.6	9.2	7.2	7.2	6.9	7.3	8.0	0.37	2.42
BH-CRT-5-P	12.7	13.6	3.8	8.7	8.5	8.6	9.0	7.1	7.3	6.7	6.7	7.3	0.72	2.65
BH-CRT-10-F	7.5	7.8	7.3	8.8	9.3	9.8	9.7	8.0	8.4	7.5	7.6	8.2	0.67	0.90
BH-CRT-10-R	10.2	11.9	3.5	8.4	8.7	9.1	9.6	7.7	7.8	6.9	7.7	8.4	-0.81	2.02
BH-CRT-10-P	13.0	8.6	7.5	8.3	8.4	8.8	8.9	7.3	7.3	6.7	7.2	7.7	2.28	1.86
BH-CRT-15-F	6.1	7.1	7.1	8.7	9.3	10.2	10.4	8.5	8.4	7.7	8.1	8.5	0.05	1.26
BH-CRT-15-R	7.3	10.6	3.4	8.5	9.1	9.7	10.4	8.1	8.2	7.8	8.2	8.5	-1.64	1.65
BH-CRT-15-P	13.5	8.1	7.0	8.1	8.5	8.9	9.1	7.4	7.5	7.0	7.2	7.8	2.56	1.77
BH-SBS-3-F	8.1	8.2	7.4	8.6	9.0	9.8	9.9	8.1	8.1	7.3	8.0	7.7	0.84	0.84
BH-SBS-3-R	10.3	12.8	3.6	8.5	8.6	9.0	9.7	7.6	7.5	6.8	7.7	7.9	-0.11	2.19
BH-SBS-3-P	9.6	8.8	7.9	8.7	8.7	9.2	9.4	7.6	7.6	7.0	7.6	7.8	0.11	0.84
BH-SBS-6-F	9.6	7.8	7.1	8.1	8.4	9.1	9.5	7.8	8.0	7.3	8.1	9.2	0.23	0.83
BH-SBS-6-R	9.8	11.3	3.3	8.0	8.3	8.9	9.9	8.1	8.2	7.5	8.1	8.8	-1.49	1.89
BH-SBS-6-P	14.7	8.5	7.3	7.9	7.8	8.3	8.6	7.4	7.5	6.8	7.1	8.2	3.01	2.08
BH-SBS-9-F	8.2	10.6	3.4	8.4	8.9	9.4	10.3	8.2	8.1	7.7	8.3	8.6	-1.92	1.79
BH-SBS-9-R	9.0	11.0	3.4	8.2	8.6	9.3	10.2	7.9	8.1	8.2	8.3	7.9	-1.70	1.63
BH-SBS-9-P	12.4	10.0	8.3	8.4	8.0	8.5	8.8	7.4	7.3	6.6	6.7	7.4	1.58	1.59
KW-CRT-5-F	16.6	9.4	8.1	8.7	7.9	7.7	7.7	6.5	6.9	6.4	6.8	7.4	2.86	2.74
KW-CRT-5-R	17.0	13.7	3.8	8.4	7.6	7.1	7.7	6.4	6.9	6.8	7.1	7.7	1.71	3.53
KW-CRT-5-P	20.1	9.4	7.9	8.2	7.4	7.1	7.2	6.3	6.6	6.1	6.7	7.0	3.14	3.82
KW-CRT-10-F	14.4	8.9	7.9	8.7	8.0	7.9	8.0	6.9	7.3	6.7	7.1	8.1	2.83	2.01
KW-CRT-10-R	13.9	12.8	3.8	8.8	8.1	7.8	8.2	6.9	7.3	6.8	7.7	8.0	0.92	2.66
KW-CRT-10-P	18.4	8.9	7.7	8.3	7.6	7.4	7.5	6.4	6.9	6.5	7.1	7.2	3.18	3.24
KW-CRT-15-F	9.6	8.4	8.2	9.3	8.8	8.6	8.6	7.4	8.0	7.4	7.8	7.9	0.39	0.70
KW-CRT-15-R	12.0	12.6	3.9	9.0	8.4	8.0	8.5	7.1	7.5	7.1	7.7	8.2	0.35	2.26
KW-CRT-15-P	16.9	8.8	7.8	8.5	7.8	7.7	7.7	6.6	7.0	6.7	7.0	7.5	3.13	2.78
KW-SBS-3-F	7.9	8.4	8.5	9.6	8.9	8.7	8.7	7.5	7.9	7.5	8.0	8.4	0.51	0.62
KW-SBS-3-R	10.2	13.4	4.1	9.3	8.6	8.2	8.7	7.3	7.7	7.1	7.6	7.8	0.58	2.17
KW-SBS-3-P	12.0	9.2	8.4	9.1	8.3	8.0	8.0	6.9	7.3	7.0	7.6	8.1	1.94	1.37
KW-SBS-6-F	12.1	8.6	8.2	9.1	8.3	8.1	8.1	7.0	7.3	7.1	7.6	8.6	2.16	1.36
KW-SBS-6-R	12.4	13.1	4.0	9.1	8.2	7.8	8.2	6.9	7.3	7.0	7.6	8.4	0.67	2.42
KW-SBS-6-P	15.6	9.3	8.3	8.9	8.0	7.7	7.7	6.6	7.0	6.5	6.9	7.5	2.73	2.45
KW-SBS-9-F	17.4	8.5	7.7	8.4	7.7	7.5	7.5	6.5	6.9	6.5	7.2	8.3	3.15	2.94
KW-SBS-9-R	12.2	12.9	4.0	9.1	8.3	7.9	8.3	7.0	7.4	7.0	7.6	8.5	0.52	2.34
KW-SBS-9-P	12.7	8.3	8.0	9.0	8.3	8.1	8.0	6.9	7.5	7.0	7.7	8.5	2.53	1.50

Appendix E

Statistical Analysis of the Produced Models

Table E-1: Correlation matrix - using three equal areas fractions.

Partition	1st	2nd	3rd	Skew	Standard
Corr. time	30.49	33.17	38.00	Factor	Deviation
PEN25	-0.6	0.3	0.5	-0.3	-0.2
PEN4	0.7	-0.4	-0.4	0.3	-0.7
SP (°C)	0.5	-0.2	-0.5	0.3	0.0
FP (°C)	-0.2	0.6	0.0	-0.4	0.1
VIS60 (Poise)	0.0	-0.4	0.2	0.4	-0.3
RV135 (cPa.s)	0.4	-0.2	-0.4	0.1	0.0
VIS135 (cSt)	-0.1	-0.3	0.2	0.4	0.2
RP25	0.4	0.0	-0.4	-0.4	-0.6
RP4	0.1	0.3	-0.3	-0.5	0.0
VR60	0.4	-0.1	-0.3	0.4	-0.3
VR135	-0.2	-0.6	0.5	0.4	0.2
PI	0.7	-0.3	-0.4	0.3	-0.7
PR	0.4	-0.3	-0.2	0.3	-0.6
PVN	0.3	-0.4	0.0	0.4	-0.2
VTs	0.1	-0.1	0.0	-0.1	-0.3
Lower grading temp. (°C)	0.3	-0.2	-0.2	0.4	0.2
Upper grading temp. (°C)	0.7	-0.3	-0.6	0.3	0.0
Gg (Gpa)	0.3	-0.4	-0.2	0.2	0.4
R	0.5	-0.1	-0.5	0.0	-0.1
ω_0 @ Td (Hz)	0.3	-0.2	-0.2	0.1	0.3
η_0 @ Td (Gpa.s)	0.0	0.0	0.0	-0.2	-0.3
$G^* / \sin \delta$ @ 64°C (MPa)	-0.1	0.1	0.1	-0.2	-0.1
$G^* \times \sin \delta$ @ 25°C (MPa)	0.3	-0.1	-0.3	0.0	-0.1
S(60) @ 0°C (MPa)	0.3	-0.1	-0.3	0.1	0.0
m(60) @ 0°C	0.4	-0.1	-0.3	0.1	0.1
1st Partition	1.0	-0.4	-0.9	0.4	0.0
2nd Partition		1.0	-0.1	-0.6	-0.3
3rd Partition			1.0	-0.1	0.1
Skew Factor				1.0	0.2
Standard Deviation					1.0

Table E-2: Correlation matrix - using three (25%, 50% & 25%) times fractions.

Partition	1st	2nd	3rd	Skew	Standard
Corr. time	26.00	34.00	38.00	Factor	Deviation
PEN25	-0.6	0.2	0.4	-0.5	0.4
PEN4	0.8	-0.1	-0.3	0.4	-0.3
SP (°C)	0.7	-0.2	-0.4	0.5	-0.4
FP (°C)	-0.1	0.3	-0.1	0.1	0.3
VIS60 (Poise)	0.0	-0.3	0.2	-0.2	-0.3
RV135 (cPa.s)	0.5	-0.1	-0.3	0.4	-0.3
VIS135 (cSt)	-0.4	-0.1	0.2	-0.3	0.0
RP25	0.8	0.0	-0.3	0.5	-0.2
RP4	0.3	0.2	-0.3	0.3	0.1
VR60	0.3	0.1	-0.3	0.3	0.1
VR135	0.0	-0.6	0.5	-0.5	-0.6
PI	0.5	0.1	-0.3	0.3	-0.1
PR	0.5	-0.1	-0.1	0.2	-0.2
PVN	0.0	0.0	0.0	0.0	0.0
VTs	0.4	-0.3	0.0	0.1	-0.4
Lower grading temp. (°C)	0.3	-0.2	-0.1	0.2	-0.3
Upper grading temp. (°C)	0.7	-0.1	-0.5	0.6	-0.4
Gg (Gpa)	0.2	-0.1	-0.2	0.2	-0.1
R	0.5	0.1	-0.5	0.5	-0.1
ω_0 @ Td (Hz)	0.3	-0.1	-0.2	0.2	-0.2
η_0 @ Td (Gpa-s)	0.0	0.0	0.0	0.1	0.0
$G^* / \sin \delta$ @ 64°C (MPa)	-0.1	0.1	0.0	-0.1	0.1
$G^* \times \sin \delta$ @ 25°C (MPa)	0.4	-0.1	-0.3	0.3	-0.2
S(60) @ 0°C (MPa)	0.4	-0.1	-0.3	0.3	-0.3
m(60) @ 0°C	0.4	0.0	-0.3	0.3	-0.2
1st Partition	1.0	-0.3	-0.6	0.8	-0.6
2nd Partition		1.0	-0.6	0.4	0.9
3rd Partition			1.0	-1.0	-0.3
Skew Factor				1.0	0.0
Standard Deviation					1.0

Table E-3: Correlation matrix -using three (25%,50% &25%) areas fractions.

Partition	1st	2nd	3rd	Skew	Standard
Corr. time	29.39	33.89	38.00	Factor	Deviation
PEN25	-0.6	0.3	0.4	0.3	0.3
PEN4	0.8	-0.5	-0.3	0.5	-0.6
SP (°C)	0.6	-0.3	-0.4	-0.1	-0.3
FP (°C)	-0.2	0.5	-0.1	0.1	0.5
VIS60 (Poise)	0.1	-0.4	0.2	0.0	-0.4
RV135 (cPa.s)	0.4	-0.2	-0.4	-0.1	-0.2
VIS135 (cSt)	-0.1	-0.2	0.2	-0.3	-0.2
RP25	0.5	-0.1	-0.3	0.6	-0.2
RP4	0.2	0.2	-0.3	0.2	0.2
VR60	0.4	-0.1	-0.3	0.3	-0.1
VR135	-0.2	-0.5	0.5	-0.5	-0.5
PI	0.7	-0.4	-0.3	0.5	-0.5
PR	0.5	-0.4	-0.1	0.4	-0.5
PVN	0.3	-0.3	0.0	0.0	-0.3
VTs	0.1	-0.2	0.0	0.2	-0.2
Lower grading temp. (°C)	0.3	-0.3	-0.2	-0.3	-0.2
Upper grading temp. (°C)	0.6	-0.3	-0.5	-0.1	-0.4
Gg (Gpa)	0.3	-0.3	-0.2	-0.5	-0.2
R	0.5	-0.1	-0.5	0.0	-0.2
ω_0 @ Td (Hz)	0.3	-0.2	-0.2	-0.3	-0.1
η_0 @ Td (Gpa-s)	0.1	0.0	0.0	0.3	-0.1
$G^* / \sin \delta$ @ 64°C (MPa)	-0.1	0.1	0.0	0.2	0.1
$G^* \times \sin \delta$ @ 25°C (MPa)	0.3	-0.2	-0.3	0.1	-0.2
S(60) @ 0°C (MPa)	0.3	-0.2	-0.3	0.0	-0.2
m(60) @ 0°C	0.3	-0.2	-0.3	-0.2	-0.1
1st Partition	1.0	-0.6	-0.8	-0.3	-0.6
2nd Partition		1.0	-0.1	0.6	1.0
3rd Partition			1.0	-0.2	-0.1
Skew Factor				1.0	0.4
Standard Deviation					1.0

Table E-4: Correlation matrix - using eight equal times fractions.

Partition	1st	2nd	3rd	4th	5th	6th	7th	8th	Skew Factor	Standard Deviation
Corr. time	24	26	28	30	32	34	36	38		
PEN25	-0.7	-0.5	-0.4	-0.3	0.0	0.6	0.5	0.2	-0.1	0.6
PEN4	0.8	0.8	0.6	0.4	-0.1	-0.7	-0.5	-0.1	-0.4	-0.8
SP (°C)	0.8	0.5	0.3	0.2	0.1	-0.5	-0.5	-0.3	0.3	-0.6
FP (°C)	0.0	-0.2	-0.3	-0.4	0.4	0.4	0.0	-0.2	0.7	0.4
VIS60 (Poise)	0.0	0.0	0.1	0.0	-0.4	-0.2	0.2	0.3	-0.4	-0.3
RV135 (cPa.s)	0.5	0.4	0.2	0.2	0.1	-0.4	-0.4	-0.3	0.2	-0.4
VIS135 (cSt)	-0.4	-0.3	0.0	0.4	-0.2	-0.2	0.2	0.2	-0.4	0.0
RP25	0.8	0.8	0.3	-0.3	0.0	-0.2	-0.5	-0.2	0.2	-0.5
RP4	0.3	0.3	0.1	-0.2	0.2	0.2	-0.3	-0.3	0.4	0.1
VR60	0.4	0.3	0.4	0.4	0.1	-0.3	-0.3	-0.2	-0.1	-0.3
VR135	0.2	-0.1	-0.3	-0.2	-0.6	-0.2	0.5	0.6	-0.4	-0.3
PI	0.3	0.5	0.7	0.6	0.0	-0.7	-0.4	-0.1	-0.5	-0.6
PR	0.4	0.5	0.5	0.2	-0.2	-0.4	-0.2	0.0	-0.3	-0.6
PVN	-0.2	0.0	0.4	0.7	-0.1	-0.5	0.0	0.0	-0.6	-0.3
VTS	0.5	0.4	0.0	-0.4	-0.2	-0.1	-0.1	0.1	0.1	-0.3
Lower grading temp. (°C)	0.5	0.2	0.2	0.1	0.0	-0.3	-0.2	-0.1	0.0	-0.3
Upper grading temp. (°C)	0.7	0.6	0.4	0.4	0.1	-0.7	-0.6	-0.3	0.1	-0.6
Gg (Gpa)	-0.2	0.4	0.4	0.3	-0.3	-0.3	-0.2	-0.1	-0.8	-0.2
R	0.2	0.6	0.5	0.3	0.2	-0.4	-0.5	-0.4	-0.1	-0.3
ω_0 @ Td (Hz)	0.4	0.2	0.2	0.1	0.0	-0.3	-0.2	-0.1	0.1	-0.3
h_0 @ Td (Gpa.s)	-0.2	0.2	0.1	-0.1	-0.1	0.0	-0.1	0.0	-0.1	-0.1
$G^* / \sin \delta$ @ 64°C (MPa)	-0.2	-0.1	-0.1	-0.1	0.0	0.2	0.0	0.0	0.1	0.1
$G^* \times \sin \delta$ @ 25°C (MPa)	0.4	0.3	0.2	0.1	0.0	-0.3	-0.3	-0.2	0.2	-0.3
S(60) @ 0°C (MPa)	0.4	0.3	0.2	0.0	0.0	-0.3	-0.3	-0.2	0.3	-0.4
m(60) @ 0°C	0.4	0.3	0.2	0.3	0.1	-0.4	-0.3	-0.2	0.0	-0.3
1st Partition	1.0	0.6	0.4	0.1	-0.2	-0.7	-0.5	-0.2	0.3	-0.8
2nd Partition		1.0	0.8	0.4	-0.1	-0.8	-0.8	-0.4	-0.1	-0.9
3rd Partition			1.0	0.8	0.1	-0.8	-0.9	-0.6	-0.2	-0.7
4th Partition				1.0	0.3	-0.6	-0.6	-0.5	-0.4	-0.3
5th Partition					1.0	0.3	-0.4	-0.7	0.5	0.5
6th Partition						1.0	0.6	0.2	0.4	0.9
7th Partition							1.0	0.8	-0.2	0.5
8th Partition								1.0	-0.5	0.1
Skew Factor									1.0	0.3
Standard Deviation										1.0

Table E-5: Correlation matrix - using eight equal areas fractions.

Partition	1st	2nd	3rd	4th	5th	6th	7th	8th	Skew Factor	Standard Deviation
Corr. time	27.64	29.39	30.90	31.89	32.98	33.89	35.28	38.00		
PEN25	-0.6	-0.2	-0.2	-0.1	0.5	0.6	0.6	0.3	-0.5	-0.3
PEN4	0.8	0.4	0.1	-0.2	-0.5	-0.8	-0.5	-0.1	0.6	-0.7
SP (°C)	0.6	0.1	0.2	0.1	-0.4	-0.6	-0.5	-0.3	0.5	0.1
FP (°C)	-0.2	-0.5	0.0	0.5	0.6	0.2	0.0	-0.2	-0.3	0.1
VIS60 (Poise)	0.0	0.1	-0.3	-0.4	-0.3	-0.1	0.1	0.3	0.6	-0.4
RV135 (cPa.s)	0.4	0.2	0.3	0.1	-0.4	-0.4	-0.4	-0.3	0.3	0.1
VIS135 (cSt)	-0.2	0.5	0.1	-0.3	-0.3	0.0	0.2	0.2	0.1	0.0
RP25	0.6	-0.3	-0.1	0.1	0.0	-0.4	-0.5	-0.2	0.2	-0.5
RP4	0.2	-0.2	0.1	0.2	0.3	0.0	-0.2	-0.3	-0.4	0.1
VR60	0.4	0.4	0.3	0.1	-0.2	-0.4	-0.4	-0.2	0.3	-0.2
VR135	-0.2	-0.2	-0.5	-0.6	-0.5	0.0	0.4	0.5	0.2	0.1
PI	0.6	0.7	0.3	-0.1	-0.5	-0.7	-0.5	-0.2	0.5	-0.7
PR	0.5	0.3	-0.1	-0.2	-0.3	-0.4	-0.3	0.0	0.7	-0.7
PVN	0.1	0.8	0.3	-0.2	-0.5	-0.4	-0.1	0.0	0.3	-0.3
VTS	0.3	-0.4	-0.4	-0.1	0.0	-0.1	-0.1	0.1	0.3	-0.3
Lower grading temp. (°C)	0.3	0.2	0.1	-0.1	-0.3	-0.4	-0.2	-0.1	0.4	0.3
Upper grading temp. (°C)	0.7	0.3	0.3	0.1	-0.5	-0.7	-0.6	-0.4	0.6	0.1
Gg (Gpa)	0.3	0.3	0.0	-0.3	-0.4	-0.2	-0.2	-0.1	0.3	0.4
R	0.5	0.3	0.3	0.2	-0.3	-0.5	-0.5	-0.4	0.4	0.0
ω_{10} @ Td (Hz)	0.3	0.1	0.1	0.0	-0.3	-0.3	-0.3	-0.2	0.3	0.3
h_0 @ Td (Gpa.s)	0.1	-0.1	-0.1	-0.1	0.1	0.0	-0.1	0.0	-0.1	-0.3
$G^* / \sin \delta$ @ 64°C (MPa)	-0.1	0.0	-0.1	0.0	0.2	0.2	0.1	0.0	-0.2	-0.2
$G^* \times \sin \delta$ @ 25°C (MPa)	0.3	0.1	0.0	0.0	-0.2	-0.3	-0.3	-0.2	0.3	0.0
S(60) @ 0°C (MPa)	0.4	0.0	0.0	0.0	-0.2	-0.3	-0.3	-0.2	0.3	0.1
m(60) @ 0°C	0.3	0.3	0.3	0.2	-0.4	-0.4	-0.4	-0.2	0.3	0.1
1st Partition	1.0	0.5	0.3	-0.1	-0.7	-0.9	-0.9	-0.6	0.8	0.3
2nd Partition		1.0	0.6	0.0	-0.6	-0.6	-0.6	-0.5	0.3	0.0
3rd Partition			1.0	0.7	0.0	-0.4	-0.6	-0.8	0.0	-0.2
4th Partition				1.0	0.6	0.1	-0.3	-0.7	-0.3	-0.3
5th Partition					1.0	0.8	0.5	-0.1	-0.7	-0.2
6th Partition						1.0	0.9	0.5	-0.8	-0.1
7th Partition							1.0	0.8	-0.6	-0.1
8th Partition								1.0	-0.2	-0.1
Skew Factor									1.0	0.4
Standard Deviation										1.0

Table E-6: Correlation matrix - using twelve equal times fractions.

Partition	1st	2nd	3rd	4th	5th	6th	7th	8th	9th	10th	11th	12th	Skew Factor	Standard Deviation
Corr. time	23.33	24.67	26.00	27.33	28.67	30.00	31.33	32.67	34.00	35.33	36.67	38.00		
PEN25	-0.7	-0.6	-0.4	-0.4	-0.2	-0.3	-0.2	0.3	0.6	0.5	0.3	0.2	-0.1	0.5
PEN4	0.7	0.8	0.8	0.7	0.4	0.4	0.0	-0.4	-0.8	-0.5	-0.2	-0.1	-0.3	-0.8
SP (°C)	0.9	0.6	0.4	0.3	0.1	0.2	0.1	-0.2	-0.6	-0.5	-0.4	-0.3	0.3	-0.6
FP (°C)	0.1	-0.2	-0.2	-0.2	-0.4	-0.4	0.2	0.6	0.3	0.0	-0.1	-0.2	0.7	0.4
VIS60 (Pulse)	0.0	-0.1	0.0	0.1	0.2	-0.1	-0.4	-0.4	-0.1	0.1	0.2	0.3	-0.4	-0.3
RV135 (cPa.s)	0.5	0.5	0.4	0.3	0.1	0.3	0.2	-0.2	-0.4	-0.4	-0.3	-0.3	0.2	-0.4
VIS135 (cst)	-0.2	-0.4	-0.3	-0.1	0.4	0.3	-0.1	-0.3	0.0	0.2	0.2	0.2	-0.5	0.0
RP25	0.7	0.8	0.8	0.4	-0.2	-0.2	0.0	0.1	-0.3	-0.5	-0.3	-0.2	0.3	-0.4
RP4	0.2	0.3	0.3	0.1	-0.2	-0.1	0.2	0.3	0.1	-0.2	-0.3	-0.2	0.4	0.1
VR60	0.5	0.3	0.3	0.4	0.4	0.3	0.2	-0.1	-0.4	-0.4	-0.2	-0.2	-0.1	-0.3
VR135	0.2	0.2	-0.1	-0.3	-0.2	-0.3	-0.6	-0.6	-0.1	0.4	0.5	0.6	-0.4	-0.3
PI	0.2	0.4	0.5	0.7	0.7	0.6	0.1	-0.4	-0.7	-0.5	-0.2	-0.1	-0.4	-0.6
PR	0.4	0.4	0.5	0.5	0.4	0.1	-0.2	-0.3	-0.5	-0.3	-0.1	0.1	-0.3	-0.6
PVN	-0.1	-0.1	0.0	0.3	0.7	0.6	0.0	-0.4	-0.4	-0.1	0.0	-0.3	-0.6	-0.3
VTS	0.3	0.5	0.4	0.1	-0.4	-0.4	-0.3	-0.1	-0.1	-0.1	0.0	0.1	0.1	-0.3
Lower grading temp. (°C)	0.5	0.3	0.1	0.1	0.2	0.1	0.0	-0.2	-0.4	-0.2	-0.1	-0.1	0.0	-0.3
Upper grading temp. (°C)	0.7	0.7	0.6	0.5	0.3	0.4	0.2	-0.3	-0.7	-0.6	-0.4	-0.3	0.2	-0.6
Gg (Gpa)	-0.3	0.2	0.4	0.4	0.3	0.2	-0.2	-0.4	-0.3	-0.2	-0.2	-0.1	-0.7	-0.2
R	0.1	0.4	0.6	0.5	0.2	0.3	0.3	-0.1	-0.5	-0.5	-0.5	-0.4	-0.1	-0.3
ω_0 @ Td (Hz)	0.4	0.3	0.2	0.2	0.1	0.1	0.1	-0.2	-0.3	-0.2	-0.2	-0.1	0.1	-0.3
h_0 @ Td (Gpa.s)	-0.2	0.0	0.2	0.1	0.0	-0.1	-0.1	0.0	0.0	-0.1	-0.1	0.0	0.0	0.0
$G^* I \sin \delta$ @ 64°C (MPa)	-0.2	-0.1	-0.1	-0.1	0.0	-0.1	0.0	0.1	0.2	0.0	0.0	0.0	0.1	0.1
$G^* \times \sin \delta$ @ 25°C (MPa)	0.4	0.4	0.3	0.2	0.1	0.1	0.0	-0.1	-0.3	-0.3	-0.2	-0.2	0.3	-0.3
$S(60)$ @ 0°C (MPa)	0.4	0.4	0.3	0.2	0.1	0.0	0.0	-0.1	-0.3	-0.3	-0.2	-0.2	0.3	-0.3
$m(60)$ @ 0°C	0.4	0.4	0.3	0.2	0.2	0.4	0.3	-0.2	-0.4	-0.3	-0.3	-0.2	0.0	-0.3
1st Partition	1.0	0.8	0.5	0.3	0.1	0.1	-0.1	-0.3	-0.6	-0.5	-0.3	-0.2	0.3	-0.7
2nd Partition		1.0	0.9	0.7	0.3	0.2	-0.1	-0.6	-0.8	-0.7	-0.5	-0.3	0.0	-0.9
3rd Partition			1.0	0.9	0.5	0.4	0.1	-0.5	-0.8	-0.9	-0.7	-0.4	-0.1	-0.8
4th Partition				1.0	0.8	0.7	0.3	-0.4	-0.8	-0.9	-0.8	-0.6	-0.2	-0.7
5th Partition					1.0	0.9	0.3	-0.4	-0.6	-0.6	-0.5	-0.4	-0.4	-0.4
6th Partition						1.0	0.6	-0.1	-0.6	-0.6	-0.6	-0.6	-0.3	-0.3
7th Partition							1.0	0.6	-0.2	-0.5	-0.7	-0.8	0.4	0.3
8th Partition								1.0	0.6	0.1	-0.2	-0.5	0.7	0.8
9th Partition									1.0	0.8	0.5	0.3	0.2	0.9
10th Partition										1.0	0.9	0.7	-0.2	0.6
11th Partition											1.0	0.9	-0.4	0.2
12th Partition												1.0	-0.5	0.0
Skew Factor													1.0	0.3
Standard Deviation														1.0

Table E-7: Correlation matrix - using twelve equal areas fractions.

Partition	1st	2nd	3rd	4th	5th	6th	7th	8th	9th	10th	11th	12th	Skew Factor	Standard Deviation
Corr. time	26.96	28.29	29.41	30.44	31.22	31.89	32.57	33.17	33.89	34.70	35.89	38.00		
PEN25	-0.6	-0.4	0.0	-0.2	-0.1	0.0	0.4	0.6	0.6	0.6	0.5	0.3	-0.4	-0.4
PEN4	0.8	0.5	0.4	0.2	0.0	-0.2	-0.5	-0.7	-0.8	-0.6	-0.4	-0.1	0.8	-0.6
SP (°C)	0.6	0.3	-0.1	0.1	0.1	0.1	-0.4	-0.5	-0.6	-0.6	-0.5	-0.3	0.4	0.3
FP (°C)	-0.2	-0.1	-0.4	-0.1	0.3	0.5	0.6	0.4	0.2	0.0	-0.1	-0.2	-0.4	0.1
VIS60 (Poise)	0.0	0.2	0.1	-0.3	-0.4	-0.4	-0.3	-0.2	-0.1	0.1	0.2	0.3	0.2	-0.4
RV135 (cPa.s)	0.5	0.1	0.1	0.2	0.1	0.0	-0.3	-0.4	-0.5	-0.4	-0.4	-0.3	0.3	0.1
VIS135 (cSt)	-0.3	0.3	0.5	0.1	-0.1	-0.3	-0.3	-0.2	0.0	0.2	0.2	0.2	-0.2	0.1
RP25	0.7	0.0	-0.3	-0.1	0.0	0.1	0.1	-0.1	-0.4	-0.5	-0.4	-0.2	0.6	-0.5
RP4	0.3	-0.1	-0.2	0.0	0.2	0.3	0.3	0.2	0.0	-0.2	-0.3	-0.3	0.0	0.0
VR60	0.4	0.4	0.4	0.3	0.1	0.1	-0.1	-0.3	-0.4	-0.4	-0.3	-0.2	0.3	-0.2
VR135	-0.1	-0.3	-0.1	-0.4	-0.6	-0.6	-0.5	-0.3	0.1	0.4	0.5	0.6	0.3	0.3
PI	0.6	0.7	0.7	0.4	0.1	-0.2	-0.4	-0.7	-0.7	-0.5	-0.3	-0.1	0.5	-0.7
PR	0.5	0.4	0.2	-0.1	-0.2	-0.3	-0.3	-0.4	-0.5	-0.4	-0.2	0.0	0.5	-0.6
PVN	0.1	0.6	0.8	0.4	0.0	-0.3	-0.5	-0.5	-0.3	-0.1	0.0	0.0	0.1	-0.3
VTS	0.3	-0.3	-0.4	-0.4	-0.3	-0.1	0.0	0.0	-0.1	-0.1	0.0	0.1	0.5	-0.3
Lower grading temp. (°C)	0.3	0.3	-0.1	0.1	0.0	-0.1	-0.3	-0.3	-0.4	-0.3	-0.2	-0.1	0.1	0.4
Upper grading temp. (°C)	0.7	0.3	0.1	0.3	0.2	0.1	-0.5	-0.6	-0.7	-0.7	-0.5	-0.3	0.4	0.2
Gg (Gpa)	0.2	0.3	0.1	0.1	-0.2	-0.4	-0.4	-0.3	-0.2	-0.2	-0.2	-0.1	0.2	0.3
R	0.5	0.3	0.1	0.3	0.3	0.1	-0.2	-0.4	-0.5	-0.5	-0.5	-0.4	0.3	0.1
ω_p @ Td (Hz)	0.3	0.1	0.1	0.1	0.1	0.0	-0.2	-0.3	-0.3	-0.3	-0.2	-0.2	0.3	0.3
h_0 @ Td (Gpa.s)	0.1	0.0	-0.1	-0.1	-0.1	0.0	0.1	0.0	0.0	-0.1	-0.1	0.0	0.1	-0.3
$G' / \sin \delta$ @ 64°C (MPa)	-0.1	-0.1	0.1	-0.1	0.0	0.0	0.2	0.2	0.2	0.1	0.0	0.0	-0.1	-0.2
$G' \times \sin \delta$ @ 25°C (MPa)	0.4	0.1	0.1	0.0	0.0	0.0	-0.2	-0.2	-0.3	-0.3	-0.3	-0.2	0.3	0.0
$S(60)$ @ 0°C (MPa)	0.4	0.0	0.1	-0.1	0.0	0.0	-0.2	-0.3	-0.3	-0.3	-0.3	-0.2	0.4	0.1
$m(60)$ @ 0°C	0.3	0.3	0.1	0.3	0.2	0.1	-0.3	-0.4	-0.4	-0.4	-0.3	-0.2	0.2	0.1
1st Partition	1.0	0.4	0.3	0.3	0.0	-0.2	-0.6	-0.8	-0.9	-0.9	-0.8	-0.5	0.8	0.4
2nd Partition		1.0	-0.4	0.5	0.4	0.2	-0.1	-0.4	-0.5	-0.6	-0.5	-0.4	0.1	0.2
3rd Partition			1.0	0.3	0.0	-0.2	-0.4	-0.3	-0.2	-0.2	-0.2	-0.2	0.4	-0.1
4th Partition				1.0	0.8	0.5	0.0	-0.3	-0.4	-0.6	-0.7	-0.7	0.0	-0.2
5th Partition					1.0	0.9	0.5	0.1	-0.2	-0.4	-0.6	-0.8	-0.3	-0.3
6th Partition						1.0	0.7	0.4	0.1	-0.2	-0.4	-0.7	-0.5	-0.4
7th Partition							1.0	0.9	0.7	0.4	0.1	-0.2	-0.8	-0.3
8th Partition								1.0	0.9	0.7	0.5	0.1	-0.8	-0.3
9th Partition									1.0	0.9	0.8	0.4	-0.8	-0.2
10th Partition										1.0	0.9	0.7	-0.7	-0.2
11th Partition											1.0	0.9	-0.5	-0.1
12th Partition												1.0	-0.1	0.0
Skew Factor													1.0	0.3
Standard Deviation														1.0

Model fitting results for (PEN25) ^{1/2}					
Independent variable	coefficient	std. error	t-value	sig.level.	
CONSTANT	-8.338437	4.940086	-1.6879	0.1015	
R-2/12	-1.059777	0.385058	-2.7237	0.0105	
R-3/12	1.395615	0.329112	4.2406	0.0002	
R-4/12	-1.336816	0.459724	-2.9079	0.0067	
R-5/12	1.283488	0.453135	2.8325	0.0080	
R-9/12	0.622393	0.169522	3.6715	0.0009	
R-SQ. (ADJ.) = 0.6828 SE= 0.617990 MAE= 0.423439 DurbWat= 2.322					
37 observations fitted. forecast(s) computed for 0 missing val. of dep. var.					
Analysis of Variance for the Full Regression					
Source	Sum of Squares	DF	Mean Square	F-Ratio	P-value
Model	31.5041	5	6.30083	16.4981	0.0000
Error	11.8393	31	0.381912		
Total (Corr.)	43.3434	36			
R-squared = 0.726849		Std. error of est. = 0.61799			
R-squared (Adj. for d f.) = 0.682793		Durbin-Watson statistic = 2.32168			

Plot of PEN25^{1/2}

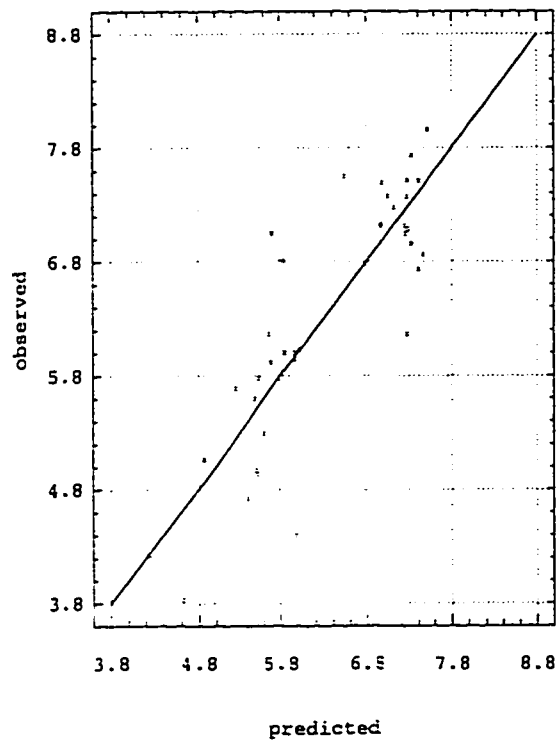
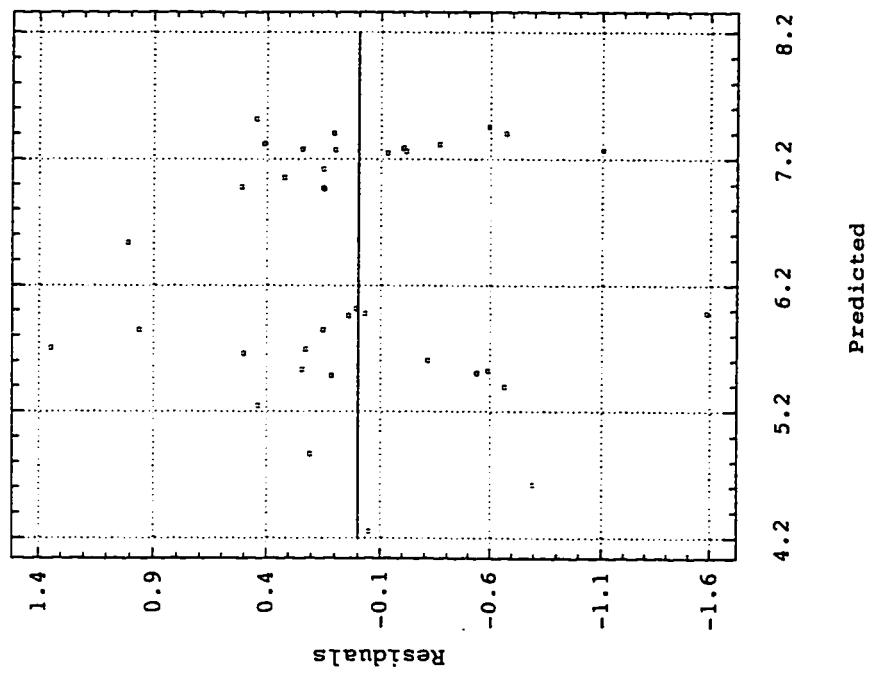


Fig. E-1

Residual Plot for $PEN25^{1/2}$



Nor. Prob. Plot for $PEN25^{1/2}$

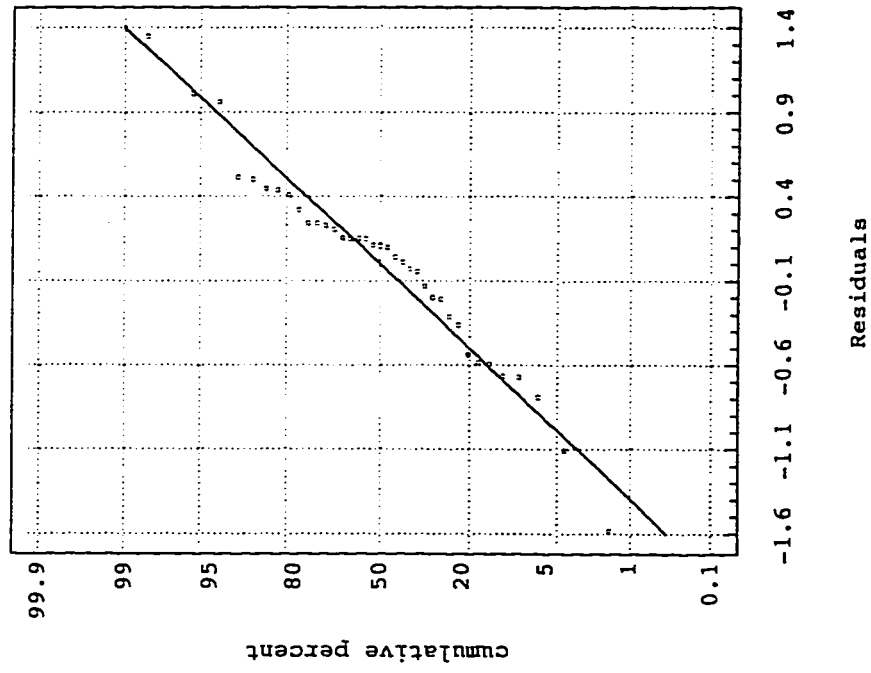


Fig. E-2

Model fitting results for: PEN4					
Independent variable	coefficient	std. error	t-value	sig.level	
CONSTANT	-5.94E+04	1.45E+04	-4.1046	0.0017	
R-4/12	1261.668666	365.073858	3.4559	0.0054	
R-5/12	2655.203166	635.768475	4.1764	0.0015	
R-7/12	-915.448466	303.208778	-3.0192	0.0117	
R-8/12	1945.648665	448.988733	4.3334	0.0012	
R-12/12	1792.496557	447.284222	4.0075	0.0021	
17 observations fitted, forecast(s) computed for 0 missing val. of dep. var.					
Analysis of Vanance for the Full Regression					
Source	Sum of Squares	DF	Mean Square	F-Ratio	P-value
Model	288.613	3	96.2043	30.0295	0.0000
Error	41.6475	13	3.2037		
Total (Corr.)	330.26	16			
R-squared = 0.873895		Std. error of est. = 1.78988			
R-squared (Adj. for d.f.) = 0.844794		Durbin-Watson statistic = 1.51353			

Plot of PEN4

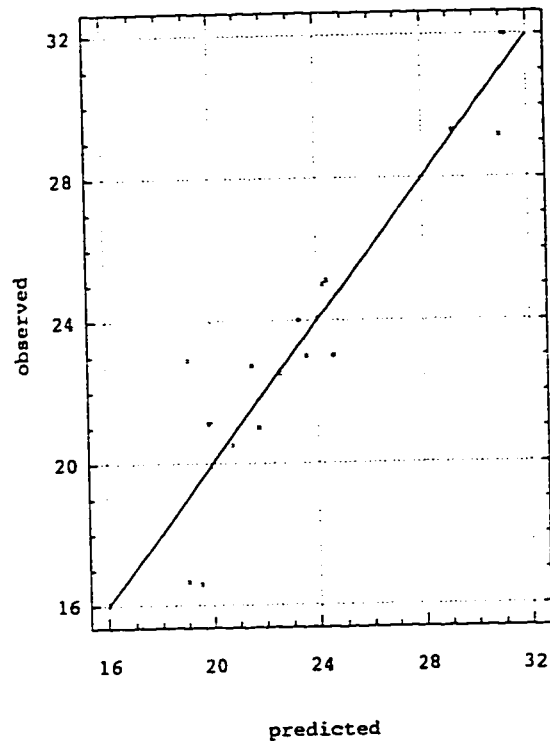
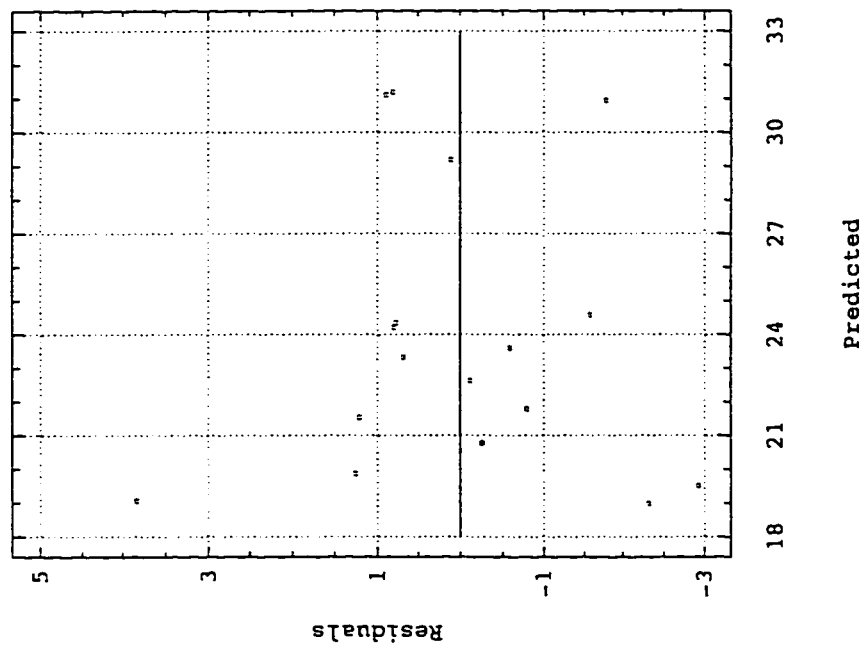


Fig. E-3

Residual Plot for PEN4



Normal Probability Plot for PEN4

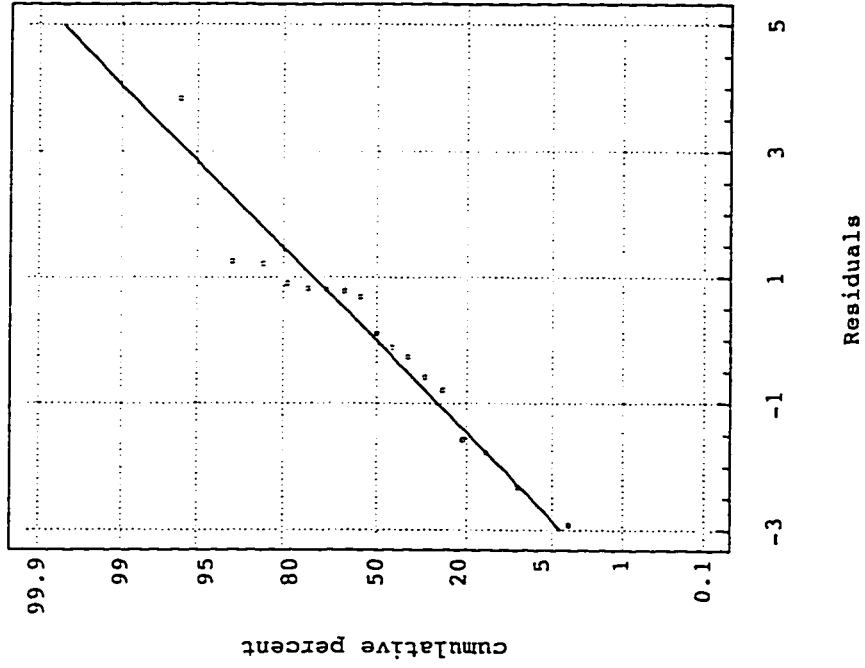


Fig. E-4

Model fitting results for: SP					
Independent variable	coefficient	std. error	t-value	sig.level	
CONSTANT	51.379462	0.839584	61.1964	0.0000	
R-1/12	15.376882	0.749562	20.5145	0.0000	
R-SQ. (ADJ.) = 0.9210 SE= 3.969458 MAE= 2.950274 DurWat= 2.280					
37 observations fitted, forecast(s) computed for 0 missing val. of dep. var.					
Analysis of Variance for the Full Regression					
Source	Sum of Squares	DF	Mean Square	F-Ratio	P-value
Model	6631.08	1	6631.08	420.8450	0.0000
Error	551.481	35	15.7566		
Total (Corr.)	7182.56	36			
R-squared = 0.923219		Std. error of est. = 3.96946			
R-squared (Adj. for d.f.) = 0.921026		Durbin-Watson statistic = 2.28024			

Plot of SP

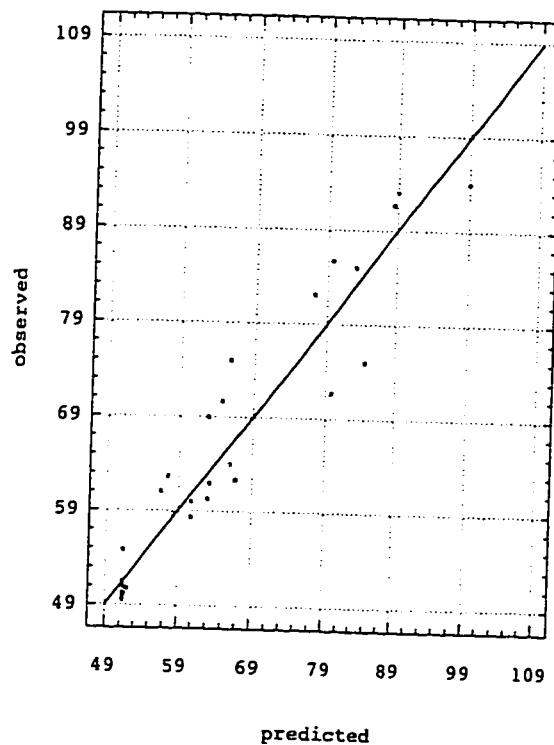
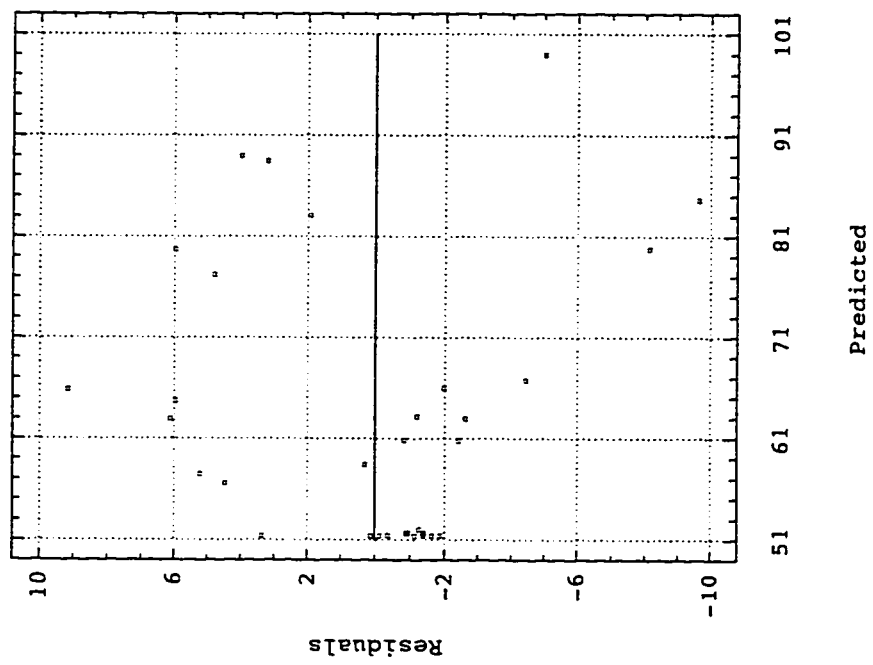


Fig. E-5

Residual Plot for SP



Normal Probability Plot for SP

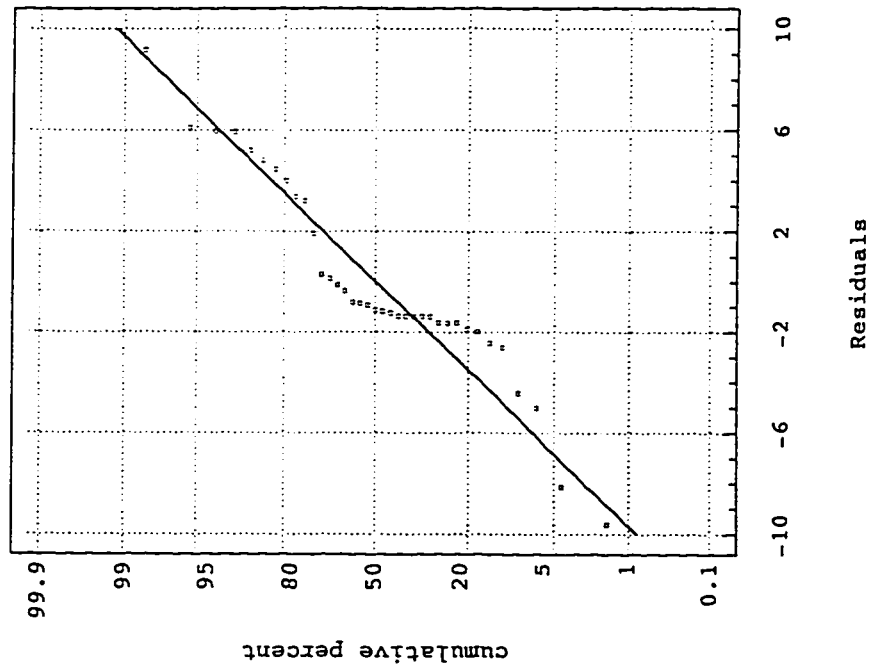


Fig. E-6

Model fitting results for: FP					
Independent variable	coefficient	std. error	t-value	sig.level	
CONSTANT	-1530.537812	302.241113	-5.0640	0.0000	
RTR-1/12	45.793995	5.091368	8.9944	0.0000	
R-2/12	40.797671	7.792445	5.2355	0.0000	
R-4/12	86.306082	10.821054	7.9758	0.0000	
R-5/12	-66.538647	9.416457	-7.0662	0.0000	
R-6/12	65.554937	13.211858	4.9618	0.0000	
R-7/12	-28.154419	6.677668	-4.2162	0.0003	
R-8/12	12.160158	4.708493	2.5826	0.0150	
R-10/12	-14.572857	4.144698	-3.5160	0.0017	
R-11/12	19.3668	3.926896	4.9318	0.0000	
R-12/12	55.546754	6.321938	8.7863	0.0000	
STANDARD DEV.	183.819019	22.127743	8.3072	0.0000	
R-SQ. (ADJ.) = 0.9015 SE= 4.584483 MAE= 2.985385 DurbWat= 2.254					
37 observations fitted, forecast(s) computed for 0 missing val. of dep. var.					
Analysis of Vanance for the Full Regression					
Source	Sum of Squares	DF	Mean Square	F-Ratio	P-value
Model	7159.37	11	650.852	30.9672	0.0000
Error	525.437	25	21.0175		
Total (Corr.)	7684.81	36			
R-squared = 0.931627		Std. error of est. = 4.58448			
R-squared (Adj. for d.f.) = 0.901542		Durbin-Watson statistic = 2.25443			

Plot of FP

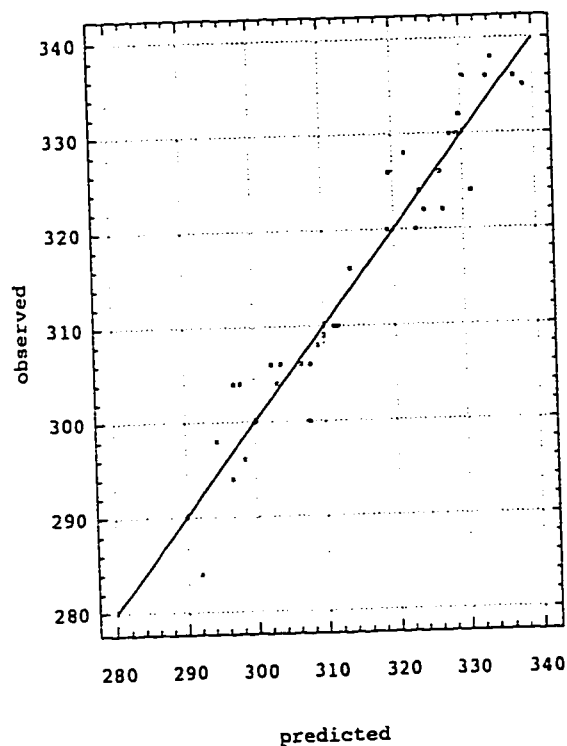
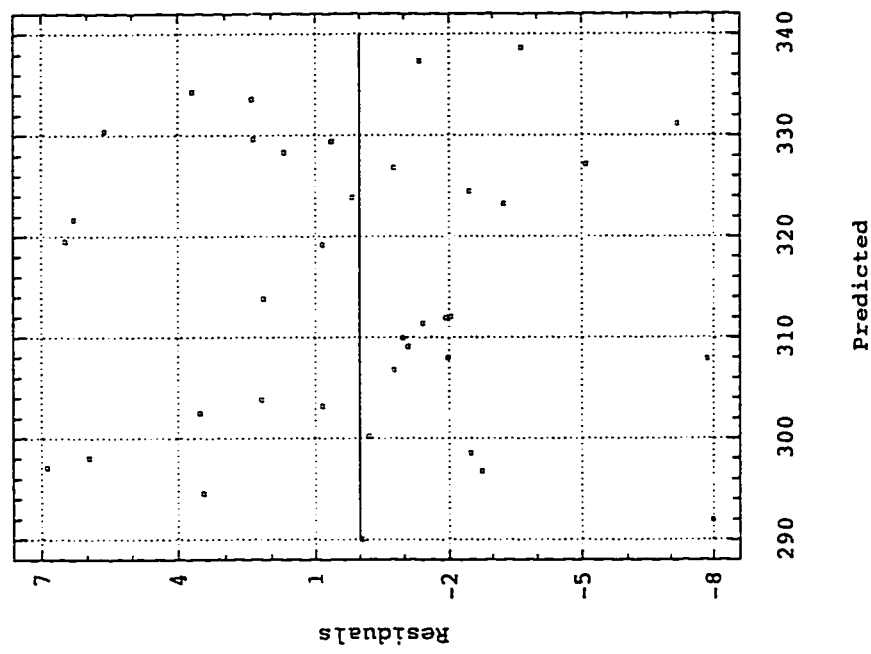


Fig. E-7

Residual Plot for FP



Normal Probability Plot for FP

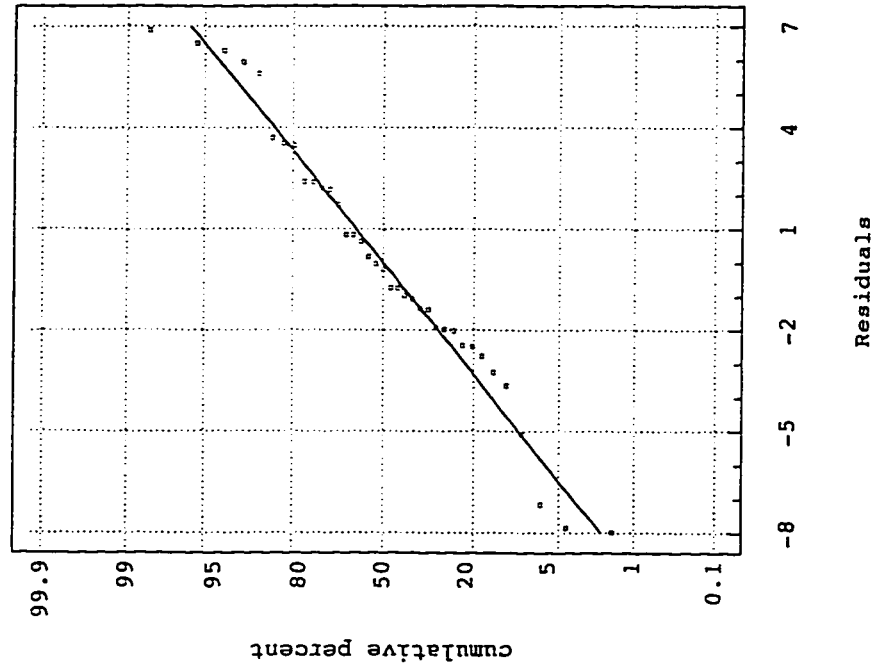


Fig. E-8

Model fitting results for: VIS60					
Independent variable	coefficient	std. error	t-value	sig.level	
CONSTANT	-5.94E+04	1.45E+04	-4.1046	0.0017	
R-4/12	1261.668666	365.073858	3.4559	0.0054	
R-5/12	2655.203166	635.768475	4.1764	0.0015	
R-7/12	-915.448466	303.208778	-3.0192	0.0117	
R-8/12	1945.648665	448.988733	4.3334	0.0012	
R-12/12	1792.496557	447.284222	4.0075	0.0021	
R-SQ. (ADJ.) = 0.5948 SE= 505.418626 MAE= 355.041528 DurbWat= 2.561					
17 observations fitted, forecast(s) computed for 0 missing val. of dep. var.					
Analysis of Vanance for the Full Regression					
Source	Sum of Squares	DF	Mean Square	F-Ratio	P-value
Model	7276589	5	1455318	5.6971	0.0078
Error	2809928	11	255448		
Total (Corr.)	10086517	16			
R-squared = 0.721417					Std. error of est. = 505.419
R-squared (Adj. for d.f.) = 0.594789					Durbin-Watson statistic = 2.56059

Residual Plot for VIS60

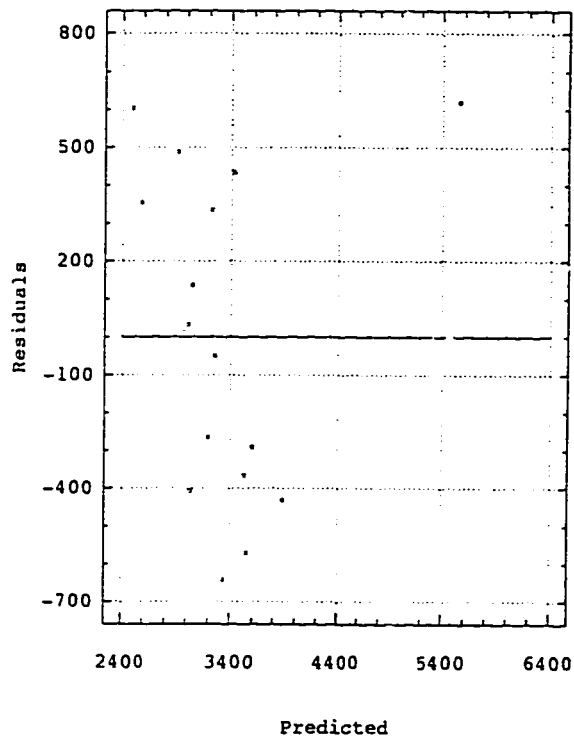
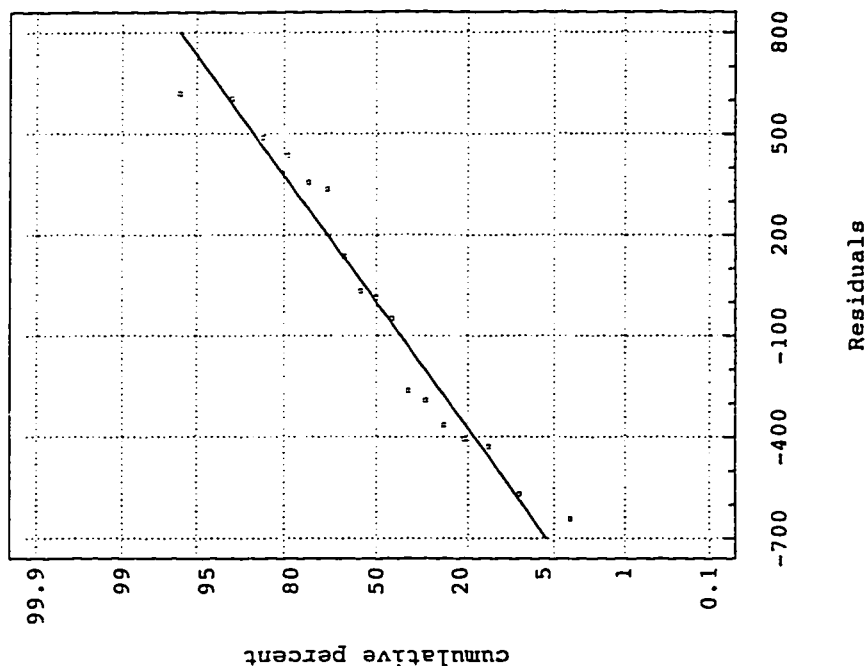


Fig. E-9

Normal Probability Plot for VIS60



Plot of VIS60

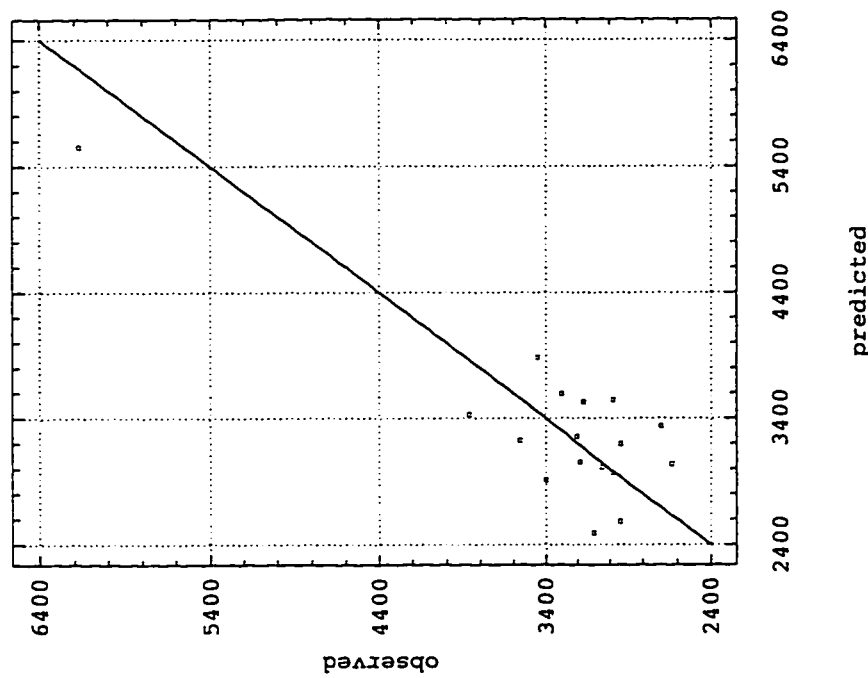


Fig. E-10

Model fitting results for: LN(RV135)					
Independent variable	coefficient	std. error	t-value	sig.level	
CONSTANT	69.804433	13.694064	5.0974	0.0000	
R-1/12	-1.129092	0.371586	-3.0386	0.0052	
R-3/12	-1.789359	0.434479	-4.1184	0.0003	
R-5/12	-2.038812	0.247158	-8.2490	0.0000	
R-6/12	0.327292	0.272365	1.2017	0.2399	
R-9/12	-0.408675	0.169924	-2.4050	0.0233	
R-10/12	0.305342	0.196705	1.5523	0.1322	
R-11/12	-0.527991	0.311098	-1.6972	0.1012	
R-12/12	-1.283875	0.203823	-6.2990	0.0000	
STANDARD DEV	-5.216869	1.058925	-4.9266	0.0000	
R-SQ. (ADJ.) = 0.9024 SE= 0.340920 MAE= 0.222644 DurbWat= 2.194					
37 observations fitted, forecast(s) computed for 0 missing val. of dep. var.					
Analysis of Variance for the Full Regression					
Source	Sum of Squares	DF	Mean Square	F-Ratio	P-value
Model	39.729	9	4.41433	37.9804	0.0000
Error	3.13812	27	0.116227		
Total (Corr.)	42.8671	36			
R-squared = 0.926794		Std. error of est. = 0.34092			
R-squared (Adj. for d.f.) = 0.902392		Durbin-Watson statistic = 2.19424			

Plot of LN(RV135)

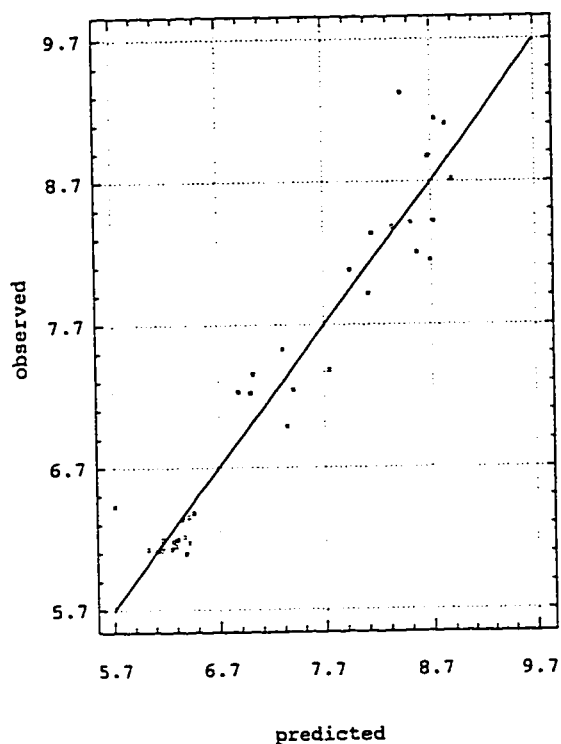
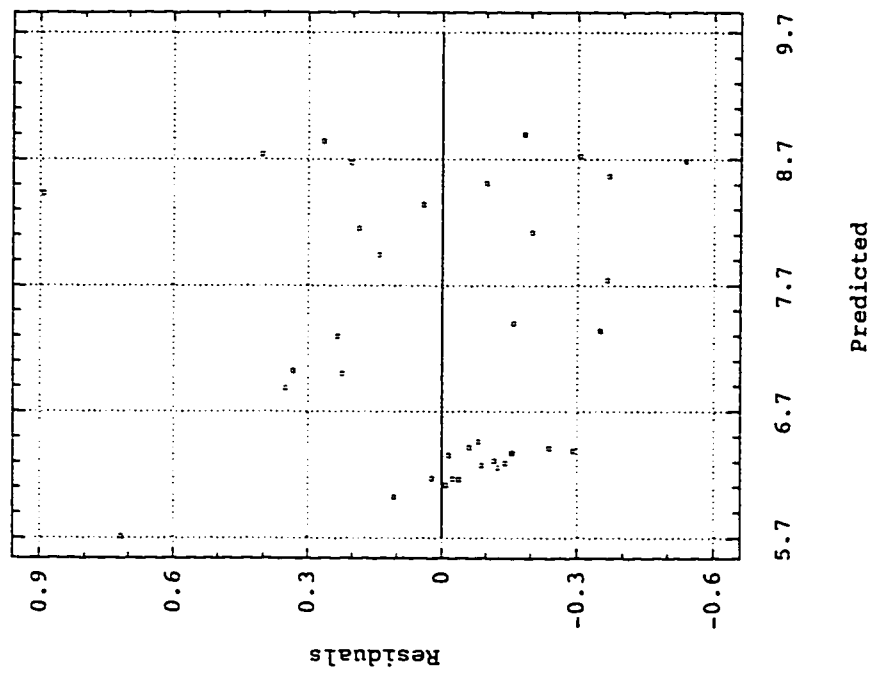


Fig. E-11

Residual Plot for LN(RV135)



Norm. Prob. Plot for LN(RV135)

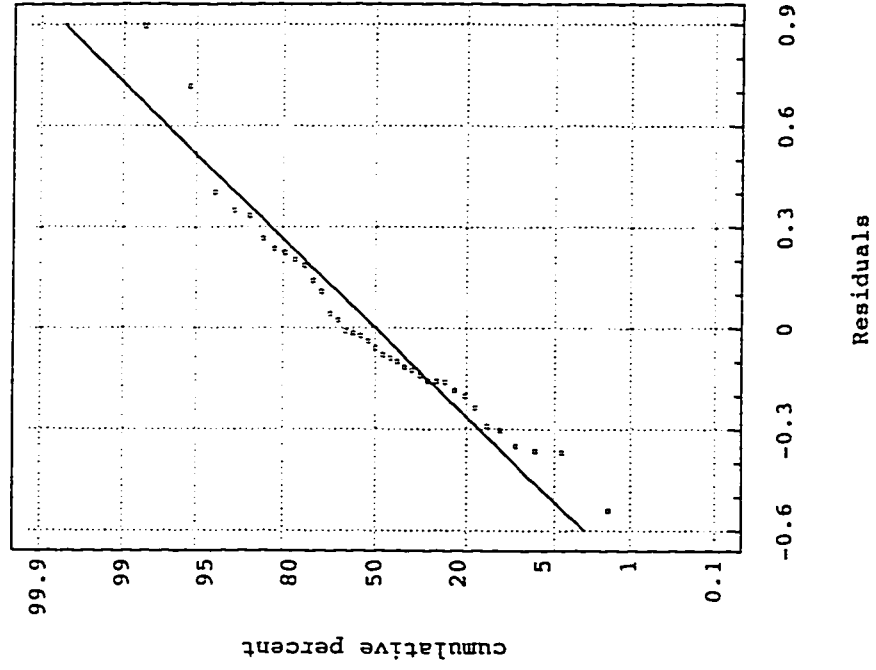


Fig. E-12

Model fitting results for: VIS135					
Independent variable	coefficient	std. error	t-value	sig.level	
CONSTANT	7100.710009	3569.407606	1.9893	0.0779	
R-1/12	3542.734205	1411.432482	2.5100	0.0333	
R-2/12	-385.748679	166.244587	-2.3204	0.0455	
R-5/12	-321.343119	183.993454	-1.7465	0.1147	
R-8/12	-96.242098	85.605958	-1.1242	0.2900	
R-10/12	-109.289421	72.47175	-1.5080	0.1658	
R-12/12	-133.739685	52.102053	-2.5669	0.0303	
SKEW	-661.480985	644.257227	-1.0267	0.3313	
R-SQ. (ADJ.) = 0.7594 SE= 23.279098 MAE= 13.687275 DurbWat= 2.050					
17 observations fitted, forecast(s) computed for 0 missing val. of dep. var.					
Analysis of Variance for the Full Regression					
Source	Sum of Squares	DF	Mean Square	F-Ratio	P-value
Model	31159.8	7	4451.4000	8.2142	0.0027
Error	4877.25	9	541.9160		
Total (Corr.)	36037.1	16			
R-squared = 0.86466		Std. error of est. = 23.2791			
R-squared (Adj. for d.f.) = 0.759396		Durbin-Watson statistic = 2.04979			

Plot of VIS135

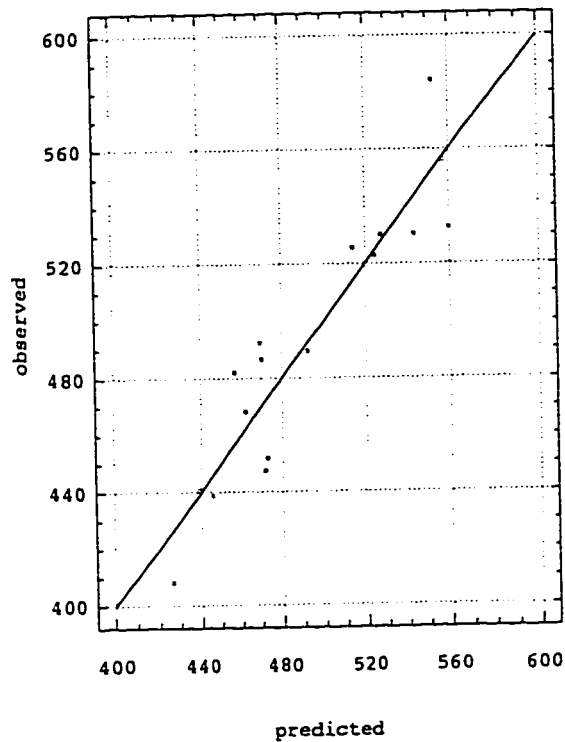
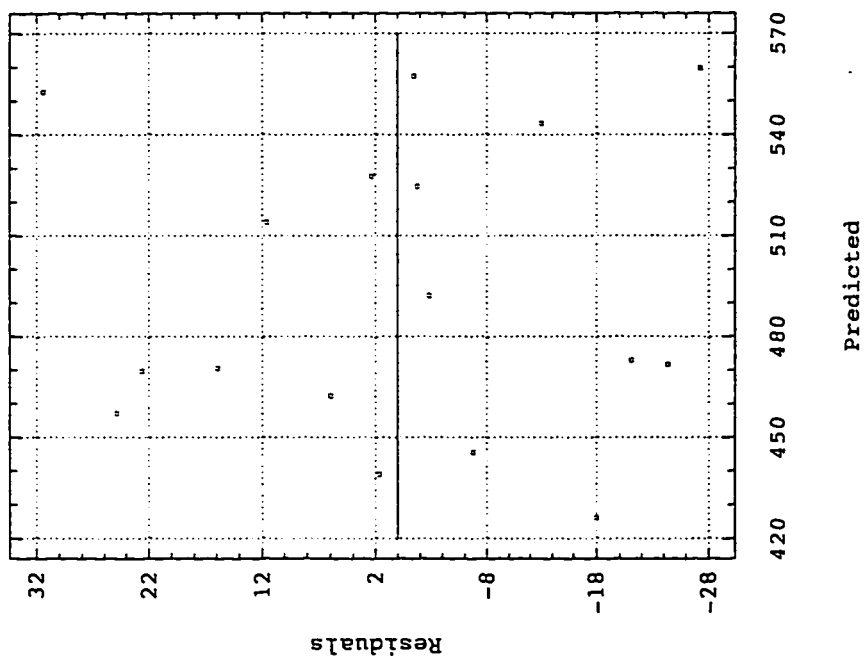


Fig. E-13

Residual Plot for VIS135



Normal Probability Plot for VIS135

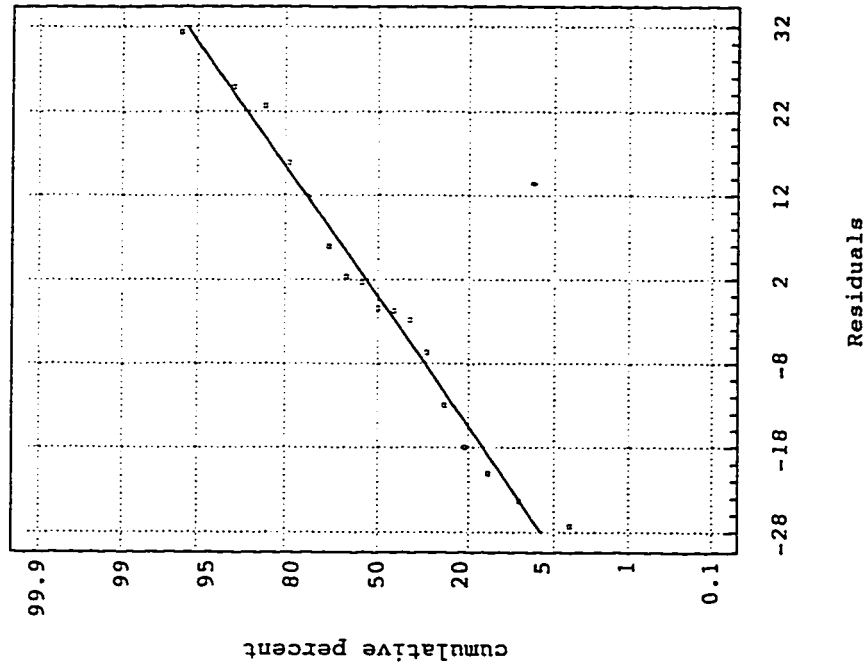


Fig. E-14

Model fitting results for: RP25					
independent variable	coefficient	std. error	t-value	sig.level	
CONSTANT	0.604596	0.059962	10.0830	0.0000	
R-2/12	0.150314	0.019516	7.7020	0.0000	
R-12/12	0.018077	0.0108	1.6738	0.1180	
SKEW	0.231887	0.062773	3.6941	0.0027	
R-SQ. (ADJ.) = 0.8103 SE= 0.039895 MAE= 0.028626 DurbWat= 2.222					
17 observations fitted, forecast(s) computed for 0 missing val. of dep. var.					
Analysis of Variance for the Full Regression					
Source	Sum of Squares	DF	Mean Square	F-Ratio	P-value
Model	0.113228	5	0.0226455	4.83682	0.0139
Error	0.0515009	11	0.0046819		
Total (Corr.)	0.164728	16			
R-squared = 0.845868		Std. error of est. = 0.039895			
R-squared (Adj. for d.f.) = 0.810299		Durbin-Watson statistic = 2.22176			

Plot of RP25

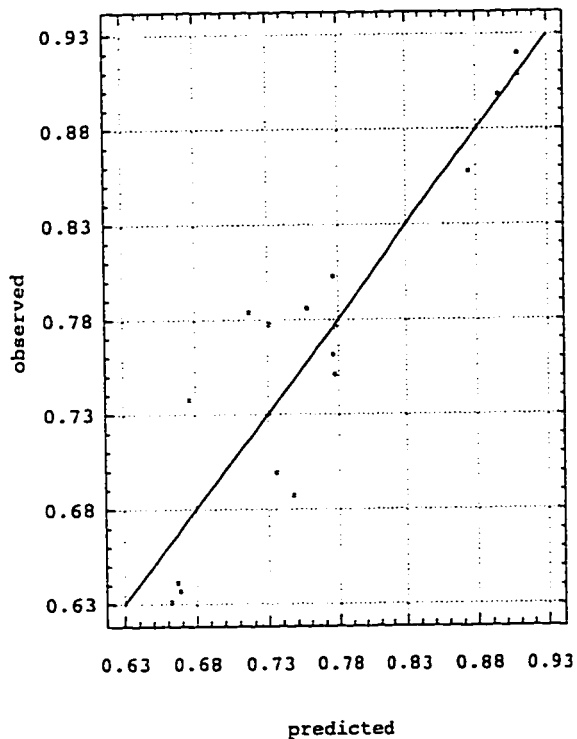
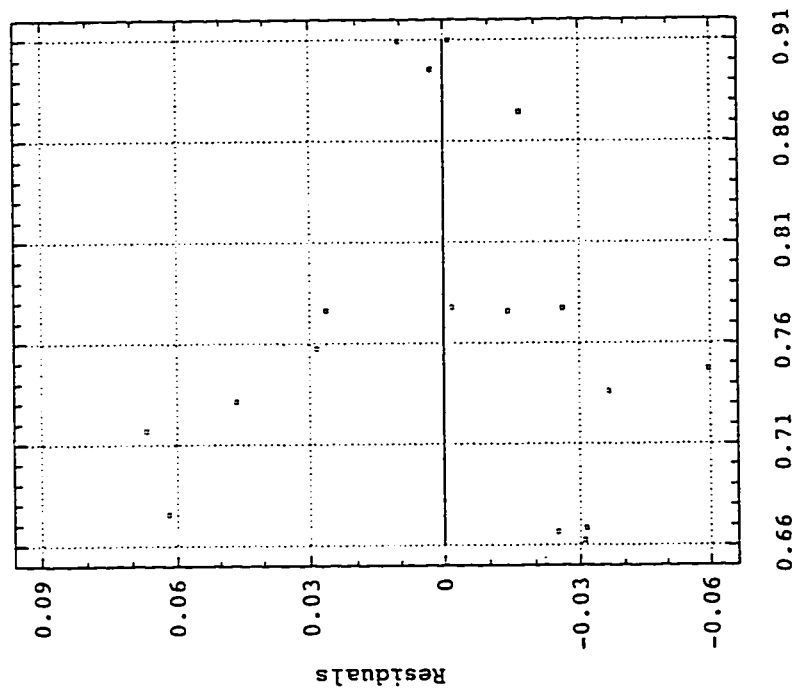


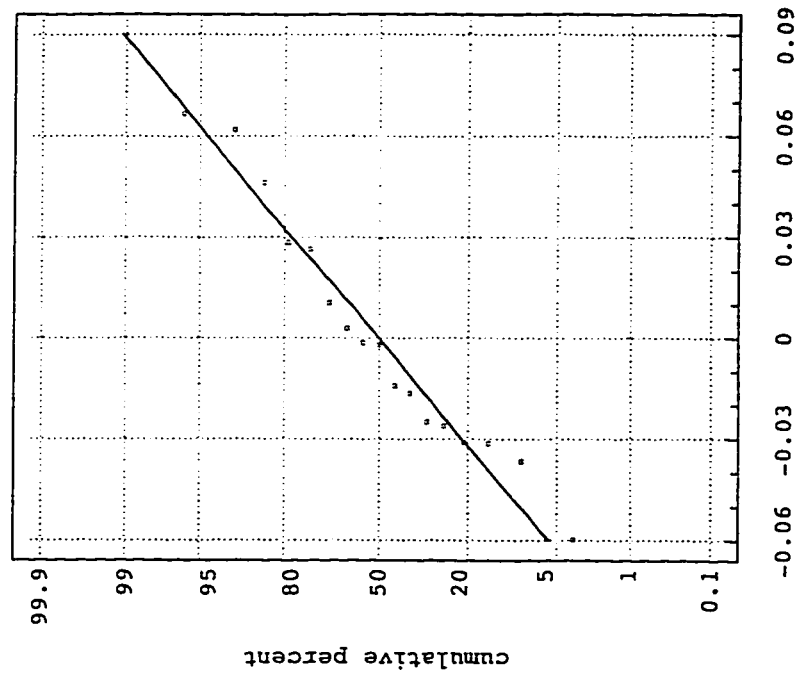
Fig. E-15

Residual Plot for RP25



Predicted

Normal Probability Plot for RP25



Residuals

Fig. E-16

Model fitting results for: RP4					
Independent variable	coefficient	std. error	t-value	sig.level	
CONSTANT	-7.911192	2.480352	-3.1895	0.0086	
R-1/12	-3.75044	3.364267	-1.1148	0.2887	
R-3/12	0.253185	0.067885	3.7296	0.0033	
R-6/12	0.365376	0.109263	3.3440	0.0065	
R-10/12	0.375408	0.105767	3.5494	0.0046	
SKEW	1.124531	0.270892	4.1512	0.0016	
R-SQ (ADJ.) = 0.5452 SE= 0.068424 MAE= 0.043456 DurbWat= 2.164					
17 observations fitted, forecast(s) computed for 0 missing val. of dep. var.					
Analysis of Vanance for the Full Regression					
Source	Sum of Squares	DF	Mean Square	F-Ratio	P-value
Model	0.113228	5	0.0226455	4.83682	0.0139
Error	0.0515009	11	0.0046819		
Total (Corr.)	0.164728	16			
R-squared = 0.687359					Std. error of est. = 0.0684244
R-squared (Adj. for d.f.) = 0.545249					Durbin-Watson statistic = 2.16444

Plot of RP4

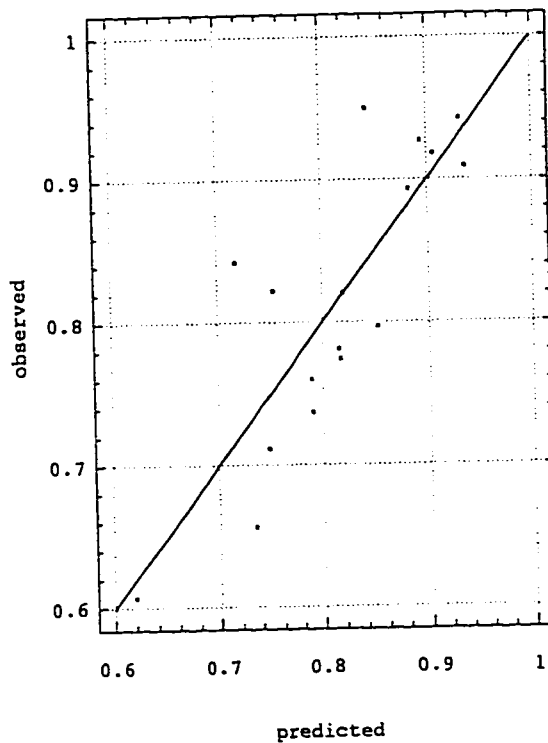
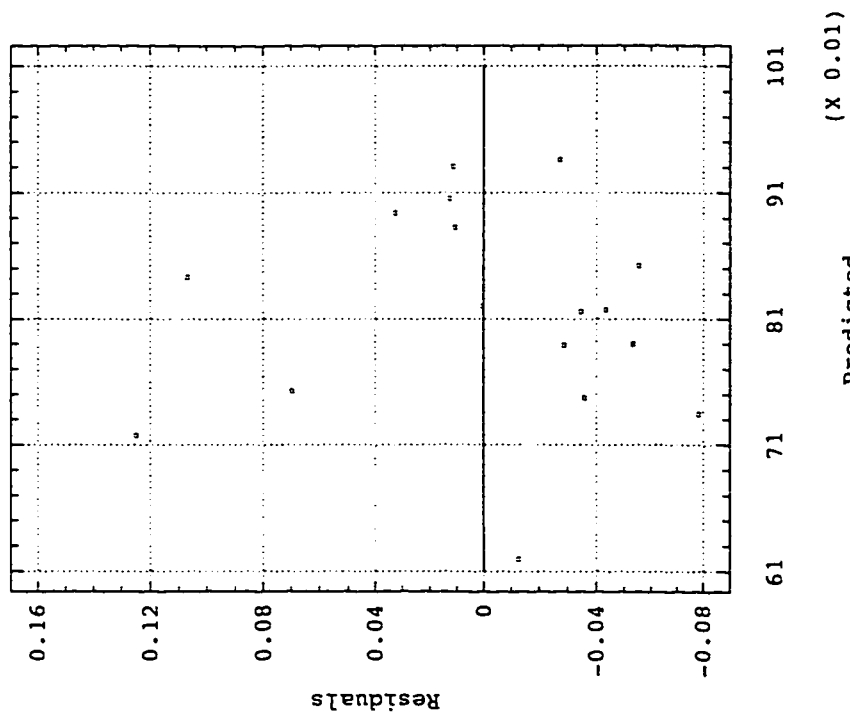


Fig. E-17

Residual Plot for RP4



Normal Probability Plot for RP4

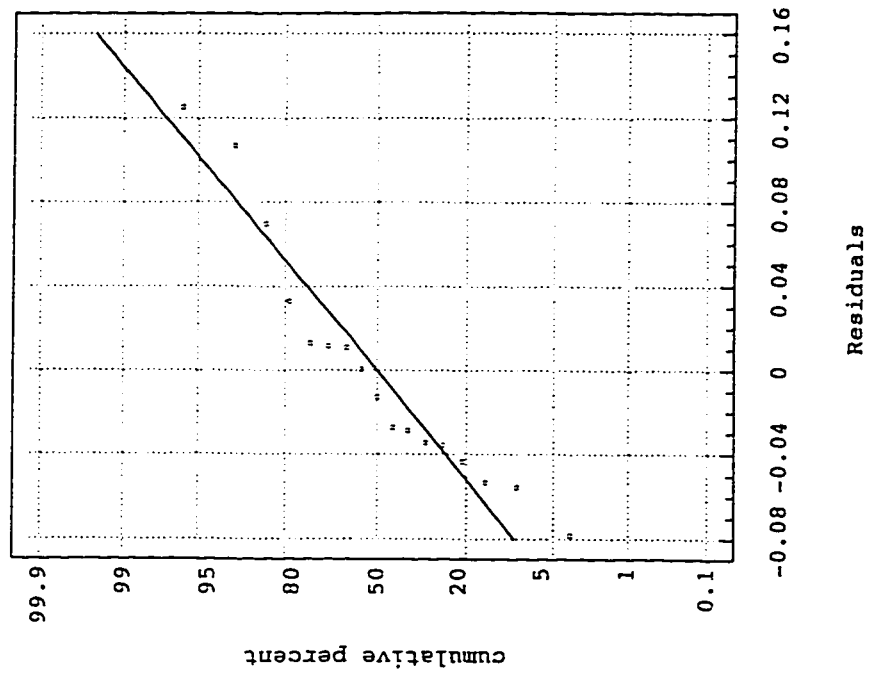


Fig. E-18

Model fitting results for: VR60					
Independent variable	coefficient	std. error	t-value	sig.level	
CONSTANT	0.763582	0.729261	1.0471	0.3141	
R-1/12	28.751761	12.308128	2.3360	0.0362	
R-2/12	-0.412458	0.264472	-1.5596	0.1429	
R-6/12	0.120322	0.073483	1.6374	0.1255	
R-SQ. (ADJ.) = 0.2992 SE= 0.221874 MAE= 0.157572 DurbWat= 1.645					
17 observations fitted, forecast(s) computed for 0 missing val. of dep. var					
Analysis of Vanance for the Full Regression					
Source	Sum of Squares	DF	Mean Square	F-Ratio	P-value
Model	0.484001	3	0.161334	3.27726	0.0555
Error	0.639967	13	0.0492283		
Total (Corr.)	1.12397	16			
R-squared = 0.430618		Std. error of est. = 0.221874			
R-squared (Adj. for d.f.) = 0.299222		Durbin-Watson statistic = 1.64494			

Plot of VR60

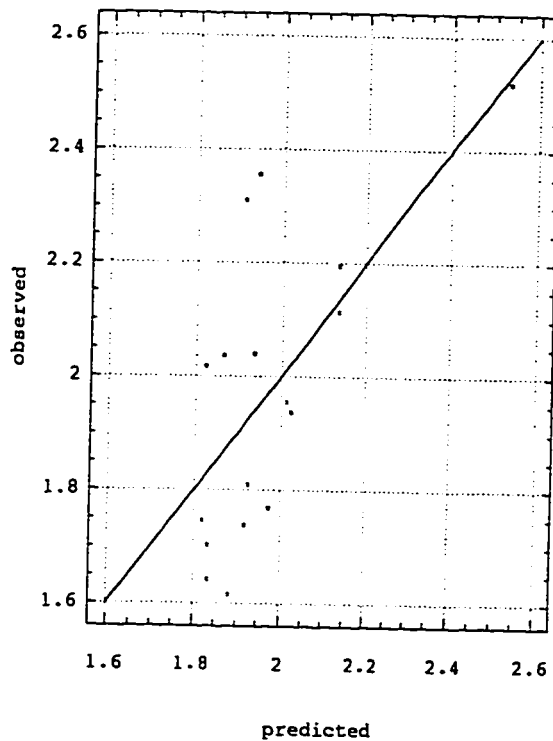
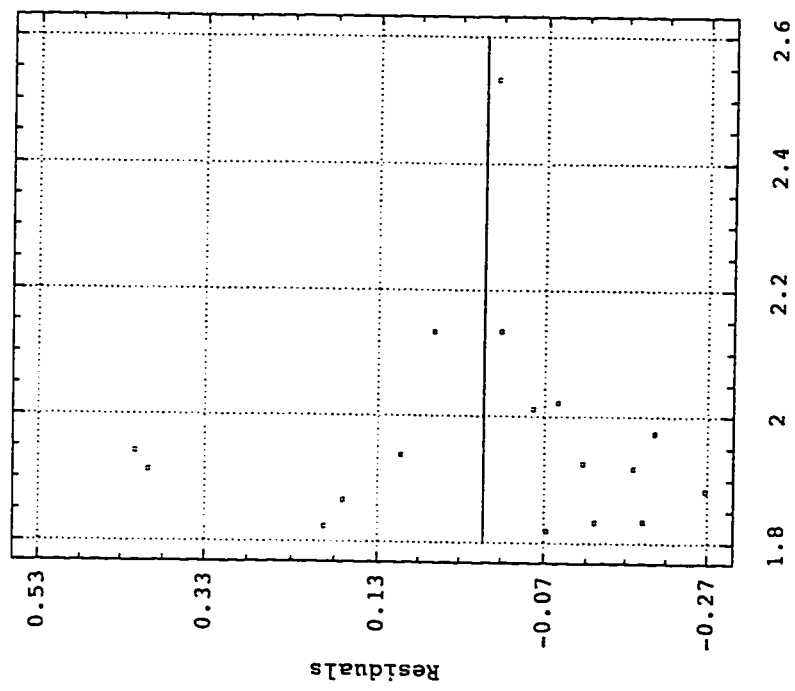


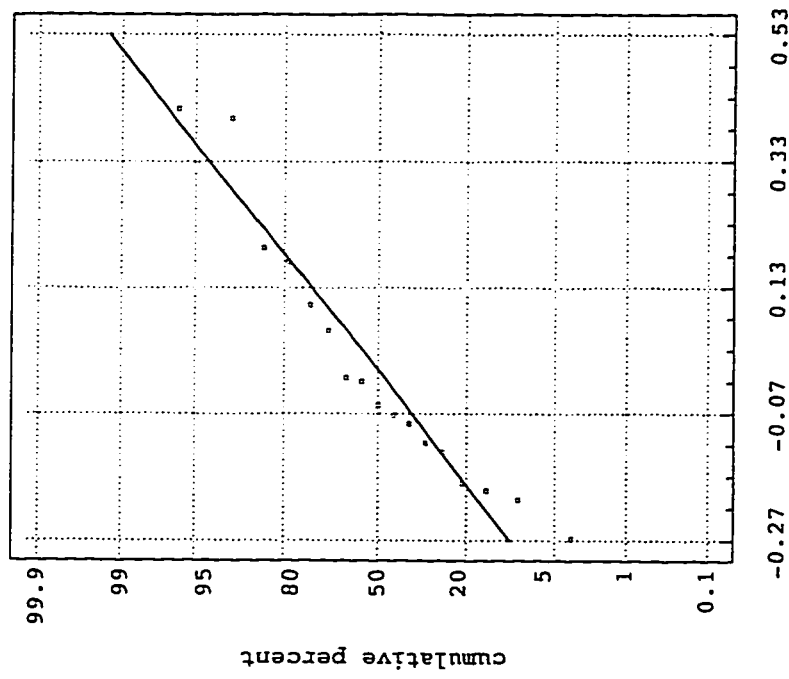
Fig. E-19

Residual Plot for VR60



Predicted

Normal Probability Plot for VR60



Residuals

Fig. E-20

Model fitting results for: VR135					
Independent variable	coefficient	std. error	t-value	sig.level	
CONSTANT	-5.096803	3.112335	-1.6376	0.1298	
R-1/12	4.381242	4.018894	1.0902	0.2989	
R-3/12	0.139167	0.089512	1.5547	0.1483	
R-7/12	0.214071	0.106691	2.0065	0.0700	
R-10/12	0.223762	0.122044	1.8335	0.0939	
R-12/12	0.109058	0.029896	3.6479	0.0038	
R-SQ. (ADJ.) = 0.5868 SE= 0.080491 MAE= 0.047955 DurbWat= 2.333					
17 observations fitted, forecast(s) computed for 0 missing val. of dep. var.					
Analysis of Variance for the Full Regression					
Source	Sum of Squares	DF	Mean Square	F-Ratio	P-value
Model	0.179586	5	0.0359172	5.54383	0.0086
Error	0.0712664	11	0.00647876		
Total (Corr.)	0.250852	16			
R-squared = 0.715903		Std. error of est. = 0.0804908			
R-squared (Adj. for d.f.) = 0.586768		Durbin-Watson statistic = 2.33322			

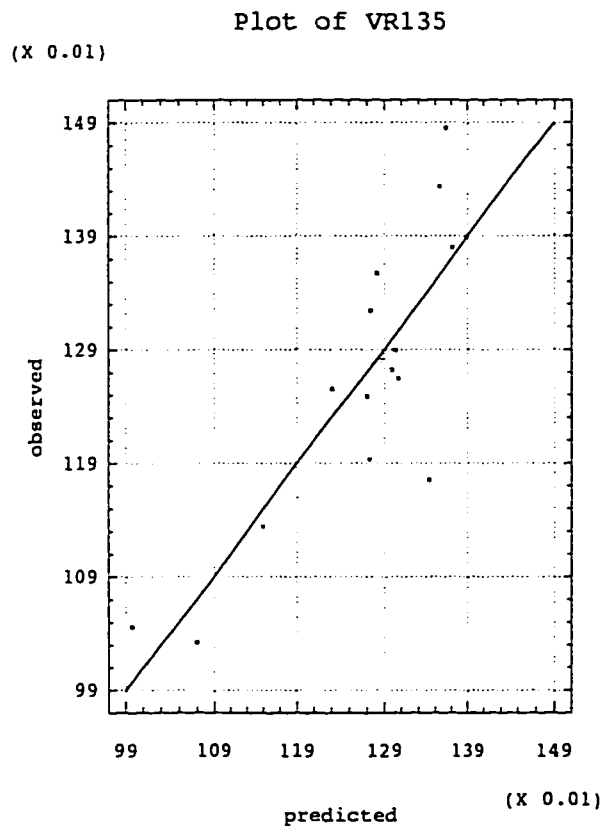
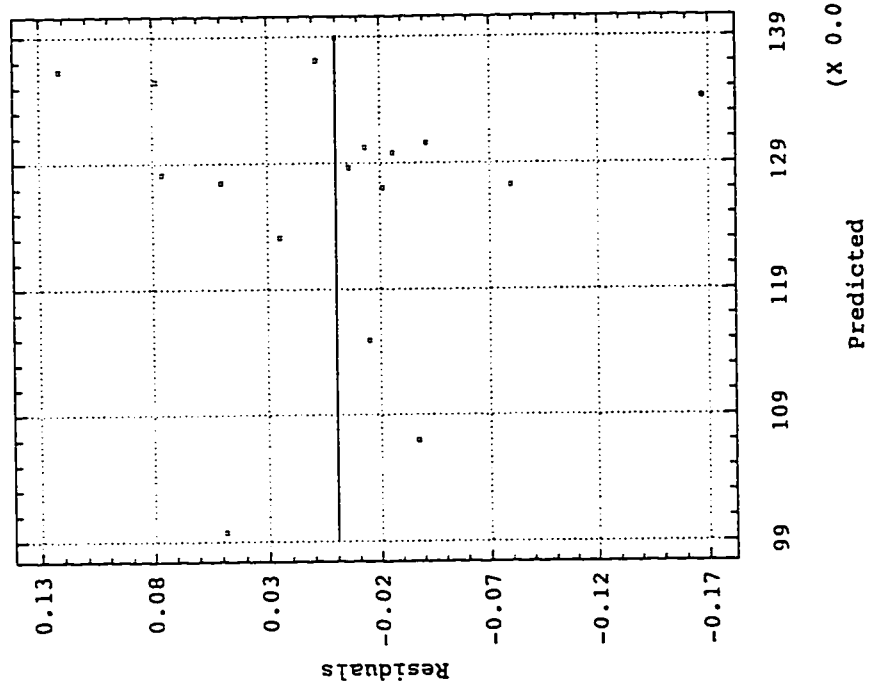


Fig. E-21

Residual Plot for VR135



Normal Probability Plot for VR135

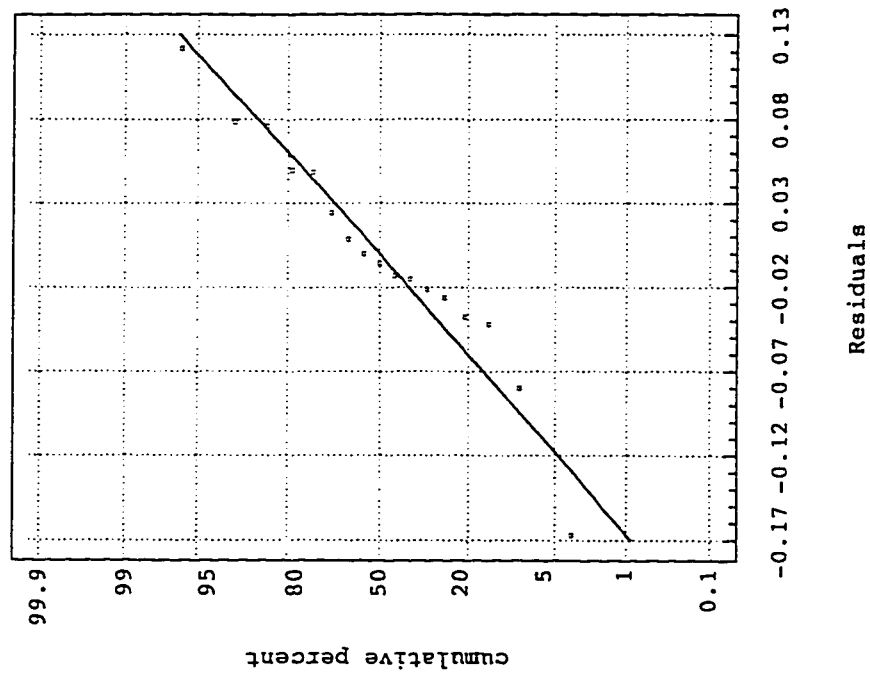


Fig. E-22

Model fitting results for: PI					
Independent variable	coefficient	std. error	t-value	sig.level	
CONSTANT	-1.82027	1.183907	-1.5375	0.1501	
R-1/12	-15.438427	4.885854	-3.1598	0.0082	
R-4/12	0.347251	0.065823	5.2755	0.0002	
R-9/12	-0.103134	0.051211	-2.0139	0.0670	
R-11/12	0.03493	0.029365	1.1895	0.2572	
R-SQ. (ADJ.) = 0.7518 SE= 0.146046 MAE= 0.104487 DurbWat= 2.985					
17 observations fitted, forecast(s) computed for 0 missing val. of dep. var.					
Analysis of Vanance for the Full Regression					
Source	Sum of Squares	DF	Mean Square	F-Ratio	P-value
Model	1.11879	4	0.279697	13.1132	0.0002
Error	0.255954	12	0.0213295		
Total (Corr.)	1.37474	16			
R-squared = 0.813817		Std. error of est. = 0.146046			
R-squared (Adj. for d.f.) = 0.751756		Durbin-Watson statistic = 2.98527			

Normal Probability Plot for PI

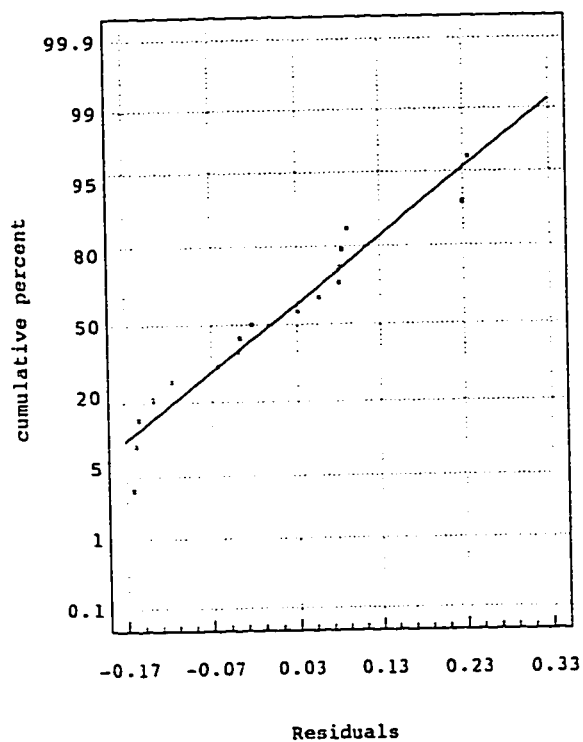
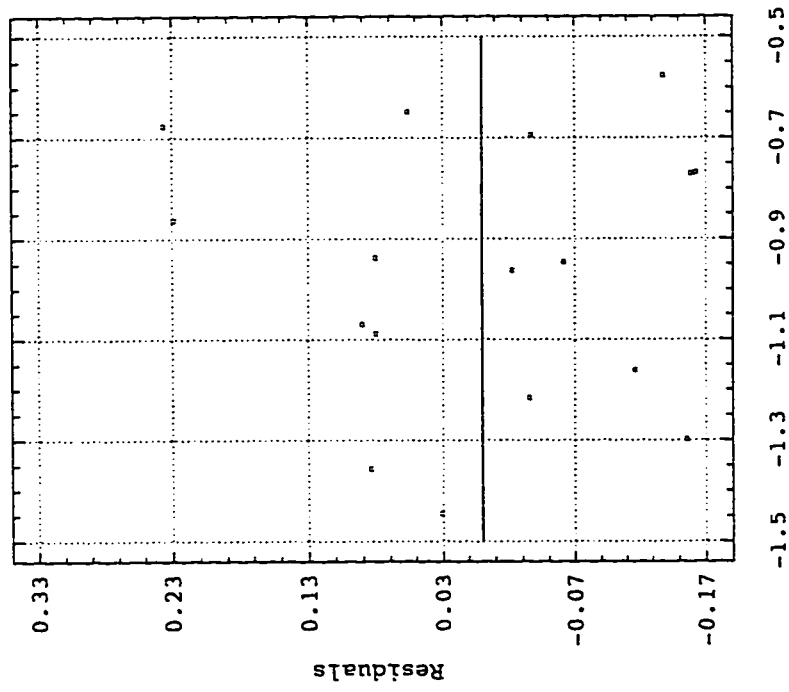


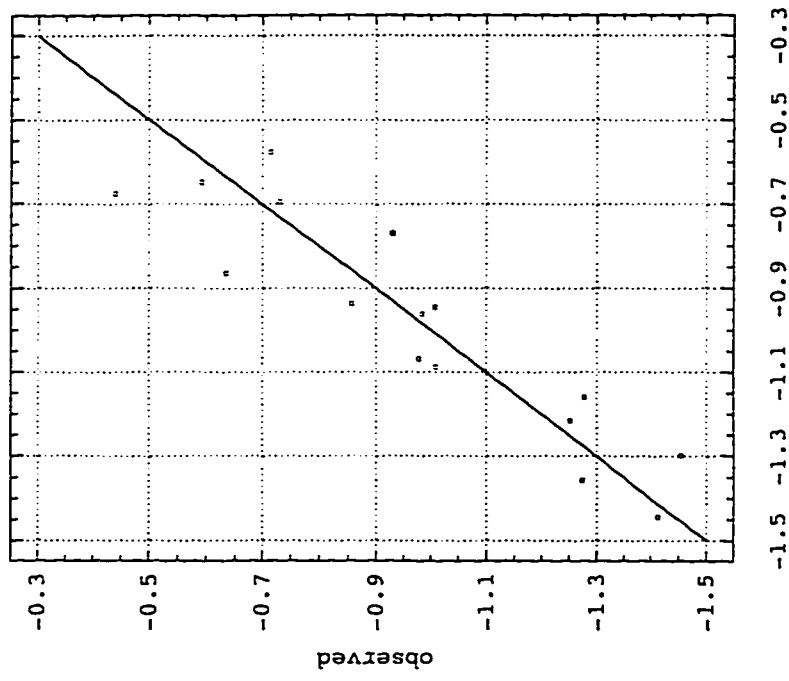
Fig. E-23

Residual Plot for PI



Predicted

Plot of PI



predicted

Fig. E-24

Model fitting results for PR					
Independent variable	coefficient	std. error	t-value	sig. level	
CONSTANT	-925.416151	269.756391	-3.4306	0.0064	
R-1/12	649.389344	317.714135	2.0439	0.0682	
R-3/12	-6.484008	6.111165	-1.0610	0.3136	
R-4/12	34.847538	9.061167	3.8458	0.0032	
R-8/12	35.469176	13.449009	2.6373	0.0248	
R-12/12	27.232232	6.239044	4.3648	0.0014	
SKEW	-125.971905	78.716353	-1.6003	0.1406	
R-SQ (ADJ) = 0.6612 SE= 6.120492 MAE= 4.078656 DurbWat= 2.398					
17 observations fitted. forecast(s) computed for 0 missing val. of dep. var					
Analysis of Varnance for the Full Regression					
Source	Sum of Squares	DF	Mean Square	F-Ratio	P-value
Model	1394.28	6	232.38	6.20336	0.0061
Error	374.604	10	37.4604		
Total (Corr.)	1768.89	16			
R-squared = 0.788226		Std. error of est. = 6.12049			
R-squared (Adj. for d.f.) = 0.661161		Durbin-Watson statistic = 2.35767			

Plot of PR

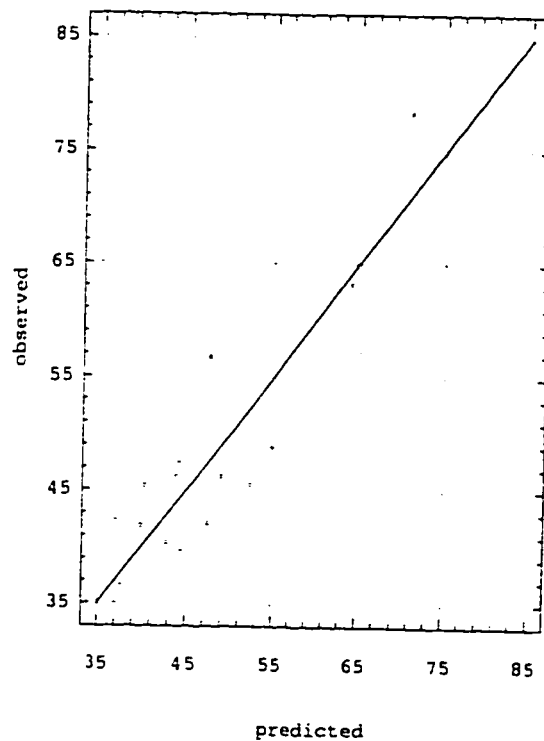
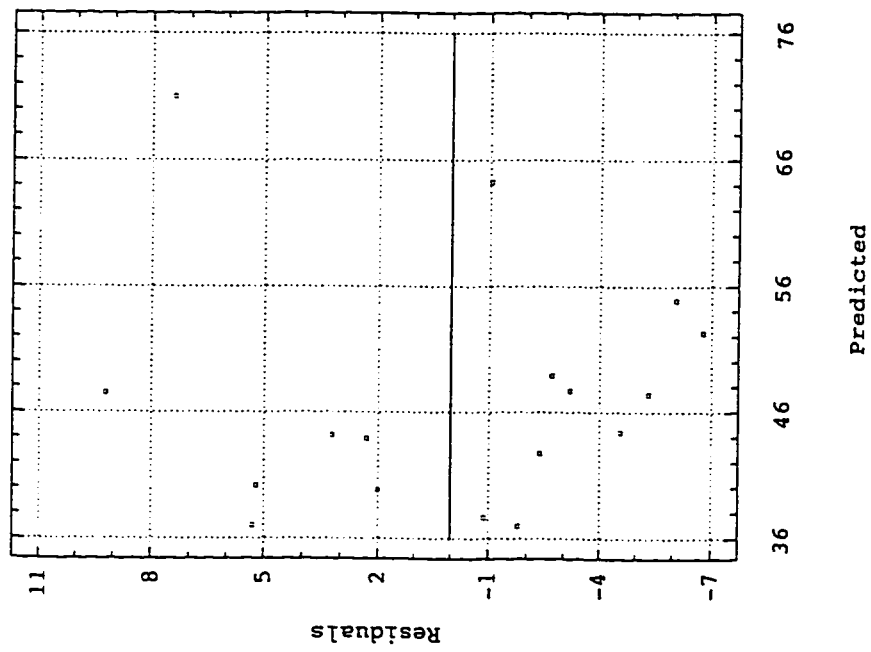


Fig. E-25

Residual Plot for PR



Normal Probability Plot for PR

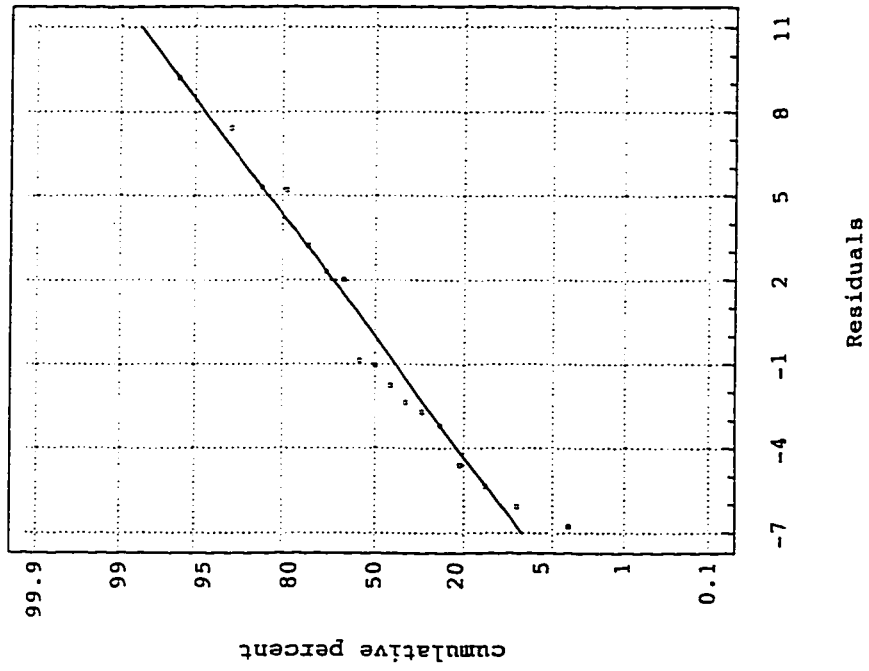


Fig. E-26

Model fitting results for: PVN					
Independent variable	coefficient	std. error	t-value	sig.level.	
CONSTANT	-3.480438	0.702473	-4.9546	0.0003	
R-5/12	0.376845	0.058197	6.4753	0.0000	
R-6/12	-0.120092	0.035453	-3.3873	0.0049	
R-9/12	0.046007	0.024253	1.8970	0.0803	
R-SQ. (ADJ.) = 0.7220 SE= 0.078671 MAE= 0.041537 DurbWat= 2.464					
17 observations fitted. forecast(s) computed for 0 missing val. of dep. var.					
Analysis of Vancane for the Full Regression					
Source	Sum of Squares	DF	Mean Square	F-Ratio	P-value
Model	0.275708	3	0.0919026	14.8490	0.0002
Error	0.080459	13	0.00618915		
Total (Corr.)	0.356167	16			
R-squared = 0.774098		Std. error of est. = 0.0786712			
R-squared (Adj. for d.f.) = 0.721966		Durbin-Watson statistic = 2.46437			

Plot of PVN

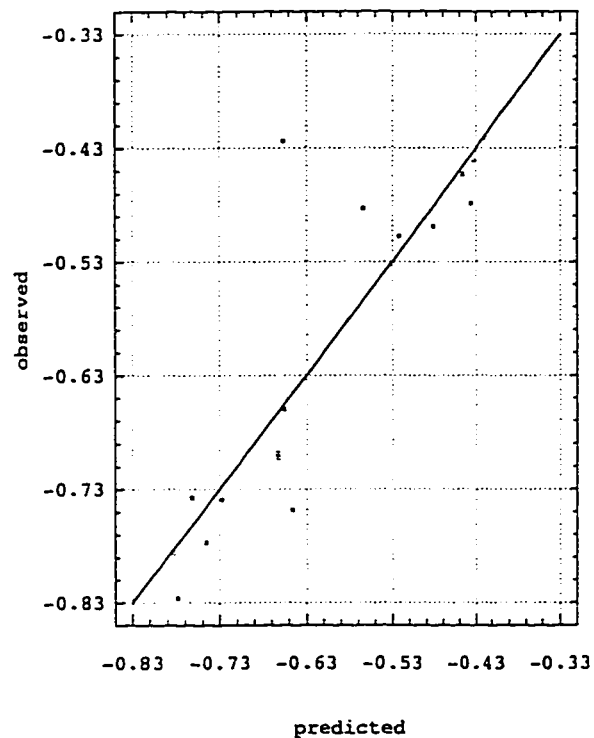
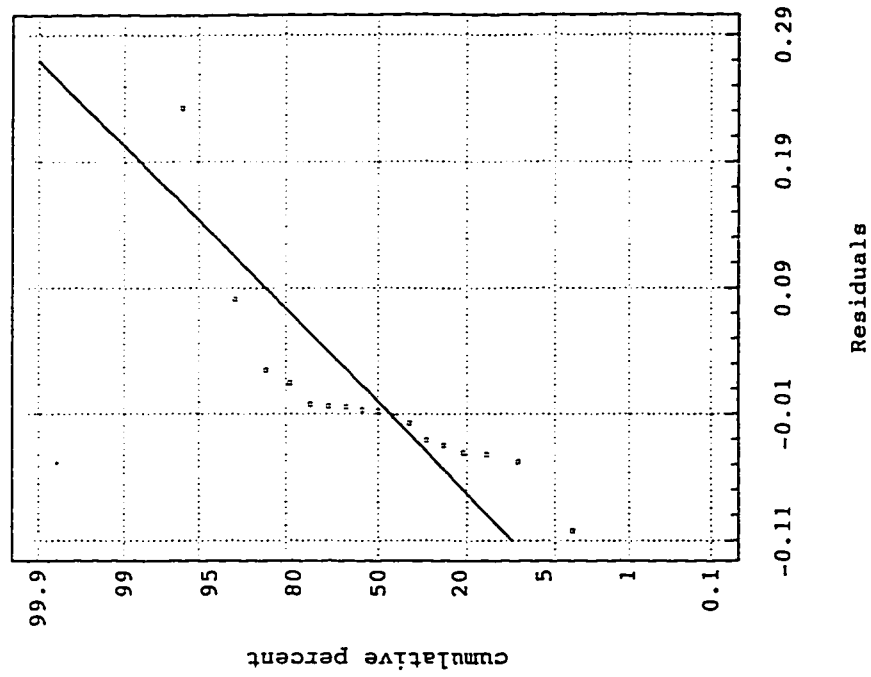
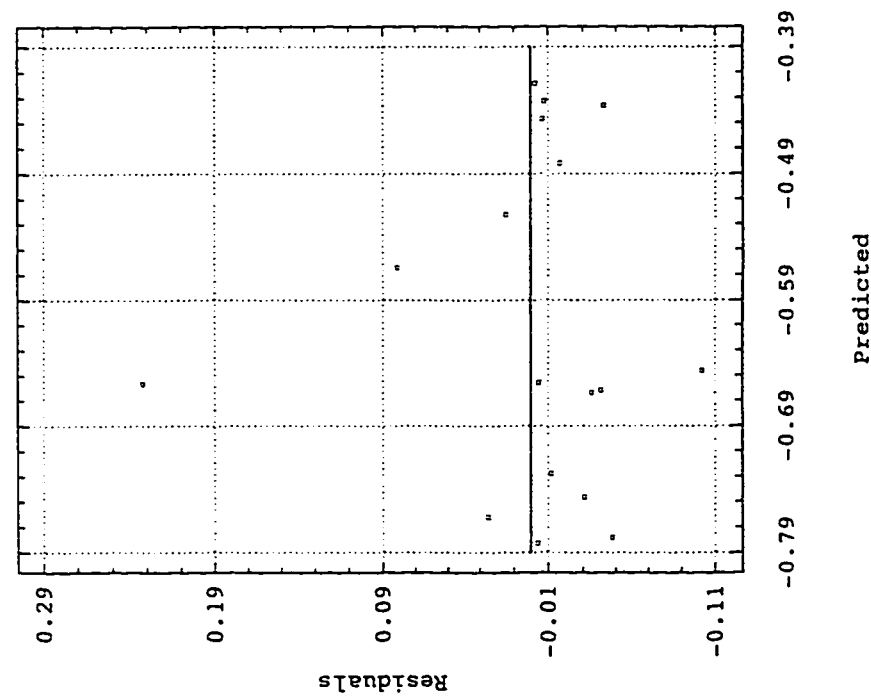


Fig. E-27

Normal Probability Plot for PVN



Residual Plot for PVN



Residuals

Predicted

Fig. E-28

Model fitting results for: VTS					
Independent variable	coefficient	std. error	t-value	sig.level	
CONSTANT	4.406966	0.354735	12.4233	0.0000	
R-2/12	-0.240523	0.150749	-1.5955	0.1366	
R-3/12	0.169393	0.063137	2.6829	0.0199	
R-4/12	-0.129049	0.031922	-4.0426	0.0016	
R-9/12	-0.022569	0.017018	-1.3261	0.2095	
R-SQ. (ADJ.) = 0.6018 SE= 0.047059 MAE= 0.028658 DurbWat= 2.522					
17 observations fitted, forecast(s) computed for 0 missing val. of dep. var.					
Analysis of Variance for the Full Regression					
Source	Sum of Squares	DF	Mean Square	F-Ratio	P-value
Model	0.0624091	4	0.0156023	7.04546	0.0037
Error	0.0265742	12	0.00221451		
Total (Corr.)	0.0889832	16			
R-squared = 0.701358		Std. error of est. = 0.0470586			
R-squared (Adj. for d.f.) = 0.60181		Durbin-Watson statistic = 2.52215			

Plot of VTS

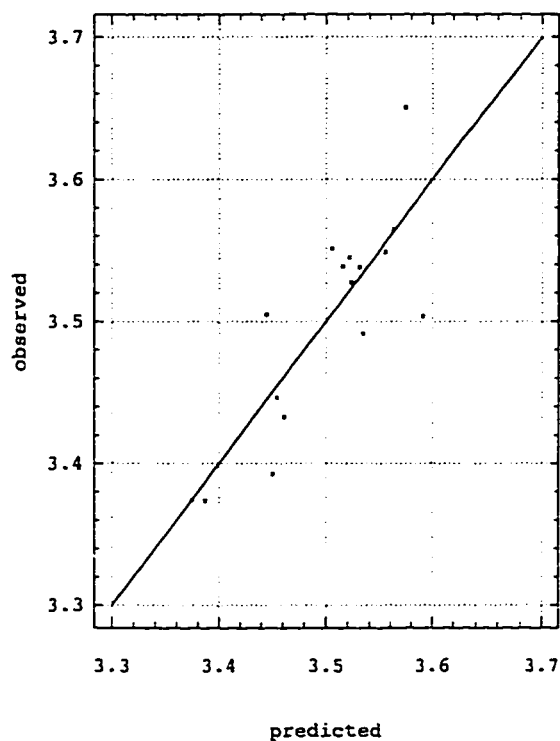
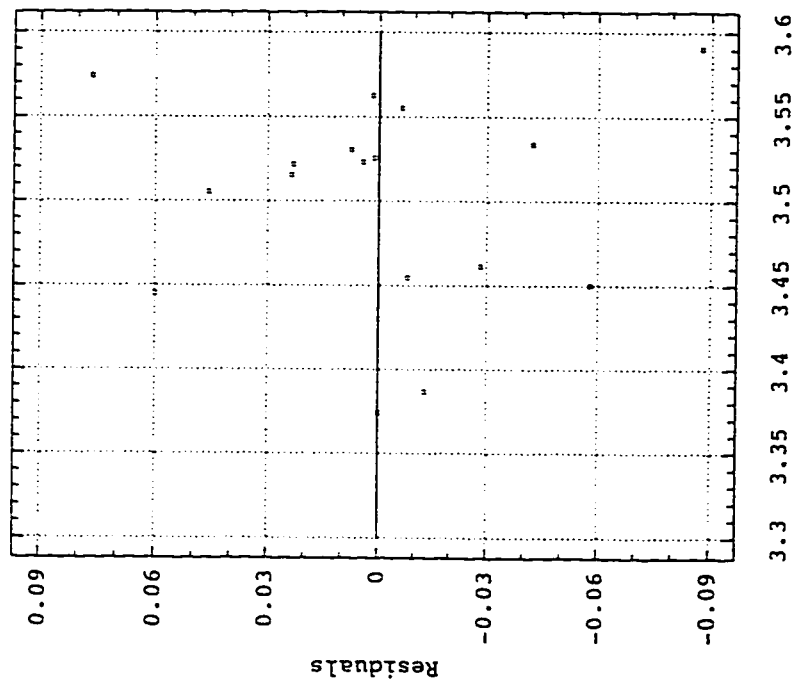


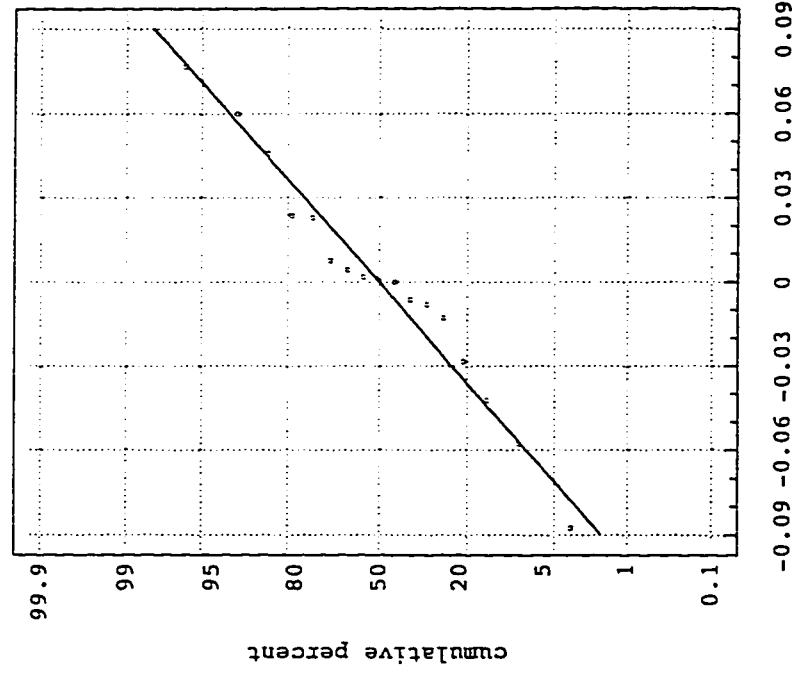
Fig. E-29

Residual Plot for ALL VTS



Predicted

Normal Probability Plotfor VTS



Residuals

Fig. E-30

Model fitting results for: 1/(LOWER)					
Independent variable	coefficient	std. error	t-value	sig.level	
CONSTANT	-0.191277	0.0954381	-2.0042	0.0545	
R-1/12	-0.016962	0.002298	-7.3819	0.0000	
R-4/12	0.00545	0.002499	2.1809	0.0374	
R-6/12	0.013623	0.004	3.4059	0.0020	
R-8/12	-0.003589	0.003225	-1.1128	0.2749	
R-10/12	0.011919	0.004013	2.9705	0.0059	
STANDARD DEV.	-0.018301	0.008159	-2.2430	0.0327	
SKEW	0.089852	0.015405	5.8325	0.0000	
R-SQ. (ADJ.) = 0.6185 SE= 0.004607 MAE= 0.003280 DurWat= 2.515					
37 observations fitted, forecast(s) computed for 0 missing val. of dep. var.					
Analysis of Variance for the Full Regression					
Source	Sum of Squares	DF	Mean Square	F-Ratio	P-value
Model	0.00138707	7	0.000198153	9.33605	0.0000
Error	0.000615511	29	2.12245E-05		
Total (Corr.)	0.00200258	36			
R-squared = 0.692641					Std. error of est. = 0.00460701
R-squared (Adj. for d.f.) = 0.618451					Durbin-Watson statistic = 2.51532

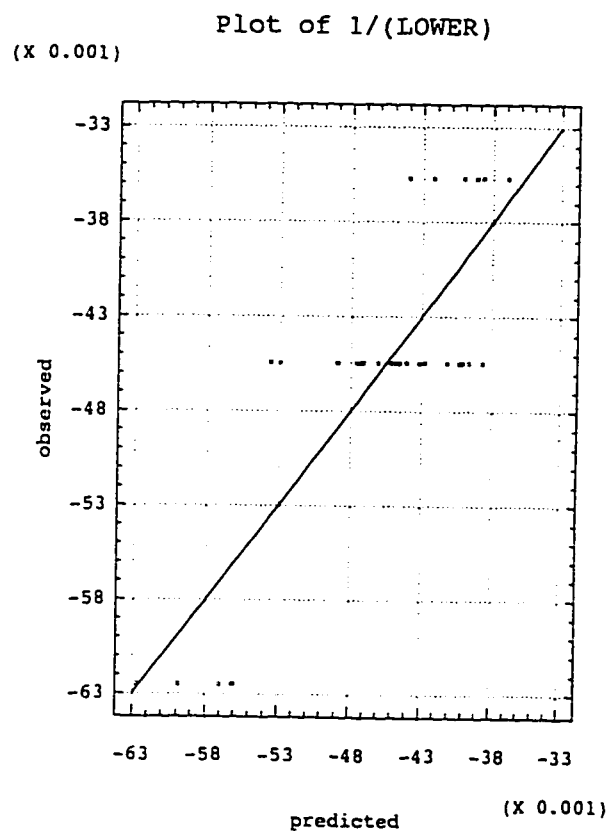
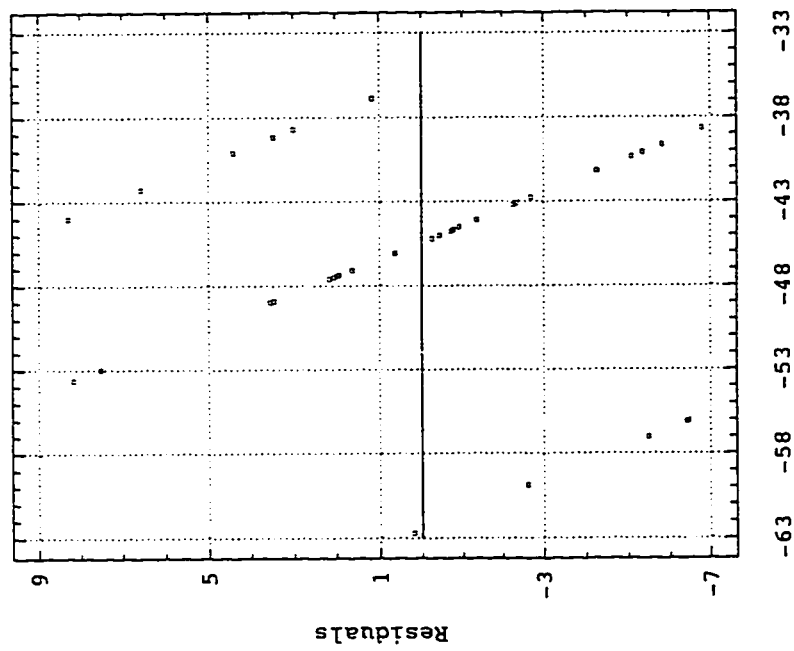


Fig. E-31

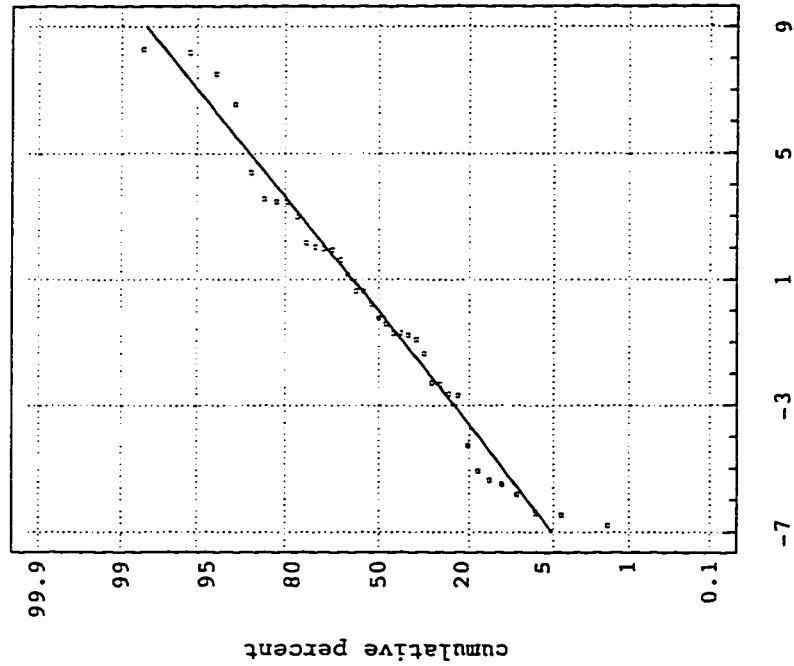
Residual Plot for 1/(LOWER)

(X 0.001)



Predicted (X 0.001)

Norm. Prob. Plot for 1/(LOWER)



Residuals (X 0.001)

Fig. E-32

Model fitting results for: Gg					
Independent variable	coefficient	std. error	t-value	sig.level	
CONSTANT	126.506227	18.889833	6.6971	0.0001	
R-3/12	-1.330358	0.42823	-3.1066	0.0111	
R-5/12	-4.112983	1.236507	-3.3263	0.0077	
R-6/12	-6.816957	1.955003	-3.4869	0.0059	
R-7/12	2.719568	1.309713	2.0765	0.0646	
R-8/12	-1.125474	0.971133	-1.1589	0.2734	
R-9/12	-1.954437	0.785951	-2.4867	0.0322	
SKEW	-22.904258	2.06313	-11.1017	0.0000	
R-SQ. (ADJ.) = 0.9027 SE= 0.767411 MAE= 0.486446 DurbWat= 2.555					
18 observations fitted, forecast(s) computed for 19 missing val. of dep. var.					
Analysis of Vanance for the Full Regression					
Source	Sum of Squares	DF	Mean Square	F-Ratio	P-value
Model	96.9632	7	13.8519	23.5208	0.0000
Error	5.8892	10	0.58892		
Total (Corr.)	102.852	17			
R-squared = 0.942741		Std. error of est. = 0.767411			
R-squared (Adj. for d.f.) = 0.90266		Durbin-Watson statistic = 2.55535			

Plot of GG

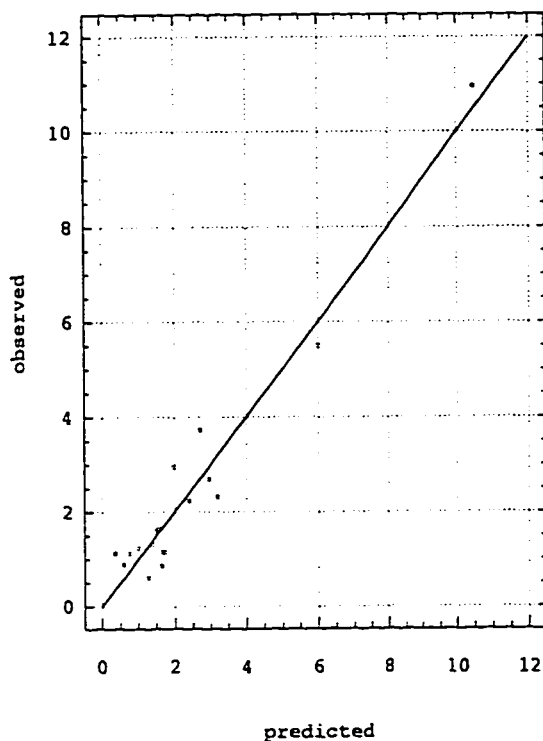
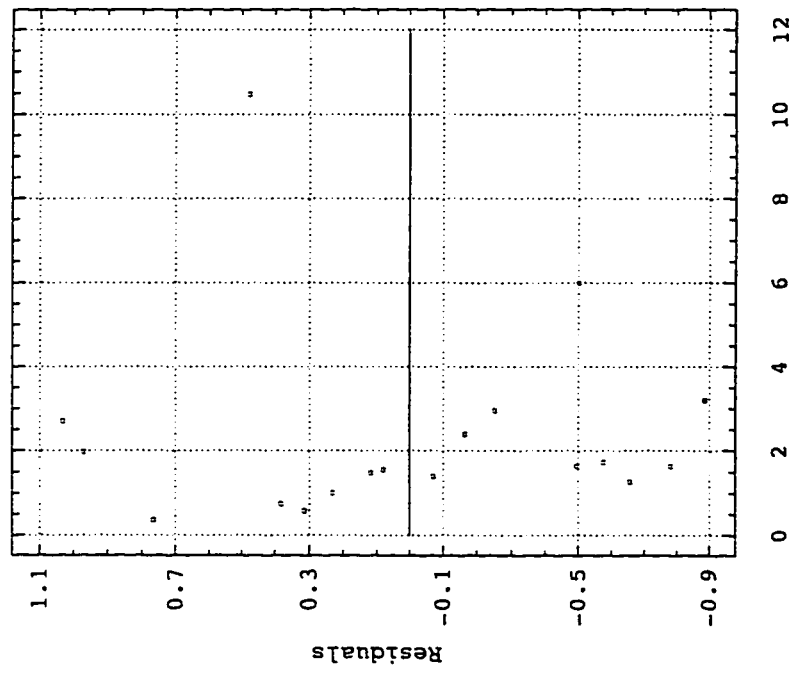


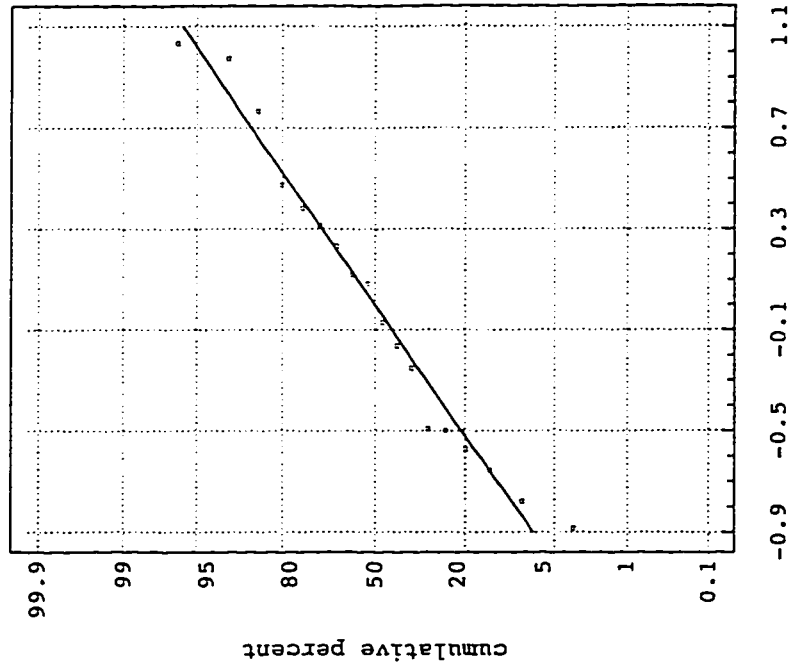
Fig. E-33

Residual Plot for GG



Predicted

Normal Probability Plot for Gg



Residuals

Fig. E-34

Model fitting results for:			LN(R)		
Independent variable	coefficient	std. error	t-value	sig.level	
CONSTANT	5.698026	0.648938	8.7805	0.0000	
R-5/12	-0.338751	0.058585	-5.7823	0.0000	
R-9/12	-0.057005	0.011655	-4.8911	0.0000	
R-12/12	-0.16282	0.025369	-6.4181	0.0000	
SKEW	-0.793361	0.142496	-5.5676	0.0000	
R-SQ. (ADJ.) = 0.6777 SE= 0.096113 MAE= 0.070771 DurbWat= 1.955					
35 observations fitted, forecast(s) computed for 2 missing val. of dep. var.					
Analysis of Vanance for the Full Regression					
Source	Sum of Squares	DF	Mean Square	F-Ratio	P-value
Model	0.697259	4	0.174315	18.8700	0.0000
Error	0.277129	30	0.00923765		
Total (Corr.)	0.974388	34			
R-squared = 0.715586		Std. error of est. = 0.0961127			
R-squared (Adj. for d.f.) = 0.677664		Durbin-Watson statistic = 1.95461			

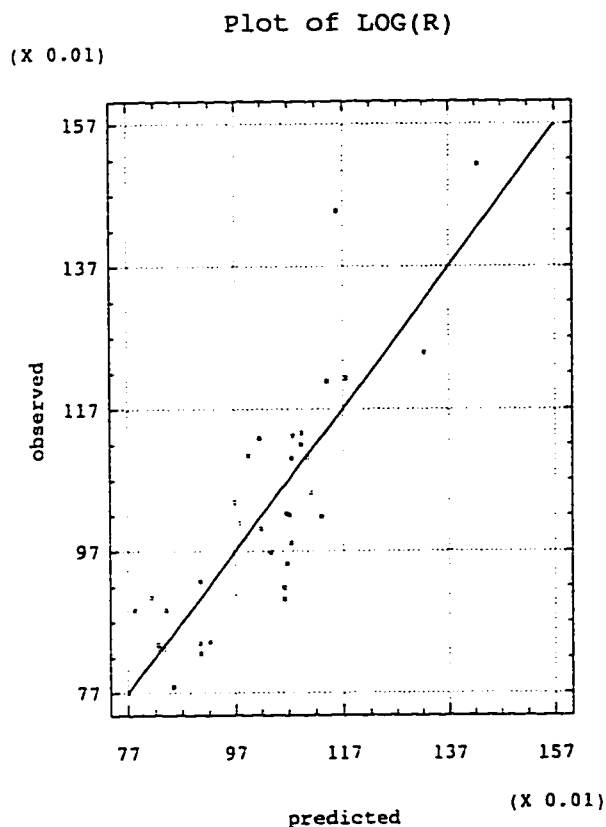
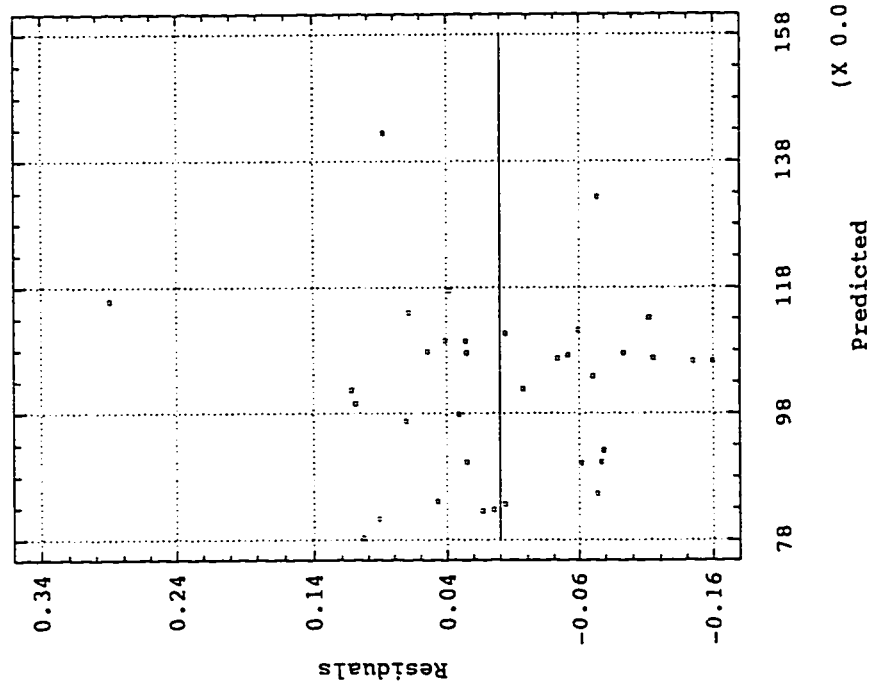


Fig. E-35

Residual Plot for LOG(R)



Norm. Prob. Plot for LOG(R)

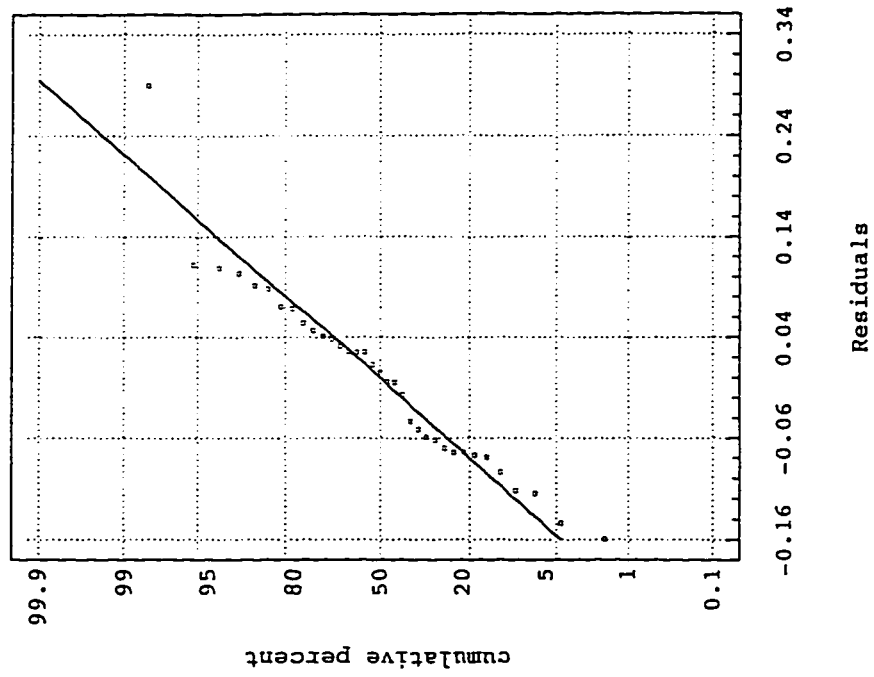


Fig. E-36

Model fitting results for: 1/(ω₀)					
Independent variable	coefficient	std. error	t-value	sig.level	
CONSTANT	1.34E+08	8.19E+07	1.6296	0.1144	
R-2/12	-4.05E+07	1.10E+07	-3.6666	0.0010	
R-3/12	3.53E+07	7.01E+06	5.0390	0.0000	
R-4/12	-1.40E+07	7.05E+06	-1.9931	0.0561	
R-8/12	-1.37E+07	9.02E+06	-1.5223	0.1392	
STANDARD DEV.	2.30E+07	2.15E+07	1.0699	0.2938	
SKEW	7.08E+07	3.69E+07	1.9211	0.0650	
R-SQ. (ADJ.) = 0.4453 SE=14559783.904047 MAE= 9295993.449872 DurbWat= 1.449					
35 observations fitted, forecast(s) computed for 2 missing val. of dep. var.					
Analysis of Variance for the Full Regression					
Source	Sum of Squares	DF	Mean Square	F-Ratio	P-value
Model	7.06E+15	6	1.18E+15	5.54906	0.0007
Error	5.94E+15	28	2.12E+14		
Total (Corr.)	1.30E+16	34			
R-squared = 0.543188					Std. error of est. = 1.45598E7
R-squared (Adj. for d.f.) = 0.4453					Durbin-Watson statistic = 1.44875

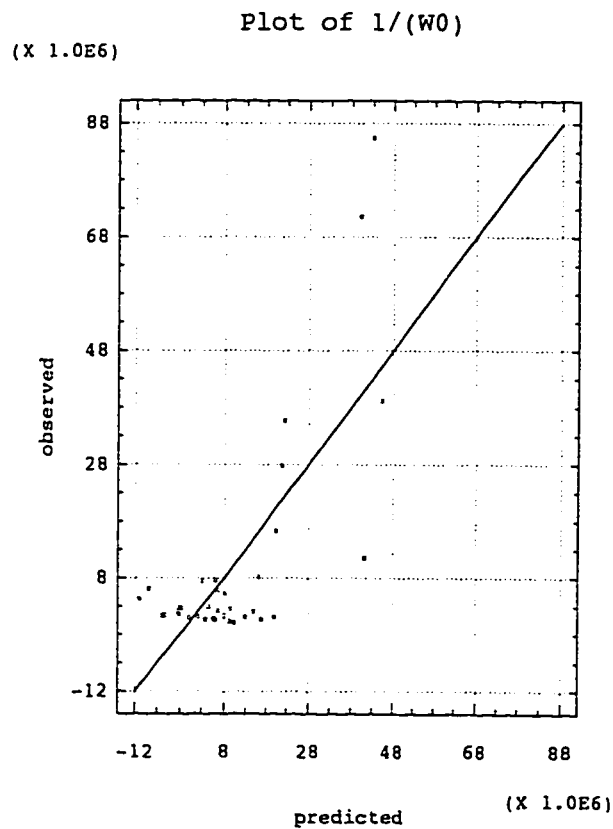
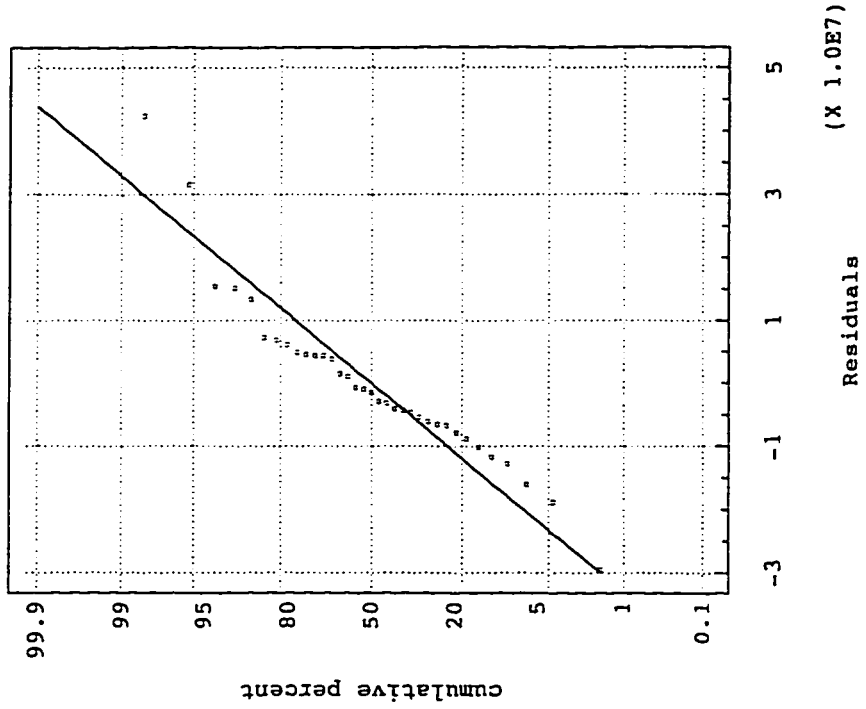


Fig. E-37

Normal Probability Plot for 1/W0



Residual Plot for 1/(W0)

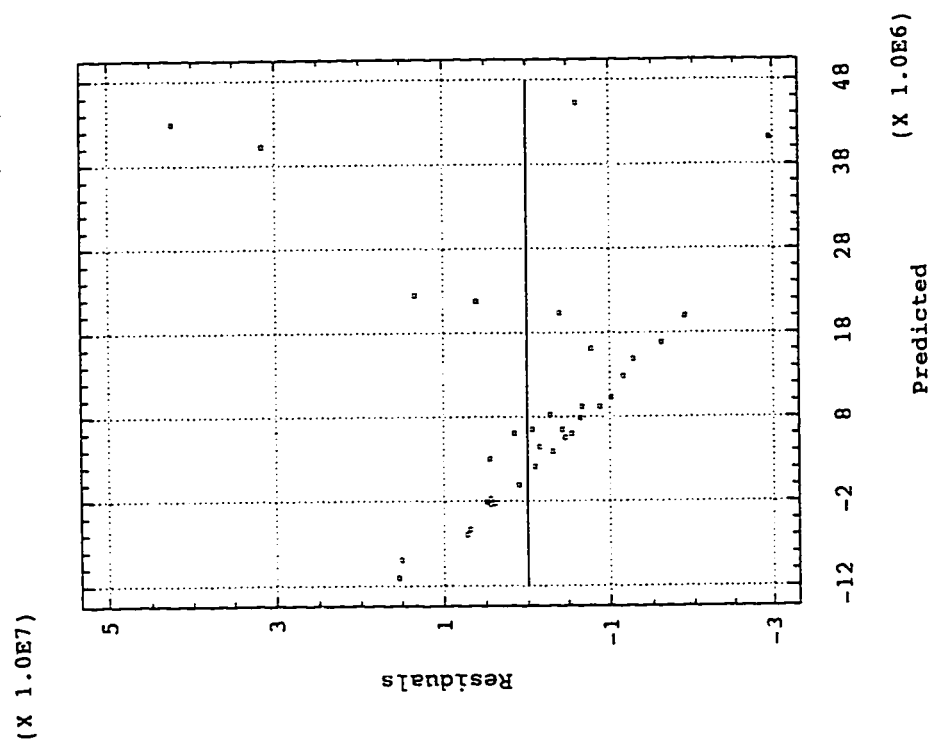


Fig. E-38

Model fitting results for: η_1					
Independent variable	coefficient	std. error	t-value	sig.level	
CONSTANT	5.04E+07	3.75E+07	1.3457	0.1885	
R-2/12	-3.62E+07	7.22E+06	-5.0081	0.0000	
R-3/12	3.11E+07	6.56E+06	4.7445	0.0000	
R-4/12	-1.53E+07	6.98E+06	-2.1975	0.0358	
SKEW	1.60E+07	1.24E+07	1.2855	0.2085	
R-SQ. (ADJ.) = 0.4335 SE=14611413.057497 MAE= 9598242.351509 DurbWat= 1.576					
35 observations fitted, forecast(s) computed for 2 missing val. of dep. var.					
Analysis of Vancane for the Full Regression					
Source	Sum of Squares	DF	Mean Square	F-Ratio	P-value
Model	6.41E+15	4	1.60E+15	7.50429	0.0003
Error	6.40E+15	30	2.13E+14		
Total (Corr.)	1.28E+16	34			
R-squared = 0.500143		Std. error of est. = 1.46114E7			
R-squared (Adj. for d.f.) = 0.433495		Durbin-Watson statistic = 1.57614			

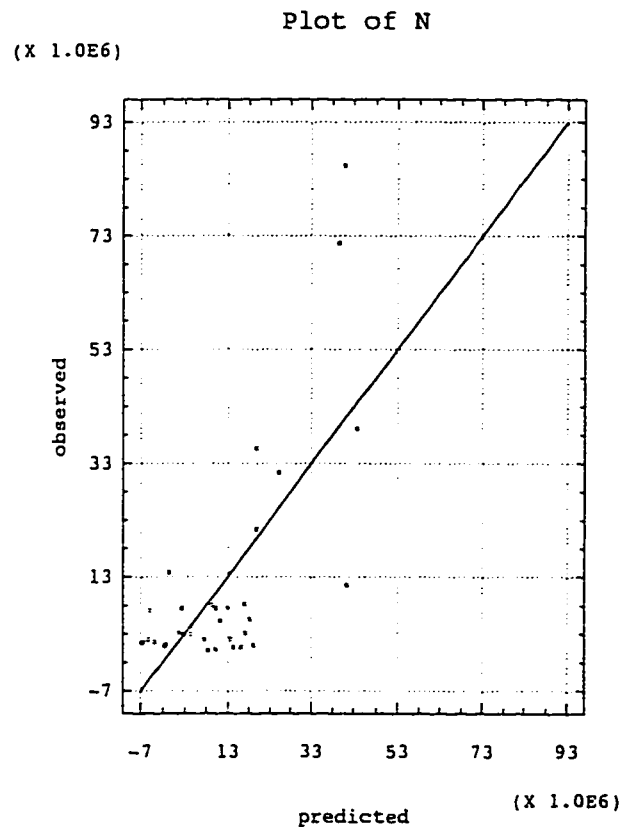


Fig. E-39

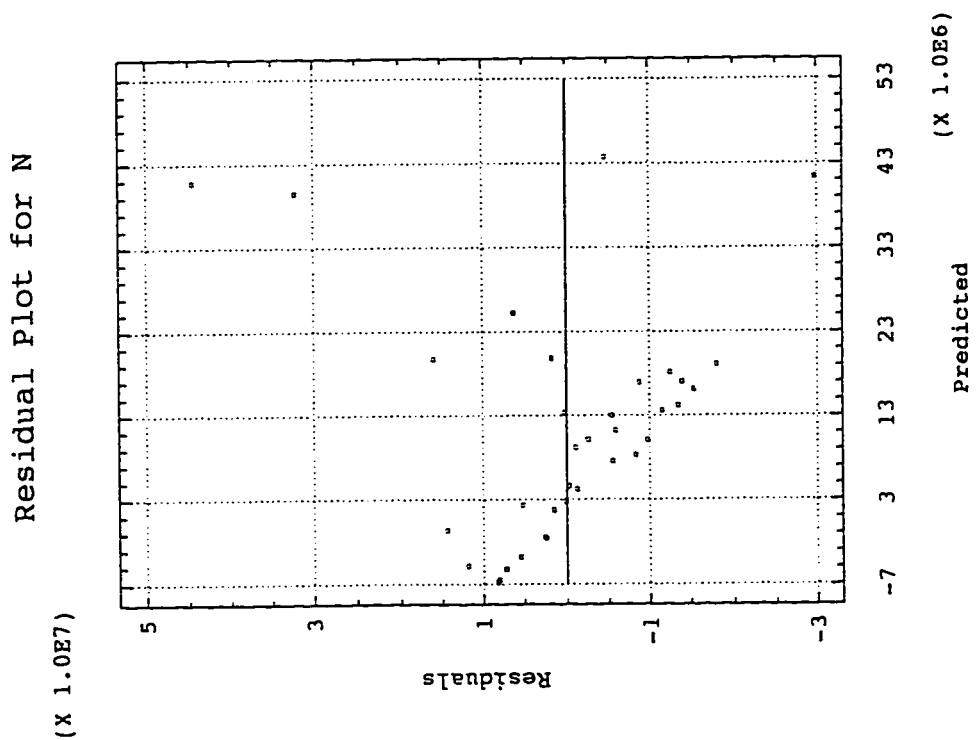
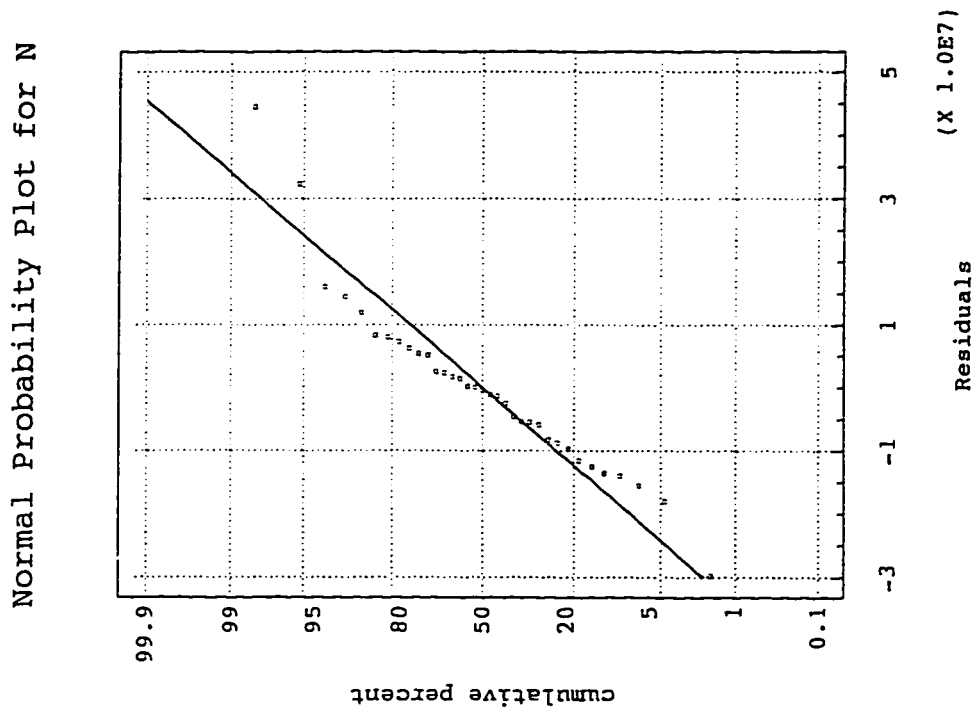


Fig. E-40

Model fitting results for: LN(G* / sin δ)					
Independent variable	coefficient	std. error	t-value	sig.level	
CONSTANT	51.210207	16.750732	3.0572	0.0050	
R-2/12	-1.61515	0.86776	-1.8613	0.0736	
R-3/12	2.434106	0.717176	3.3940	0.0021	
R-4/12	-6.698443	1.296911	-5.1649	0.0000	
R-5/12	9.953518	1.594007	6.2443	0.0000	
R-6/12	-6.421931	1.072204	-5.9895	0.0000	
R-9/12	-1.00771	0.474413	-2.1241	0.0430	
R-11/12	-2.604	0.464175	-5.6100	0.0000	
R-SQ. (ADJ.) = 0.5425 SE= 1.243030 MAE= 0.768360 DurbWat= 2.171					
35 observations fitted, forecast(s) computed for 2 missing val. of dep. var					
Analysis of Varnance for the Full Regression					
Source	Sum of Squares	DF	Mean Square	F-Ratio	P-value
Model	73.1094	7	10.4442	6.75945	0.0001
Error	41.7184	27	1.54512		
Total (Corr.)	114.828	34			
R-squared = 0.636687		Std. error of est. = 1.24303			
R-squared (Adj. for d.f.) = 0.542495		Durbin-Watson statistic = 2.17116			

Plot of $\text{LOG}(G/\sin d)$

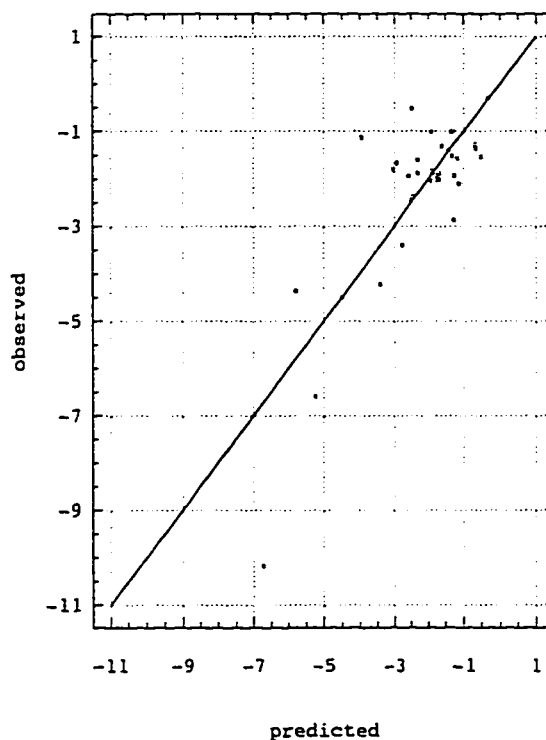
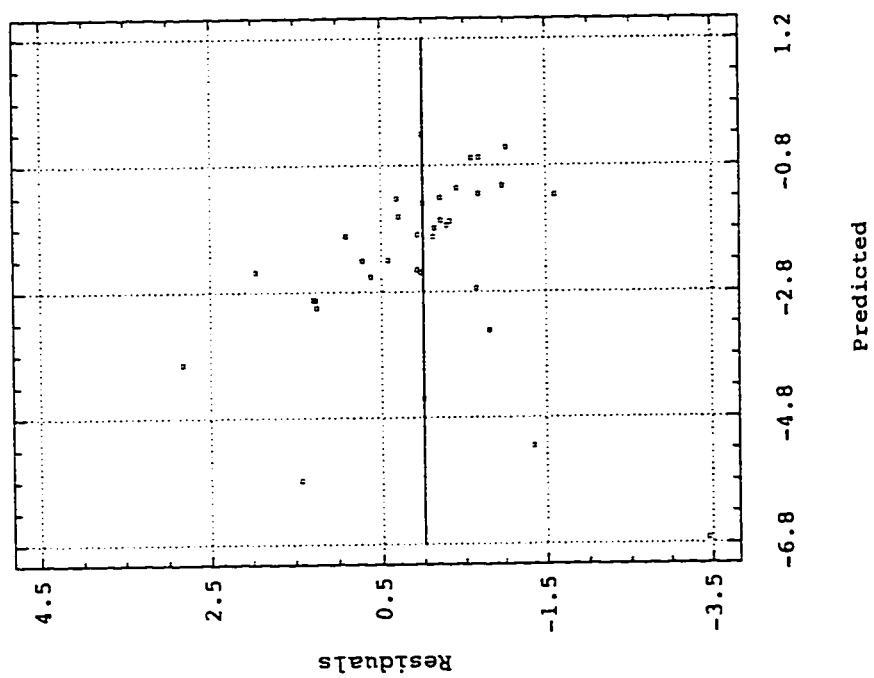


Fig. E-41

Residual Plot for LOG(G/sin d)



Norm. Prob. Plot for LOG(G/sin d)

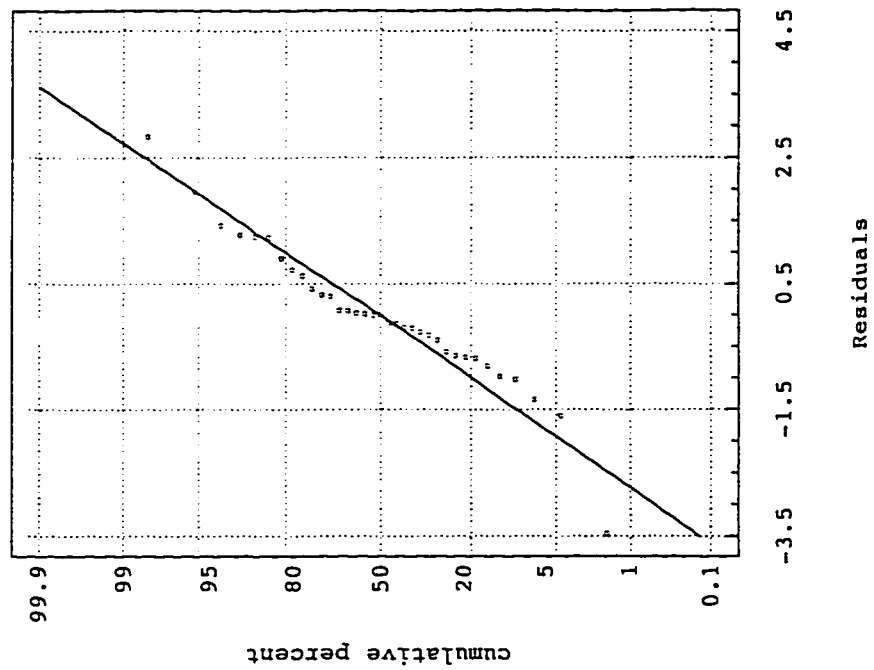


Fig. E-42

Model fitting results for: LN(G* X sin δ)					
Independent variable	coefficient	std. error	t-value	sig.level	
CONSTANT	-176.867978	34.372007	-5.1457	0.0000	
R-2/12	2.99396	1.185403	2.5257	0.0177	
R-3/12	1.460473	0.491818	2.9695	0.0062	
R-5/12	9.33847	1.583098	5.8989	0.0000	
R-8/12	2.253596	0.769323	2.9293	0.0068	
R-10/12	3.075994	0.731703	4.2039	0.0003	
R-12/12	3.010177	0.636002	4.7330	0.0001	
SKEW	15.23095	3.418587	4.4553	0.0001	
R-SQ. (ADJ.) = 0.5425 SE= 1.364741 MAE= 0.840762 DurbWat= 2.065					
35 observations fitted, forecast(s) computed for 2 missing val. of dep. var.					
Analysis of Vanance for the Full Regression					
Source	Sum of Squares	DF	Mean Square	F-Ratio	P-value
Model	88.1256	7	12.5894	6.75933	0.0001
Error	50.288	27	1.86252		
Total (Corr.)	138.414	34			
R-squared = 0.636683		Std. error of est. = 1.36474			
R-squared (Adj. for d.f.) = 0.54249		Durbin-Watson statistic = 2.06489			

Plot of LOG(GXSIND)

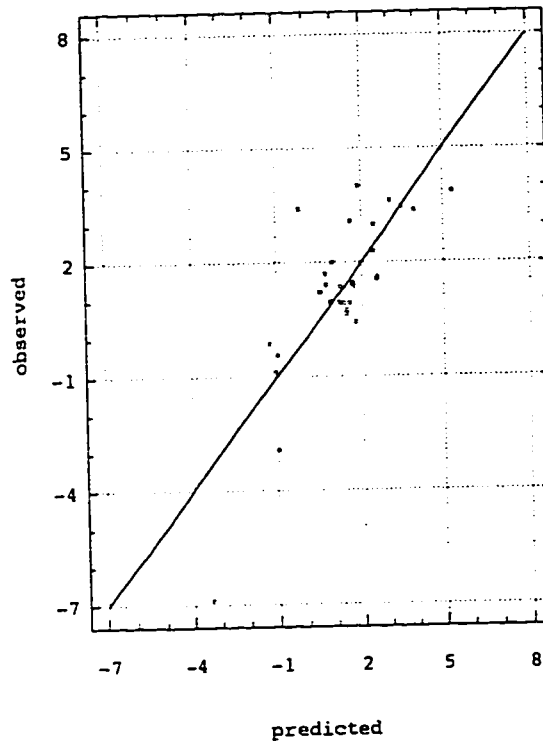
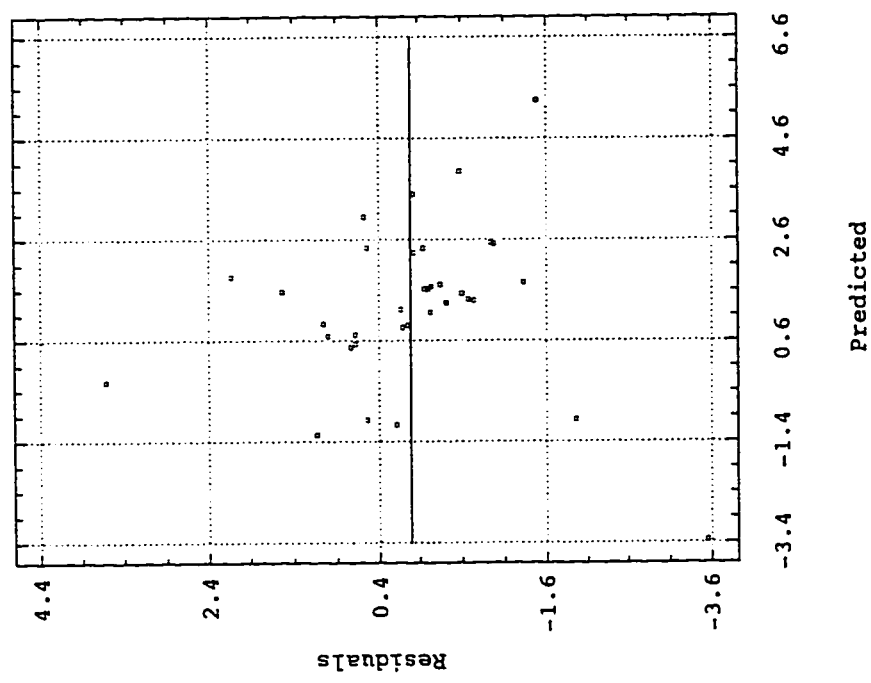


Fig. E-43

Residual Plot for LOG(GXSIND)



Norm. Prob. Plot LOG(G X sin d)

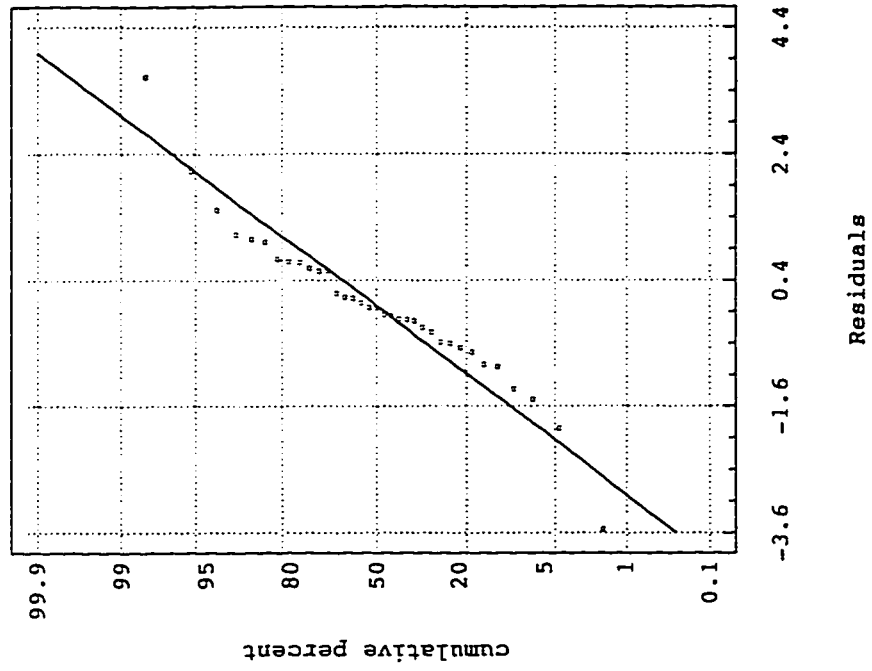


Fig. E-44

Model fitting results for: 1/(S)					
Independent variable	coefficient	std. error	t-value	sig.level	
CONSTANT	-7.43E+08	1.08E+08	-6.9135	0.0000	
R-1/12	2.13E+07	4.71E+06	4.5202	0.0001	
R-2/12	3.35E+07	4.44E+06	7.5513	0.0000	
R-8/12	3.21E+07	4.59E+06	6.9899	0.0000	
R-9/12	1.37E+07	4.21E+06	3.2668	0.0030	
R-10/12	-8.33E+06	4.50E+06	-1.8511	0.0751	
R-12/12	1.19E+07	3.51E+06	3.3873	0.0022	
SKEW	-2.24E+08	2.92E+07	-7.6883	0.0000	
R-SQ. (ADJ.) = 0.7214 SE= 7546059.781668 MAE= 4994485.578884 DurbWat= 2.101					
35 observations fitted, forecast(s) computed for 2 missing val. of dep. var.					
Analysis of Vanance for the Full Regression					
Source	Sum of Squares	DF	Mean Square	F-Ratio	P-value
Model	5.41E+15	7	7.73E+14	13.5788	0.0000
Error	1.54E+15	27	5.69E+13		
Total (Corr.)	6.95E+15	34			
R-squared = 0.778782					Std. error of est. = 7.54606E6
R-squared (Adj. for d.f.) = 0.721429					Durbin-Watson statistic = 2.1008

Plot of LOG(S)

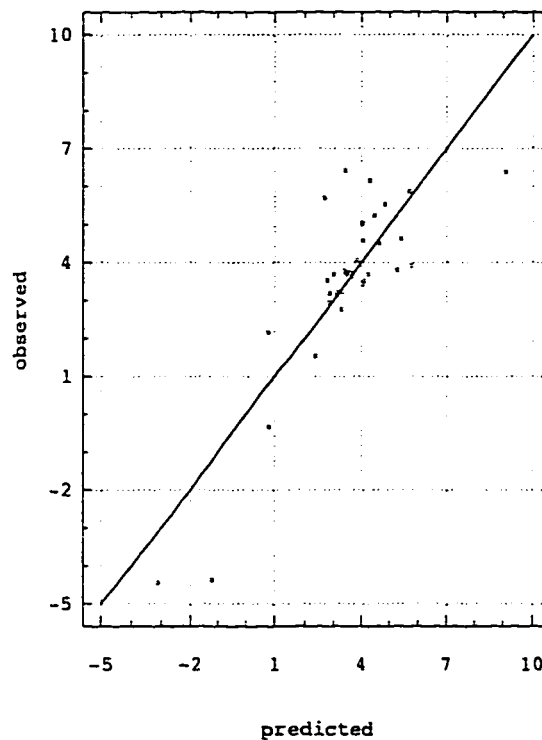
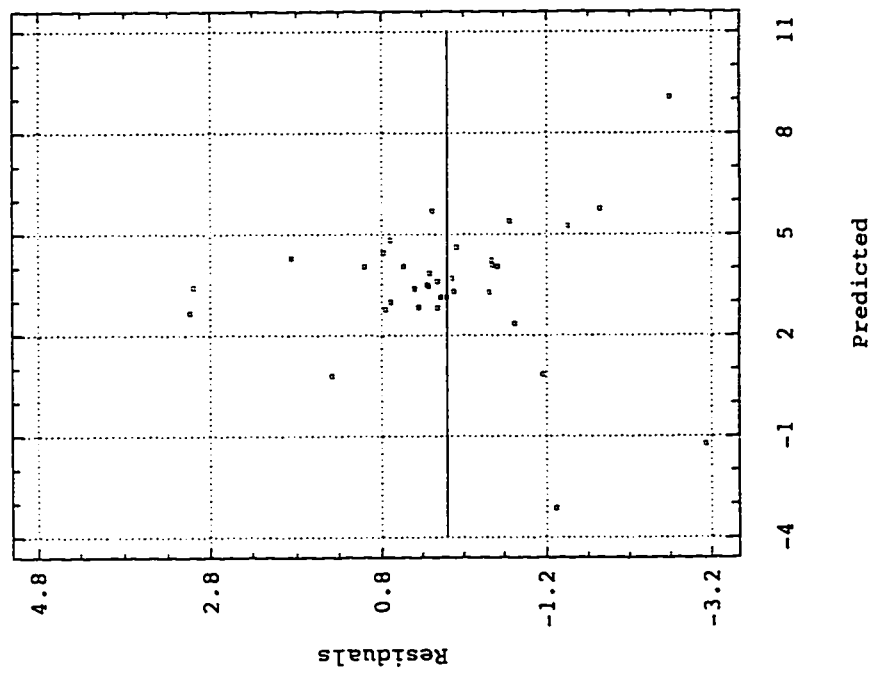


Fig. E-45

Residual Plot for LOG(S)



Normal Probability Plot for LOG(S)

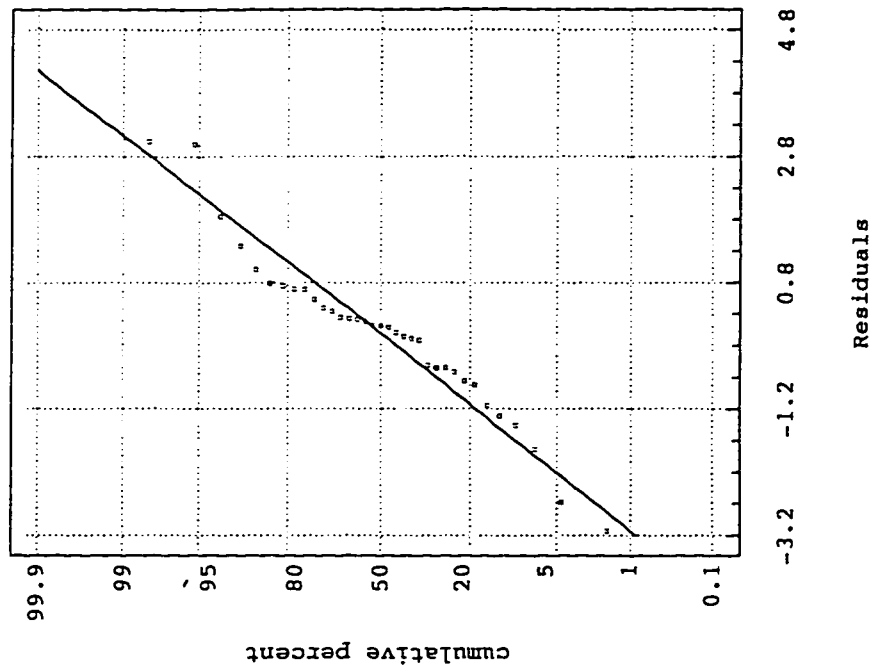


Fig. E-46

Model fitting results for: 1/(m)					
Independent variable	coefficient	std. error	t-value	sig.level	
CONSTANT	4.784595	1.666889	2.8704	0.0076	
R-2/12	-0.15463	0.091407	-1.6917	0.1014	
R-7/12	-0.099901	0.074919	-1.3335	0.1928	
R-8/12	-0.091977	0.049835	-1.8456	0.0752	
R-9/12	0.263462	0.069739	3.7778	0.0007	
R-10/12	-0.319226	0.074216	-4.3013	0.0002	
R-SQ. (ADJ.) = 0.5266 SE= 0.179151 MAE= 0.128317 DurbWat= 1.862					
35 observations fitted, forecast(s) computed for 2 missing vai. of dep. var.					
Analysis of Variance for the Full Regression					
Source	Sum of Squares	DF	Mean Square	F-Ratio	P-value
Model	1.37446	5	0.274891	8.56487	0.0000
Error	0.93076	29	0.0320952		
Total (Corr.)	2.30522	34			
R-squared = 0.596237 Stnd. error of est. = 0.179151					
R-squared (Adj. for d.f.) = 0.526623 Durbin-Watson statistic = 1.86166					

Normal Probability Plot for 1/M

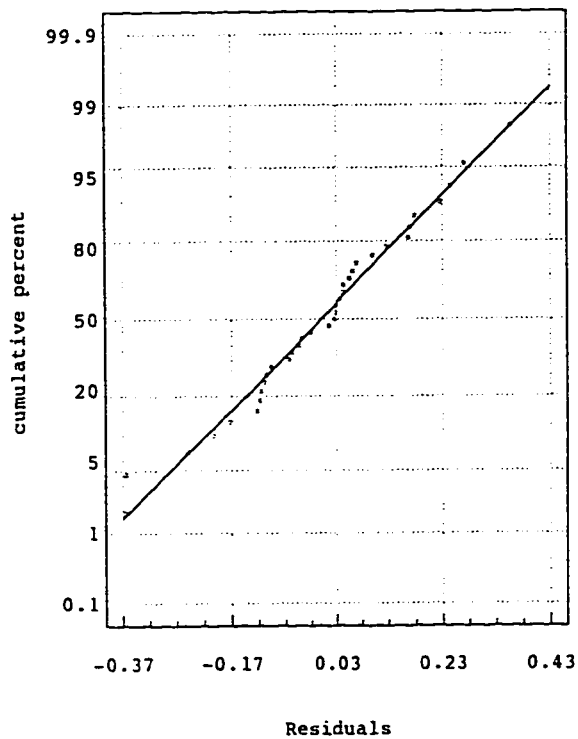
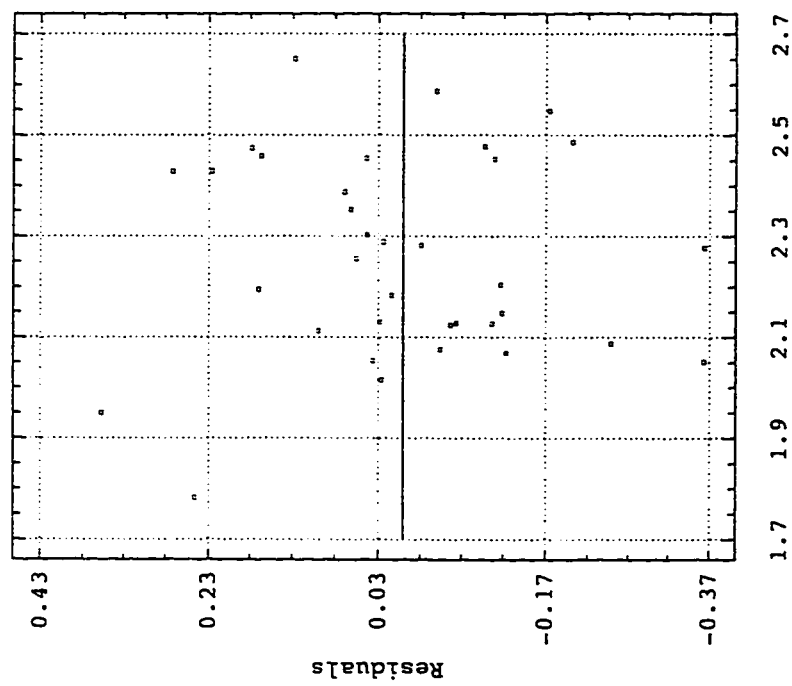


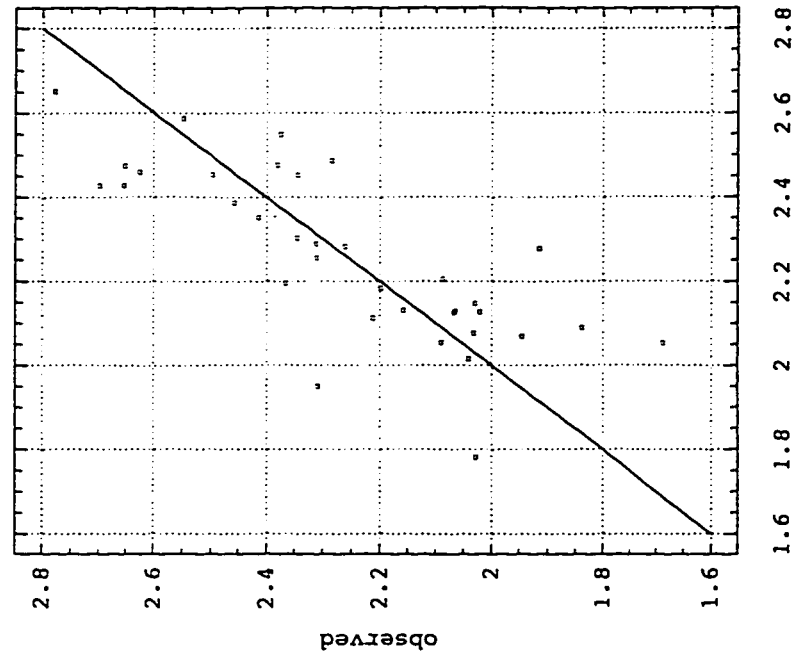
Fig. E-47

Residual Plot for $1/(M)$



Predicted

Plot of $1/(M)$



predicted

Fig. E-48